CYCLIC STRESS-STRAIN BEHAVIOR OF SAND IN OFFSHORE ENVIRONMENT

by

JAN HEDBERG

Dipl.-Ing., Technische Hochschule Darmstadt
(1972)

S.M., Massachusetts Institute of Technology
(1975)

SUBMITTED IN PARTIAL FULFILLMENT

OF THE REQUIREMENTS FOR THE

DEGREE OF

DOCTOR OF PHILOSOPHY

at the

MASSACHUSETTS INSTITUTE OF TECHNOLOGY

October, 1977

Signature of Author.....
Department of Civil Engineering, October 3, 1977

Certified by.....
Thesis Supervisor

Accepted by.....
Chairman, Department Committee

To Mimi

CYCLIC STRESS-STRAIN BEHAVIOR OF SAND IN OFFSHORE ENVIRONMENT

by

JAN HEDBERG

Submitted to the Department of Civil Engineering on October 3, 1977 in partial fulfillment of the requirements for the Degree of Doctor of Philosophy.

ABSTRACT

Behavior of sand subjected to cyclic loading has been investigated based on results from 80 cyclic tests and 75 static tests. The test program concentrated on the influence of stress path on behavior of undrained sand at different densities. Most tests were performed in triaxial cells.

A tendency to volume increase was demonstrated for the combination of dense sand and small cyclic shear stress ratio. Cyclic loading under all other conditions yielded a tendency for the sand to decrease in volume. Very loose samples could suddenly lose strength and collapse during one load cycle.

The average shear stress in cyclic triaxial test samples has a profound influence on strain and pore pressure development. Isotropic cyclic tests with zero average shear stress developed rapidly large strains (reversing direction each cycle) after the generated pore pressure reached the value of the confining stress. Anisotropic cyclic tests with vertical stress larger than horizontal stress throughout the cycle slowly accumulated vertical compression strains. Anisotropic cyclic tests with horizontal stress always exceeding vertical stress developed rapidly large vertical extension strains.

Detailed test results are presented that related the influence of density, cyclic shear stress ratio, mean normal stress, average shear stress and the number of load cycles to the development of strain and pore pressure. Based on those results, a procedure to predict strain and pore pressure development for different values of the above variables is presented.

In addition, effects of stress history, partial drainage and testing conditions on strain and pore pressure development were investigated.

Thesis Supervisor: T. William Lambe
Title: Professor of Civil Engineering

ACKNOWLEDGEMENTS

I am grateful to Professor T. William Lambe, my faculty advisor and thesis supervisor, for both his guidance in this investigation and his interest in my educational and professional development. His suggestions and valuable encouragement are deeply appreciated.

I greatly enjoyed working with Dr. W. Allen Marr, co-supervisor of this thesis, and the source of daily comments and challenges. His frequent reviews contributed much to the final version of the thesis.

I would also like to express my sincere thanks to Professor Charles C. Ladd for reviewing the thesis and for valuable comments and encouragement. Mr. Oddvin Tokheim and Dr. Robert T. Martin made valuable suggestions in discussions of aspects of the investigation. Dr. Fransisco Silva assisted in building the cyclic testing machine and writing the data reduction program. The large amount of work reported in the thesis was made possible by the patient help of Mr. Todd Dickson in the laboratory, and Mrs. Dominique Caillaux, Mr. Keith Johson and Mr. Ralph Grismala. Thank you all!

Miss Phyllis Cusanelli did an excellent job in typing this thesis, as did Ms. Micheline Papadakau with the hundreds of figures.

The Dutch Government, through its agency Rijkswaterstaat Deltadienst, and in particular Mr. Jan Willum Boehmer, the geotechnical head of that agency, supported this laboratory investigation. Additional financial support for my studies was provided by the Philips Petroleum Company Fellowship in Civil Engineering at M.I.T., Maria and Helmich Jansons Legat, Oslo and Det norske Veritas' Utdannelsesstipend, for all of which I am greatly indebted.

But most of all I thank M.I.T. for an exciting growth environment, and my wife and children for spiritual support, joy and keeping up with me.

Table of Contents

Page

APPENDICES

List of Tables

List of Figures

LIST OF SYMBOLS

A	-	Pore pressure parameter = $\frac{\Delta u - \Delta\sigma_3}{\Delta\sigma_1 - \Delta\sigma_3}$
A_m	-	Area in middle of sample after deformation.
A_o	-	Initial sample area.
AR	-	Area ratio = $\frac{A_m - A_o}{A_o}$
a	-	Slope of strain or pore pressure contour.
B	-	Pore pressure coefficient for isotropic stress, $B = \Delta u/\Delta\sigma_c$.
b	-	Slope of strain or pore pressure contour.
CAD	-	Anisotropically consolidated drained test.
CID	-	Isotropically consolidated drained test.
$\overline{\text{CID}}$pp	-	Isotropically consolidated drained test with pore pressure increase.
CID-U	-	Isotropically consolidated drained unloading test.
$\overline{\text{CIU}}$	-	Isotropically consolidated undrained test.
CMEM	-	Membrane correction factor.
COMPR	-	Compression deformation.
C_n	-	Porosity correction factor.
$C_{\bar{p}}$	-	Mean consolidation stress correction factor.
$C_{\Delta q}$	-	Cyclic stress correction factor.
cm	-	Centimeter
DEF	-	Cyclic mobility deformation.
D_{10}	-	Grain diameter at which 10% is finer.
D_{50}	-	Mean grain diameter

D_{90} - Grain diameter at which 90% is finer.

d - Slope of strain or pore pressure contour.

E_c - Modulus to describe accumulated strain.

$$E_c = \frac{2}{\varepsilon_{vres}} (q_m + \Delta q_{cy})$$

E_{sec} - Secant modulus.

E_{sec}^{50} - Secant modulus at 50% of maximum strength.

ESP - Effective Stress Path.

EXT - Extension failure.

e - Void ratio.

e_o - Initial void ratio.

F.S. - Fine Oosterschelde Sand

G - Specific gravity.

in - Inch.

K_c - Consolidation stress ratio.

K_o - Coefficient of lateral stress at rest.

k - Coefficient of permeability.

kg - Kilogram.

LC - Lambe Cyclic test.

L.C. - Load Controlled Triaxial Test.

LS - Lambe Static test.

M - Pore pressure ratio, = $\Delta u / u_f$

M* - Membrane modulus.

M.S. - Medium Oosterschelde sand.

m - Meter.

mm - Millimeter.

min - Minute.

N - Number of cycles.

$N_{(\varepsilon_v = 1\%)}$ Number of cycles to ($\pm$) 1% strain.

N_ε or N_u Normalized number of cycles.

n - Porosity.

n_c - Porosity after consolidation.

n_{setup} Porosity at which sample is set up.

OCR - Over Consolidation Ratio.

p - $\frac{\sigma_v + \sigma_h}{2}$, "p-value," mean normal stress.

$\bar{p}$ - $\frac{\bar{\sigma}_v + \bar{\sigma}_h}{2}$, mean effective normal stress.

$\bar{p}_o$ - Initial mean effective normal stress.

psi - Pounds per square inch.

q - $\frac{\sigma_1 - \sigma_3}{2}$, "q-value," mean shear stress.

q_m - Mean shear stress about which a cyclic test is run.

$q_m/\bar{p}_o$ - Mean shear stress ratio in cyclic test.

Δq_{cy} - Half the total change in shear stress in a cyclic test.

$\Delta q_{cy}/\bar{p}_o$ Shear stress ratio in cyclic test.

R_d - Relative density.

sec - Second

S.C. - Strain Controlled Triaxial Test

T - Cyclic loading period, seconds.

TSP - Total Stress Path.

t - Ton.

t - Time.

t_m - Membrane thickness.

U - Coefficient of Uniformity.

u - Pore pressure.

u_b - Back pressure in triaxial test.

u_i^* - Degree of undercompaction.

u_f - Excess pore pressure at K_ε-line.

u_s - Steady-state pore pressure.

Δu - Pore pressure change.

V_c - Volume after consolidation

V_i - Initial volume.

V_{end} - Final volume

ΔV - Volume change.

W_c - Total cyclic hanger weight in kg.

W_h - Static hanger weight in kg.

W_s - Deadweight on static hanger in kg.

α^* - Angle of rotation on flywheel.

α - Inclination of the K_f-line.

β - Inclination of the K_ε-line.

γ - Shear strain.

γ_t - Total unit weight.

γ_d - Dry unit weight.

γ_w - Unit weight of water.

ε - Strain (see subscripts).

ε_{hcorr} - Horizontal strain corrected for anisotropy.

ε_m - Membrane strain.

ε_{acc} - Accumulated (residual) strain.

ε_{vol} - Volumetric strain ($=\Delta V/V$)

μ - Poisson's ratio.

θ - Inclination of the effective stress path of a load cycle.

σ - Total stress (see subscripts).

$\bar{\sigma}$ - Effective stress (denoted by bar).

$\bar{\sigma}_c$ - Effective consolidation stress.

$\bar{\sigma}_f$ - Effective stress at failure.

$\bar{\sigma}_{vm}$ - Mean vertical effective stress in oedometer tests.

$\Delta\sigma$ - Change in stress.

$\Delta\sigma_c$ - Change in cell pressure.

$\Delta\sigma_v$ - Vertical cyclic stress.

τ - Shear stress (see subscripts).

$\bar{\phi}$ - Angle of internal friction.

$\bar{\phi}_{cycl}$ - Angle of friction form cyclic tests.

$\bar{\phi}_{stat}$ - Angle of friction from static loading after cyclic test.

FREQUENTLY USED SUBSCRIPTS

v,h - Denotes stresses or strains in vertical and horizontal direction.

pp - Denotes peak-to-peak strains.

o - Denotes initial stress state.

c - Denotes consolidation stress.

ref - Denotes reference value.

ε - Denotes strain.

u - Denotes pore pressure.

res - Denotes residual strain.

LIST OF DEFINITIONS

- Coefficient of Lateral Stress at Rest: K_o, the ratio of horizontal to vertical effective stress acting in the ground where there has been no lateral strain = $\bar{\sigma}_h/\bar{\sigma}_v$

- Consolidation Stress Ratio: K_c, the ratio of horizontal to vertical stress at end of consolidation = $\bar{\sigma}_{hc}/\bar{\sigma}_{vc}$

- Contraction: (Webster (1966)): "The action or process of becoming smaller, shorter or pressed together". In this work contraction describes the tendency of soils to decrease in volume under stress changes. In undrained conditions, contraction leads to positive pore pressure. In drained conditions, contraction leads to a volume decrease.

- Cyclic: (Webster (1966)): "Moving in cycles"

- Cyclic Compression Test: Cyclic triaxial test where vertical stress always exceeds horizontal stress ($K_c < 1$)

- Cyclic Extension Test: Cyclic triaxial test where horizontal stress is always greater than vertical stress ($K_c > 1$)

- Cyclic Isotropic Test: Cyclic test consolidated to the same vertical and horizontal stress, and where the cyclic shear stress alternates between the same positive and

and negative value ($K_c = 1$)

- Cyclic Mobility: (Castro (1969)): Cyclically induced pore pressures and strains, characterized by zero effective stress and large recoverable strains, limited by pore pressure reduction during loading and unloading in every cycle.

- Cyclic Shear Stress: $\pm \Delta q_{cy}$, one half of the vertical stress amplitude in a cyclic triaxial test, $= \pm \Delta \sigma_v / 2$

- Cyclic Shear Stress Ratio: $\Delta q_{cy} / \bar{p}_o$, the ratio of cyclic shear stress to mean normal stress at consolidation, $= \frac{\Delta \sigma_v}{\bar{\sigma}_{vc} + \bar{\sigma}_{hc}}$

- Dilation: (Webster (1966)): "The act of increasing in volume when changed in shape because of an increase in space between the particles." In this work dilation describes the tendency of soils to increase in volume under stress changes. For undrained conditions, a dilative tendency produces negative pore pressures. In drained conditions, a dilative tendency produces a volume increase.

- K_f-line: The line drawn through the peak values of q in a $\bar{p}$-q-diagram ($\bar{p} = \frac{\bar{\sigma}_v + \bar{\sigma}_h}{2}$, $q = \frac{\sigma_v - \sigma_h}{2}$), i.e., a plot of q versus $\bar{p}$ at failure.

- K_ε- line: A plot of maximum q versus $\bar{p}$ at 1% vertical residual strain or $\pm$ 1% vertical peak to peak strain.

- Liquefaction: (Webster (1966)): "The process of making or becoming liquid. The state of being liquid." In this work liquefaction describes the rapid loss of strength and resulting large strain that develops primarily in loose samples during a monotonic shear stress increase for static tests, or in one particular cycle in a cyclic test.

- Mean Consolidation Stress: $\bar{p}_o$, one half of the sum of vertical and horizontal stress at consolidation, = $\frac{\bar{\sigma}_{vc} + \bar{\sigma}_{hc}}{2}$

- Mean Shear Stress: q_m, one half of the difference of vertical and horizontal stress at consolidation, = $\frac{\sigma_{vc} - \sigma_{hc}}{2}$, also $[(\frac{\sigma_v - \sigma_h}{2})^2 + \tau_{vh}^2]^{0.5}$

- Mean Shear Stress Ratio: = $q_m/\bar{p}_o$, the ratio of mean shear stress to mean normal stress at consolidation, = $\frac{\sigma_{vc} - \sigma_{hc}}{\bar{\sigma}_{vc} + \bar{\sigma}_{hc}}$

- Peak to Peak Vertical Strain: ε_{vpp}, the maximum difference between two vertical strain values recorded within one load cycle.

- Pore Pressure Ratio: M, the ratio between the excess pore pressure measured at the end of a load cycle to the excess pore pressure measured at the end of the first load cycle reaching the K_ε-line, = $\Delta u/u_f$

- Relative Density: $R_d = \frac{e_{max} - e}{e_{max} - e_{min}} \cdot 100\%$, where e_{max} is

the void ratio of soil in loosest condition, e is in-place void ratio and e_{min} is void ratio of soil in densest condition.

- Residual Vertical Strain: ε_{vres}, the accumulated vertical strain measured at the end of a load cycle.

- Shear Stress Reversal: Change in direction of shear stresses within a sample during cyclic loading.

- Stress Path: The past, present and future stresses acting in a soil element. In this work, stress path for the case of static loading denotes the line connecting points of maximum shear stress in subsequent Mohr circles during a stress change. Stress path for the case of cyclic loading includes the mean normal stress at consolidation, the mean shear stress and the cyclic shear stress under which the cyclic loading takes place.

Chapter I

INTRODUCTION

During the past decade, the geotechnical profession has seen great increase in interest and work on the behavior of soils for cyclic loading conditions. This situation can be attributed to the increasing involvement of geotechnical engineers in the fields of earthquake and offshore engineering. Common to both these areas of activity is that the stresses induced in the ground below engineered facilities, whether by earthquake shaking or ocean waters, are cyclic in nature. These cyclic stresses often represent a loading condition of major concern to geotechnical engineers, and therefore the determination of soil response to such cyclic stresses has great importance.

The extensive damage caused by ground failures during the Alaska and Niigata earthquakes of 1964 (Coulter and Migliaccio (1966), Hansen (1965), Kawakami and Asada (1966) and Yamada (1966)*) and the deployment of offshore gravity structures for petroleum production and coastal protection in the North Sea the last five years (Bjerrum (1973), Clausen (1975), Eide (1974), Ferguson (1972), de Leeuw (1976) and Høeg (1976)) have significantly contributed to the recent surge

---

*A List of References and Bibliography is presented at the end of the main body.

of research work on cyclic soil behavior. The body of knowledge existing in this area today is the result of the efforts of many researchers. Notable contributions have been made by Andersen, Bjerrum, Casagrande, Castro, Finn, Huang, Ishihara, Ladd, Lee, Seed, Silver, Yoshimi and Youd, among others.

Although both earthquakes and ocean waves can induce cyclic stresses in foundation soils, there are certain important differences between the two load cases. An earthquake generates shear waves (among others) which propagate in all directions from the point of energy release. The foundation soil below level ground is very often assumed to be initially under hydrostatic stresses, and during an earthquake to experience cyclic shear stresses on horizontal and vertical planes (Seed and Lee (1966)). Earthquake shaking typically lasts from 5 to 40 seconds, and may contain 2 to 60 major stress cycles (Yegian (1976)). In contrast to earthquake loading where the cyclic stresses come from the ground to the foundation soils, wave loading on structures induce cyclic stresses in the foundation soils through and by the structure. A storm, generating waves, can last anywhere from 6 to 48 hours and contains thousands of waves with period from 5 to 15 seconds (Hoffman (1974)). The cyclic shear stresses acting below wave loaded structures are not restricted to horizontal and vertical planes, nor are the initial stresses assumed to be hydrostatic. (This is treated in Chapter II.) Whereas

loss of strength and large deformations in soil due to pore pressure increase during cyclic loading are of concern both under wave and earthquake loads, the offshore soil engineer in addition must consider long-term deformations caused by the large number of waves in each of many subsequent storms. Another characteristic of ocean storms is the occurrence of very many each year, in all oceans. Large earthquakes, however, occur much less frequently and predictably. Constructed offshore facilities will, therefore, experience cyclic loads each year on the order of 1/2 the design loads or more, whereas an earthquake never may strike a constructed facility during its design life.

In summary, cyclic stresses induced by earthquakes are characterized by relatively few high frequency cycles at high shear stress levels occurring within a short period of time. Wave induced cyclic stresses are characterized by a great number of low frequency cycles at moderate shear stress levels occurring over a much longer period of time, and reoccurring with intervals.

This thesis will address itself to the effects of cyclic loading on sand under conditions pertinent to wave loaded offshore gravity structures as modeled in laboratory tests.

The objectives guiding the experimental investigation reported in this thesis were three-fold:

1) to determine undrained stress-strain behavior of a sand in cyclic triaxial tests

2) to determine the influence of porosity and stress path on strain and pore pressure development in undrained cyclic triaxial tests on a sand.

3) to develope a method to predict strain and pore pressure development in undrained cyclic triaxial tests on a sand at various porosities and subjected to different stress paths.

In order to achieve these objectives, a laboratory test was necessary, which allowed the application of a large variety of well-controlled cyclic stress paths, but was simple to perform. The triaxial test met these requirements. A low-cost automatic loading device with a remote controlled data acquisition system was constructed. A testing procedure was derived to yield reproducible results. A cyclic test program was devised to determine the influence of various parameters pertinent to soil foundations of wave loaded structures. The cyclic tests were supplemented by static tests in order to relate observations of cyclic behavior of sand to sand behavior under static loads.

The investigation results indicate that dependent on the porosity of the sand and the stress path followed, undrained cyclic loading can cause negative pore pressure, i.e.,

a tendency to volume increase (dilation*), or positive pore pressure, i.e., a tendency to volume decrease in the sand (contraction*). Contraction can be followed by a nearly total strength loss and large deformations (liquefaction*). The amount of shear stress about which the cyclic stress alternates has a profound influence on the development of strain and pore pressure in undrained tests. The rate at which strain and pore pressure accumulates per cycle is dependent on parameters such as density, cyclic shear stress, normal consolidation stress and mean shear stress of the sand.

The stress-strain behavior of sand under undrained cyclic loading is described in Chapter II. A summary of previous work on cyclic sand behavior is extracted from the published literature, and followed by an investigation of dilation, contraction and liquefaction of an offshore sand from Holland, Oosterschelde Fine Sand. The stress situation below offshore gravity structures is analyzed. The fundamental influence of the magnitude of shear stress at consolidation on strain and pore pressure development in undrained cyclic triaxial tests are demonstrated based on performed tests. Chapter III discusses factors such as test conditions, sample condition, stress history and drainage, that all have been found to influence cyclic tests results, based both on

---

*Explained in List of Definitions and in detail in Chapter II.

published work and on experimental findings during this research effort. Measurements of strain and pore pressure in undrained cyclic triaxial tests were made; in which porosity, cyclic shear stress, mean consolidations stress and initial shear stress were varied. Based on these measurements reported in Chapter IV, a method to predict strain and pore pressure in undrained cyclic triaxial tests is suggested in Chapter V. Chapter VI presents recommendations based on the experience and findings during this work for planning cyclic laboratory test programs. Chapter VII concludes this thesis with a summary of the experimental findings. The Appendices present sand description, testing procedures, triaxial test discussion, static test results, cyclic triaxial test results, cyclic oedometer test results and an example of the prediction procedure.

Chapter II

UNDRAINED CYCLIC BEHAVIOR OF SAND

When soil is loaded cyclically, elastic and plastic deformations result. If the time required for drainage is long compared to the loading time, changes in pore water pressure result. If the drainage time is short, volume changes occur. The amount and nature of deformation, pore pressure and volume change depend, among other factors, on:

(1) the effective stresses in the soil,

(2) the magnitude and number of the cyclic stress applications, and

(3) the soil characteristics, notably soil type, grain size and distribution, porosity, permeability, degree of saturation and stress history.

This chapter describes the typical stress conditions in the foundation soil below offshore gravity structures to define the stress paths which model foundation conditions. The results of previous investigations of undrained sand behavior under cyclic loads are summarized. Undrained cyclic behavior of saturated sand in the laboratory is examined, concentrating on the distinction between dilative and contractive* behavior. The fundamental influence of mean shear stress on undrained

---

*Explained in List of Definitions.

cyclic behavior of saturated sand is demonstrated.

2.1 Stress Conditions in Offshore Foundations

The response of sand to cyclic loading depends on the stress system acting on the sand during loading. In order to properly define the stress conditions prevailing under an offshore structure during storm loading, the following steps are necessary:

(1) Determine the likely and possible range of stresses existing in the sea bed before placement of the structure.

(2) Determine typical stress increases resulting from structure's weight.

(3) Determine stresses induced in the foundation soil by the structure during design storm conditions.

(4) Superpose the above stresses to give possible and likely foundation stress states during storm loading.

Figure II-1 shows an element of soil below the sea bed. The stresses acting on that element are given in Figure II-1b. The coefficient of lateral stress at rest, K_o, is a major unknown. K_o is difficult to measure reliably, and very little information exists to estimate its magnitude in offshore deposits. For normally consolidated sands, K_o is commonly assumed equal to $[1-\sin\bar{\phi}]$ (Jaky (1944), where $\bar{\phi}$ = effective

angle of friction), which gives values of 0.4 to 0.6. Larger values of K_o result from overconsolidation, e.g., an OCR of 4 to 6 (OCR = Overconsolidation Ratio, defined as ratio of maximum previous vertical effective stress to present vertical effective stress) would typically give K_o of 1. Overconsolidation of the sea bottom can result from glaciation, erosion of overburden, major sea level changes, etc. In addition, soil deposits below the sea level can experience shear stresses from passing waves (Bjerrum (1973), Moshagen and Tørum (1975)), that may cause an increase in horizontal stress with time. The net effect is that K_o may have a value anywhere from 0.4 to more than 2 in offshore deposits. In situ measurements of lateral stress seem required to make a reasonable estimate of the magnitude of K_o.

Figure II.1c shows Mohr circles and stress points associated with K_o of 0.4, 1 and 2. A stress point (with the coordinates $q = \frac{\sigma_v - \sigma_h}{2}$ and $p = \frac{\sigma_v + \sigma_h}{2}$) is the point of maximum shear stress on the circle, and can replace the Mohr circle to describe a state of stress (consult Figure II-2 for definition). For cohesionless soils, a line through the origin and the stress points on Mohr circles at failure is called the K_f-line, and is inclided α degrees to the horizontal. A line connecting stress points for an element is called a stress path, which, when plotted in a p-q diagram, is capable of showing stress changes in a very simple way (Lambe and

Whitman (1969) and Lambe (1967) give further explanations). The 45 degree inclined line connecting the stress points in Figure II-1c is the location of possible stress states in situ at a given value of vertical stress, and different values of K_o. The intermediate principal stress is not included in these considerations; however, its importance to soil behavior is generally secondary.

Figure II-3a shows a gravity structure placed on a level sea bed. If the sediments are cohesionless, full drainage of excess pore pressures will take place within hours to a few days. The stresses acting on soil elements A (below centerline of structure), B and C (below structure edge) will be as given in Figure II-3b. In elements B and C, a rotation of principal stress directions will result from the weight of the structure. Horizontal and vertical planes will therefore experience both an increase in normal stress and shear stress, so q and p, based on horizontal and vertical normal stress, will no longer be the peak point on the Mohr Circle.

Qualitative indications of stress paths for element A, B and C under the static structure load are given in the p-q diagram in Figure II.3c for initial K_o - values of 0.4, 1 and 2. Typical surface load from a submerged offshore gravity structure is 30 t/m^2 over an area of about 100 m in diameter. If the elements are deep (say depth 1/2 of foundation diameter), the initial stresses are high and the stress increments

relatively small. The solid drawn arrows on Figure II-3c indicate the stress paths for the three elements for that case. If the elements are shallow (say depth 1/10 of foundation diameter), the initial stresses will be much smaller than the stress increments. That is qualitatively indicated by the dashed stress paths in Figure II-3c. From this figure, the following observations can be made:

(1) Whatever magnitude of lateral stress coefficient at rest (K_o) exists in shallow sediments below offshore structures, the consolidation stress ratio ($K_c = \bar{\sigma}_{hc}/\bar{\sigma}_{vc}$) after placement of a structure will be less than one.

(2) Only in deeper soils with a K_o larger than one, K_c might remain greater than one after loading.

Static forces from wind and current and cyclic forces from the waves act on the offshore structure as indicated in Figure II-4a. Figure II-4b shows the stresses induced in elements A, B and C under that load. Vertical and horizontal cyclic normal stresses will be small on element A and large on element B and C, whereas cyclic shear stresses on horizontal and vertical planes will be large on element A and somewhat smaller on elements B and C. Figure II-4c presents typical qualitative stress paths for static loading (solid arrows) and cyclic loading (dashed arrows) of elements that started out with different K_o-values.

If the stress paths of Figure II-4 are modeled in the laboratory, element A would be most closely modeled by a simple shear apparatus whereas elements B and C have stress paths more closely resembling those that can be obtained in a triaxial apparatus. Stress paths on other elements are between those of the simple shear and triaxial tests.

The qualitative stresses shown in Figure II-4 result from considering the foundation as an elastic material. Since soil is known to be inelastic, particularly during cyclic loading, these stress paths must change during the course of a storm hitting the structure. The stress redistribution in the foundation with time depends on the pattern of strain and pore pressure that develope with cycling. For the purpose of this investigation, the stress distribution is considered constant during cycling.

From the preceeding discussion of stress states below offshore gravity structures, the following general statements can be made:

(1) The state of stress below an offshore structure is not known with certainty.

(2) At shallow depths (less than about 1/4 of the foundation width) the vertical stress is very likely larger than the horizontal.

(3) At larger depths the vertical stress still increases more than the horizontal, however the uncertainty in K_o becomes important in determining

the final stress state.

(4) Storm loading causes cyclic stresses in the soil below offshore structures, superposed on the static stress state.

(5) The manner in which the normal stress ratio below a wave loaded structure changes during cyclic loading is not known.

In order to predict strain and pore pressure in offshore foundations, a knowledge of soil behavior under cyclic loading is thus essential.

2.2 Summary of Previous Investigations

Having acknowledged the importance of cyclic soil behavior for performance prediction of wave loaded structures, the next step is to examine what is available in the geotechnical literature on the subject. Cyclic behavior of soils, particularly sands, has concerned geotechnical engineers since the early days of soil mechanics (Hertwig et al. (1933), Lorenz (1934)). The topic has received increased attention in the last ten years, due primarily to questions about seismic response of soils and foundations, but recently also from foundation problems of wave loaded offshore structures.

Huang (1961) reported cyclic tests on silty sand (mean grain size, D_{50} = 0.09 mm, coefficient of uniformity, U = 1.4), performed in a triaxial cell placed on a vertically

vibrating table. Using the triaxial cell allowed much better stress control and a wider range of stress paths than earlier investigations in laterally confined cylinders (Maslow (1957)). Huang measured pore pressure development in the sand samples at different consolidation stress ratios, densities, cyclic shear stresses and confining stresses. His results, which are widely accepted now, were:

(1) Increasing density decreases excess pore pressure generation,

(2) Increasing consolidation stress ratio decreases excess pore pressure generation,

(3) Increasing cyclic shear stress increases excess pore pressure generation, and

(4) Increasing consolidation stress level decreases excess pore pressure generation.

His paper does not report the number of stress cycles or any strain measurements in the tests.

Following the widespread damage in the 1964 Alaska and Niigata earthquakes, Seed and Lee (1966) published their first work on cyclic sand behavior under earthquake induced stresses. They considered soil elements below level ground under an isotropic stress state, and assumed earthquake motion to cause shear stresses on horizontal and vertical planes only. That loading condition could be modeled in a triaxial test sample, consolidated isotropically and with cycling of only

vertical stress to produce the desired magnitude of shear stresses on a plane inclined 45 degrees to the sample axis. Tests performed this way accumulated excess pore pressure each load cycle, until the excess pore pressure value became equal to the confining stress. Large, recoverable strains then developed rapidly. This test condition is hereafter referred to as "cyclic isotropic test". Triaxial test modeling of seismic loading assumes that the magnitude of shear stress rather than rotation of principal stress direction is important in governing soil behavior under cyclic loads.

Seed and Lee's conclusions, that cyclic behavior in terms of strain and pore pressure development depends on soil density, cyclic shear stress, confining stress and number of load cycles, supported Huang's 1961 findings. In a companion paper (Lee and Seed (1976a)), they quantified their results and added failure criterion to the list of factors influencing cyclic behavior because the number of load cycles varied with failure definition. The cyclic shear stress required to reach failure was found to increase approximately linearly with confining stress. This observation was confirmed by other researchers (Peacock and Seed (1968), Finn et al. (1971)). However, Mulilis, Chan and Seed (1975), Castro and Poulos (1976) and Meehan (1976) presented results on a variety of sands indicating no linear relationship. Rather, the number of load cycles to failure

decreased with confining stress for a constant shear stress ratio.

Lee and Seed (1967b) reported results from triaxial cyclic tests on anisotropically consolidated sand samples. Tests with shear stresses reversing directions during cyclic loading showed a rapid increase in peak to peak strains in the sample, once the generated pore pressure equalled the confining stresses (cyclic isotropic tests). Tests not experiencing shear stress reversal (vertical stress is always larger than horizontal stress) accumulated axial strain at a relatively slow and approximately constant rate throughout the test. In that case it was noted that: "the pore pressure simply cycled up and down, but never quite reached the value of the cell pressure (which would have produced a liquefaction condition)". The authors found development of a predetermined compressive axial strain to be the most useful failure criterion. This type of test will hereafter be referred to as "cyclic compression test".

The above tests were performed to model seismic loading of sloping ground. One of Lee and Seed's conclusions was that the cyclic strength of sand (the shear stress ratio required to produce a predetermined strain or pore pressure state in a certain number of cycles) increased with decreasing consolidation ratio (= K_c, the ratio of horizontal to vertical

consolidation stress). This confirmed the earlier findings of Huang (1961). In other words, a steep slope would exhibit larger resistance to cyclic failure than a gentle slope. (However, it seems unlikely that the soil mass in a slope would respond undrained as the laboratory sample does and have a relatively uniform stress field. A thin failure zone in the slope would probably dilate, suck up water, and fail under drained conditions.)

Schroeder and Schuster (1969) also reported anisotropic tests, confirming the conclusions of Huang (1961) and Lee and Seed (1967a) that stress-strain behavior of sand under cyclic loading depends on the consolidation stress ratio. With decreasing consolidation stress ratio, the rate of strain and pore pressure accumulation per cycle decreases substantially. In addition, Schroeder and Schuster found by testing two sands with identical grain size curves (Ottawa Sand and Platte River Sand), that cyclic behavior depends very much on sand type. The angular Platte River Sand strained 2 to 4 times more than the rounded Ottawa Sand under comparable test conditions.

Castro's (1969) data show, contrary to Huang's, Lee and Seed's and Schroeder and Schuster's findings, that cyclic tests on loose samples exhibit about the same resistance to failure (defined in terms of strain) whether shear stresses reverse or not. He reported that the samples suddenly collapsed, and developed large strains only limited by the test equipment

when the generated pore pressure equalled 50 to 80% of the confining stress. In all cases, the pore pressure increased simultaneously with the collapse to a value almost equal to the confining stress. Based on his cyclic and additional static test results, Castro concluded that both increasing confining stress and consolitaion ratio led to increased failure susceptability. These observations conflict with the previous reported data.

The reason for this conflict in conclusions about anisotropic cyclic test behavior lies in the fundamentally different response of the samples tested by Castro and the previous investigators. All researchers reported tests on anisotropic samples that generated positive pore pressures under the cyclic loading. But only Castro's samples were so loose that they liquefied* when approaching the failure line (at effective friction angles, $\bar{\phi}$ = 25 to 30°). Lee and Seed's samples dilated** at the failure line. Because the anisotropic

---

From List of Definitions:

*Liquefaction describes the rapid loss of strength and resulting large strain that develops primarily in loose samples during a monotonic shear stress increase for static tests, or in one particular cycle in a cyclic test.

**Dilation describes the tendency of soils to increase in volume under stress changes. For undrained conditions, a dilative tendency produces negative pore pressures.

tests did not reverse shear stress direction, the pore pressure value could not become equal to the confining stress, with the accompanying large strains. Therefore, Lee and Seed concluded that an increase in consolidation stress ratio led to slower strain accumulation. Because anisotropic samples are consolidated at a higher shear stress ratio than isotropic samples, they are nearer to the failure line, and thus require less pore pressure generation to reach the failure line where loose sand will liquefy. Therefore, Castro concluded that an increase in consolidation stress ratio led to increased failure susceptability. Based on the fact that the porosity at which sand will liquefy (denoted critical state or critical void ratio, Casagrande (1936)) decreases with increasing confining stress, Castro stated that increasing the confining stress will increase the failure susceptability.

Adding to the confusion caused by the different responses of the samples tested by Castro and Lee/Seed, both used the term liquefaction to describe failure, although the behavior of the samples at failure were quite different. Over the years this terminology conflict has contributed greatly to misunderstandings and communication difficulties, which still persist to date (1977). In this thesis, the term liquefaction will be limited to the definition given above. The large, recoverable deformations developing in cyclic isotropic tests when the pore pressure equals the confining stress,

will be termed cyclic mobility (consult List of Definitions for further description).

Since 1969, the geotechnical literature indicates research focusing on the factors influencing cyclic and behavior in laboratory tests such as testing procedures, sand characteristics, sample condition, stress and strain history, and drainage. The effect of these factors and relevant literature will be discussed in Chapter III.

In addition to cyclic triaxial tests, cyclic simple shear tests (Thiers and Seed (1968), Peacock and Seed (1968), Finn et al. (1971), and Seed and Peacock (1971)) and large scale shaking table tests (Finn et al. (1971), O'Hara (1972) and De Alba et al. (1975)) have been employed for cyclic testing. These tests allow rotation of principal stress directions, and were therefore found to be more representative for earthquake induced cyclic loading in the field. Recently also drained tests have been used to predict undrained behavior (Martin et al. (1975)). De Alba et al (1975) give recommended design curves for cyclic sand strength at different relative densities. Based upon simple shear and shaking table tests, a correction factor ranging from .55 to 1.0 (Seed (1976a)) is used to adjust cyclic strengths from triaxial tests to "in situ conditions".

In addition to the above three test types, various other cyclic testing methods have been developed (Ishihara and Li

(1975), Ishibashi and Sherif (1974), Ishihara and Yasuda (1975), Yoshimi and Oh-Oka (1975), Casagrande (1976) and Wolfe et al. (1977)), but have not yet added any new information as to the fundamental factors controlling cyclic sand behavior.

Stoll and Kald (1976) report stress controlled cyclic triaxial tests on silt at small cyclic shear stress ratios. From strain measurements, the conclude there is a threshold shear strain level, about $5 \cdot 10^{-5}$, below which the soil does not contract under cyclic loading. Gupta and Prakash (1977) report shaking table tests on fine sand and gravel. Samples of fine sand prepared to relative densities exceeding 65% were observed to dilate and develop negative pore pressures. At lower relative densities, positive pore pressures were recorded. They therefore concluded that saturated sands can not liquefy if the relative density exceeds 65%. These two cases are isolated in reporting dilation under cyclic loading, however, it is possible that other investigations have used too high shear stress ratios to obtain dilation. Then it is commonly found that plots of cyclic shear stress ratio versus log number of cycles flattens off to a horizontal line at small shear stress ratios. Even smaller values of shear stress ratio could produce dilation.

Castro (1969) and Casagrande (1976) reported the presence of large density differences within cyclic test samples after failure. Bjerrum (1973) concluded that due to void redistribution, the pore pressure buildup at small strains (< 1 to 2%) is

the only reliable parameter to quantify undrained cyclic behavior of a medium dense to dense sand. Because of the now well-investigated effects of sample preparation and stress history, both Casagrande (1976) and Seed (1976b) recommend using the best possible undisturbed samples for cyclic testing to simulate field behavior. In situ measurement confirm the fact that strain and pore pressure accumulate in sand subjected to cyclic loading (e.g. Clausen et al. (1975), Høeg (1976) and de Leeuw (1976)). However, quantitative data to correlate laboratory test results with field behavior are scarce.

The most important conclusion that can be stated after reviewing published literature on sand behavior in undrained cyclic laboratory tests, is that the behavior is much more complex than pioneering work suggested. Both strain and pore pressure response to cyclic loads and the terminology to describe response need clarification. Therefore, the author decided early in this research work to carry out an investigation aimed at giving a complete picture of undrained cyclic stress-strain behavior of sand in triaxial laboratory tests. The literature summary suggests the following tentative conclusions about cyclic sand behavior:

(1) Sand subjected to undrained cyclic loading in the laboratory can dilate or contract.

(2) Contracting sand can dilate or liquefy at the failure line.

(3) Increasing density, decreasing cyclic shear stress and increasing consolidation stress lead to a decrease in the rate of strain and pore pressure accumulation per cycle.

(4) Strain and pore pressure accumulation in sand is dependent on the number of load cycles.

(5) Strain and pore pressure measurements in laboratory test samples can be erroneous for strains exceeding 1 to 2% due to pore redistribution.

2.3 Dilation, Contraction and Liquefaction

In order to describe the volume change response of sand under monotonic (static) loading, Casagrande (1936) developed the concept of the critical void ratio (often termed "critical state"). The critical void ratio separates approximate samples that liquefy from those that dilate in static loading. The distinction is made based on the response of the sand at the failure line and not the initial response at the start of the loading.

From the 30 effective stress paths on loose sand in Appendix D, the difference in pore pressure and strain response of both dilating and liquefying samples in undrained static triaxial tests can be examined. Figure II.5 presents typical effective stress paths for a very loose sand that liquefies (1), a loose sand that dilates (2) and a dense sand that dilates (3).

The dotted line is the total stress path (TSP) for standard triaxial loading tests. The effective stress space is limited by the failure line, where the distinction between dilation and liquefaction is made. All samples contracted before they reached the failure line. Figures D-11 and D-12 in Appendix D present the critical void ratio line for load controlled tests on Oosterschelde sand.

The effective stress paths for an undrained loading and an unloading test were found to be very similar (Appendix D). In accordance with the effective stress principle,the sand behavior did not seem to be influenced appreciably by whether the pore pressure was negative or positive.

The conclusion from the test data in Appendix D confirms Casagrande's (1936) findings:

> There is a fundamental difference in sand behavior between samples that liquefy and dilate under static loading. Dilating samples increase in strength at the failure line due to negative pore pressures, and strain moderately. Liquefying samples lose strength and collapse with large strains at the failure line.

The influence of volume change tendency is less clear for cyclic tests than for static tests. The reason for this is the basic difference in effective stress paths. Effective stress paths for static triaxial shear tests, whether loading or unloading, dilation or contraction, finally always end on

the failure line. This is not so in cyclic triaxial tests, which can be demonstrated with Figure II.6. The total stress path from a cyclic triaxial test is given by the dotted arrow. The total stress condition will move back and forth on this arrow throughout the cyclic test. The effective stress path is therefore limited by the horizontal lines at the tips of the total stress path. If the sample dilates; i.e., develop negative pore pressure during cyclic loading, the effective stress path for one cycle will, after a number of load applications, be given by ESP (1). The effective stress path will therefore move further and further away from the failure line, and can never reach the failure line. Only small strains will accumulate. This is denoted dilation. Samples that contract during cyclic loading and develop positive pore pressure (ESP (2) is an example of the effective stress path for one load cycle), will reach the failure line. Therefore, a fundamental difference in behavior results between cyclic test samples that dilate and contract initially, in contrast to what was found in static tests.

When the effective stress path of a contractive sample in a cyclic triaxial test reaches the failure line, one of two things can occur, analog to the behavior of static tests. A very loose sample may collapse, which is characterized by a sudden loss of strength and large, non-recoverable strains within one particular load cycle. This is denoted liquefaction.

A medium dense sample may dilate at the failure line, which is characterized by a cease in the pore pressure accumulation, such that the effective stress path becomes stationary with its upper tip on the failure line. Strains will then accumulate uniformly with further cyclic loading. This is denoted contraction.

If the initial stress point had been located on the p-axis in Figure II.6, a dilating sample would have behaved similarly, and only accumulated small strains, if any at all. A contracting sample that is very loose and liquefies, will also behave as described above. The major difference is found in contracting samples that dilate at the failure line. Once they reach the failure line, the pore pressure will rapidly increase until the effective stress path follows the failure line both during loading and unloading. Each time the effective stress path crosses the p-line (and only then), the pore pressure magnitude equals the effective confining stress, and the sample develops large recoverable strains. This is what Seed, Lee and their co-workers termed "initial liquefaction", which with strain developed to "partial" and "complete" liquefaction (Lee and Seed (1967a)). The definitions were later changed to "initial liquefaction with limited strain potential" (Seed et al. (1975)). Castro (1969) denotes this phenomenon "cyclic mobility".

There are two major reasons for making the distinction

between dilation, contraction and liquefaction in cyclic tests. One is the fundamentally different pore pressure response of the sand to loading. Another and probably more important reason is the resulting difference in strain behavior. The increasing effective stress in undrained, dilating sand gives very small strain accumulation. The decreasing effective stresses in contractive sand may lead to large strain accumulation with time; however, dilation at the failure line limits sudden development of large strains as long as shear stresses do not reverse. Sand that liquefies (after some strain accumulation during the preceeding contraction) will strain to the limits of the testing equipment in less than a second.

Sudden collapse of samples in cyclic triaxial tests was demonstrated by Castro (1969). Both isotropically and anisotropically consolidated specimens failed suddenly and never showed signs of dilation during failure. He found the critical void ratio line to be the same for cyclic and static tests. In both test types the critical void ratio line divides between samples that liquefy and samples that dilate at the failure line.

Only five cyclic tests were run on Oosterschelde sand to examine the critical void ratio for cyclic tests, one of which liquefied. Eight cyclic test samples dilated and ended with negative pore pressures, most of them after initially having contracted slightly. Appendix F presents detailed plots and tabulations of the cyclic triaxial tests.

A summary of all the undrained cyclic triaxial tests is presented in Figure II-7, in a plot of porosity and relative density versus cyclic stress ratio. The open points signify samples that dilated during cyclic loading, the closed points samples that contracted. The figure shows the three different types of response, divided by two tentative lines (dotted): the upper dotted line divides between tests that liquefy and tests that contract. The lower dotted line divides between tests that contract (positive pore pressure) and dilate (negative pore pressure). The fine sand evidently dilates at 42% porosity with a cyclic stress ratio less than 0.05, and at 37% porosity with a stress ratio less than 0.2.

Further investigation of the exact location of these lines are required; however, results from this investigation clearly show that such a division in fundamental cyclic behavior occurs. The most likely explanation why the phenomenon of dilation with negative pore pressures has not been commonly reported for cyclic tests, is that the cyclic shear stress ratio leading to dilation is much smaller than the values usually selected in cyclic testing for earthquake design at various soil densities. Data from Lee and Seed (1967a) can serve as an example. The point where Lee and Seed's values of cyclic shear stress ratios at different relative densities indicate an infinite number of cycles to cause liquefaction can be taken as conditions just beginning to produce dilation. An interpretation of their data in the form of Figure II-7 produces

Figure II-8. The line for minimum stress ratio causing contraction for cyclic loading of Sacramento River Sand correspond well to the tentative dividing line between contraction and dilation for Oosterschelde sand. Since cyclic testing of sand for earthquake design concentrates on test conditions leading to failure in relatively few cycles, it is unlikely that tests where negative pore pressures can be expected, have been performed at all.

To summarize, cyclic tests on sand can be divided in three different types based on the pore pressure response of the sand to loading:

(1) Liquefaction: Contraction followed by strength loss and collapse at the failure line. Large strains occurring suddenly.

(2) Contraction: Positive pore pressure generation followed by dilation at the failure line. Strains accumulating with time.

(3) Dilation: Negative pore pressure generation. Very small strain accumulation.

2.4 Cyclic Triaxial Tests

The literature review indicated a behavioral difference between cyclic test samples consolidated to various stress ratios. However, this difference is not well described and portrayed in the literature. This subchapter will discuss the

influence of consolidation stress ratio on the behavior of contractive sand samples loaded cyclically in undrained triaxial tests.

Having established the static and cyclic stress paths for typical elements *in situ*, the next task is to run laboratory tests along those stress paths. Deformations and pore pressures or volume changes can then be measured. If the tested soil is representative of the soil conditions *in situ* (this is a very important question; however, beyond the scope of this investigation), a good estimate of *in situ* strains and pore pressures can be made. This is the stress path method of Lambe (1967) in a nutshell.

Triaxial testing was selected for the experimental investigation after an examination of the various possibilities. This was done in spite of its shortcomings in modeling rotation of principal stress directions, and the intermediate stress always being equal to the maximum or minimum normal stress. The main reasons for this choice were the relative simplicity of running triaxial tests and interpreting test results, and a wide range of possible and well-controlled stress paths. The stress modeling of field elements is done by consolidating the laboratory sample to stresses equal to the estimated maximum and minimum principal stress *in situ*, and applying a cyclic shear stress equal to the maximum cyclic shear stress for the *in situ* element. The cylic shear stress was achieved by

cycling only the vertical stress on the triaxial sample, as additional cycling of horizontal stress is complicated and only adds a change in all around pressure for a fully saturated specimen. Appendix B presents the cyclic loading frame, the cyclic testing procedure and the data recording and reduction method.

Figure II-9 defines the variables used to describe the state of stress in a cyclic triaxial test. Before structure placement, the initial effective vertical stress in the ground is $\bar{\sigma}_v$, the horizontal stress $\bar{\sigma}_h = K_o \cdot \bar{\sigma}_v$. With the additional stresses from the submerged structure weight, the vertical consolidation stress ($\bar{\sigma}_{vc}$) and the horizontal consolidation stress ($\bar{\sigma}_{hc} = K_c \cdot \bar{\sigma}_{vc}$) for the triaxial test samples are found. The mean consolidation stress is $\bar{p}_o$, equal to half the sum of normal consolidation stresses. Adding the static pore pressure ($u_s = u_b$ = back pressure) to the mean consolidation stress gives the mean total stress, p_o. The mean shear stress (q_m) equals half the difference of the principal normal stresses. The vertical stress change ($\pm \Delta\sigma_v$) produces a cyclic shear stress half as large ($\pm \Delta q_{cy}$). The stress path for a cyclic test is defined as the combination of mean consolidation stress, mean shear stress and cyclic shear stress. Figure II-9 gives for a cyclic test the total stress path (TSP), the total stress path minus static pore pressure (TSP-u_s) and two effective stress paths (ESP) at different number of cycles.

Both mean and cyclic shear stress remains approximately constant throughout a cyclic triaxial test. Due to contraction tendency, positive pore pressure is accumulated in cyclic tests (Δu), which reduces the mean consolidation stress to a smaller mean effective stress ($\bar{p}$). A K_ε-line has been defined to enable comparison of different tests. The accumulated pore pressure when the K_ε-line is reached, is denoted u_f. We define the K_ε-line (inclined β degrees to the horizontal) for cyclic tests based on vertical strain, which was suggested by previous investigators. Lee and Seed (1967b) wrote about anisotropically consolidated cyclic tests: "A quantitative analysis of the results of anisotropic pulsating loading tests required that a criterion for failure be established. Of the several possibilities it was finally decided that the most useful failure criterion would be the development of a predetermined compressive axial strain." Lee and Focht (1975) wrote: "For ocean structures on sands, designs should be based on cyclic strength data defined from initial liquefaction or from very low, e.g., 1% to 2%, axial strain conditions."

From the examination of 60 - 70 effective stress paths from all types of cyclic triaxial tests, 1% accumulated axial strain or $\pm$ 1% peak to peak strain was found to be a suitable basis for defining the location of the K_ε-line. The friction angles for the first load cycle reaching 1% vertical strain in cyclic compression tests at different porosities are

plotted in Figure II-10 along with friction angles from drained static tests. The two sets of data correspond very closely, suggesting a consistent relationship between the K_f- and the K_ε-line. That the effective stress path reaches the K_ε-line does not necessarily mean failure (unless the sample is very loose and liquefies), but the behavior changes markedly. In contractive anisotropic tests little additional pore pressure builds up, and strain accumulation usually stabilizes to a constant rate per cycle. Isotropic tests undergo cyclic mobility, with large peak to peak strains under zero effective stress. This is discussed in detail in the following sections. The K_ε-line is defined as a plot of maximum q versus $\bar{p}$ at 1% vertical residual strain or $\pm$ 1% vertical peak to peak strain. The ratio of accumulated pore pressure (Δu) and the pore pressure when the K_ε-line is reached (u_f), is denoted pore pressure ratio, $M = \Delta u/u_f$. The pore pressure ratio is 1 at the K_ε-line.

Cyclic Isotropic Tests

Cyclic tests on specimens consolidated to an isotropic state of stress and loaded cyclically about that stress state, are denoted "cyclic isotropic tests". Seed and Lee (1966) present the basis for considering this stress condition as representative of conditions beneath level ground during seismic loading.

Figure II-11 presents a typical effective stress path

plot of representative cycles for an isotropically consolidated triaxial test on Oosterschelde sand. This plot is very similar to an effective stress path presented by Shibata et al. (1972). Figure II-12 shows a stress-strain plot of the load cycles from Figure II-11. Maximum, mean and minimum values of shear stress and corresponding vertical strain, pore water pressure and mean effective stress, $\bar{p}$, versus number of cycles on a linear scale, are given in Figure II-13. The plots of these three figures, typical for cyclic isotropic tests on contractive sand, allow the following statements about sand behavior in such tests:

(1) Pore pressure increases, decreasing the effective stress with each additional cycle (Figures II-11 and II-13).

(2) The first cycle produces a larger increment of residual pore pressure (i.e., pore pressure that remains the end of the cycle) than do subsequent cycles (Figure II-13).

(3) The pore pressure builds up at an approximate constant rate after the first cycle, until the effective stress path approaches the K_f-line during unloading (Figure II-11 and II-13).

(4) The pore pressure then increases rapidly until the effective stress path follows the K_f-line, which is the limiting stress condition for a

contractive sample (Figures II-11 and II-13).

(5) When and only when $q = 0$, does the pore pressure equal the confining stress. For positive and negative values of q, the effective confining stress is larger than zero (Figures II-11 and II-13).

(6) Both peak to peak and accumulated strains remain essentially unchanged from the first cycle until the effective stress path approaches the K_f-line in extension (Figure II-12).

(7) Peak to peak strains then increase suddenly, and develop within a few load cycles to large peak to peak strains, mainly occurring at zero effective stress, and commonly around a small residual extension strain. Castro (1969) defined this condition as cyclic mobility (Figure II-12). In dense sands the number of load cycles to produce large strains after large pore pressures are developed, increases, and the maximum cyclic strain can be limited by dilation.

(8) The major part of the cyclic strains occur when q and $\bar{p}$ are at or near zero. As the absolute value of q increases, dilatancy leads to an increase in $\bar{p}$ as well, and an arrest of the cyclic strains (Figures II-11 and II.12).

(9) The stress-strain curve at the end of the test is clearly hysteretic, indicating energy is required for dilatancy and particle rearrangement (Figure II-12). A stress-strain curve from Lee (1976b), shows large strains taking place at exactly zero shear stress towards the end of the test.

(10) Since the K_f-line is inclined about 25 to 35° and the total stress path 45° to the horizontal (Figure II-6), the pore pressure (= the distance between effective and total stress) near failure will <u>decrease</u> when the shear stress increases, and then <u>increase</u> when the shear stress decreases to zero again. Thus, the pore pressure will have two peaks (with values equal to the confining stress) at mean load in each cycle, and be smaller at maximum load and also minimum load. This causes the so-called "double peaking" of pore pressure in isotropic cyclic tests.

(11) The A-parameter for the cyclic loading ($A = \frac{\Delta u - \Delta\sigma_3}{\Delta\sigma_1 - \Delta\sigma_s}$, here the ratio of pore pressure change to vertical stress change during a cycle) in isotropic cyclic tests is typically about .25 until the K_f-line is approached.

In Figure II-13 the test has been divided into Stage I and Stage II. Stage I is the part of the test where the pore

pressure increases at very small and approximately constant strains. Stage II is where the pore pressure development is being influenced by the K_f-line, and the peak to peak strains increase to a large value. The dividing line between Stage I and II is located at the end of the cycle where the effective stress path first reached the K_ε-line, i.e. according to our definition at $\pm$ 1% peak to peak strain.

Cyclic Compression Tests

Cyclic tests on a specimen consolidated and loaded cyclically such that the vertical stress always remains larger than the horizontal stress ($\bar{\sigma}_{vc} > \bar{\sigma}_{hc}$), are denoted cyclic compression tests. These tests represent the best triaxial test modeling of shallow elements under an offshore gravity structure during storm conditions.

Figure II-14 presents a typical effective stress path plot of representative cycles from an anisotropically consolidated sand sample tested in compression. Figure II-15 shows a stress-strain plot of the same cycles, and corresponding values of vertical strain, pore pressure and mean effective stress throughout the test is given in Figure II-16. These plots, typical for cyclic compression tests on contractive sand, allow the following statements about sand behavior in such tests:

(1) Pore pressure increases, decreasing the effective

stress with each additional cycle (Figures II-14 and II-16).

(2) The first cycle produces a larger increment of residual pore pressure than does any subsequent cycle (Figure II-14 and II-16).

(3) The rate of pore pressure buildup per cycle decreases with the number of load cycles in Stage I (Figure II-16).

(4) In Stage II the pore pressure remains essentially constant throughout the test (Figure II-16). (The borderline between Stage I and II is at the end of the load cycle where 1% vertical residual strain is reached for the first time.)

(5) The value of the accumulated pore pressure can never reach the value of the confining stress as the shear stress does not reverse, and the K_f-line limits the pore pressure buildup in contractive sand (Figure II-14).

(6) The cyclic peak to peak strains remain very small throughout the tests, typically less than 0.1%. The maximum shear stress during the test decreases slightly because of the increase in sample area with vertical strain accumulation and corresponding horizontal bulging (Figure II-15).

(7) The stress-strain curves show a very small

hysteresis (Figure II-15).

(8) The A-parameter for each individual cycle varies from about .15 in the first cycle to about .05 at 10% vertical strain.

The basic difference in strain and pore pressure response between the isotropic and compression cyclic tests is that the compression test can never reach zero effective stress as the shear stresses never reach zero. Therefore, cyclic mobility type failure never can occur in cyclic compression tests on contractive sand. However, large accumulated strains can develop with sufficient cycling.

Cyclic Extension Tests

Cyclic tests on specimens consolidated to a higher horizontal than vertical stress ($\bar{\sigma}_{hc} > \bar{\sigma}_{vc}$) and cycled about that stress state such that the horizontal stress always remains larger than the vertical are denoted cyclic extension tests. This is not a common stress state below a structure, and is only possible at large depths where stress increments from loading are small compared to the initial stresses, and K_o is greater than one. These deep soil layers will have considerably less influence on the structure's performance than the shallow layers beneath the foundation, where larger vertical than horizontal stresses prevail, independent of K_o. However, an example of a cyclic extension test is included to

complete the picture of stress path influence on cyclic sand behavior.

Figure II-17 presents a typical effective stress path plot of representative cycles from an anisotropically consolidated sand sample tested in cyclic extension. Figure II-18 shows a stress-strain plot of the same load cycles. A summary plot of maximum and minimum values of shear stress, vertical strain, pore pressure and mean normal effective stress throughout the test is given in Figure II-19. All three figures are typical for cyclic extension tests on contractive sand, and allow the following statements about sand behavior in such tests:

(1) Similar to contractive sand behavior in compression and isotropic cyclic tests, the pore pressure increases, decreasing effective stresses (Figures II-17 and II-19).

(2) Again the first cycle produces a much larger increment of pore pressure than does any subsequent cycle (Figures II-17 and II-19).

(3) The rate of pore pressure build-up decreases with the number of load cycles in Stage I (Figure II-19).

(4) In Stage II, the residual pore pressure dropped after initially increasing and leveling off. That happened in all the extension tests, and

could be caused by dilatancy as well as a decrease in strength of the sample (Figure II-19).

(5) The K_f-line again limits the pore pressure development, and the effective stress cannot reach zero (Figures II-17 and II-19).

(6) The peak to peak strains are somewhat larger than in compression tests, and also increase towards the end of the test (Figure II-18). They, however, never become as large as the peak to peak strains during cyclic mobility.

(7) Residual vertical extension strains build up with an increasing rate per cycle throughout the test (Figure II-19).

(8) The stress-strain curves are hysteretic (Figure II-18).

(9) The A-parameter for individual cycles changes from about .25 in the first load cycle to about 1.0 at the end of the test (Figure II-17).

The important similarity between cyclic extension and compression tests on contractive sand, is that neither one can reach zero effective stress in a triaxial test, as long as the shear stress direction does not reverse. Therefore, both develop residual strains, respectively in extension and compression. The vertical strains are aligned with σ_1 in compression tests and σ_3 in

extension tests. The special characteristic of isotropic consolidated cyclic test specimens, is that zero effective stress is reached at zero shear stress, and large cyclic strains then occur rapidly. An anisotropically consolidated contractive sample with shear stress reversal starts out behaving similarly to compression or extension tests. As the effective stress path approaches the K_f-line, the pore pressure at zero shear stress increases in a few load cycles to equal the confining stress. Simultaneously cyclic mobility leads to large peak to peak strains that overshadow the residual strain component, and the sample behaves much like the isotropically consolidated sample described above. Tests LC71, LC75 and LC143 (Appendix F) are examples of this behavior.

The most important difference between cyclic extension and compression tests can be explained with Figure II-20. The total stress paths for two cyclic tests at the same porosity are drawn, one cyclic extension test and one cyclic compression test. Both tests are starting about equally far away from the lines indicating 30° friction angle. The cyclic shear stress is, however, 3 1/2 times higher in the compression tests than the extension test. Even so, the cyclic extension sample reaches 5% accumulated strain in one-third as many cycles as the compression test. The main reason for this behavioral difference is the difference in

stress paths, but it is also likely that sample anisotropy plays some role (anisotropy in the triaxial samples is discussed in Appendix C).

Figure II.21 presents total stress paths for three cyclic tests that are identical except for the value of mean shear stress. Figure II-22 compares strain and pore pressure development in those tests. All were performed undrained on contractive sand at about 41.2% porosity (46% relative density), with 2.50 kg/cm^2 mean consolidation stress and with 0.45 kg/cm^2 cyclic shear stress (i.e., cyclic shear stress ratio = $\Delta q_{cy}/\bar{p}_o$ = 0.18). The stress history, the testing procedure and the sample preparation method were identical in all tests. The cyclic isotropic test (upper plot, q_m = 0 kg/cm^2) reached zero effective stress in 203 load cycles, and the peak to peak strains exceeded $\pm$ 5% in 206 cycles. The cyclic compression test (middle plot, q_m = 0.5 kg/cm^2) developed a pore pressure ratio of 0.8 in 1000 load cycles. (The pore pressure ratio, M, is defined in Figure II-9). Only 0.5% vertical compression strain accumulated in the 1000 load cycles. The cyclic extension test (bottom plot in Figure II-22, q_m = -0.5 kg/cm^2) reached the K_ε-line (M = 1.0) in 5 cycles, and 10% residual extension strain in 22 cycles.

2.5 General Observations

After termination of each cyclic test, the sample was reconsolidated to initial consolidation stresses. The purpose of this reconsolidation was to investigate possible correlations between pore pressure development (dilation - contraction - liquefaction), test type, density and volume change. The measured volumetric strains are plotted in Figure II.23 versus the pore pressure generated during the cyclic test. Different points are used to differentiate between cyclic compression, extension, and isotropic tests, as well as indicate porosity and the occurrence of cyclic mobility. The generation of positive pore pressure indicates contraction and negative pore pressure dilation. All samples that contracted, expelled water upon consolidation, and decreased in volume (positive volumetric strain). The samples that dilated, increased in volume upon consolidation by absorbing water.

Cyclic compression tests show a dependence on the amount of volumetric strain on the generated pore pressure and the sample porosity. For a porosity of 39%, the volumetric strain is about 0.1%. For 41% porosity, the volumetric strain varies from about -0.25 to +0.3% for generated pore pressures from -2 kg/cm^2 to +2 kg/cm^2. Compression test samples at 43% porosity showed 0.4% volumetric strain at 1 kg/cm^2 generated pore pressure, and samples at 47%

porosity showed 1.8% strain at 2.5 kg/cm^2 pore pressure. Two loose samples that liquefied at the K_f-line showed volumetric strains of 2 and 4%.

Three cyclic isotropic tests consolidated at a pore pressure ratio of 0.4 to 0.6 before reaching cyclic mobility failure, correspond well to the compression test results at the same porosity (n = 41%). However, the large number of isotropic tests at 41% porosity experiencing cyclic mobility developed much larger volumetric strains, from 2 to 4%, apparently independent of the value of generated pore pressure. This suggests that a radical change in sand structure takes place during cyclic mobility, resulting in a very compressible soil sceleton.

Cyclic extension tests at 41% porosity developed about 0.7% volumetric strain, three times as much as the compression tests at the same generated pore pressure of about 1 kg/cm^2.

Two anisotropically consolidated static tests were performed in which the back pressure was increased, decreasing the effective stress until failure. The effective stress paths of the tests thus were horizontal lines to the left in $\bar{p}$ - q - diagram, both at 0.5 kg/cm^2 static shear stress. Figure II.24 presents a plot of vertical strain versus shear stress divided by effective stress for those two static tests and four more cyclic tests with the same mean shear stress, 0.5 kg/cm^2. The accumulated vertical strains in the cyclic

tests were 3 to 10 times larger than in the static tests at all effective stress levels. This suggests that strains are not uniquely related to decrease in effective stress, but also depends on how the effective stress decrease was achieved.

Lee ([1976b) and (1976d)] maintains the view that cyclic strain amplitude (peak to peak strain) rather than cyclic stress amplitude governs the behavior of cohesionless soils subjected to cyclic loading. When comparing tests performed with varying stress paths, that is in accordance with the findings herein. Figure II.25 presents a plot of peak to peak strains at a pore pressure ratio of 0.5, versus the number of cycles required to reach 1% strain. Three series of tests with varying cyclic shear stresses are plotted. The open points indicate measured values, and the solid points next to them values corrected for porosity deviations. Four further plots given in Appendix E show very similar effects of the cyclic strain amplitude. Clearly the number of cycles to reach 1% strain decreases as the peak to peak strain increases. The variations in peak to peak strains are caused by the variations in cyclic stress conditions, not by performing strain controlled tests.

If, however, tests at the same cyclic stress condition but with varying porosity, loading period and stress history are performed, the variations in strain amplitude are given

by Figure II.26. The number of load cycles does not seem to depend on the peak to peak strain in this case, suggesting that the cyclic strain amplitude not always governs cyclic behavior.

2.6 Summary of Undrained Cyclic Sand Behavior

When a sand sample in a triaxial test is loaded with a vertical cyclic stress component superposed on an acting static stress condition, the sample might, under undrained conditions, develop negative pore pressures (dilation), develop positive pore pressures until the effective stress path reaches the K_f-line (contraction), or generate positive pore pressures followed by collapse at the K_f-line and almost total loss of strength (liquefaction). Judging from the cyclic tests performed in this investigation, the type of pore pressure response to cyclic loading seems to be governed by the sand porosity and the cyclic shear stress ratio. The importance of the volume change tendency and thus the pore pressure response lies in the accompanying strains: Samples that developed negative pore pressure and thus experienced increased effective stresses, accumulated less than 0.2% vertical strain, even after as many as 30,000 load cycles. Samples which liquefied, suddenly collapsed and strained until limited by the testing equipment.

Comparing tests LC133 that dilated and LC134 that

contracted under similar conditions (Appendix F), an increase in strain by a factor of 5 is found between the dilating and contracting test. The difference between contraction (LC156) and liquefaction (LC155) is a stunning 32 load cycles to 1 load cycle to reach 10% vertical strain under virtually identical conditions.

Samples that contracted in triaxial tests were very dependent on the stress path, particularly on whether the shear stress became equal to zero at any time during cyclic loading. Three different types of strain and pore pressure response of cyclic triaxial tests were identified based on the acting mean shear stresses: Cyclic compression tests have positive shear stresses, and accumulate vertical strain at an approximate constant rate per cycle throughout the test. Cyclic extension tests have negative shear stresses, and accumulate vertical strain rapidly, but at an approximately constant rate per cycle. Cyclic isotropic tests have shear stress reversal, and will, after reaching the K_f-line, experience cyclic mobility with rapid development of large peak to peak strains in the sample.

The importance of reaching zero shear stress or not during cyclic loading can be demonstrated by the following comparison: the cyclic compression tests LC148 accumulated 10% vertical strain in about 12,000 laod cycles, whereas the almost identical test LC75 with slight shear stress reversal

experienced cyclic mobility and 10% peak to peak strain after 420 load cycles (Appendix F).

The behavior of samples that liquefy are probably only slightly influenced by the mean shear stress acting in the sample. The reason is that the K_f-line does not limit the pore pressure development, since the samples collapse and the effective stress drops almost to zero, regardless of what mean shear stress existed. This is supported by Castro's (1969) cyclic test results from samples that liquefied.

The behavior of samples that dilate appears equally insensitive to the mean shear stress. The effective stress path will not in any way be influenced by the K_f-lines, since the path moves towards larger effective stresses.

The rest of this thesis is devoted mainly to contractive cyclic behavior. All results are for contractive conditions with no liquefaction possible unless otherwise stated.

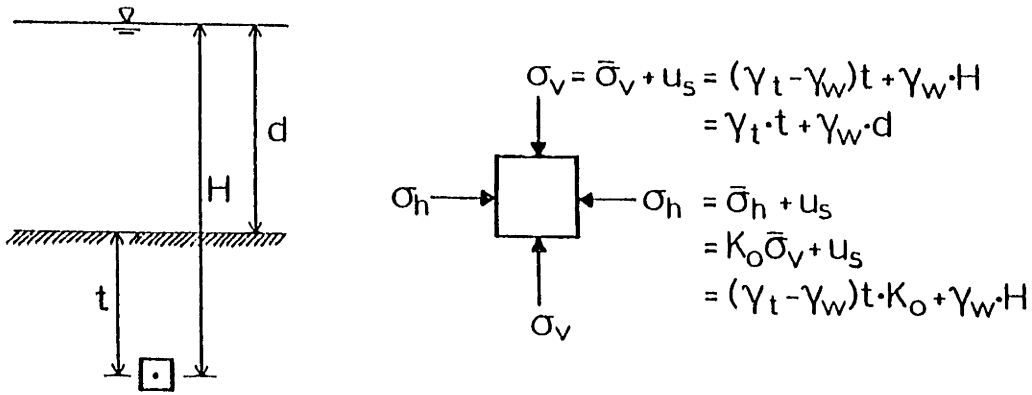

a. GEOMETRY b. STRESSES ON SOIL ELEMENT

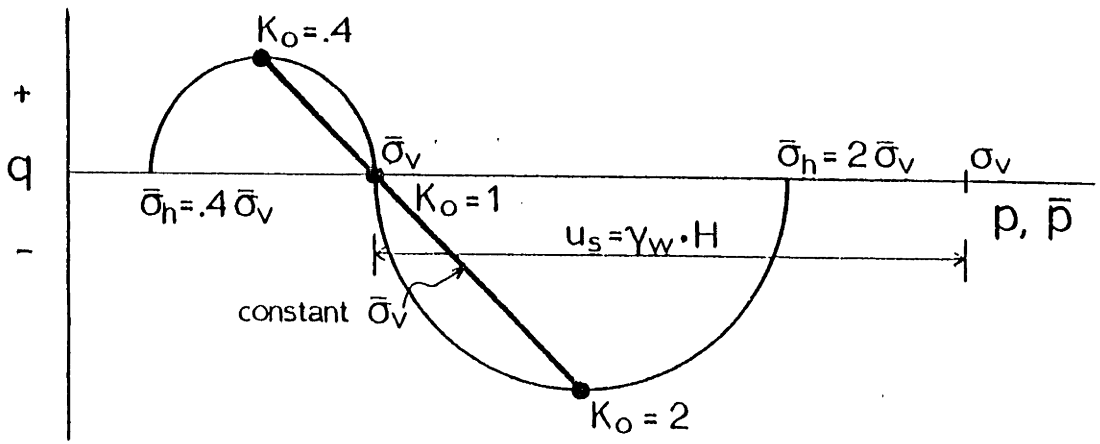

c. STRESS POINTS

FIGURE II-1

IN SITU STRESS CONDITION

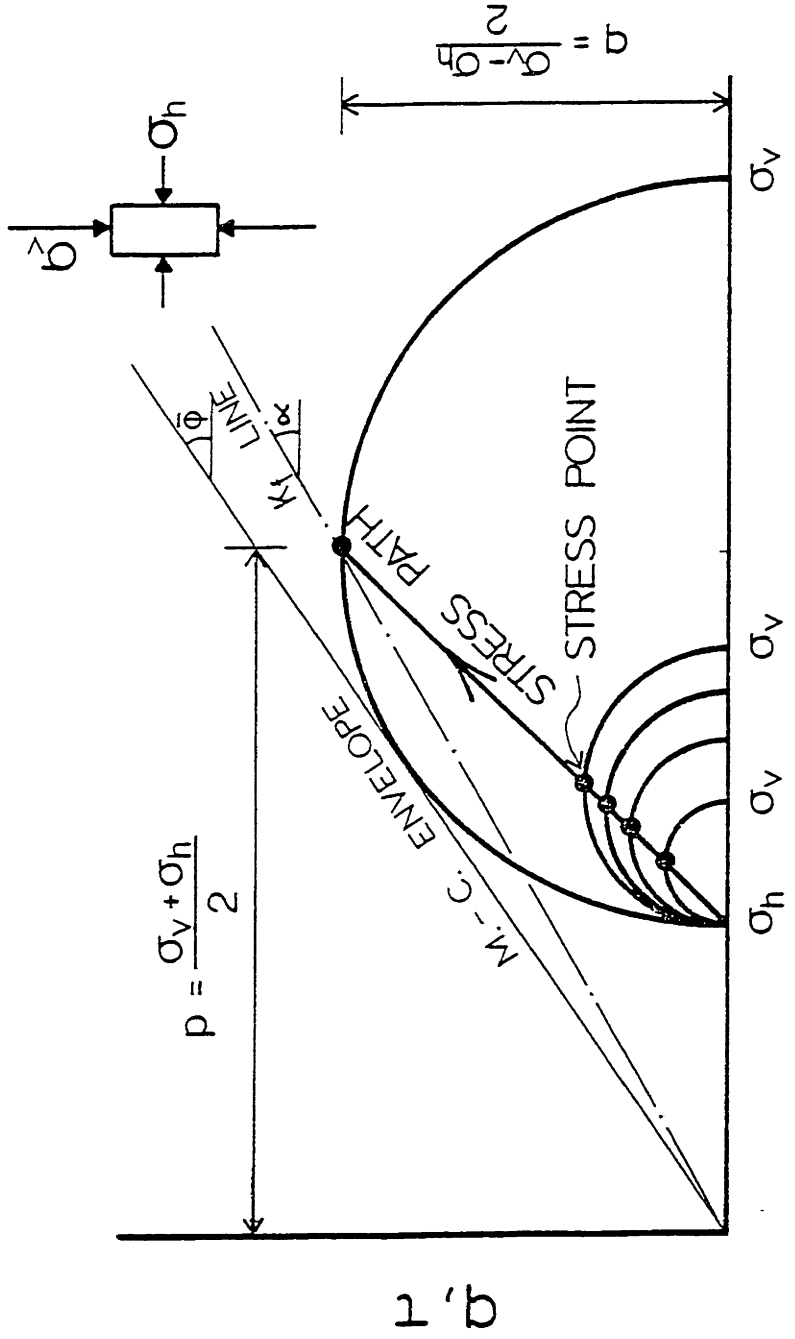

STRESS POINTS AND STRESS PATH

FIGURE II-2

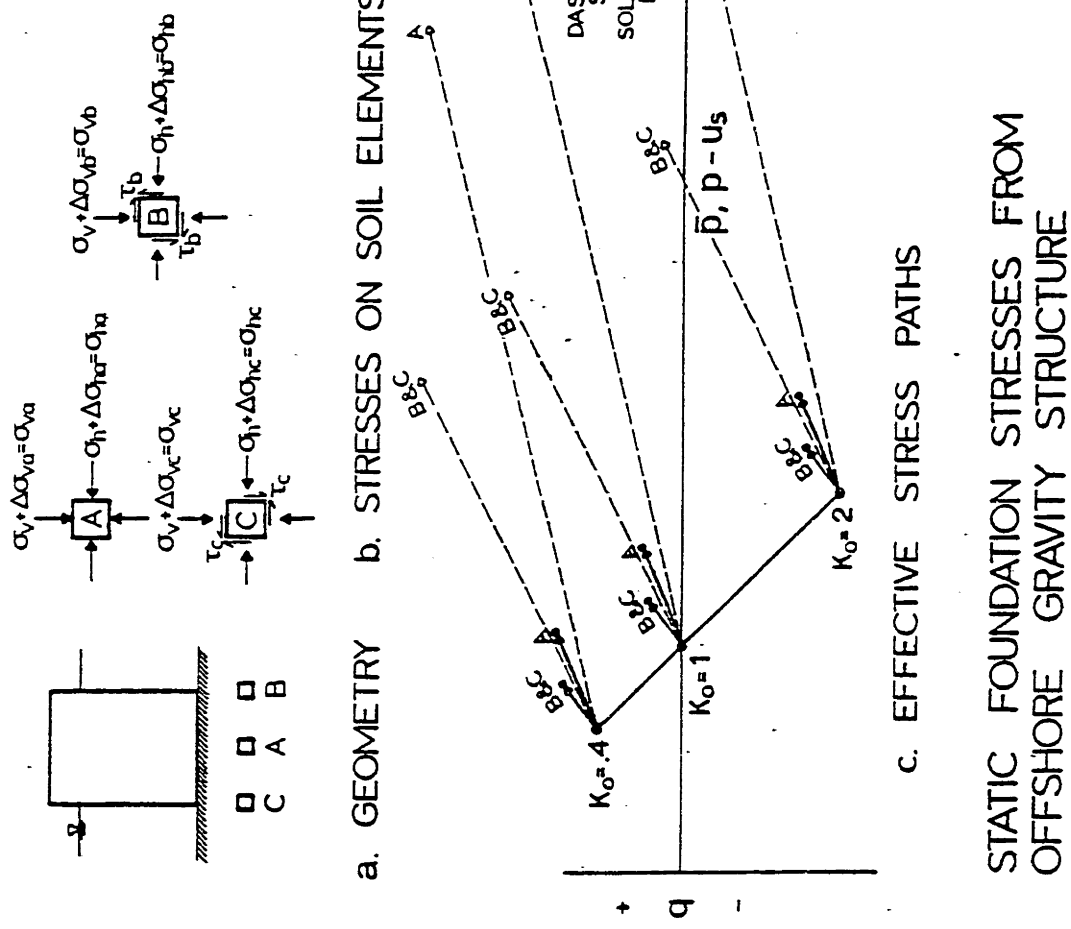

FIGURE II-3

STATIC FOUNDATION STRESSES FROM OFFSHORE GRAVITY STRUCTURE

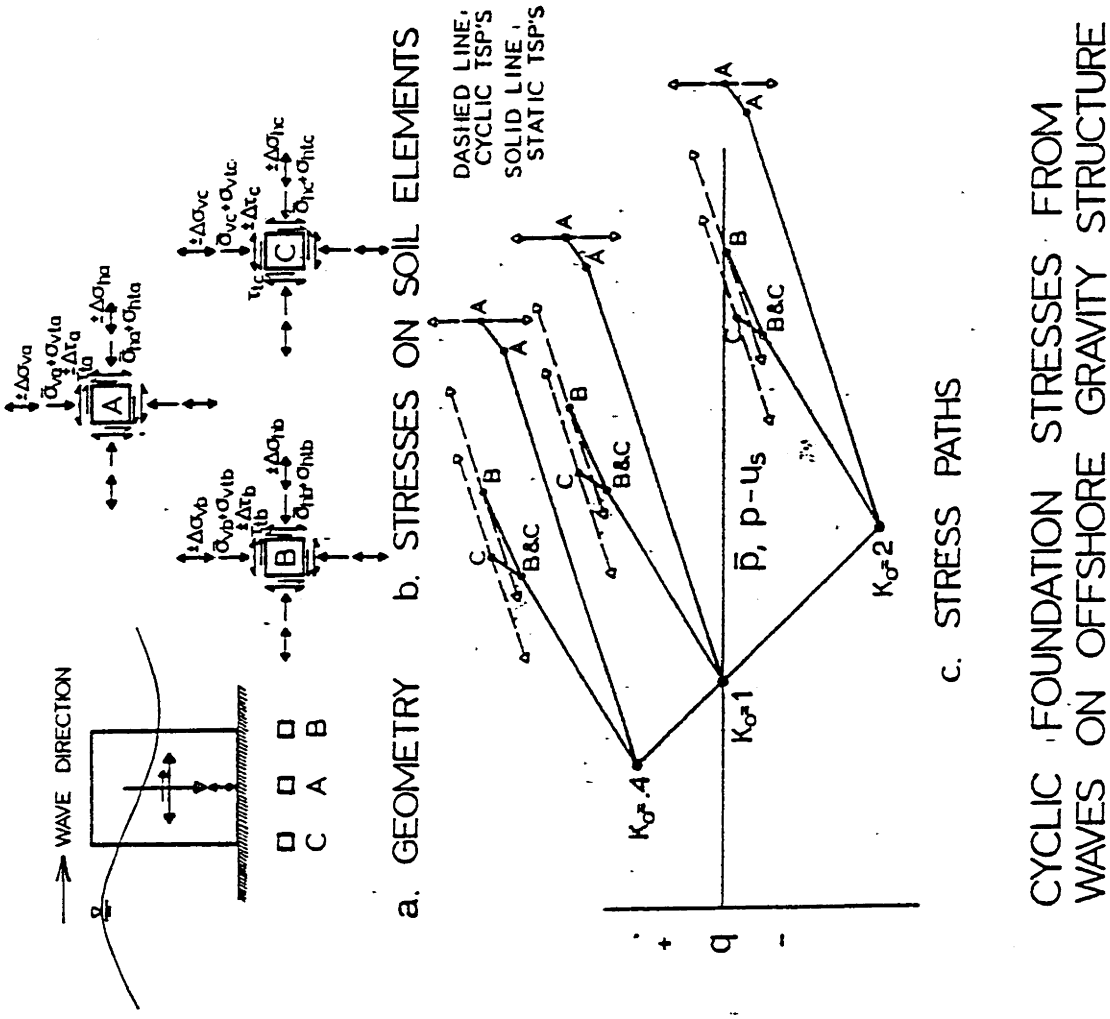

CYCLIC FOUNDATION STRESSES FROM WAVES ON OFFSHORE GRAVITY STRUCTURE

FIGURE II-4

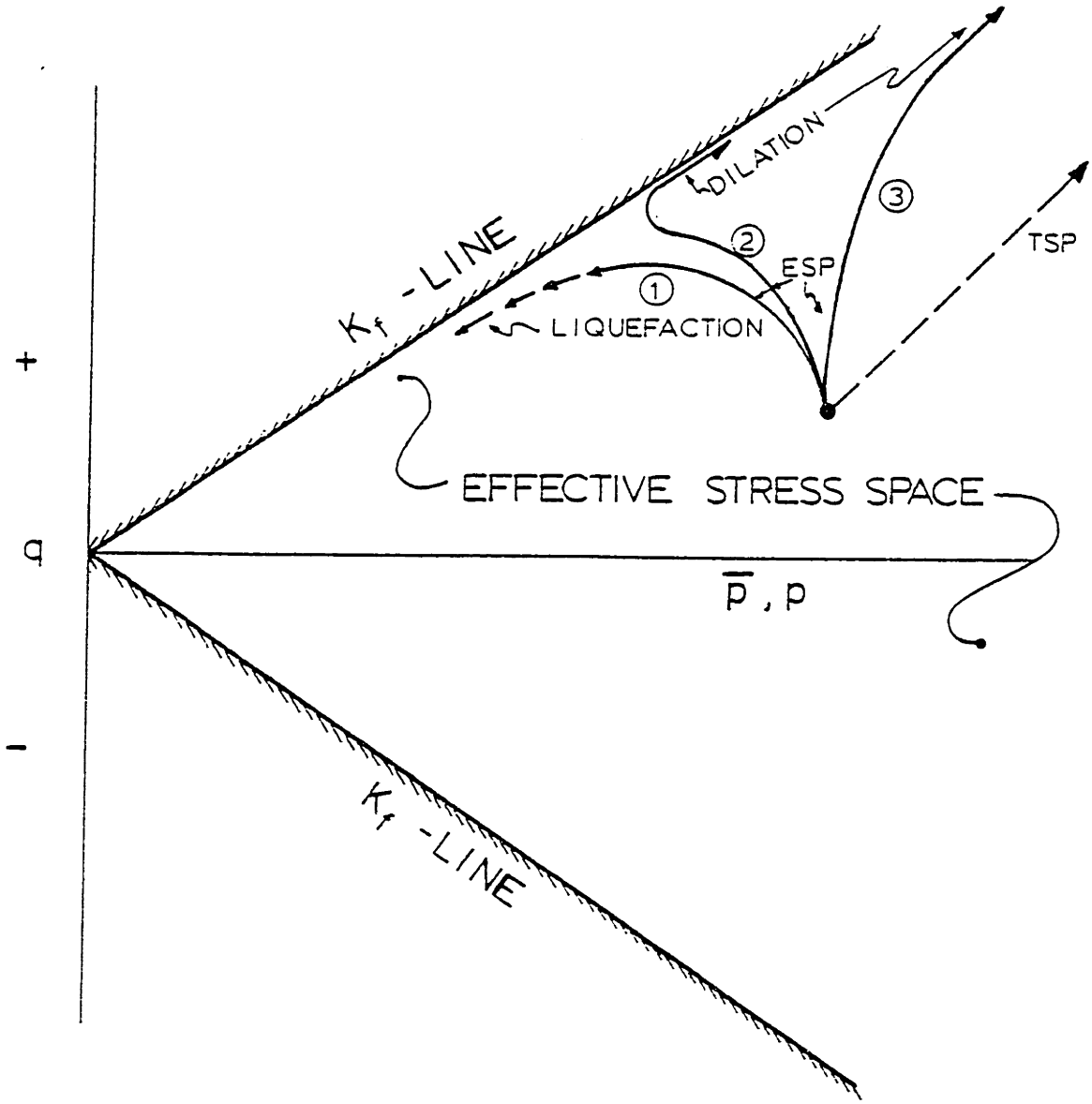

TYPICAL STRESS PATHS FOR UNDRAINED STATIC TESTS AT DIFFERENT DENSITIES

FIGURE II-5

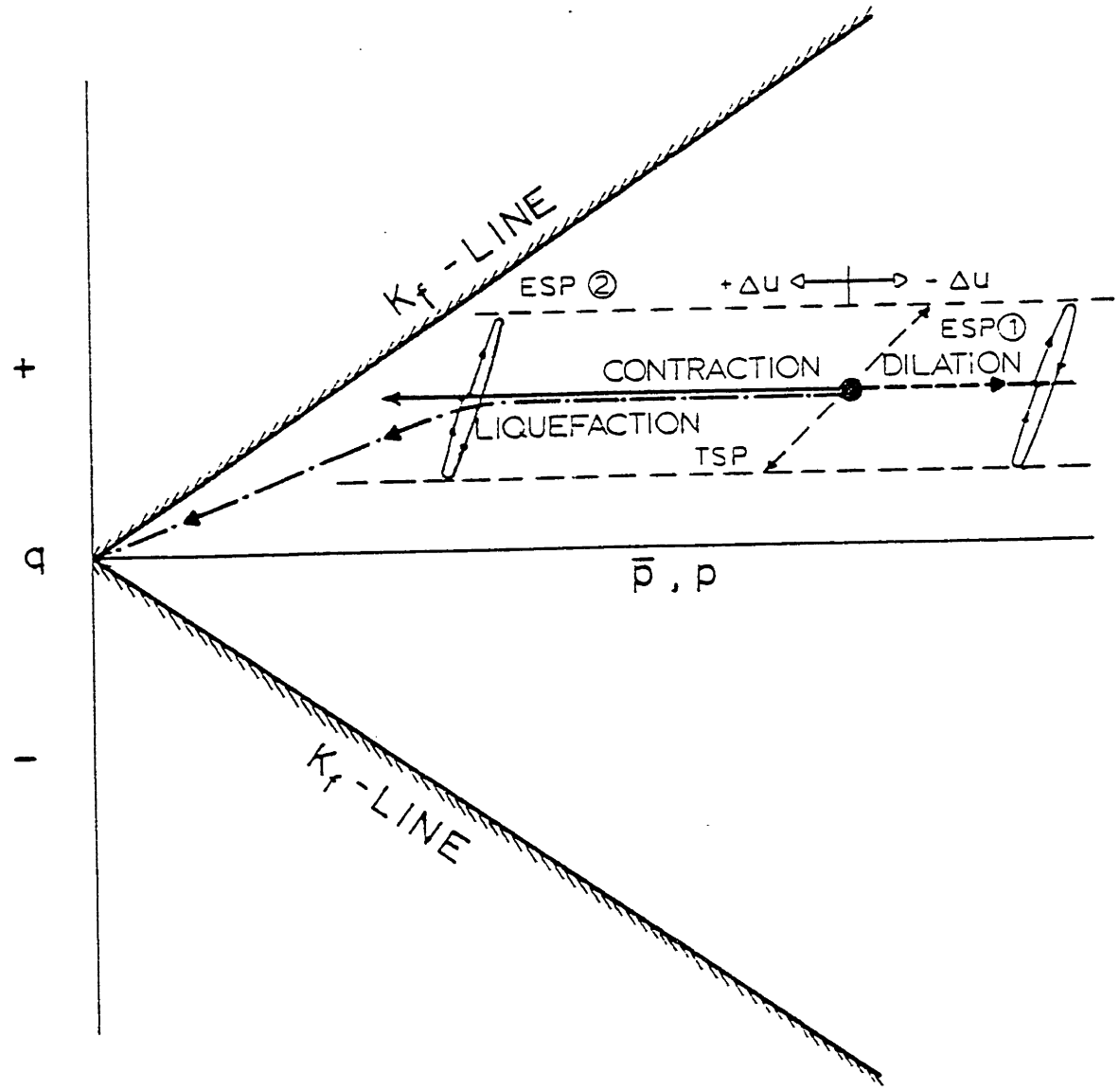

LIQUEFACTION, CONTRACTION AND DILATION IN CYCLIC TRIAXIAL TESTS

FIGURE II-6

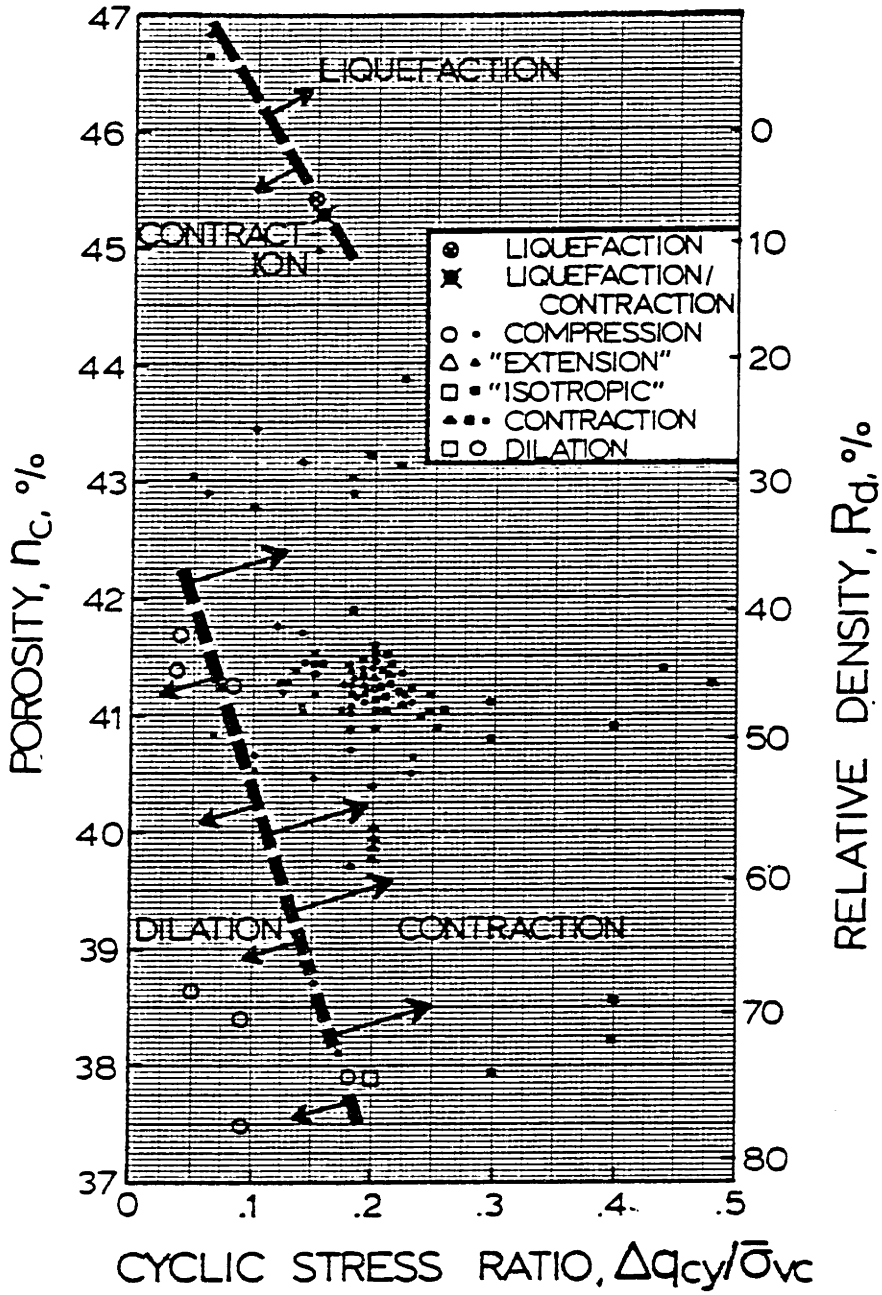

SUMMARY OF CYCLIC TRIAXIAL TESTS

FIGURE II-7

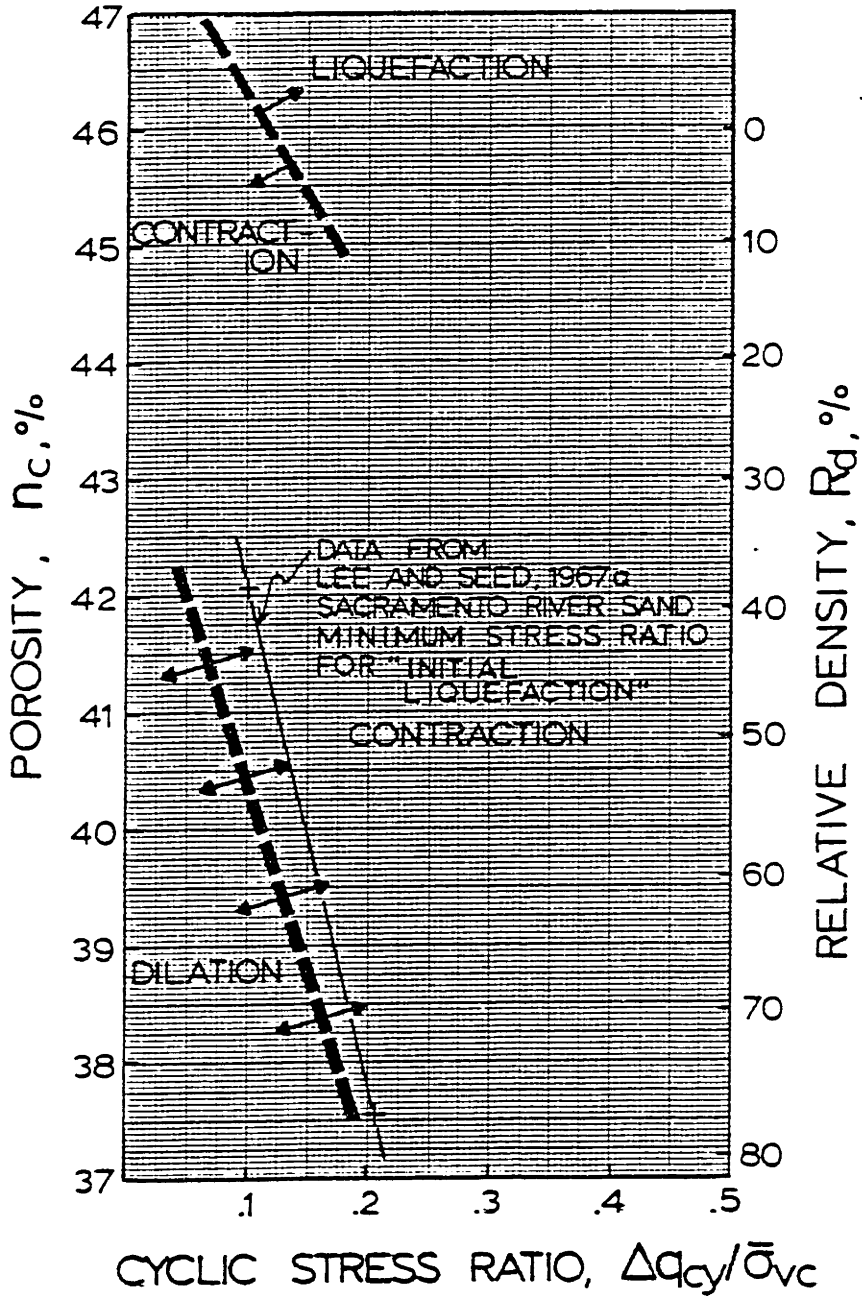

DILATION, CONTRACTION AND LIQUEFACTION IN CYCLIC TRIAXIAL TESTS

FIGURE II-8

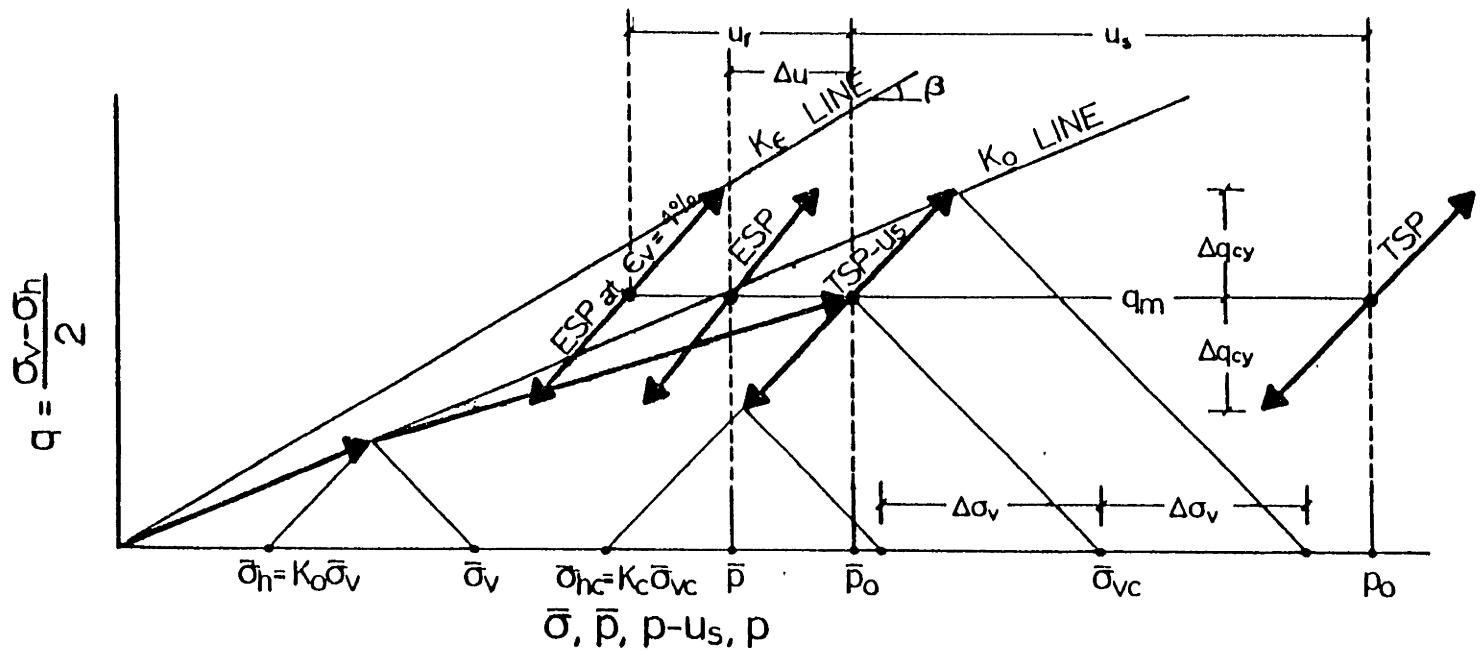

$\bar{\sigma}_{vc}$ & $\bar{\sigma}_{hc}$ = EFFECTIVE STRESSES BELOW STRUCTURE
$\bar{\sigma}_v$ & $\bar{\sigma}_h$ = IN SITU EFFECTIVE STRESSES
ESP = EFFECTIVE STRESS PATH
TSP - u_s = TOTAL STRESS PATH - STATIC PORE PRESSURE
TSP = TOTAL STRESS PATH
u_f = PORE PRESSURE AT 1% VERTICAL STRAIN
$\Delta q_{cy} = \frac{\Delta\sigma_y}{2}$ = CYCLIC SHEAR STRESS
$q_m = \frac{\sigma_{va} - \sigma_{ha}}{2}$ = MEAN SHEAR STRESS DURING CYCLIC TEST
$\bar{p}_o = \frac{\sigma_{va} + \sigma_{ha}}{2}$ = MEAN NORMAL STRESS AT CONSOLIDATION
$M = \frac{\Delta u}{u_f}$ = PORE PRESSURE RATIO

FIGURE II-9

STRESS PATH DIAGRAM WITH DEFINITION OF SYMBOLS TO DESCRIBE STRESS STATE IN CYCLIC TRIAXIAL TESTS

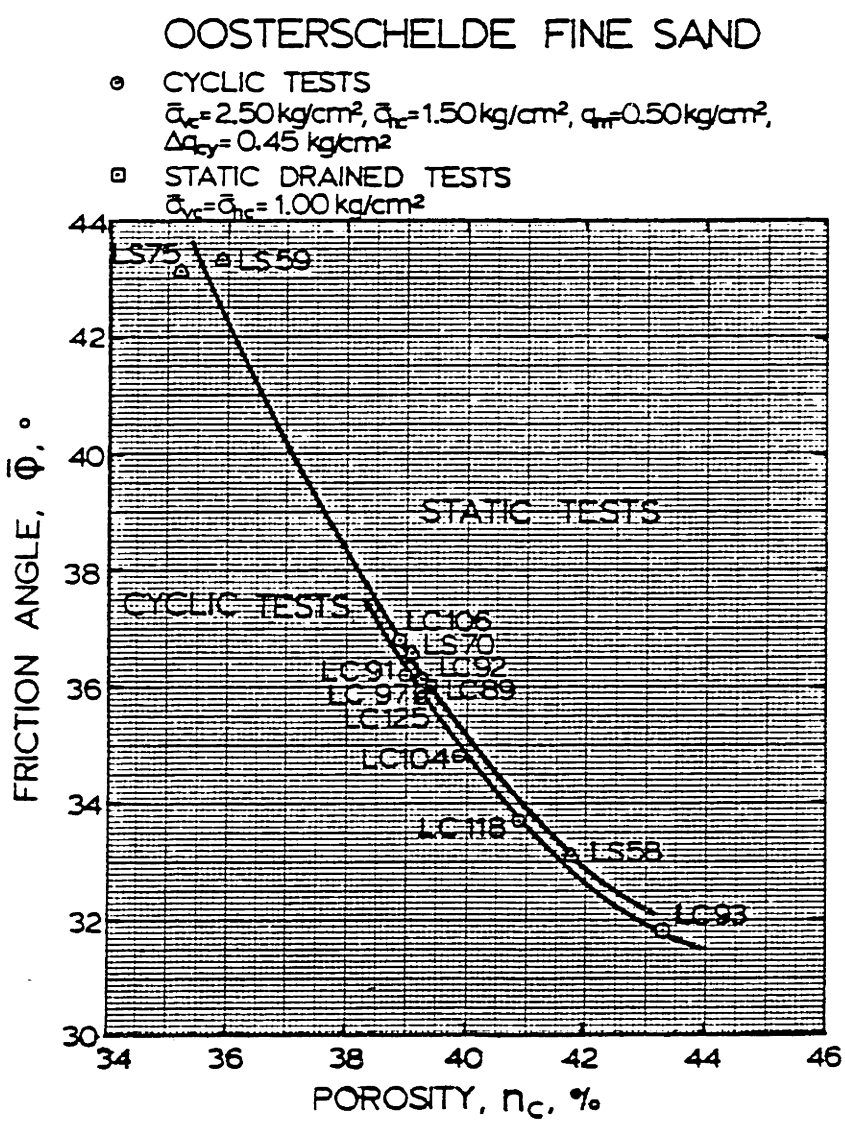

FRICTION ANGLE MEASURED IN UNDRAINED CYCLIC COMPRESSION TESTS AT ϵ_v=1% AND IN DRAINED STATIC TESTS

FIGURE II-10

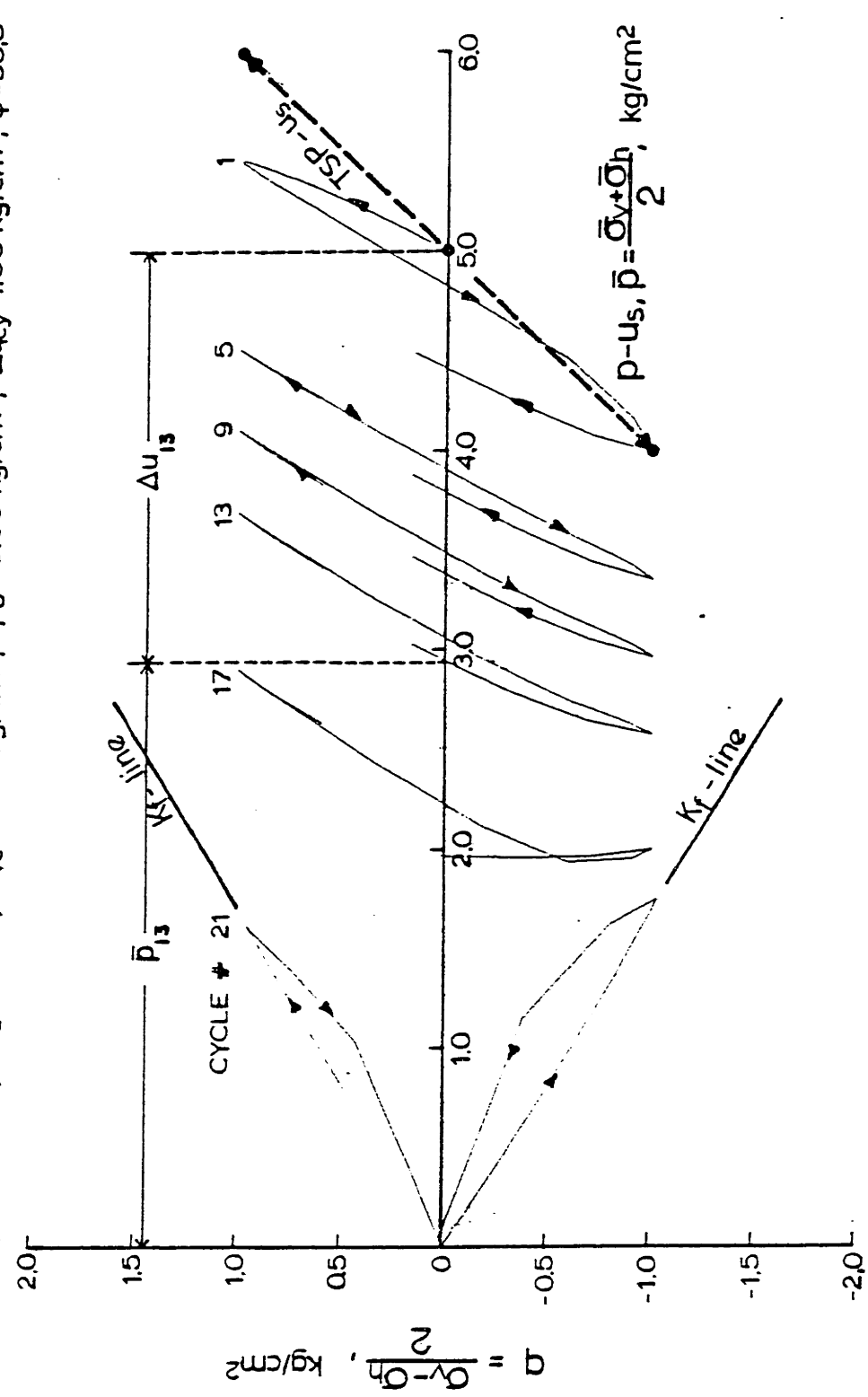

EFFECTIVE STRESS PATH FOR ISOTROPICALLY CONSOLIDATED SAND SAMPLE IN CYCLIC TRIAXIAL TEST

FIGURE II-11

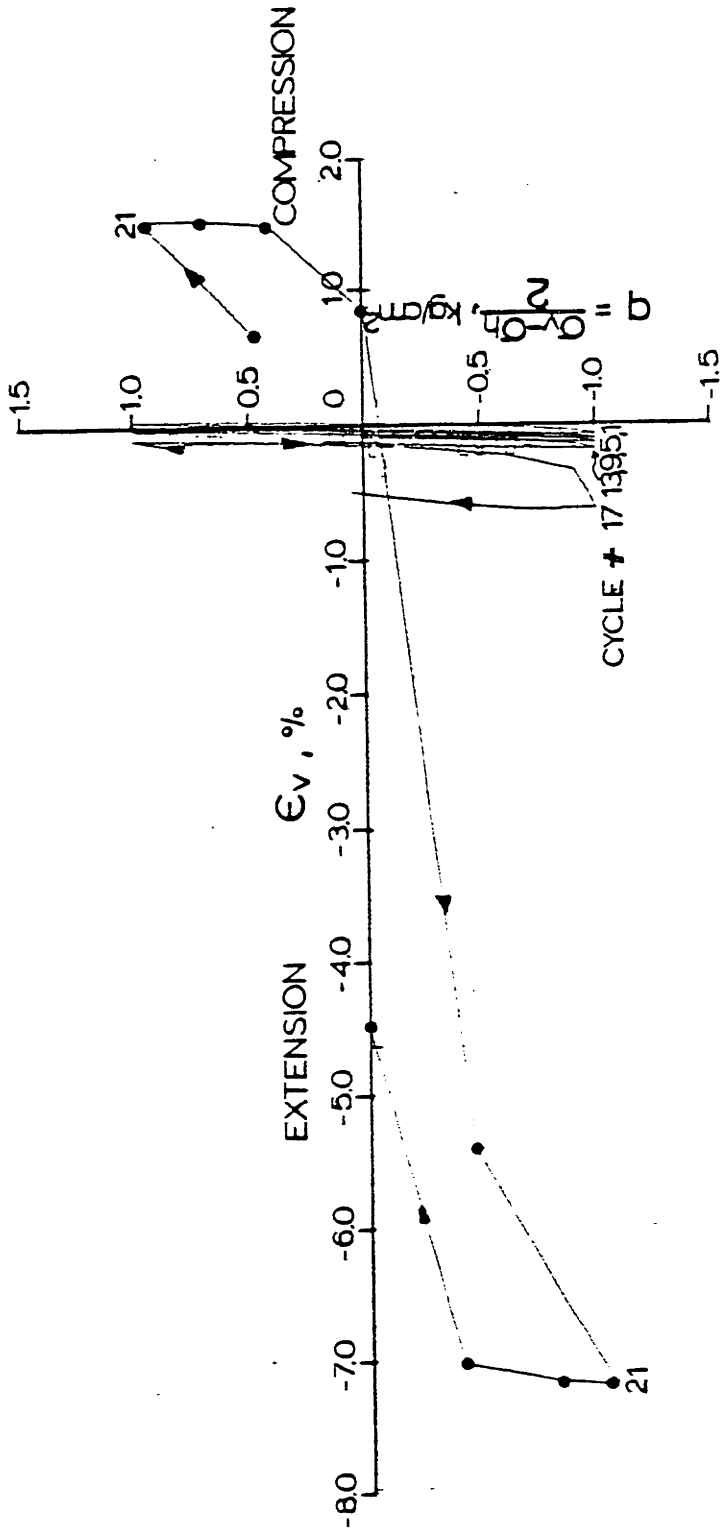

STRESS-STRAIN PLOT FOR ISOTROPICALLY CONSOLIDATED SAND SAMPLE IN CYCLIC TRIAXIAL TEST

FIGURE II-12

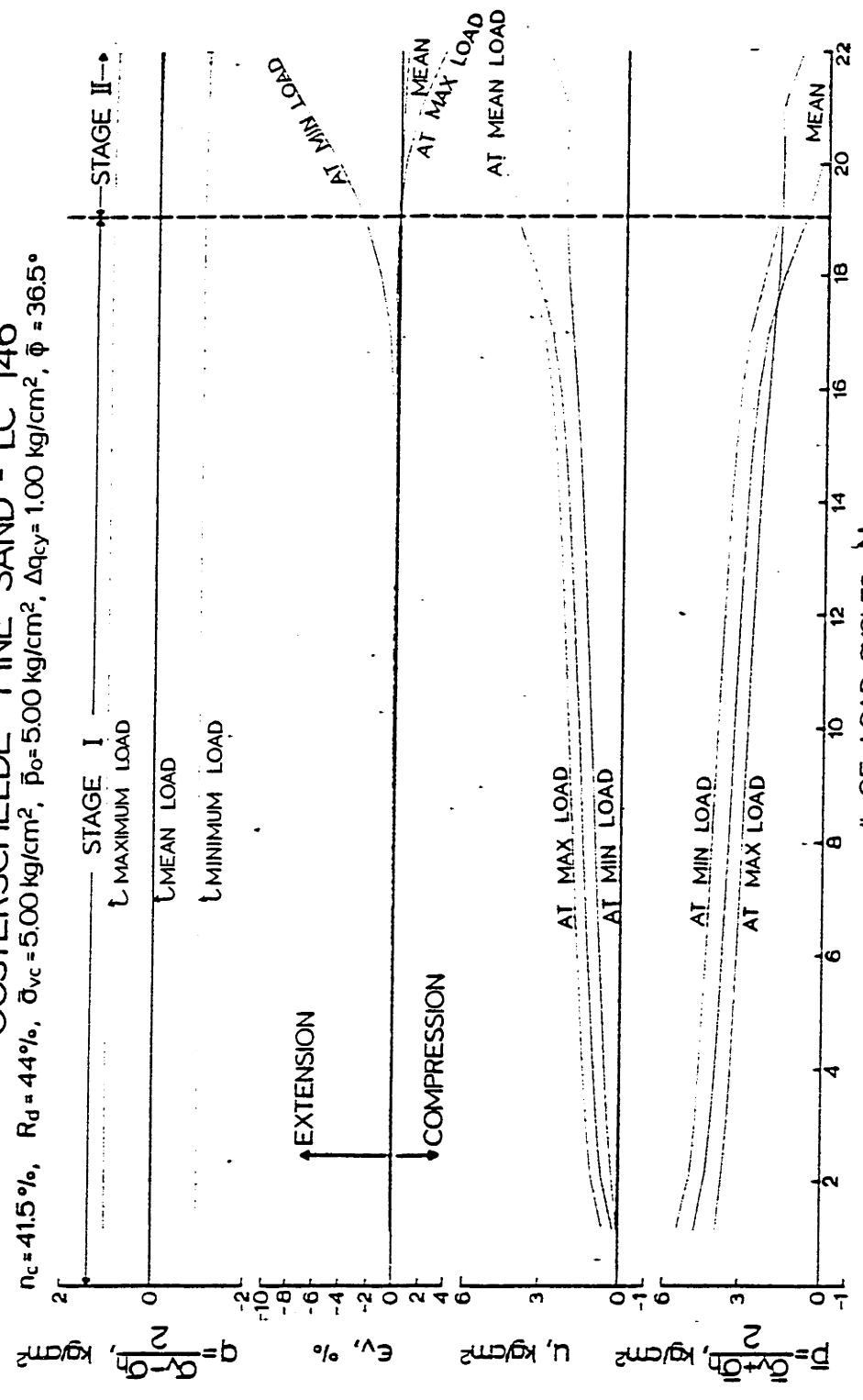

SUMMARY OF STRESS, STRAIN AND PORE PRESSURE DEVELOPMENT FOR ISOTROPICALLY CONSOLIDATED SAND SAMPLE IN CYCLIC TRIAXIAL TEST

FIGURE II-13

OOSTERSCHELDE FINE SAND - LC 142

$n_c = 41.7\ \%$, $R_d = 42\ \%$, $\bar{\sigma}_{vc} = 2.50\ kg/cm^2$, $\bar{p}_o = 2.00\ kg/cm^2$, $\Delta q_{cy} = 0.35\ kg/cm^2$, $q_m = 0.50\ kg/cm^2$, $\bar{\varphi} = 36.4°$

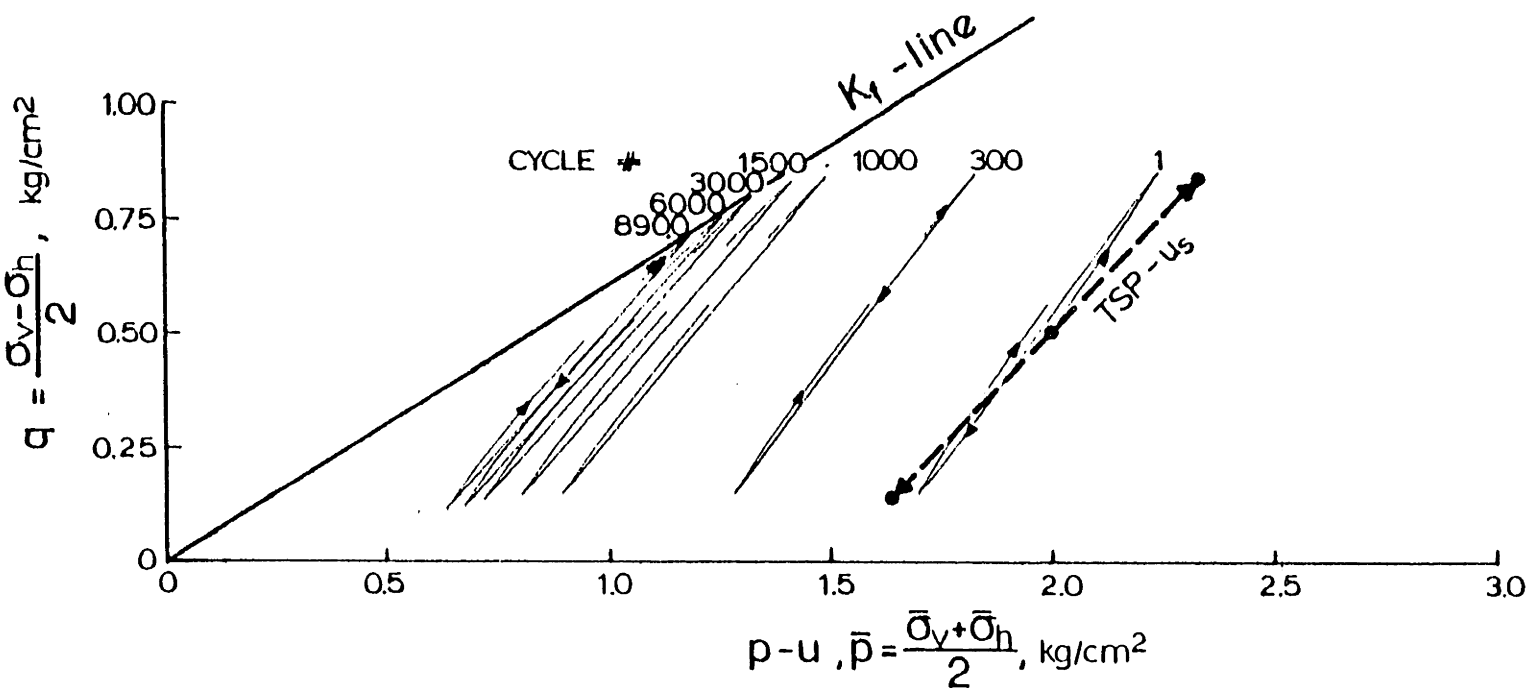

EFFECTIVE STRESS PATH FOR ANISOTROPICALLY CONSOLIDATED SAND SAMPLE IN CYCLIC TRIAXIAL COMPRESSION TEST

FIGURE II-14

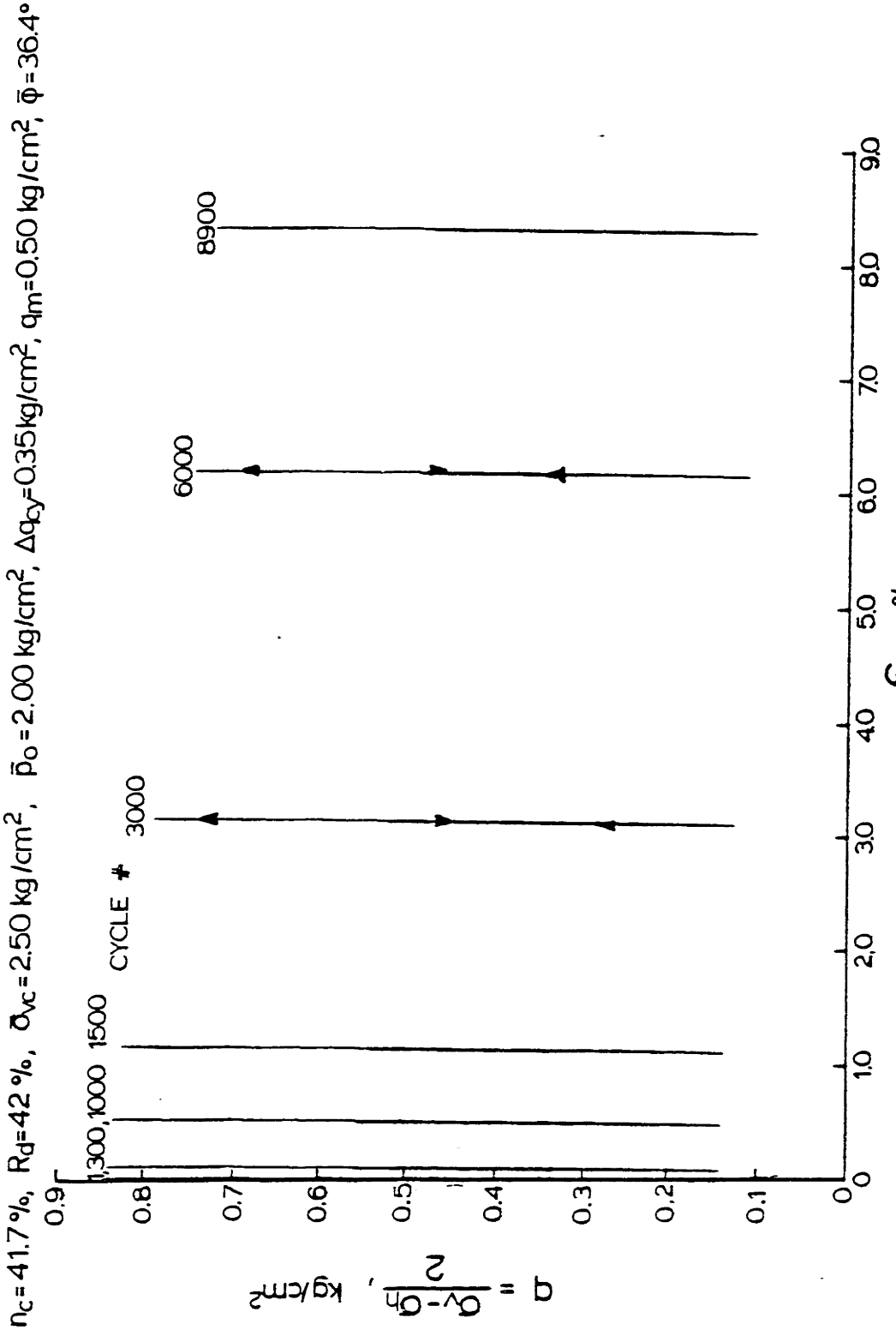

STRESS-STRAIN PLOT FOR ANISOTROPICALLY CONSOLIDATED SAND SAMPLE IN CYCLIC TRIAXIAL COMPRESSION TEST

FIGURE II-15

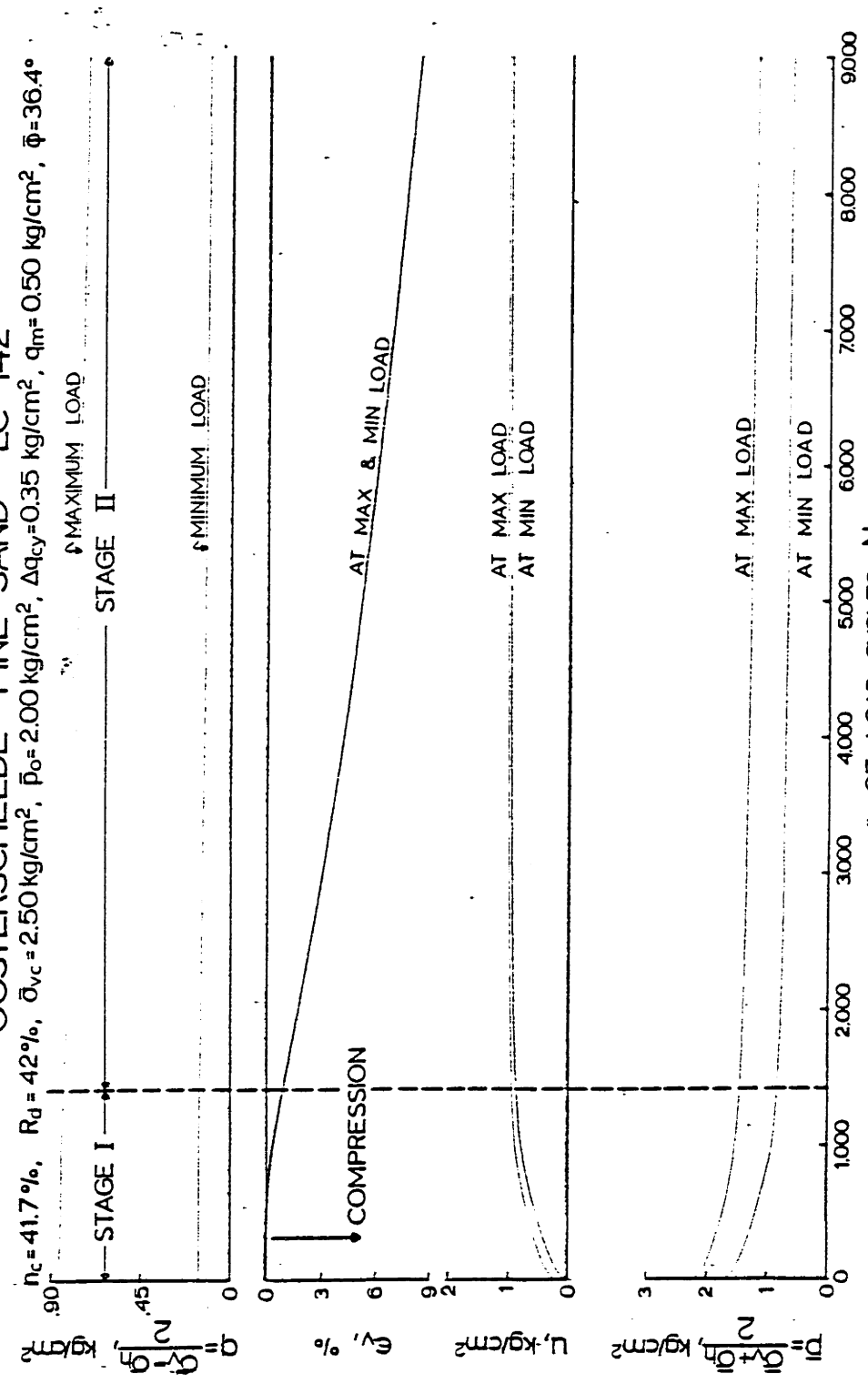

FIGURE II-16

SUMMARY OF STRESS, STRAIN AND PORE PRESSURE DEVELOPMENT FOR ANISOTROPICALLY CONSOLIDATED SAND SAMPLE IN CYCLIC TRIAXIAL COMPRESSION TEST

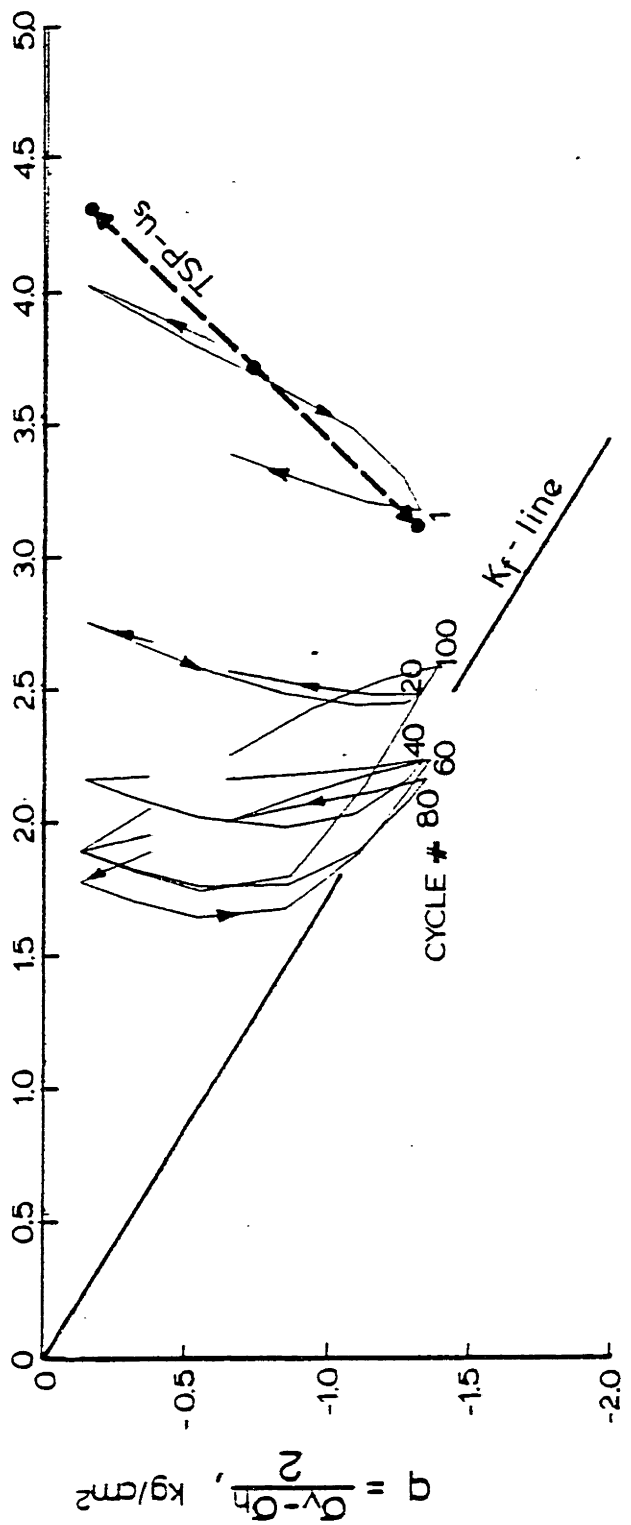

EFFECTIVE STRESS PATH FOR ANISOTROPICALLY CONSOLIDATED SAND SAMPLE IN CYCLIC TRIAXIAL EXTENSION TEST

FIGURE II-17

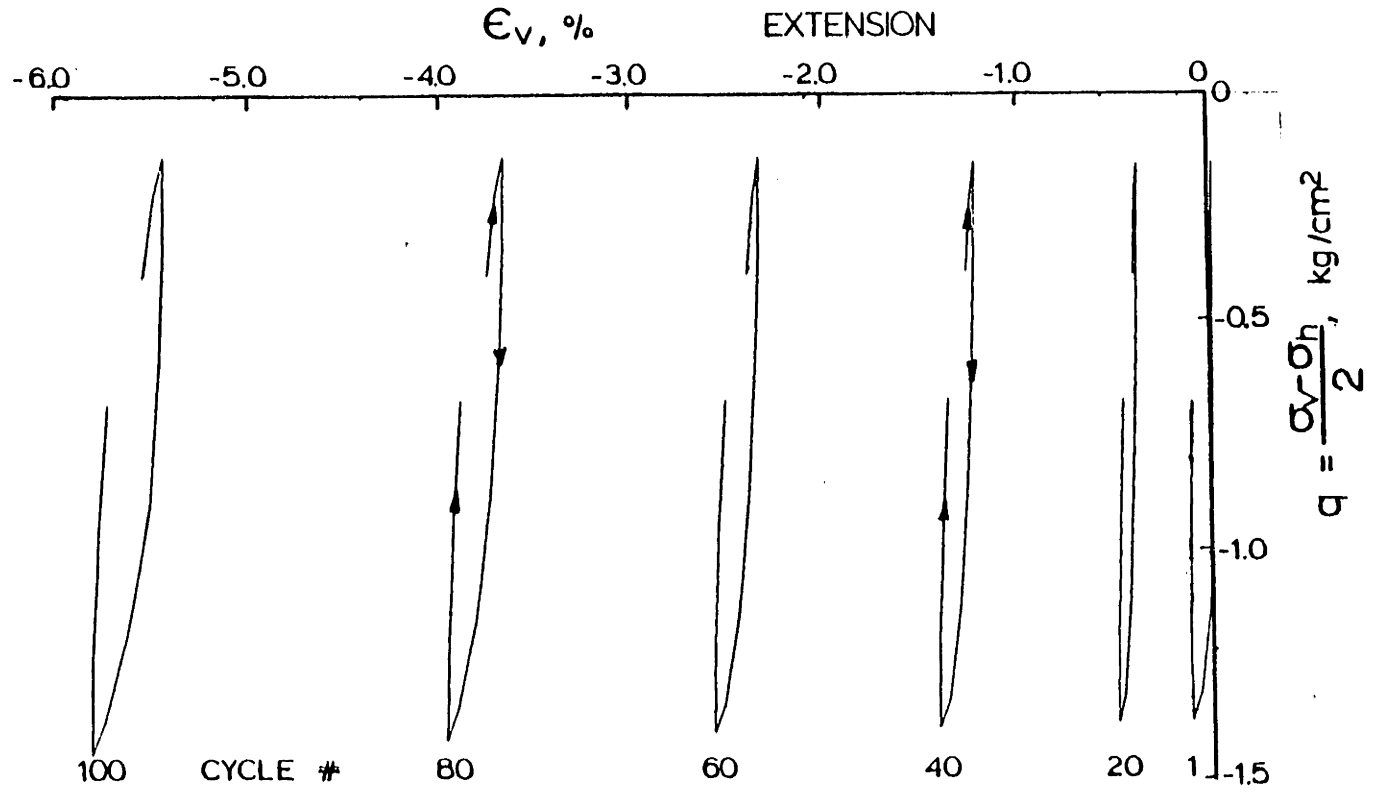

FIGURE II-18

STRESS - STRAIN PLOT FOR ANISOTROPICALLY CONSOLIDATED SAND SAMPLE IN CYCLIC TRIAXIAL EXTENSION TEST

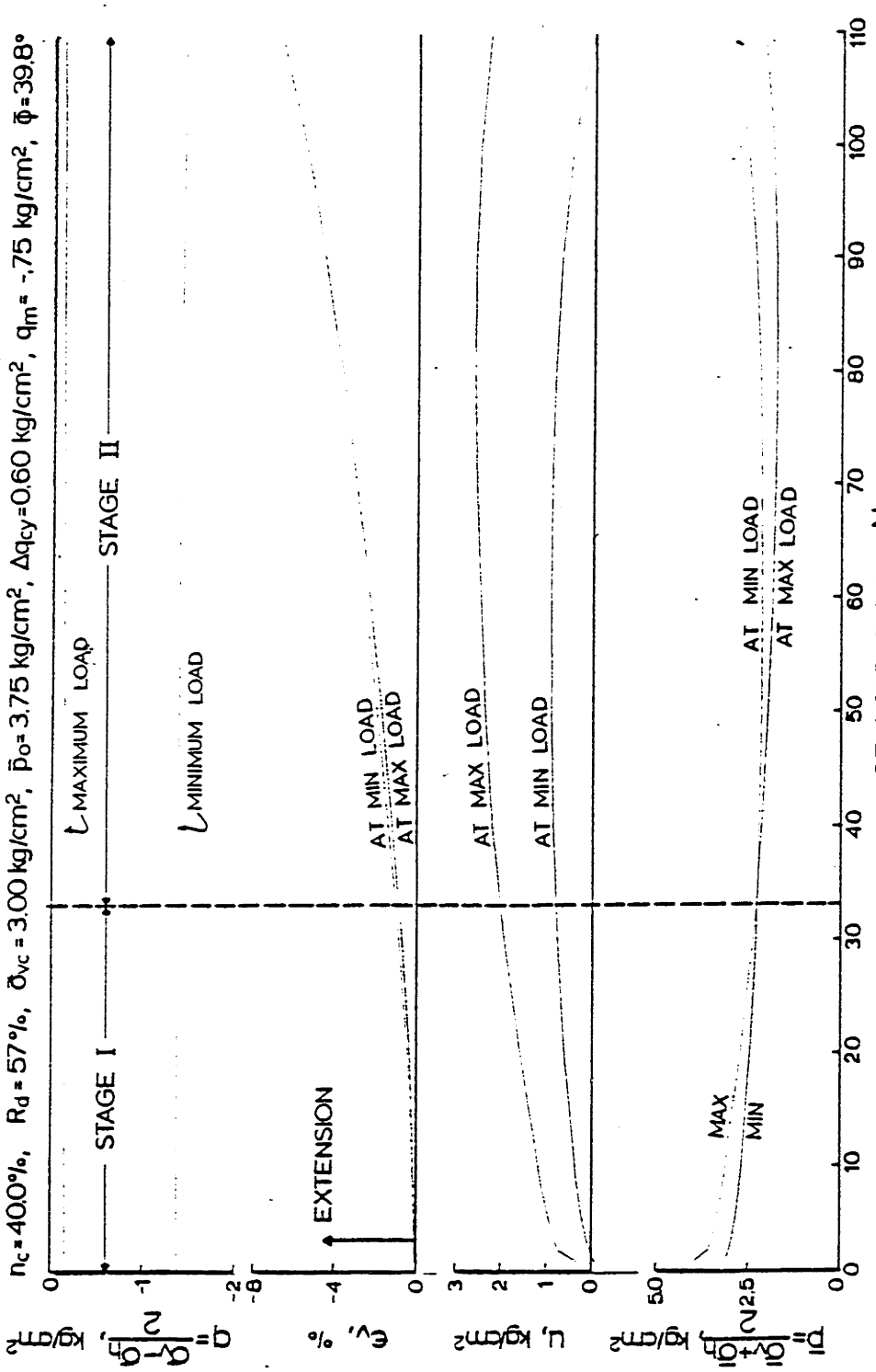

FIGURE II-19 SUMMARY OF STRESS, STRAIN AND PORE PRESSURE DEVELOPMENT FOR ANISOTROPICALLY CONSOLIDATED SAND SAMPLE IN CYCLIC TRIAXIAL EXTENSION TEST

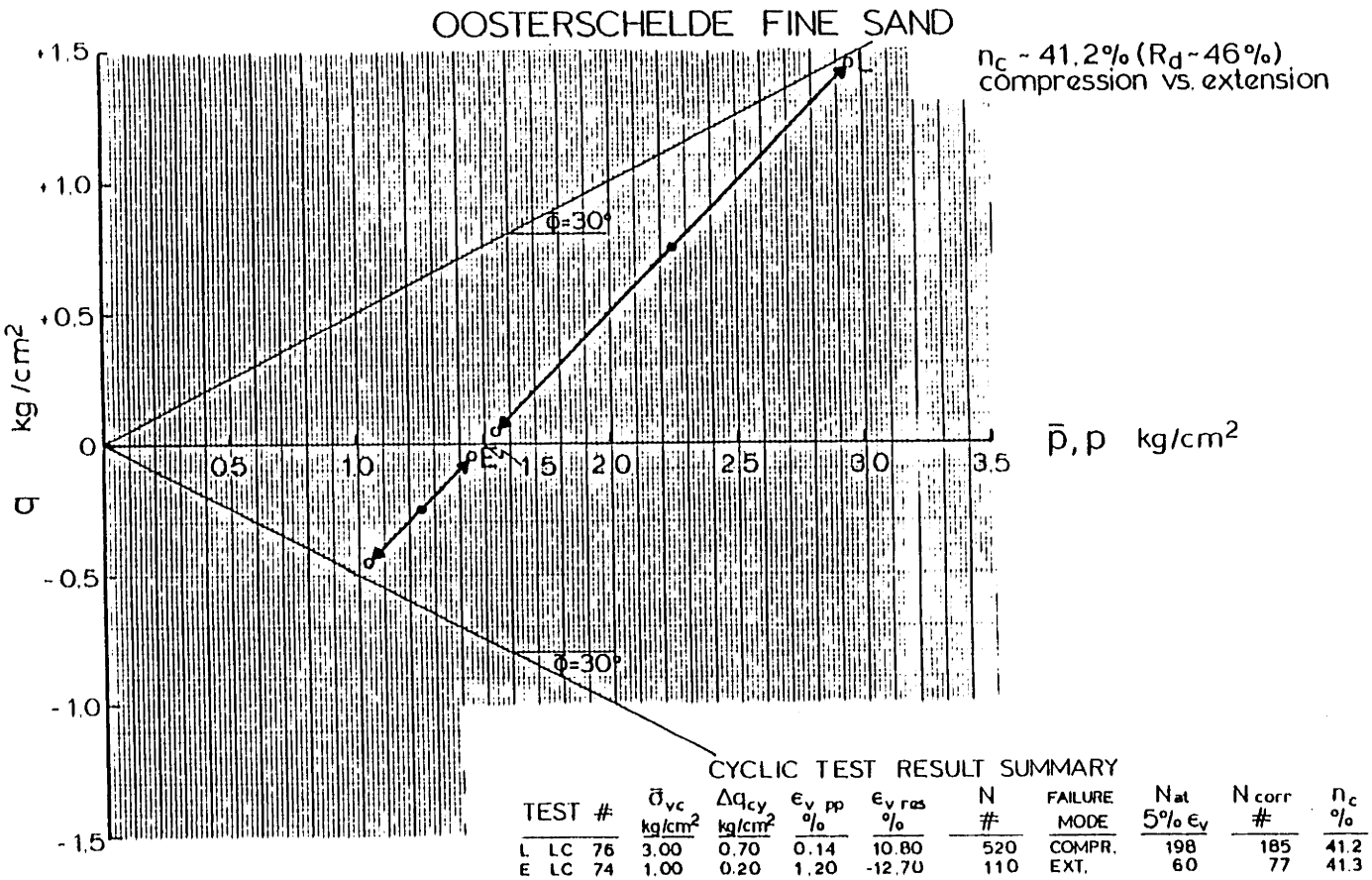

TEST #	$\bar{\sigma}_{vc}$ kg/cm²	Δq_{cy} kg/cm²	$\epsilon_{v\ pp}$ %	$\epsilon_{v\ res}$ %	N #	FAILURE MODE	N_{at} 5% ϵ_v	N_{corr} #	n_c %
L LC 76	3.00	0.70	0.14	10.80	520	COMPR.	198	185	41.2
E LC 74	1.00	0.20	1.20	-12.70	110	EXT.	60	77	41.3

TOTAL STRESS PATHS (TSP-u_B) FOR CYCLIC TRIAXIAL TESTS.
INFLUENCE OF EXTENSION STRESSES

FIGURE II-20

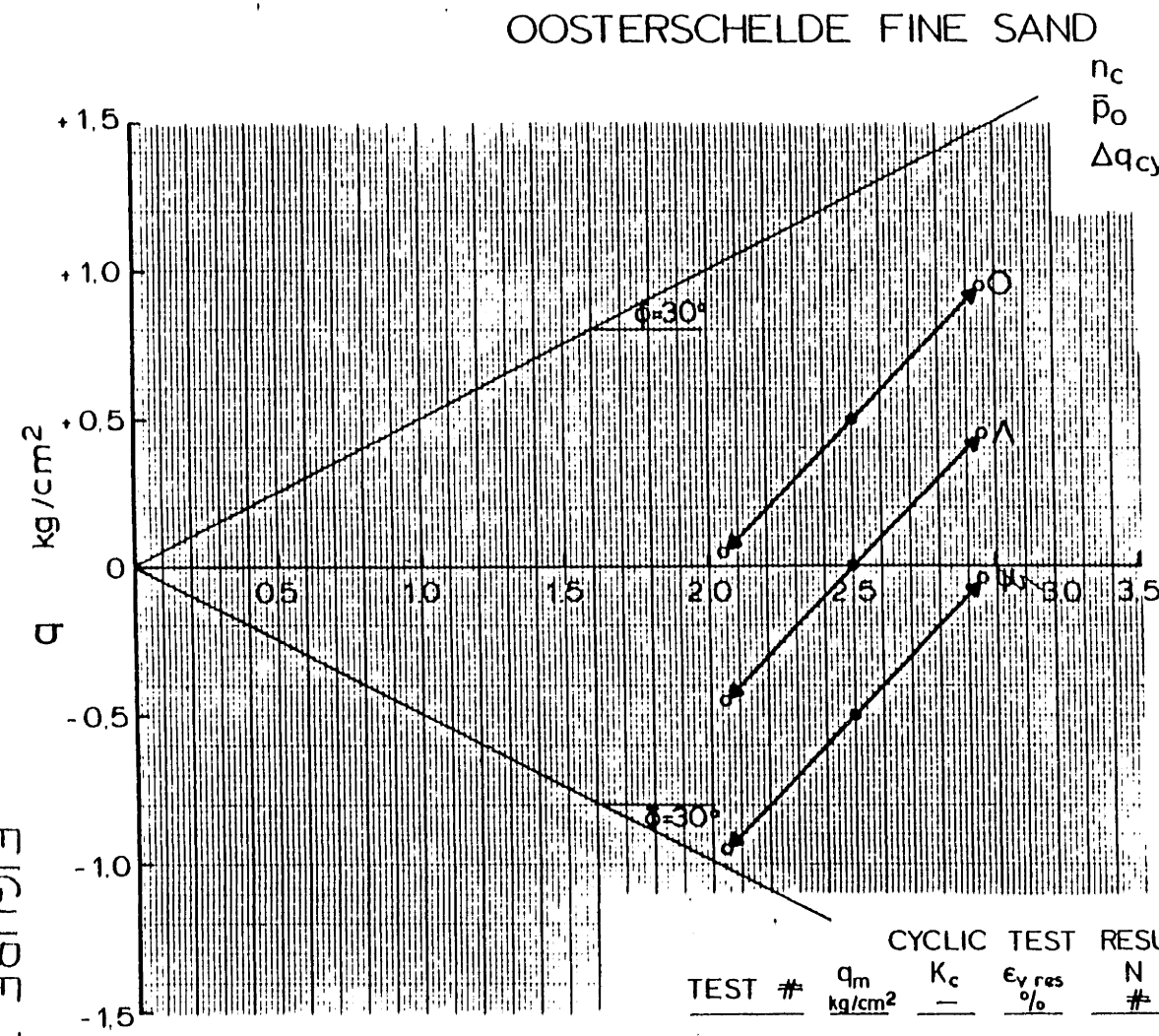

CYCLIC TEST RESULT SUMMARY

TEST #	q_m kg/cm²	K_c —	$\epsilon_{v\,res}$ %	N #	FAILURE MODE	N_{at} 5% ϵ_v	N_{corr} #	n_c %
O LC 135	0.50	0.67	12.80	3000	COMPR.	1855	1855	41.2
Λ LC 144	0	1.00	10.03*	206	DEF.	205	258	41.4
Ψ LC 145	-0.50	1.50	-8.00	20	EXT.	16	14	41.1

*$\epsilon_{v\,pp}$

FIGURE II-21

TOTAL STRESS PATHS (TSP-u_B) FOR CYCLIC TESTS WITH DIFFERENT MEAN SHEAR STRESS, $q_m/\bar{p}_o$

OOSTERSCHELDE FINE SAND

$\bar{p}_o$ = 2.50 kg/cm², n_c~41.2%, Δq_{cy}= 0.45 kg/cm²

CYCLIC ISOTROPIC TEST

q_m = 0 kg/cm²

CYCLIC COMPRESSION TEST

q_m = 0.5 kg/cm²

CYCLIC EXTENSION TEST

q_m = -.5 kg/cm²

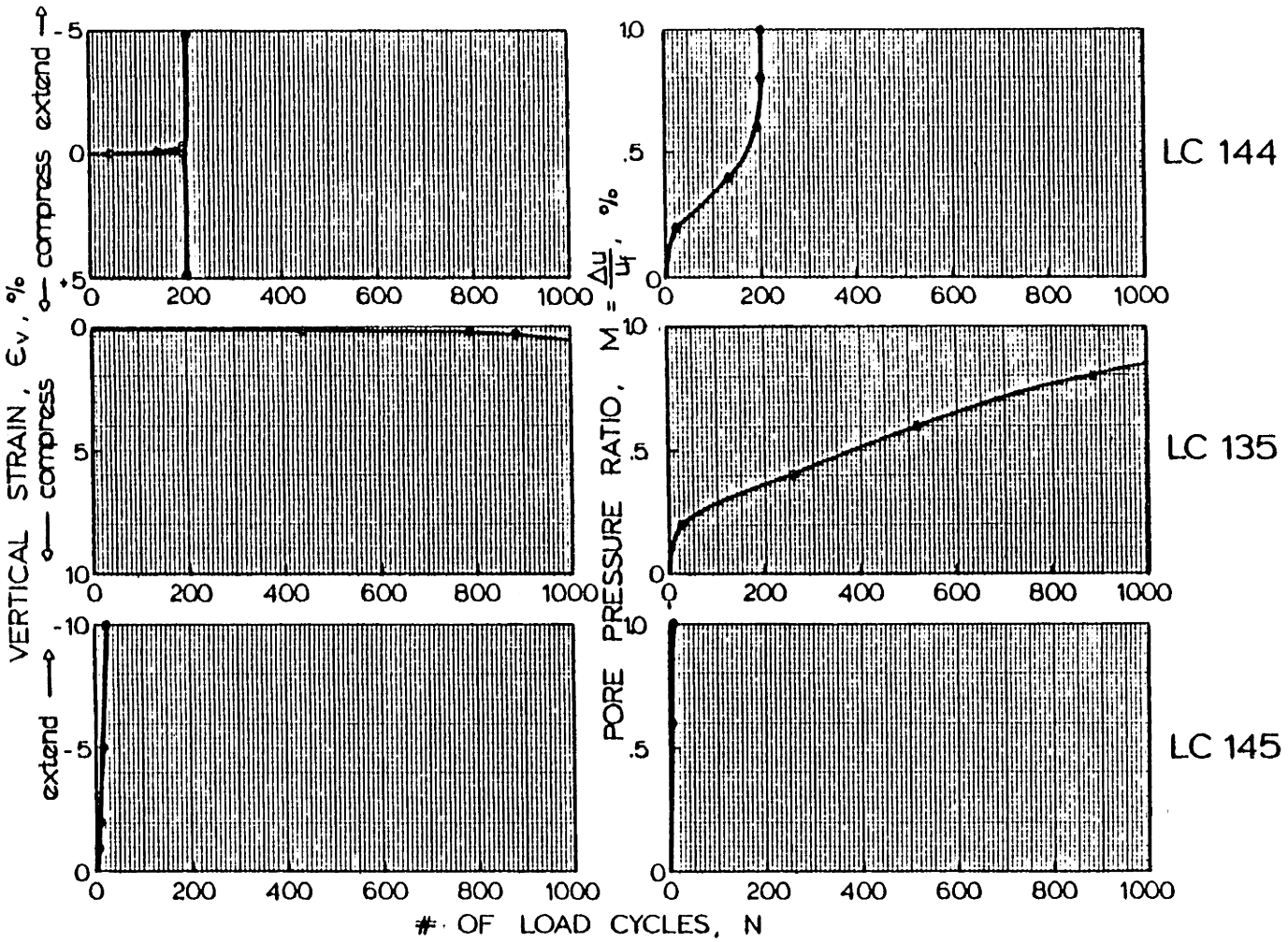

STRAIN AND PORE PRESSURE DEVELOPMENT MEASURED IN ISOTROPIC, COMPRESSION AND EXTENSION CYCLIC TESTS

FIGURE II-22

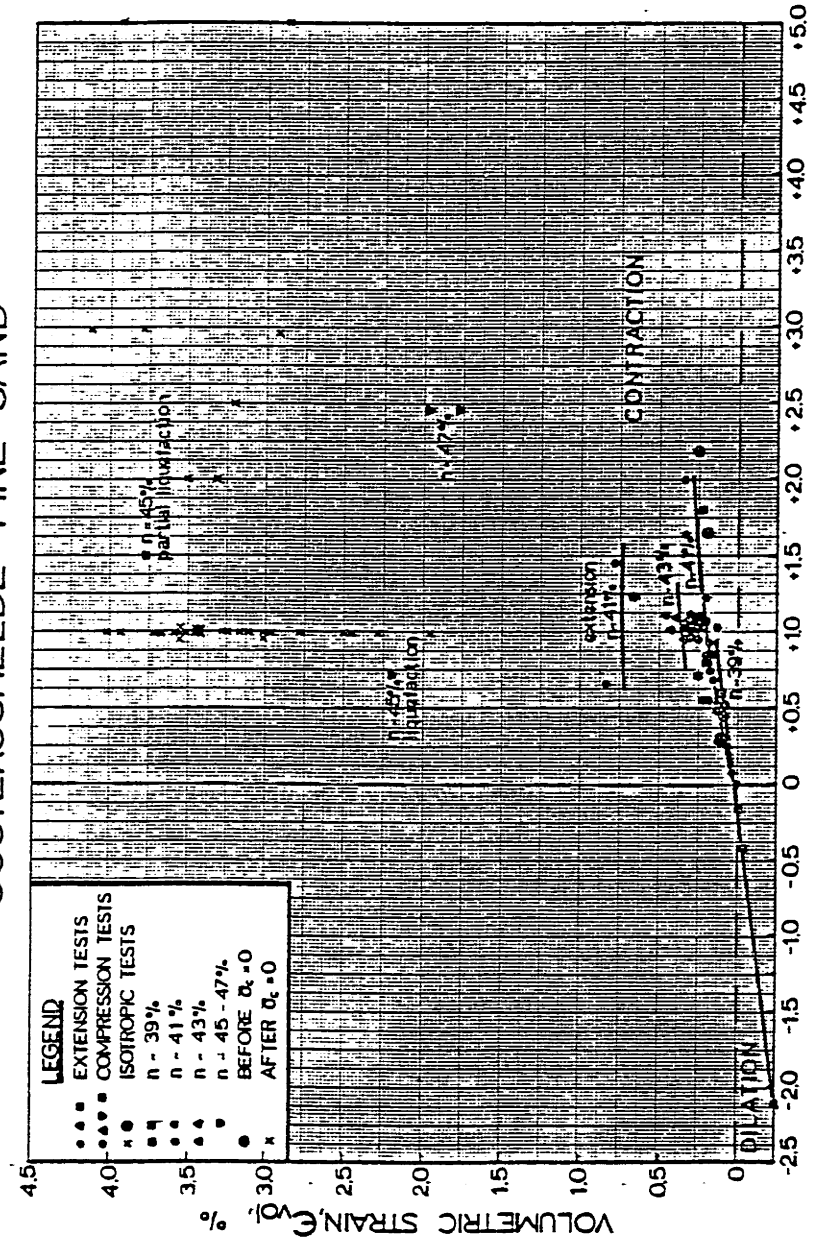

VOLUMETRIC STRAINS MEASURED DURING CONSOLIDATION FOLLOWING CYCLIC TESTING

FIGURE II-23

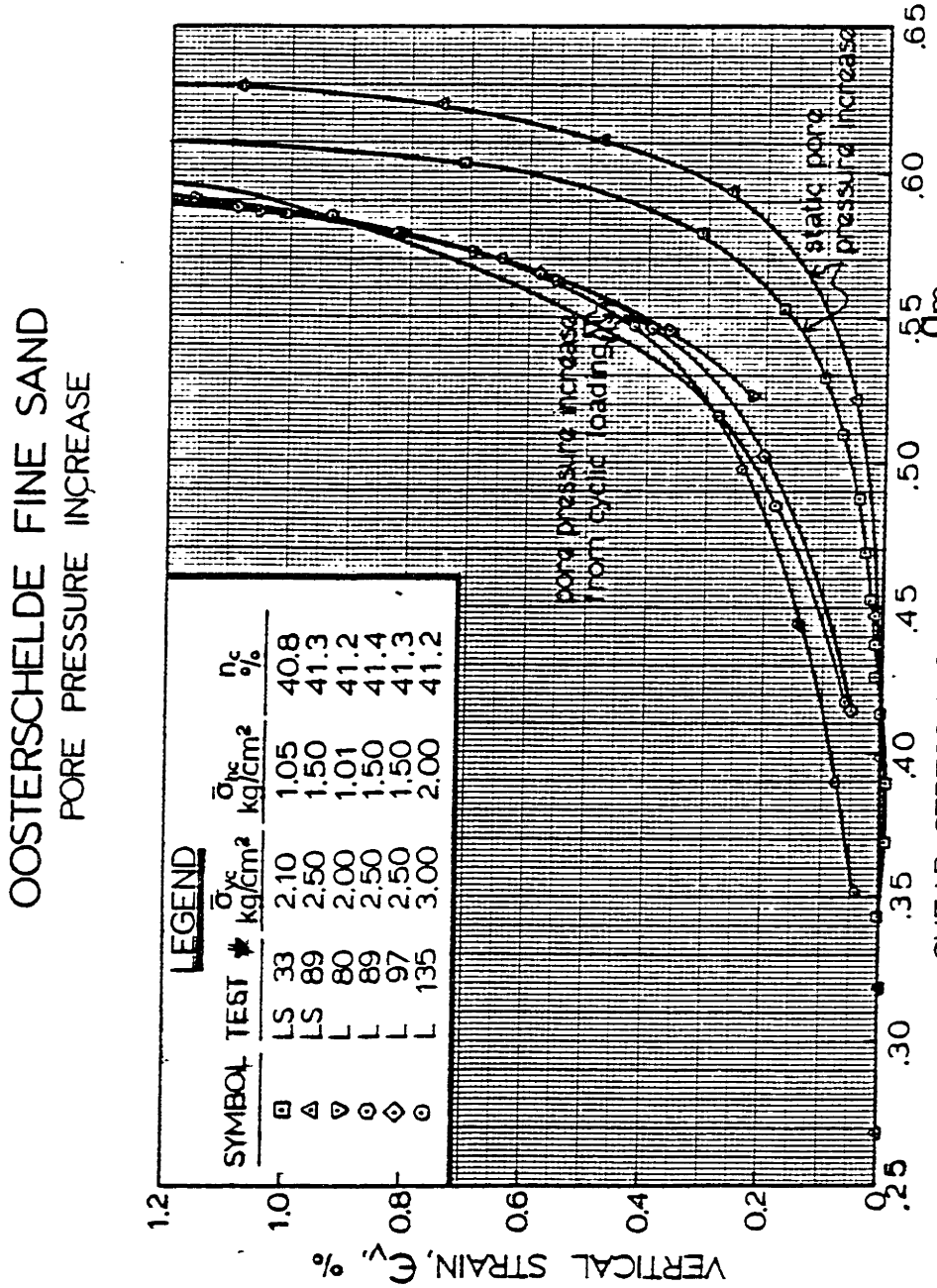

COMPARISON OF GENERATED STRAIN IN CYCLIC TRIAXIAL TESTS AND TESTS WITH STATIC PORE PRESSURE INCREASE AT SAME MEAN SHEAR STRESS LEVEL

FIGURE II-24

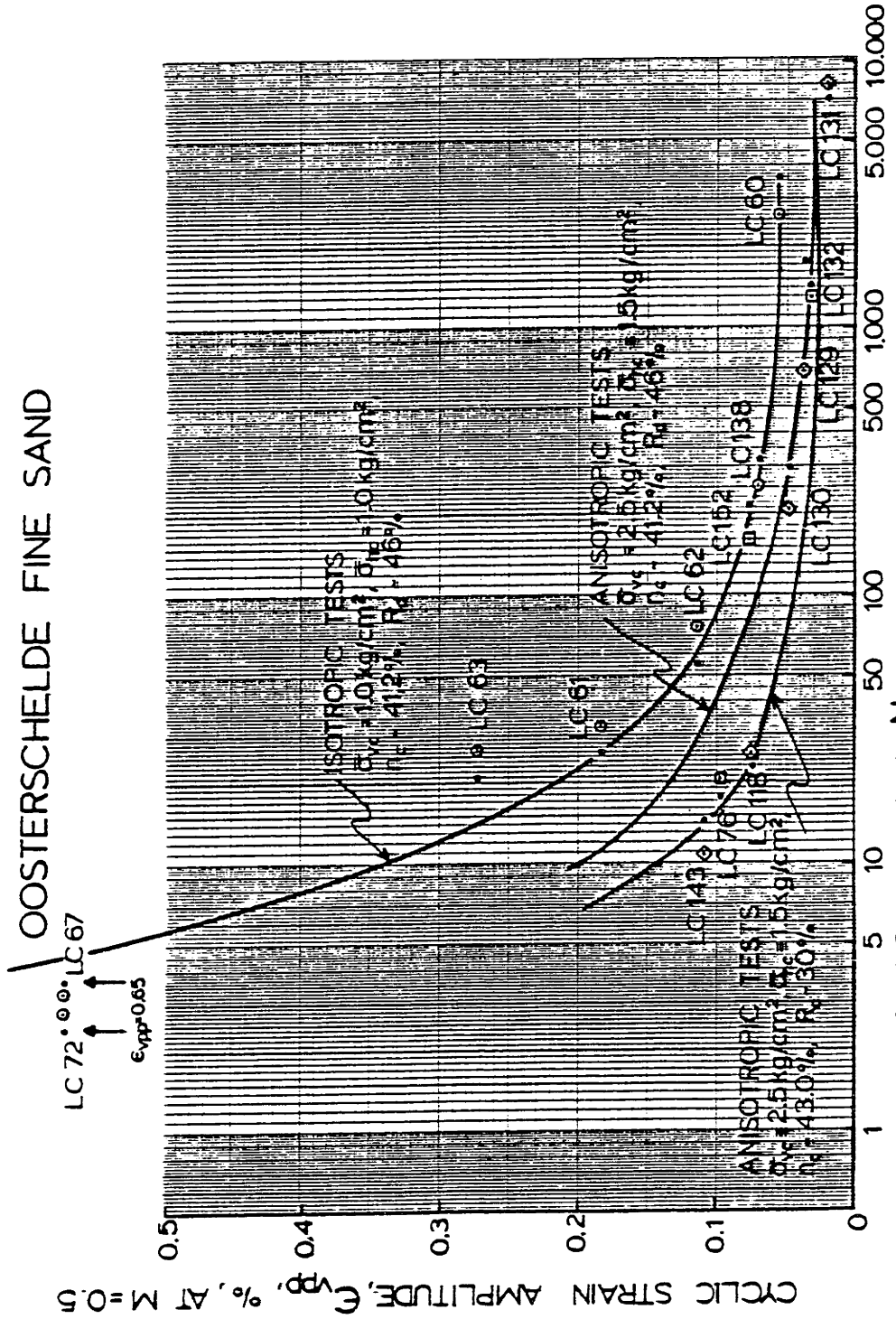

INFLUENCE OF CYCLIC STRAIN AMPLITUDE ON STRAIN DEVELOPMENT IN TESTS WITH VARYING CYCLIC SHEAR STRESS

FIGURE II-25

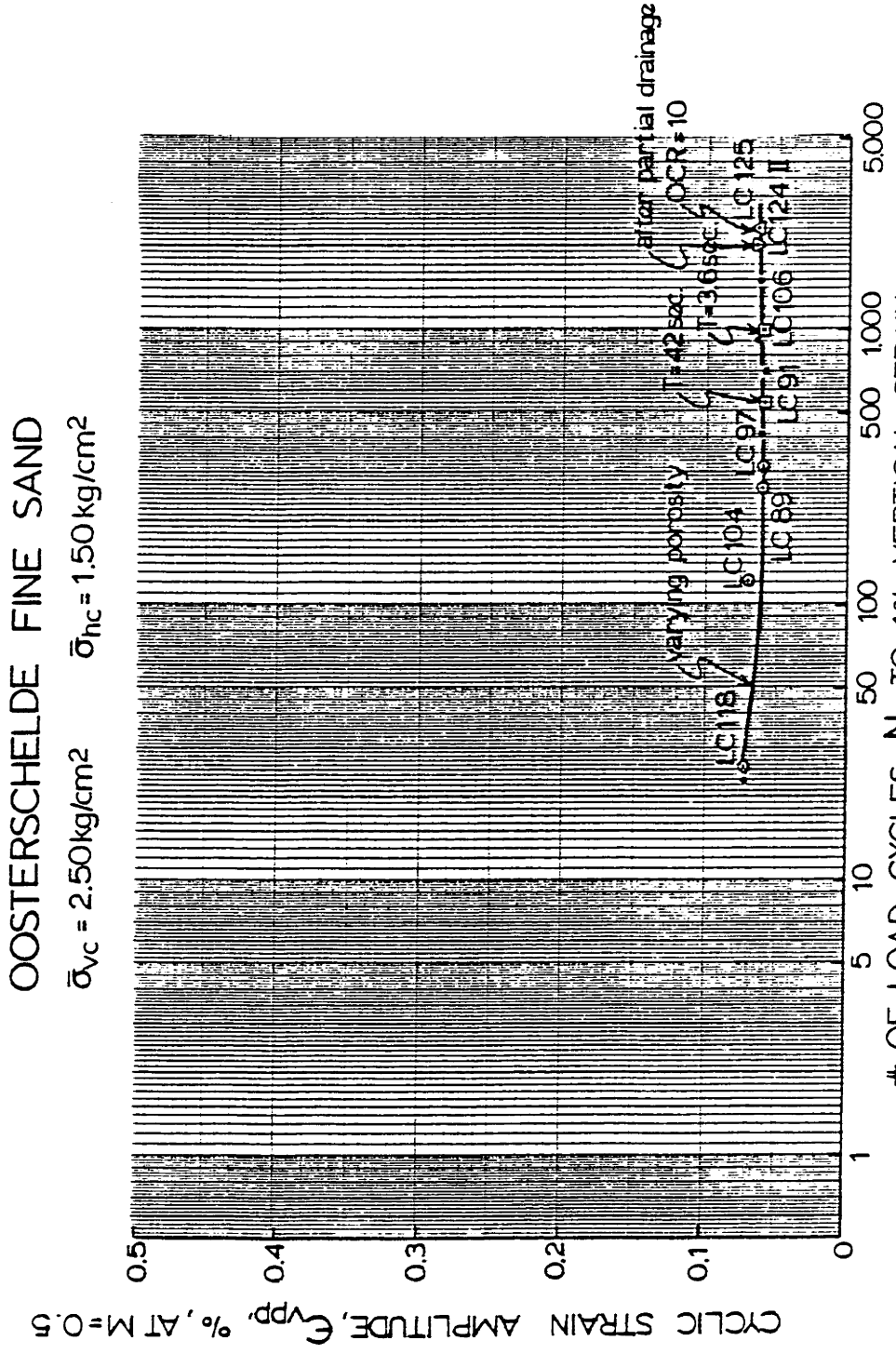

INFLUENCE OF CYCLIC STRAIN AMPLITUDE ON STRAIN DEVELOPMENT IN TESTS WITH VARYING POROSITY, LOAD PERIOD AND STRESS HISTORY

FIGURE II-26

Chapter III

FACTORS INFLUENCING CYCLIC SAND BEHAVIOR

Experimental investigations of cyclic behavior of sand published in the last ten years indicate a large sensitivity of strain and pore pressure development to almost all changes in test or sample condition. Apart from porosity and stress path, factors such as test conditions (cyclic load period, load pulse shape, end restraints, sample size, etc.), sample condition (mean grain size, grain shape, sample preparation procedure) stress-strain history and drainage have profound influences on the rate of strain and pore pressure development in cyclic tests. These influences are discussed below, mainly to determine procedures to test sand which might produce behavior most representative of field behavior. The influence of various parameters are generally reported in the literature in terms of effect on cyclic strength, where cyclic strength is defined as the cyclic shear stress ratio required to produce "failure" in a specified number of cycles.

3.1 Test Conditions

This section examines the effects of end restraints, sample size, height to diameter ratio, membrane penetration, loading frequency and the shape of the load pattern on cyclic behavior in triaxial tests.

The non-uniform stresses produced by rigid end caps has concerned several investigators. Lee (1976a) reports a 25 - 40% increase of the cyclic strength when testing samples (H/D = 2) in a triaxial cell with frictionless ends. Mulilis (1975) found only a slight difference in cyclic strength between frictionless and conventional end caps (H/D = 2). Geotechnical Engineers, Inc. (1975) found no effect of the frictionless caps, both for 1.4 and 2.8 in. samples (H/D = 1.5). Present methods for producing frictionless ends induce additional problems. Rubber strips separated by vacuum grease tend to compress with time leading to an erroneous measure of strain, possible clogging of porous stones and loss of the lubricating effect (Lee (1976a)). Cince typical cyclic tests in this investigation run 4 - 10 hours, with some running as long as 11 days, the lubricated ends would be destroyed. Therefore, it was decided to use conventional end caps.

The possible influence of the end cap restrains on triaxial sample behavior was qualitatively examined by photographing the deformation patterns in cyclic test samples. A square grid was drawn on many sample membranes, and pictures taken initially, at the end of the test and 5 to 6 times in between. Photos and sample measurements are given in Appendix C. Since zero effective stress never was reached in contractive compression tests, contact between membrane and sand

was never lost, thus the membrane deformations reflected the deformations of the sand sample. Due to the curvature of the lucite triaxial cell, only vertical deformations could be measured from the pictures, and vertical strains calculated for each sample section between grid lines. Assuming constant volume of each of the sections between grid lines, radial strains can be calculated from the vertical strains. By comparing these calculated strains with radial measurements of the sample sections at the beginning and the end of the test, it was apparent that the middle of the sample expanded more radially and the ends less than what is required to maintain constant volume throughout the sample (Figure III.1). Thus the ends contracted and the middle of the samples dilated. This is very likely caused by end effects, and indicates a non-uniform stress distribution in the sample.

Appendix C reports several more measurements of sample deformation, suggesting that the void redistribution becomes severe only at vertical strains exceeding 5%. From the literature review in Chapter II, it was found that void redistribution does not occur below 1 to 2% vertical strain (Bjerrum (1973)). It would therefore seem warranted to suggest that conclusions about cyclic sand behavior from this triaxial test investigation should primarily be based on measurements taken before 1% vertical strain is reached in the sample. Results beyond 1% vertical strain should be used with caution.

Lee and Fitton (1968) found little effect of sample size on cyclic behavior. Annaki and Lee (1975) found, however, 2.8 in. and 12 in. diameter samples to have respectively 30 and 40% lower cyclic strength than 1.4 in diameter samples. Geotechnical Engineers, Inc. (1975) found 2.8 in. diameter samples to have 20% lower strength than 1.4 in diameter ones. Effect of sample size may partly result from differences in membrane penetration (Annaki and Lee (1975)). Cyclic tests in the U.S. have usually employed 1.4 in. diameter samples, 2.8 in. high, to use existing equipment and ease sample preparation. All tests in this investigation were performed on 1.4 in. diameter samples.

Little is known about the effect of height to diameter ratio in cyclic triaxial tests. Geotechnical Engineers' (1975) data for values of H/D from 1.5 to 2.3 on 2.8 in. diameter samples with rigid end caps show the same cyclic behavior.

The effects of membrane penetration on pore pressure have concerned some investigators. Judging from Lade and Hernandez (1977), a sand with 0.2 mm average particle diameter allows negligible membrane penetration, and one with 1.2 mm diameter particles shows penetration effects at 5 kg/cm^2 effective confining stress, but negligible effects at 1 kg/cm^2. The fine sand utilized for the cyclic testing herein has an average grain diameter of 0.17 mm; therefore, membrane penetration does not occur for effective confining stresses below

5 kg/cm^2.

Several investigators considered the effect of load frequency on cyclic behavior. Lee and Fitton (1969), Seed and Peacock (1967), Peacock and Seed (1968), Yoshimi and Oh-Oka (1975), Lee and Focht (1975) and Wong et al. (1975) report either none or very slight dependence of the cyclic strength on loading frequency. Silver et al. (1976) show a reduced cyclic strength for frequencies greater than 2 hz. Figure III.2 shows results on Oosterschelde sand for load periods of 3.6, 8 and 42 seconds. The open circles indicate measured values whereas the solid points are values corrected for variations in porosity, since a given porosity after consolidation is difficult to obtain exactly. Relatively small differences in strain accumulation were found. The pore pressure parameter, A, for individual cycles in these tests were virtually identical for all periods, indicating no lag in pore pressure response (Appendix C).

The shape of the loading pattern was found to have a negligible influence on the sample behavior (Lee and Fitton (1969)). Newer data, however, suggest that a square load form leads to strength values about 15% lower than a sinusoidal changing cyclic load (Silver et al. (1976)). The general consensus of the profession seems to suggest avoiding load shapes with rapid changes, such as the square wave.

The reported tests herein employ a triaxial cell with

a fixed top cap, linear piston bearings to reduce friction, 1.4 in. diameter samples, a height to diameter ratio of 2.1, 8 seconds loading period and an almost sinusoidal loading pattern. A standard operating procedure for testing was worked out, aimed at keeping all test conditions as nearly constant and identical as possible in all cyclic tests. Appendix B gives detailed testing procedures.

The repeatability of test results in terms of strain and pore pressure is quite satisfactory. Duplicate tests LC80 and 120, LC89 and 97, LC61 and 63 and LC136 and 147 are plotted and tabulated in Appendix F. The repeatability obtained in these tests is discussed in Appendix C. The number of load cycles to reach a certain level of strain varies from 3% to 17% in the four pairs of duplicate tests.

3.2 Sample Condition

There is insufficient data available at present to relate cyclic behavior to sand characteristics such as angularity, sand minerals, and coefficient of uniformity. Results reported by Marcuson and Townsend (1976), Castro and Poulos (1976) and Schroeder and Schuster (1969) indicate a wide variation in cyclic strengths and strain accumulation for different sands at the same density and under the same stress path. Generally, angular or "soft" grained sands tend to crush; consequently, they are more contractive and build

up pore pressure and strain more rapidly. Coarser sands and gravels where fewer grain contacts have to carry the effective stresses should, therefore, be more sensitive to cyclic loading. Fine Oosterschelde sand with .17 mm mean grain size has about 3000 grains per cm^2. A gravel with 2 mm mean grain size has only an average of 17 grains per cm^2. However, both laboratory and field experience indicate that pore pressures develop slower in gravel than in sand. This could be attributed to membrane penetration effects in the laboratory and high permeability in the field (Wong et al. (1975)).

Lee and Fitton's (1969) results demonstrated a dependence of cyclic behavior on the mean grain size, showing find sand and silt to be less resistent to cyclic loading than sand and gravel. Again membrane penetration might have influenced the results and the conclusions.

Most of the laboratory work to date has been performed on uniform sands often washed and sieved to remove fine and coarse fractions. Wong et al. (1975) report that well-graded soils are weaker than uniform soils at a given relative density. The reason for this can be that relative density is not an appropriate measure to compare behavior of uniform and well-graded sands. The fact that well-graded deposits historically have been less susceptible to liquefaction failures (Kishida (1969)), may be due to the gradation, but can also be the result of a different sedimentation process. Shen et al. (1977)

reports for constant void ratio an increase in cyclic strength with increase in amount of fines.

Investigations of cyclic behavior have usually been performed on reconstituted samples. Ladd (1974b) and (1976b), Mulilis et al. (1975) and Marcuson and Townsend (1976) all showed significantly greater resistance to cyclic loading for samples that were prepared moist rather than dry. Not only presence of water but also compaction procedure greatly influenced the measured cyclic strengths, with differences exceeding 100%. Undisturbed samples have been shown to exceed the strength of samples tamped moist by as much as 50% (Mulilis et al. (1975)). Since the emphasis of this investigation was to determine cyclic sand behavior and effects of stress path rather than trying to obtain in situ behavior, sample preparation effects were not investigated.

The cyclic tests were all performed on reconstituted samples, tamped moist, a procedure which yields sand fabric with high resistance to cyclic loading. Appendix B gives further information about the compaction procedure, the so-called undercompaction technique (Ladd (1974b)). This technique produces uniform samples in the vertical direction, with behavior which is highly reproducible. The deformation characteristics in horizontal and vertical direction are, however, greatly different (Appendix C), suggesting the samples are anisotropic.

3.3 Stress and Strain History

An important fact to bear in mind when quantifying the effect of stress and strain history is the initial condition of the specimen. Dry compacted samples, above found to be less resistant to cyclic loads, are probably more sensitive to stress and strain history than moist compacted samples. This difference in stress history effects has, however, not been investigated, and is purely a hypothesis.

Figure III.3 shows the influence of overconsolidation on strain development. Both for isotropically and anisotropically consolidated samples, the number of cycles to reach a given strain increases with overconsolidation. The value of K_c, the consolidation stress ratio, is the same for over-consolidated and the normally consolidated samples. Lee and Focht (1975) indicate a strength increase of 30% at an over-consolidation ratio of 3. Geotechnical Engineers, Inc. (1976b) report more than 100% increase in strength for an OCR of 15 in tests on undisturbed samples. Ladd et al. (1977) reported major change in sand behavior for an OCR of 1.5.

Another form of overconsolidation results from prior cyclic loading. A sand sample loaded cyclically in the laboratory, under drained or undrained conditions, and followed by consolidation, will show an increase in cyclic strength in a subsequent undrained test (provided no cyclic mobility failure occurred!). This has been reported by Finn et al. (1970), Bjerrum (1973), Seed et al. (1975), Lee and Focht

(1975) and Moussa (1975).

During this investigation, the following observations were made where a sample with overconsolidation is compared to a standard test without overconsolidation. Note that all results are given in terms of number of cycles, which is much more sensitive to sample behavior than is cyclic strength. Appendix F contains plots, tables and further description of the following tests:

(a) 50 drained cycles (LC54), increased the number of cycles to produce 5% peak to peak strain from 59 (Test LC62) to 249.

(b) About 1000 load cycles (before main test), where 10% of the accumulated pore pressures was drained off each 50th cycle, caused the number of cycles to increase by a factor of four in subsequent undrained cyclic loading test (LC128 versus 129, LC124 versus 89/98).

(c) Samples reconsolidated after reaching a pore pressure ratio, M, of 0.4 to 0.65, required 4 to 10 times more cycles to reach a given strain (LC100, 103, 117 and 119).

(d) Figure III.4 presents total stress paths for four cyclic compression tests consolidated at different mean normal stress ($\bar{p}_o$). All samples behaved contractively, such that the effective stress paths

moved towards the left as the pore pressure increased. The four tests were compared when their effective stress paths reached the stress path location (1) in Figure III.4, and proceeded to (2). Thus, the effect of the varying change in effective stress and number of load cycles required to reach the effective stress path location (1) can be estimated. The percent vertical strain per load cycle between the effective stress path locations (1) and (2), is .002 for the test initially consolidated to $\bar{p}_o$ = 3.00 kg/cm^2, and .013 for the test initially consolidated to $\bar{p}_o$ = 1.50 kg/cm^2. Thus, although we compare strains developed over the same change in effective stress, the strains are much different. This indicates the important influence of prior cyclic stress history.

(e) If the magnitude of cyclic shear stress is changed during a laboratory test, the strain and pore pressure response is found to depend on whether the smaller or larger cyclic stresses come first. Two hundred cycles with a cyclic stress ratio of 0.23 were followed by cyclic loading with a stress ratio of 0.18. The number of load cycles increased by a factor of 5 in the second

part of the test (LC121 and 142). Fifteen hundred cycles of the smaller stress ratio of 0.18 were preceeding testing with a cyclic shear stress ratio of 0.23. This led to less than a doubling of the number of cycles in the second part of the test (LC122 and 89/97). This tentatively suggests that the sequence of smaller and larger cyclic stresses during a storm could influence the total amount of generated strain and pore pressure.

Figure III.5 presents the development of strain and pore pressure for a cyclic compression test with "no" stress history (LC97); an identical test except for an overconsolidation ratio of 5 (LC125); one with 900 partially drained cycles (10% of Δu drained off each 50 cycles, LC124); and one with reconsolidation after reaching a pore pressure ratio of 0.69 (LC117).

The upper plot in Figure III.5 gives vertical strain from 0 to 1%, plotted versus the "normalized" number of load cycles, N, divided by N at 1% vertical strain. The lwoer plot gives the pore pressure ratio from 0 to 1, again versus the normalized number of load cycles. The number of load cycles at 1% strain are for the tests: LC94: 320, LC117: 942, LC124: 2030, LC125: 2340. Since the pore pressure ratio is defined equal to 1 at 1% vertical strain, all curves in both plots have to pass through 0,0 and 1,1. Several important

observations can be made from the two plots:

Whether the stress history of the sand sample was an overconsolidation (LC125), or a "precycling" with partial drainage (LC124) or undrained cyclic loading (LC117), both followed by consolidation, the effects on strain and pore pressure development were of the same nature. The rate of pore pressure accumulation per cycle in the "virgin" sample was large in the beginning of the test (M = 0.4 reached at $N/N_{(\varepsilon_v = 1)} = 0.1$), and decreased gradually until M = 1 and thus the K_ε-line was reached. The strains accumulated a little faster at the very beginning of the test than during the following third of the load cycles. At a pore pressure ratio of 0.6 to 0.8, the strain accumulation accelerated again. The three prestressed samples show almost a constant rate of pore pressure increase. The prestressed samples require 3 times more normalized cycles to reach M = 0.5 than the virgin sample, which actually corresponds to about 10 - 30 times as many load cycles when the normalizing effect is accounted for. The strain accumulation of the prestressed samples is extremely slow during the first part of the cyclic test. The initial "jump" in strain disappears, and the samples do not reach 0.1% vertical strain until the pore pressure ratio equals 0.6. Like the virgin sample, the strain accumulation per cycle accelerates between M = 0.6 and 0.8.

Triaxial sand samples that are reconsolidated after cyclic mobility failure ($\bar{\sigma}_c = 0$, large peak to peak strains) show drastic reduction in strength (Finn et al. (1970), Finn (1972)). Tests on cubical triaxial samples by Wolfe et al. (1977) did not show a reduction in strength after cyclic mobility and reconsolidation. The test results herein are similar to those of Finn et al. (Table F.4 in Appendix F). From the sample measurements reported in Appendix C and the large volume changes during consolidation after cyclic mobility failure, it seems likely that this results from redistribution of pore spaces within the sample. In addition, some change in the sand fabric throughout the sample is conceivable, in which case the sample preparation procedure may influence the magnitude of strength change produced by cyclic mobility followed by reconsolidation.

The important effect of prior stress history is further demonstrated by a test (LC58) which was unloaded (drained) from the consolidation stress to zero effective confining stress by increasing the back pressure. As soon as the sample started deforming under zero effective stress, the drainage valve was closed, so dilation led to negative pore pressure and arrest of the deformation. The sample was then reconsolidated to its initial stress condition and loaded cyclically. Strains and pore pressures generated 10 times faster per cycle than in a "virgin" sample.

The possible effects of time of consolidation was not investigated during this work. Seed (1976b) reports a strength increase of 25% for reconstituted samples that had been kept 100 days under consolidation stress before cyclic loading.

From the observations described above, one main conclusion can be drawn: Any type of stress history, precycling or overconsolidation increases the resistance of sand to strain and pore pressure accumulation under cyclic loading. The only exception is when the stress history includes cyclic mobility, which seems to drastically weaken the sand sample by a redistribution of voids. Ladd et al (1977) distinguish between large and small prestraining, dependent on the effects on the soil fabric.

3.4 Drainage

This investigation focuses on cyclic behavior for undrained conditions; however, a few partially drained (LC124 and 128) and drained tests (LC126, 127 and 141) were performed. The drained samples strained substantially slower than undrained ones, and after a few thousand cycles, the rate of strain per cycle had decreased to almost zero. This is demonstrated in Figure III.6, where accumulated vertical strain is plotted versus the number of cycles for two identical cyclic compression tests except for drainage condition. LC118

is an undrained test where the sample contracted, with decreasing effective stress until the K_f-line was reached, and underwent a vertical strain of 10% in 130 cycles at a fairly constant rate per cycle. LC141 is a drained test where the sample contracted (0.6% volumetric strain in 30,000 cycles), but of course remained at the same effective stress. The strain rate decreased with increasing number of cycles, and the sample accumulated 2.2% vertical strain in 30,000 load cycles.

3.5 Summary

Figures III.7 and III.8 summarize the effects of drainage, stress-strain history and sample condition on the recorded number of load cycles to some measured value of vertical strain, using the laboratory results from this investigation. Both figures compare two tests, one performed according to normal testing procedure (Appendix B) and one that has a different stress history, drainage condition or sample condition than the standard test. Figure III.7 shows circles where arrows start and end, above a scale of number of load cycles. The starting point for each arrow signifies the number of cycles a standard test took to reach some level of strain or cyclic mobility. The end point of each arrow gives the number of cycles a similar test with different stress history or drainage condition required to reach the

same strain level or failure condition. Thus the length of the arrow gives some quantitative measure for the influence of the stress history or drainage. The vertical column on the left side of the figure gives a short description of the deviation from the standard test procedure for the arrows.

The same data are redrawn in Figure III.8, above a scale in "order of magnitude", signifying increasing or decreasing effects on the number of load cycles. All points on the vertical line in the middle represents cyclic tests under standard conditions. The arrow length again is a measure of the influence. Arrows pointing to the right signify an increase in sample resistance to cyclic loading, arrows pointing to the left a decrease in resistance. The beneficial effects of drainage and stress history, and the detrimental effect of cyclic mobility and non-uniform samples are clearly demonstrated.

In summary, stress history including the condition of zero effective stress on the sample with large peak to peak strains (cyclic mobility) causes a large decrease in cyclic strength. All other investigated types of stress history strengthen the sample. A non-uniform sample is weaker than a uniform sample with the same average density. Any degree of drainage greatly decreases the rate of strain per cycle.

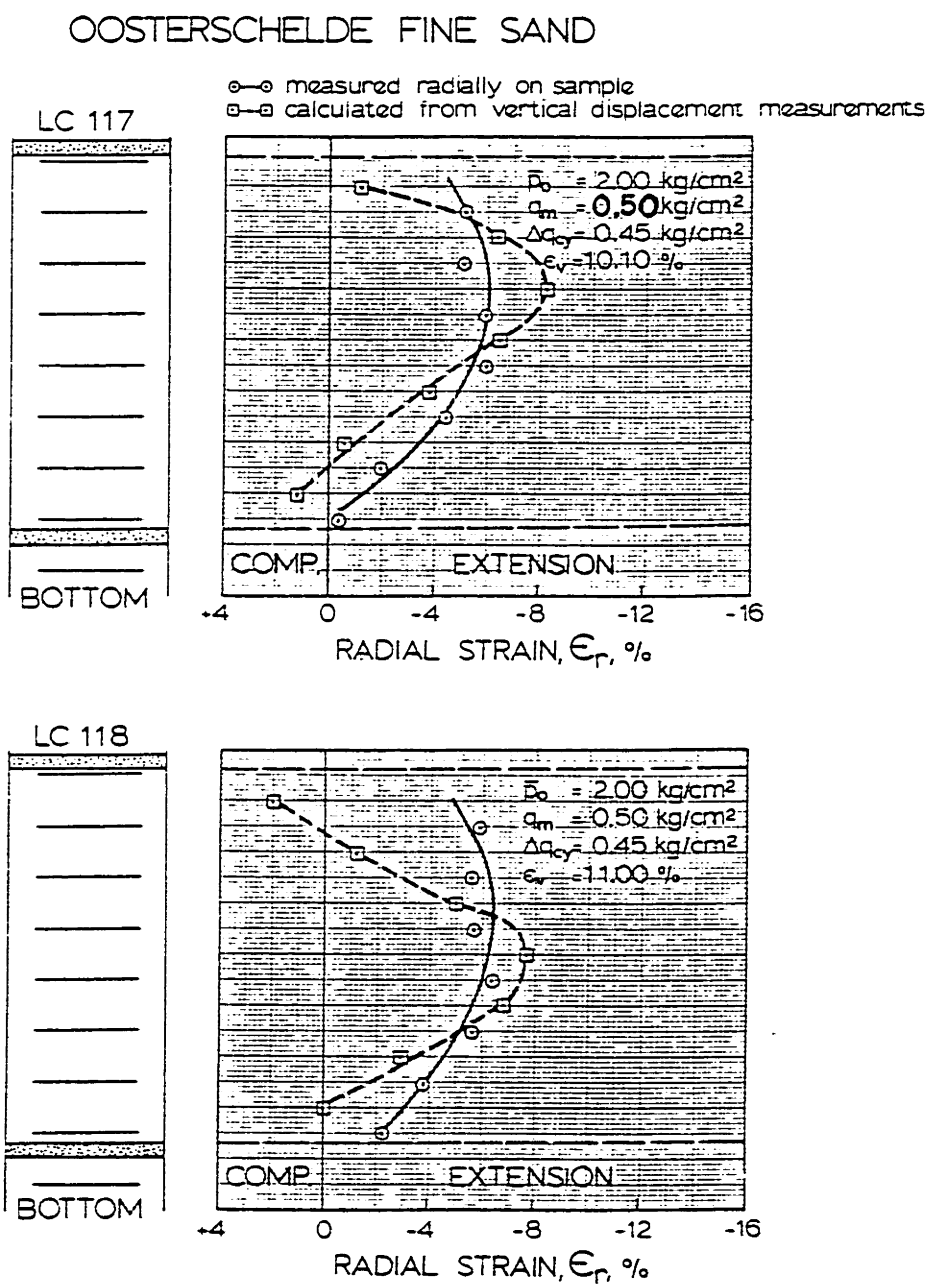

COMPARISON OF MEASURED AND CALCULATED RADIAL STRAINS IN CYCLIC COMPRESSION TESTS

FIGURE III-1

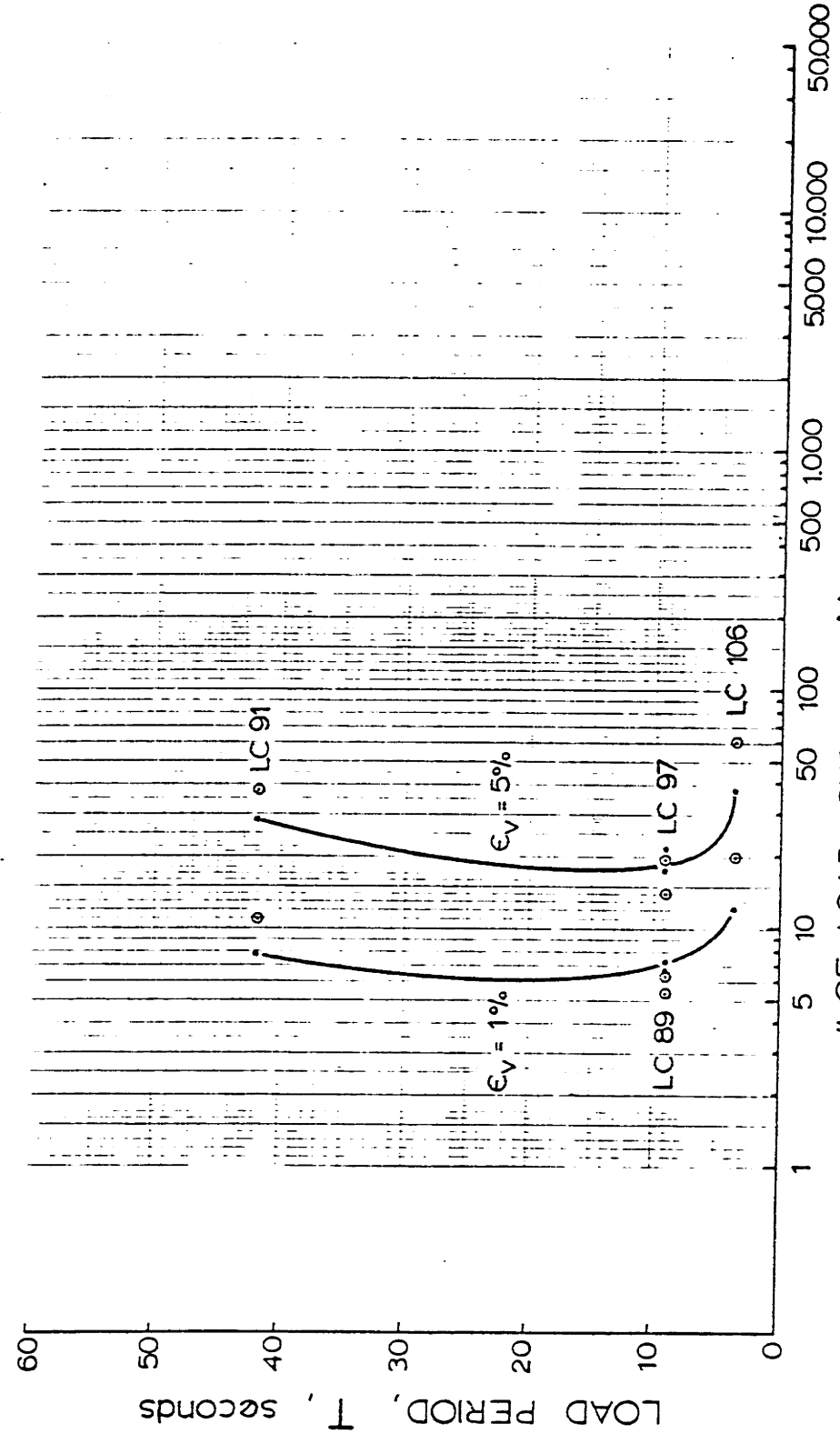

INFLUENCE OF LOAD PERIOD T ON STRAIN DEVELOPMENT IN CYCLIC TRIAXIAL COMPRESSION TESTS

FIGURE III-2

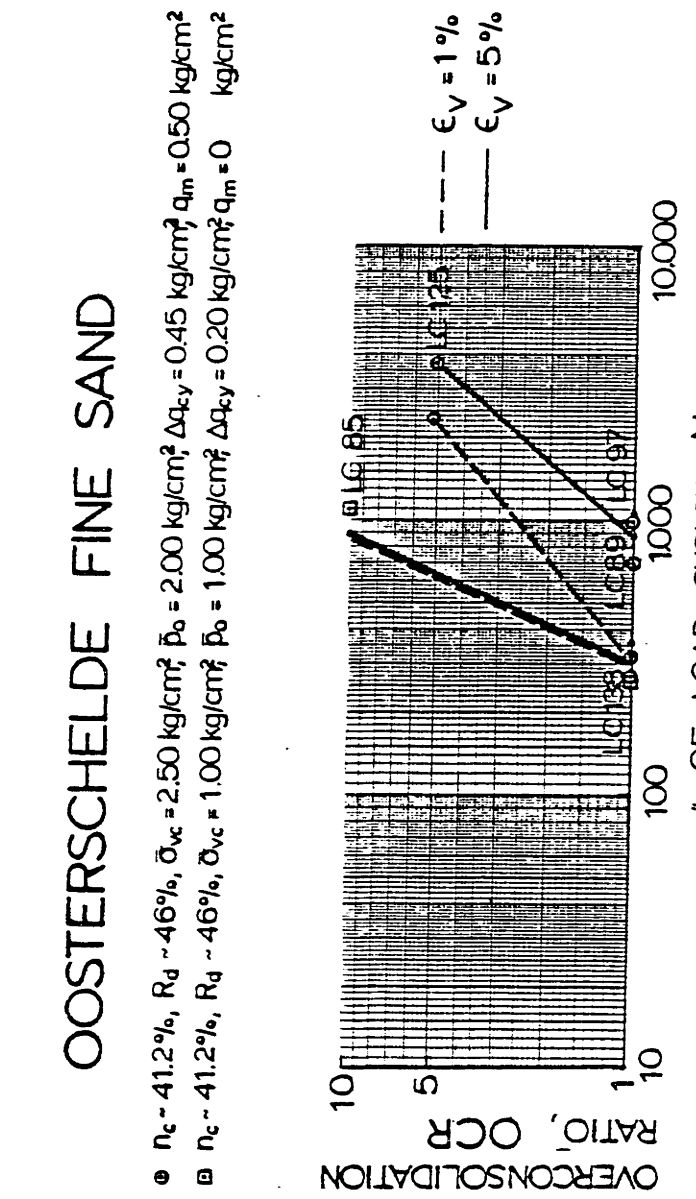

INFLUENCE OF OVERCONSOLIDATION RATIO ON STRAIN DEVELOPMENT IN CYCLIC TRIAXIAL TESTS

FIGURE III-3

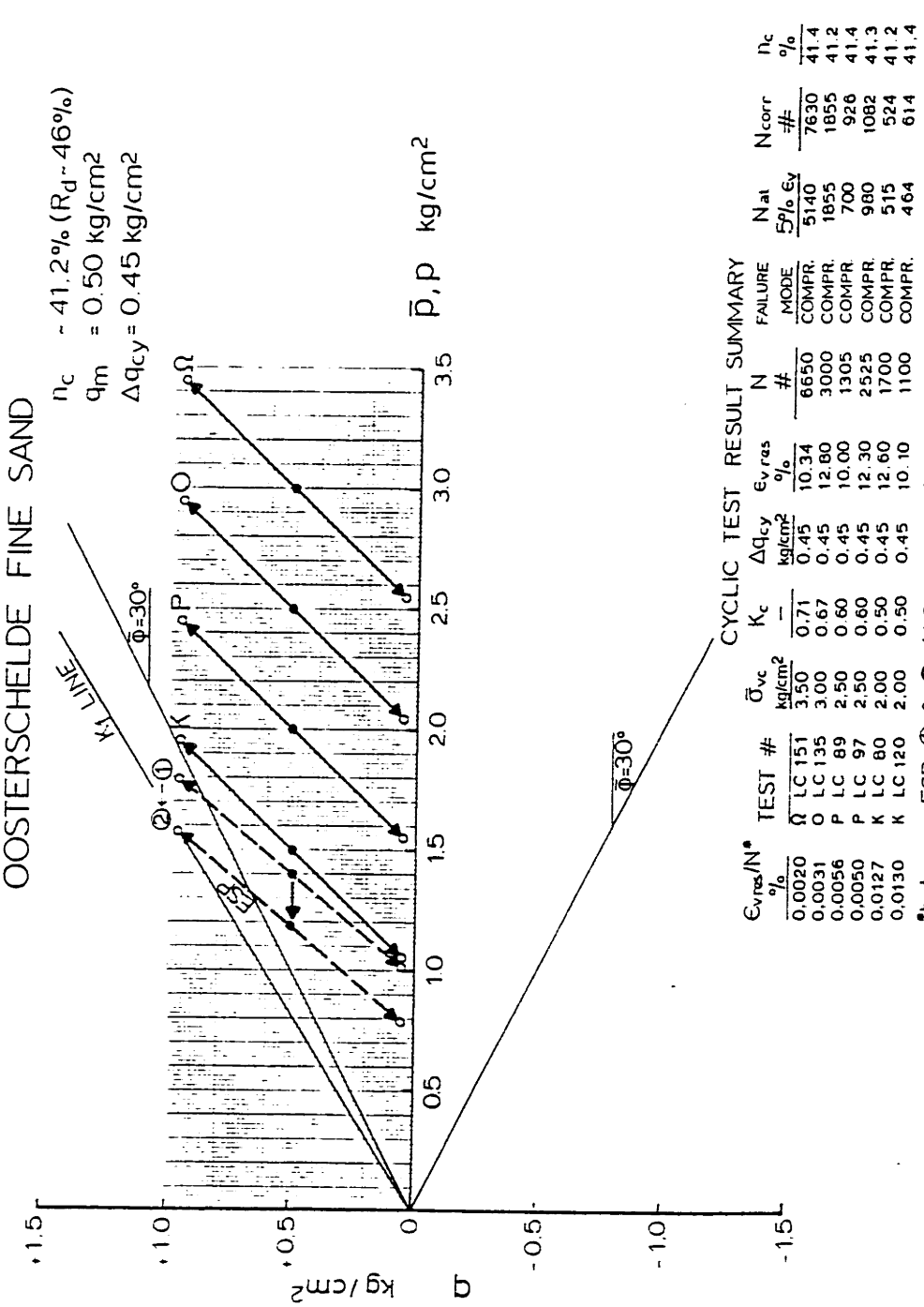

ϵ_{vras}/N^* %	TEST #	$\bar{\sigma}_{vc}$ kg/cm²	K_c –	Δq_{cy} kg/cm²	ϵ_{vras} %	N #	FAILURE MODE	N_{at} 5% ϵ_v	N_{corr} #	n_c %
0.0020	Ω LC 151	3.50	0.71	0.45	10.34	6650	COMPR.	5140	7630	41.4
0.0031	O LC 135	3.00	0.67	0.45	12.80	3000	COMPR.	1855	1855	41.2
0.0056	P LC 89	2.50	0.60	0.45	10.00	1305	COMPR.	700	926	41.4
0.0050	P LC 97	2.50	0.60	0.45	12.30	2525	COMPR.	980	1082	41.3
0.0127	K LC 80	2.00	0.50	0.45	12.60	1700	COMPR.	515	524	41.2
0.0130	K LC 120	2.00	0.50	0.45	10.10	1100	COMPR.	464	614	41.4

*between ESP ① & ② ($\Delta\epsilon_{vras}$=1-1.5%)

FIGURE III-4

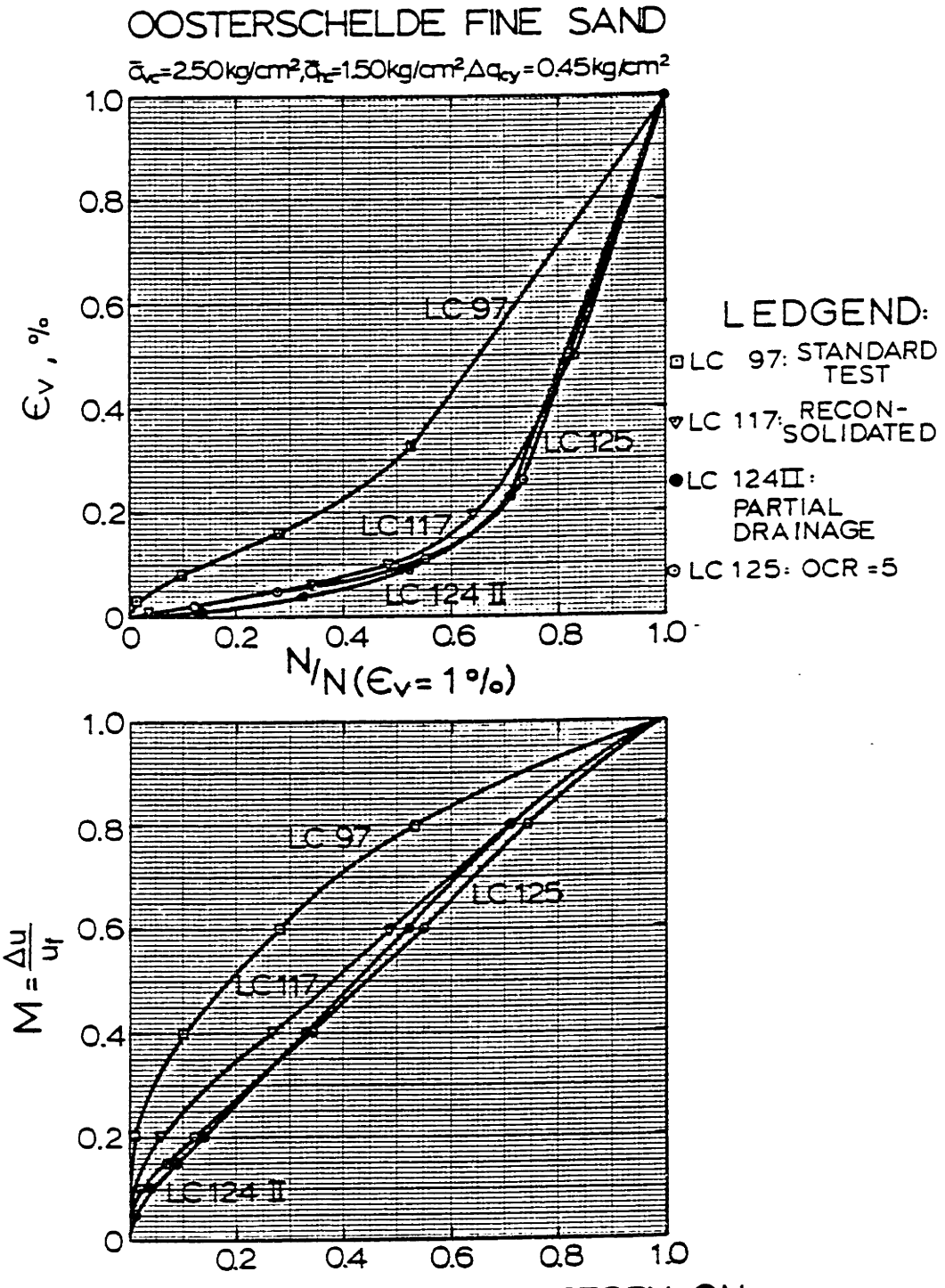

INFLUENCE OF STRESS HISTORY ON STRAIN AND PORE PRESSURE DEVELOPMENT

FIGURE III-5

OOSTERSCHELDE FINE SAND

n_c ~ 43 % $\bar{p}_o$ = 2.00 kg/cm²

Δq_{cy} = 0.45 kg/cm² q_m = 0.50 kg/cm²

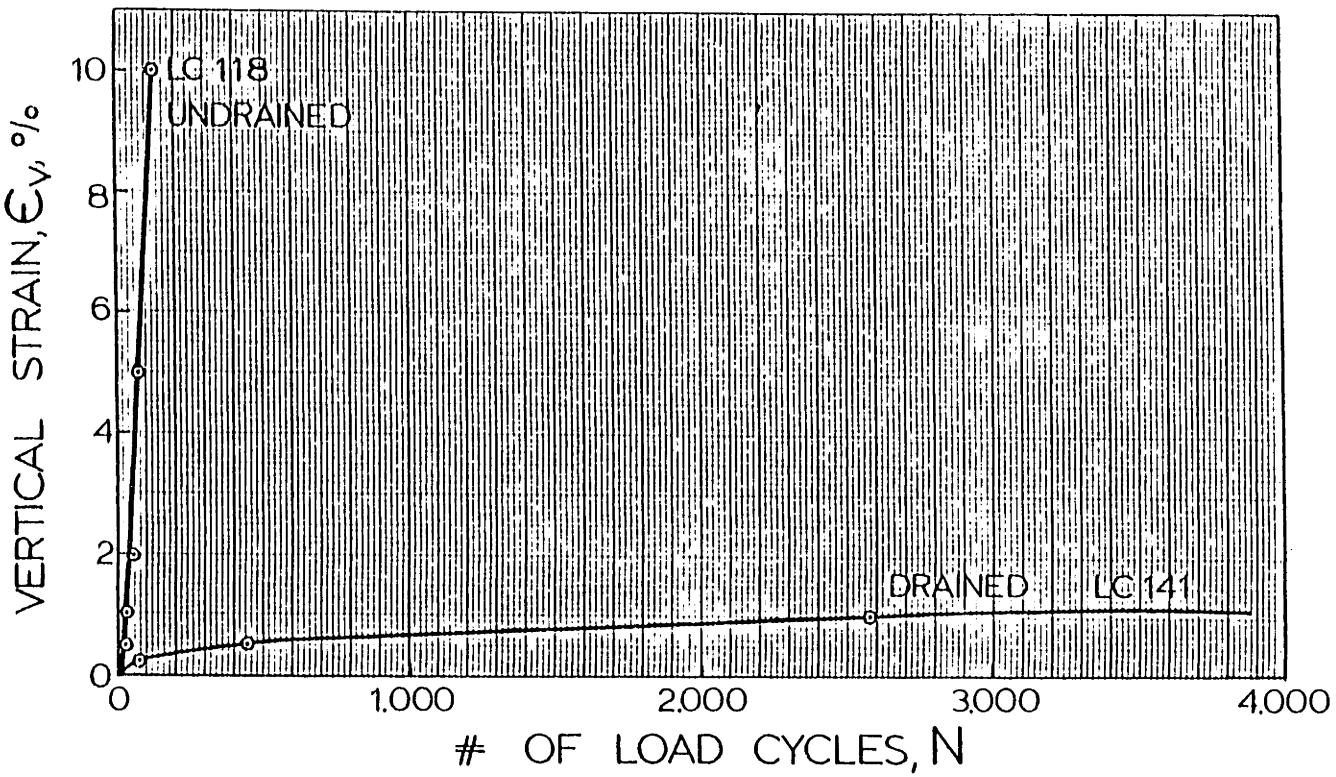

INFLUENCE OF DRAINAGE ON STRAIN DEVELOPMENT IN CYCLIC TRIAXIAL TESTS

FIGURE III-5

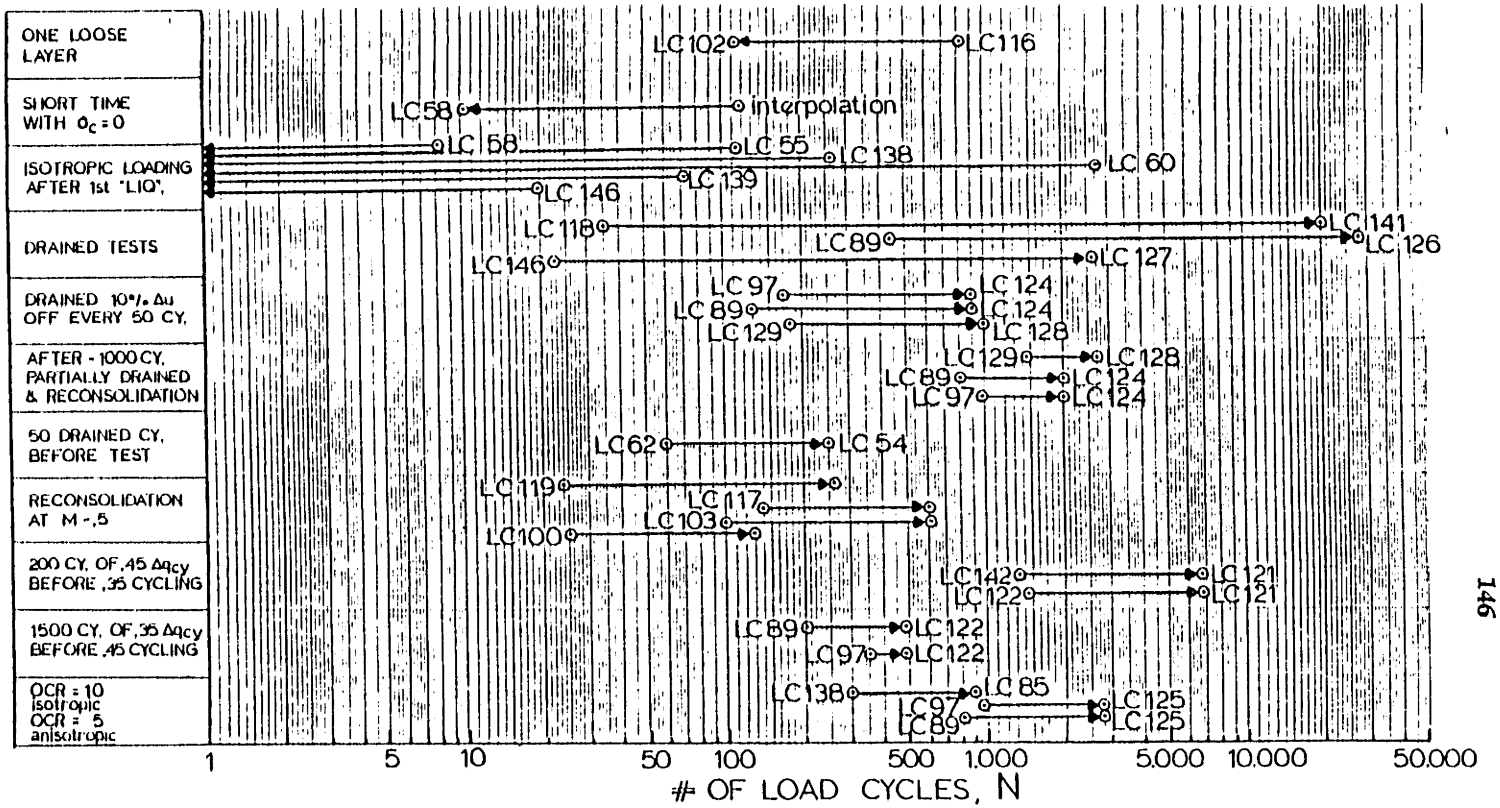

EFFECT OF DRAINAGE, STRESS HISTORY AND SAMPLE CONDITION ON THE NUMBER OF LOAD CYCLES TO REACH SOME STRAIN LEVEL OR FAILURE CONDITION

FIGURE III-7

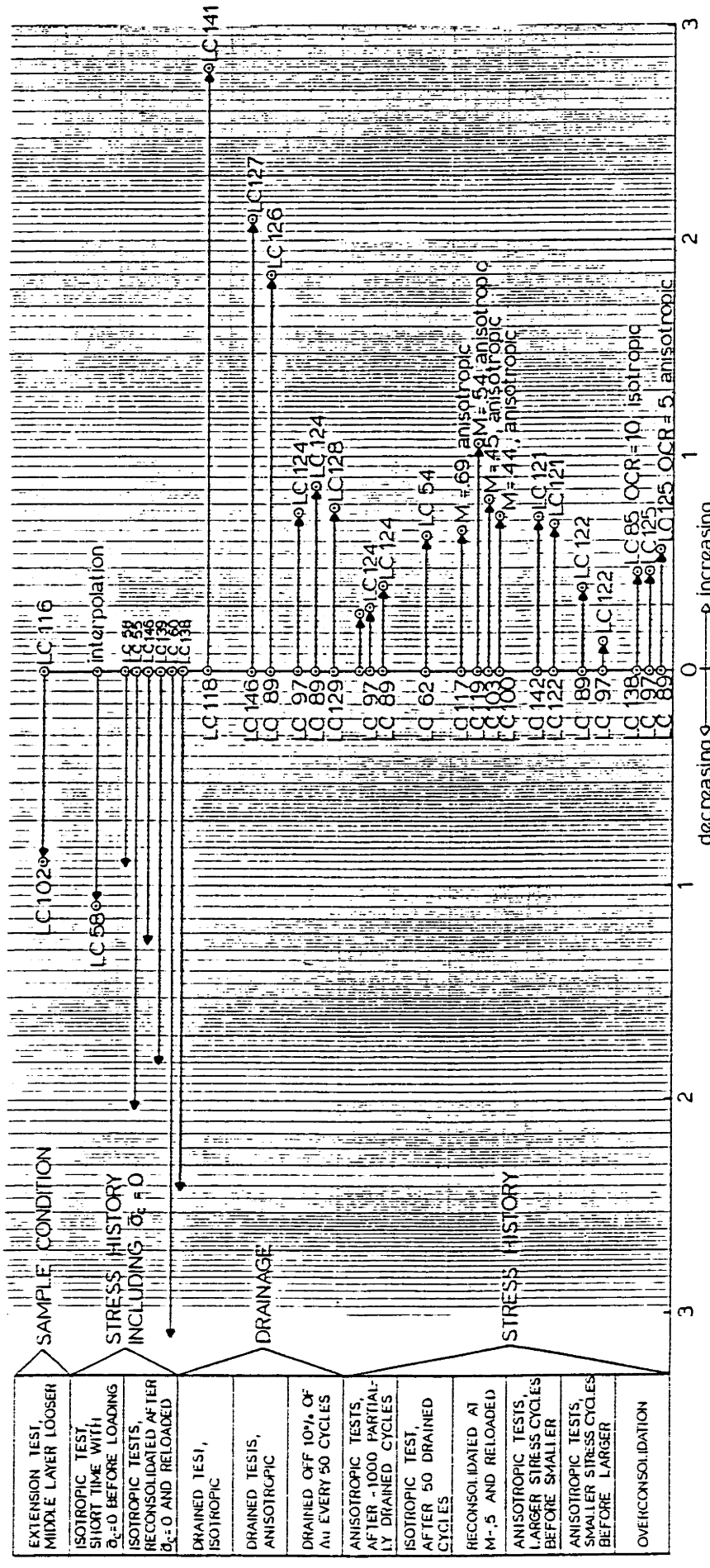

EFFECT OF DRAINAGE, STRESS HISTORY AND SAMPLE CONDITION ON THE NUMBER OF LOAD CYCLES IN ORDERS OF MAGNITUDE

FIGURE III-8

Chapter IV

STRAIN AND PORE PRESSURE DEVELOPMENT IN UNDRAINED CYCLIC TRIAXIAL TESTS

This chapter quantifies the influence of stress path on the development of pore pressure and strain in undrained cyclic tests on samples of varying porosity. The stress path includes consideration of cyclic shear stress, mean consolidation stress and shear stress at consolidation. Emphasis is on cyclic compression tests, since they model the stress system in the upper soil layers below an offshore structure, which have the most important influence on stability and deformations of the structure. The influence of each parameter was determined by performing tests where only that parameter was varied while all other factors and parameters were kept unchanged. Results from cyclic compression and isotropic tests are treated separately due to their different cyclic behavior. For reasons of comparison, static test results from the same sand is reported in Appendix D.

4.1 Soil Porosity

Compactness or denseness of soil can be expressed several different ways. Porosity (n) relates the void volume of the soil to the total soil volume. Relative density (R_d) relates the density to a maximum and a minimum value experimentally found by a prescribed method (Appendix A). Dry unit

weight (γ_d) gives the weight of the soil particles per unit of volume. Void ratio (e) relates the void volume in the soil to the volume of the soil particles. Figure IV.1 shows the range in densities of tested samples during this investigation, along with the four different ways to express the density. Results presented herein are all given in terms of porosity (n).

Cyclic Compression Tests

Figure IV.2 shows the effect of porosity on the number of load cycles required to produce 1% residual strain in a set of cyclic compression tests. This plot is analogous to the common cyclic test summary plots, reporting cyclic shear stress ratio versus log number of cycles. The shear stress ratio has simply been replaced by porosity. All the other parameters investigated below will be displayed versus log number of cycles in this same manner. A legend on each plot indicates the sample conditions in the test series.

Figure IV.3 presents the total stress paths for the tests in Figure IV.2. The stress paths are all identical. The figure also gives test conditions and a summary of the cyclic test results. All total stress paths for the following test series will be presented in this manner.

Figure IV.4 presents vertical strain and pore pressure ratio versus the normalized number of load cycles for the

cyclic test series with differing porosity. All tests develop strain and pore pressure almost identically. This type plot also appears for each following test series.

Figure IV.5 shows five test series in addition to the one given in Figure IV.2, all with different stress paths, but where porosity is the only variable within each series. The test series have been plotted at residual vertical strain levels from .03% to 1.0%, because some of the tests never reached 1% residual vertical strain. All the following test data describing strain and pore pressure development in cyclic triaxial tests will be presented in this form. Figure IV.5 suggests that the variation in the number of load cycles to reach a given level of strain at various sample porosities is log-linear in cyclic compression tests. The parallel lines imply that the effect of porosity on strain accumulation is the same under a variety of stress paths, i.e., the porosity effect is independent and can be separated from all other parameter effects. Since the pore pressure ratio, M, is defined equal to 1.0 at 1.0% vertical strain, the above observations are also valid for pore pressure development.

Figure IV.6 presents contours of equal strain for one test series in a porosity versus log number of cycles diagram. The contours are linear and reasonably parallel, indicating that the influence of porosity on strain development does not change with the strain level in cyclic compression tests.

Figure IV.7 shows contours of generated pore pressure for the same test series in a porosity vs. log number of cycles diagram. Again the contours are reasonably log-linear and parallel, until the soil porosity reaches a value where the sample dilates for the stress path employed for the tests. Strain and pore pressure contours for all the other test series are given in Appendix E. Due to the relative parallel and log-linear shape of both sets of contours, all of them can be expressed by a simple logarithmic function of the form:

$$N = N_{ref} \cdot 10^{\frac{n-n_{ref}}{a}} \qquad \text{Eq. IV.1}$$

where

N = the number of load cycles to reach a given strain or pore pressure level at the porosity n.

N_{ref} = a "reference" number of load cycles to reach the same strain or pore pressure at a "reference" porosity n_{ref}. (This reference porosity is arbitrarily selected.)

n = porosity in %.

n_{ref} = reference porosity in %.

a = average slope of strain contour (a_ε) or average slope of pore pressure contour (a_u).

Rearranging the equation yields the slope of the contours:

$$a = \frac{n-n_{ref}}{\log N/N_{ref}} \qquad \text{Eq. IV.2}$$

Figure IV.8 gives values of a_ε for all available strain contours where porosity is the series variable. Figure IV.9 gives values of a_u for the available pore pressure contours. Average values of a_ε and a_u were selected by weighing the influence of different contours based upon how many tests define the contours. Values of a_ε = -1.5% porosity per log cycle and a_u = -1.75% porosity per log cycle result. Equation IV.1 therefore takes the form:

$$N_\varepsilon = N_{ref} \cdot 10^{\frac{n-n_{ref}}{-1.5}} \qquad \text{Eq. IV.3}$$

and

$$N_u = N_{ref} \cdot 10^{\frac{n-n_{ref}}{-1.75}} \qquad \text{Eq. IV.4}$$

where Equation IV.3 is valid for vertical strain accumulation and Equation IV.4 for residual pore pressure. These two equations allow calculation of strain and pore pressure at any porosity from 39 to 45% from one test, provided the test to be predicted for has the same stress path ($\bar{p}_o$, $\Delta q_{cy}/\bar{p}_o$ and $q_m/\bar{p}_o$). The increase in number of cycles for decreasing

porosity seems logical based on the static tests in Appendix D.

Cyclic Isotropic Tests

Figure IV.10 presents peak to peak strain and pore pressure developed in two cyclic isotropic tests at different densities (note M = 1.0 for $\varepsilon_{vpp} = \pm 1.0\%$). The large difference in behavior of the two test samples is mainly caused by the rapid failure of test LC67 (3 cycles) compared to 62 cycles for LC123. Strain contours of peak to peak strains are given in Figure IV.11 for the two tests. Insufficient data are available to define a log-linear realtion between porosity and number of cycles for isotropic tests.

Data from Lee and Seed (1967a) for cyclic isotropic tests on Sacremento River sand, an angular, uniform fine sand, are added to Figure IV.11 to supplement the available data. Their data plot on approximately straight lines, indicating a log-linear relation between porosity and number of cycles exists for isotropic tests.

Pore pressure contours for LC67 and LC123 are plotted in Figure IV.12.

Although these are the only data available for isotropic tests, the pore pressure contours are assumed to be linear and parallel, and independent of the stress condition. A similar assumption for the strain contours are not made, as

the rate of peak to peak strain development per cycle in isotropic cyclic tests is not log-linear (Chapter II). Figure IV.13 presents a plot of the slope of the residual pore pressure contours, and the following relationship for isotropic tests can be written based on that plot:

$$N_u = N_{ref} \cdot 10^{\frac{n-n_{ref}}{-1.8}} \qquad \text{Eq. IV.5}$$

Thus, residual pore pressures can be calculated for tests at any density from one performed test, provided all have the same stress path. Peak to peak strains cannot be calculated this way. Chapter V will present an alternative prediction method based on strain-pore pressure relations.

4.2 Cyclic Shear Stress

Since several researchers (notably Seed, Lee and co-workers, see Chapter II) found the cyclic shear stress effects on cohesionless soil to vary linearly with confining stress, it became customary to present the effects of cyclic shear stress in a normalized manner, as cyclic shear stress ratio ($\pm \tau/\bar{\sigma}_{co}$). The cyclic shear stress is also normalized as $\Delta q_{cy}/\bar{p}_o$ to simplify the prediction procedure presented in Chapter V. Later a correction to the results for stress level, $\bar{p}_o$, is made to account for the experimental finding that cyclic results do not uniquely normalized as ($\Delta q_{cy}/\bar{p}_o$).

Cyclic Compression Tests

Figure IV.14 presents the total stress paths of five anisotropically consolidated cyclic tests, all with the same consolidation stresses and porosity, but varying cyclic shear stresses. The test with the largest shear stress amplitude undergoes shear stress reversal during unloading. The strain and pore pressure development in the cyclic test series is found to be almost identical for all five tests (Figure IV.15).

Figure IV.16 compares the influence of cyclic stress ratio on the number of load cycles to 1% vertical strain for four different cyclic compression test series. The lines are approximately linear and parallel. Note that each test result is given by two points. The open points indicate the actual measured data in the performed tests. The solid points are corrected number of cycles based on the difference between measured porosity and the porosity the test series was to be performed at (usually n = 41.2%). All following drawings of this type will have both measured and corrected points, since it is very difficult to set up a sample to be at an exact porosity value after consolidation.

Figure IV.17 presents the strain contours for the test series given in Figure IV.14. The strain level is given below each open point. The contours can be approximated as linear and parallel. Figure IV.18 shows contours of pore pressure generation for the same tests, again allowing approximation

by a log-linear relation.

A plot of the strain contour slopes b_ε from the one test series above and additional data from Appendix E, is given in Figure IV.19. The weighted average of b_ε is -.057. The average of the pore pressure contour slopes given in Figure IV.20 is b_u = -.062. Thus, the following expression results for predicting the effects of cyclic stress ratio on strain development:

$$N_\varepsilon = N_{ref} \cdot 10^{\frac{(\frac{\Delta q_{cy}}{\bar{p}_o}) - (\frac{\Delta q_{cy}}{\bar{p}_o})_{ref}}{-0.57}} \qquad \text{Eq. IV.6}$$

and for residual pore pressure

$$N_u = N_{ref} \cdot 10^{\frac{(\frac{\Delta q_{cy}}{\bar{p}_o}) - (\frac{\Delta q_{cy}}{\bar{p}_o})_{ref}}{-.062}} \qquad \text{Eq. IV.7}$$

where $\frac{\Delta q_{cy}}{\bar{p}_o}$ = cyclic shear stress ratio.

Strain and pore pressure can be calculated from these equations for all cyclic stress ratios between 0.075 and 0.275, based on one test with the same porosity, mean normal stress and mean shear stress.

Cyclic Isotropic Tests

Figure IV.21 gives the total stress paths for tests

in an isotropic cyclic test series with different cyclic shear stresses. Vertical strain (peak to peak) and accumulated pore pressure are presented in Figure IV.22 for the above tests. All tests except LC67 and LC72 show similar behavior. The two exceptions fail in a few cycles so that a general pattern of pore pressure and strain development is not established.

Figure IV.23 shows the influence of cyclic stress ratio on the number of load cycles to reach $\pm$ 1% peak to peak strain in two cyclic isotropic test series. Additional data from Lee and Seed (1967a) are also given on the figure. The lines are reasonably parallel, but not log-linear. Figure IV.24 presents strain contours for one of the series, and Figure IV.25 pore pressure contours. Again a log-linear relation between cyclic stress ratio and number of cycles does not apply. The effects of cyclic stress ratio on residual strain and pore pressure can therefore not be calculated by a simple formula based on one cyclic test. Instead, values will have to be obtained from plots like those of Figures IV.24 and IV.25.

4.3 Mean Consolidation Stress

Reported research conclusions are divided on the issue of whether or not strain and pore pressure behavior is linearly dependent on consolidation stress. Figure IV.26 presents a plot of vertical strain versus number of load cycles for

compression tests performed during this investigation. The tests had a constant mean and cyclic shear stress ratio, but varying mean consolidation stress ($\bar{p}_o$). The rate of strain per cycle clearly increases with increasing mean consolidation stress. Based on static test results in Appendix D, Rowe (1962) and Ladd et al. (1977), this effect of stress level is consistent with static behavior as the increasing normal stress causes a decrease in dilatancy. The influence of mean normal stress on strain and pore pressure accumulation will be determined for constant mean and cyclic shear stress ratio to simplify the prediction procedure.

Cyclic Compression Tests

Figure IV.27 presents total stress paths for 4 cyclic compression tests with the same porosity and shear stress ratios, but different mean consolidation stresses. Strain and pore pressure development in the samples are similar in all tests (Figure IV.28). The number of load cycles to reach 1% vertical strain is given in Figure IV.29 for two test series with varying mean normal stress. The curves are reasonably log-linear, but not parallel. Figure IV.30 shows strain contours for one of the series. The contours are reasonably log-linear, but change inclination somewhat, to become flatter at smaller strain levels. The pore pressure contours are both log-linear and parallel (Figure IV.31).

Contour slopes are plotted in Figure IV.32 (strains) and Figure IV.33 (pore pressures). The strain contour slopes vary with strain level, but an average value has been chosen to simplify the prediction procedure outlined in the next chapter. The logarithmic function relating various mean normal stresses will therefore be for accumulated strains:

$$N_\varepsilon = N_{ref} \cdot 10^{\frac{\bar{p}_o - \bar{p}_{o\,ref}}{-1.8}} \qquad \text{Eq. IV.8}$$

and for accumulated pore pressures:

$$N_u = N_{ref} \cdot 10^{\frac{\bar{p}_o - \bar{p}_{o\,ref}}{-2.0}} \qquad \text{Eq. IV.9}$$

Thus, again strain and pore pressure development can be calculated from one experimental test, as long as the mean consolidation stress is the only varied parameter, and the tests have the same porosity, cyclic stress ratio and mean stress ratio. These values will, however, be approximate, as the slopes were not quite parallel.

Cyclic Isotropic Tests

Figure IV.34 presents five total stress paths of cyclic isotropic tests at varying mean consolidation stress and

constant cyclic shear stress ratio. (One of the tests plots outside the figure.) The strain and pore pressure development for the five tests, presented in Figure IV.35, is similar for all tests, unlike Figure IV.22, because sufficient cycles were required to reach failure in all tests so the general pattern of pore pressure and strain could develop.

Figure IV.36 gives the number of load cycles to reach $\pm$ 1% peak to peak strain in two cyclic isotropic test series with varying mean consolidation stress. Below a stress of 3 kg/cm^2 the curves are parallel and linear. Test LC146 indicates no further variation in strain development above 3 kg/cm^2. Figure IV.37 gives strain contours for one of the isotropic test series. The curves are neither linear nor parallel. The pore pressure contours in Figure IV.38 are approximately linear and parallel below a mean normal stress of 3 kg/cm^2.

A plot of the slopes of the pore pressure contours for all test series is given in Figure IV.39 and yield the logarithmic function

$$N_u = N_{ref} \cdot 10^{\frac{\bar{p}_o - \bar{p}_{o\,ref}}{-1.9}} \quad (\text{for } \bar{p}_o < 3 \text{ kg/cm}^2)$$

Eq. IV.10

for pore pressure generation. Thus pore pressures in tests consolidated below 3 kg/cm^2 can be calculated from one performed

test, provided porosity and cyclic shear stress ratio are the same.

4.4 Mean Shear Stress

Mean shear stress normalized by mean consolidation stress ($q_m/\bar{p}_o$) is termed mean shear stress ratio and is equivalent to the consolidation stress ratio, K_c. Mean shear stress ratio is a convenient measure to relate shear stress dependent behavior of soil.

The influence of mean shear stress ratio on behavior in cyclic triaxial tests is complicated to express, both due to the behavioral differences between isotropic and anisotropic cyclic tests, and the influence of the K_f-line. Figure IV.40 presents a comparison of strain accumulation in two identical cyclic tests (on contractive sand) except for the mean shear stress ratio. Note that the sample consolidated at the higher mean shear stress ratio strains faster in the beginning of the test. The test starting at a high mean shear stress ratio is close to the K_f-line (see Figure IV.41, total stress path R). Consequently, only a small pore pressure can develop before the sample dilates at the K_f-line, therefore, the effective stress cannot decrease much. The test at smaller mean shear stress starts further from the K_f-line and undergoes a larger decrease in effective stress (Figure IV.41, total stress path D). Once at the K_f-line, the sample with the smaller shear stress ratio has a smaller effective confining

stress, and thus a greater effective cyclic shear stress ratio (0.32 versus 0.18). Therefore, its strain rate accelerates and consequently the test with the smaller initial mean shear stress ends up straining faster.

Figure IV.41 presents total stress paths from one test series with varying mean shear stress ratio. From the plots of strain (ε_{vres} or $\pm \varepsilon_{vpp}$) and pore pressure development in Figure IV.42, it is apparent that tests at varying shear stress ratios behave completely different with respect to strain and pore pressure development. Figure IV.42 presents the influence of mean shear stress ratio on the number of cycles required to reach 1% accumulated vertical strain or $\pm$ 1% peak to peak strain in two test series. The curves are neither parallel nor linear, however, they suggest a smooth transition in behavior between cyclic compression, isotropic and extension tests. This is, however, very dependent on strain level. Figure IV.43 gives strain contours for a test series with varying mean shear stress ratio. The lines are far from being linear and parallel. The same can be said about the pore pressure contours in Figure IV.44. Prediction of the effects of mean shear stress ratio will, therefore, require use of plots rather than the simple log-linear equation used for other parameters. Tests at negative shear stress ratios (cyclic extension tests) strain much faster than isotropic tests ($q_m = 0$) or compression tests ($q_m > 0$). This

was noted already in Chapter II. From Figure IV.42 it is also evident that the compression test at the higher shear stress ratio strains faster in the beginning and slower at the end of the test than the test with lower shear stress ratio, as found in Figure IV.40.

4.5 Summary of Strain and Pore Pressure Development

Both strain contours and pore pressure contours in cyclic compression tests were found to be approximately linear and parallel when plotted on a logarithmic scale of number of load cycles versus porosity (n), cyclic shear stress ratio $(\frac{\Delta q_{cy}}{\bar{p}_o})$, and mean consolidation stress $(\bar{p}_o)$ to a linear scale. The significance of this is that all the parallel and log-linear contours can be expressed by one simple logarithmic function for each variable. Furthermore, our test data show that the effects of porosity, cyclic shear stress ratio and consolidation stress on strain and pore pressure development are independent, i.e., if the effect of porosity on residual strain for one cyclic shear stress ratio is known, the effects on another value of cyclic shear stress ratio is also known. Contours of strain and pore pressure for variations in mean shear stress ratio are neither parallel nor log-linear; consequently, prediction of its effects will require a more complicated form than the simple log-linear relation.

In cyclic isotropic tests, only pore pressure contours

under varying porosity and mean consolidation stress below 3 kg/cm^2 were found to be approximately log-linear and parallel. Thus, the contours could be expressed by the same type of simple log-linear functions as above. The pore pressure contours for cyclic shear stress were not linear and parallel; neither were all the strain contours. Procedures to predict these nonlinearities are described in Chapter V.

In order to investigate if the qualitative effects of cyclic shear stress ratio and mean shear stress were the same in a totally different test type, cyclic oedometer tests were performed (detailed results in Appendix G). Figure IV.46 summarizes the results in terms of vertical strain versus log number of cycles. The curves vary widely in average accumulated strain per log cycle (given in legend), although all started with the same initial porosity. The numbers on the curves give the ratio of cyclic to mean vertical stress ($\Delta\bar{\sigma}_v/\bar{\sigma}_{vm}$), which is analog to cyclic shear stress ratio in triaxial tests. The strain rate increases with increasing shear stress ratio. D'Appolonia (1970) presented similar data. The break in the lines for $\Delta\bar{\sigma}_v/\bar{\sigma}_{vm}$ = 0.17, 0.33 and 0.71, is caused by a decrease in vertical stress such that the shear stress ratio increases to 0.98. Tests LC-4-0 and 6-0 both have a shear stress ratio of 0.98, but a vertical stress of 1.24 and 0.62 kg/cm^2, respectively. LC-4-0 with the higher effective stress also has a higher strain rate. Both

the effect of cyclic shear stress ratio and of effective stress level is the same as found in triaxial tests.

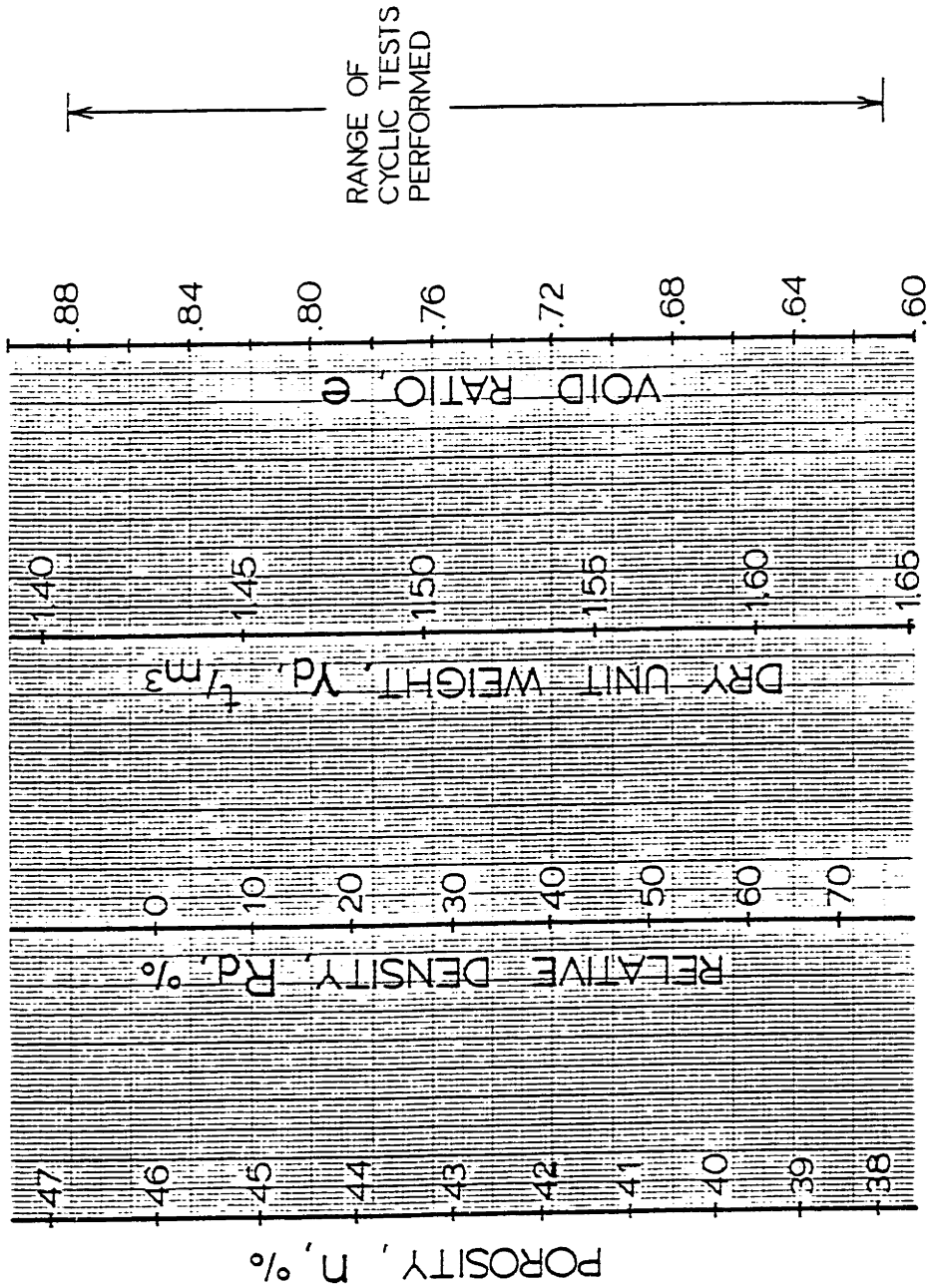

COMPARISON OF DIFFERENT MEASURES FOR SOIL DENSITY OF OOSTERSCHELDE FINE SAND

FIGURE IV-1

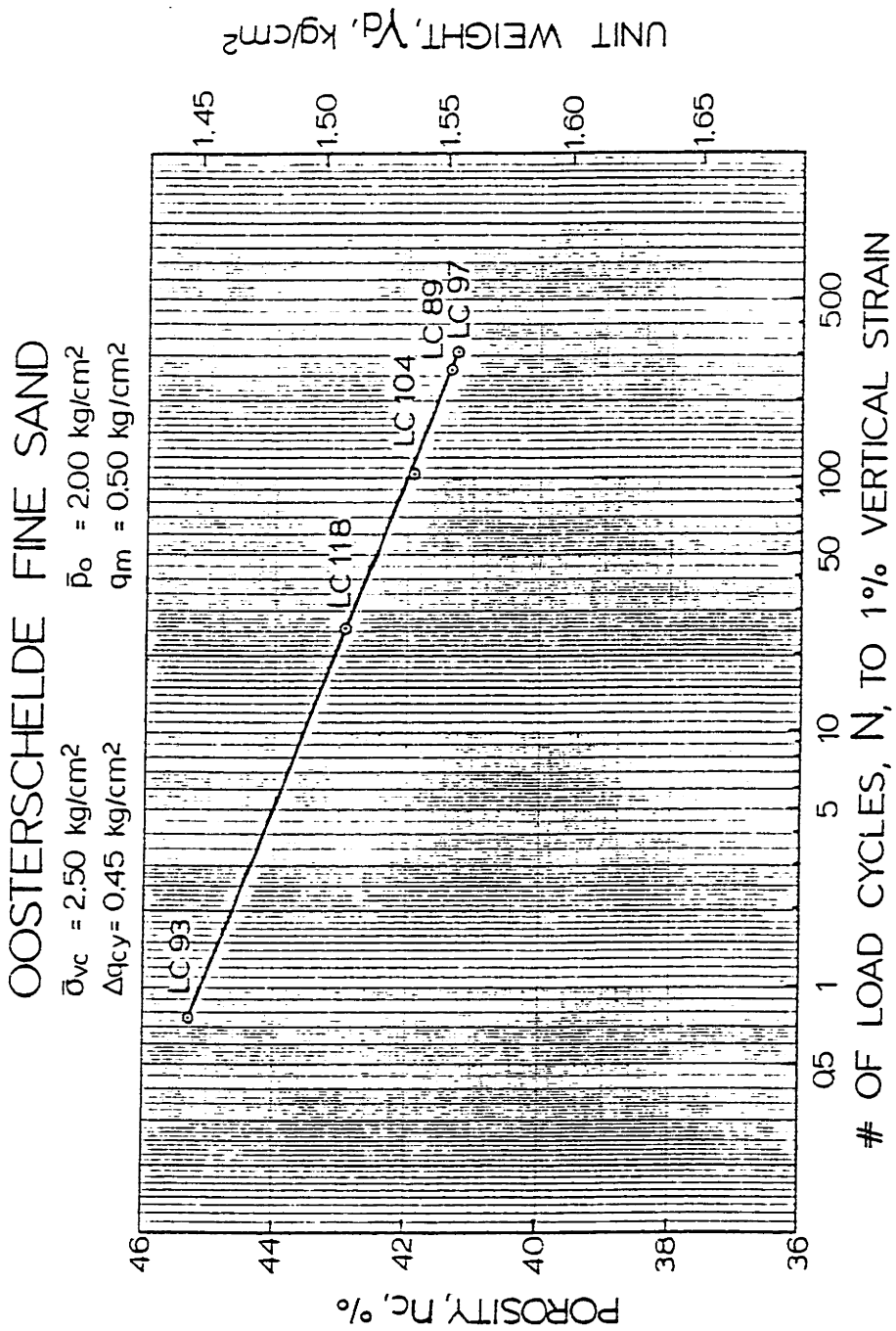

INFLUENCE OF SOIL DENSITY ON STRAIN DEVELOPMENT IN CYCLIC TRIAXIAL COMPRESSION TESTS

FIGURE IV-2

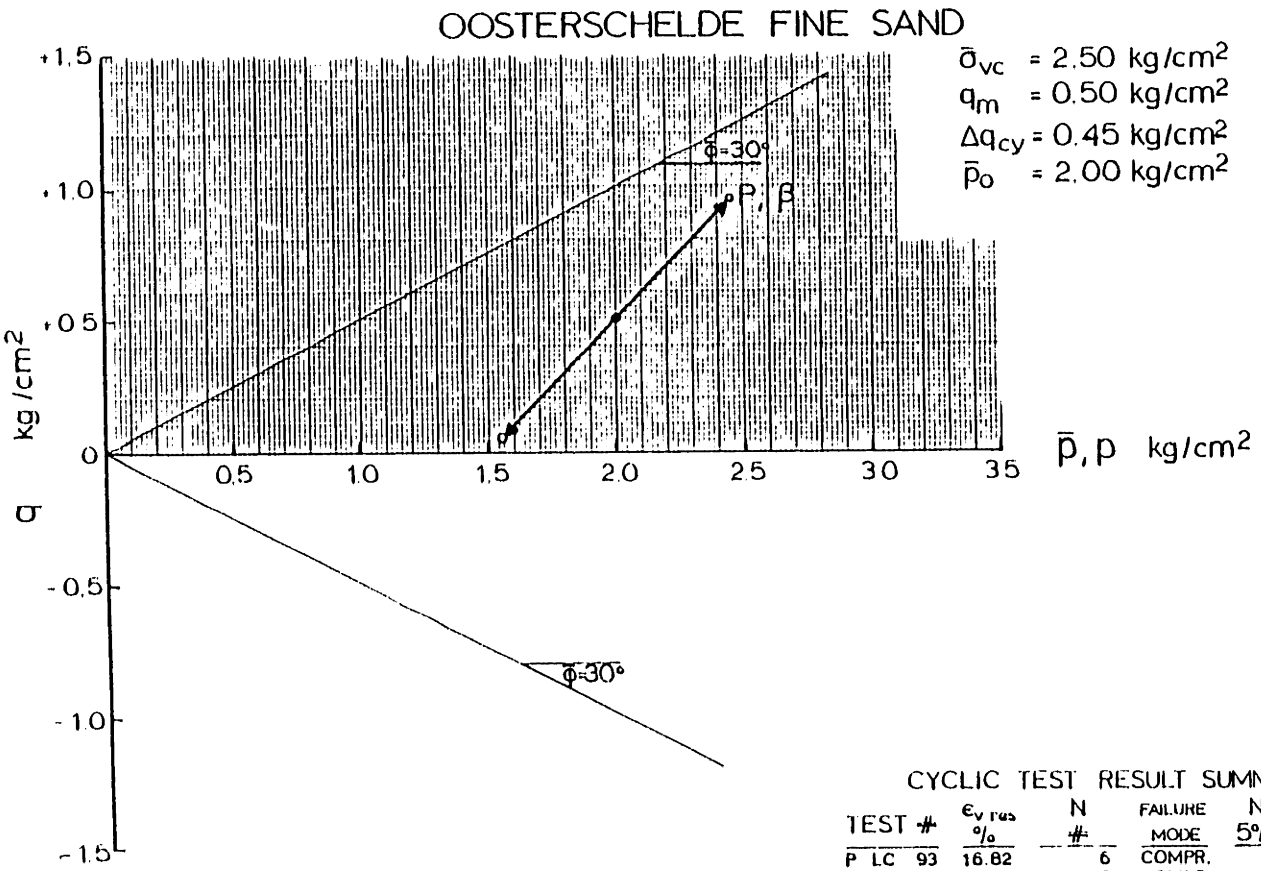

CYCLIC TEST RESULT SUMMARY

TEST #	$\epsilon_{v\,res}$ %	N #	FAILURE MODE	N_{at} 5% ϵ_v	n_c %
P LC 93	16.82	6	COMPR.	1	45.3
β LC 118	11.03	130	COMPR.	72	42.9
P LC 104	8.37	650	COMPR.	410	41.9
P LC 89	10.00	1305	COMPR.	700	41.4
P LC 97	12.30	2525	COMPR.	980	41.3
P LC 105	0.36	9500	COMPR.	–	39.7
P LC 94	0.12	10000	COMPR.	–	37.9

TOTAL STRESS PATHS (TSP-u_B) FOR ANISOTROPIC CYCLIC TESTS WITH DIFFERENT POROSITY, n_c

FIGURE IV-61

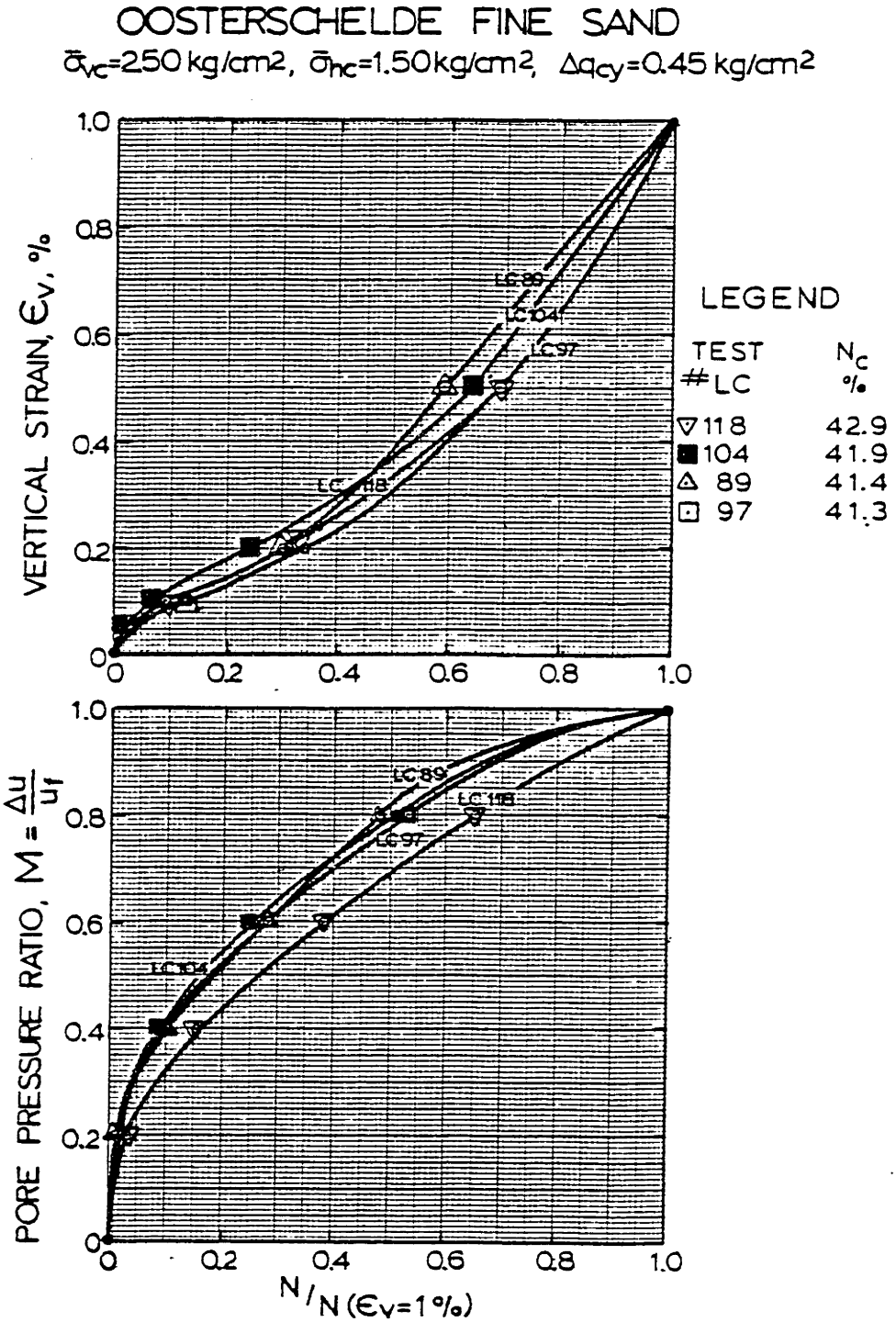

NORMALIZED STRAIN AND PORE PRESSURE DEVELOPMENT FOR CYCLIC COMPRESSION TESTS WITH DIFFERENT POROSITIES, n_c

FIGURE IV-4

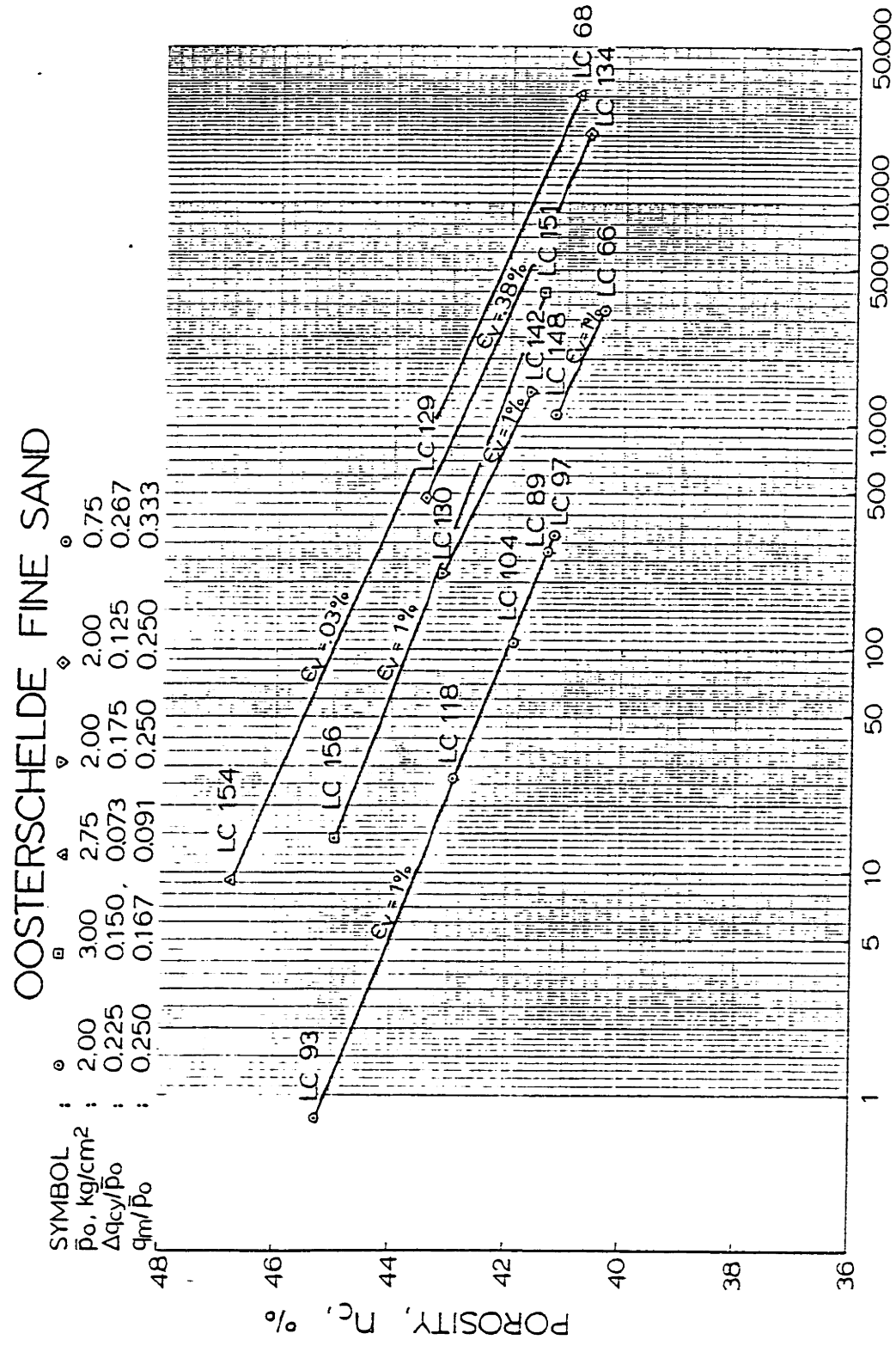

INFLUENCE OF POROSITY ON THE NUMBER OF LOAD CYCLES TO REACH SOME VERTICAL STRAIN IN CYCLIC TRIAXIAL COMPRESSION TESTS UNDER VARIOUS CONDITIONS

FIGURE IV-5

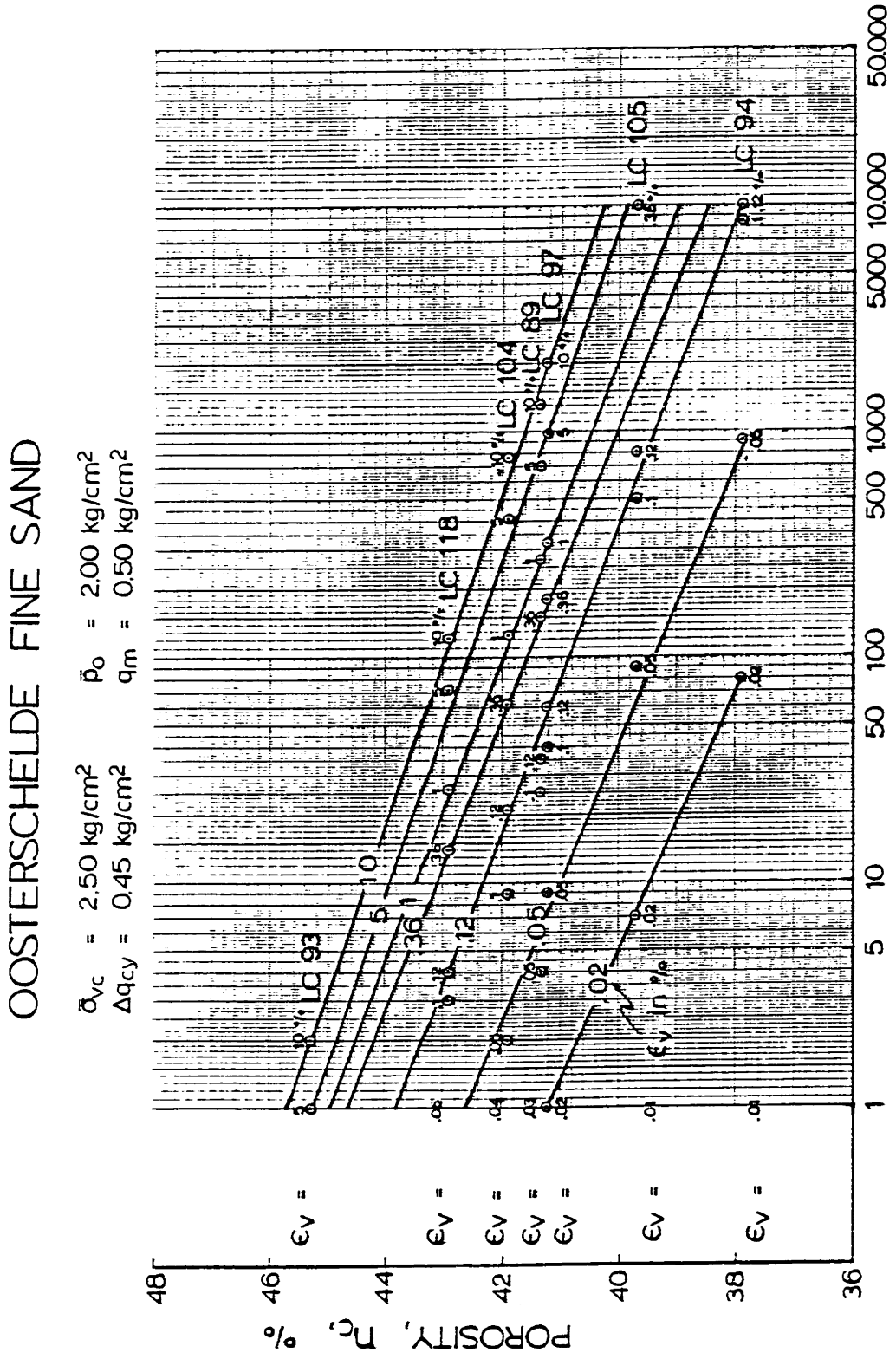

STRAIN CONTOURS FOR COMPRESSION CYCLIC TESTS ON SAMPLES AT DIFFERENT POROSITIES

FIGURE IV-6

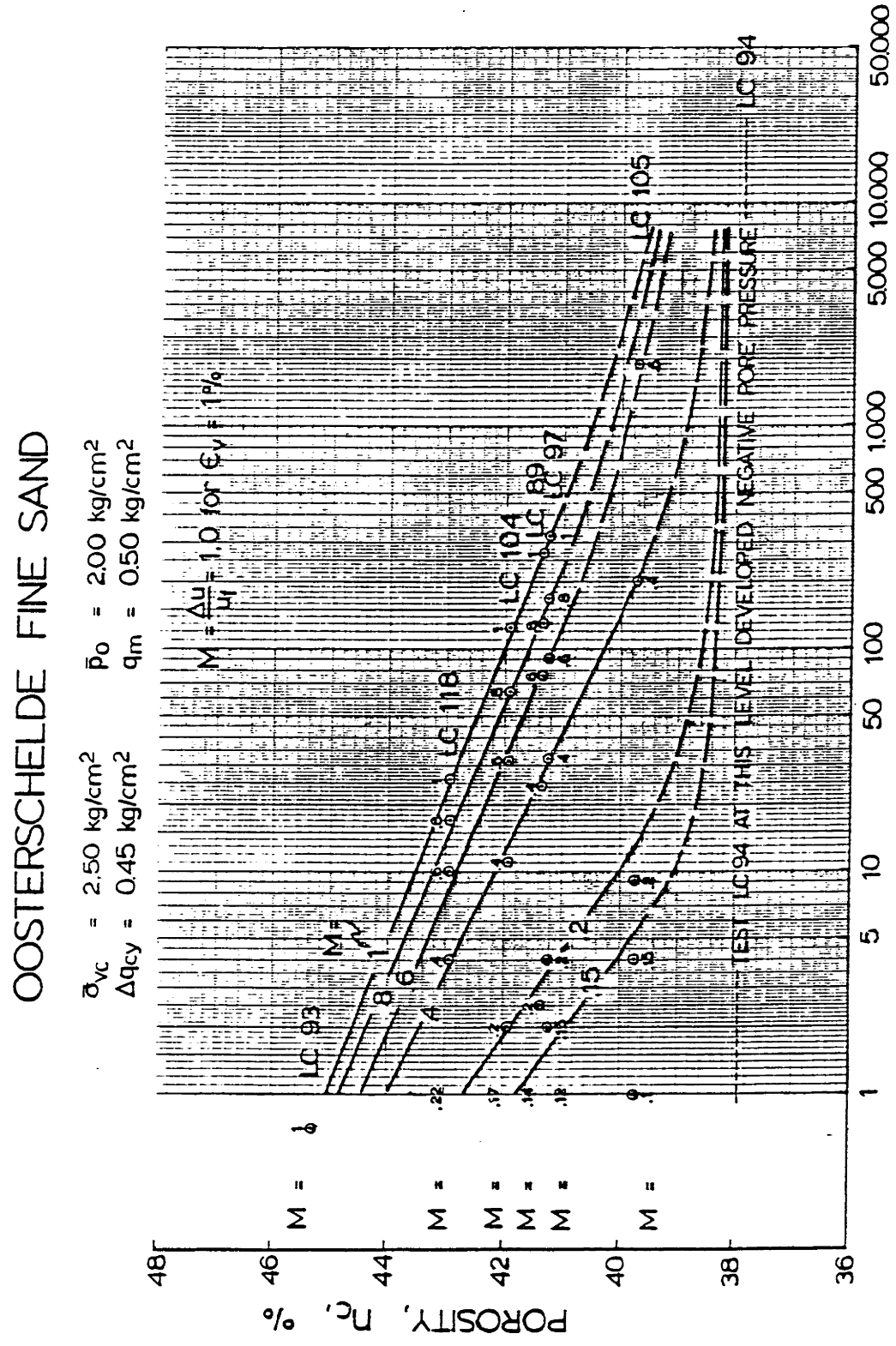

PORE PRESSURE CONTOURS FOR COMPRESSION CYCLIC TESTS ON SAMPLES AT DIFFERENT POROSITIES

FIGURE IV-7

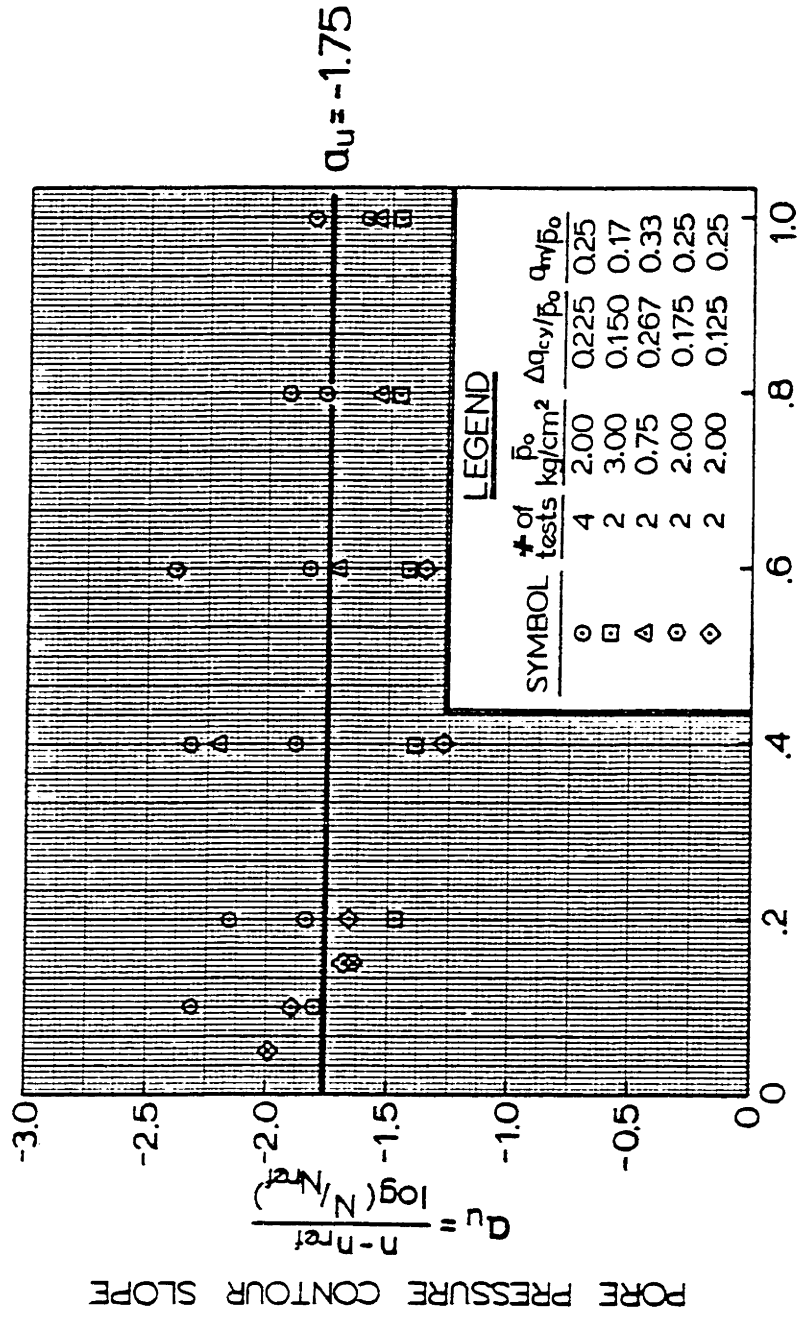

VARIATION IN THE SLOPE OF PORE PRESSURE CONTOURS FOR CYCLIC COMPRESSION TESTS AT DIFFERENT POROSITIES

FIGURE IV-6

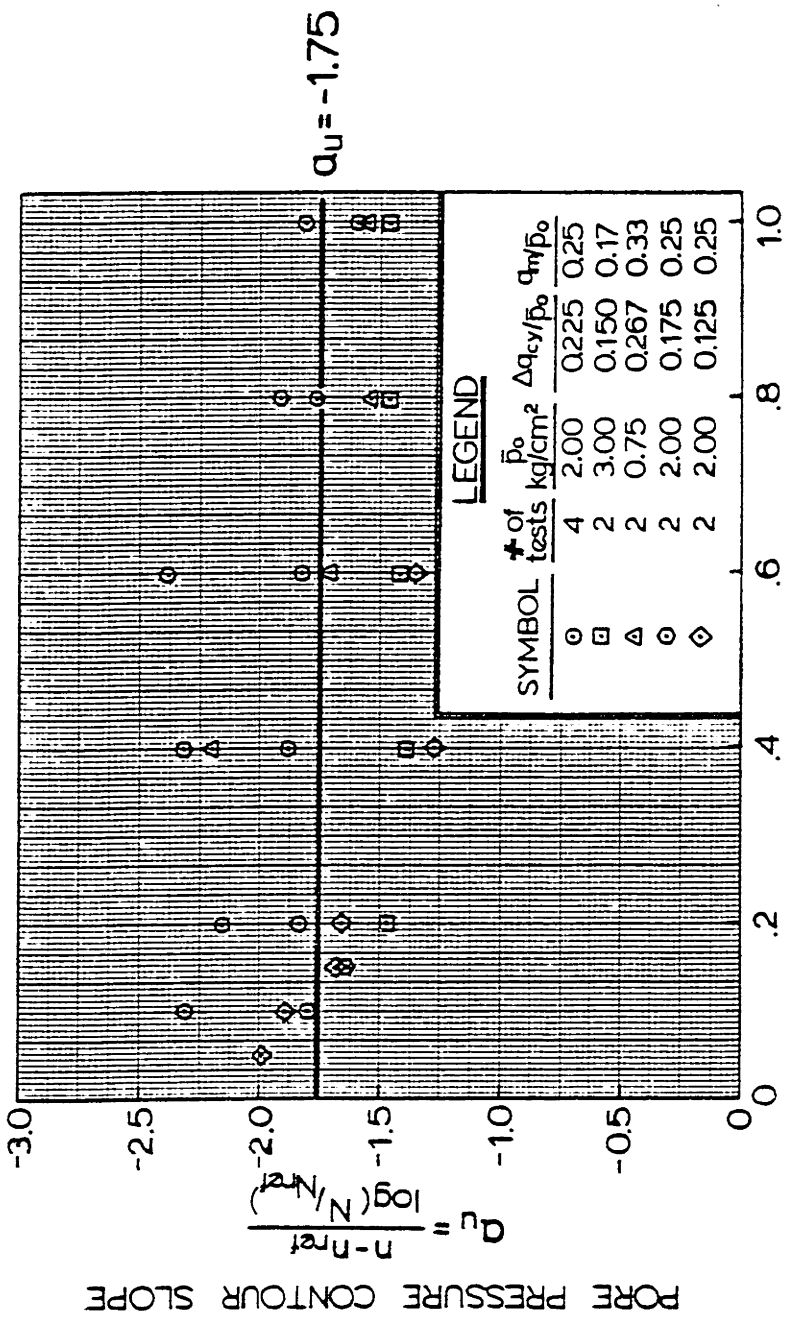

VARIATION IN THE SLOPE OF PORE PRESSURE CONTOURS FOR CYCLIC COMPRESSION TESTS AT DIFFERENT POROSITIES

FIGURE IV-9

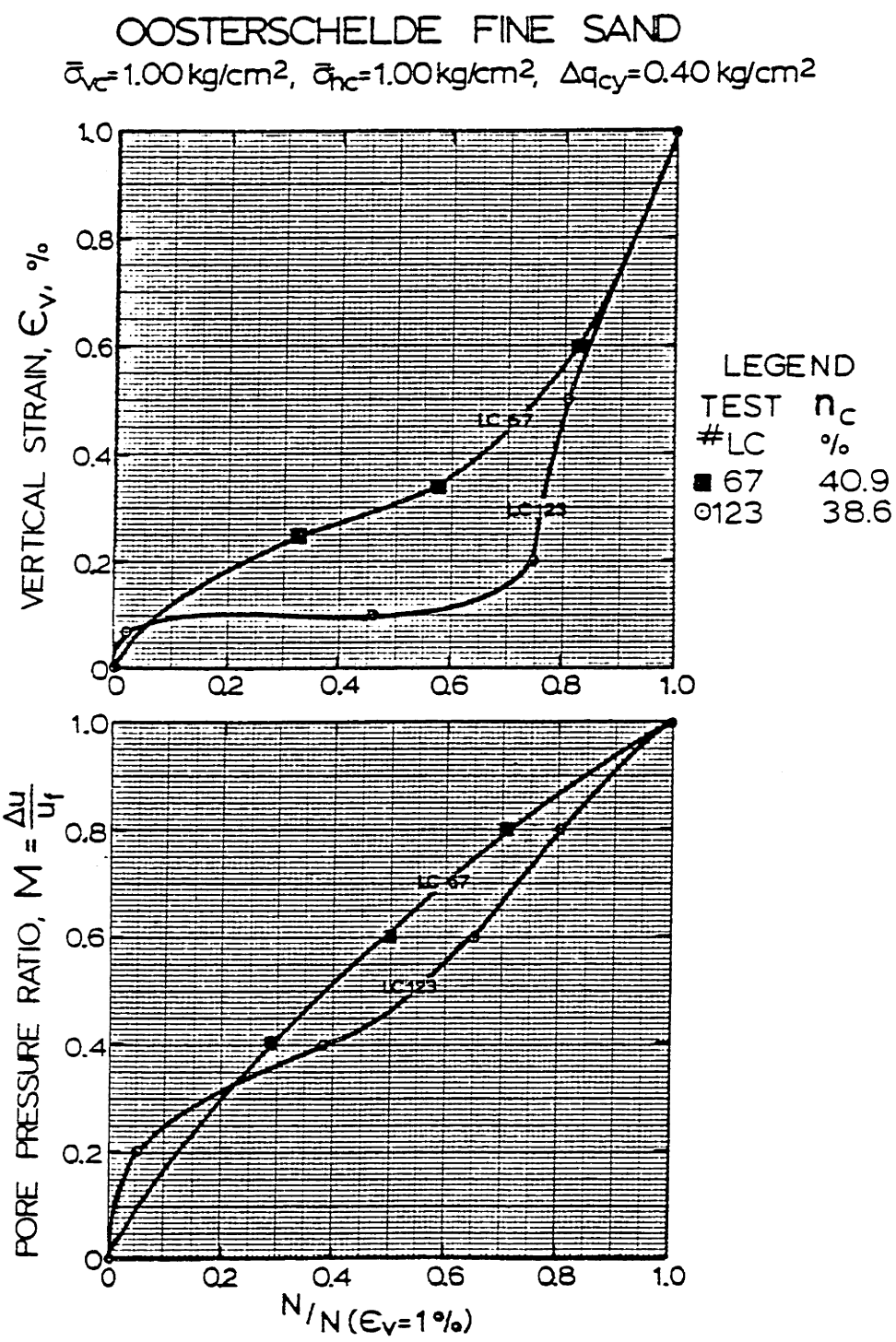

NORMALIZED STRAIN AND PORE PRESSURE DEVELOPMENT FOR CYCLIC ISOTROPIC TESTS WITH DIFFERENT POROSITIES, n_c

FIGURE IV-10

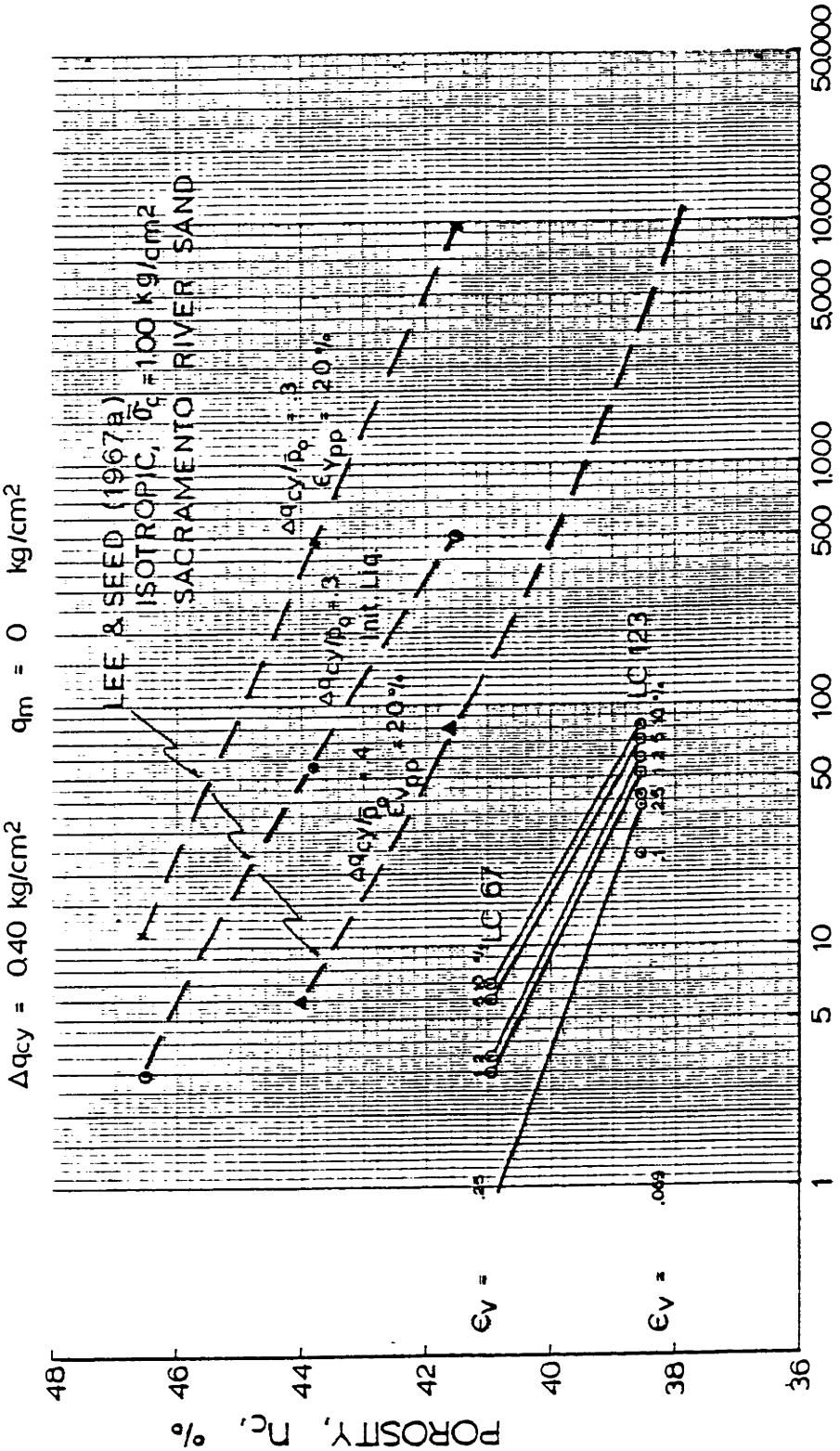

STRAIN CONTOURS FOR ISOTROPIC CYCLIC TESTS ON SAMPLES AT DIFFERENT POROSITIES

FIGURE IV-11

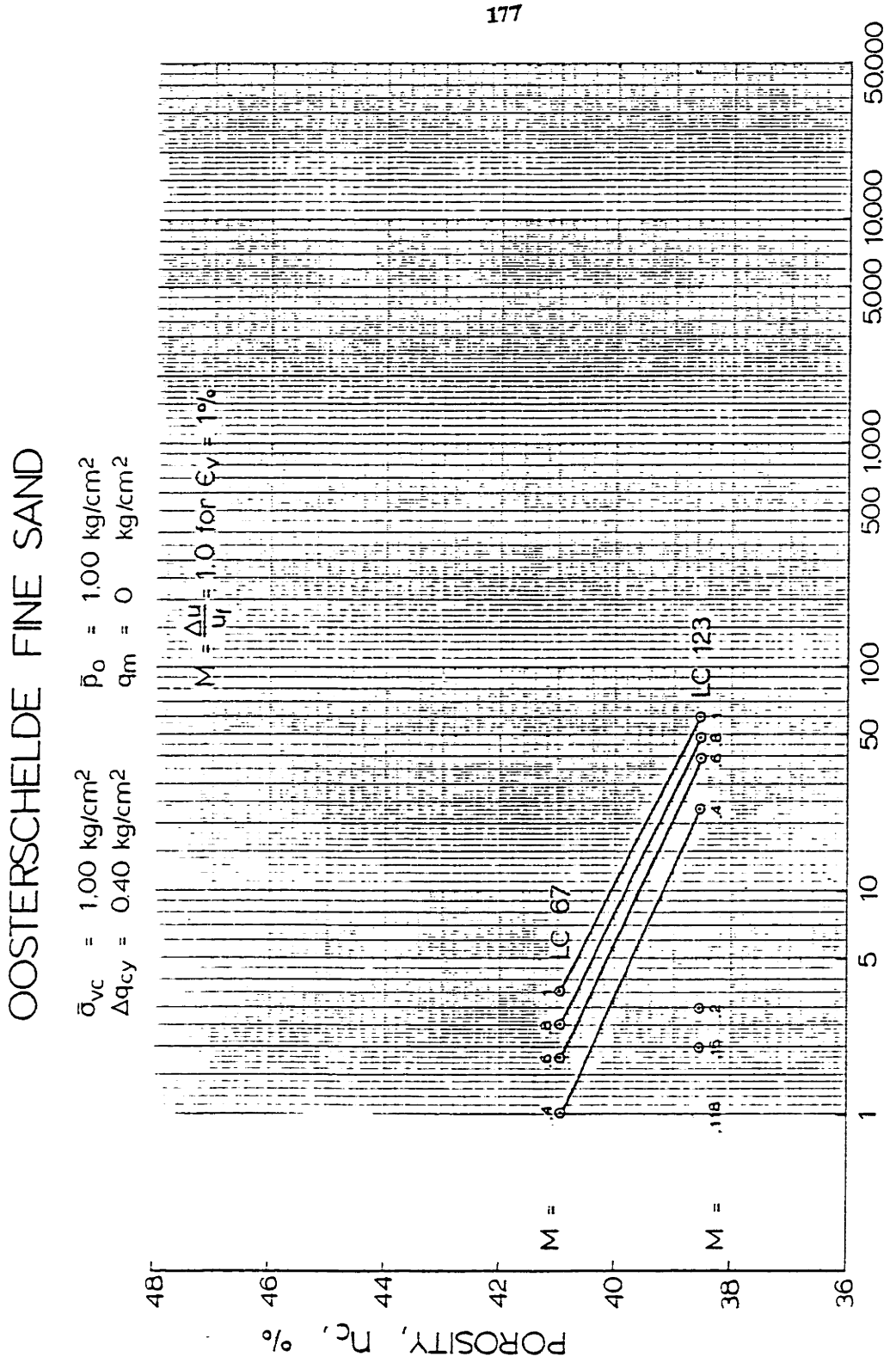

PORE PRESSURE CONTOURS FOR ISOTROPIC CYCLIC TESTS ON SAMPLES AT DIFFERENT POROSITIES

FIGURE IV-12

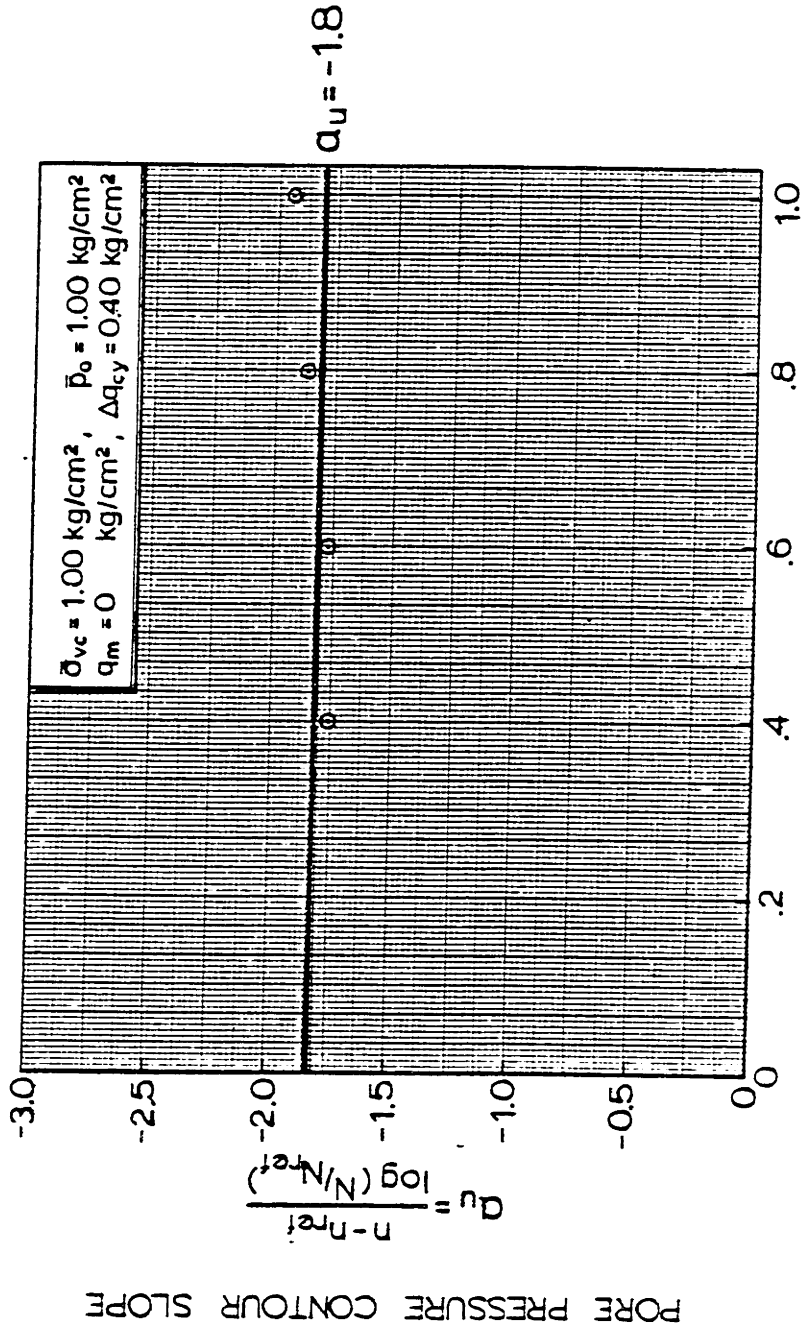

VARIATION IN THE SLOPE OF PORE PRESSURE CONTOURS FOR CYCLIC ISOTROPIC TESTS AT DIFFERENT POROSITIES

FIGURE IV-13

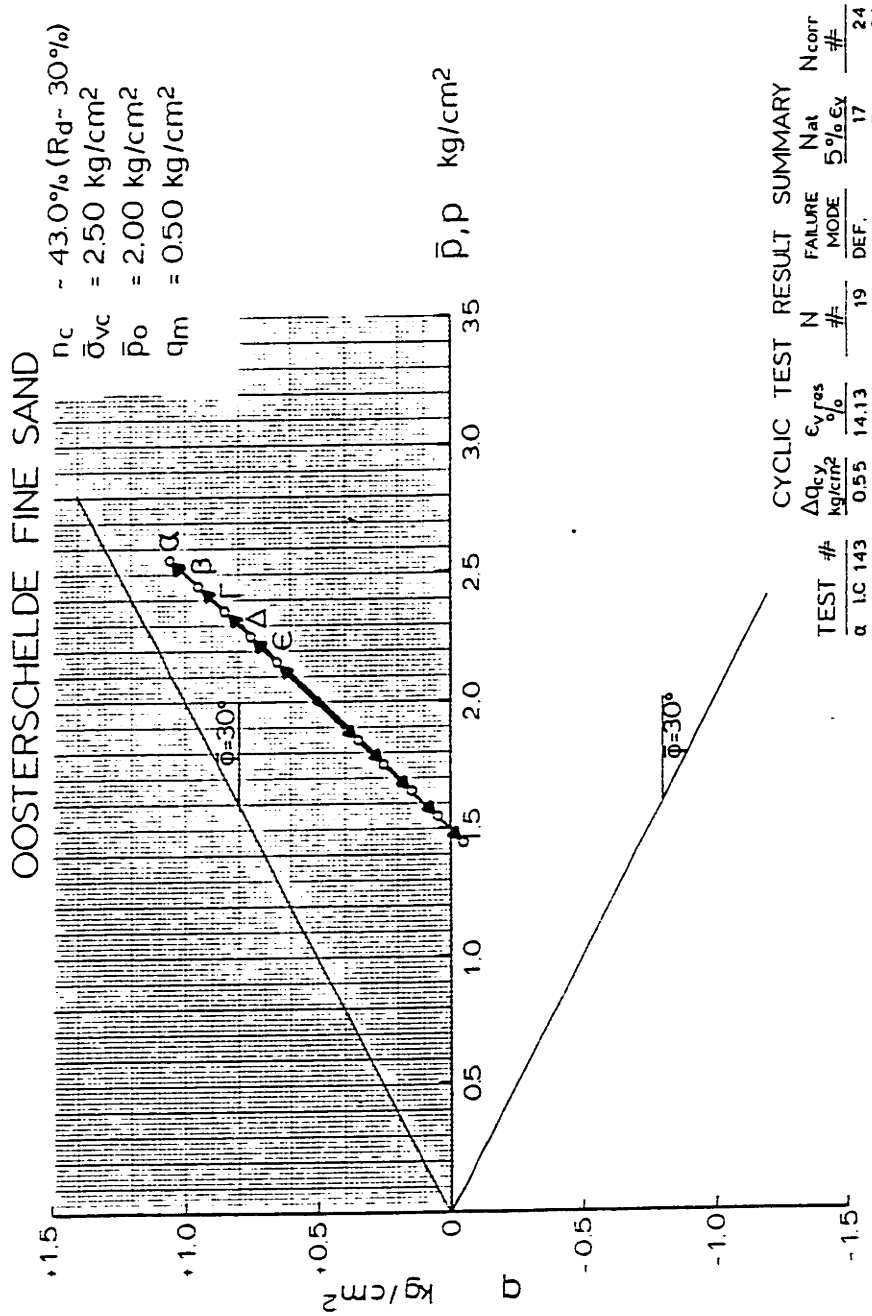

CYCLIC TEST RESULT SUMMARY

TEST #	Δq_{cy} kg/cm²	$\epsilon_{v\,res}$ %	N #	FAILURE MODE	N_{at} $5\%\,\epsilon_v$	N_{corr} #	n_c %
α LC 143	0.55	14.13	19	DEF.	17	24	43.2
β LC 118	0.45	11.03	130	COMPR.	72	84	42.9
Γ LC 130	0.35	10.20	1000	COMPR.	546	746	43.2
Δ LC 129	0.25	13.50	3600	COMPR.	1440	3170	43.5
ε LC 131	0.15	1.75	10700	COMPR.	—	—	42.9

TOTAL STRESS PATHS (TSP-u_B) FOR ANISOTROPIC CYCLIC TESTS WITH DIFFERENT CYCLIC SHEAR STRESS RATIO, $\Delta q_{cy}/\bar{p}_o$

FIGURE IV-14

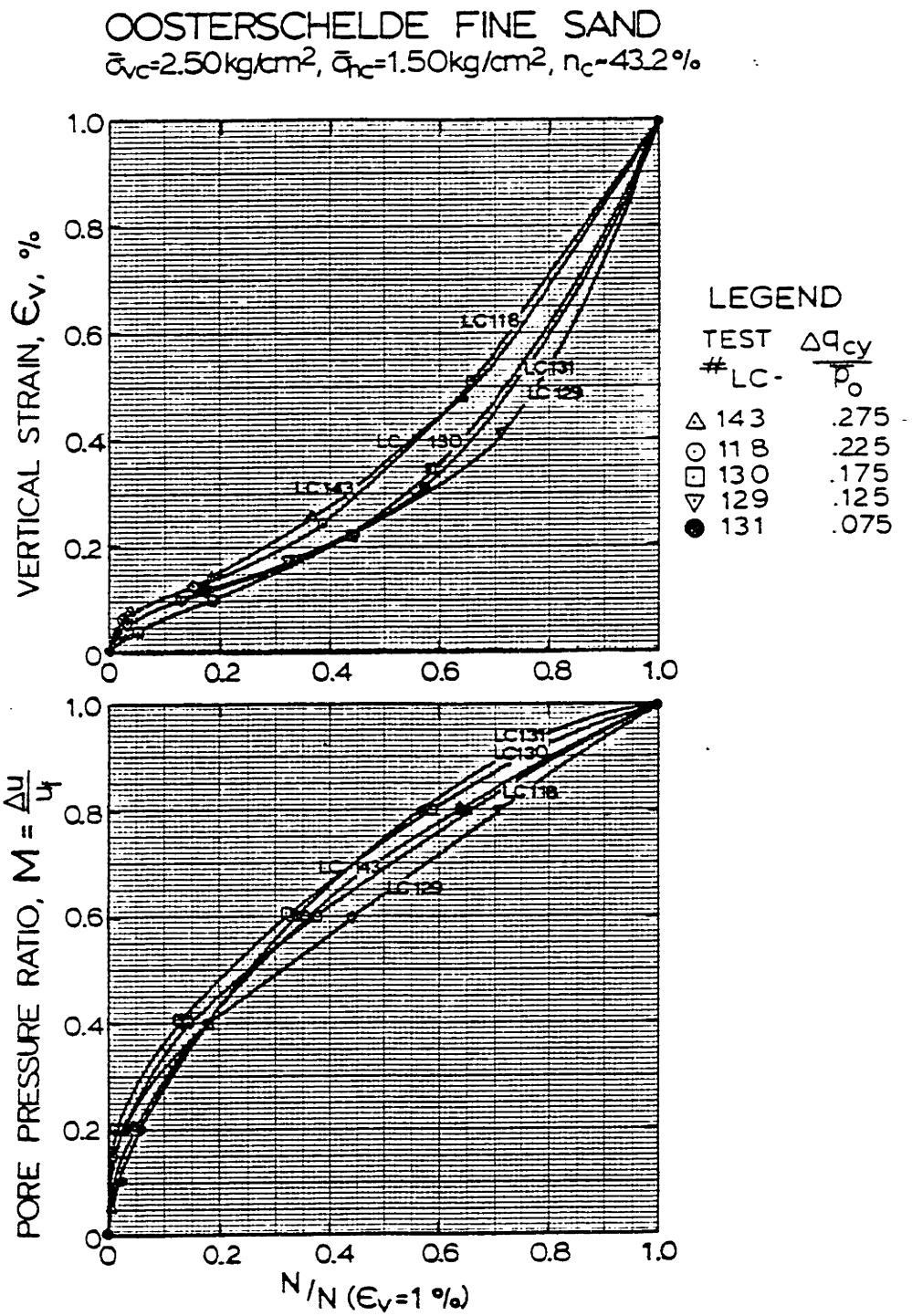

NORMALIZED STRAIN AND PORE PRESSURE DEVELOPMENT FOR CYCLIC COMPRESSION TESTS WITH DIFFERENT CYCLIC SHEAR STRESSES, Δq_{cy}

FIGURE IV-15

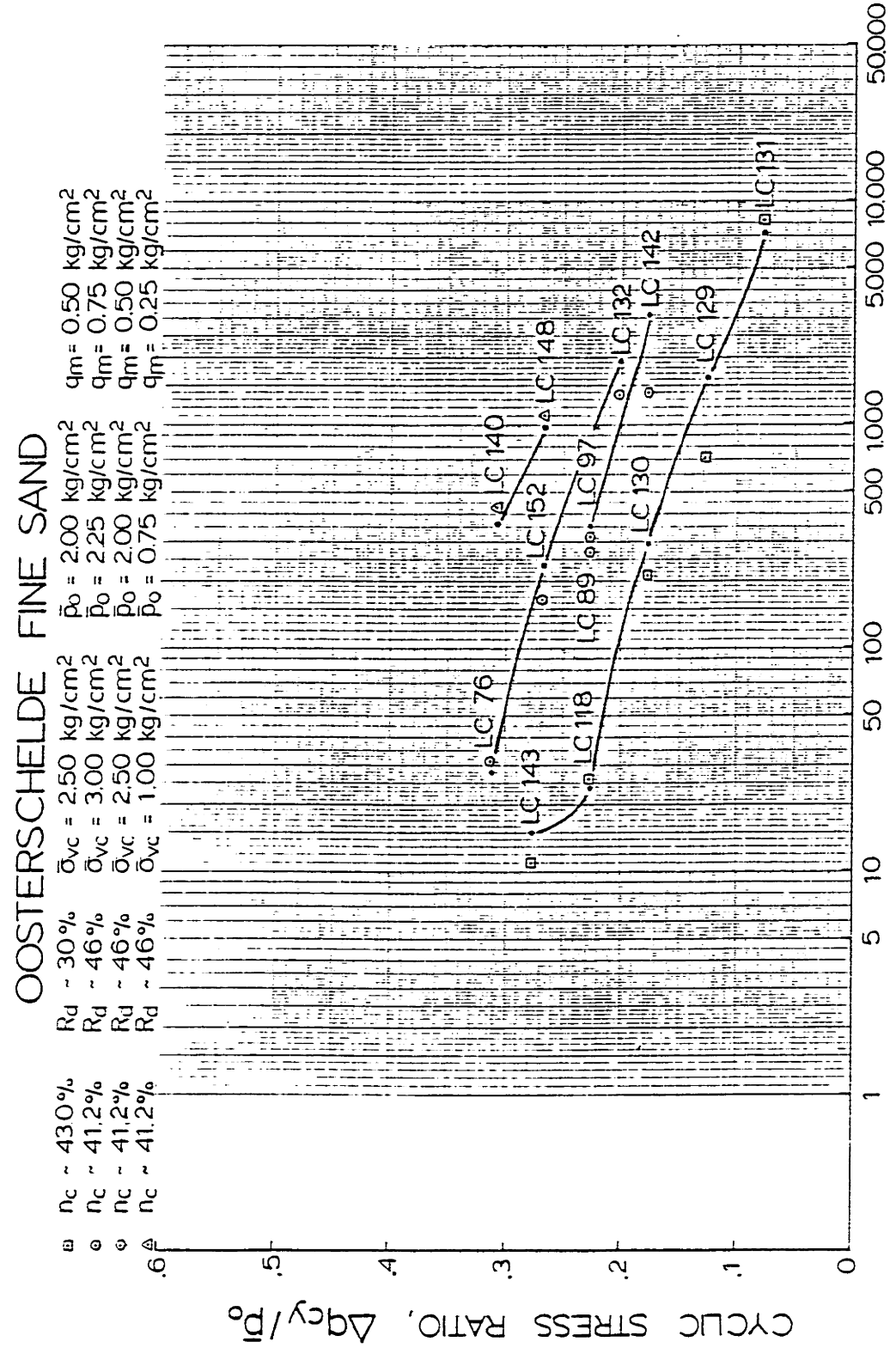

INFLUENCE OF CYCLIC STRESS RATIO ON NUMBER OF LOAD CYCLES TO REACH 1% VERTICAL STRAIN IN CYCLIC TRIAXIAL COMPRESSION TESTS UNDER VARIOUS CONDITIONS

FIGURE IV-16

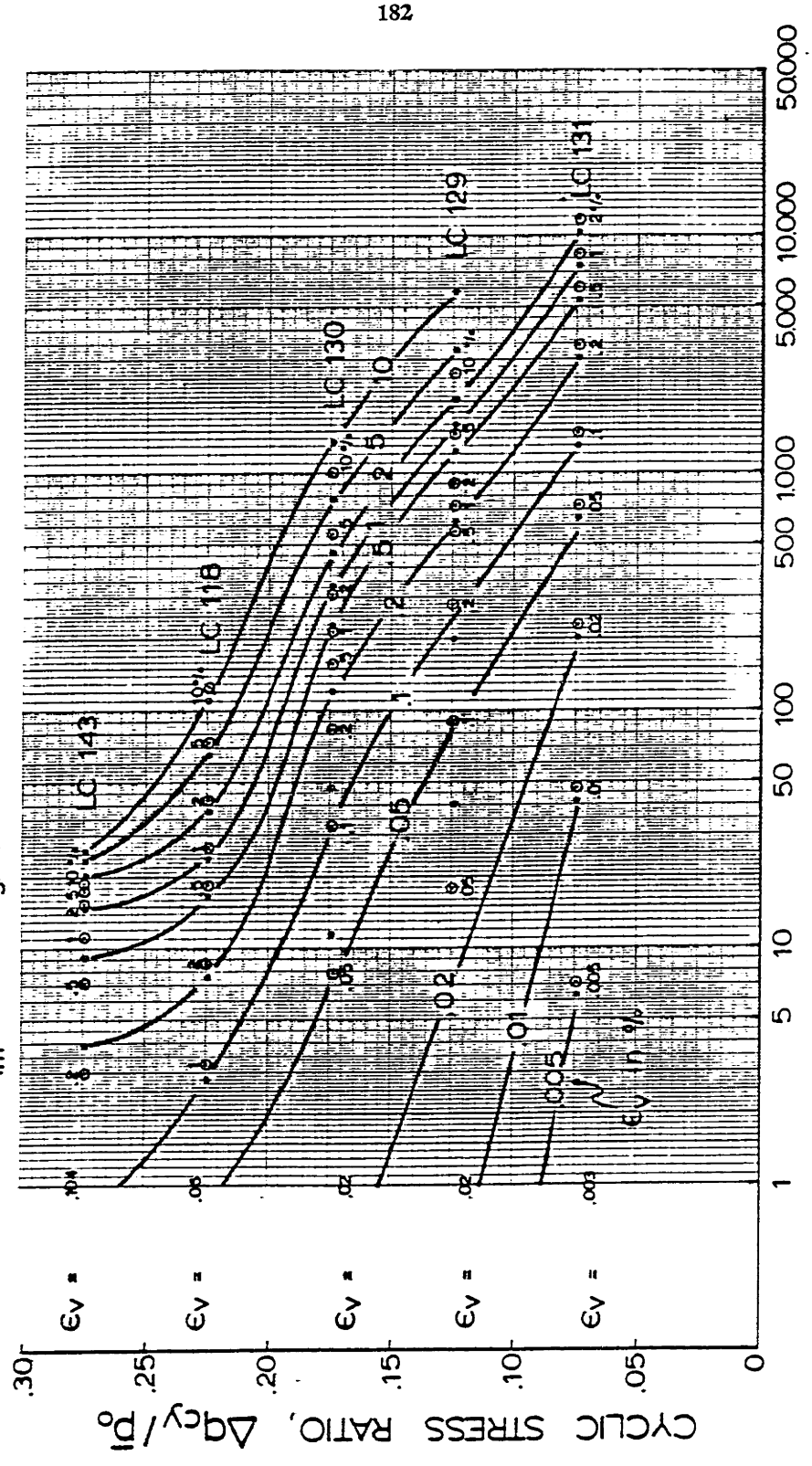

FIGURE IV-17

STRAIN CONTOURS FOR COMPRESSION CYCLIC TESTS WITH DIFFERENT CYCLIC STRESS RATIOS

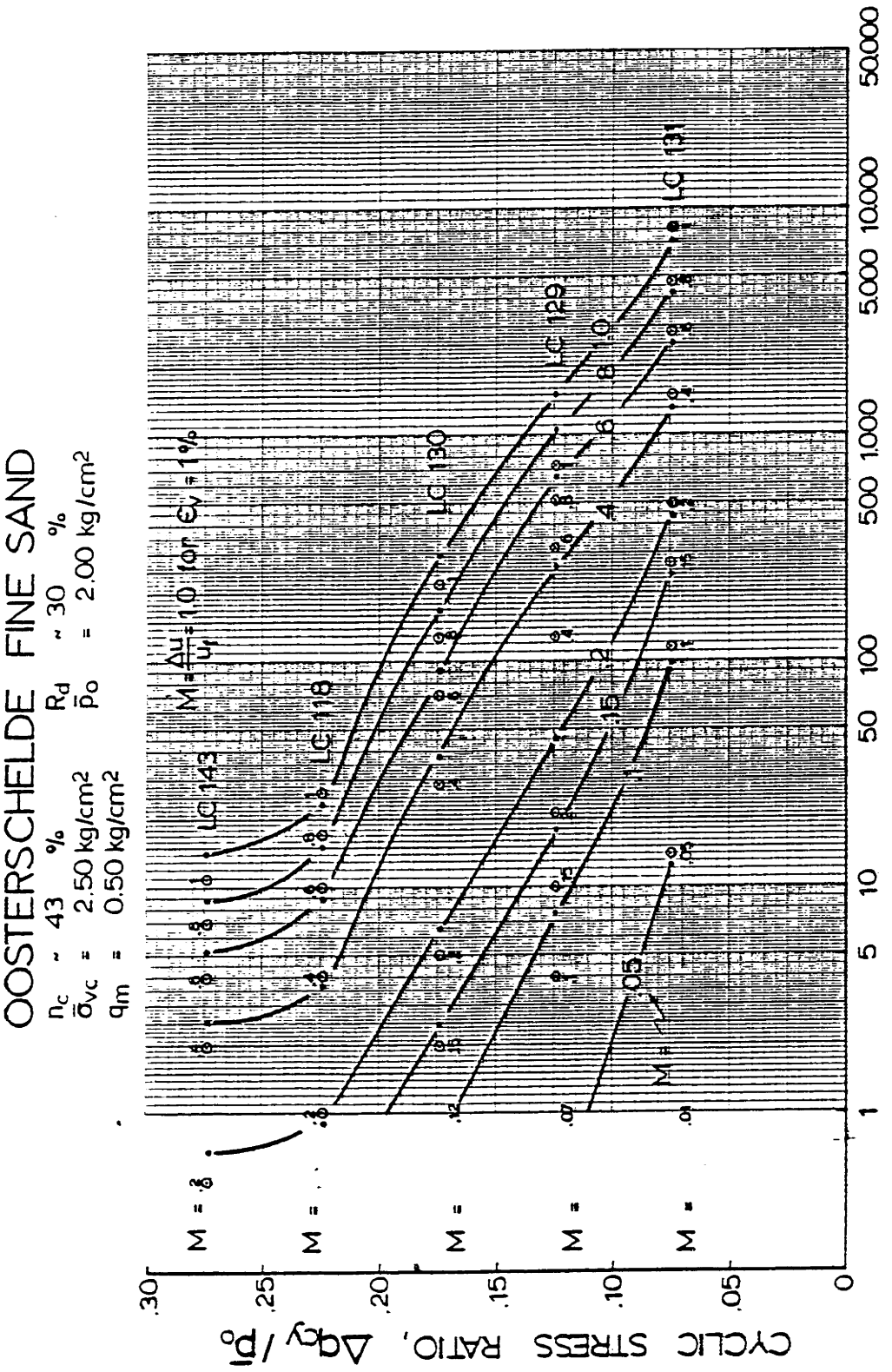

PORE PRESSURE CONTOURS FOR COMPRESSION CYCLIC TESTS WITH DIFFERENT CYCLIC STRESS RATIOS

FIGURE IV-18

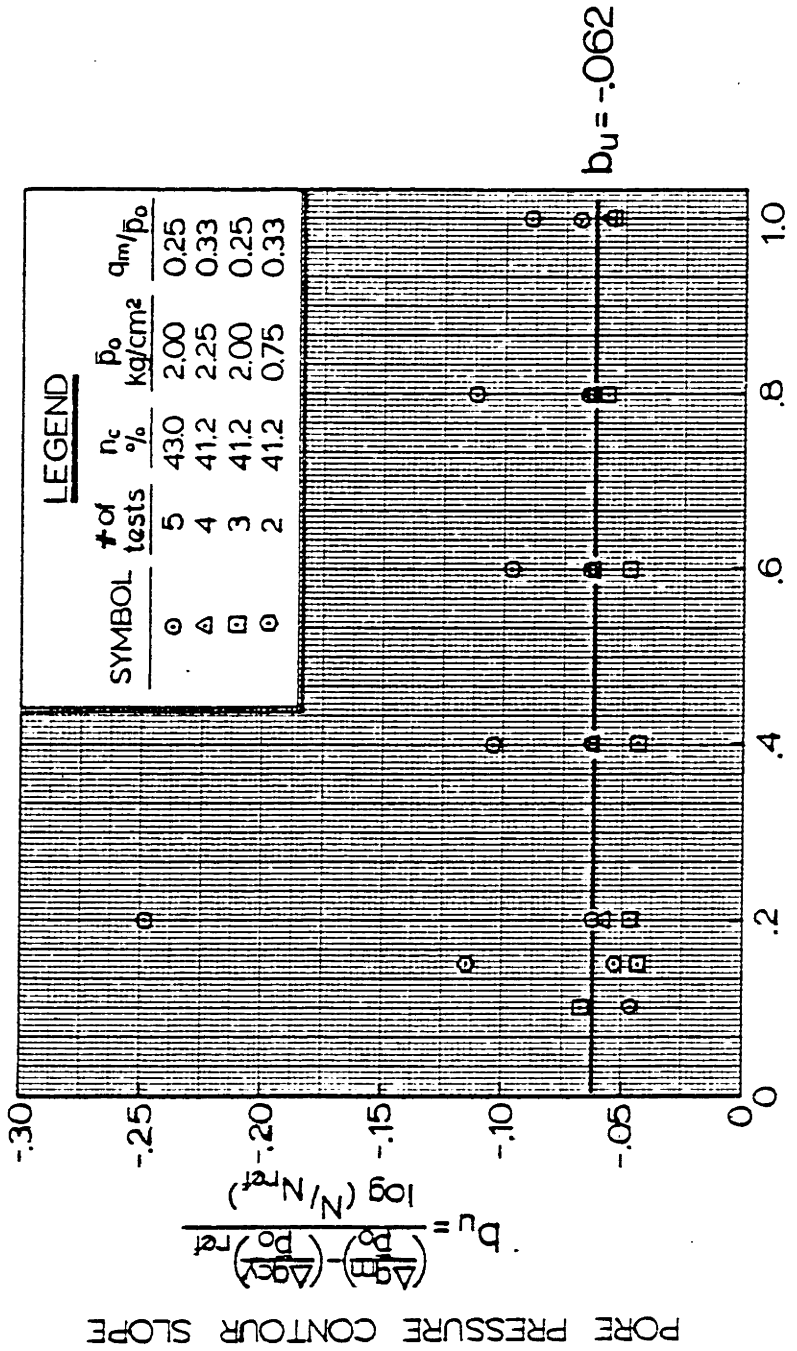

VARIATION IN THE SLOPE OF PORE PRESSURE CONTOURS FOR COMPRESSION TESTS AT DIFFERENT CYCLIC STRESS RATIOS

FIGURE IV-19

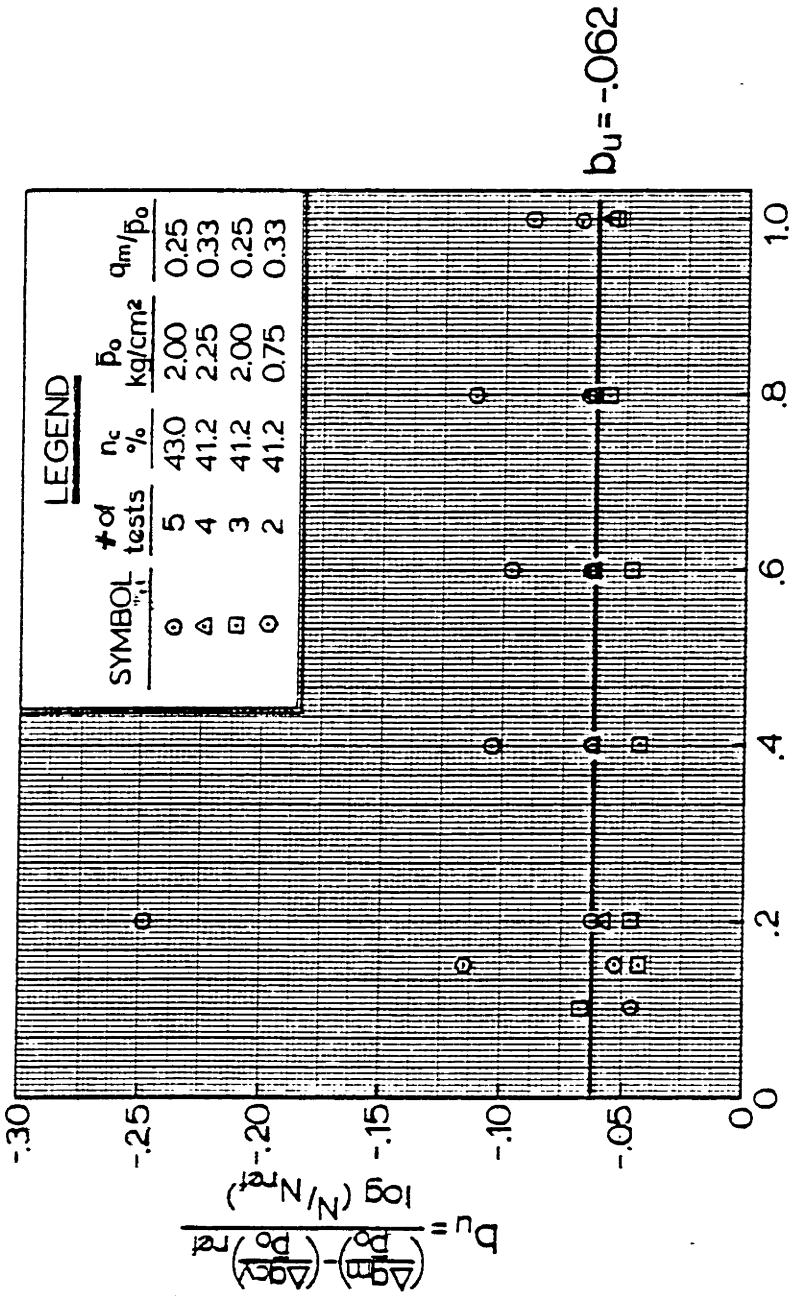

VARIATION IN THE SLOPE OF PORE PRESSURE CONTOURS FOR COMPRESSION TESTS AT DIFFERENT CYCLIC STRESS RATIOS

FIGURE IV-20

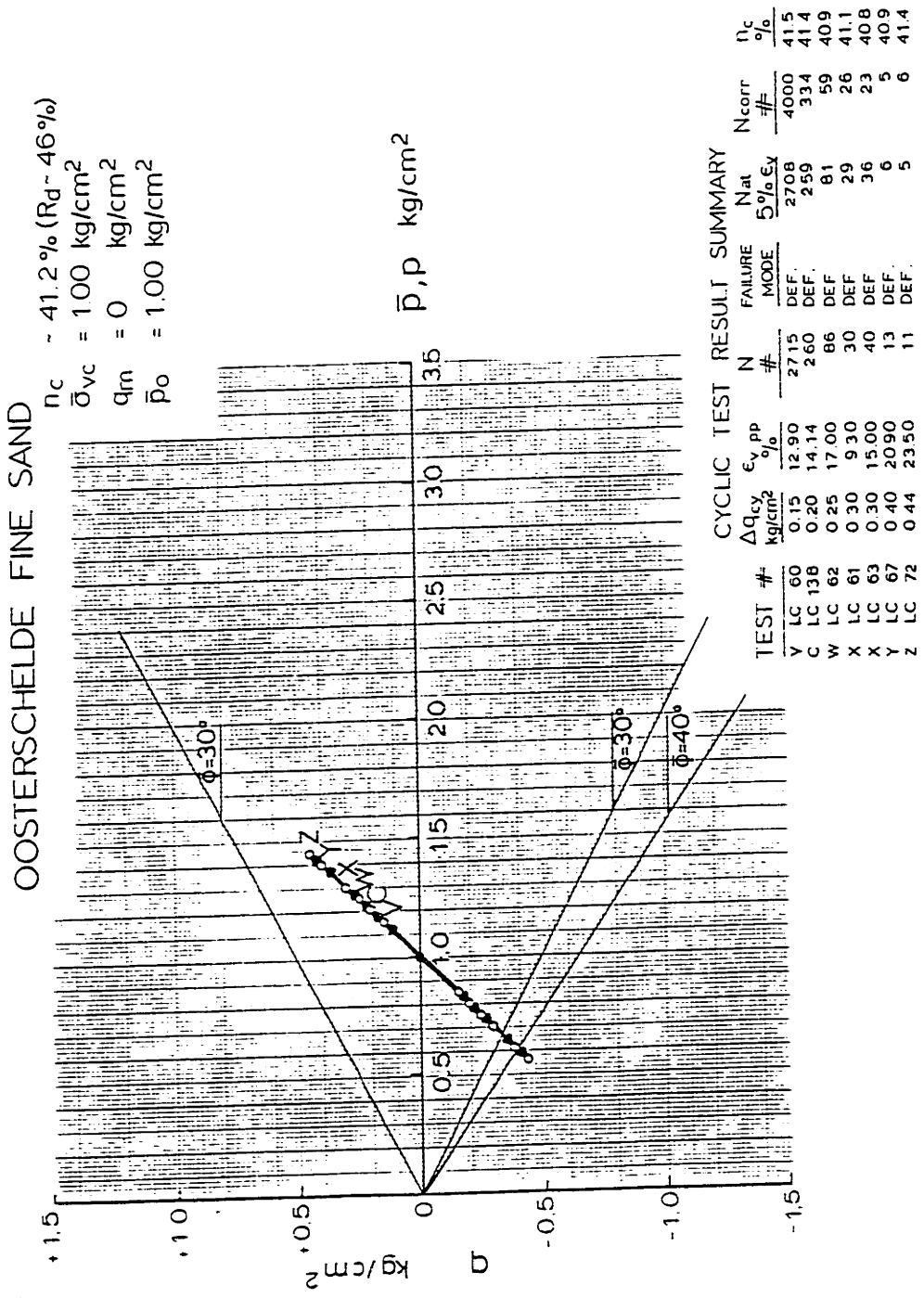

CYCLIC TEST RESULT SUMMARY

TEST #	Δq_{cy} kg/cm²	$\epsilon_{v\,pp}$ %	N #	FAILURE MODE	Nat 5% ϵ_v #	N_{corr} #	n_c %
V LC 60	0.15	12.90	2715	DEF.	2708	4000	41.5
C LC 138	0.20	14.14	260	DEF.	259	334	41.4
W LC 62	0.25	17.00	86	DEF	81	59	40.9
X LC 61	0.30	9.30	30	DEF	29	26	41.1
X LC 63	0.30	15.00	40	DEF	36	23	40.8
Y LC 67	0.40	20.90	13	DEF.	6	5	40.9
Z LC 72	0.44	23.50	11	DEF.	5	6	41.4

TOTAL STRESS PATHS (TSP-u_B) FOR ISOTROPIC CYCLIC TESTS WITH DIFFERENT CYCLIC SHEAR STRESS RATIO, $\Delta q_{cy}/\bar{p}_o$

FIGURE IV-21

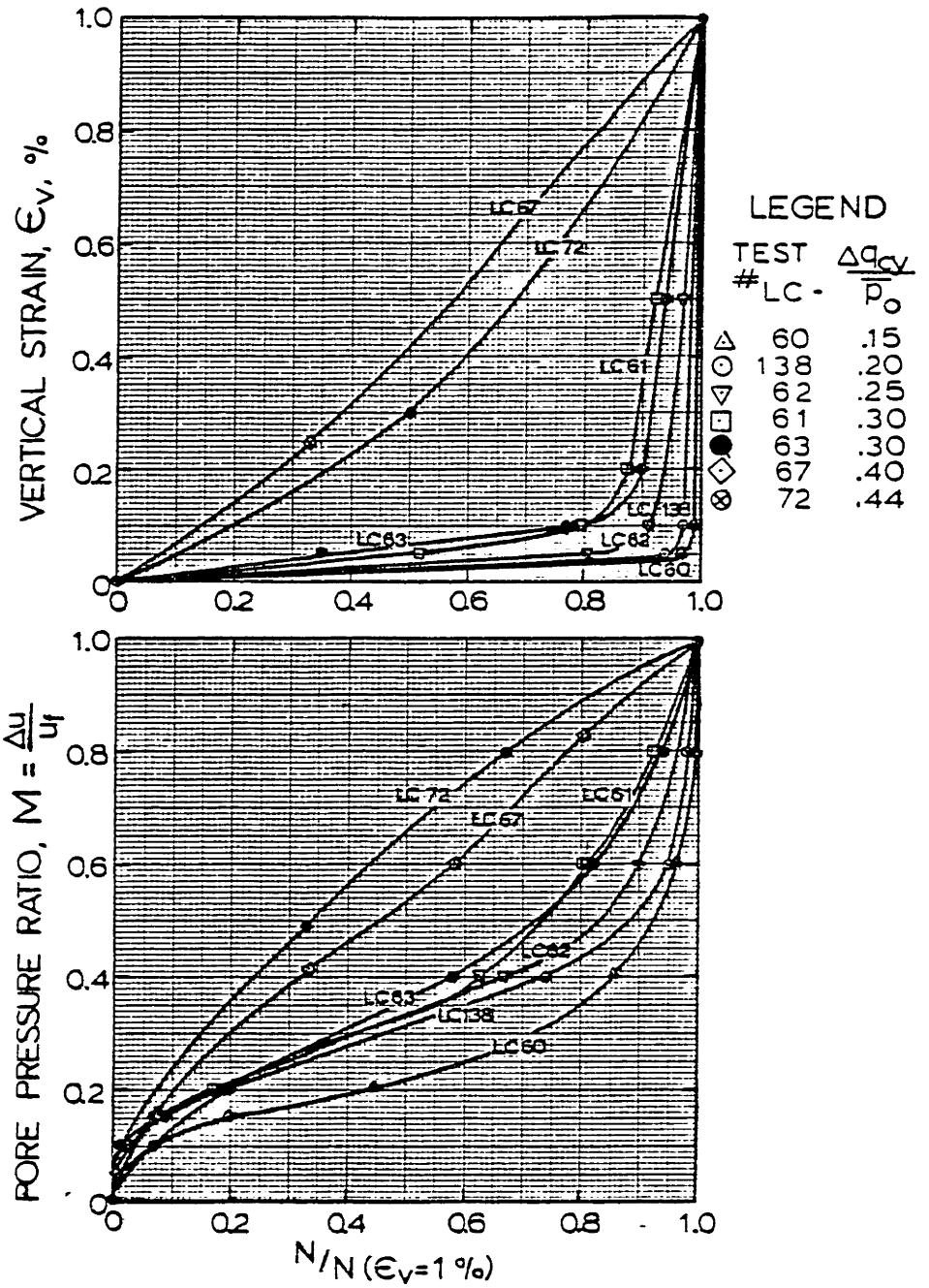

NORMALIZED STRAIN AND PORE PRESSURE DEVELOPMENT FOR CYCLIC ISOTROPIC TESTS WITH DIFFERENT CYCLIC SHEAR STRESSES, Δq_{cy}

FIGURE IV-22

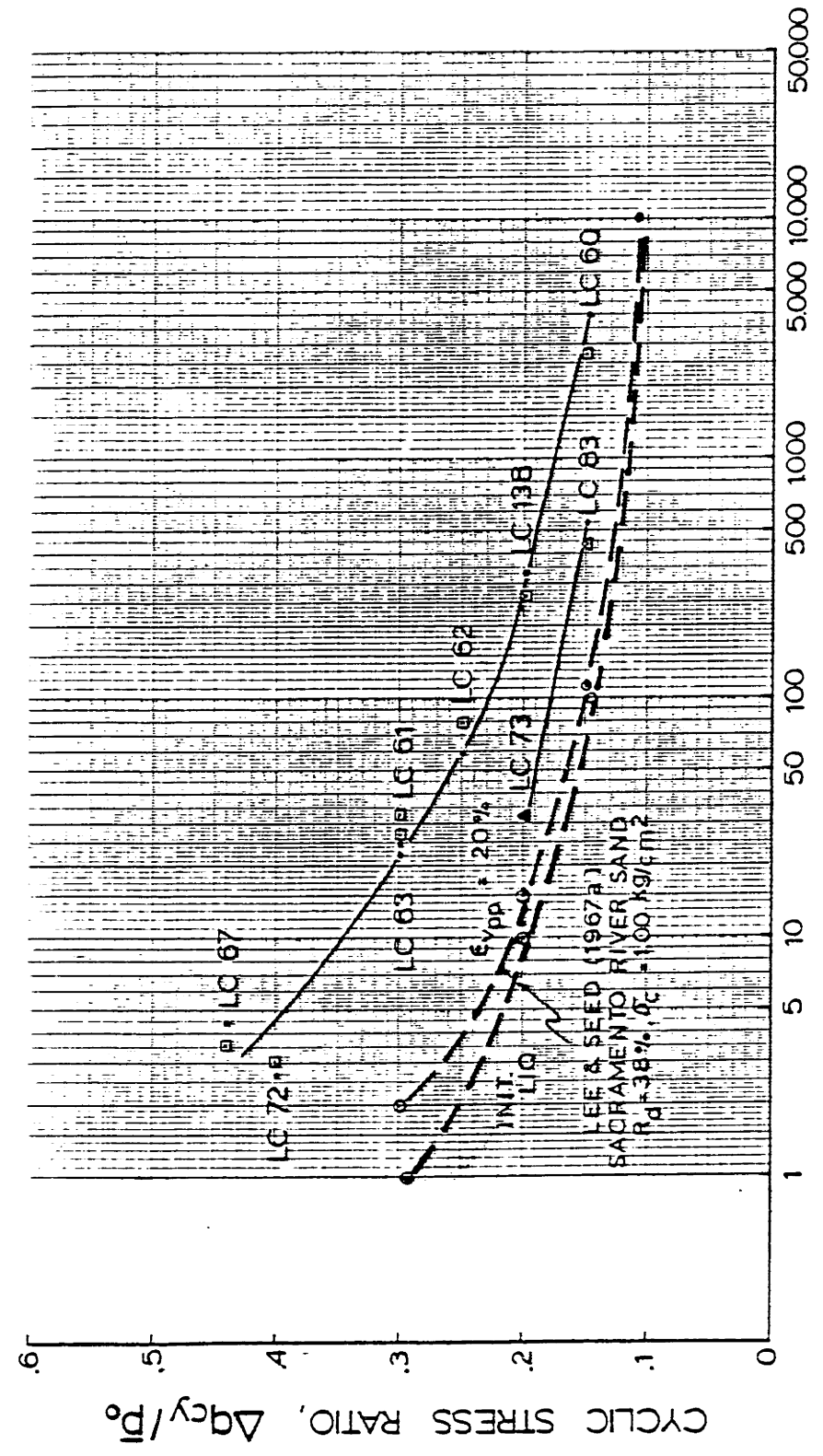

INFLUENCE OF CYCLIC STRESS RATIO ON NUMBER OF LOAD CYCLES TO REACH 1% VERTICAL STRAIN IN CYCLIC TRIAXIAL ISOTROPIC TESTS UNDER VARIOUS CONDITIONS

FIGURE IV-23

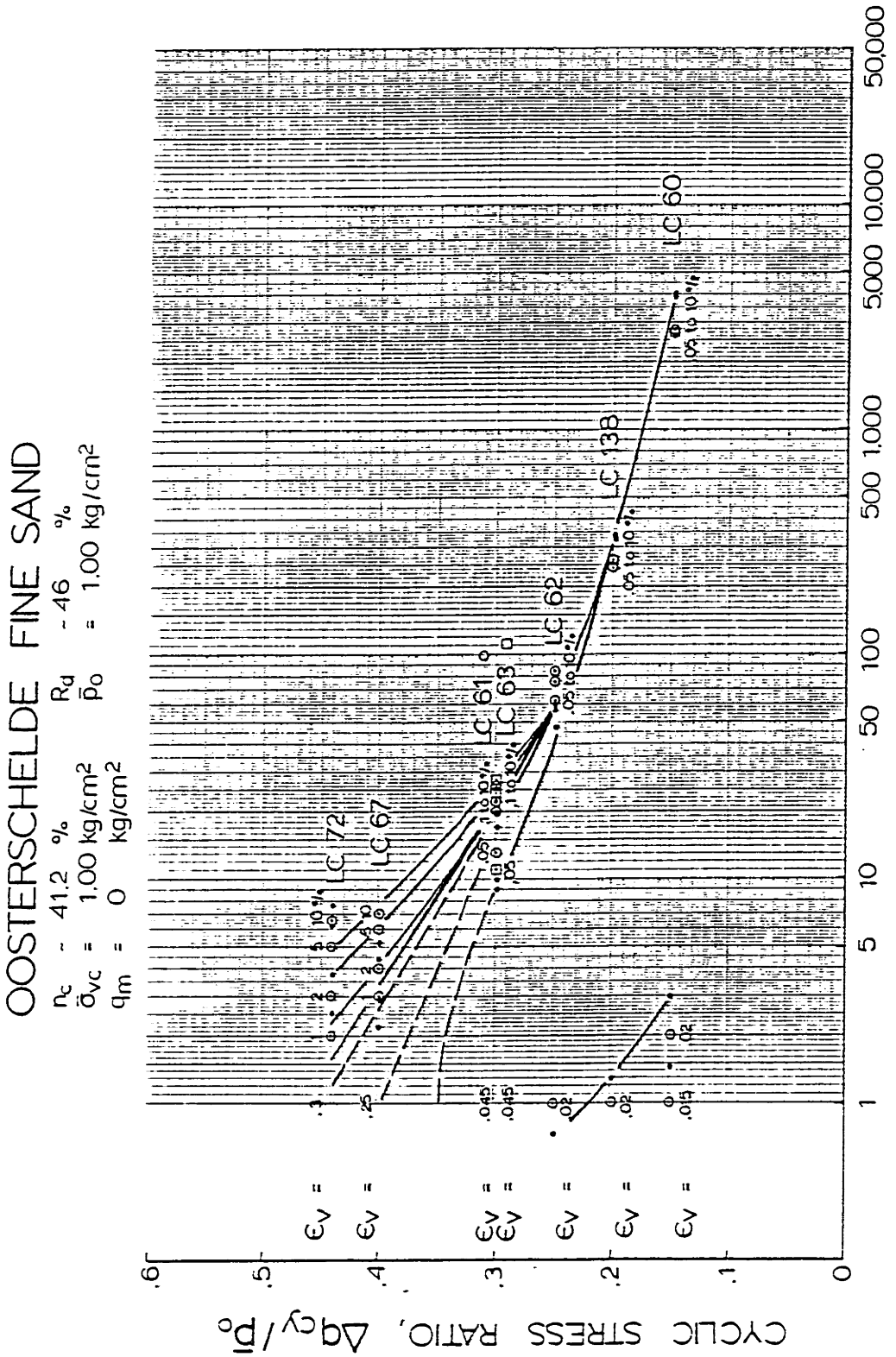

STRAIN CONTOURS FOR ISOTROPIC CYCLIC TESTS WITH DIFFERENT CYCLIC STRESS RATIOS

FIGURE IV-24

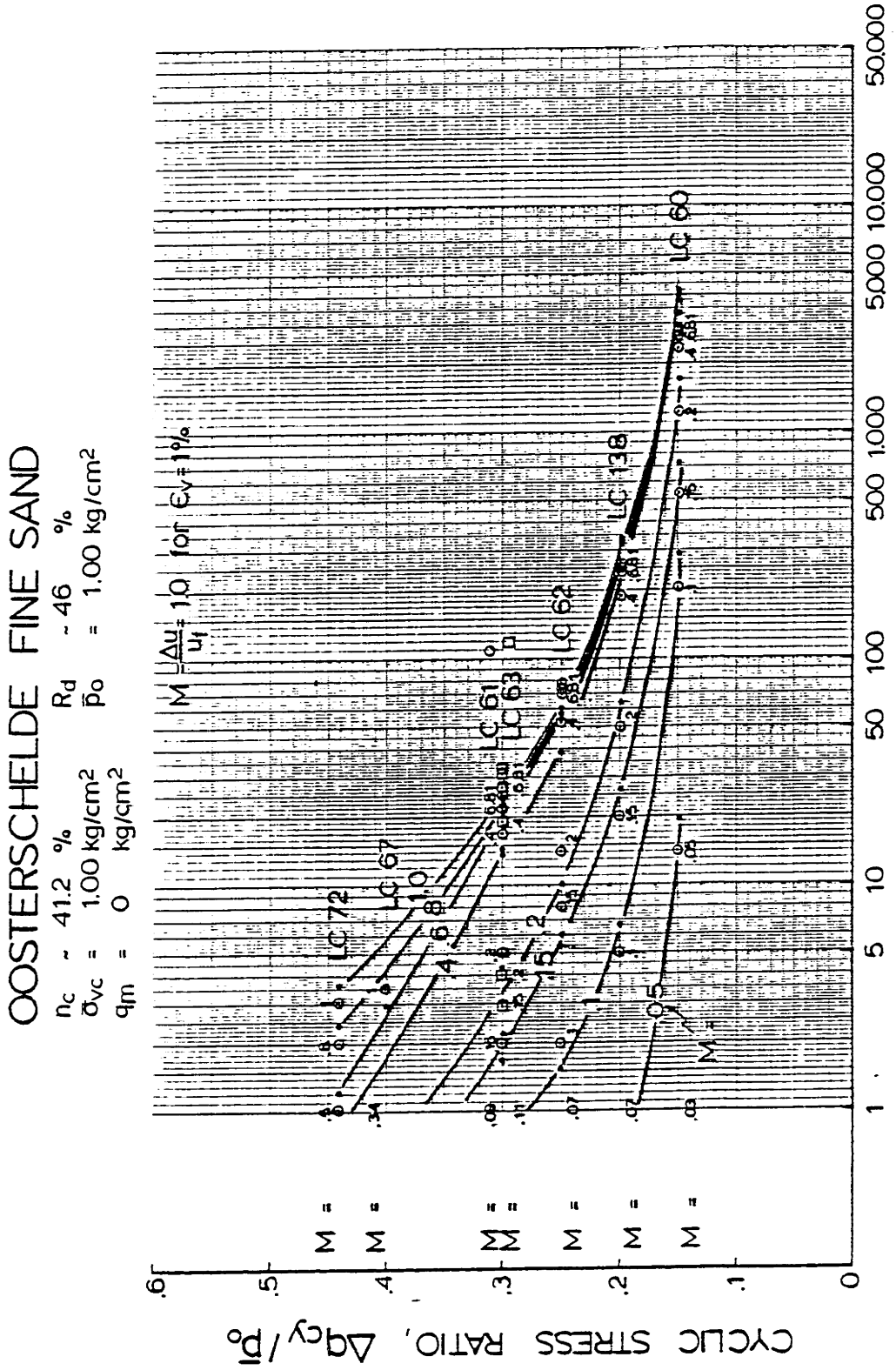

PORE PRESSURE CONTOURS FOR ISOTROPIC CYCLIC TESTS WITH DIFFERENT CYCLIC STRESS RATIOS

FIGURE IV-25

OOSTERSCHELDE FINE SAND

n_c ~ 41.2%, R_d ~ 46%, $\Delta q_{cy}/\bar{p}_o$ = 0.26, $q_m/\bar{p}_o$ = 0.33

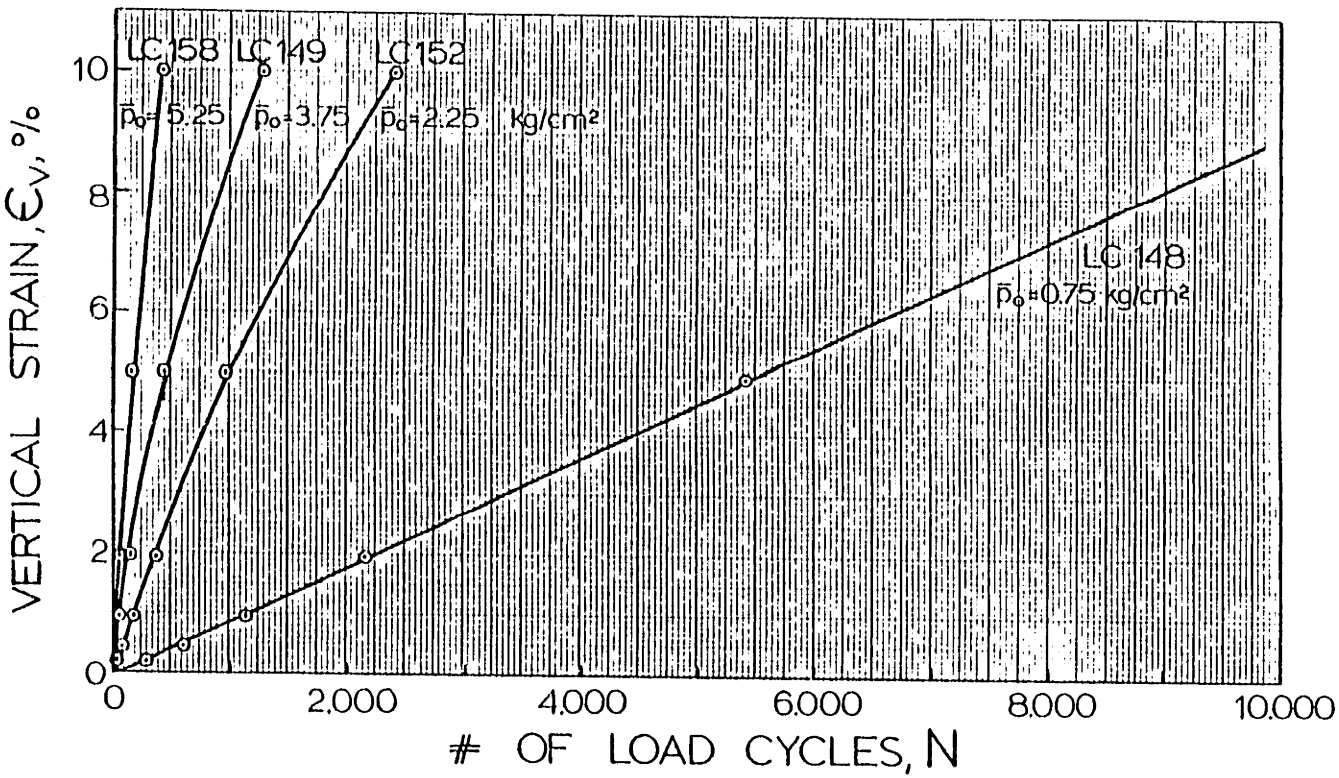

INFLUENCE OF MEAN NORMAL STRESS ON STRAIN DEVELOPMENT IN CYCLIC COMPRESSION TESTS

FIGURE IV-26

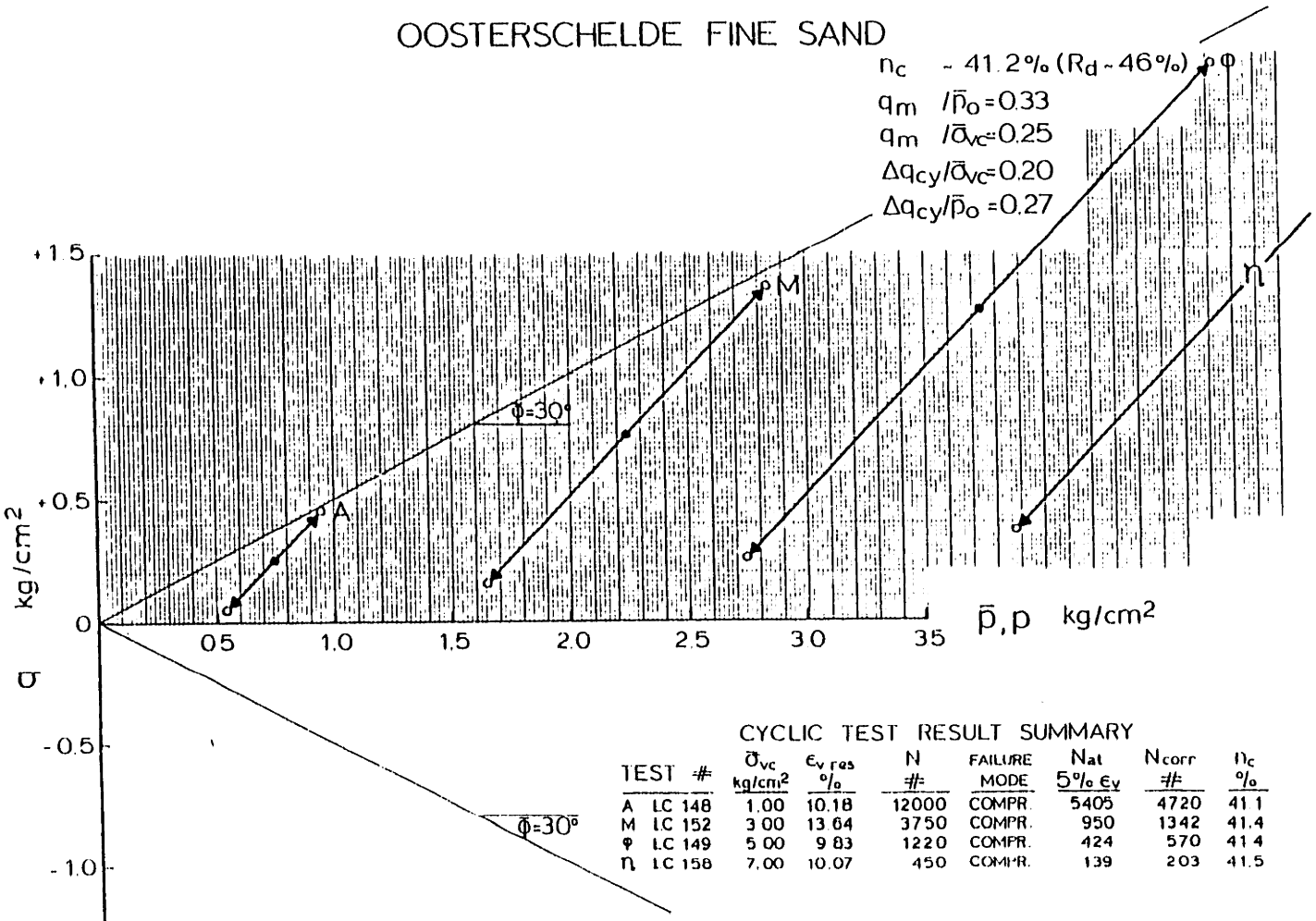

CYCLIC TEST RESULT SUMMARY

TEST #	$\bar{\sigma}_{vc}$ kg/cm²	$\epsilon_{v\,res}$ %	N #	FAILURE MODE	N_{at} 5% ϵ_v	N_{corr} #	n_c %
A LC 148	1.00	10.18	12000	COMPR.	5405	4720	41.1
M LC 152	3.00	13.64	3750	COMPR.	950	1342	41.4
φ LC 149	5.00	9.83	1220	COMPR.	424	570	41.4
η LC 158	7.00	10.07	450	COMPR.	139	203	41.5

FIGURE IV-27 TOTAL STRESS PATHS (TSP-u_B) FOR ANISOTROPIC CYCLIC TESTS WITH DIFFERENT MEAN NORMAL STRESS, $\bar{p}_o$

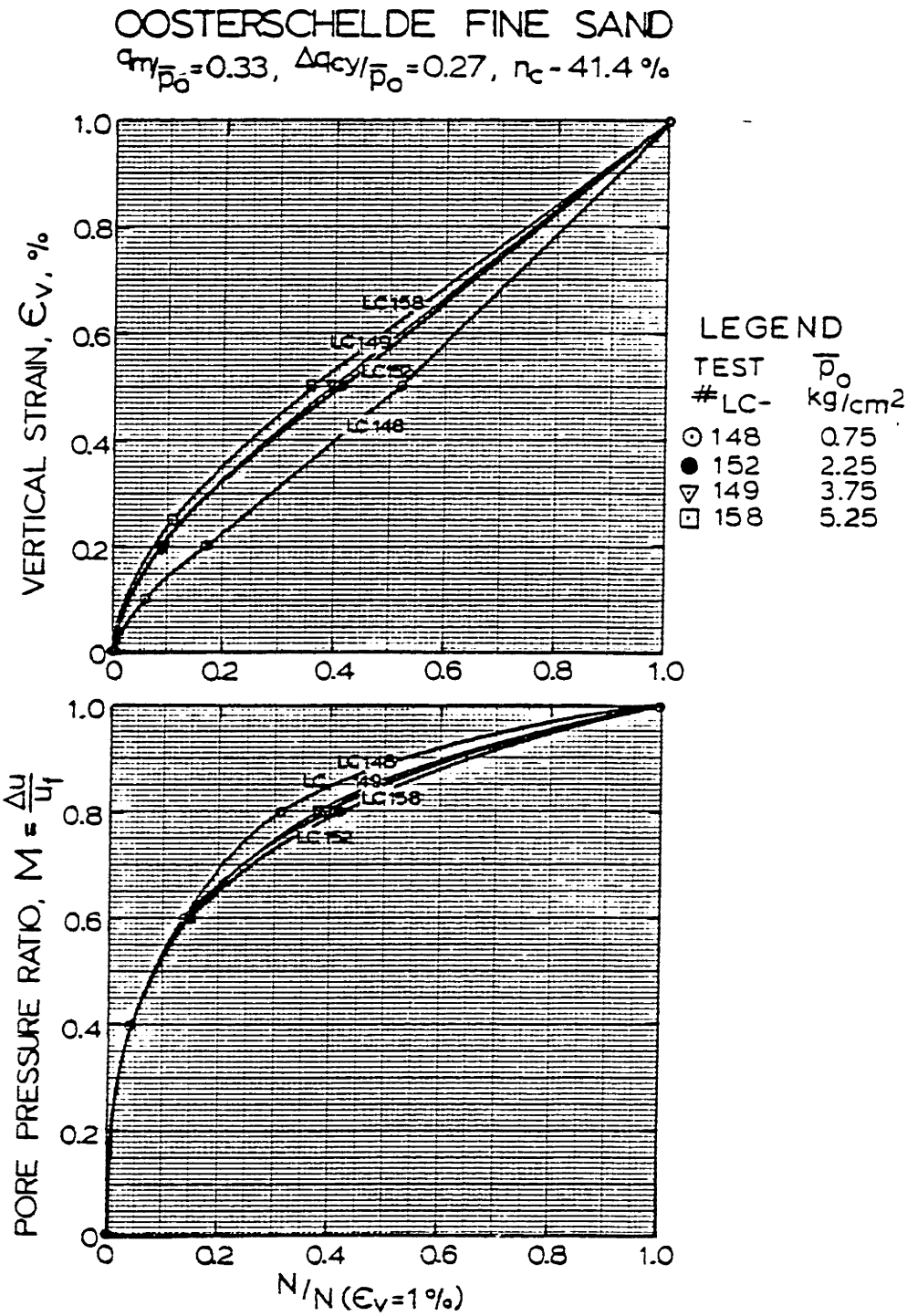

NORMALIZED STRAIN AND PORE PRESSURE DEVELOPMENT FOR CYCLIC COMPRESSION TESTS WITH DIFFERENT MEAN NORMAL STRESSES, $\bar{p}_o$

FIGURE IV-28

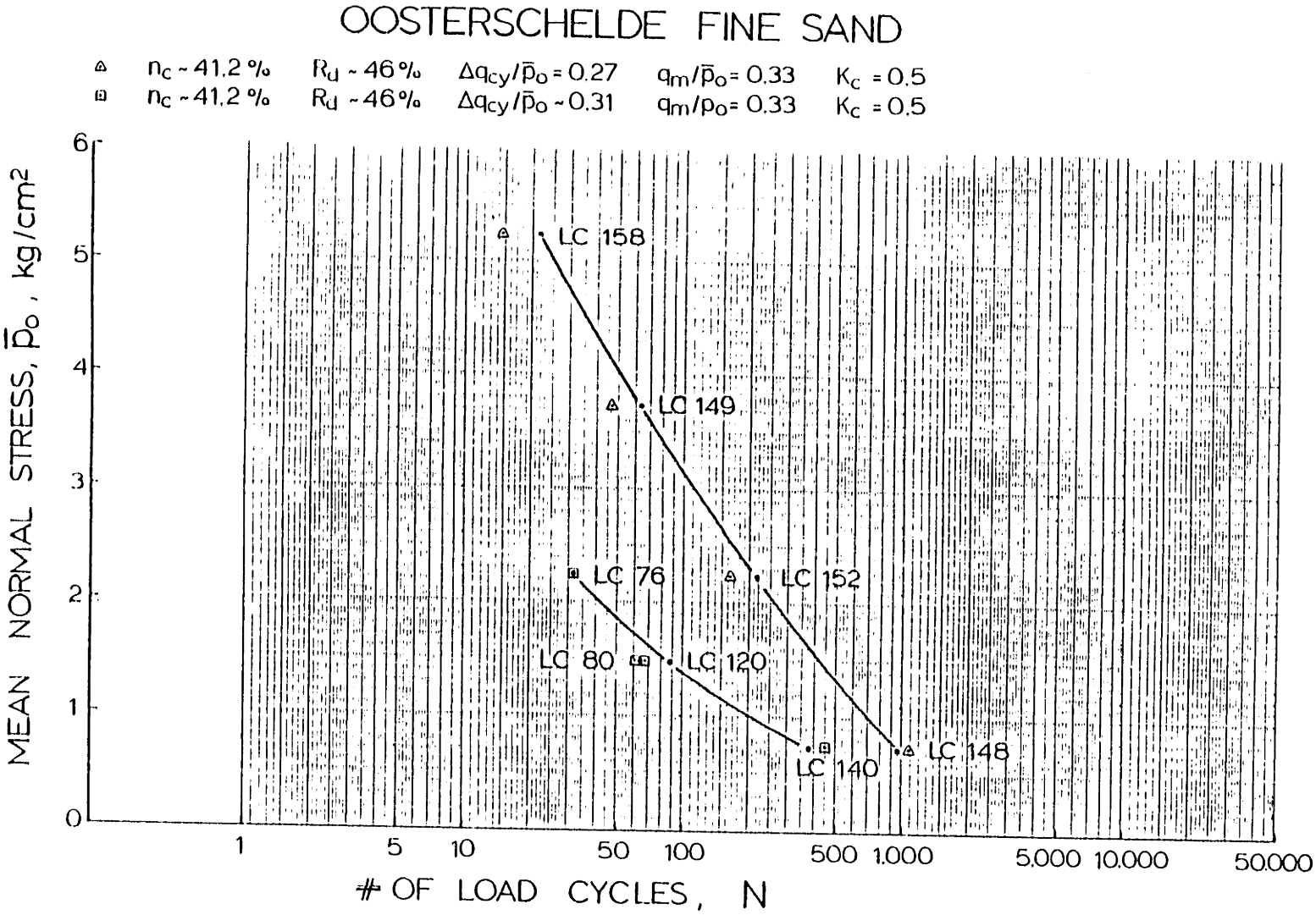

FIGURE TE29

INFLUENCE OF MEAN NORMAL STRESS ON NUMBER OF LOAD CYCLES TO REACH 1% VERTICAL STRAIN IN CYCLIC TRIAXIAL COMPRESSION TESTS UNDER VARIOUS CONDITIONS

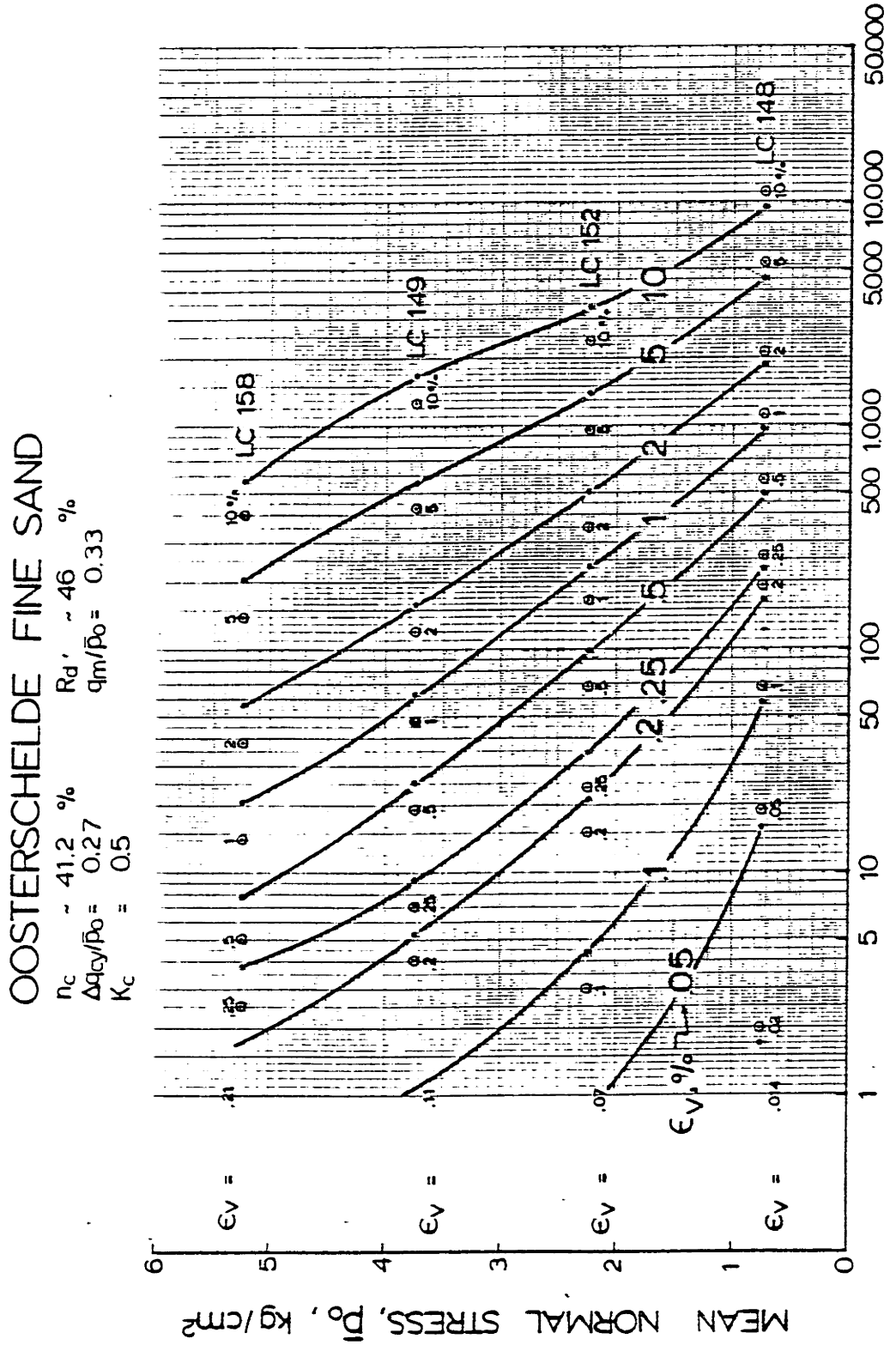

STRAIN CONTOURS FOR COMPRESSION CYCLIC TESTS WITH DIFFERENT MEAN NORMAL STRESSES

FIGURE IV-30

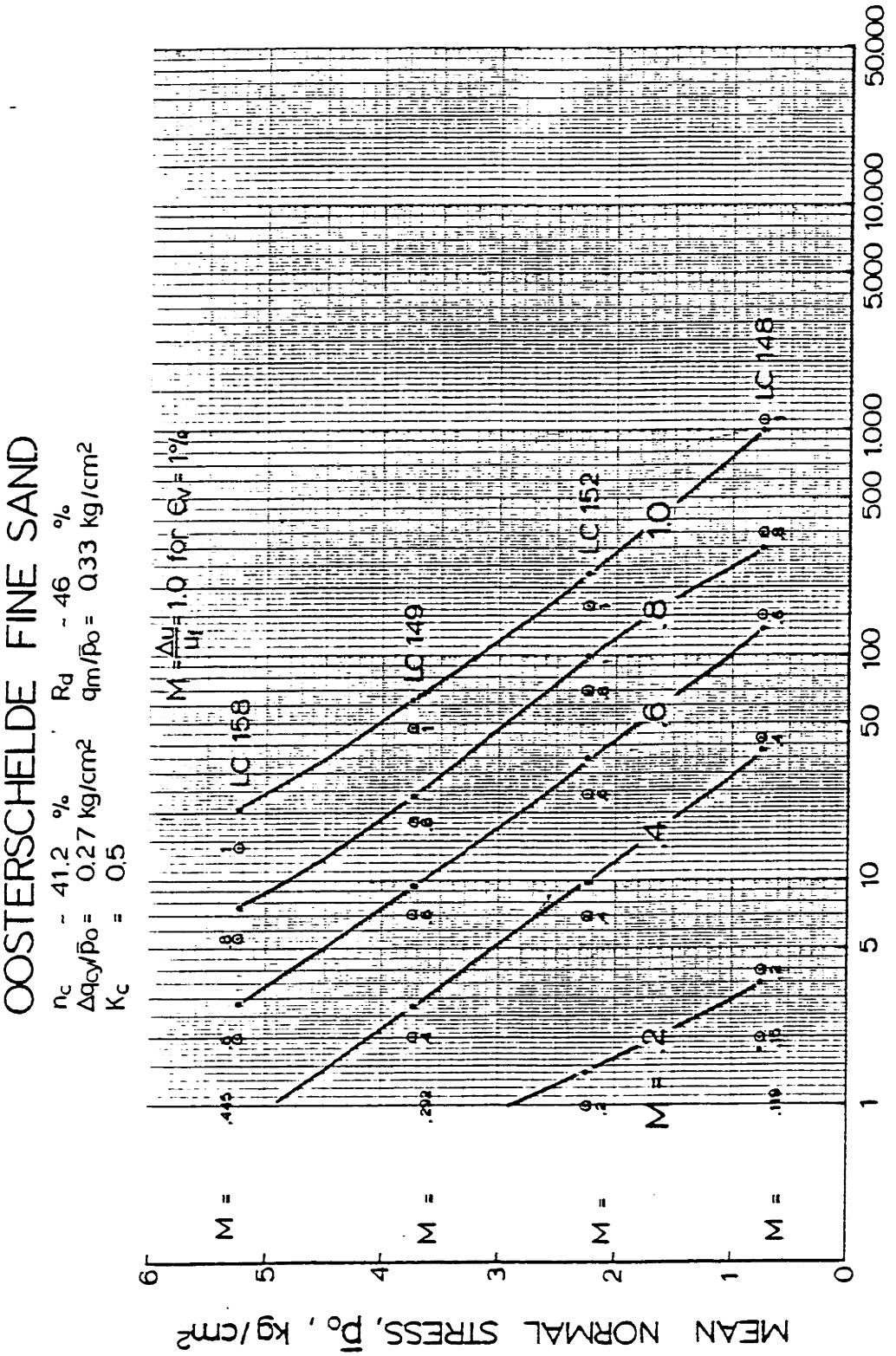

PORE PRESSURE CONTOURS FOR COMPRESSION CYCLIC TESTS WITH DIFFERENT MEAN NORMAL STRESSES

FIGURE IV-31

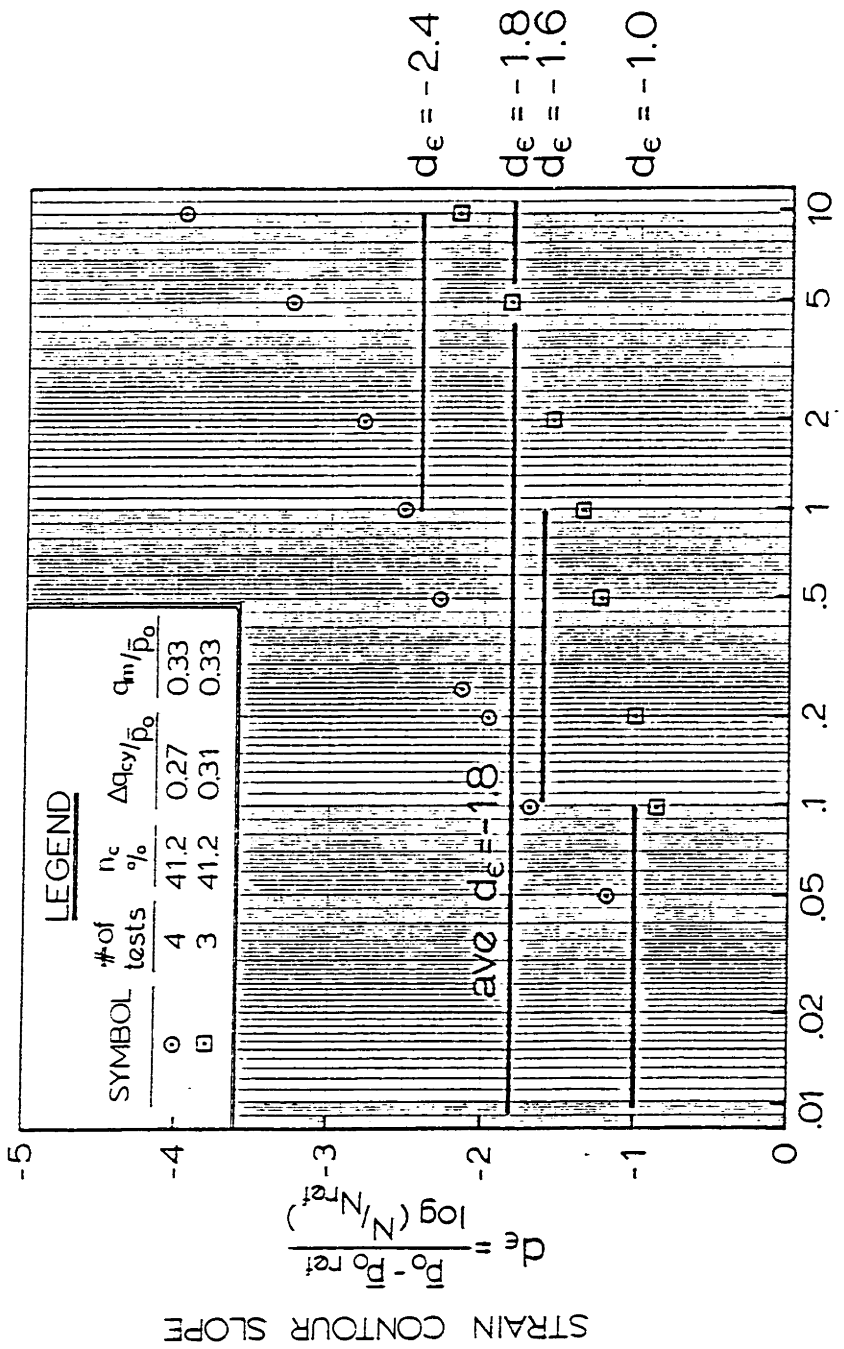

VARIATION IN THE SLOPE OF STRAIN CONTOURS FOR CYCLIC COMPRESSION TESTS AT DIFFERENT MEAN NORMAL STRESS

FIGURE IV-32

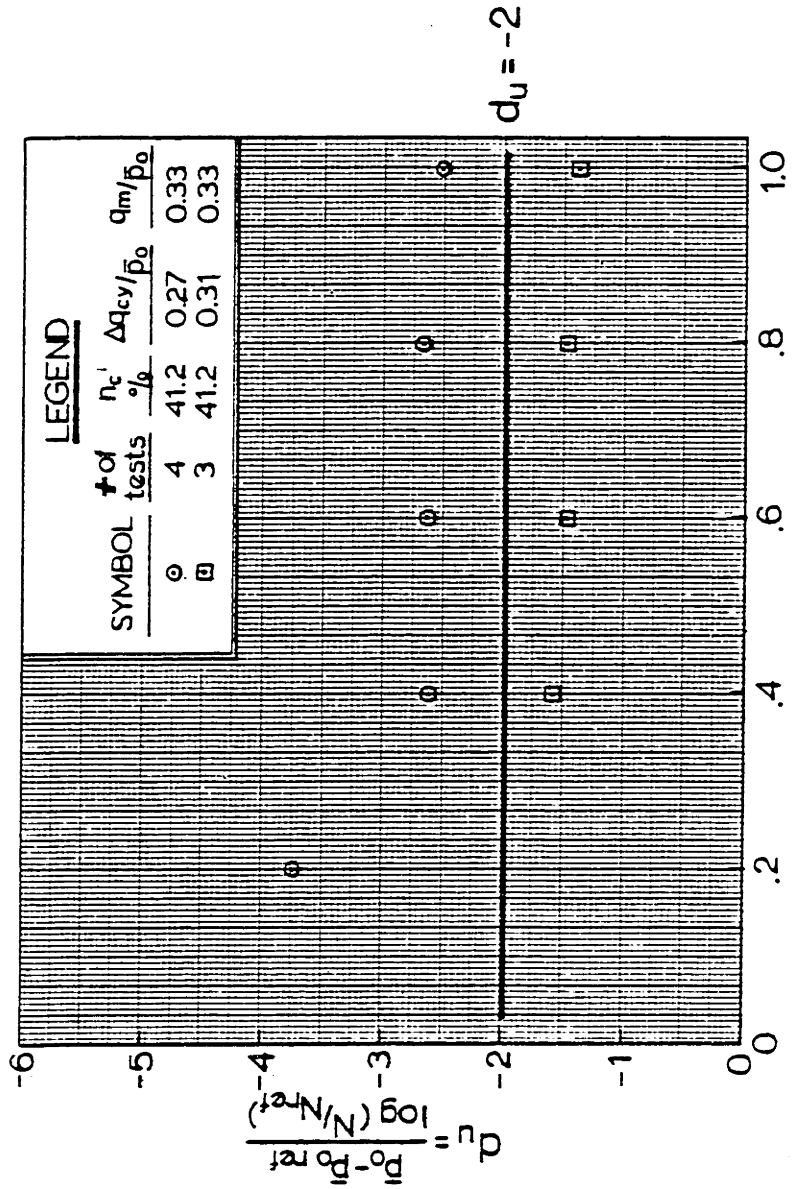

VARIATION IN THE SLOPE OF PORE PRESSURE CONTOURS FOR CYCLIC COMPRESSION TESTS AT DIFFERENT MEAN NORMAL STRESS

FIGURE IV-33

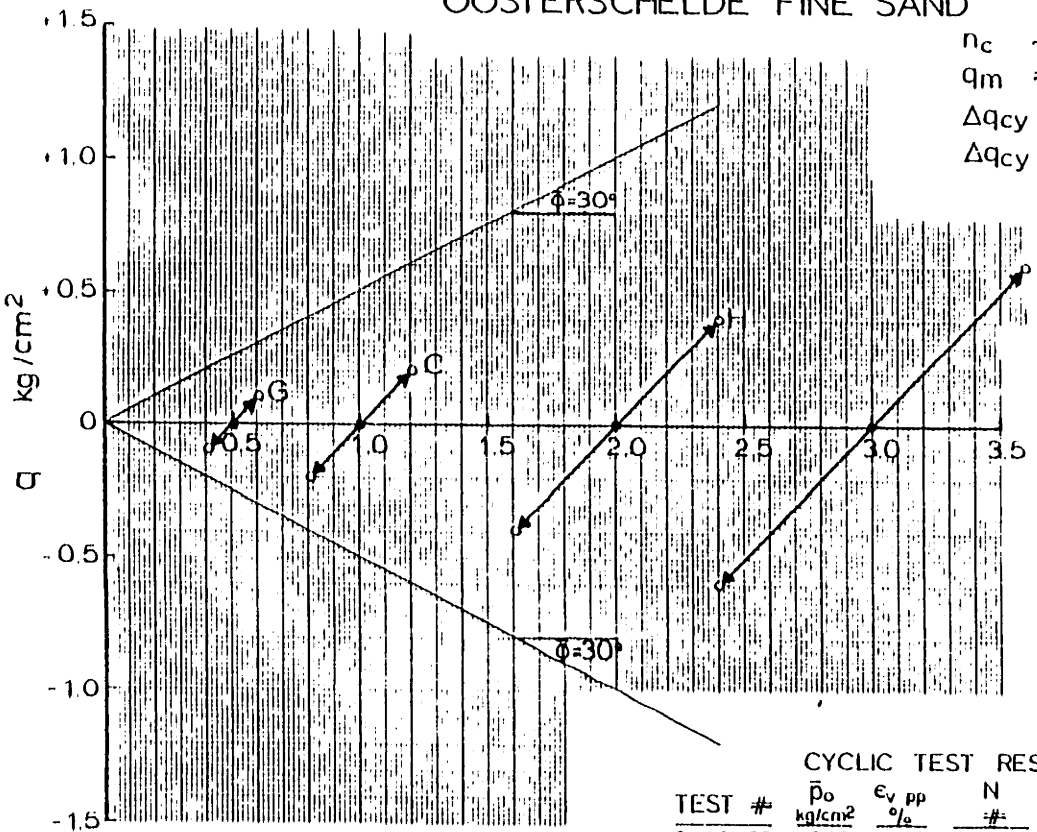

CYCLIC TEST RESULT SUMMARY

TEST #	$\bar{p}_o$ kg/cm²	$\epsilon_{v\,pp}$ %	N #=	FAILURE MODE	N_{at} 5% ϵ_v	N_{corr} #=	n_c %
G LC 78.	0.50	17.70	540	DEF.	536	548	41.2
C LC 138	1.00	14.14	260	DEF.	259	341	41.4
H LC 139	2.00	10.99	70	DEF.	69	97	41.5
I LC 73	3.00	21.20	39	DEF.	34	35	41.2
Σ LC 146	5.00	13.25	21	DEF.	20	31	41.5

TOTAL STRESS PATHS (TSP-u_B) FOR ISOTROPIC CYCLIC TESTS WITH DIFFERENT MEAN NORMAL STRESS, $\bar{p}_o$

FIGURE IV-34

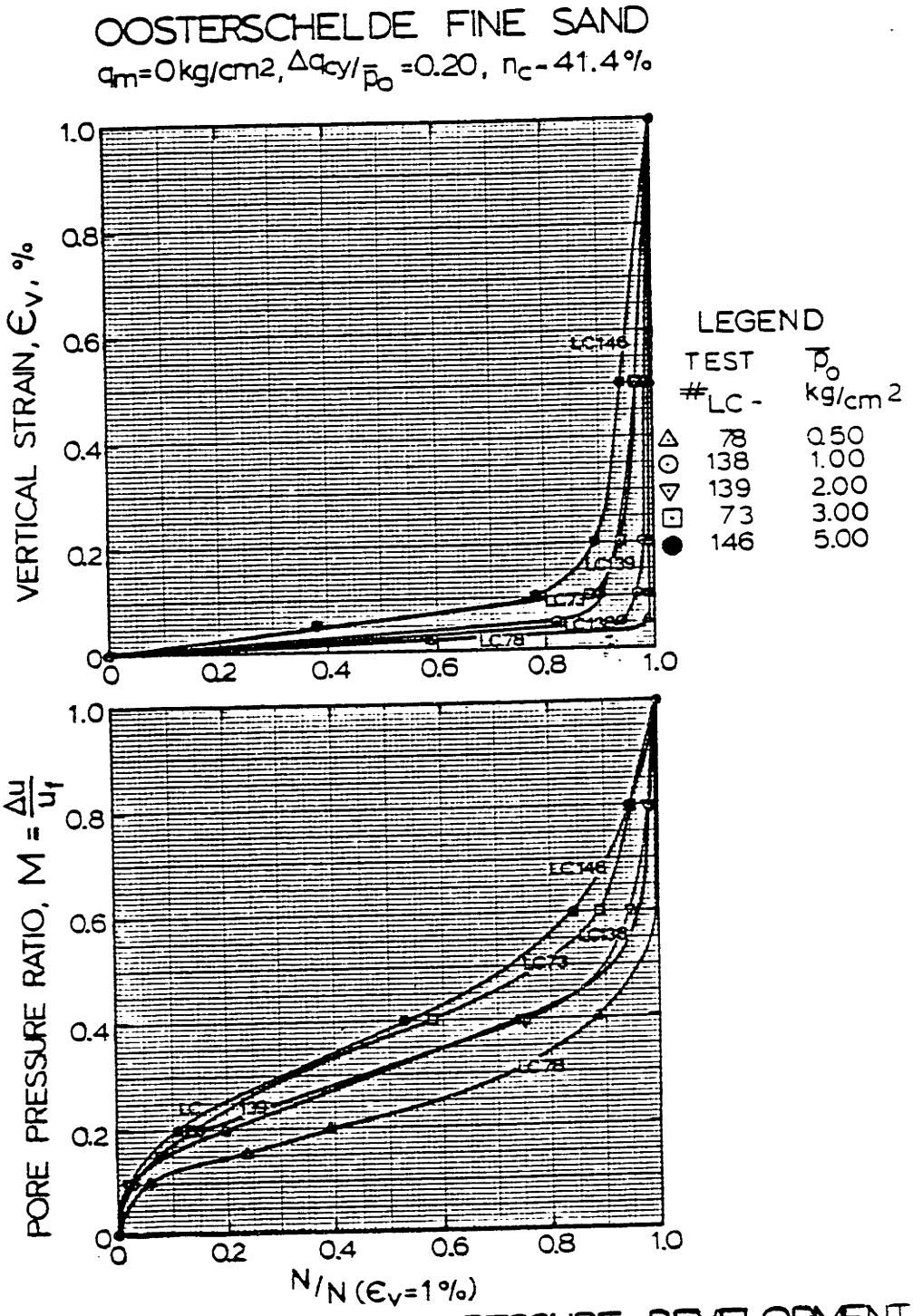

NORMALIZED STRAIN AND PORE PRESSURE DEVELOPMENT FOR CYCLIC ISOTROPIC TESTS WITH DIFFERENT MEAN NORMAL STRESSES, $\bar{p}_o$

FIGURE IV-35

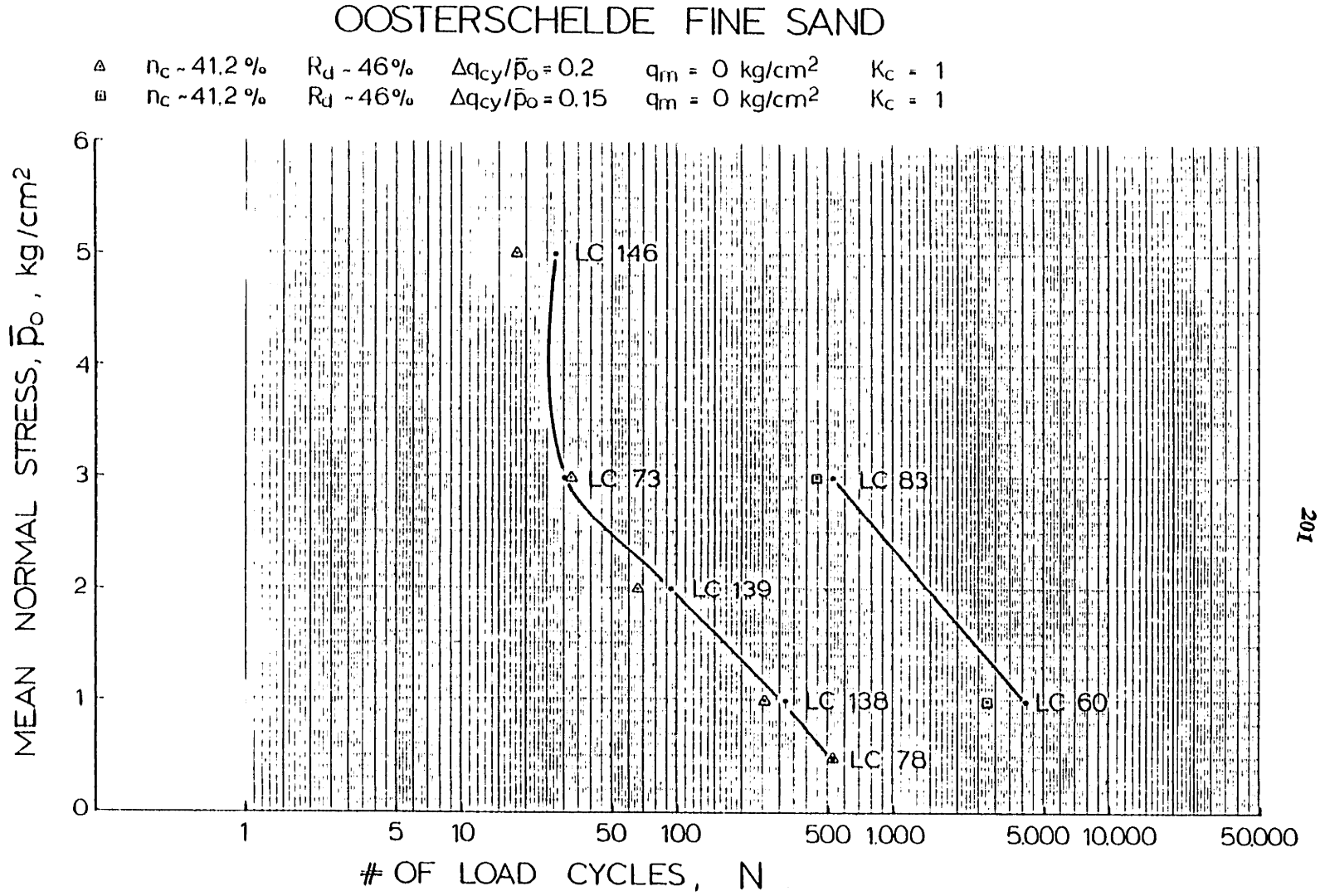

INFLUENCE OF MEAN NORMAL STRESS ON NUMBER OF LOAD CYCLES TO REACH 1% VERTICAL STRAIN IN CYCLIC TRIAXIAL ISOTROPIC TESTS UNDER VARIOUS CONDITIONS

FIGURE IV-36

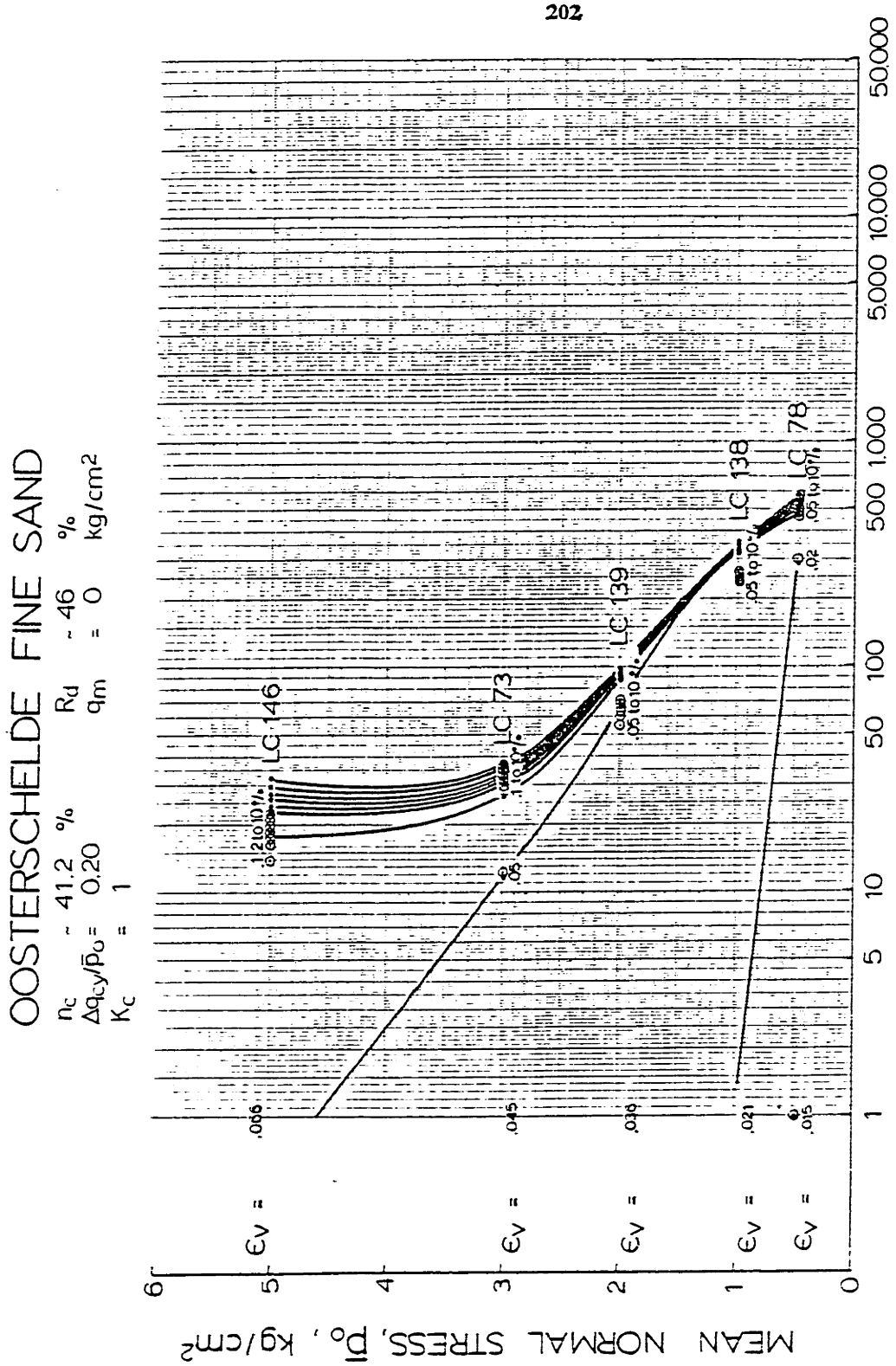

STRAIN CONTOURS FOR ISOTROPIC CYCLIC TESTS WITH DIFFERENT MEAN NORMAL STRESSES

FIGURE IV-37

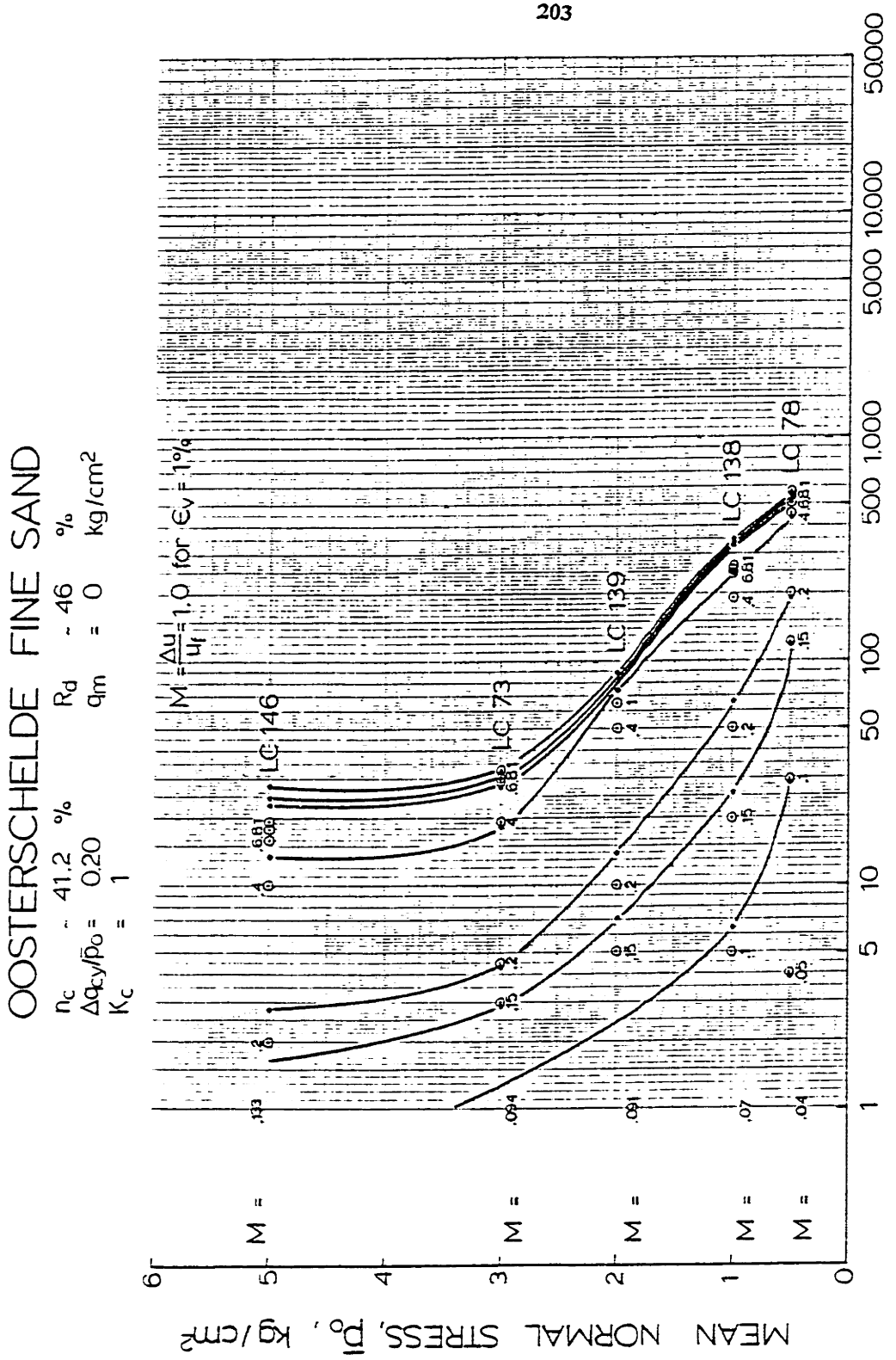

FIGURE IV-38

PORE PRESSURE CONTOURS FOR ISOTROPIC CYCLIC TESTS WITH DIFFERENT MEAN NORMAL STRESSES

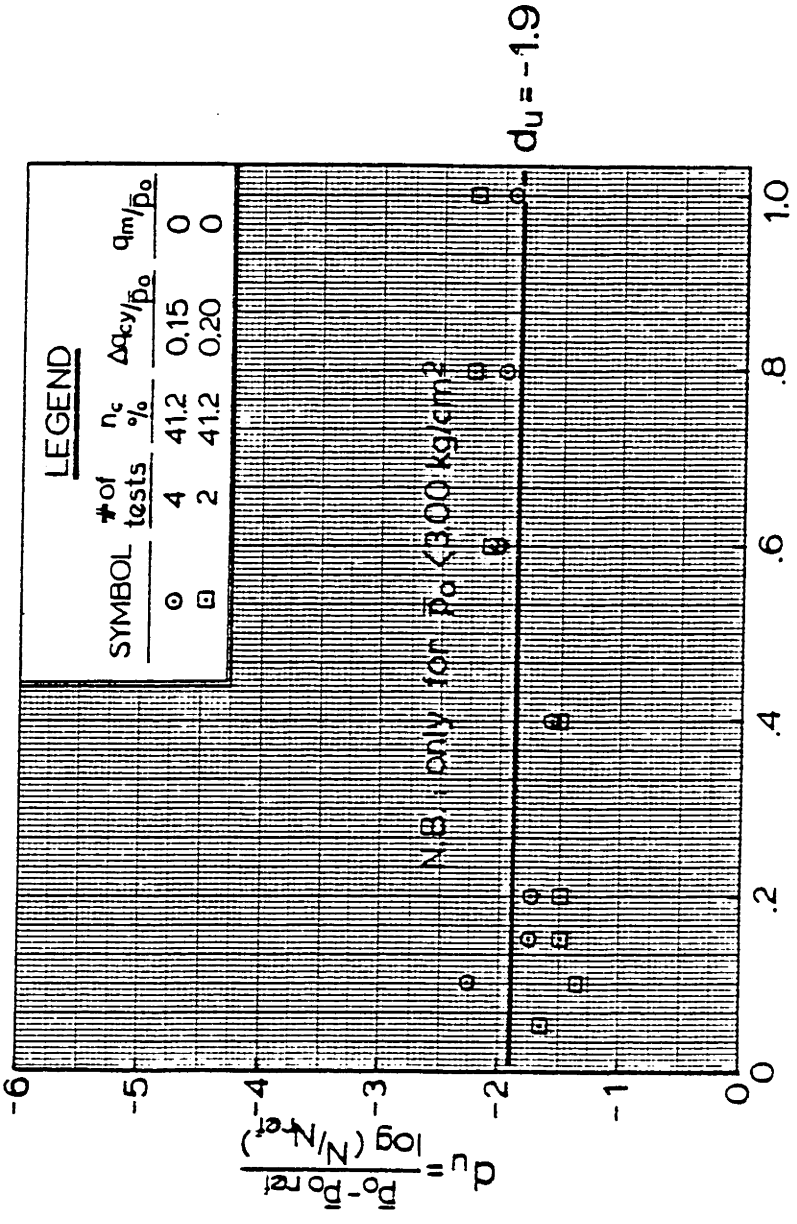

VARIATION IN THE SLOPE OF PORE PRESSURE CONTOURS FOR ISOTROPIC CYCLIC TESTS AT DIFFERENT MEAN NORMAL STRESS

FIGURE IV-39

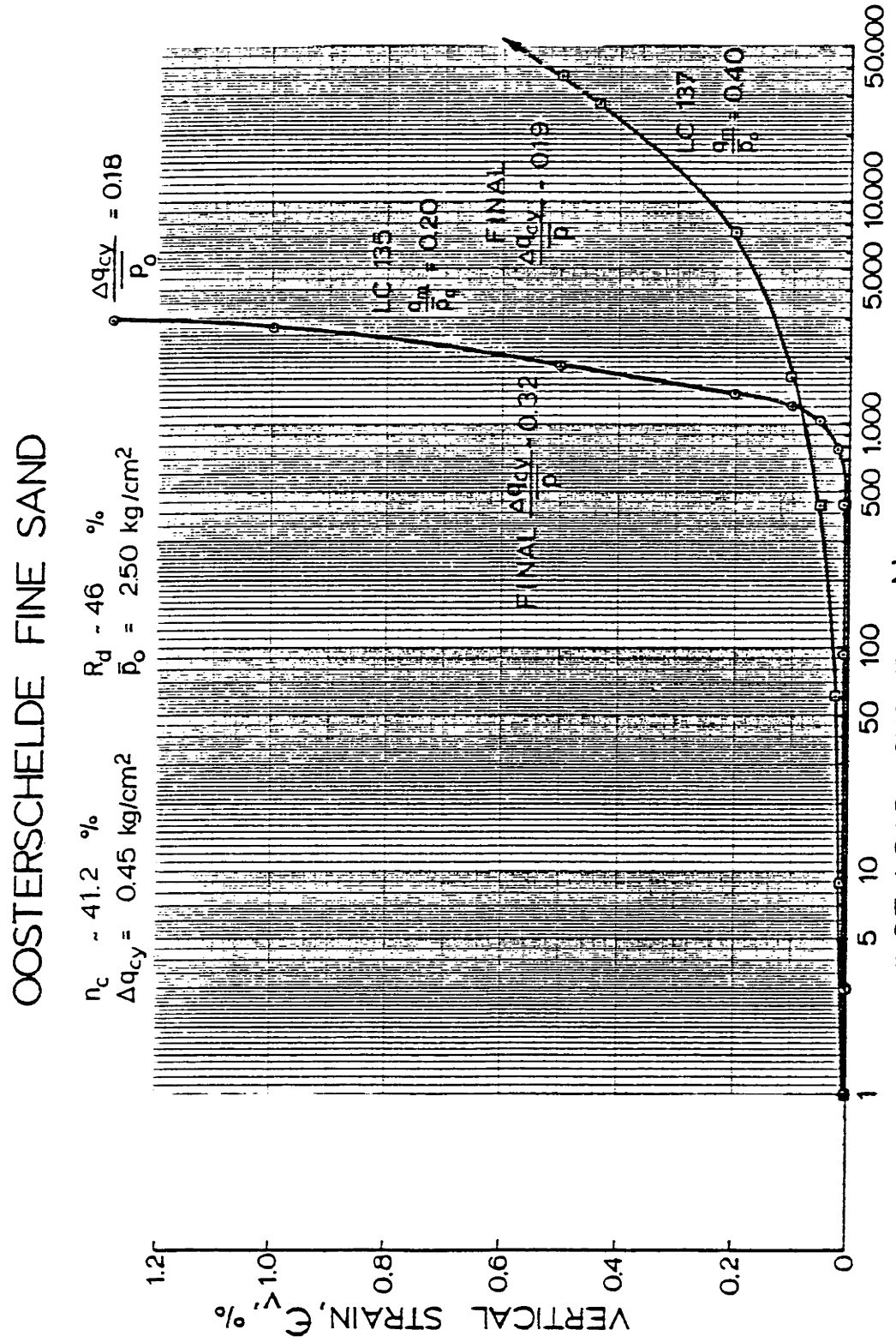

STRAIN DEVELOPMENT IN CYCLIC COMPRESSION TESTS WITH DIFFERENT MEAN SHEAR STRESS RATIOS

FIGURE IV-40

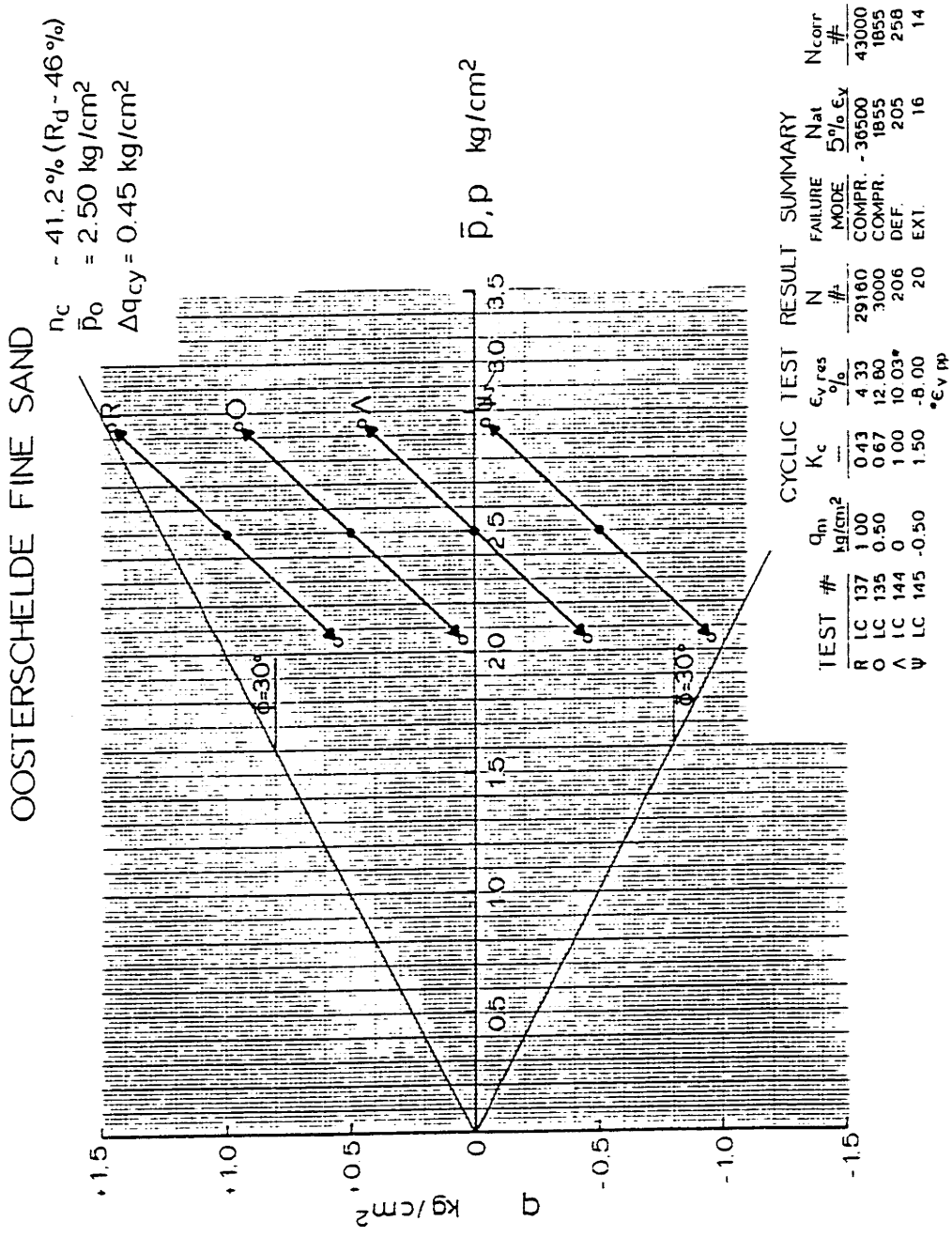

TOTAL STRESS PATHS (TSP-u_B) FOR CYCLIC TESTS
WITH DIFFERENT MEAN SHEAR STRESS, $q_m/\bar{p}_o$

FIGURE IV-41

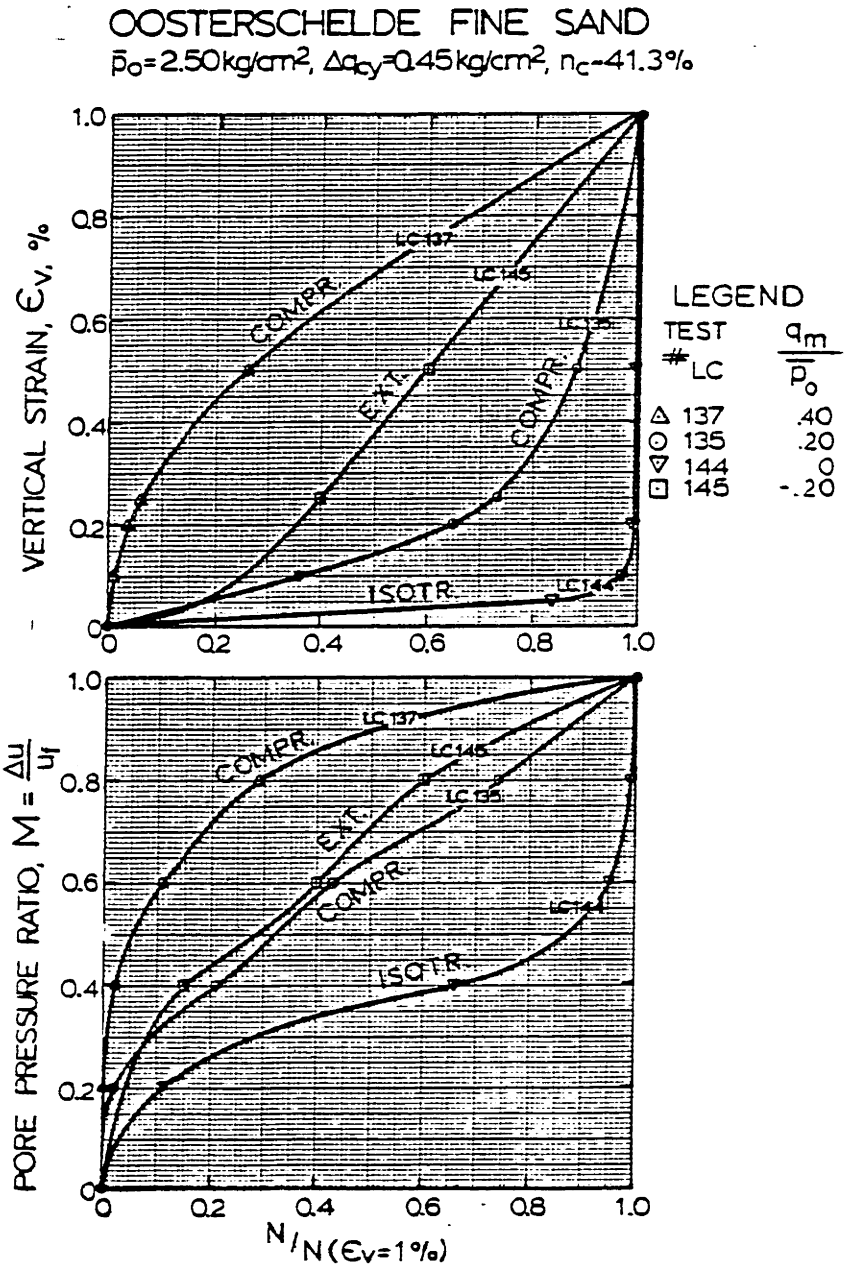

NORMALIZED STRAIN AND PORE PRESSURE DEVELOPMENT FOR CYCLIC TESTS WITH DIFFERENT MEAN SHEAR STRESSES, q_m

FIGURE IV-42

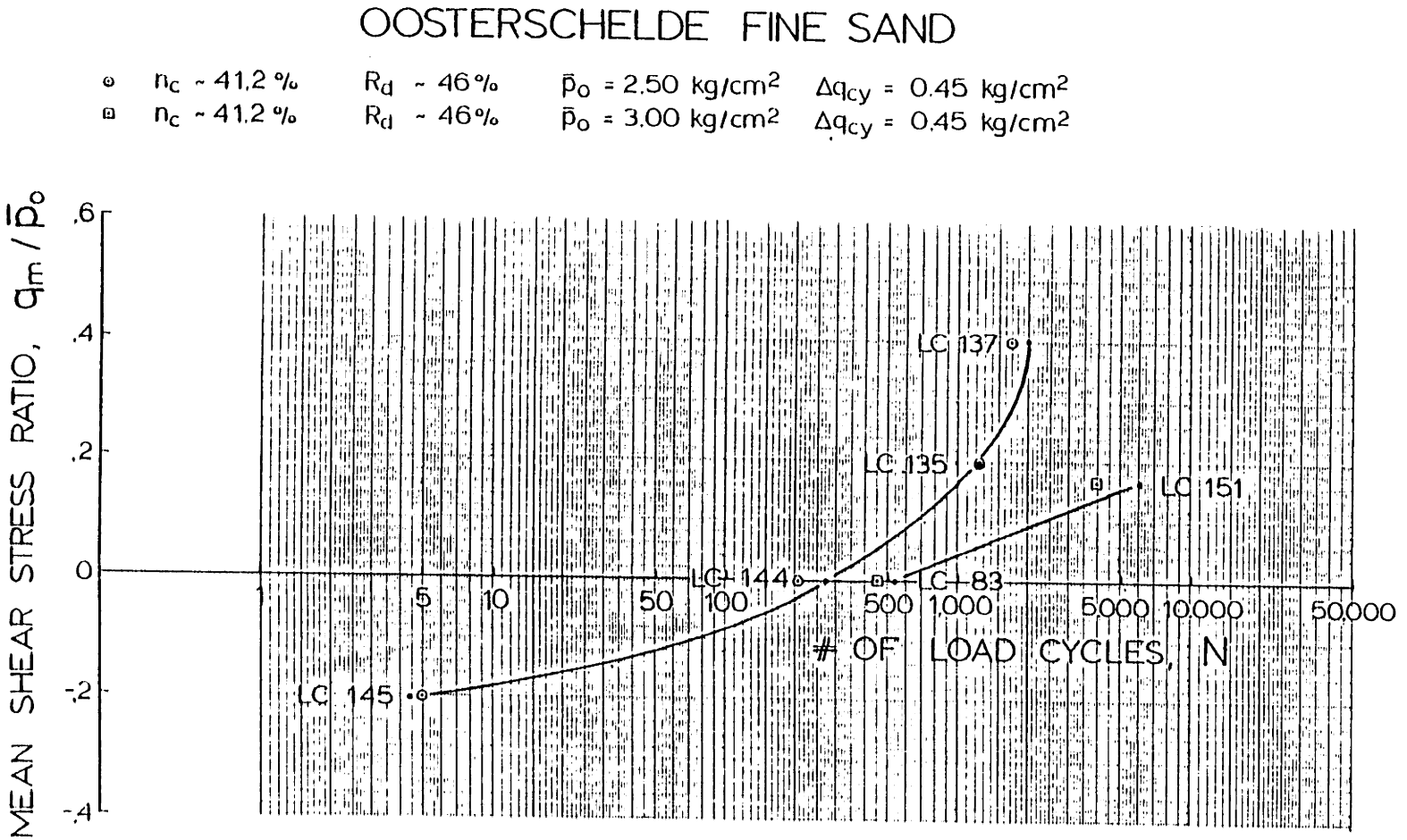

FIGURE IV-43

INFLUENCE OF MEAN SHEAR STRESS RATIO ON NUMBER OF LOAD CYCLES TO REACH 1% VERTICAL STRAIN IN CYCLIC TRIAXIAL TESTS UNDER DIFFERENT CONDITIONS

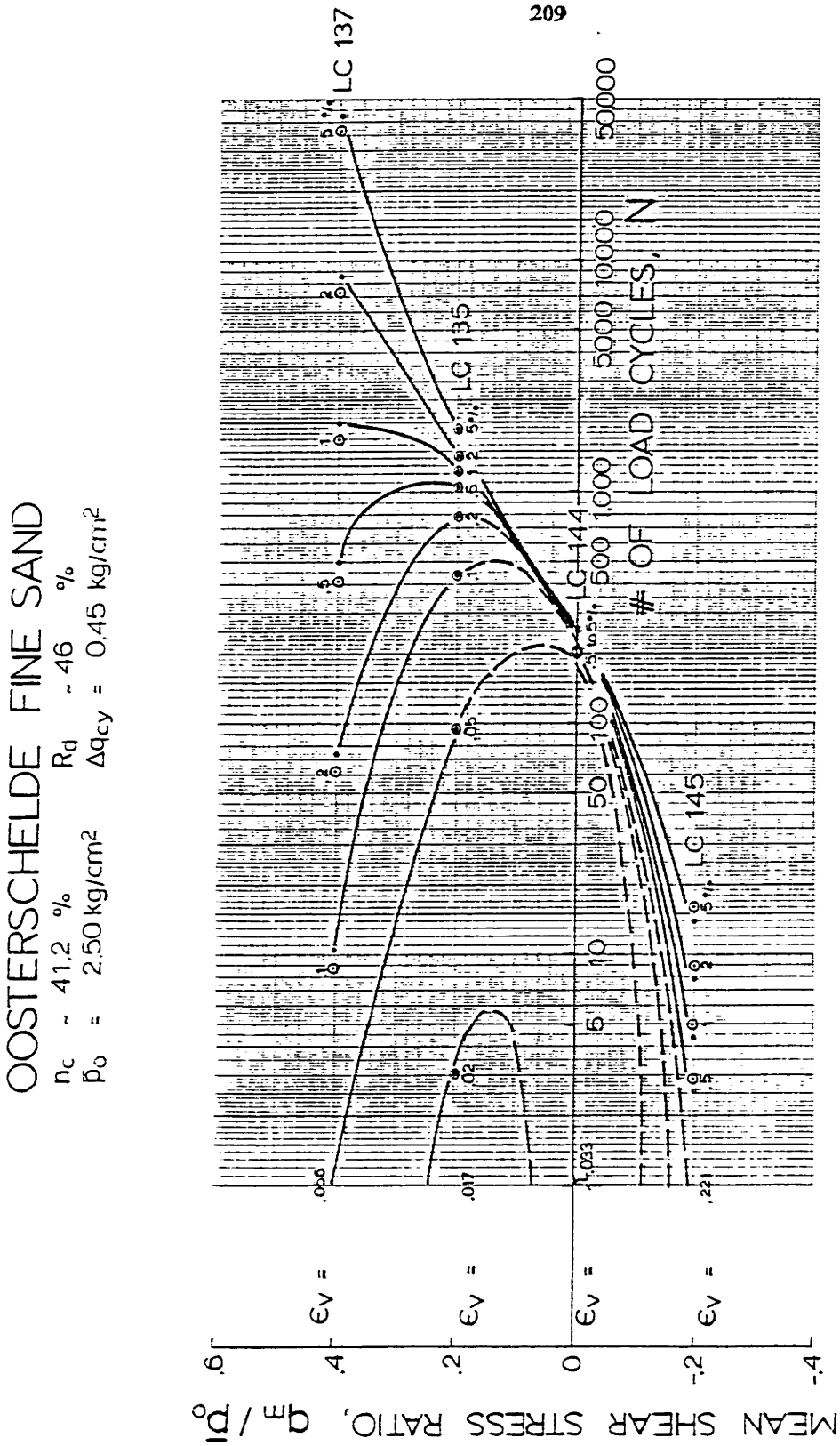

STRAIN CONTOURS FOR CYCLIC TRIAXIAL TESTS WITH DIFFERENT MEAN SHEAR STRESS RATIOS

FIGURE IV-44

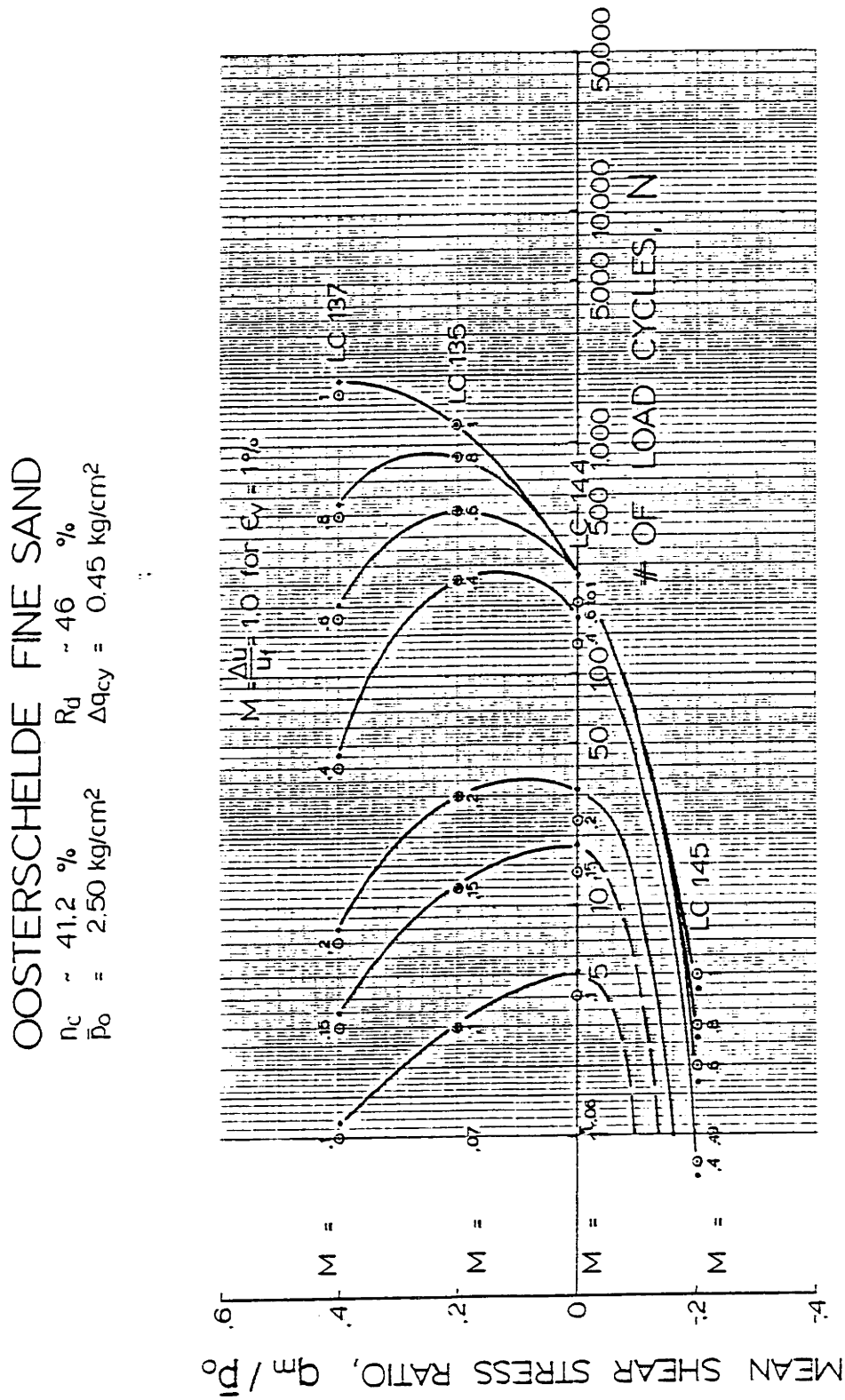

PORE PRESSURE CONTOURS FOR CYCLIC TRIAXIAL TESTS WITH DIFFERENT MEAN SHEAR STRESS RATIOS

FIGURE IV-45

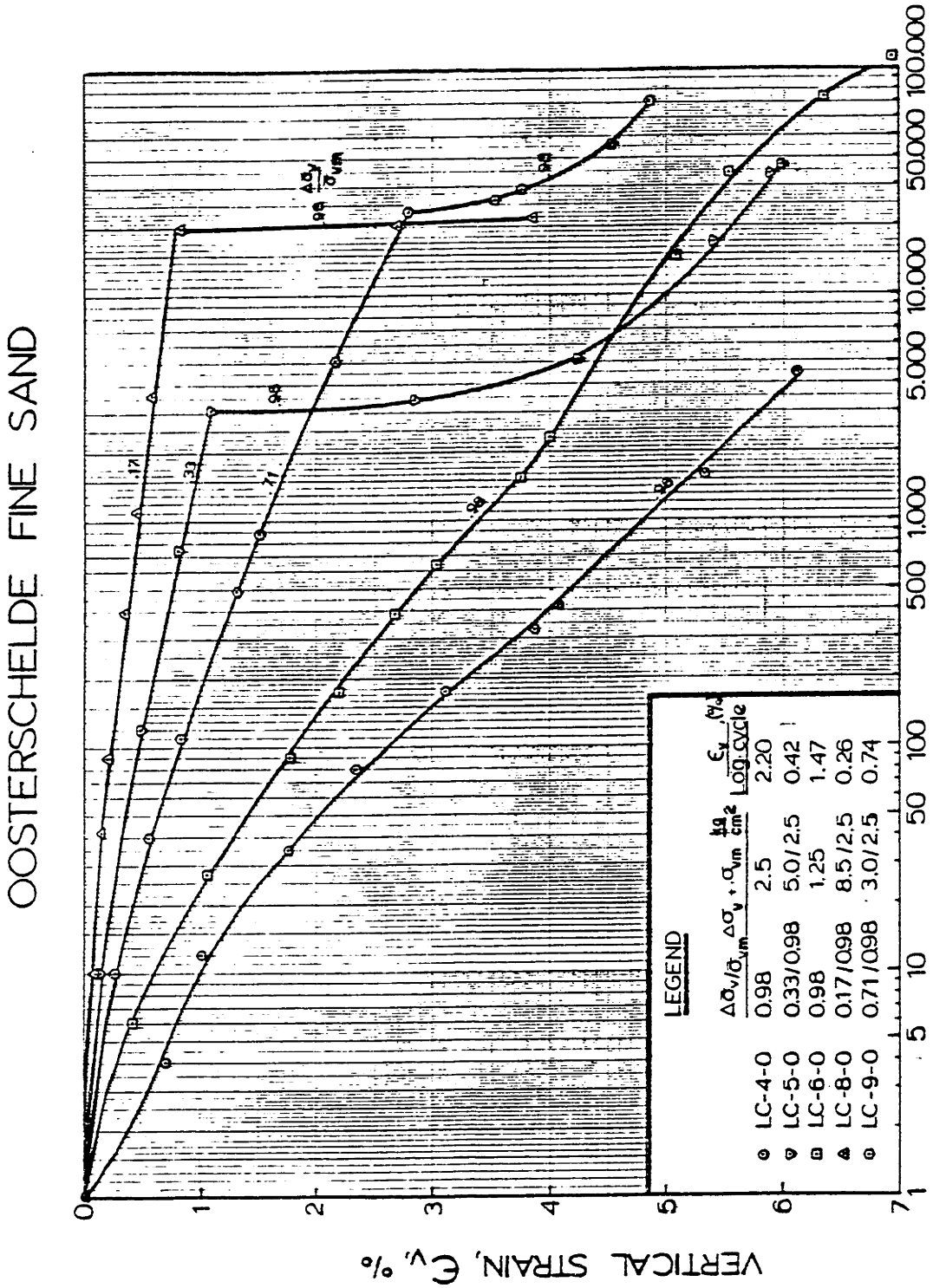
OOSTERSCHELDE FINE SAND
VERTICAL STRAIN, ε_v, %
OF LOAD CYCLES, N
SUMMARY OF CYCLIC OEDOMETER TESTS
LEGEND
$\Delta\sigma_v/\sigma_{vm}$ $\Delta\sigma_v + \sigma_{vm}$ kg/cm² ε_v (%) Log cycle
LC-4-0 0.98 2.5 2.20
LC-5-0 0.33/0.98 5.0/2.5 0.42
LC-6-0 0.98 1.25 1.47
LC-8-0 0.17/0.98 8.5/2.5 0.26
LC-9-0 0.71/0.98 3.0/2.5 0.74

FIGURE IV-46

Chapter V

PREDICTION OF STRAIN AND PORE PRESSURE FOR UNDRAINED CYCLIC LOADING

The influence of porosity, cyclic shear stress, mean normal stress, mean shear stress and the number of load cycles on the development of strain and pore pressure in cyclic triaxial tests was quantified in Chapter IV. In this chapter, the relationships established among these variables and strain and pore pressure are incorporated into an overall procedure for predicting strain and pore pressure in cyclic triaxial tests.

If the number of variables in cyclic compression tests is limited to the ones described above, it follows that:

$$\varepsilon_v = f(N, q_m/\bar{p}_o, \bar{p}_o, \Delta q_{cy}/\bar{p}_o, n) \qquad \text{Eq. V.1}$$

and

$$M = g(N, q_m/\bar{p}_o, \bar{p}_o, \Delta q_{cy}/\bar{p}_o, n) \qquad \text{Eq. V.2}$$

For cyclic isotropic tests the expressions are analogous, but without the term $q_m/\bar{p}_o$.

In Chapter IV were found that for most variables, strain and pore pressure contours were approximately linear and parallel when plotted in semi-logarithmic plots of stress or

porosity versus log N. In order to exploit this mathematical advantage, Equation V.1 and V.2 were inverted to obtain:

$$N = f'(\varepsilon_v, q_m/\bar{p}_o, \bar{p}_o, \Delta q_{cy}/\bar{p}_o, n) \qquad \text{Eq. V.3}$$

and

$$N = g'(M, q_m/\bar{p}_o, \bar{p}_o, \Delta q_{cy}/\bar{p}_o, n) \qquad \text{Eq. V.4}$$

The functional form of Equations V.3 and V.4 may be complex and of little use unless independence of variables can be established. The discussion in Chapter IV and test results like Figure IV.5, IV.6 and IV.7 indicated that for all different combinations of ε_v, $q_m/\bar{p}_o$, $\bar{p}_o$, $\Delta q_{cy}/\bar{p}_o$ and M, the relationships between porosity and log number of cycles were linear and parallel. This result implies that porosity can be treated as an independent variable. Similarly, other sections of Chapter IV showed that $\Delta q_{cy}/\bar{p}_o$ and $\bar{p}_o$ also can be treated as independent variables. The above equations can therefore be rewritten with these three factors separated from the main functions:

$$N = f''(\varepsilon_v, q_m/\bar{p}_o) \cdot r(n) \cdot s(\Delta q_{cy}/\bar{p}_o) \cdot t(\bar{p}_o) \qquad \text{Eq. V.5}$$

and

$$N = g''(M, q_m/\bar{p}_o) \cdot r'(n) \cdot s'(\Delta q_{cy}/\bar{p}_o) \cdot t'(\bar{p}_o) \qquad \text{Eq. V.6}$$

This means that the effects of porosity, cyclic shear stress ratio and mean consolidation stress can be treated individually and independently from the other factors influencing strain and pore pressure behavior. Their functional forms will resemble the log-linear functions found in Chapter IV. Chapter IV also showed that the relationship among log N, ε_v and $q_m/\bar{p}_o$ is not linear, so another way to relate them must be found.

Note that the following prediction method is based upon test results from contractive tests only, and there are not enough test results available to prove validity for samples that liquefy or dilate under cyclic loading. The first step in the prediction procedure will therefore be to check if the test conditions to be predicted for (porosity and cyclic shear stress ratio) are within the contractive range in Figure II.7.

5.1 Cyclic Compression Tests

Assume two identical cyclic tests except for porosity (and then, of course, the number of cycles required to reach specified strain values), one characterized by the subscript 1, the other by 2. From Equation V.5 follows:

$$\frac{N_1}{N_2} = \frac{f(\varepsilon_{v1},\ q_m/\bar{p}_o)}{F(\varepsilon_{v2},\ q_m/\bar{p}_o} \cdot \frac{r(n_1)}{r(n_2)} \qquad \text{Eq. V.7}$$

where terms with $\bar{p}_o$ and $q_{cy}/\bar{p}_o$ in Equation V.5 drop out since

they have identical values in the two tests.

Chapter IV showed that strain contours were straight parallel lines on a plot of log N versus n. This fact tells that Equation V.7 is a logarithmic function, so for the same magnitude of strain in the two tests follows:

$$\frac{N_1}{N_2} = \frac{r(n_1)}{r(n_2)} = 10^{\frac{n_1 - n_2}{a}} \qquad \text{Eq. V.8}$$

Equation V.8 in turns says that if a relationship between strain and number of cycles at some arbitrary reference porosity is available, the relationship between strain and number of cycles for any other porosity can be predicted by the expression

$$N = N_{ref} \cdot 10^{\frac{n - n_{ref}}{a}} \qquad \text{Eq. V.9}$$

which is identical to Equation IV.1 in Chapter IV. Using the same considerations for cyclic shear stress ratio, follows (analog to Equation IV.6):

$$N = N_{ref} \frac{s(\Delta q_{cy}/\bar{p}_o)}{s[(\Delta q_{cy}/\bar{p}_o)_{ref}]} = N_{ref} \cdot 10^{\frac{(\Delta q_{cy}/\bar{p}_o) - (\Delta q_{cy}/\bar{p}_o)_{ref}}{b}} \qquad \text{Eq. V.10}$$

and for mean normal stress (analog to Equation IV.8):

$$N = N_{ref} \frac{t(\bar{p}_o)}{t[(\bar{p}_o)_{ref}]} = N_{ref} \cdot 10^{\frac{\bar{p}_o - \bar{p}_{o\,ref}}{d}} \qquad \text{Eq. V.11}$$

A close examination of these expressions reveals that the effects of porosity, cyclic shear stress and mean normal stress can be accounted for by revising the number of load cycles. The right side of Equations V.9, V.10 and V.11 become correction factors to the reference number of cycles to account for variations of n, $\Delta q_{cy}/\bar{p}_o$ and $\bar{p}_o$ from reference conditions. These corrections will be defined as:

$$C_n \equiv 10^{\frac{n-n_{ref}}{a}} \qquad \text{Eq. V.12}$$

$$C_{\Delta q} \equiv 10^{\frac{(\Delta q_{cy}/\bar{p}_o)-(\Delta q_{cy}/\bar{p}_o)_{ref}}{b}} \qquad \text{Eq. V.13}$$

$$C_{\bar{p}} \equiv 10^{\frac{(\bar{p}_o)-(\bar{p}_o)_{ref}}{d}} \qquad \text{Eq. V.14}$$

where a, b and d are the slopes of the log-linear strain and pore pressure contours found in Chapter IV.

Selecting $n_{ref} = 41\%$, $(\Delta q_{cy}/\bar{p}_o)_{ref} = 0.2$ and $\bar{p}_{o\,ref} = 2.0$ kg/cm^2, the correction factors for both strain and pore pressure can be plotted. These reference values correspond to the mean values of each parameter in the test program. Figure V.1 gives equations and plots for porosity correction

factors. Figure V.2 and V.3 give the same for cyclic stress ratio and mean normal stress correction factors. The interpretation of Equation V.12 is that a test at porosity n, cycled N times, develops as much strain as a test at porosity n_{ref}, cycled N_{ref} times.

Rearranging Equation V.5 gives:

$$\frac{N}{r(n) \cdot s(\Delta q_{cy}/\bar{p}_o) \cdot t(\bar{p}_o)} = f''(\varepsilon_v, q_m/\bar{p}_o)$$

Substituting the correction factors into this equation yields:

$$\frac{N}{C_n \cdot C_{\Delta q} \cdot C_{\bar{p}} \cdot r(n_{ref}) \cdot s[(\Delta q_{cy}/\bar{p}_o)_{ref}] \cdot t[(\bar{p}_o)_{ref}]}$$

$$= f''(\varepsilon_v, q_m/\bar{p}_o)$$

For $n = n_{ref}$, $\Delta q_{cy}/\bar{p}_o = (\Delta q_{cy}/\bar{p}_o)_{ref}$ and $\bar{p}_o = (\bar{p}_o)_{ref}$; $r(n_{ref})$, $s[(\Delta q_{cy}/\bar{p}_o)_{ref}]$ and $t[(\bar{p}_o)_{ref}]$ will all be equal to 1, and the above equation reduces to

$$\frac{N}{C_n \cdot C_{\Delta q} \cdot C_{\bar{p}}} = f'''(\varepsilon_v, q_m/\bar{p}_o) \qquad \text{Eq. V.15}$$

which is the equation for tests corrected or "normalized" to the reference conditions.

First examining one value of $q_m/\bar{p}_o$, N versus ε_v is measured in a test as shown in Figure V.4. The number

of cycles can now be normalized to reference conditions by dividing N with $C_n \cdot C_{\Delta q} \cdot C_{\bar{p}}$ to obtain the reference curve shown in Figure V.4. If additional tests at the same $q_m/\bar{p}_o$ but various porosities, cyclic stress ratios and mean consolidation stresses are included, approximately the same reference curve should result because of the approximately log-linear relationships established earlier. Figure V.5 shows that this is indeed the case. Similar curves can be established for other values of $q_m/\bar{p}_o$ with the summarized results shown in Figure V.6. Appendix E gives the data for each value of $q_m/\bar{p}_o$ used to establish the average lines in Figure V.6.

Since prediction of accumulated vertical strain is the goal, Equation V.15 is inverted to

$$\varepsilon_v = f'''(N_\varepsilon, q_m/\bar{p}_o) \qquad \text{Eq. V.16}$$

where

$$N_\varepsilon = N/C_{n\varepsilon'}, C_{\Delta q\varepsilon'}, C_{\bar{p}\varepsilon} \qquad \text{Eq. V.17}$$

Figure V.6 describes the function of Equation V.16. A similar procedure can be followed for residual pore pressure with the result that

$$M = g'''(N_u, q_m/\bar{p}_o) \qquad \text{Eq. V.18}$$

where the function of Equation V.18 is given in Figure V.7. Appendix E contains the detailed results used to arrive at Figure V.7. N_u is equal to $N/C_{nu} \cdot C_{\Delta qu} \cdot C_{\bar{p}u}$.

These equations indicate that generated strain and pore pressure are a function of an normalized number of load cycles (N_ε or N_u) and the mean shear stress ratio ($q_m/\bar{p}_o$). Examination of Figure V.6 indicates that the curves for high shear stress ratios cross the ones for smaller ratios, analogous to the tests plotted in Figure IV.40. The reason for this was explained in Chapter IV in terms of differences in initial shear stress ratio and the amount of effective stress changes.

In order to predict pore pressures and strains developed in a contractive triaxial cyclic compression test on Oosterschelde Fine Sand, the following steps have to be performed:

1. Check if the test sample will behave contractively at selected porosity and cyclic shear stress ratio by entering Figure II.7. If yes, proceed to (2). If dilatant, residual pore pressures will be negative and residual strains very small (measured values less than 0.2% ε_v). If liquefaction is indicated, large strains and pore pressures will develop very rapidly.
2. Find correction factors C_n, $C_{\Delta q}$ and $C_{\bar{p}}$ for strain

and pore pressure from Figures V.1, 2 and 3 for the selected conditions.

3. Calculate the normalized number of load cycles for both strain and pore pressure development by dividing the number of load cycles to be predicted for by the corresponding product of the correction factors.

4. Enter Figures V.6 and V.7 at the respective equivalent number of load cycles, and read off strain and pore pressure ratio by going horizontally from the intersection with the appropriate value of mean shear stress ratio.

The prediction procedure is limited to the range of test conditions used to construct Figures V.6 and V.7, which are:

Porosity: $37.9\% < n_c < 46.8\%$

Cyclic shear stress ratio: $0.09 < \Delta q_{cy}/\bar{p}_o < 0.36$

Mean consolidation stress: $0.75\ kg/cm^2 < \bar{p}_o < 5.00\ kg/cm^2$

Mean shear stress ratio: $0.09 < q_m/\bar{p}_o < 0.40$

In addition this procedure is only valid for normally consolidated undrained triaxial samples, behaving contractively, and wet compacted by the undercompaction procedure.

This prediction approach assumes that the effects of porosity, cyclic shear stress and mean consolidation stress on

undrained cyclic behavior are perfectly described by Equations V.12, V.13 and V.14. This forces all of the scatter in the data from these relations into the final plots of strain and pore pressure ratio versus normalized number of cycles, e.g. Figure V.6, for each value of $q_m/\bar{p}_o$.

Appendix E gives the data for all tests where strain and pore pressure are plotted versus equivalent number of cycles for several values of $q_m/\bar{p}_o$. One of these plots is presented in Figure V.5. The scatter of data about the selected curve for each $q_m/\bar{p}_o$ is the complete scatter in the whole prediction method. Study of these curves shows that the scatter in the prediction method is surprisingly small considering the complexity of cyclic behavior. The lines of Figures V.6 and V.7 are best fit lines for the available test. From Figure V.5 and corresponding figures in Appendix E, it is found that strains and pore pressures typically scatter by a factor of two.

Figure V.8 presents a plot of pore pressure ratio from 0 to 1.0 versus vertical strain from 0 to 1.0%. This plot can be used to check if predicted values of strain below 1% compare reasonably with the predicted pore pressure values.

5.2 Cyclic Isotropic Tests

Results in Chapter IV for isotropic tests indicate a procedure similar to that followed for compression test was

feasible to predict pore pressure generation for isotropic tests. A similar procedure can not be used to predict peak to peak cyclic strain because the strain contours given in Chapter IV were not log-linear or parallel.

Following similar logic as above for compression tests, it can easily be established for isotropic tests:

$$\frac{N}{C_{nu} \cdot C_{\bar{p}u}} = N_u = h(M, \Delta q_{cy}/\bar{p}_o) \qquad \text{Eq. V.19}$$

which can be inverted to:

$$M = h'(N_u, \Delta q_{cy}/\bar{p}_o) \qquad \text{Eq. V.20}$$

Figure V.9 gives the equation and a plot of the correction factor, C_{nu}, for porosity. Figure V.10 gives the same for the mean consolidation stress correction factor, $C_{\bar{p}u}$. Curves of equal cyclic shear stress ratio ($\Delta q_{cy}/\bar{p}_o$) have been plotted in Figure V.11 by exactly the same procedure as the mean shear stress ratio curves for the compression tests in Figures V.6 and V.7.

Similar plots for strain cannot be developed. Instead, use must be made of the observation that in isotropic cyclic tests, peak to peak strains are reasonably related to the residual pore pressure. Figure V.12 presents a plot of peak to peak strain versus pore pressure ratio for all isotropic

test data. Accumulated strain cannot be predicted for isotropic tests.

The procedure for prediction of residual pore pressure and peak to peak strain in cyclic isotropic tests is analogous to the procedure given above for cyclic compression tests:

1. Check if the test sample will behave contractively by entering Figure II.7. If yes, proceed to (2). If dilatant, residual pore pressures will be negative and both residual and peak to peak strains very small (values measured in one dilating test: $\varepsilon_{vpp} = 0.05\%$ and $\varepsilon_{vres} = -0.04\%$). If liquefaction is indicated, large strains and pore pressures will develop very rapidly.
2. Find correction factors C_{nu} and $C_{\overline{pu}}$ from Figures V.9 and V.10 for the selected conditions.
3. Calculate the normalized number of load cycles by dividing the number of load cycles to be predicted for by the product of the correction factors.
4. Enter Figure V.11 at the normalized number of cycles, and read off the pore pressure ratio by going horizontally from the intersection with the appropriate value of cyclic shear stress ratio.
5. With the pore pressure ratio, peak to peak strains

are obtained from Figure V.12. If the predicted pore pressure ratio is 1.0 or larger, the sample will suffer a cyclic mobility failure with correspondingly large cyclic strains.

The prediction procedure for isotropic tests is limited to the following values, which is the range of test data:

Porosity: $38.6\% < n_c < 42.1\%$

Mean consolidation stress: $0.50\ kg/cm^2 < \bar{p}_o < 3.00\ kg/cm^2$

Cyclic shear stress ratio: $0.15 < \Delta q_{cy}/\bar{p}_o < 0.40$

In addition, the procedure is only valid for normally consolidated undrained triaxial samples, behaving contractively, and wet compacted by the undercompaction procedure.

From the test data reported in Appendix E, a scatter in test results by a factor of 1.7 was found. The scatter would very likely have been larger if more tests at a greater range of test conditions had been performed.

5.3 Summary

A procedure to predict the effects of porosity and stress path on strain and pore pressure development in cyclic triaxial tests has been devised. The procedure is developed in detail for contractive behavior and isotropic and compressive stress conditions. Conditions producing dilatant behavior or liquefaction are identified, but a prediction

procedure is not established due to lack of test data. The procedure is only valid for normally consolidated undrained triaxial samples of Oosterschelde Fine Sand, wet compacted by the undercompaction procedure.

Appendix H presents an example of the prediction procedure for a cyclic compression test.

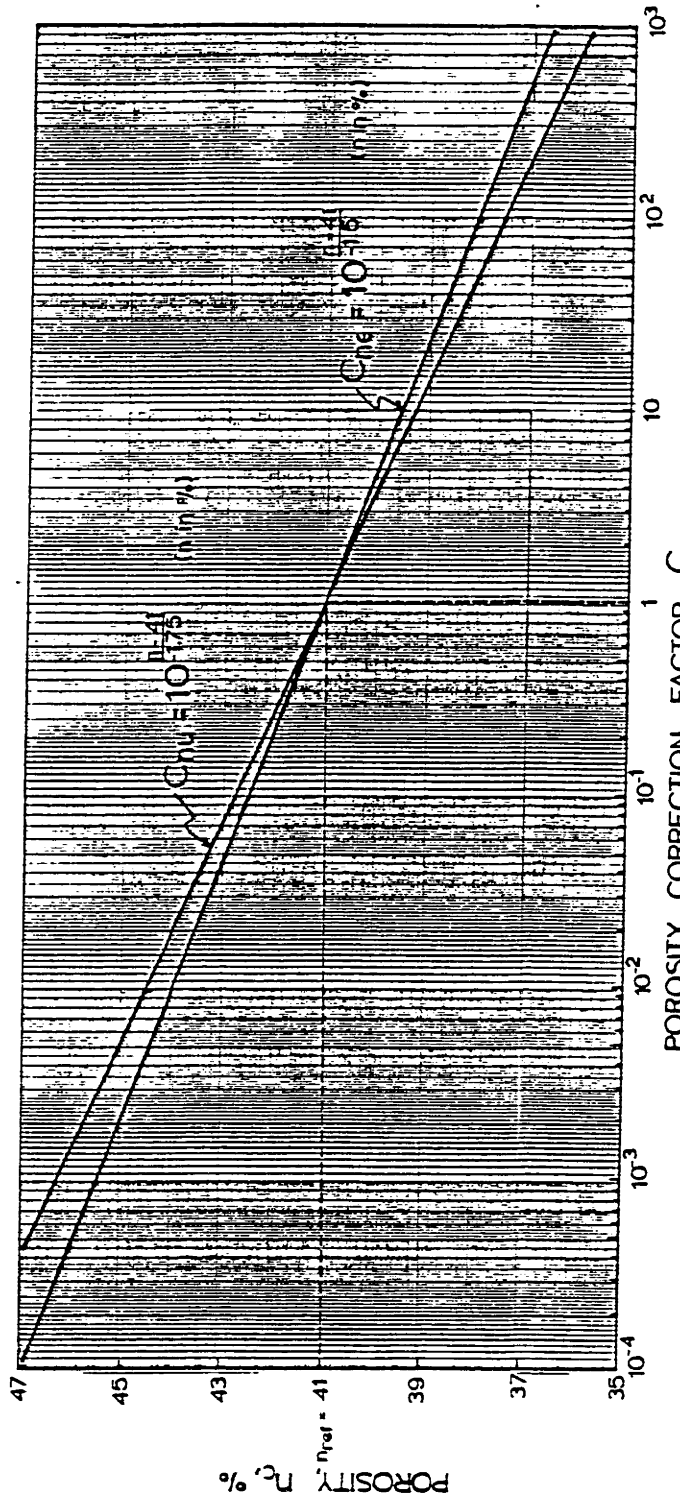

POROSITY CORRECTION FACTORS FOR CYCLIC COMPRESSION TESTS

FIGURE V-1

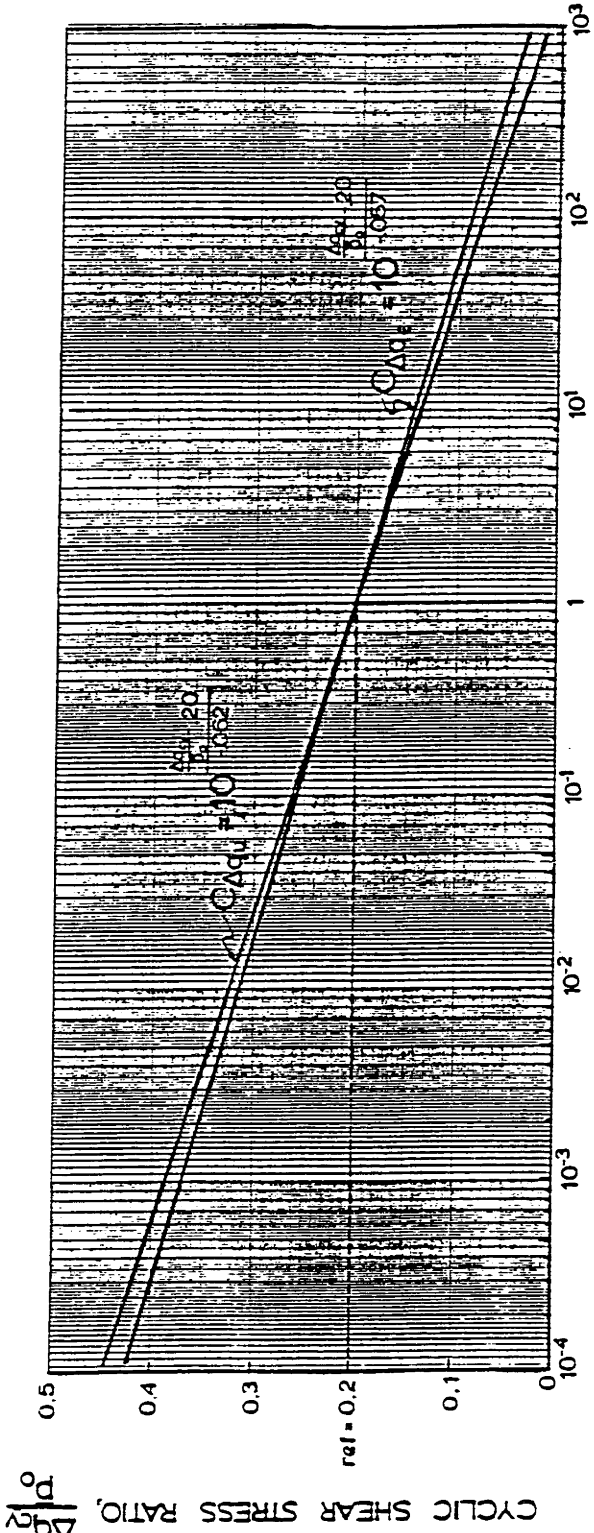

CYCLIC SHEAR STRESS RATIO CORRECTION FACTORS FOR CYCLIC COMPRESSION TESTS

FIGURE V-2

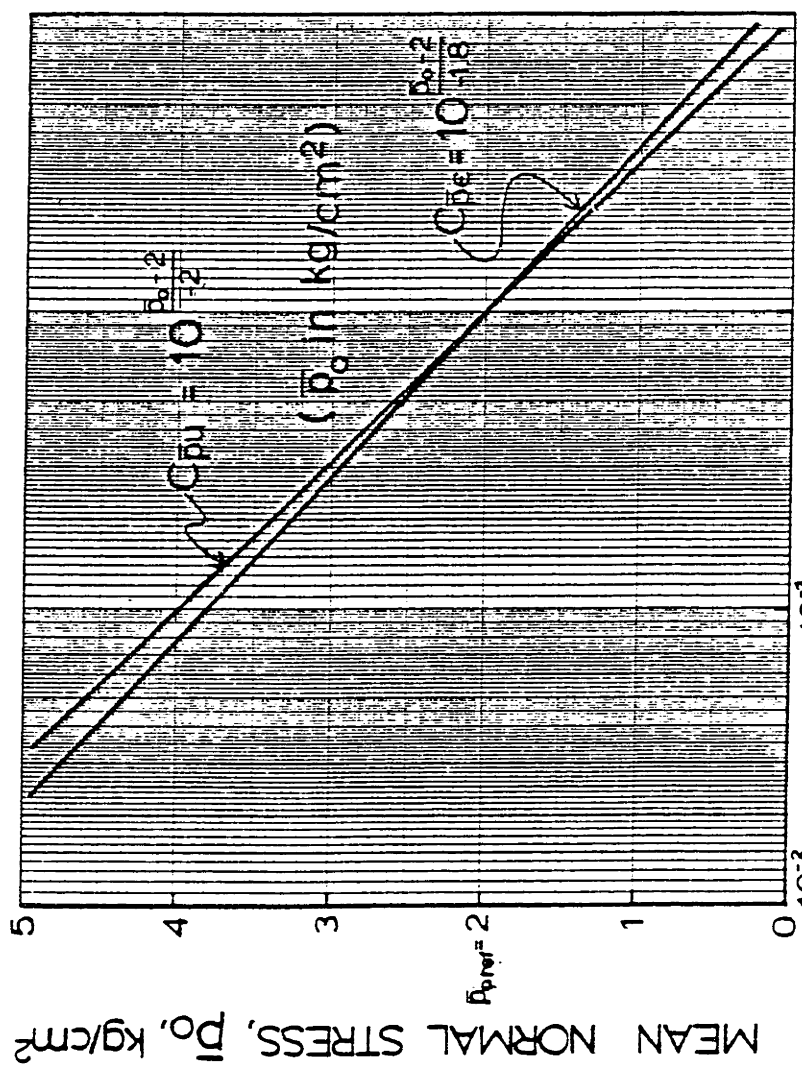

MEAN NORMAL STRESS CORRECTION FACTOR FOR CYCLIC COMPRESSION TESTS

FIGURE V-3

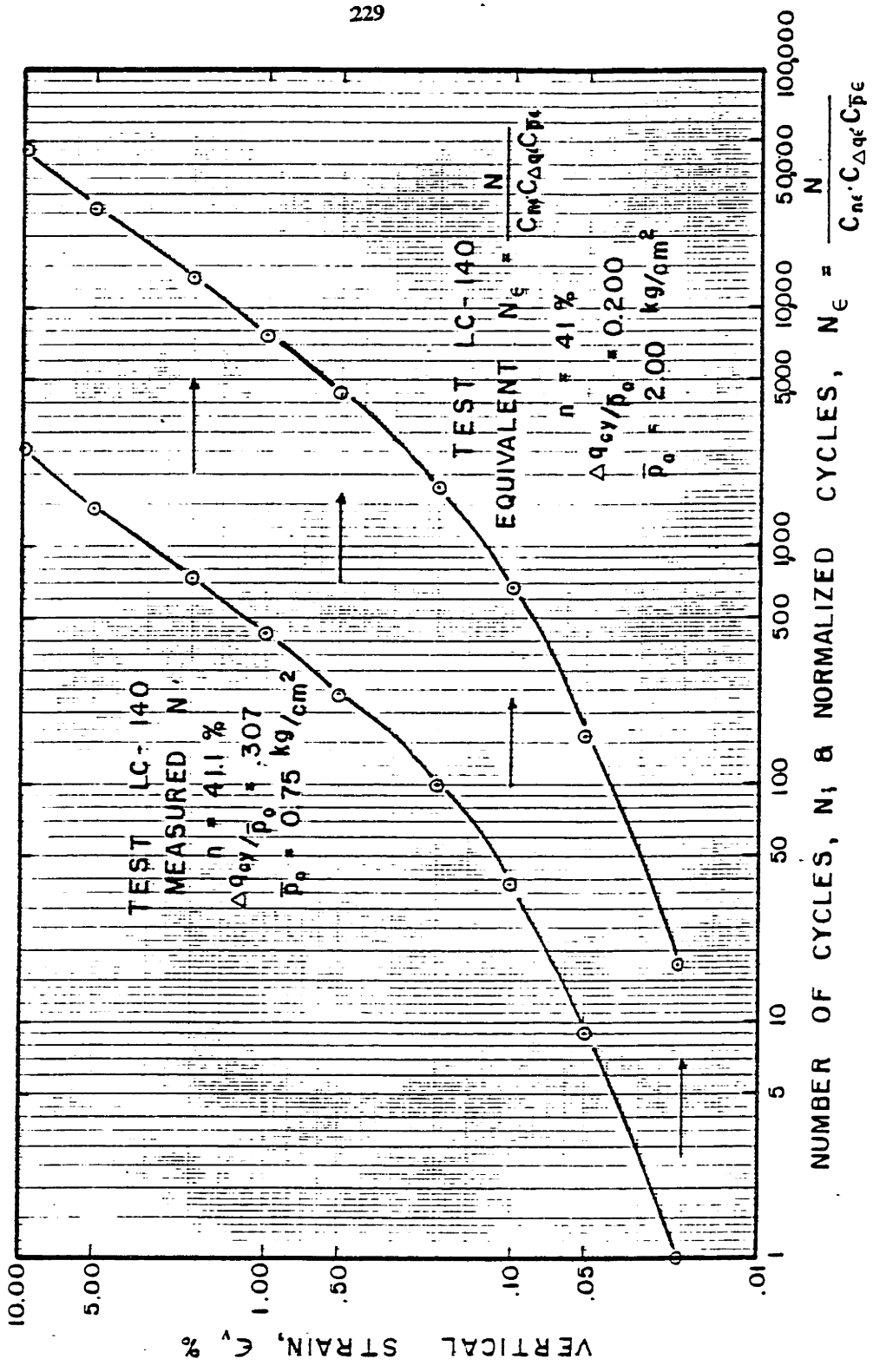

MEASURED AND NORMALIZED LOAD CYCLES

FIGURE V-4

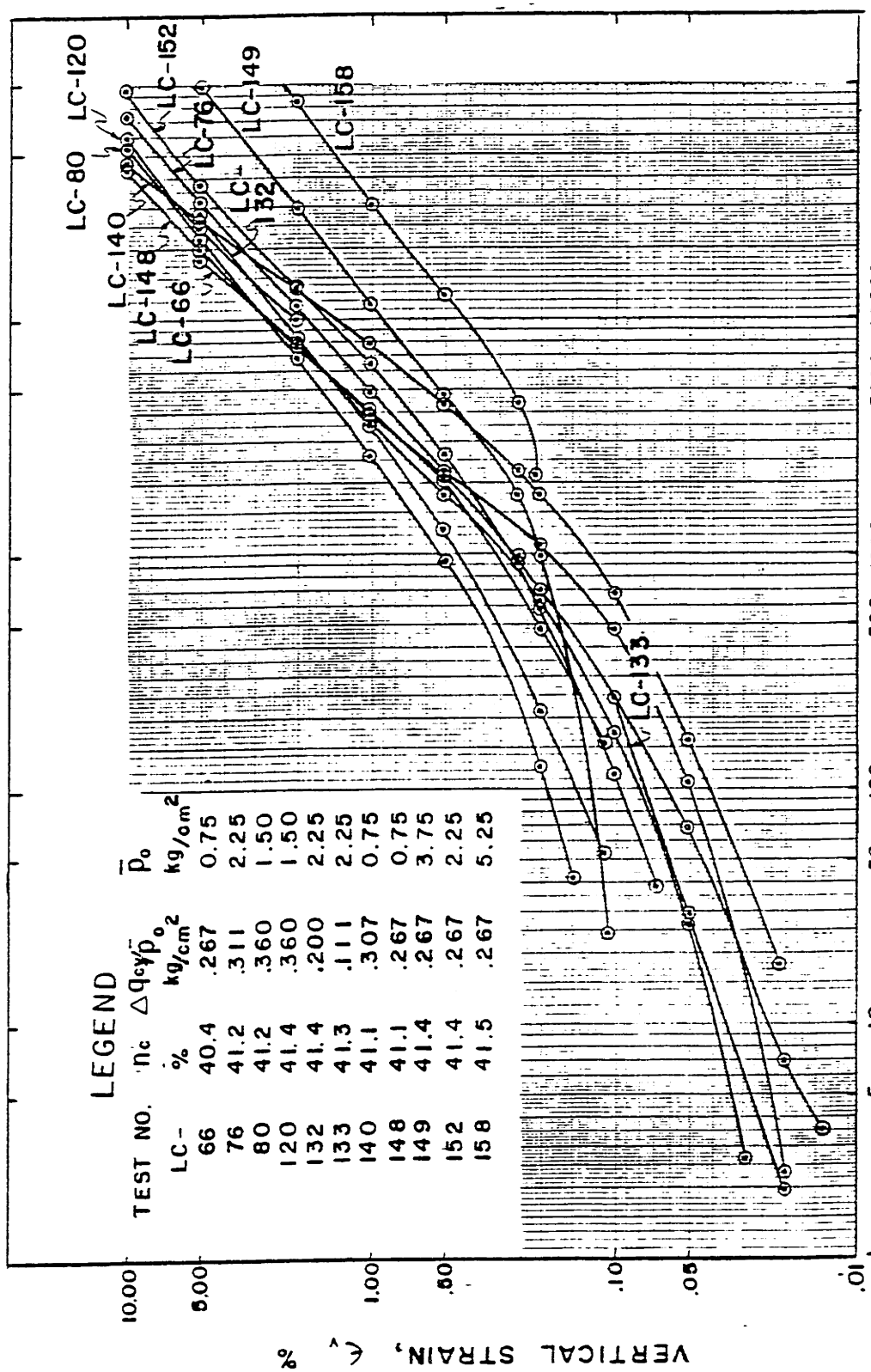

STRAIN VERSUS NUMBER OF NORMALIZED LOAD CYCLES IN TESTS WITH $q_m/\bar{p}_o$ = .33

FIGURE V-5

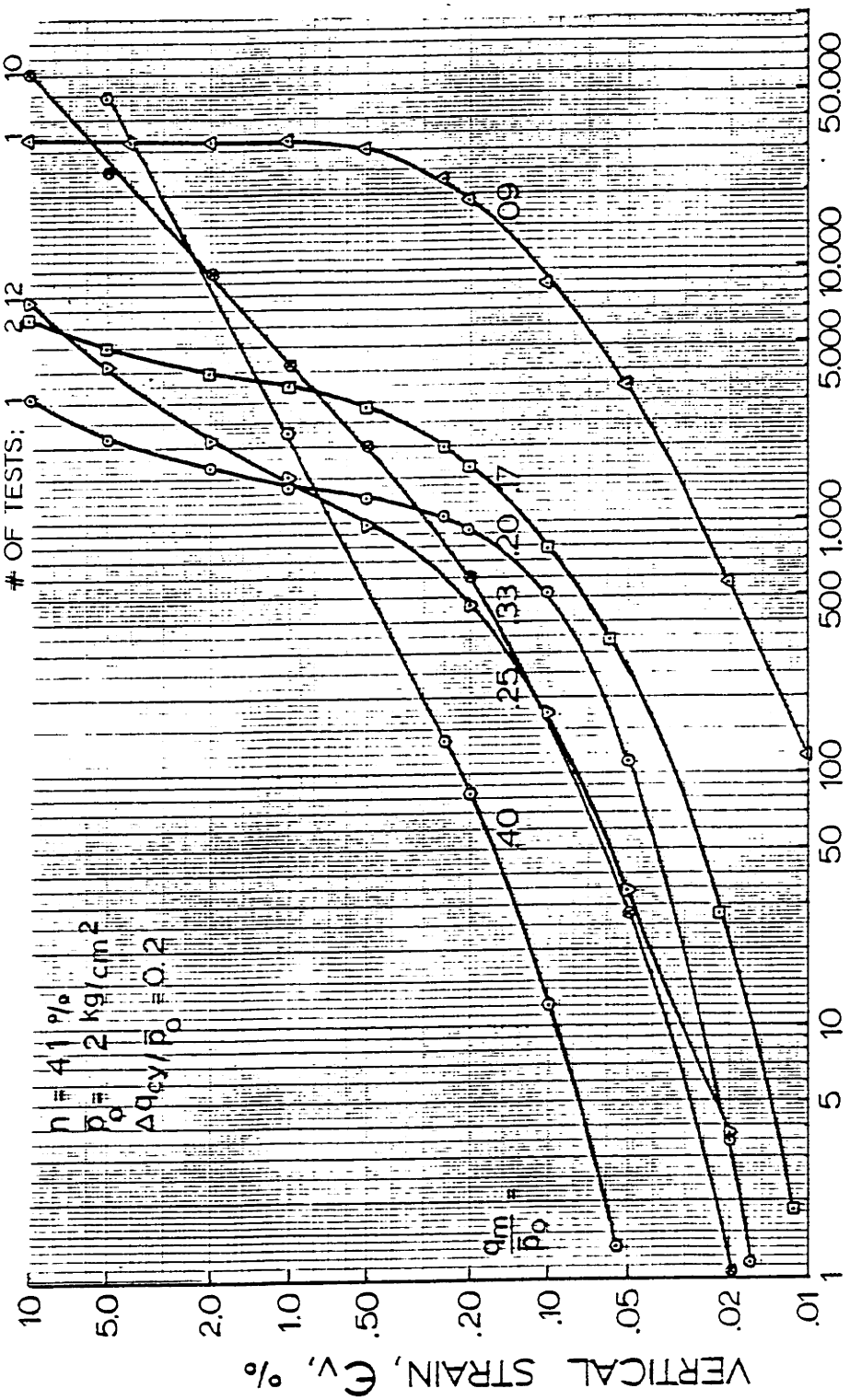

STRAIN PREDICTION PLOT FOR COMPRESSIVE STRESS STATE

FIGURE V-6

OOSTERSCHELDE FINE SAND

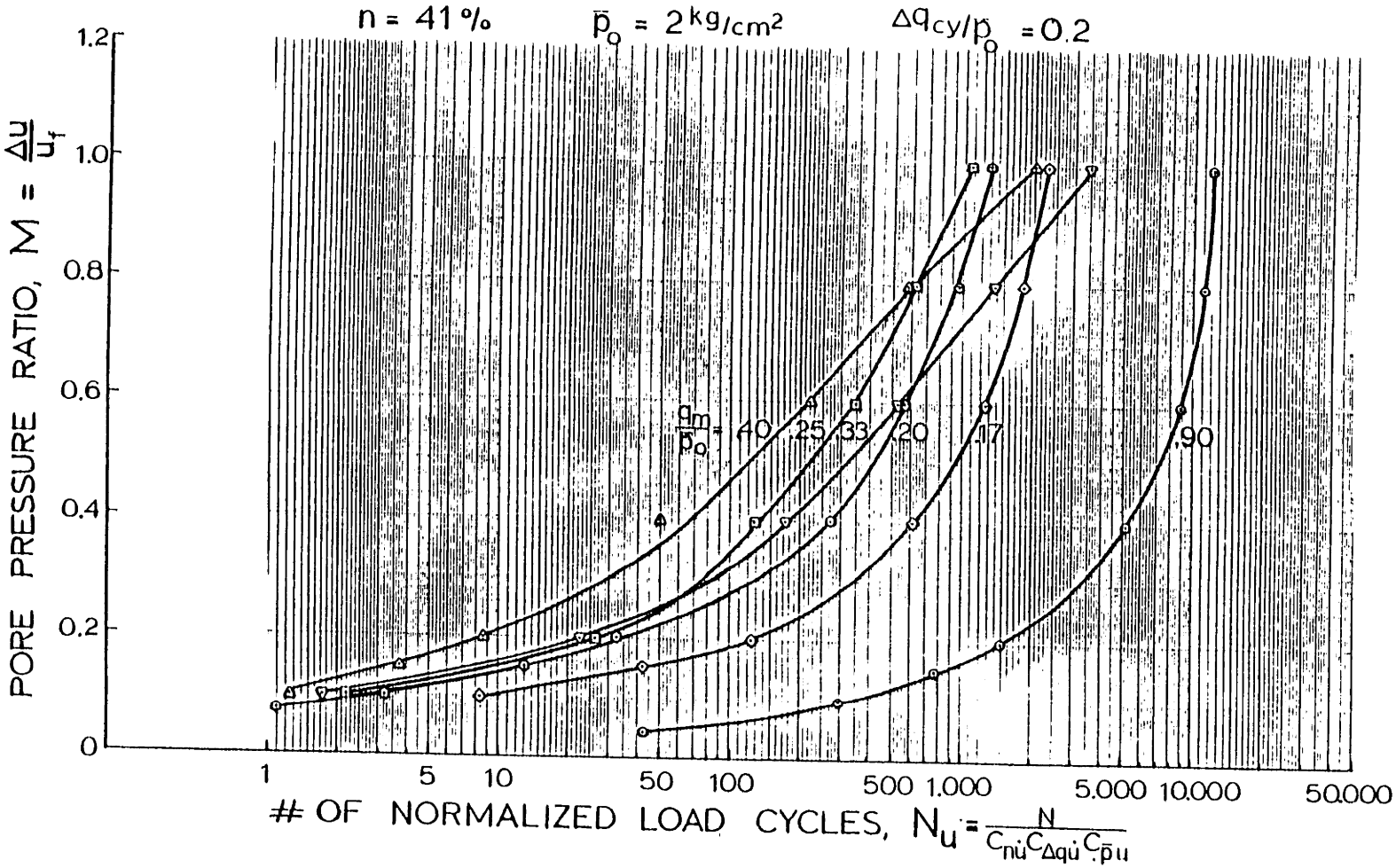

FIGURE Y-7

PORE PRESSURE PREDICTION PLOT FOR COMPRESSIVE STRESS STATE

OOSTERSCHELDE FINE SAND
ANISOTROPIC CYCLIC TRIAXIAL TESTS

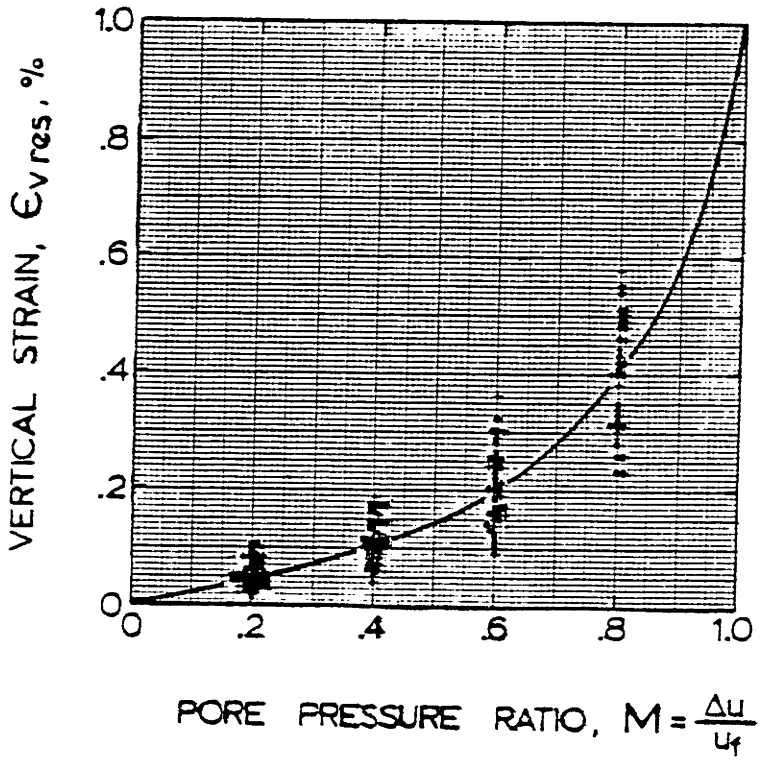

PORE PRESSURE DEVELOPMENT AS A FUNCTION OF VERTICAL STRAIN

FIGURE I-3

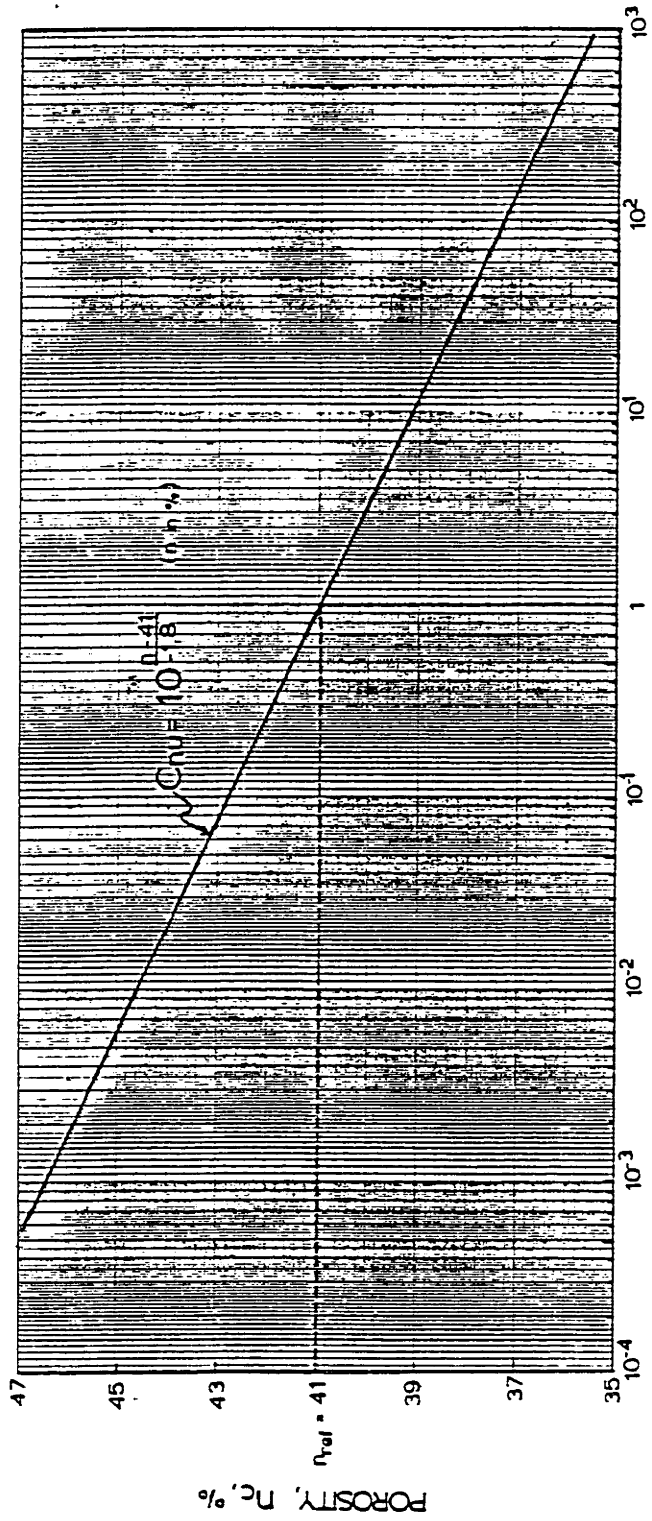

POROSITY CORRECTION FACTOR FOR ISOTROPIC CYCLIC TESTS

FIGURE V-3

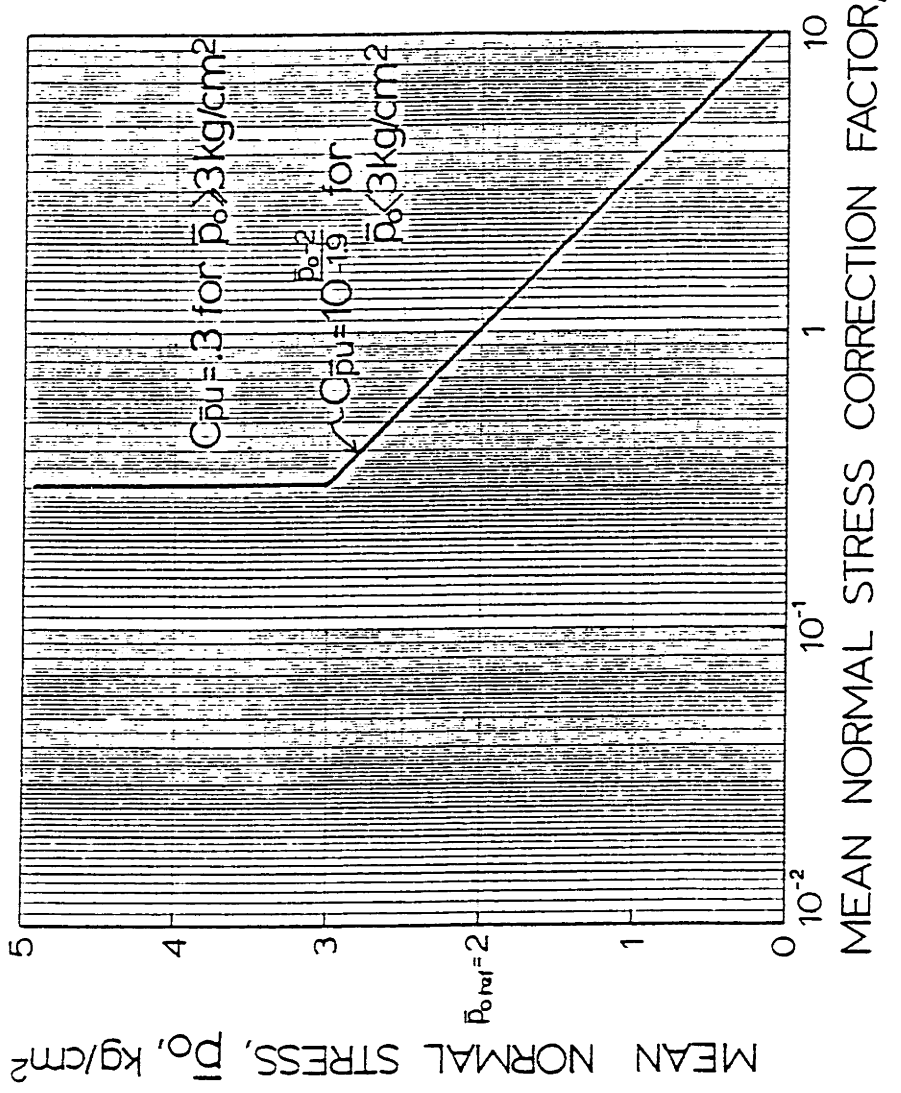

MEAN NORMAL STRESS CORRECTION FACTOR $C_{\bar{p}u}$ FOR CYCLIC ISOTROPIC TESTS

FIGURE V-10

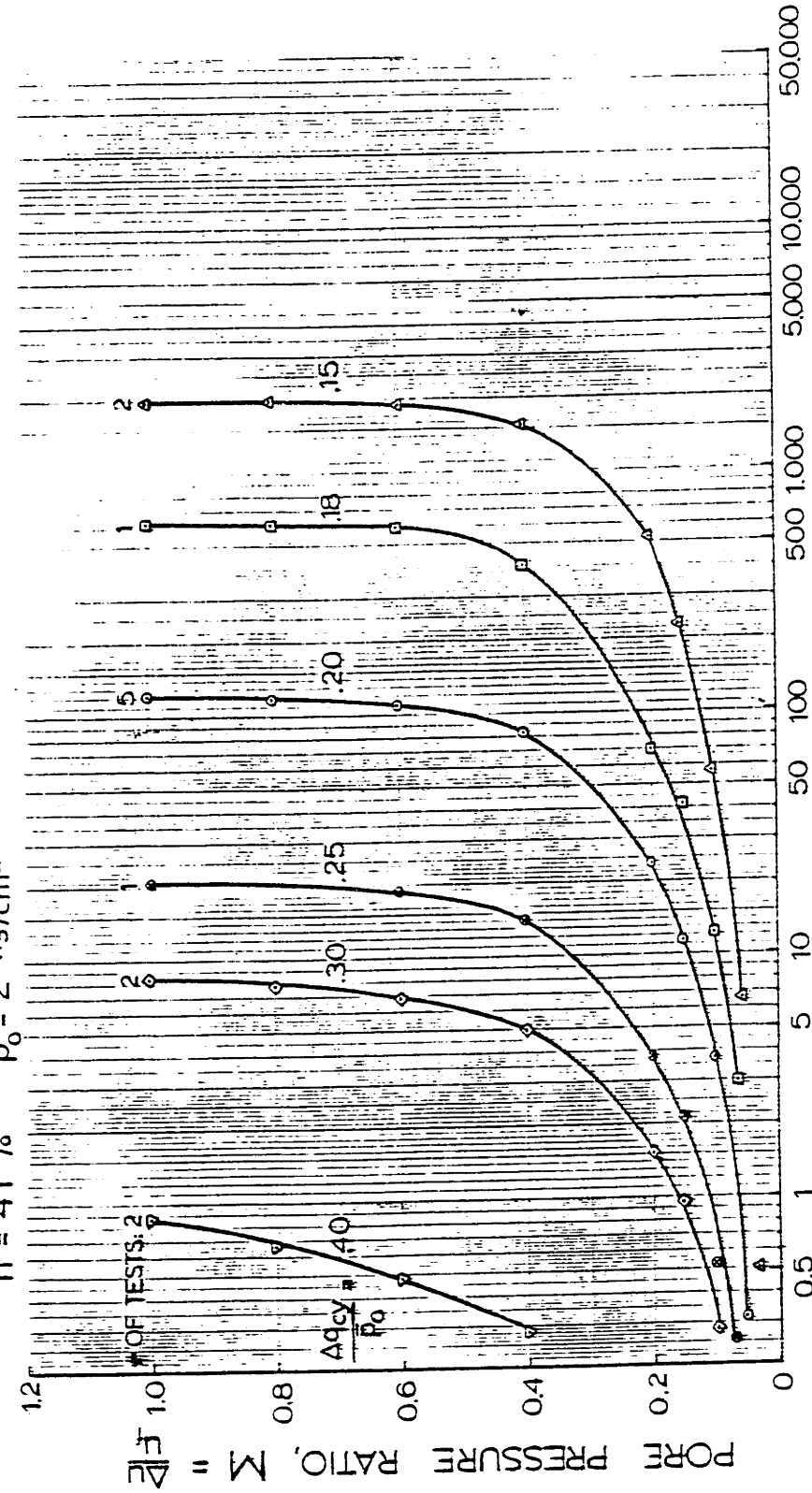

PORE PRESSURE PREDICTION PLOT FOR ISOTROPIC STRESS STATE

FIGURE V-11

OOSTERSCHELDE FINE SAND
ISOTROPIC CYCLIC TRIAXIAL TESTS

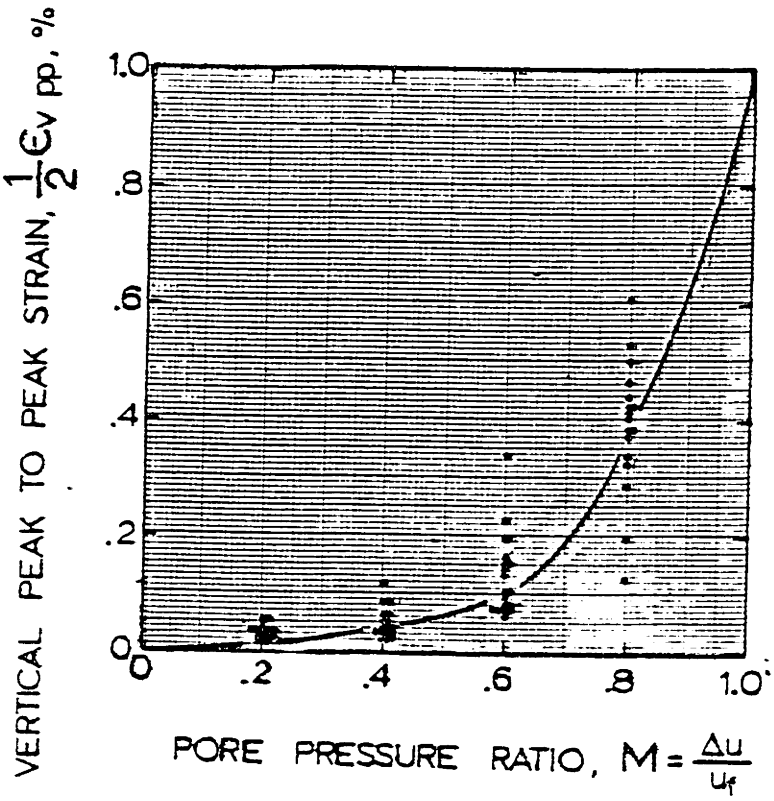

PORE PRESSURE DEVELOPMENT AS A FUNCTION OF STRAIN AMPLITUDE

FIGURE V-12

Chapter VI

LABORATORY INVESTIGATION PROCEDURE FOR OTHER SANDS

The purpose of this chapter is to give a procedure to plan a laboratory investigation that will yield the necessary results to establish correction factors for porosity, cyclic shear stress ratio and mean consolidation stress, and the relationship between mean shear stress ratios and the number of load cycles (Chapter V gives a complete description of the prediction procedure).

The goal of the laboratory tests is to obtain parameters to use in foundation design. One critical question is then, of course, how well the compacted samples in the laboratory compare to in situ soil. That is beyond the scope of this thesis. However, tests comparing different sample preparation procedures (Mulilis et al. (1975), Ladd (1976b) and Marcuson and Townsend (1976)), indicate a large sensitivity of cyclic sand behavior to preparation procedure. Undisturbed samples have been shown to exceed the strength of samples tamped moist by as much as 50% (Mulilis et al. (1975), see also Chapter III). The condition of the tested samples are therefore very important. The present state of the art is to use the best possible undisturbed samples in laboratory testing for field design (Casagrande (1976) and Seed (1976a)). It

it however uncertain how well these samples compare to in situ soil. The assumption underlying the use of reconstituted samples for the prediction procedure is that the pattern of strain and pore pressure predicted will be representative and reliable. The absolute values predicted may differ from field behavior.

The following information concerning the field conditions is desirable for the planning of the laboratory tests:

(1) In situ porosity

(2) The stress condition in the foundation soil after placement of the structure (e.g. from finite element analysis)

(3) The stress changes in the foundation soil under a static load on the structure, equal to the maximum expected environmental forces acting on the structure (e.g. from finite element analysis)

With this information, the average field stress condition, with associated porosity and stress path, can be identified. These average conditions are the basis for selecting the laboratory test conditions.

As an example, let the heavy drawn arrow in Figure VI.1 represent the total stress path for the average field condition and the associated average porosity. A cyclic triaxial test can then be run under those conditions. This will be denoted the "standard" test, representative for the average

field conditions. In order to obtain the influence of cyclic shear stress on stress-strain behavior, three more tests with smaller and larger cyclic shear stress amplitudes than the standard test are performed (see Figure VI.1). The effect of mean consolidation stress is investigated by further three tests at varying consolidation stress, but constant mean and cyclic shear stress ratio (Figure VI.1). The effect of mean shear stress is investigated by three tests at constant cyclic shear stress and mean consolidation stress, but varying mean shear stress level. All these tests are performed at the average porosity. The influence of porosity is found by running three more tests at the standard stress path (heavy arrow in Figure VI.1), but with porosities smaller and larger than the standard porosity. A total of thirteen cyclic tests thus have to be performed to obtain four tests in each series.

If 1% vertical strain takes too long to reach, all tests to establish the influence of the stress path can be performed at a higher than the standard porosity. From the test results, the correction factors C_n, $C_{\Delta q}$ and $C_{\bar{p}}$ can be established by the procedure outlined in Chapter V. Prediction plots similar to Figures V.6 and V.7 can then be plotted for the four different values of mean shear stress ratio and used to predict strain and pore pressure for all desired cyclic triaxial test conditions.

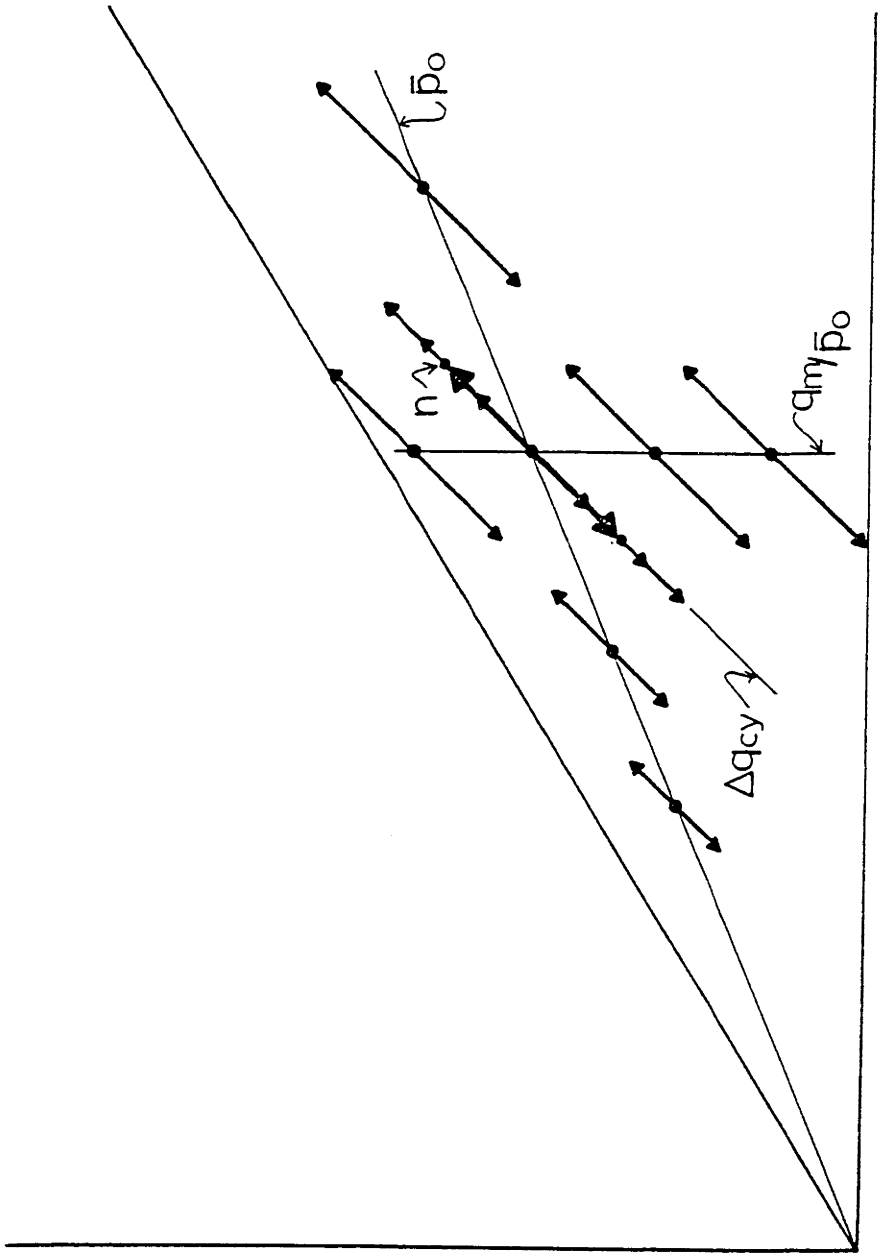

TOTAL STRESS PATHS (TSP-u_s) FOR TYPICAL TEST PROGRAM TO OBTAIN CORRECTION FACTORS FOR STRAIN AND PORE PRESSURE PREDICTION

FIGURE VI-1

CHAPTER VII

Summary, Conclusions and Recommendations

The objectives guiding the experimental investigation reported in this thesis were three-fold:

1) to determine undrained stress-strain behavior of a sand in cyclic triaxial tests,
2) to determine the influence of porosity and stress path on strain and pore pressure development in undrained cyclic triaxial tests on a sand,
3) to develop a method to predict strain and pore pressure development in undrained cyclic triaxial tests on a sand at various porosities and subjected to different stress paths.

In order to meet these objectives, experimental investigations were carried out to measure laboratory behavior of sand samples subjected to cyclic loading in triaxial tests under a variety of soil conditions and stress paths. Emphasis was primarily placed on determining strain and pore pressure development to aid in prediction of these quantities for laboratory triaxial samples subjected to undrained cyclic loading conditions. Efforts were also made to find a basic understanding of sand response to cyclic loading.

Undrained cyclic triaxial tests on reconstituted sand samples comprised the major part of the experimental work. They were supplemented by static triaxial tests in an attempt to relate cyclic sand behavior to known and accepted patterns of sand behavior under static loads.

The adopted investigation procedure was to perform a series of cyclic and static triaxial tests, where all test conditions and soil parameters but one were kept constant within each series. Thus the influence of the one varied parameter on the sand behavior could be assessed. However, the magnitude of that influence would not necessarily be the same under another set of test conditions and soil parameters. Therefore several test series under various conditions were run to examine each parameter. Only a fine, uniform sand was utilized for the cyclic testing.

Three key findings result from this investigation of undrained cyclic behavior:

1. Volume change tendency under cyclic loading is found to be more complicated than previously demonstrated;
2. The average shear stress on an element of soil significantly affects cyclic strain and pore pressure behavior; and
3. The influences of porosity, cyclic shear stress, mean normal stress and mean shear stress on strain

and pore pressure development under cyclic loads can be separated.

The test results show that undrained cyclic loading can cause either a decrease in excess pore pressure (termed dilation) or an increase in excess pore pressure (termed contraction). Contraction may be followed by a near total loss of strength and large strains within one load application (termed liquefaction) or by continued straining but no loss of strength. The response type is apparently governed mainly by soil porosity and cyclic shear stress ratio. Dilation prevails under the combination of dense samples and small cyclic shear stress ratios. Liquefaction prevails in very loose samples subjected to larger cyclic shear stresses. Contractive behavior prevails over a substantial range of intermediate conditions.

The mean shear stress about which cycling occurs has an important influence on the strain and pore pressure that develop in undrained cyclic tests on contractive sand. Figure VII.1 illustrates typical test results. For mean shear stresses that always remain positive (i.e., the vertical normal stress is always larger than the horizontal normal stress), compressive axial strains develop and accumulate with each cycle, provided liquefaction does not occur. Pore pressures reach a maximum value controlled by the Mohr-Coulomb failure envelope; however, the sample retains strength

and stiffness. Similar behavior occurs for conditions where the mean shear stresses on an element always remain negative (i.e., the horizontal normal stress is always larger than the vertical normal stress), except strains and pore pressures develop much more rapidly and the axial strains are extensive. For mean shear stresses which allow shear stress reversal, the major strains occur within the cycle and are recovered. The sample develops large excess pore pressures followed by large cyclic strains. It eventually becomes very compressible, although the sample always retains ability to develop strength if strained sufficiently.

The fact that the influences of porosity, cyclic shear stress, mean normal stress and mean shear stress on strain and pore pressure can be separated, is exploited by making plots that allow an estimate of the influence of each of the above factors on strain and pore pressure development in undrained cyclic triaxial tests. An example of such a plot for the influence of porosity in the case that vertical stress always remains larger than horizontal stress is presented in Figure VII.2. The net result of this possible separation of influences is that a procedure for prediction of strain and pore pressure in undrained cyclic tests, taking porosity and stress path into account, can be established. Figures VII.3 and VII.4 present plots to predict strain and pore pressure respectively, at selected reference conditions

for porosity, cyclic shear stress ratio and mean normal stress. The number of load cycles and the conditions to be predicted for are adjusted to a normalized number of load cycles at selected reference conditions by Figure VII.2 and two similar plots given in Chapter V. With the normalized number of load cycles, strain and pore pressure can be predicted for the given mean shear stress ratio by entering Figures VII.3 and VII.4. Appendix H gives an example of the prediction procedure.

Figures VII.2, VII.3 and VII.4 are only valid for conditions where the vertical stress always remains larger than the horizontal stress. For cases where horizontal and vertical stress alternates as the largest stress, plots in Chapter V are utilized to estimate strain and pore pressure development.

In addition to the undrained cyclic triaxial tests on normally consolidated samples, several tests were performed on samples with stress history or partial drainage. The results of those tests are summarized in Figure III.8 in Chapter III.

Questions as drainage effects, irregular load pattern, time under sustained load, compaction procedure and effect of principal stress rotation deserve closer attention. The large, overriding question remaining, however, is how these laboratory results relate to field behavior. That is the

primary area where future effort is required. It seems likely that the qualitative trends of cyclic sand behavior obtained in the laboratory, as "decreasing porosity leads to decreasing strain and pore pressure development", also should hold for field behavior. However, quantitative findings from laboratory tests, as "decreasing the sample porosity 1.5% leads to one order of magnitude more stress cycles to reach a given strain", are less likely to be true in the field. When uncertainty about the values of in situ parameters as soil porosity or coefficient of lateral stress at rest are added to the uncertainty of the soil response to random, wave induced loads, the selection of soil parameters for design is at best very difficult. The most promising way to obtain reliable soil parameters for design could therefore be to "calibrate" laboratory results by field exploration and subsequent measurements on constructed facilities. In any event, the coherent body of information about sand behavior under cyclic loads in the laboratory and the prediction procedure described in this work, will hopefully be of help to understand and predict behavior of constructed facilities subjected to wave loading.

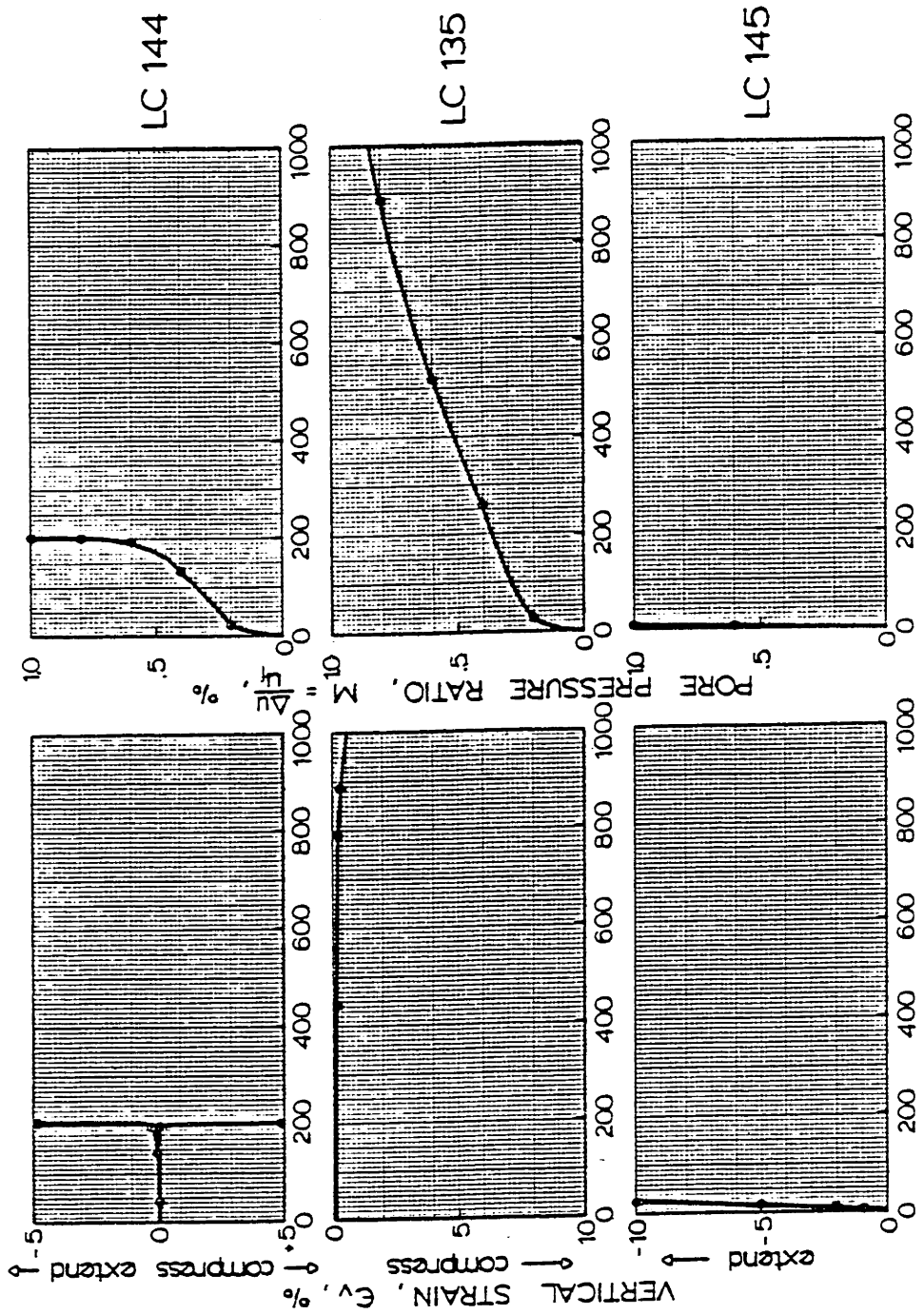

STRAIN AND PORE PRESSURE DEVELOPMENT MEASURED IN ISOTROPIC, COMPRESSION AND EXTENSION CYCLIC TESTS

FIGURE VII-1

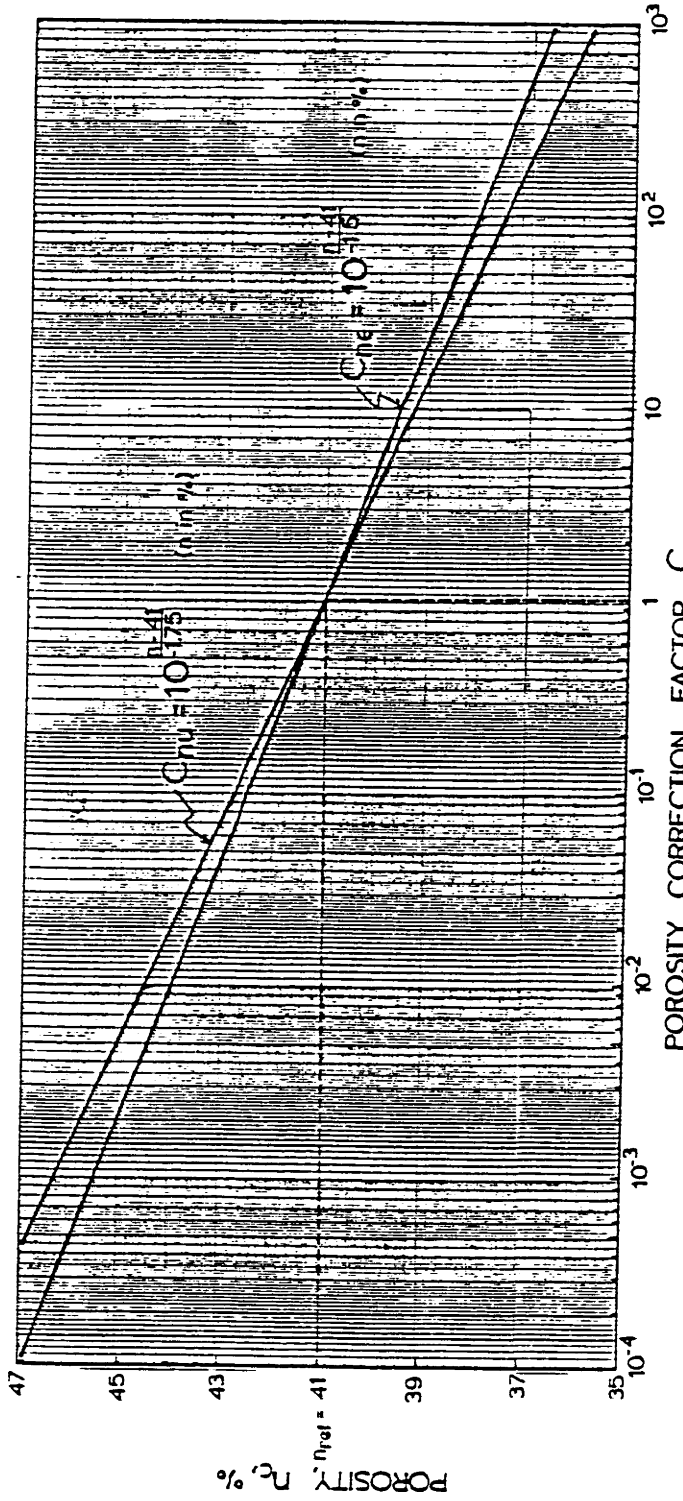

POROSITY CORRECTION FACTORS FOR CYCLIC COMPRESSION TESTS

FIGURE VII - 2

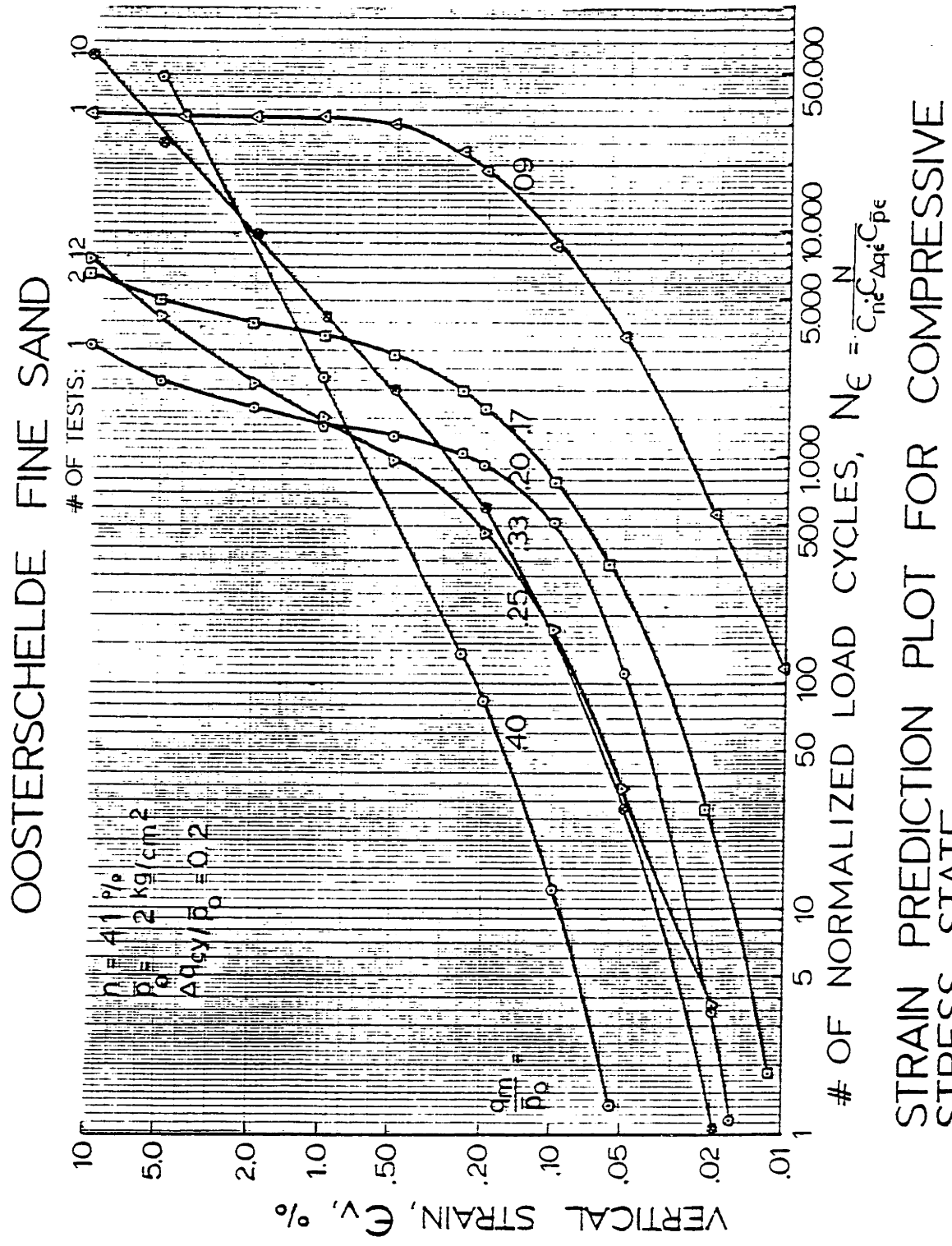
OOSTERSCHELDE FINE SAND
# OF TESTS: 1 2 12 1 10
n = 41 %
ρd = 2 kg/cm²
Δσcy/p'o = 0.2
dm/p'o =
.09
.17
.20
.33
.25
.40
VERTICAL STRAIN, εv, %
10 5.0 2.0 1.0 .50 .20 .10 .05 .02 .01
OF NORMALIZED LOAD CYCLES, Nε = N / Cnε Cσqε Cρε
1 5 10 50 100 500 1.000 5.000 10.000 50.000
STRAIN PREDICTION PLOT FOR COMPRESSIVE STRESS STATE

FIGURE VII-3

OOSTERSCHELDE FINE SAND

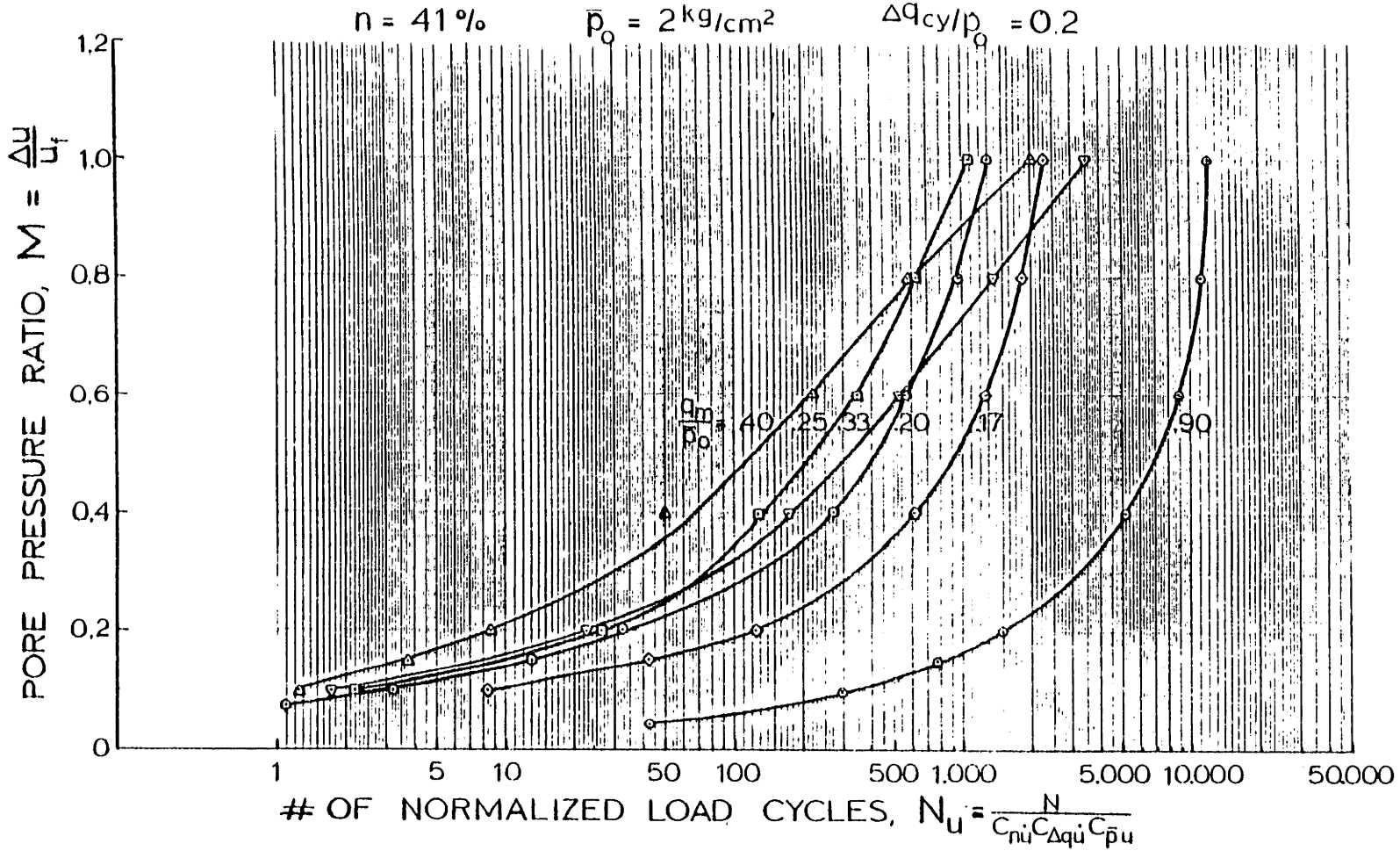

FIGURE VII-4

PORE PRESSURE PREDICTION PLOT FOR COMPRESSIVE STRESS STATE

LIST OF REFERENCES AND BIBLIOGRAPHY

ABBREVIATIONS

AIME	American Institution of Mining Engineers
ASCE	American Society of Civil Engineers
ASTM	American Society for Testing and Materials
BOSS'76	Behavior of Offshore Structures, 1st Symposium, 1976
CSMFE	Conference on Soil Mechanics and Foundation Engineering
EERC	Earthquake Engineering Research Center
ICSMFE	International Conference on Soil Mechanics and Foundation Engineering
JGED	Journal of the Geotechnical Engineering Division
JHD	Journal of the Hydraulic Division
JSMFD	Journal of the Soil Mechanics and Foundation Division
JWW	Journal of the Waterways, Harbors and Coastal Engineering Division
MIT	Massachusetts Institute of Technology
NCLPGE	National Convention on Liquefaction Problems in Geotechnical Engineering
NGI	Norwegian Geotechnical Institute
OTC	Offshore Technology Conference
SMFE	Soil Mechanics and Foundation Engineering
STP	Special Technical Publication
UCLA	University of California at Los Angeles
WCEE	World Conference on Earthquake Engineering
WES	Waterways Experiment Station

REFERENCES

Al-Hussaini, M.M. (1973), "Influence of Relative Density on the Strength and Deformation of Sand Under Plane Strain Conditions", Evaluation Properties Involving Cohesionless Soils, ASTM, STP 523, American Society for Testing and Materials.

Allen, J.J. and Thompson, M.R. (1974), "Significance of Variable Confined Triaxial Testing", Transportation Engineering Journal, ASCE, 100, No. TE4, pp. 827-843.

Ambraseys, N. and Sarma, S. (1969), "Liquefaction of Soils induced by Earthquakes", Bulletin of the Seismological Society of America, 59, No. 2, pp. 651-664.

Andersen, K.H. (1976), "Behavior of Clay Subjected to Undrained Cyclic Loading", Proc. BOSS'76, 1, pp. 392-403, Trondheim, Norway.

Andersen, K.H., Brown, S.F., Foss, I., Pool, J.H. and Rosenbrand, W.F. (1976), "Effect of Cyclic Loading on Clay Behavior", NGI Publication 113, pp. 1-6.

Andersen, K.H., Hansteen, O.E., Hoeg, K., and Prevost, J.H. (1977) "Soil Deformations Due to Cyclic Loads on Offshore Structures", NGI Report 52412-6.

Annaki, M. and Lee, K.L. (1976), "Equivalent Uniform Cycle Concept for Soil Dynamics", ASCE, pp. 227-254.

Arthur, J.R.F. (1976), "Discussion of Lee's Paper", Proc. BOSS'76, 2, pp. 427-429.

Arthur, J.R.F. (1976), "Discussion of Seed's Paper", Proc. BOSS-76, 2, p. 432.

Arthur. J.F. and Menzies, B.K. (1972), "Inherent Anistropy in a Sand", Geotechnique, 22, No. 1, pp. 115-128.

Arulanandan, K. (1975), "Influence of Sample Preparation on Pore Structure of Sand", Technical Publication, University of California, Davis.

ATSM, "Test for Relative Density of Cohesionless Soils", ASTM, D2049-69.

Baligh, M. and Levadoux, J. (1977) "Nonlinear Consolidation Theory for Cyclic Loading", MIT Report R77-10, March.

Banister, J.R., Pyke, R., Ellett, D.M., Winters, L. (1975), "In-Situ Pore Pressure Measurements at Rio Blanco", ASCE National Convention, Nov. 3-7, Denver, Colorado.

Banister, J.R., Pyke, R. Ellett, D.M. and Winters, L., "In-Situ Pore Pressure Measurements at Rio Blanco", JGED, ASCE 102, GT. 10, pp. 1073-1092.

Barden, L. and McDermott, J.W. (1965), "The Use of Free Ends in Triaxial Testing in Clays,", JSMFD, ASCE, 91, SM6, pp. 1-23.

Bazant, Z.P. and Krizek, R.J. (1976a), "Densification and Hysteresis of Sand Under Cyclic Shear", Report S-76-8, WES, Vicksburg, Miss.

Bazant, Z.P. and Krizek, R.J. (1976b), "Endochronic Constitutive Law for Liquefaction of Sand", Report S-76-9, WES, Vicksburg, Miss.

Bishop, A.W. and Green, G.E. (1965), "The Influence of End Restraint on the Compression Strength of a Cohesionless Soil", Geotechnique, 15, No. 3, pp. 243-266.

Bishop, A.W. and Henkel, D.J. (1962), The Measurements of Soil Properties in the Triaxial Test", A. Arnold, London.

Bjerrum, L. (1973), "Geotechnical Problems Involved in Foundations of Structures in the North Sea", Geotechnique, 23, No. 3, pp. 319-358.

Bjerrum, L., Kringstad, S. and Kummeneje, O. (1961), "The Shear Strength of a Fine Sand", Proceedings, 5th ICSMFE, 1, pp. 29-37, Paris.

Black, D.K. and Lee, K.L. (1973) "Saturating Laboratory Samples by Back Pressure", JSMFE, ASCE, 99, SM1, pp. 75-93.

Blight, G.E. (1965), "Shear Stress and Pore Pressure in Triaxial Testing", JSMFD, ASCE, 91, SM6, pp. 25-39.

Bonin, J.P., Deleuil, G. and Zaleski-Samenhof, L.C. (1976), "Foundation Analysis of Marine Gravity Structures Submitted to Cyclic Loading", Proceeding OTC, Paper No. 2475, Houston, May.

Borowicka, D.H. (1976), "Seminar at M.I.T.", November 2, Cambridge, Mass.

Brandt, E.W. (1973), "Some Observations on the Control of Density by Vibration", ASTM, STP 523, pp. 121-132.

Breth, H. and Schwab, H.H. (1977), "Liquefaction of a Fully Saturated Sand Under Anisotropic Initial State of Stress in a Controlled Drainage System", to be published at June ASTM Meeting, Denver, Colorado.

Brown, S. (1974), "Repeated Load Testing of a Granular Material", JSMFD, ASCE, 101, GT 7, pp. 825-841.

Carstens, T., Brebner, A., Kamphuis, J.W. (1976), "Seabed Mobility under Vertical Pressure Gradients", Proc. BOSS'76, 1, pp. 423-438, Trondheim, Norway.

Casagrande, A. (1936), "Characteristics of Cohesionless Soils Affecting the Stability of Slopes and Earth Fills", Contributions to Soil Mechanics, 1925-1940, Boston Society of Civil Engineers, Oct. 1940.

Casagrande, A. (1971), "On Liquefaction Phenomena: A Lecture to the ENCOLD and the British Geotechnical Society", Geo-Technique, 21, No. 3, pp. 197-202.

Casagrande, A. (1976), "Liquefaction and Cyclic Deformation of Sands, A Critical Review", Harvard Soil Mechanics Series No. 88.

Castro, G. (1969), "Liquefaction of Sands", PhD Dissertation, Harvard University.

Castro, G. (1975), "Liquefaction and Cyclic Mobility of Saturated Sands", JGED, ASCE, 101, No. GT6, pp. 551-570.

Castro, G. and Christian, J.T. (1976), "Shear Strength of Soils and Cyclic Loading", JGED, ASCE, 102 GT9, pp. 887-894.

Castro, G. and Poulos, J. (1976), "Factors Affecting Liquefaction and Cyclic Mobility", ASCE NCLPGE, pp. 105-137.

Chan, C.K., (1975), "Low-Friction Seal System", JGED, ASCE, 101 GT9, pp. 991-995.

Cho, Y., Rizzo, P.C. and Humphoier, W.K. (1976), "Saturated Sand and Cyclic Dynamic Tests", ASCE NCLPGE, pp. 285-312.

Christian, J.T. and Boehmer, J.W. (1970), "Plane Strain Consolidation of Finite Elements", JSMFD, ASCE, 96, SM4, pp. 1435-1457.

Clausen, C.J.F. (1975), "Fundamentering av gravitasjonsplattformer i Nordsjøen", NGI, Publication 110.

Clausen, C.J.F., DiBiagio, E., Duncan, J.M. and Andersen, K.H. (1975), "Observed Behavior of the Ekofisk Oil Storage Tank Foundation", NGI Pubilicatoin No. 108, pp. 1-8.

Cornforth, D.H. (1964), "Some Experiments on the Influence of Strain Conditions on the Strength of Sand", Geotechnique, 14, No. 2, pp. 143-167.

Cornforth,D.H., (1973) "Prediction of Drained Strength of Sands from Relative Density Measurement," ASTM STP 523, pp. 281-303.

Coulter, H.W. and Migliaccio, R.R. (1966), "Effects of the Earthquake of March 27, 1964 at Valdez, Alaska", Geological Survey Professional Paper 542-C, U.S. Dept. of the Interior, Washington, D.C.

Crandell, F.J. (1949), "Ground Vibration Due to Blasting and its Effect upon Structures", Jour. of Boston Soc. of Civ. Eng. Vol 27, pp. 6-27

D'Appolonia, E. (1970), "Dynamic Loadings", JGED, ASCE, 97, SM1, pp. 49-72.

De Alba, P.A., Chan, C.K. and Seed, H.B. (1975), "Determination of Soil Liquefaction Characteristics by Large-Scale Laboratory Tests", Report No. EERC 75-14.

DiBiagio, E., Myrvoll, F. and Borg-Hansen, S. (1976), "Instrumentation of Gravity Platforms for Performance Observations", Proc. BOSS'76, 1, pp. 516-527.

Dickin, E.A. (1973a), "Use of Lubicated and Conventional End Platens in Triaxial Tests on Sands", Soil and Foundations, 13, No. 4, pp. 87-89.

Dickin, E.A. (1973b), "Influence of Grain Shape and Size Upon the Limiting Porosities of Sands", ASTM STP 523, pp. 113-120.

Dobry, R. and Whitman, R.V. (1972), "Compaction of Sand on a Vertically Vibrating Table", MIT Soils Publicaton, No. 302, May.

Donovan, N.C. and Singh, S. (1976), "Liquefaction Criteria for the Trans-Alaska Pipeline", ASCE NCLPGE, pp. 139-168.

Drnevich, V.P. (1972), "Undrained Cyclic Shear of Saturated Sand", JSMFD, ASCE, 98, No. SM8, pp. 807-825.

Drnevich, V.P., Hall, J.R., Jr. and Richard F.E., Jr. (1966), "Large Amplitude Vibration Effects on the Shear Modulus of Sand", U.S. Army Engineer Waterways Experiment Station, Vicksburg, MS, Contract Report No. 3-161.

Drnevich, V.P., Hall, J.R., Jr. and Richart, F.E., Jr. (1967), "Effects of Amplitude of Vibration on the Shear Modulus of Sand", Proc. International Symposium on Wave Propagation and Dynamic Properties of Earth Materials, New Mexico, pp. 189-199.

Drnevich, V.P. and Richard, F.E., Jr. (1970), "Dynamic Prestraining of Dry Sand", JSMFD, ASCE, 96, No. SM2, pp. 253-469.

Duncan, J.M. and Dunlop, P. (1968), "The Significance of Cap and Base Restraint", JSMFD, ASCE, 94, SM1, pp. 271-290.

Durham, G.N. (1971), "A Study of the Liquefaction Phenomena of a Fine Sand Utilizing the Consolidated Undrained Triaxial Compression Test Under Controlled Stress Loading", MSc Thesis, Mississippi State University, August.

Durham, G.N. and Townsend, F.C. (1973), "Effect of Relative Density on the Liquefaction Susceptability of a Fine Sand Under Controlled Stress Loading", ASTM STP 523, pp. 319-331.

Edgers, L., Ladd, C.C. and Christian, J.T. (1973), "Undrained Creep of Atchafalaya Levee Foundation Clays", MIT Research Report R73-16, Dept. of Civil Engineering.

Eekelen, H.A.M. van (1976a), "Discussion of Smits' Paper", Proc. BOSS'76, 2, p. 449.

Eekelen, H.A.M. van (1976b), "Discussion of Janbu's Paper", Proc. BOSS'76, 2, pp. 450-451.

Eekelen, H.A.M. van (1976c), "Discussion of Foss' Paper", Proc. BOSS'76, 2, p. 474.

Eide, O. (1974), "Marine Soil Mechanics", NGI Publication, No. 103.

Eide, O. (1976), "Chairman's Report; Performance of Platforms", Proc. BOSS'76, 2, pp. 465-468.

Ellis, W. and Hartman, V.B. (1967), "Dynamic Soil Strength and Slope Stability", JSMFD, ASCE, 93, SM7.

El-Sohby, M.A. and Andrawes, K.Z. (1973), "Experimental Examination of Sand Anisotropy", Proc. 8th ICSMFE, Moscow, Vol. 1.1, pp. 103-109.

Emery, J.J., Finn, W.D.L. and Lee, K.L. (1972), "Uniformity of Saturated Sand Samples", Soil Mechanics Series, University of British Columbia.

Faccioli, F. and Resendiz, D. (1975), "Soil Dynamics", Seismic Risk and Engineering Decisions, Elsevier, Amsterdam.

Farrell, E.R. (1970), "A Study of the Behavior of Saturated Sand during Repeated Loading", MSc Thesis, Cornell University, Ithaca, New York.

Ferguson, H.A. (1972), "The netherlands Delta Project: Problems and Lessons", Proc. Inst. for Civil Engineers, 51, pp. 465-478, March.

Finn, W.D.L. (1972), "Soil Dynamics Liquefaction of Sands", Proc. Microzonation Conference Seattle, 1, pp. 87-111.

Finn, W.D.L., Bransby, P.L. and Pickering, D.J. (1970), "Effect of Strain History on Liquefaction of Sand", JSMFD, ASCE, 96, No. SM6, pp. 1917-1934.

Finn, W.D.L., Byrne, P.M. and Martin, G.R. (1976), "Seismic Response and Liquefaction of Sands", JGED, ASCE, 102, GT8, pp. 841-856.

Finn, W.D.L., Emergy, J.J. and Gupta, Y.P. (1971), "Liquefaction of Large Samples of Saturated Sand on a Shaking Table", Proc. 1st Canadian Conf. on Earthquake Engrg., Vancouver, Canada, pp. 97-110.

Finn, W.D.L., Lee, K.W. and Martin, G.R. (1976), "An Effective Stress MOdel for Liquefaction", ASCE NCLPGE, pp. 169-198.

Finn, W.D.L., Pickering, D.J. and Bransby, P.L. (1971), "Sand Liquefaction in Triaxial and Simple Shear Tests", JSMFD, ASCE, 97, No. SM4, pp. 639-659.

Finn, W.D.L. and Vaid, Y.P. (1977), "Liquefaction Potential from Drained Constant Volume Cyclic Simple Shear Tests", Proc. 6th WCEE, 6, pp. 7-12, New Dehli, India.

Florin, V.A. and Ivanov, P.L. (1961), "Liquefaction of Saturated Sandy Soils", Proc. 5th ICSMFE, Paris, France.

Foss, J. (1976), "Instrumentation for Operation Surveillance of Gravity Structures", Proc. BOSS'76, 1, pp. 545-556, Trondheim, Norway.

Gallagher, K.A. (1976), "Performance of the Foundation of the Christchurch Bay Tower", Proc. BOSS'76, 2, pp. 549-552.

Geotechnical Engineers, Inc. (1975), "Liquefaction Investigation, Athletic Facilities, Harvard University", Winchester, Mass.

Geotechnical Engineers, Inc. (1976a), "Seminar on Earthquake Analysis of Sand Foundations for Nuclear Plants and Dams", Winchester, Mass., April 20-21.

Geotechnical Engineers, Inc. (1976b), "Test Pit Investigation and Laboratory Testing, Pilgrim Nuclear Station No. 600, Unit II", Winchester, Mass.

Geuze, E. (1948), "Critical Density of Some Dutch Sands", Proceedings, 2nd ICSMFE, Rotterdam, 3, pp. 125-130.

Ghaboussi, J. and Wilson, E.L. (1973), "Liquefaction of Saturated Granular Soils", Proc. 5th WCEE, Rome, Italy, Preprint No. 44.

Gordon, B.B., Dayton, D.J. and Sadigh, K. (1974), "Seismic Stability of Upper Leandro Dam", JGED, ASCE, 100, GT. 5.

Goto, N. et al. (1977), "An Easy-Capable and High-Precise Shear Wave Measurement by Means of the Standard Penetration Test", Proc. 6th WCEE, 6, pp. 171-176, New Dehli, India.

Grande, L. and Eggereide, K. (1976), "Discussion of Janbu's Paper", Proc. BOSS'76, 2, pp. 452-461.

Gupta, M.K. and Prakash, S. (1977), "Sand Liquefaction During Shake Table Vibration", Proc. 6th WCEE, 6, pp. 19-24, New Dehli, India.

Hansen, B. (1976), "Modes of Failure Under Inclined Eccentric Laods", Proceedings, BOSS'76, 1, pp. 488-500, Trondheim, Norway.

Hansen, W.R. (1965), "Effects of the Earthquake of March, 27, 1964 at Anchorage, Alaska", Geological Survey Professional Paper 542-A, U.S. Dept. of the Interior, Wash. D.C.

Hara, A. and Kiyota, Y. (1977), "Dynamic Shear Tests of Soils for Seismic Analysis", Proceedings, 9th ICSMFE Tokyo.

Hardin, B.O. and Black, W.L. (1966), "Sand Stiffness Under Various Triaxial Stresses", JSMFD, ASCE, 92, No. SM2, pp. 27-42.

Hardin, B.O. and Drnevich, V.P. (1972a), "Shear Modulus and Damping in Soils: Measurement and Parameter Effects", JSMFD, ASCE, 98, No. SM6, pp. 603-624.

Hardin, B.O. and Drnevich, V.P. (1972b), "Shear Modulus and Damping in Soils: Design Equations and Curves", JSMFD, ASCE, 98, No. SM7, pp. 667-692.

Hardin, B.O. and Richard, F.E., Jr. (1963), "Elastic Wave Velocities in Granular Soils", JSMFD, ASCE, 89, No. SM1, pp. 33-65.

Hazen, A. (1892), "Physical Properties of Sands and Gravels with Reference to their Use in Filtration", Report Mass. State of Board of Health, p. 539.

Hendron, A.J., Jr. (1963), "The Behavior of Sand in One-Dimensional Compression", PhD Thesis, University of Illinois.

Herrmann, H.G. and Houston, W.N. (1976), "Response of Sea-floor Soils to Combined Static and Cyclic Loading", Proc. OTC, Paper No. 2428, Houston, May.

Hertwig, A., Früh, G. and Lorenz, H. (1933), "Die Ermittlung der für das Bauwesen wichtigsten Eigenschaften des Bodens duzch erzwundgende Schwingungen", Degebo, Veröffentlichung, Vol. 1.

Hicks, R.G. (1970), "Factors Influencing the Resilient Properties of Granular Materials", University of California at Berkeley.

Hoffman, D. (1974), "Analysis of Wave Records and Application to Design", International Symposium on Ocean Wave Measurement and Analysis, Vol. II, pp. 235-253.

Huang, W.-X. (1961), "Investigation on Stability of Saturated Sand Foundations and Slopes Against Liquefaction", Proc. 5th ICSMFE, 2, pp. 629-631.

Høeg, K. (1976), "Foundation Engineering for Fixed Off-Shore Structures", Proc. BOSS'76, 1, pp. 39-69, Trondheim, Norway.

Ishibashi, I. and Sherif, M.A. (1974), "Soil Liquefaction by Torsional Simple Shear Device", JGED, ASCE, 100, GT8, pp. 871-888.

Ishihara, K. (1975), "Sand Liquefaction in Hollow Cylinder Torsion Under Irregular Excitation", Soils and Foundations, 15 No. 1, pp. 45-49.

Ishihara, K. et al (1977), "Liquefaction of Anisotropically Consolidated Sand", Proceedings, 9th ICSMFE, Tokyo.

Ishihara, K. and Kawaguchi, N. (1970), "Triaxial Torsion Shear Tests on Saturated Sands Under Simulated Earthquake Loading Conditions", Proc. 3rd Japan Earthquake Engineering Symposium, Tokyo.

Ishihara, K. and Li, S.I. (1972), "Liquefaction of Saturated Sand in Triaxial Torsion Shear Test", Soils and Foundations, 12, No. 3, pp. 19-39.

Ishihara, K. and Takatsu, H. (1977), "Pore Pressure Buildup in Initially Sheared Sand Subjected to Irregular Excitation", Proc. 6th WCEE, 6, pp. 13-18, New Dehli, India.

Ishihara, K. and Yasuda, S. (1972), "Sand Liquefaction Due to Irregular Excitation", Soils and Foundations, 12, No. 4, pp. 65-78.

Ishihara, K. and Yasuda, S. (1973), "Sand Liquefaction Under Random Earthquake Loading Condition", Proc. 5th WCEE, Rome, Preprint No. 38.

Jaky, F. (1944), "The Coefficient of Earth Pressure at Rest", Journal of the Society of Hungarian Architects and Engineers, pp. 355-358.

Janbu, N. (1976), "Chairman's Summary", Proc. BOSS'76, 2, pp. 373-383.

Janbu, N. (1976), "Summary of Soil Sessions", Proc. BOSS'76, 2, pp. 654-660.

Janbu, N., Grande, L., Eggereide, K. (1976), "Effective Stress Stability Analysis of Gravity Structures", Proc. BOSS'76, 1, pp. 449-466, Trondheim, Norway.

Johnston, M.M. (1973), "Laboratory Studies of Maximum and Minimum Dry Densities of Cohesionless Soils", STP 523, ASTM, pp. 133-140.

Kawakami, F. and Asada, A (1966), "Damage to the Ground and Earth Structures by the Niigata Earthquake of June 16, 1964", Soils and Foundations, Vol. 6, Na. 1.

Khosla, V.K. (1972), "Behavior of Dry Ottawa Sand Under Cyclic Loadings", PhD Thesis, Ohio State University, Columbus, Ohio.

Khosla, V.K. and Wu, T.H. (1976), "Stress-Strain Behavior of Sand", JGED, ASCE, 102, GT4, pp. 303-321.

Kirkpatrick, W.M. Seals, R.K. and Newman, F.B. (1974), "Stress Distributions in Triaxial Compression Samples", JGED, ASCE, 100, GT2, pp. 190-196.

Kishida (1969), "Characteristics of Liquefied Sands During Mino-Owari, Tohnankai and Fukui Earthquakes", Soils and Foundations, Vol. 6, No. 2, pp. 38-44.

Kishida, H. (1970), "Characteristics of Liquefaction of Level Sandy Ground During the Tokachioki Earthquake", Soils and Foundations, 10, No. 2.

Klein, K. Michaelsen, M. and DiBiagio, E. (1976), "A System for Full Scale Measurements and Continuous Monitoring of Gravity Platform Behavior in the North Sea", Platform Instrumentation Consultants, PI-Group, Report.

Kolbuszewski, J.J. (1948), "An Experimental Study of the Maximum and Minimum Porosities of Sands", Proc. 2nd ICSMFE, 1, Rotterdam.

Kolbuszewski, J.J. (1948), "General Investigation of the Fundamental Factors Controlling Loose Packings of Sand", Proceedings, 2nd ICSMFE, Rotterdam.

Koppejan, A.W., Wamelen, B.M. and Weinberg, L.J. (1948), "Coastal Flow Slides in the Dutch Providence of Zeeland", Proceedings, 2nd ICSMFE, Rotterdam, 5, pp. 89-96.

Krizek, J.R. (1971), "Rheologic Behavior of Cohesionless Soils Subjected to Dynamic Loads", Transactions of the Society of Rheologie, 15, No. 3, pp. 491-540.

Kurzeme, M. (1971), "Liquefaction of Saturated Granular Soils", Proceedings, Australia-New Zealand Conference on Geomechanics, 1, Melbourne, pp. 45-53.

Lacroix, Y. and Horn, H.M. (1973), "Direct Determination and Indirect Evaluation of Relative Density and Its Use on Earth-work Construction Projects", ASTM STP 523, pp. 251-280.

Ladd, C.C. (1964), "Stress-Strain Behavior of Saturated Clay and Basic Strength Principles", Research Report R64-17, M.I.T., Cambridge, Mass.

Ladd, C.C. and Edgers, L. (1972), "Consolidated-Undrained Direct-Simple Shear Tests on Saturated Clays", Soils Publication No. 284, M.I.T.

Ladd, C.C. et al. (1977), "Stress-Deformation and Strength Characteristics", Proceedings, 9th ICSMFE, Vol. I, pp 421-494, Tokyo.

Ladd, R.S. (1974a), "Liquefaction Behavior of Sands as Determined in the Laboratory", Lecture Notes, Columbia University Seminar.

Ladd, R.S. (1974b), "Specimen Preparation and Liquefaction of Sands", JGED, ASCE, 100, No. GT10, pp. 1180-1184.

Ladd, R.S. (1976a), "Effects of Specimen Preparation on the Cyclic Structural Stability of Sands", unpublished.

Ladd, R.S. (1976b), "Specimen Preparation and Cyclic Stability of Sands", ASCE NCLPGE, pp. 199-226.

Ladd, R.S. (1976c), "Cyclic Behavior of Sands as Determined in the Laboratory for Earthquake Analysis", Lecture Notes, Short Course Univ. of Miss., Rolla, May.

Lade, P.V. and Duncan, J.M. (1975), "Elastoplastic Stress-Strain Theory for Cohesionless Soil", JGED, ASCE, 101, GT10, pp. 1037-1053.

Lade, P.V. and Duncan, J.M. (1976), "Stress-Path Dependent Behavior of Cohesionless Soil", JGED, ASCE, 102, GT1, pp. 51-68.

Lade, P.V. and Hernandez, S.B. (1977), "Membrane Penetration Effects in Undrained Tests", JGED, ASCE, 103, pp. 109-125.

Lambe, T.W. (1951), "Soil Testing for Engineers", John Wiley & Sons, Inc., New York.

Lambe, T.W. (1967), "Stress Path Method", JSMFD, ASCE, 93, SM6, pp. 309-339.

Lambe, T.W. and Associates (1976), "Prediction of Performance of the in Situ Test Caisson", Carlisle, Mass.

Lambe, T.W. and Whitman, R.V. (1969), Soil Mechanics, John Wiley and Sons, Inc., New York.

Lauritzen, R. and Schjetne, K. (1976), "Stability Calculations for Offshore Gravity Structures", NGI Publication 113, pp. 7-16.

Lee, K.L. (1970), "Triaxial Compressive Strength of Saturated Sands Under Seismic Loading", University of California, Berkeley, PhD Thesis.

Lee, K.L. (1971), "Characteristics of Liquefaction of Level Sandy Ground During the Tokachioki Earthquake", Discussion, Soils and Foundations, 11, pp. 65-68.

Lee, K.L. (1976a), "Influence of End Restraint in Cyclic Triaxial Tests", UCLA and WES, Vicksburg, Report S-76-1.

Lee, K.L. (1976b), "Fundamental Considerations for Cyclic Triaxial Tests on Saturated Sand", Proc. BOSS'76, 1, pp. 355-373, Trondheim, Norway.

Lee, K.L. (1976c), "Predicted and Measured Pore Pressures in the Ekofisk Tank Foundation", Proc. BOSS'76, 2, pp. 384-398.

Lee, K.L. (1976d), "Authors Reply to Discussion by Sequin", Proc. BOSS'76, 1, pp. 430-431.

Lee, K.L. (1977), "Adhesion Bonds in Sands at High Pressures", ASCE, JGED, Vol. 103, GT8 pp. 908-913.

Lee, K.L. and Albaisa, A. (1974), "Earthquake Induced Settlements in Saturated Sands", JGED, ASCE, 100, GT4, Proc. Paper 10496, pp. 387-406.

Lee, K.L. and Farhoomand, I. (1967), "Compressibility and Crushing of Granular Soil in Anisotropic Triaxial Compression", Canadian Geotechnical Journal, 4, No. 1, pp. 68-86.

Lee, K.L. and Fitton, J.A. (1969), "Factors Affecting the Cyclic Loading Strength of Soil", Vibration Effects of Earthquakes on Soils and Foundations, ASTM Special Technical Publication, 450, Phildelphia, Pa., pp. 71-95.

Lee, K.L. and Focht, J.A., Jr. (1975), "Liquefaction Potential at Ekofisk Tank in North Sea", JSMFD, ASCE, 101, GT1, pp. 1-18.

Lee, K.L. and Seed, H.B. (1967a), "Cyclic Stress Conditions Causing Liquefaction of Sand", JSMFD, ASCE, 93, No. SM1, pp. 47-70.

Lee, K.L. and Seed, H.B. (1967b), "Dynamic Strength of Anisotropically Consolidated Sand", JSMFD, ASCE, 93, No. SM5, pp. 169-190.

Lee, K.L. and Seed, H.B. (1967c), "Drained Strength Characteristics of Sands", JSMFD, ASCE, 93, SM6, pp. 117-141.

Lee, K.L. and Seed, H.B. (1970), "Undrained Strength of Anisotropically Consolidated Sand", JSMFD, ASCE, 96, SM2, pp. 411-428.

Lee, K.L. and Singh, A. (1971), "Relative Density and Relative Compaction", JSMFD, ASCE, 97, SM7, pp. 1049-1052.

Leeuw, E.H. de (1976), "Results of Large Scale Liquefaction Tests", Proc. BOSS'76, 2, pp. 65-84.

Lion, C.P., Streeter, V. and Richart, F.E., Jr. (1976), "A Numerical Model for Liquefaction", ASCE NCLPGE, pp. 313-342.

Lorenz, H. (1934), "Newe Ergebnisse der dynamischen Bangrunduntersuchung", Zeitschrift des Vereins deutscher Ingeniere, Vol. 78, pp. 379-385.

Ludes, A.S., Christian, F.T., Brandow, G.E. and Høeg, K. (1973), "Stress Conditions in NGI Simple Shear Test", N.G.I. Pubication No. 96, pp. 1-3.

Luscher, U., Ortiogosa, P., Rocker, K. and Whitman, R.V. (1967), "Repeated Load and Vibration Tests Upon Sand", Progress Report No. 1, Research Report R67-29, MIT.

Mahmood, A. (1973), "Fabric-Mechnical Properties Relationships in Fine Granular Soils", PhD Dissertation, University of California, Berkeley.

Marcuson, S.F. III and Krinitzsky, E.L. (1976), "Dynamic Analysis of Fort Peck Dam", U.S. Army WES, Vicksburg, Miss., Report No. 5-76-1.

Marcuson, S.F. III and Townsend, F.C. (1974), "The Effects of Reconstitution on Cyclic Triaxial Results", Preliminary Report, U.S. Army Corps of Engineers, WES, Vicksburg, Miss.

Marcuson, W.F. and Bieganousky, W.A. (1976), "Laboratory Standard Penetration Tests on Fine Sands", ASCE NCLPGE, pp. 255-284.

Martin, G.R., Finn, W.D.L. and Seed, H.B. (1975), "Fundamentals of Liquefaction Under Cyclic Loading", JGED, ASCE, 101, No. GT5 Proc. Paper 11285, pp. 423-438.

Maslov, M.N. (1957), "Questions of Seismic Stability of Submerged Sandy Foundations and Structures", Proc. 4th ICSMFE, Vol. 1, pp. 368-371, London.

McClelland, B. and Cox, W.R. (1976), "Performance of Pile Foundations for Fixed Offshore Structures", Proc. BOSS'76, 1, pp. 528-544, Trondheim, Norway.

Meehan, R.L. (1976), "Dynamic Strength of Hydraulic Fill", JGED, ASCE, 102, GT6, pp. 641-646.

Mitchell, J.K. (1976), Fundamentals of Soil Behavior, John Wiley & Sons, INc., New York.

Mori, K. (1976), "Factors Affecting the Liquefaction Behavior of Saturated Sands", PhD Dissertation, University of California, Berkeley.

Moshagen, H. and Tørum, A. (1975), "Wave Induced Pressures in Permeable Seabeds", JWW, ASCE, 101 WW1, pp. 49-57.

Moussa, A.A. (1975), "Equivalent Drained-Undrained Shearing Resistance of Sand to Cyclic Simple Shear Loading", Geotechnique, 25, No. 3, pp. 485-494.

Mulilis, J.P. (1975), "The Effect of Sample Preparation on the Cyclic Stress-Strain Behavior of Sands", PhD Thesis, University of California, Berkeley.

Mulilis, J.P. Chan, C.J. and Seed, H.B. (1975), "The Effects of Method of Sample Preparation on the Cyclic Stress-Strain Behavior of Sands", Report no. EERC75-18.

Mulilis, J.P., Horz, R.Z. and Townsend, F.C. (1976), "The Effects of Cyclic Triaxial Testing Techniques on the Liquefaction Behavior of Monterey No. 0 Sand", U.S. Army Corps of Engineers, WES, Vicksburg, Miss.

Mulilis, J.P. et al. (1977), "Effects of Sample Preparation on Sand Liquefaction", JGED, ASCE, 103, GT2, pp. 91-108.

Nishiyama, H. et al. (1977), "Practical Method of Predicting Sand Liquefaction", Proceedings, 9th ICSMFE, Tokyo.

Norris, G. (1975), "The Effect of Particle Size and the Natural Variation in Particle Shape and Surface Roughness on the Stress-Strain and Strength Behavior of Uniform Quartz Sands", PhD Thesis, University of California, Berkeley.

Norwegian Geotechnical Institute (1975a), "Research Project, Repeated Loading on Clay, Literature Review", Technical Information II, September.

Norwegian Geotechnical Institute (1975b), "Research Project, Repeated Loading on Clay, Summary and Interpretation of Test Results", Report No. 74037-9, 15 October.

Nunnally, S.W. (1966), "Development of a Liquefaction Index for Cohesionless Soils", PhD Thesis, Northwestern University.

Oda, M. (1972a), "Initial Fabrics and Their Relations to Mechanical Properties of Granular Material", Soils and Foundations, March, 12, NO. 1, pp. 17-36.

Oda, M. (1972b), "The Mechanism of Fabric Changes During Compressional Deformation of Sand", Soils and Foundations, June, 12, No. 2, pp. 1-18.

Oda, M. (1972c), "Deformation Mechanism of Sand in Triaxial Compression Tests", Soils and Foundations, December, 12, NO. 4, pp. 45-63.

O'Hara, S. (1972), "The Results of Experiment on the Liquefaction of Saturated Sands with a Shaking Box; Comparison with Other Methods", Technology Reports of The Yamaguchi University, 6, No. 2, pp. 14-37.

Ohsaki, Y. (1969), "Effects of Sand Compaction on Liquefaction During the Tokachioki Earthquake", Proc. 2nd Seminar on Soil Behavior and Ground Response During Earthquakes.

Ortigosa, P. (1968), "Densification of Sand by Vertical Vibrations with Almost Constant Stresses", Progress Report No. 2, Research Report, R68-2, MIT.

Park, T.K. and Sliver, M.L. (1975), "Dynamic Triaxial and Simple Shear Behavior of Sand", JGED, ASCE, 101, No. GT6, pp. 513-530.

Peacock, W.H. and Seed, H.B. (1968), "Sand Liquefaction Under Cyclic Loading Simple Shear Conditions", JSMFD, ASCE, 94, No. SM3, pp. 689-707.

Pender, M.J. (1977), "MOdelling Soil Behavior Under Cyclic Loading", Proceedings, 9th ICSMFE, Tokyo.

Pickering, D.J. (1973), "Drained Liquefaction Testing in Simple Shear", JSMFD, ASCE, 99, No. SM12, pp. 1179-1184.

Prevost, J.-H. and Høeg, K. (1975), "Mathematical Model for Static and Cyclic Undrained Clay Behavior", NGI Internal Report, 52412.

Procter, D.C. (1974), "An Upper Bound Value of ϕ_f in the Stress-Dilatancy Equation", Geotechnique, 24, No. 3, pp. 269-288.

Poulos, S.J. (1964), "Control of Leakage in the Triaxial Test", Harvard Soil Mechanics Series No. 71.

Pyke, R.M., Seed, H.B. and Chan, C.K. (1975), "Settlement of Sands under Multidirectional Shaking", JGED, ASCE, 101, No. GT4, Proc. Paper 11251, pp. 379-398.

Poulos, S.J. (1964), "Control of Leakage in the Triaxial Test", Harvard Soil Mechanics Series No. 71.

Pyke, R.M., Seed, H.B. and Chan, C.K. (1975), "Settlement of Sands under Multidirectional Shaking", JGED, ASCE, 101, No. GT4, Proc. Paper 11251, pp. 379-398.

Rahman, M.S., Seed, H.B and Booker, J.R. (1977), "Liquefaction Analysis for Offshore Oil Tanks", Unpublished.

Raju, V.S., Sadasivan, S.K. and Venkataraman, M. (1972), "Use of Lubricated and Conventional End Platens in Triaxial Tests on Sands", Soils and Foundations, 12, No. 4, pp. 35-43.

Richart, F.E., Jr. (1975), "Some Effects of Dynamic Soil Properties on Soil-Structure Interaction", JGED, ASCE, 101, GT12, pp. 1193-1240.

Richart, F.E., Jr., Anderson, D.G. and Stokoe, K.H. II (1977), "Predicting in situ Strain-Dependent Shear Moduli of Soil", Proc. 6th WCEE, 6, pp. 159-164, New Dehli, India.

Richart, F.E., Jr., Hall, J.R. and Woods, R.D. (1970), Vibrations of Soils and Foundations, Prentice-Hall, Inc., Englewood Cliffs, New Jersey.

Rocker, K., Jr. (1968), "The Liquefaction Behavior of Sands Subjected to Cyclic Loading", MIT Soils Publication No. 221.

Roscoe, K.H., Schofield, A.N. and Wroth, C.P. (1958), "On the Yielding of Soils", Geotechnique, 8, No. 1, pp. 22-57.

Rowe, P.W. (1962), "The Stress-Dilatancy Relations for Static Equilibrium of an Assembly of Particles in Contant", Proc., Royal Society of London, 269, Series A, pp. 500-527.

Rowe, P.W. (1972), "The Relevance of Soil Fabric to Site Investigation Practice", Geotechnique, 22, No. 2.

Rowe, P.W. and Barden, L. (1964), "The Importance of Free Ends in Triaxial Testing", JSMFD, ASCE, 90, SM1, pp. 1-27.

Rowe, P.W. and Proctor, D.C. (1976), "Cyclic Triaxial Tests with and without Lubricated Ends", unpublished.

Roy, M. and Lo, K.Y. (1971), "Effect of End Restraint on High Pressure Tests of Granular Materials", Revue Canadienne de Geotechnique, 8, No. 4, pp. 579-588.

Rutledge, P.C. (1974), "Cooperative Triaxial Shear Research Program", Progress Report on Soil Mechanics Fact Finding Survey, U.S. Army Engineer WES, Civil Engineering, Vicksburg, Miss.

Sangrey, D.A. (1968), "The Behavior of Soils Subjected to Repeated Loading", Thesis, Ithaca, New York.

Saxena, S.K., Hedberg, J. and Ladd, C.C. (1974), "Results of Special Laboratory Testing Program on Hackensack Valley Varved Clay", MIT Research Report R74-66, Soils Publication 342, Cambridge, Mass.

Schjetne, J. (1976), "Foundation Engineering for Gravity Structures in the North Sea", NGI Publication 113, pp. 23-33.

Schmertmann, J.H., (1970), "Static Cone to Compute Static Settlement over Sand," JSMFD, ASCE, Vol. 96, SM3, pp. 1011-1043.

Schofield, A. and Wroth, P., (1968), "Critical State Soil Mechanics, McGraw-Hill, New York.

Schroeder, W.L. and Schuster, R.L., (1969), "Laboratory Simulation of Seismic Activity in Saturated Sands," Vibration Effects of Earthquakes on Soils and Foundations, ASTM, STP 450, pp. 54-70.

Seed, H.B. (1968), "Landslides During Earthquakes Due to Soil Liquefaction", JSMFD, ASCE, 94, SM9.

Seed, H.B. (1976a), "Evaluation of Soil Liquefaction Effects on Level Ground During Earthquakes", ASCE NGLPGE, pp. 1-104.

Seed, H.B. (1976b), "Some Aspects of Sand Liquefaction Under Cyclic Loading", Proc. BOSS'76, Norway, 1, pp. 374-391.

Seed, H.B., Arango, J. and Chan, C.K. (1975), "Evaluation of Soil Liquefaction Potential During Earthquakes", Report No. EERC 75-28, University of California, Berkeley, October.

Seed, H.B. and Fead, J.W.N. (1959), "Apparatus for Repeated Load Tests on Soils", ASTM STP 254.

Seed, H.B. and Idriss, I.M. (1967), "Analysis of Soil Liquefaction, Niigata Earthquake", JSMFD, ASCE, 93, SM3.

Seed, H.B. and Idriss, I.M. (1969), "Influence of Soil Conditions on Ground Motions During Earthquakes", JSMFD, ASCE, 95, No. SM1, pp. 99-137.

Seed, H.B. and Idriss, I.M. (1970), "Soil Moduli and Damping Factors for Dynamic Response Analysis", Report No. EERC 70-10, University of California, Earthquake Engineering Center, Berkeley, California.

Seed, H.B. and Idriss, I.M. (1971), "Simplified Procedure for Evaluating Soil Liquefaction Potential", JSMFD, ASCE, 97, No. SM9, pp. 1249-1273.

Seed, H.B., Idriss, I.M., Makdisi, F. and Banerjee, N. (1975), "Representation of Irregular Stress Time Histories by Equivalet Uniform Stress Series in Liquefaction Analysis", Report No. EERC 75-29, University of California, Berkeley, October.

Seed, H.B. and Lee, K.L. (1966), "Liquefaction of Saturated Sands During Cyclic Loading", JSMFD, ASCE, 92, No. SM6, pp. 105-134.

Seed, H.B. and Lee, K.L. (1967), "Undrained Strength Characteritics of Cohesionless Soils", JSMFD, ASCE, 93, SM6, pp. 333-360.

Seed, H.B., Lee, K.L. and Idriss, I.M. (1969), "Analysis of Sheffield Dam Failure", JSMFD, ASCE, 95, SM6, pp. 1453-1490.

Seed, H.B., Lee, K.L., Idriss, I.M. and Makdisi, F.I. (1973), "Analysis of the Slides in the San Fernando Dams During the Earthquake of 9 February 1971", Report No. EERC 73-2, University of California, Berkeley.

Seed, H.B., Lysmer, J. and Hwang, R. (1975), "Soil Structure Interaction Analyses for Seismic Response", JGED, ASCE, 101, GT5, pp. 439-457.

Seed, H.B., Martin, P.P. and Lysmer, J. (1975), "The Generation and Dissipation of Pore Water Pressures During Soil Liquefaction", Report No. EERC 75-26.

Seed, H.B., Martin, P.P. and Lysmer, J. (1976), "Pore-Water Pressure Changes During Soil Liquefaction", JGED, ASCE, 102, GT4, pp. 323-346.

Seed, H.B., Mori, K. and Chan, C.K. (1975), "Influence of Seismic History on the Liquefaction Characteristics of Sands", Report No. EERC 75-25.

Seed, H.B., Mori, K. and Chan, C.K. (1977), "Influence of Seismic History on Liquefaction of Sands", JGED, ASCE, 103, GT4, pp. 257-270.

Seed, H.B. and Peacock, W.H. (1970), "Applicability of Laboratory Test Procedures for Measuring Soil Liquefaction Characteristics under Cyclic Loading", Report No. EERC 70-8, University of California, Berkeley, November.

Seed, H.B. and Peacock, W.H. (1971), "Test Procedures for Measuring Soil Liquefaction Characteristics", JSMFD, ASCE, 97, No. SM8, pp. 1099-1119.

Seed, H.B. and Silver, M.L. (1972), "Settlement of Dry Sands During Earthquakes", JSMFD, ASCE, 98, No. SM4, Proc. Paper 8844, pp. 381-397.

Selico, E.T. (1963), "Effect of Vibration on Density of Sand", Proc. 2nd Pan American CSMFE, 1, pp. 129-144.

Selig, E.T. and Ladd, R.S. (1973), "Evaluation of Relative Density Measurements and Applications", ASTM STP 523, pp. 487-504.

Shen, C.K., Vrymoed, F.L. and Uyeno, C.K. (1977), "The Effect of Fines on Liquefaction of Sands", Proceedings, 9th ICSMFE, Tokyo.

Sherif, M.A., Ishibashi, I. and Tsuchiya, C. (1977a), "Influence of Pore-Pressure Coefficient $\bar{B}$ on Soil Liquefaction Potential", Proc. 6th WCEE, 6, pp. 25-30, New Dehli, India.

Sherif, M.A., Ishibashi, I. and Tsuchiya, C. (1977b), "Saturation Effects on Initial Soil Liquefaction", ASCE, JGED, Vol. 103, GT8, pp. 914-917.

Shibata, T. (1970), "Liquefaction of Saturated Sands During Cyclic Loading", Proc. 3rd Japan Earthquake Engineering Symposium. Tokyo.

Shibata, T., Yukitomo, H. and Miyoshi, M. (1972), "Liquefaction Process of Sand During Cyclic Loading", Soils and Foundations, 12, No. 1, Tokyo, pp. 1-16.

Shockley, W.G. (1953), "The Effect of Stress History on the Relation Between ϕ and Porosity in Sand", Proc. 3rd ISCMFE, 3, p. 121.

Silver, M.L. (1976), "Laboratory Triaxial Testing Procedures to Determine the Cyclic Strength of Soils", Report No. NUREG-31, U.S. Nuclear Regulatory Commission, Washington, D.C.

Silver, M.L., Chan, C.K., Ladd, R.S., Lee, K., Mulilis, J., Tiedemann, D., Townsend, F.C., Valera, J. and Wilson, J. (1976), "Cyclic Triaxial Strength of Standard Test Sand", JGED, ASCE, 102, GT5, pp. 511-523.

Silver, M.L. and Seed, H.B. (1971a), "Deformation Characteristics of Sands Under Cyclic Loading", JSMFD, ASCE, 97, No. SM7, pp. 1081-1098.

Silver, M.L. and Seed, H.B. (1971b), "Volume Changes in Sands During Cyclic Loading", JSMFD, ASCE, 97, No. SM9, Proc. Paper 8354, pp. 1171-1182.

Simon, R.M., Ladd, C.C. and Christian, J.T. (1972), "Finite Element Program FEECON for Undrained Deformation Analyses of Granular Embankments of Soft Clay Foundations", MIT Soils Publication No. 294.

Skoglund, G.R., Maruson, W.F. III, Cunny, R.W. (1976), "Evaluation of Resonant Column Test Devices", JGED, ASCE, 102, GT11, pp. 1147-1158.

Sleath, J.F.A. (1970), "Wave-Induced Pressures in Beds of Sand", JHD, ASCE, 96, HY2, pp. 367-378.

Smits, F.P. (1976), "Stability and Defomration Analysis for Gravity Platforms", Proc. BOSS'76, Trondheim, Norway.

Sridharan, A., Altschaeffel, A.G. and Diamond, S. (1971), "Pore Size Distribution Studies", JSMFD, ASCE, 97, SM5, pp. 771-787.

Steinbach, J. (1967), "Volume Changes Due to Membrane Penetration in Triaxial Tests on Granular Materials", MSc Thesis, Cornell University, Ithaca, New York.

Stoll, R. and Kald, L. (1976), "The Threshold of Dilation Under Cyclic Loading", ASCE NCLPGE, pp.. 343-358.

Tanimoto, K. and Suga, Y. (1970), "On the Dynamic Strength of Saturated Sand", Proc. 3rd Japan Earthquake Engineering Symposium, Tokyo.

Tanimoto, K. and Suga, Y. (1971), "Liquefying Process of Saturated Sands Subjected to Dynamic Loading", Proc. 4th Asian Regional Conf., SMFE, Bangkok, Thailand.

Tatsuoka, F. and Ishihara, K. (1973), "Stress Path and Dilatancy Performance of a Sand", Proc. 8th ICSMFE, Moscow, 1, pp. 419-424.

Tavenas, F.A. (1973), "Difficulties in the Use of Relative Density as a Soil Parameter", ASTM STP 523, pp. 478-483.

Tavenas, F.A., Ladd, R.S. and LaRochelle, P. (1973), "Accuracy of Relative Density Measurements: Results of a Comparative Test Program", ASTM, STP 523, pp. 18-60.

Tavenas, F.A. and LaRochelle, P. (1972), "Accuracy of Relative Density Measurements", Geotechnique, 22, No. 4, pp. 549-562.

Terzaghi, K. (1925), "Erdbaumechanik auf Bodenphysicalischer Grundlage", Franz Deuticke, Vienna.

Thiers, G.R. and Seed, H.B. (1968), "Cyclic Stress-Strain Characteristics of Clay", JSMFD, ASCE, 94, SM2, pp. 555-569.

Tiedemann, D.A. (1973), "Variability of Laboratory Relative Density Test Results", ASTM, STP 523, pp. 61-73.

Timmerman, D.A. and Wu, T.H. (1969), "Behavior of Sand Under Cyclic Loading", JSMFD, ASCE, 95, SM4, pp. 1097-1112.

Tinoco, F.H. (1977), "Pore Pressure Parameters and Sand Liquefaction", Proceedings, 9th ICSMFE, Tokyo.

Valera, J.E. and Donovan, N.C. (1976), "Comparison of Methods for Liquefaction Evaluation", ASCE NCLPGE, pp. 359-388.

Vaughan, P.R., et al. (1976), "Stability Analysis of Large Gravity Structures", Proc. BOSS'76, 1, pp. 467-487, Trondheim, Norway.

Wang, M.S. (1972), "Liquefaction of Triaxial Sand Samples under Different Frequencies of Cyclic Loading", MSc Thesis, University of Western Ontario, London, Canada.

Whitman, R.V. (1970), "Evaluation of Soil Properties for Site Evaluation and Dynamic Analysis of Nuclear Plants", Seismic Design for Nuclear Power Plants, R.J. Hansen, ed., The MIT Press, Cambridge, MA, pp. 250-305.

Whitman, R.V. (1971), "Resistance of Soil to Liquefaction and Settlement", Soils and Foundations, 11, No. 4, pp. 59-68.

Whitman, R.V. and Healy, K.A. (1962), "Shear Resistance of Sand During Rapid Loading", Report No. 9 on Response of Soils to Dynamic Loading, MIT, May 1962.

Whitman, R.V. and Ortigosa, P. (1968), "Densification of Sand by Vertical Vibrations", Report No. 4, Soils Publication No. 222, MIT.

Winterkorn, H.F. and Fang, H.Y. (1975), Foundation Engineering Handbook, Van Nostrand Reinhold Co.

Wissa, A.E.Z., Christian, J.T., Davis, E.H. and Heiberg, S. (1971), "Consolidation at Constant Rate of Strain", JSMFD, ASCE, 97, SM10, pp. 1393-1413.

Wolfe, W.E. (1973), "Cyclic Strength of Cubic Saturated Sand Samples", MSc Thesis, University of California, Los Angeles.

Wolfe, W.E., Annaki, M. and Lee, K.L. (1977), "Soil Liquefaction in Cyclic Cubic Test Apparatus", Proc. 6th WCEE, 6, p. 1-6, New Dehli, India.

Wong, R.T., Seed, H.B. and Chan, C.K. (1975), "Cyclic Loading Liquefaction of Gravelly Soils", JGED, ASCE, 101, No. GT6, pp. 571-583.

Webster's Third New International Dictionary of the English Language Unabridged. G&C Merriam Company, Springfield, Mass. 1966.

Yamada, G. (1966), "Damage to Earth Structures and Foundations by the Niigata Earthquake, June 16, 1964." Soils and Foundations, Vol. 6, No. 1.

Yegian, M.K. (1976), "Risk Analysis for Earthquake-Induced Ground Failure by Liquefaction", PhD Thesis, MIT, Cambridge.

Yegian, M.K. and Whitman, R.V., (1977), "Soil Liquefaction Analysis Based on Field Observations", to be published.

Yoshimi, Y. (1967), "An Experimental Study of Liquefaction of Saturated Sands", Soils and Foundations, 7, No. 2, pp. 20-32.

Yoshimi, Y. et al. (1977), "Soil Dynamics and its Application to Foundation Engineering", Proceedings, 9th ICSMFE, Tokyo.

Yoshimi, Y. Kuwabara, F. (1973), "Effect of Subsurface Liquefaction on the Strength of Surface Soil", Soils and Foundations, 13, No. 2, pp. 67-81.

Yoshimi, Y. Kuwabara, F. and Tokimatsu, K. (1975), "One-Dimensional Volume Change Characteristics of Sands Under Very Low Confining Stresses", Soils and Foundations, 15, No. 3, September, pp. 51-66.

Yoshimi, Y. and Oh-Oka, H. (1970), "Liquefaction of Saturated Sand During Vibration Under Quasi-Plane-Strain Conditions", Proc. 3rd Japan Earthquake Engineering Symposium, Tokyo.

Yoshimi, Y. and Oh-Oka, H. (1973), "A Ring Torsion Apparatus for Simple Shear Tests", Proc. 8th ISCMFE, Vol. 1.2, Moscow.

Yoshimi, Y. and Oh-Oka, H. (1975), "Influence of Degree of Shear Stress Reversal on the Liquefaction Potential of Saturated Sand", Soils and Foundations, 15, No. 3.

Youd, T.L. (1970), "Densification and Shear of Sand During Vibration", JSMFD, ASCE, 96, No. SM3, Proc. Paper 7272, pp. 863-880.

Youd, T.L. (1971), "Maximum Density of Sand by Repeated Straining in Simple Shear", Highway Research Record, No. 374, pp. 1-6.

Youd, T.L. (1972), "Compaction of Sands by Repeated Shear Straining", JSMFD, ASCE, 98, N. SM7, Proc. Paper 9063, pp. 709-725.

Youd, T.L. (1973a), "Factors Controlling Maximum and Minimum Densities of Sands", ASTM, STP 523, pp. 98-112.

Youd, T.L. (1973b), "Liquefaction, Flow and Associated Ground Failure", Geological Survey Circular 688.

Youd, T.L. and Craven, T.N. (1975), "Lateral Stress in Sands During Cyclic Loading", Technical Note, JGED, ASCE, 101, GT2, pp. 217-221.

Youd, T.L., Nichols, D.R., Helley, E.J. and Lajoie, K.R. (1975), "Liquefaction Potential", Studies for Seismic Zonation, Reduction of Earthquake Hazards, San Francisco Bay Region.

Zienkiewicz, O.C., et al. (1976), "Numerical Analysis for Foundation of Offshore Structures with Special Reference to Progressive Deformation", Society of Pet. Engr. of AIME, European Spring Meeting, Proc. Paper No. 5760.

APPENDIX A

Oosterschelde Sand

All the cyclic tests were performed on one sand, Oosterschelde Fine Sand. About half of the static tests were performed on the same sand, the other half on Oosterschelde Medium Sand. Both sands are sampled at Neeltje Jans in the Oosterschelde Bay entrance, off the coast of southern Holland. Prior to all testing, the sands were sieved on a number 10 sieve (2 mm openings) to remove large shell pieces and clay lumps. Both sands are Holocene deposits.

A.1 General Description of Sand

Both the Fine and the Medium Oosterschelde sand are uniform. Figure A.1 presents the grain size distribution of the two sands. The mean grain size is .17 mm for the fine sand and .28 mm for the medium sand. The coefficient of uniformity ($U = D_{60}/D_{10}$) is 1.4 and 1.7 respectively.

Both sands have less than 0.5% fines content (passing #200 sieve, .074 mm diameter openings). The large shell pieces and clay lumps removed with the #10 sieve comprised about 1.5% of the total sand weight, they are not included in the grain size distribution curves.

Scanning electron microscope pictures were taken of the fine sand. Figure A.2 shows two pictures of sand

grains from the largest fraction of Oosterschelde Fine Sand, -#60, +#100 sieve material. The grains are subrounded, and consist of quartz with feldspars common and lesser amounts of mica, shell fragments and calcite grains. X-ray diffraction of a subsample comprising all -#10 sieve fractions indicated 65% quartz and detectable calcite, feldspars and aragonite. The percent acid soluble (calcite) was 5%. No clay was detected. X-ray diffraction of a clay lump separated off on the #10 sieve showed 30% calcite, 25% clay, 20% quartz and detectable aragonite and feldspars. The clay was an illite smectite with some chlorite and/or kaolinite. The plastic limit of a sample composed of clay lumps was 18.6%, the liquid limit 45.4% and thus the plasticity index 26.8%.

Oosterschelde Medium Sand has rounded grains which consist of quartz with feldspars common and lesser amounts of mica, shell fragments, clay and calcite grains. X-ray diffraction indicated no crystalline phases not observed with the optical microscope. The percent acid soluble was 3.3%.

Microscopic examination of the Oosterschelde Fine Sand revealed that the +#60 sieve size fractions contain abundant aggregates that break down under cyclic loading. The aggregates are quartz and feldspar grains held together by a calcium carbonate cement. Figure A.3 shows typical examples of the coarser fractions before and after cyclic testing. The nature of the cementation is clearly visible

in the upper picture.

The central particle in the lower picture of tested sand is an example of cement separated from mineral grains. A replica of a mineral grain surface is evident on the left side of the cement aggregate. The microscopic examination of sand from the +#60 sieve fractions after cyclic loading showed many cement particles but no aggregates. Dispersive X-ray analysis showed that the calcium content of the cement particle in Figure A.3 is as high as the calcium content of the shell piece next to it. Silicia content was very low, while the silicia content of the aggregates in the upper picture was very high.

No aggregates were observed in the finer sieve fractions (-#60 sieve) of the Oosterschelde Fine Sand. Also no difference was observed between cyclically tested and untested sand from the finer fractions (see Figure A.2). The coarser sieve fractions (+#60 sieve) comprises about 10% of the sand. Less than 20% of the coarse material is cemented, so less than 2% of the total sand sample consists of cemented particles.

Microscopic examination of the Oosterschelde Medium Sand revealed that the +#40 sieve size fractions contain numerous aggregates that broke down under cyclic loading. The aggregates are comprised of quartz and feldspar grains held together by a natural cement apparently high in clay and NaCl while low in carbonate minerals.

Dispersive X-ray analysis of that cement gave high silica, considerable Al, Fe, Na and Cl, but very low Ca. The quartz grains to which the cement adheres gave only silica. Powder X-ray diffraction indicated that the crystalline carbonate phases were calcite, aragonite and a trace of dolomite; all of which are high in calcium. Therefore, it was concluded that the cement in the medium sand was high in clay and NaCl, but low in carbonate.

No aggregates were observed in the finer sieve fractions (-#40 sieve) of the Oosterschelde Medium Sand. Also no difference was observed between cyclically tested and untested sand from the finer fractions. As the coarser sieve fractions (+#40 sieve) comprises only about 3-4% of the total sand weight, it was estimated that less than 1% of the Oosterschelde Medium Sand is made up of cemented particles.

A.2 Relative Density

The relative density tests on Oosterschelde Fine Sand were performed according to ASTM D-2049-69, "Standard Method of Test for Relative Density of Cohesionless Soils" with the following modifications: The sand was air dried prior to testing, not oven dried as specified in the standard. The cylinder on top of the 1/2 inch funnel was 3 inches in diameter and 30 inches high. The Soiltest vibratory table used for maximum density determination does not quite meet the standard's requirements for velocity and acceleration.

The relative density tests on Oosterschelde Medium Sand were not performed according to ASTM standards. The minimum density was determined by pouring sand directly from a bucket into the 0.1 ft^3 mold, or by pouring from the bucket through a 1/2 inch funnel into the same mold. Maximum density was determined by hammering on the base and the sides of the mold. Table A.1 gives the results from all relative density tests, and some remarks about how they were performed. The following values for maximum and minimum relative density were found:

Fine sand: 0% R_d at n = 46.0% or γ_d = 1.428 t/m^3

100% R_d at n = 34.5% or γ_d = 1.732 t/m^3

Medium sand: 0% R_d at n = 45.0% or γ_d = 1.454 t/m^3

100% R_d at n = 34.5° or γ_d = 1.732 t/m^3

Figure A.4 gives a plot of porosity versus relative density for both sands.

A.3 Specific Gravity

All specific gravity determinations were performed according to Lambe (1951). One determination on each of the fine and medium sands were performed on unwashed samples, where salt present in the sand dissolved in the water, and increased its unit weight. Both determinations gave a specific gravity G = 2.62. All other samples were carefully washed through filter paper to remove the salt without loss of any

sand fractions. Three determinations on desalted medium sand gave G = 2.649, G = 2.636, and G = 2.643. Two determinations on desalted fine sand gave G = 2.646 and G = 2.643. Both Fine and Medium Oosterschelde Sand thus have an average specific gravity value G = 2.64.

A.4 Sand Permeability

Permeability tests were performed on both Fine and Medium Oosterschelde Sand. Samples about 26 cm long and with an area of 5 cm^2 were tested under a gradient of 0.5 and a back pressure of 40 psi. No loss of fines during the tests was observed. The setup of the test allowed for densification with a vibratory tool, such that one sample could be tested at various densities.

Figure A.5 presents the measured values of permeability coefficients (k) versus the sample porosity. Hazen's (1892) empirical correlation for the permeability of loose, uniform sand, k (cm/sec) = 100 to 150 · D_{10}^2 (cm), yield for the Fine Ooosterschelde Sand k = 0.017 to 0.025 cm/sec and for the Medium Sand k = 0.029 to 0.044 cm/sec. Both values correspond very well to the measured values of permeability.

Test #	Sand Type	Maximum density n%	Minimum density n%	Remarks
1	M.S.*	-	44.68	Poured into mold
2	M.S.	-	45.06	Poured into mold
3	M.S.	-	44.90	Poured into mold
4	M.S.	-	44.92	Poured into mold
5	M.S.	-	44.99	Pour through funnel
6	M.S.	-	45.10	Pour through funnel
7	M.S.	37.97	-	Hammer on mold, no surcharge
8	M.S.	35.85	-	Hammer on mold with surcharge
9	M.S.	34.64	-	Hammer, 10 layers, surcharge
10	M.S.	34.38	-	As 9, also hammer on base
11	M.S.	35.02	-	As 9
12	M.S.	34.72	-	Test #11, hammer on base
13	F.S.**	-	46.03	ASTM Procedure
14	F.S.	34.83	-	ASTM Procedure
15	F.S.	-	45.88	ASTM Procedure
16	F.S.	34.34	-	ASTM Procedure
17	F.S.	-	46.10	Poured into mold
18	F.S.	35.14	-	ASTM, wet sand

*M.S.= Oosterschelde Medium Sand

**F.S.= Oosterschelde Fine Sand

SUMMARY OF RELATIVE DENSITY TESTS

TABLE A.1

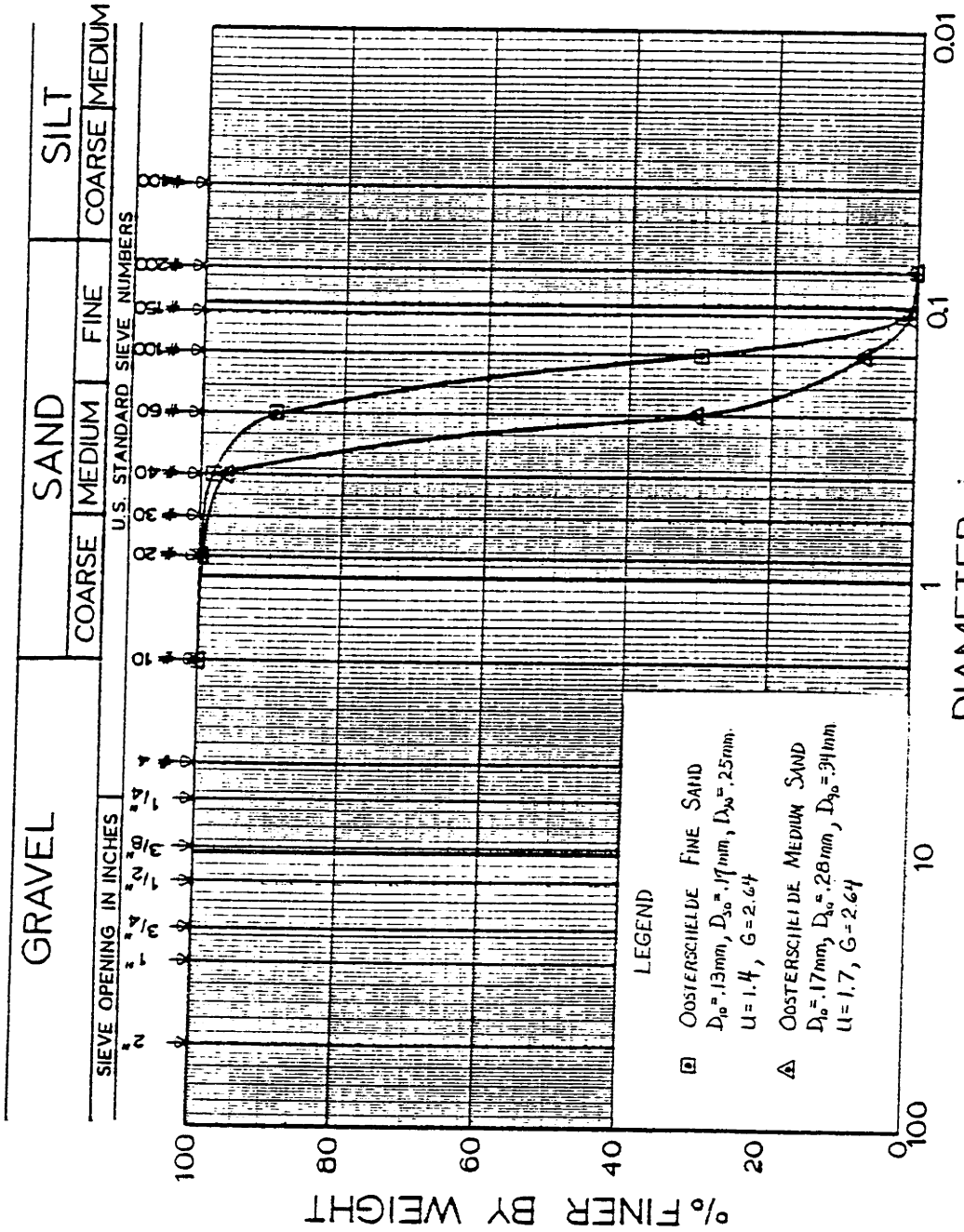

GRAIN SIZE DISTRIBUTION

FIGURE A-1

SAND BEFORE TESTING

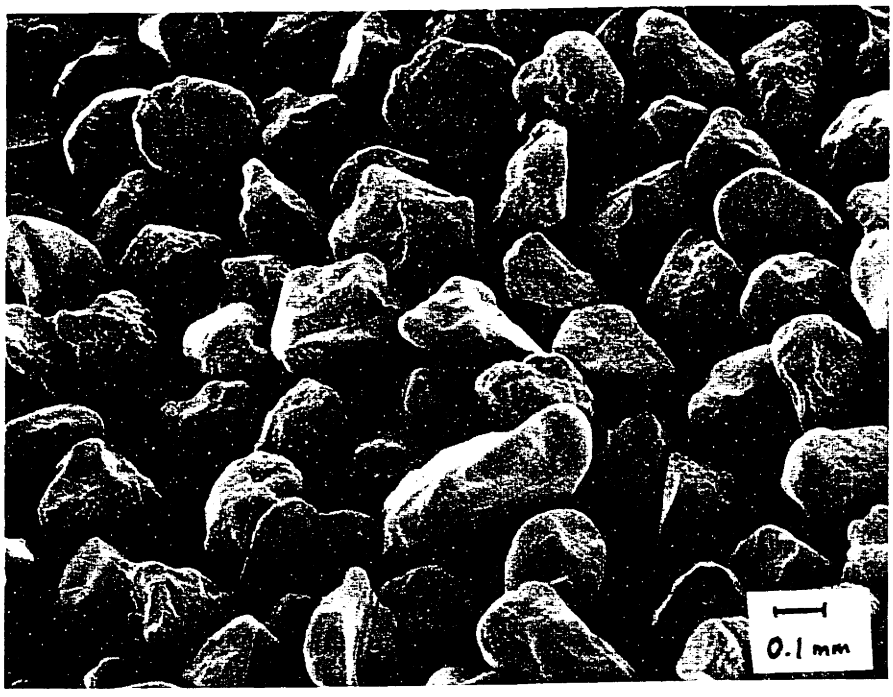

SAND AFTER TESTING

SCANNING ELECTRON MICROSCOPE PICTURES OF - #60, - #100 SIEVE FRACTION OF FINE OOSTERSCHELDE SAND.

FIGURE A. 2

SAND BEFORE TESTING

SAND AFTER TESTING

SCANNING ELECTRON MICROSCOPE PICTURES OF - #40, + #60 SIEVE FRACTION OF OOSTERSCHELDE FINE SAND.

FIGURE A. 3

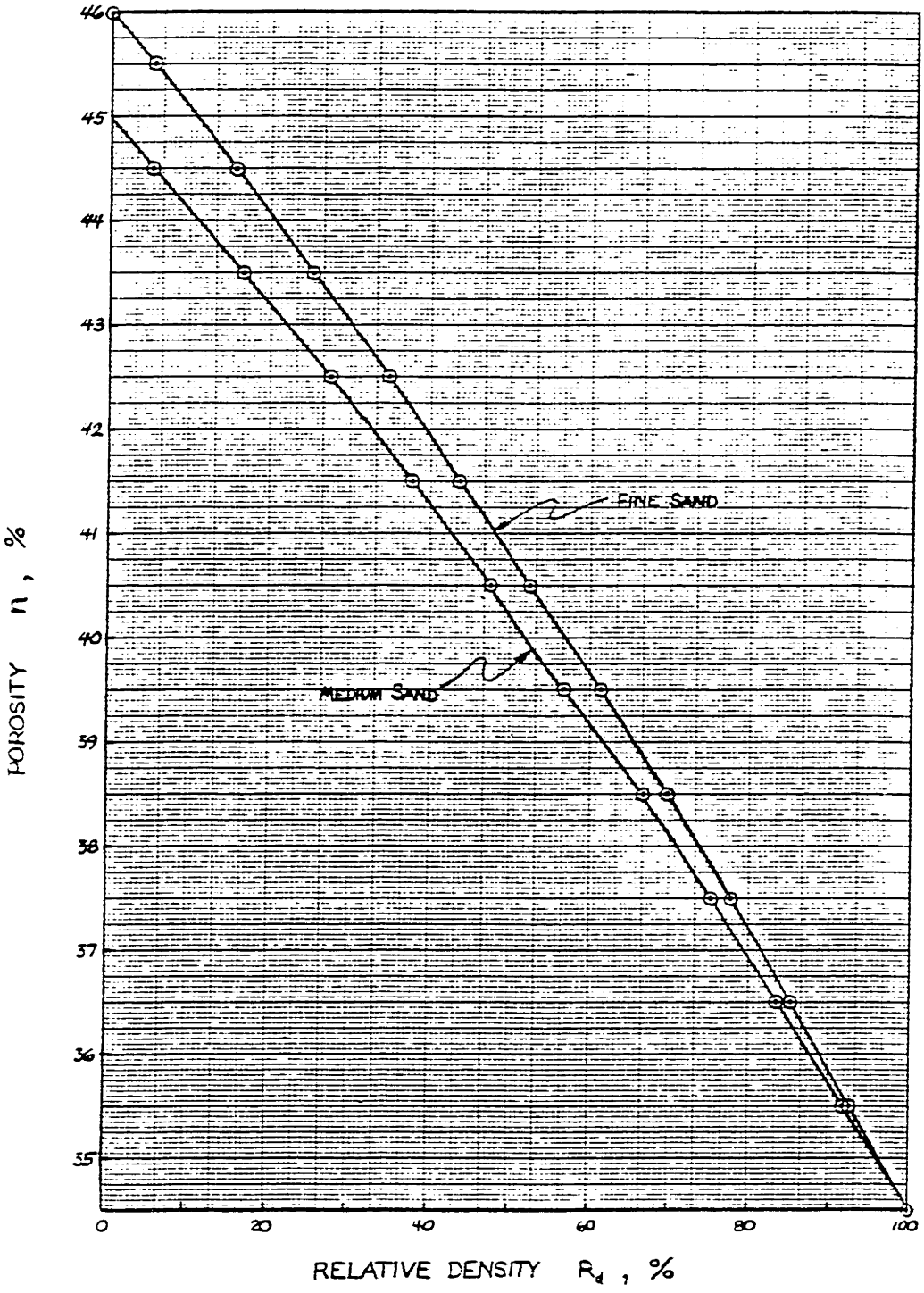

RELATIVE DENSITY VERSUS POROSITY FOR OOSTERSCHELDE SAND

FIGURE A-4

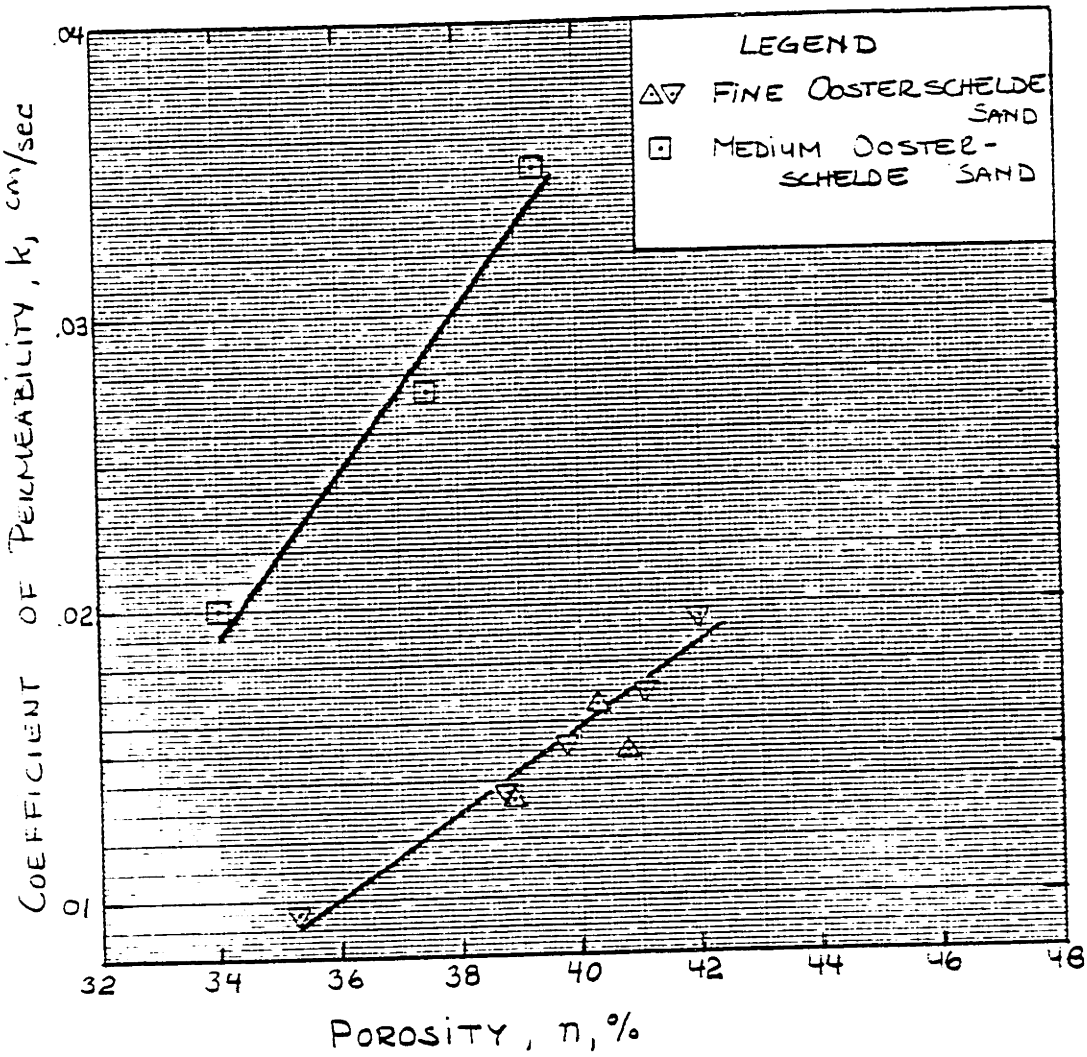

OOSTERSCHELDE SAND PERMEABILITY.

FIGURE A-5

APPENDIX B

Laboratory Testing Procedures

B.1 Triaxial Testing

Triaxial tests are performed on cylindrical soil samples inside a pressure chamber (cell). The sample is oriented with its axis vertical. Load in the vertical direction is applied by a loading ram (piston) protruding into the cell, and in horizontal direction by the cell pressure. Thus, the triaxial test is an axisymmetric test. Individual regulation of vertical and horizontal load allows for testing under a variety of stress paths.

Two load frame types were used for vertical loading, one for sample consolidation and constant rate of strain shearing, a second for cyclic tests and load controlled shearing. Air pressure or mercury pot systems supplied horizontal stresses.

Cyclic Triaxial Tests

This section describes the triaxial cell, the cyclic loading frame and the data acquisition system, discusses the sample preparation techniques and testing procedure and presents the data reduction method. Triaxial test specimens are prepared from a bulk sample using a tamping method to compact moist sand, then saturated under a backpressure, consolidated and finally subjected to the desired stress

conditions. The cyclic triaxial testing procedure and equipment are described under ten headings: (1) Triaxial cell, (2) Sample preparation, (3) Saturation, (4) Consolidation, (5) Cyclic load frame, (6) Cyclic loading, (7) Transducers, (8) Data acquisition, (9) Data reduction and (10) Display of test results. Standardized test forms were worked out to ensure that all steps were performed correctly and in the right order.

(1) Triaxial Cell

Triaxial cells, model WF10200 from Wykeham Farrance Eng., Ltd., Weston Rd., Trading Estate, Slough, SL14HW, England, were modified to perform cyclic tests. These modifications were made to reduce friction on the piston and to allow better construction of samples of known dimensions. The cell takes samples with a diameter of 3.5 cm and a height of 7.5 cm, i.e., a H/D ratio of 2.1/1.

Figure B.1 illustrates the modified cell. Friction is reduced by placing linear ball bearings around the piston. A frictionless rolling diaphragm provides an impermeable seal between the piston and the chamber, so no sealing oil is necessary in the cell. Maximum measured piston friction is less than 100 grams under normal operating conditions.

An alignment frame for the top cap/piston assembly inside the plexiglass cylinder allows connection of the piston and top cap to the sample and membrane while the sample is

still in the compaction mold. Good seating between the sample and top cap is achieved by compacting the final 0.6 mm by pushing the top cap down with a force on the piston. A piston clamping system will fix the piston in any desired position.

Porous sintered bronze disks are used at the top and bottom of the sample to assist water flow. A top drainage line allows carbon dioxide (CO_2) and deaired water to permeate through the sample and displace trapped air.

The triaxial cell is calibrated w.r.t. sample measurements, piston friction and piston area at 30- to 60-day intervals.

(2) Sample Preparation

The amount of dry soil required for a test specimen is calculated from the desired porosity of the specimen and the volume of the compaction mold. The correct amount of air-dried soil is weighed and water added to bring the mixture to a 10% moisture content. The wet soil is then divided into five parts of equal weight.

The main rubber membrane to contain the sample is first sealed to the bottom of the pedestal with o-rings. The split mold is then placed over the pedestal and the membrane stretched tight against the sides of the mold by means of vacuum.

The soil is tamped into the mold in five layers. The

thickness of each layer is controlled by a tamping tool which fits over the top of the mold and has an adjustable length of stroke. The undercompaction technique recommended by Silver et al. (1976) is used to yield a sample of uniform density by correcting for the fact that compacting an upper layer induces additional compaction of the layers below it. The degree of undercompaction for each porosity was determined experimentally by observing sample behavior during static tests over a range of undercompaction values. The percent undercompaction to yield uniformly bulging samples at axial strains of 5 to 10% was 4% for specimens compacted to a porosity of 38%, 5% for specimens compacted to a porosity of 41% and 6% for specimens compacted to a porosity of 45%. This is the value for the first layer. The degree of undercompaction decreases linearly with each layer to zero for the last one.

Once the optimum degree of undercompaction is known, the individual layer heights are given by:

$$h_i = \frac{h_t}{m} \left[(i-1) + \left(1 + \frac{u_i^*}{100}\right) \right]$$

where:

h_i = height of layer i

h_t = total height of specimen

m = total number of layers

i = number of layer being considered and

u_i^* = degree of undercompaction of the layer being considered (decreases linearly to zero at the top layer).

Upon completion of tamping, the surface of the compacted layer is scarified and the soil for the next layer poured into the mold and tamped. All five layers are compacted in like fashion. The soil surface at the top of the mold is made flat and 0.6 mm higher than the top of the mold.

The top cap/piston assembly is then affixed to the cell base and the final 0.6 mm compaction is performed by pushing the piston down until stopped by the preset piston clamp. The main membrane can now be sealed to the top cap with o-rings, a 0.2 kg/cm^2 vacuum applied to the sample and the split mold removed.

An additional membrane, 0.06 mm thick, is then placed around the sample and the 0.32 mm thick main membrane to ensure no leakage. Before the remainder of the cell is assembled and the cell filled with water, the circumference of the sample is measured with an accuracy of $\pm$ 0.05 mm. The main membrane is manufactured by Troxler Electronic Laboratories, Inc., PO Box 12057, Research Triangle Park, North Carolina 27709, and the additional membrane is a Trojans Latex Condom No. 70, Young's Drug Products Corp., Piscataway, New Jersey 08854.

Once placed in the consolidation frame (Wykeham Farrance Eng., Ltd.), the cell is pressurized to 0.2 kg/cm^2 as the vacuum on the sample is released. The piston clamp is

released, exact sample height measured on the piston stick-up and a DCDT (Direct Current Linear Variable Differential Transformer) mounted along with an AMES displacement dial measuring to .0025 mm for visual monitoring of displacements.

(3) Saturation

To provide better saturation more quickly, use is made of the fact that carbon dioxide (CO_2) dissolves more readily in water than does air. CO_2 is slowly flushed through the sample in an upward direction, displacing the air trapped in the sample. The flushing rate varies from 5 to 10 cm^3 CO_2 per minute and is terminated after 30 - 60 minutes, when about 10 times the sample void volume has passed through. De-aired water is then flushed through the sample in the same manner, displacing CO_2 and remaining air. The flushing rate is about 1 - 1 1/2 cm^3 per minute. The water flow is stopped when 30 cm^3 has passed through the sample after the last gas bubbles appeared in the effluent water. Both CO_2 and water are flushed under heads smaller than 0.05 kg/cm^2.

The cell pressure and back pressure are then raised simultaneously to 5.8 kg/cm^2 and 5.6 kg/cm^2, respectively. Pore pressure response is measured with the cell and pore pressure transducer by obtaining $B = \Delta u/\Delta\sigma_c$ for a $\Delta\sigma_c$ of 0.2 kg/cm^2. B values greater than 0.98 are required before shearing the sample in undrained tests. Saturation generally takes from 2 to 6 hours. Cell and back pressure are applied by a mercury pot system. Most samples sit under the backpressure for one day before consolidation and shearing.

(4) Consolidation

Vertical load on the triaxial cell piston in the consolidation frame (WF10021) is supplied by a proving ring readable to .0005 mm and sensitive to 0.10 kg. Once the specimen is fully saturated, the cell pressure and proving ring force are adjusted to obtain the desired isotropic or anisoptropic consolidation stresses. The volume changes during the consolidation stage are measured with a burette sensitive to 0.01 cm^3. The last part of the consolidation for cyclic tests ($\Delta\bar{\sigma}_{vc}$ = 0.5 kg/cm^2, $\Delta\bar{\sigma}_{hc} = K_c \cdot \Delta\bar{\sigma}_{vc}$) is performed after moving the triaxial cell with the sample to the cyclic load frame.

(5) Cyclic Load Frame

Figure B.2a presents a schematic of the M.I.T.-built cyclic load frame. A motor-driven rotating wheel moves a load back and forth on a lever arm that is connected to the load hanger on the triaxial cell. The load pattern is almost sinusodial, as shown in Figure B.2b. The vertical load on the piston at any one time is given by:

$$W_{TOTAL} = W_H + W_S + W_C \cdot 1/8(24 \pm 4 \cos\alpha^* - \sqrt{400 - 16 \sin^2\alpha^*})$$

where

W_H = Static hanger weight in kg

W_S = Deadload on static hanger in kg

W_C = Total cyclic hanger weight in kg

α^* = Angle of rotation on the flywheel measured from maximum load position (see Figure B.2a)

$\pm$ = + for $0 < \alpha^* < 90°$ and $270° < \alpha^* 360°$, - for $90 < \alpha^* < 270°$

This expression is valid when the counterweights balance the cyclic weights in the minimum load position.

The cycle period can be varied continuously from 3.6 seconds to 65 seconds with the standard gears. Changing gears will extend this range substantially in both directions; however, oscillation of the cyclic hanger limits the minimum period to about two seconds. The standard testing period of 8 seconds results from limits on how fast the digital data recorder can operate.

(6) Cyclic Loading

The transport of the triaxial cell from the consolidation frame to the cyclic frame is enabled by securing the piston with the clamp so that no vertical displacement can occur, and closing off all valves on the cell. The last part of the consolidation is performed in the cyclic frame. Deadloads corresponding to the desired consolidation stress and cyclic shear stress amplitude for the sample are placed on the static, cyclic and counterweight hangers. As the axial

load is carefully lowered onto the piston, the clamp is released to keep the length of the sample constant. The cell pressure is maintained with pressurized air regulated by a Bellofram reduction valve and the top 1 cm of the cell water is replaced by an air pocket to maintain constant cell pressure even when the piston is moving in and out of the cell. In drained tests, the backpressure is also maintained by pressurized air acting on an electrically reading volume change device.

The tests are started at mean shear stress with the cyclic load hanger in mean position on the lever arm. Loading period and reading interval can be changed at any time during the test. Termination of a test is based on reaching a certain peak to peak cyclic strain amplitude (normally 15 to 20%) or an accumulated (residual) strain (normally 10 to 12%). Undrained tests are consolidated after termination and loaded axially under drained conditions to obtain a friction angle. Some samples had a grid drawn on the main membrane so that deformations could be recorded on film during the test. The dimensions of most samples were recorded after test termination.

(7) Transducers

Four transducers are monitored during undrained cyclic triaxial tests. Vertical displacement of the loading piston relative to the cell base is measured with a DCDT (Direct Current Linear Variable Displacement Transformer), manufactured

by Hewlett Packard, Medical Electronics Division, 175 Wyman Street, Waltham, Massachusetts 02154. The currently used type is 7DCDT-250, with a specified nonlinearity less than $\pm$ 0.5 percent within $\pm$ 12.5 mm travel, i.e., an accuracy better than $\pm$ 0.05 percent strain at 10% vertical strain. Comparison of calibration data for the DCDT suggests a maximum error of $\pm$ 0.017 percent strain at 1 percent vertical strain accumulation, and $\pm$ 0.09 percent strain at 10 percent vertical strain. The sensitivity of strain measurements are $\pm$ 0.003%.

Pore pressure is measured at the base porous disk with a Tyco Model AB pressure transducer, manufactured by Tyco Instrument Division, 4 Hartwell Place, Lexington, Massachusetts 02173. The transducer has a linear range from 0 to 14 kg/cm^2 with a given maximum nonlinearity of 0.1% of full scale. Cell pressure is monitored with the same type transducer. These devices read pressure to within $\pm$ 0.002 kg/cm^2. Calibration data for the pressure transducers indicate a maximum error of $\pm$ 0.024 kg/cm^2 at 5.5 $kg.cm^2$ (typical back pressure value), and $\pm$ 0.007 kg/cm^2 maximum error at 15 kg/cm^2 (typical excess pore pressure value).

The vertical load on the piston is recorded by a Tyco model FP load cell, with a capacity of $\pm$ 450 kg and a nonlinearity less than $\pm$ 0.1% of full range. Calibration data for the load cell suggest a maximum error of $\pm$ 0.06 kg at a load reading of 50 kg. The sensitivity of the load cell is $\pm$ 0.013 kg.

During drained tests, an electrical volume change device

replaces the pore pressure transducer. The device has a total range of 160 cm^3 and a sensitivity of .002 cm^3 over a range of $\pm$ 6 cm^3. It was designed at MIT by Dr. R.T. Martin. All transducers are calibrated every 30 to 60 days.

(8) Data Acquisition

The number of load cycles is counted by a mechanical counter and a photo-electric switch. The switch is connected to a reading control box that counts the cycles and closes a reading command circuit each time the number of cycles equals a preset value. Another photo-electric switch can then transmit scanning command pulses at up to 20 preselected points within each the load cycle. The output voltage of all four transducers (load, displacement, cell pressure and pore pressure or volume change) are read in each scan. The scanning is performed by a Fluke Model 2240A Data Logger, manufactured by John Fluke Mfg. Co., PO Box 43210, Mountlake Terrace, Washington 98043. Digital readings of date, time and transducers from the logger are then transferred to a Kennedy Model 1600 Incremental Magnetic Tape Recorder, manufactured by Kennedy Co., 540 West Woodbury Road, Altadena, California. The test data stored on the tape are then reduced and the results plotted at MIT's Information Processing Center. Immediate visual display and monitoring of the sample behavior during the cyclic test is obtained with a four-channel heat stylus stripchart recorder.

(9) Data Reduction

All digital data collected on magnetic tape during the cyclic test are reduced by a computer program that reads the tape, maps the readings in cycles and numbers the cycles. The stresses, strains and moduli are calculated and the results tabulated and plotted.

The vertical stress on the sample is corrected for membrane stiffness based on stretching tests of the membranes (see Figure B.3). An experimentally verified area correction for undrained cyclic tests, $A_{corr} = \frac{1}{(1-4/3\varepsilon_v)}$ yields changes in the cross-sectional area in the middle of the sample during straining (see Figure B.4). Calculation of vertical stress is always based on the corrected sample area.

(10) Display of Test Results

All recorded test data on the magnetic tape is computer-listed by a tape analysis program. The data reduction program yields a second printed tabulation with all calculated strains, stresses, moduli, etc.

Plotted versus time for each logged cycle is $\bar{p}$ $(\frac{\bar{\sigma}_v + \bar{\sigma}_h}{2})$, $q(\frac{\sigma_v - \sigma_h}{2})$, ε_v (vertical strain) and u (pore pressure) or $\Delta V/V$ (volumetric strain). Figure B.5 presents a 15 inch-long portion of the often 200 - 300 inch-long plot. In addition, the same four quantities at maximum and minimum shear stress is displayed in a summary plot versus number of cycles (Figure B.6).

Finally, the computer program plots the effective stress path ($\bar{p}$ - q plot, see Figure B.7) and the stress-strain curve

($q - \varepsilon_v$ plot, in Figure B.8), for selected cycles during the cyclic test.

Static Triaxial Tests

The static tests are performed with much of the same equipment and transducer types as the cyclic tests. Several of the steps are identical, and can be found in the preceeding subchapter. The static triaxial testing procedure and equipment are described under eleven headings:

(1) Triaxial cell.

As (1) Triaxial cell for cyclic tests

(2) Sample preparation.

As (2) Sample preparation for cyclic tests

(3) Saturation.

As (3) Saturation for cyclic tests

(4) Consolidation.

As (4) Consolidation for cyclic tests.

(5) Transducers.

As (7) Transducers for cyclic tests

However, in strain controlled drained tests, the volume changes during shear were measured with a burette sensitive to 0.01 cm^3, the vertical load with a proving ring readable to .0005 mm and sensitive to 0.10 kg, and the displacement with an AMES displacement dial measuring to .0025 mm. No electrical transducers were employed.

(6) Strain controlled tests.

Strain controlled tests are consolidated and sheared in the same frame, a Wykeham Farrance Model WF 10021 loading

frame. The rate of shearing for all strain controlled tests performed was 1/3% per minute.

(7) Load controlled tests.

Load controlled tests are sheared in the cyclic load frame (see cyclic triaxial test, (5) Cyclic Load Frame and (6) Cyclic Loading). The cyclic hanger is then started off from the minimum load position on the lever arm. The hanger is moved a few millimeters, stopped, and a reading is taken immediately and another after 60 seconds at the new position. This is repeated until the end of the test.

(8) Pore pressure controlled tests.

This is a special kind of drained test where the external loads are being kept constant and the pore pressure increased in steps until failure. Both pore pressure and volume change is recorded during the test, which is performed in the cyclic load frame under load control.

(9) Data acquisition.

All readings in strain controlled tests are recorded by hand. In pore pressure and load controlled tests the data acquisition system (described under cyclic tests, (8) Data Acquistion) is utilized.

(10) Data reduction.

Hand readings from strain controlled tests are punched onto computer cards and reduced by the same data reduction program as readings stored on magnetic tape (see under cyclic tests (9) Data Reduction). Stress and pore pressure controlled tests are recorded on magnetic tape and computer reduced.

The vertical stresses are corrected with an experimentally found area correction factor, $A_{corr} = \frac{1}{1 - 5/3\ \varepsilon_v}$.

(11) Display of test results.

The results from static tests are hand-plotted from the computer tabulations. The tabulations are identical to the ones printed for cyclic tests.

B.2 Cyclic Oedometer Tests

The first 9 oedometer tests were performed in a standard oedometer. Dry sand was poured into the ring in the loosest possible state, and about 1/2 cm higher than the ring top. The excess sand was subsequently carefully trimmed down to the ring level with a polished steel straight-edge. After measuring the sample height with an AMES displacement dial reading to .0025 mm, the top cap was placed directly on the sand surface. The initial displacement reading under the .02 kg/cm^2 top cap stress was recorded.

Four additional tests were run in the MIT K_o-oedometer ring, shown in Figure B.9. The testing procedure was the same, apart from measurements of temperature and fluid pressure in the ring chamber in addition to load and displacement. In two of the K_o-oedometer tests the sand was tamped in at 10% water content in one layer to a porosity of about 47.5%.

All cyclic oedometer tests were run in the MIT-built cyclic load frame (see Figure B.2a). In all tests the static hanger weight was counter-balanced by a deadweight loaded wire running over pulleys on the frame top. After the initial displacement readings, the hanger was carefully lowered

onto the top cap ball. At this point the sand was saturated by slowly letting water flow up through the bottom porous stone into the sand, until the entire sample was submerged.

The cyclic load hanger always started from the minimum load position, where it was balanced by the counter-balance hanger. During virgin loadings, displacement dial and load cell was read continuously. At maximum load, the deadweights on the three hangers were rearranged to achieve the desired mean stress

$$\bar{\sigma}_{vm} = \frac{\max \bar{\sigma}_v + \min \bar{\sigma}_v}{2}$$

and cyclic stress

$$\Delta\bar{\sigma}_v = \frac{\max \bar{\sigma}_v - \min \bar{\sigma}_v}{2}$$

The oedometer tests were run at 3.6 sec loading period, as the drainage path was short and the sand and porous stone relatively permeable. Readings of load and displacement at selected cycle numbers were taken by hand. The system compliance for a stress change from 0 to 2.5 kg/cm^2 on the sample area was .02 mm, which was subtracted from the peak to peak strains.

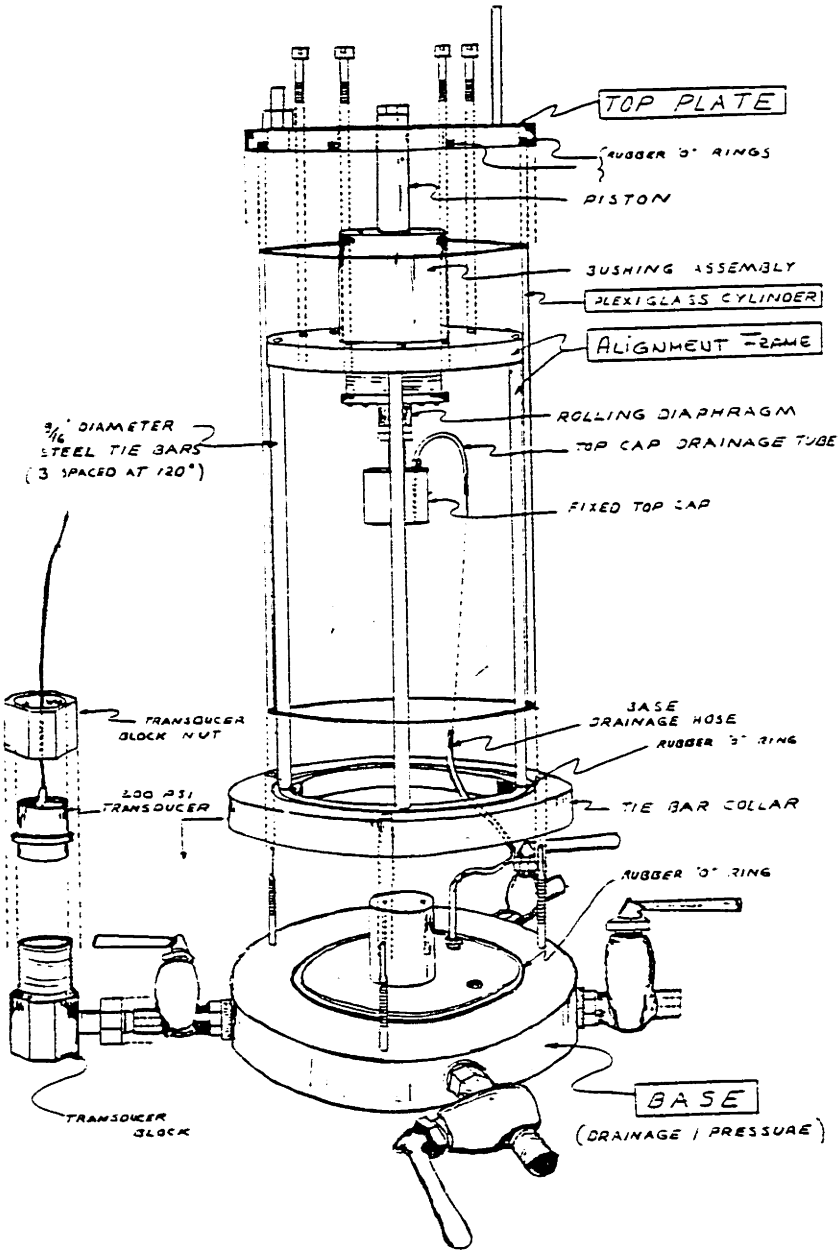

TRIAXIAL CELL

FIGURE B-1

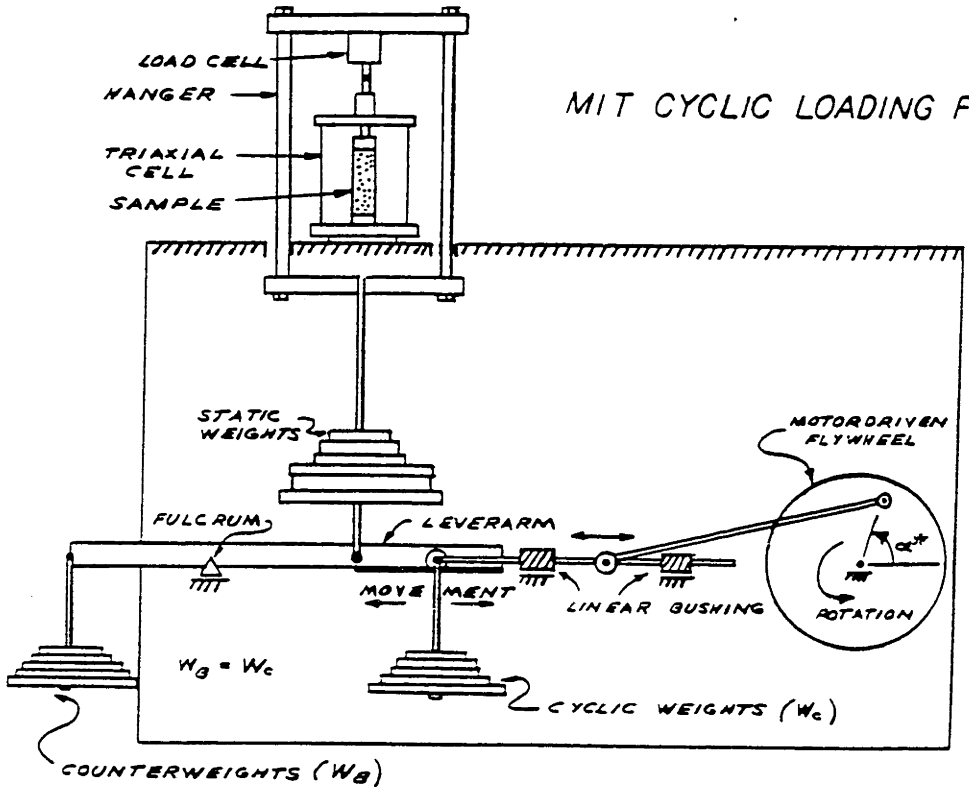

MIT CYCLIC LOADING FRAME

TOTAL LOAD ON PISTON

HANGER WEIGHT + $W_S + W_C - \frac{L}{B}\left(24 \pm 4\cos\alpha^* - \sqrt{400 - 16\sin^2\alpha^*}\right)$

WHERE: − FOR $90° < \alpha^* < 270°$ } −

\+ FOR $0° < \alpha^* < 90°$, $270° < \alpha^* < 360°$ } +

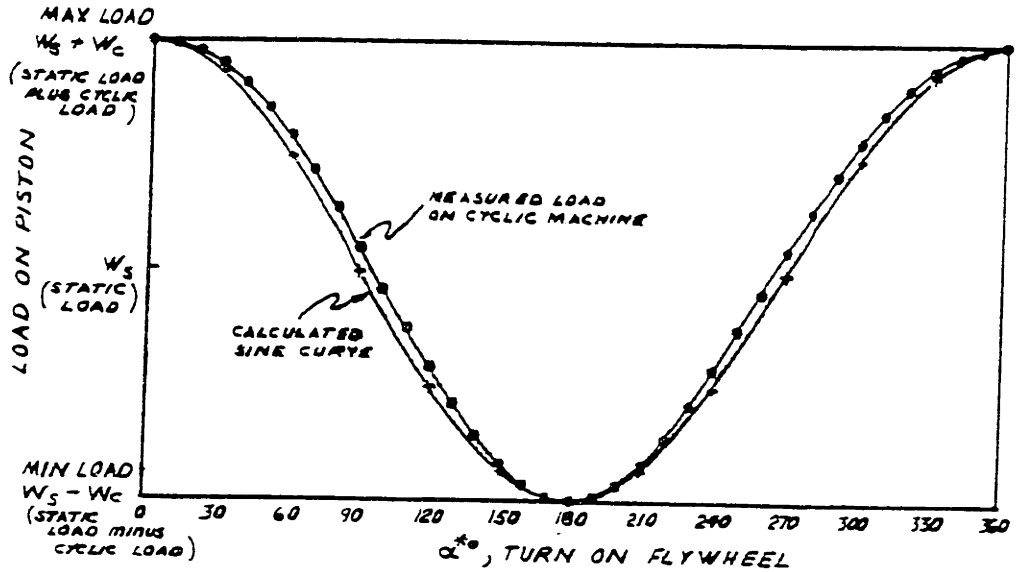

CYCLIC MACHINE LOAD PATTERN

FIGURE B-2

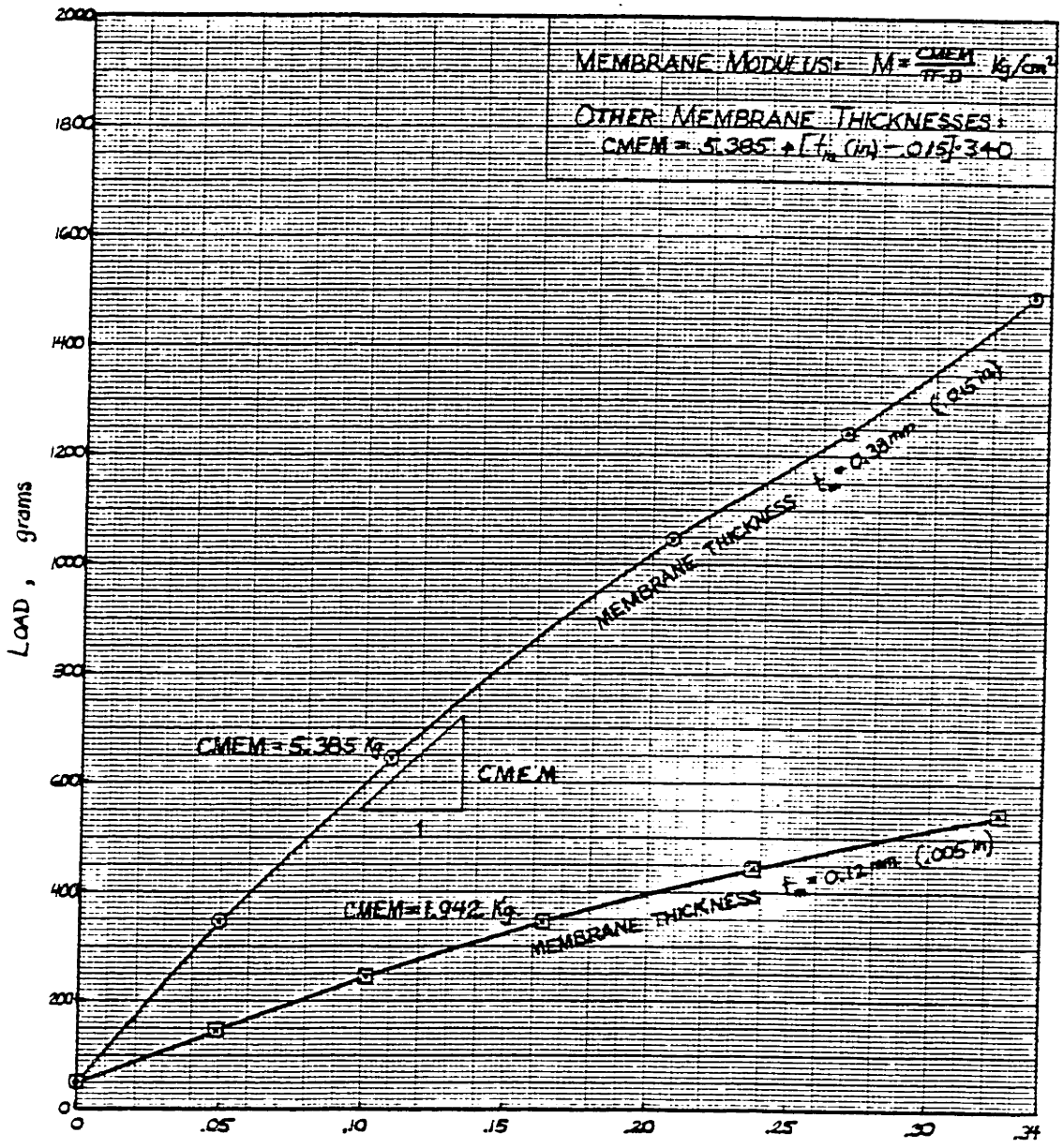

MEMBRANE CORRECTION FACTORS

FIGURE B-3

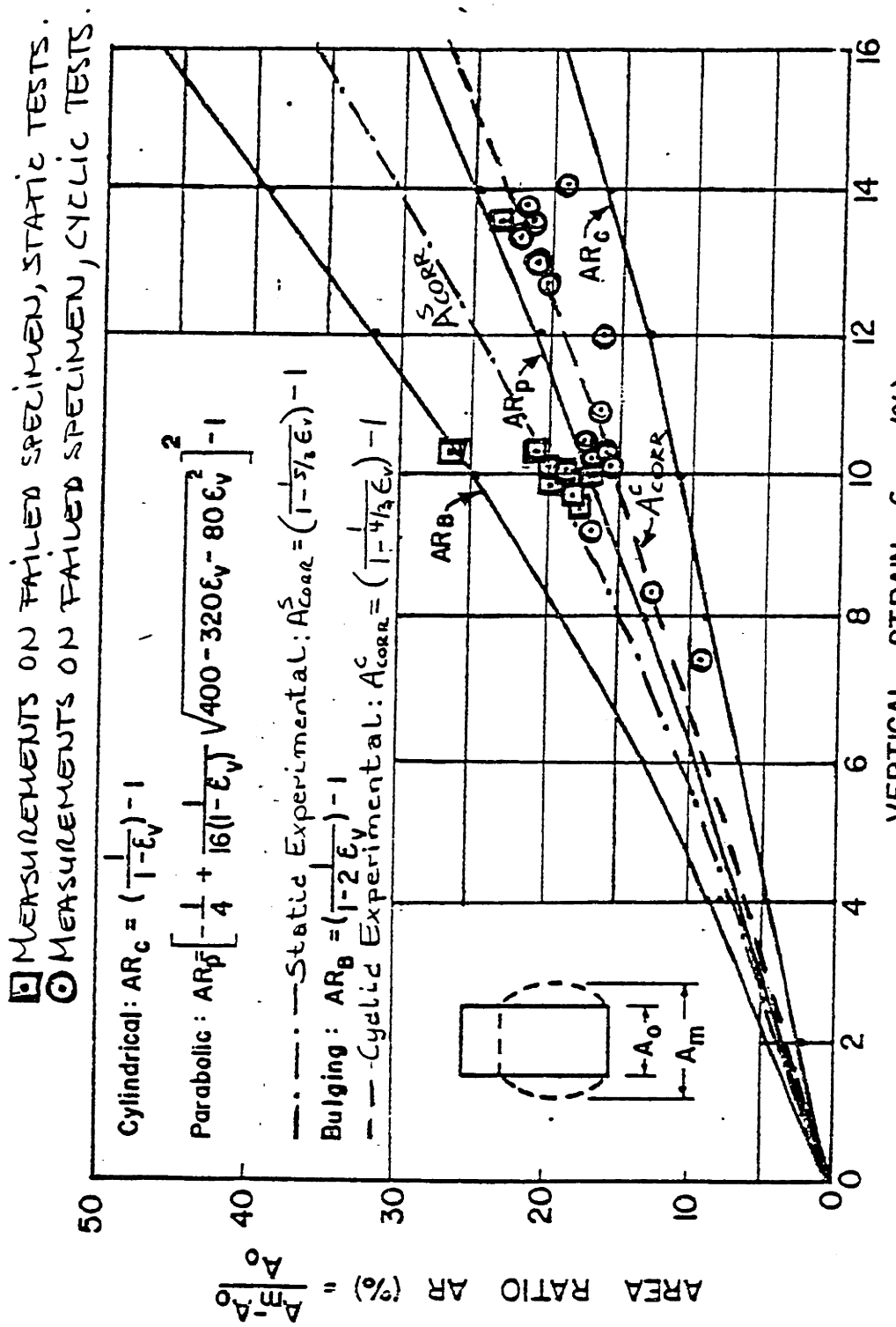

AREA CORRECTIONS IN THE TRIAXIAL COMPRESSION TEST

FIGURE B-4

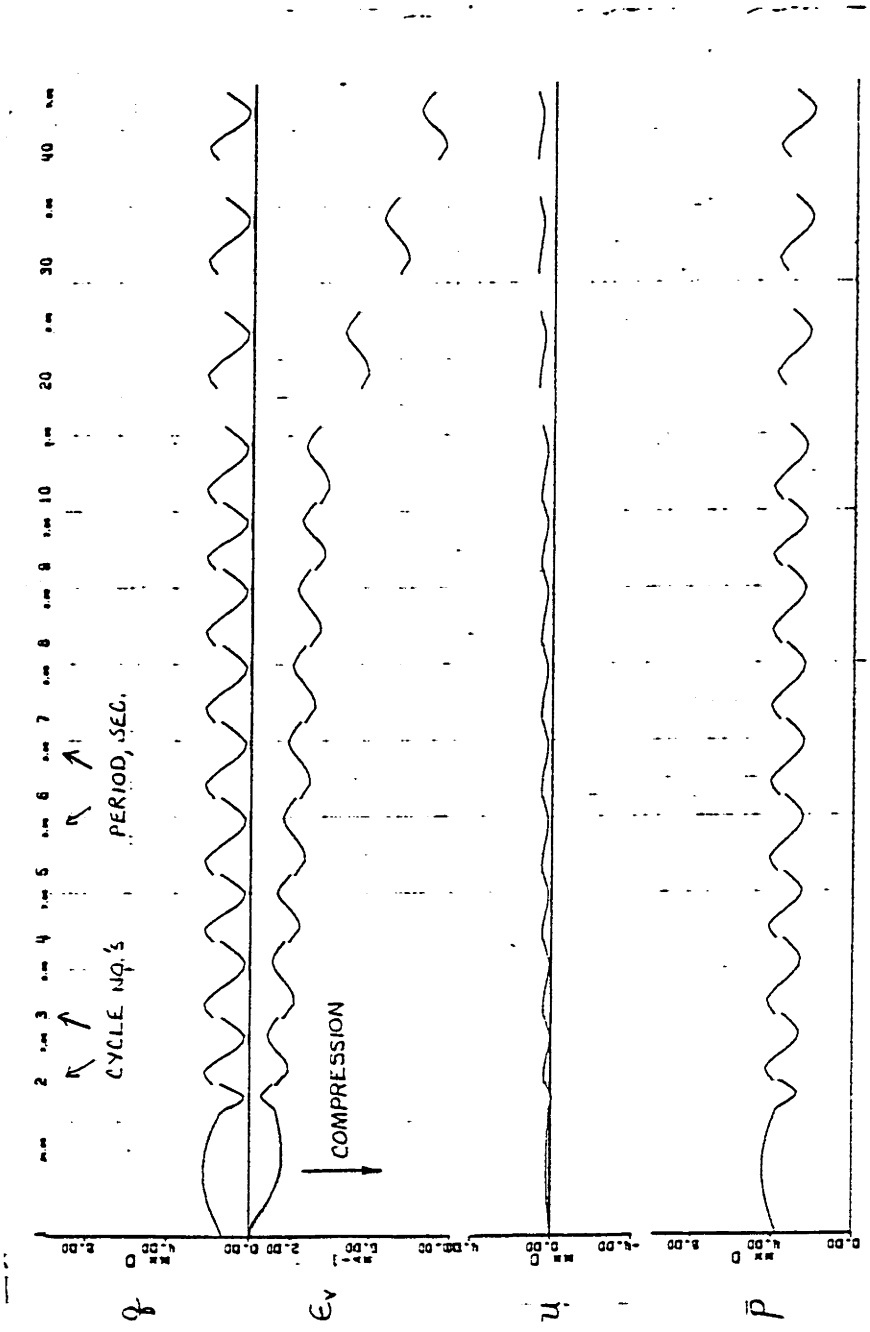

PLOTS OF SHEAR STRESS, VERTICAL STRAIN, PORE PRESSURE AND MEAN EFFECTIVE STRESS FOR INDIVIDUAL CYCLES

FIGURE B-5

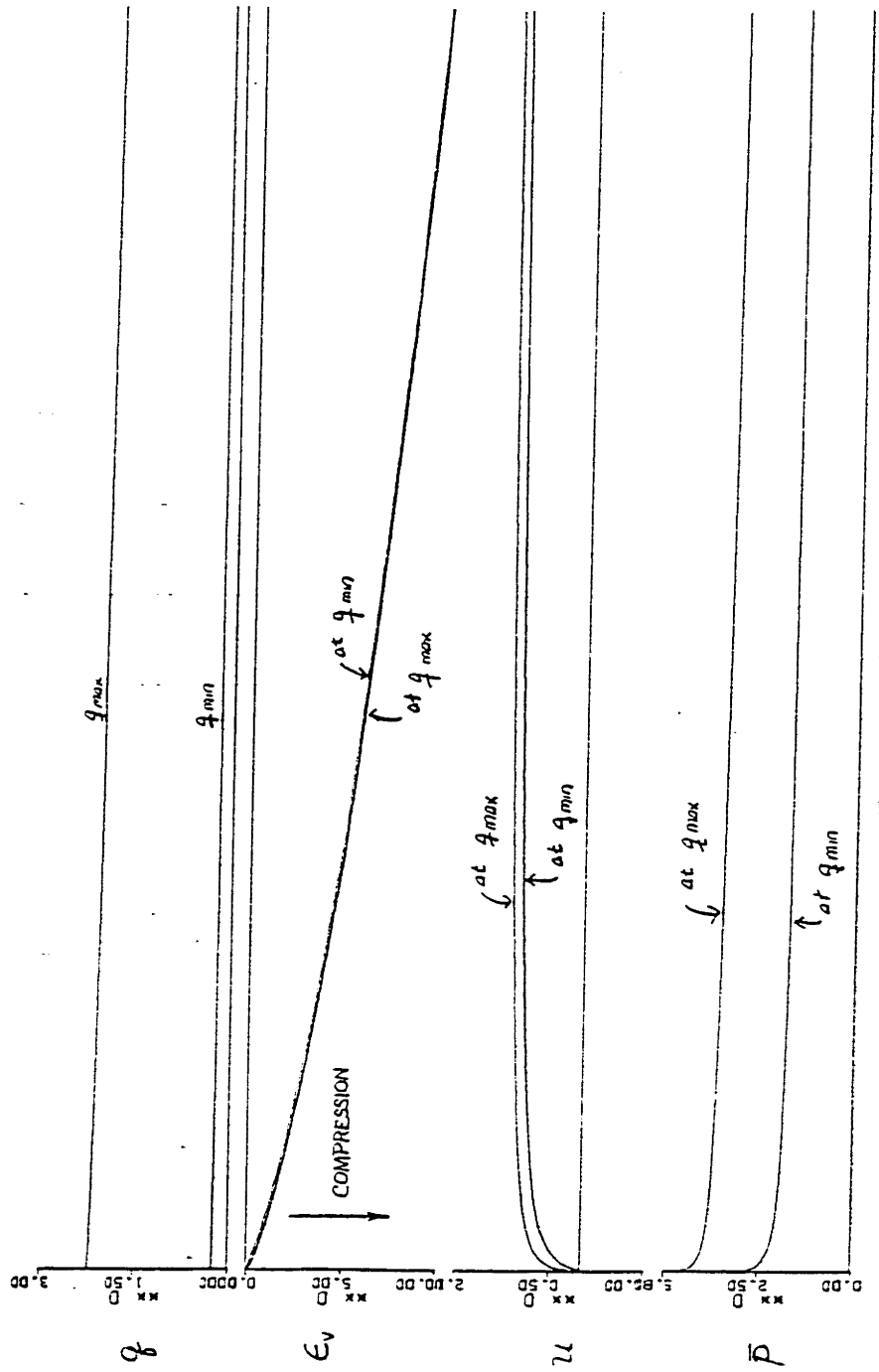

SHEAR STRESS, VERTICAL STRAIN, PORE PRESSURE AND MEAN EFFECTIVE STRESS

FIGURE B-6

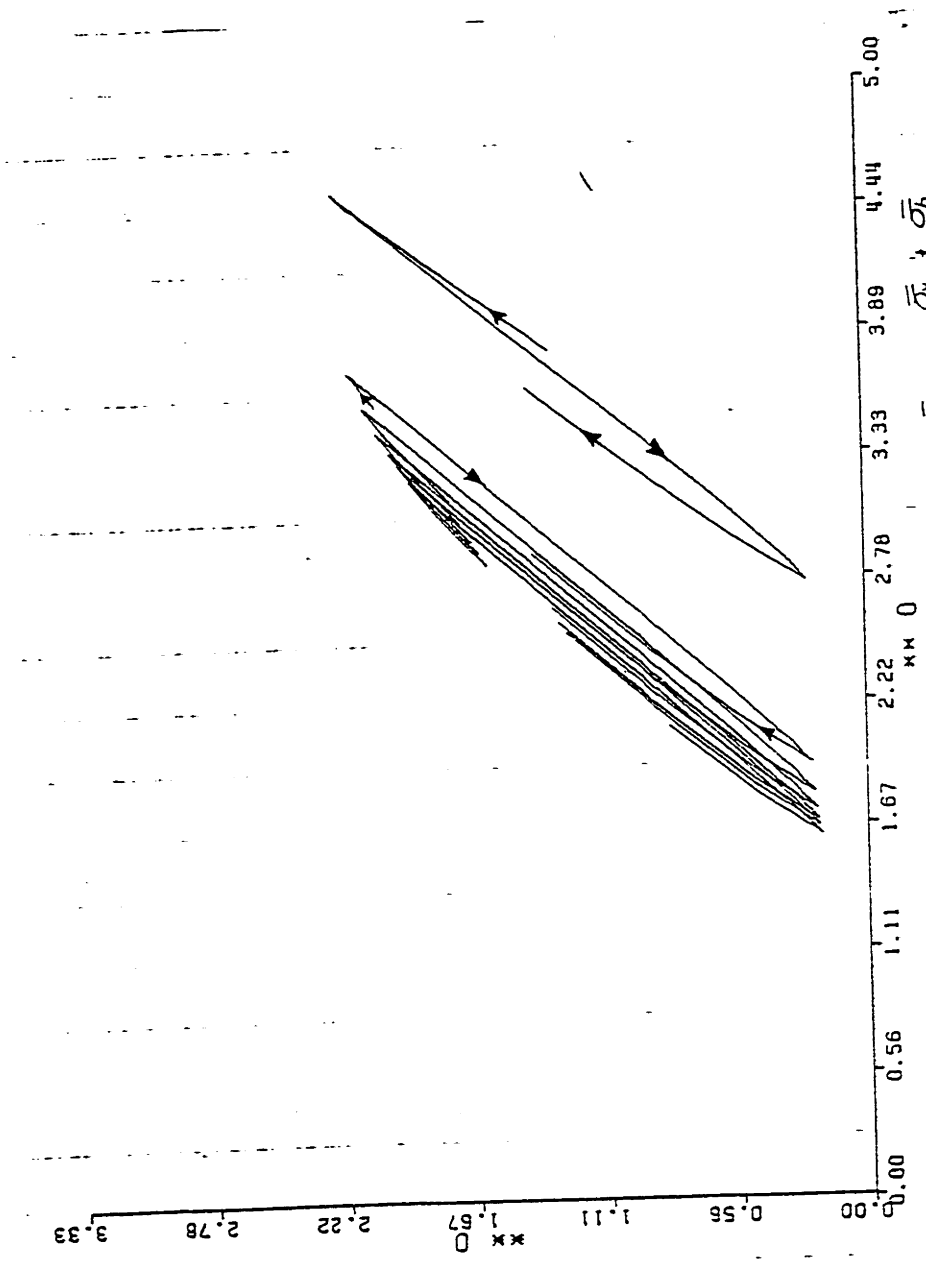

EFFECTIVE STRESS PATH

FIGURE B-7

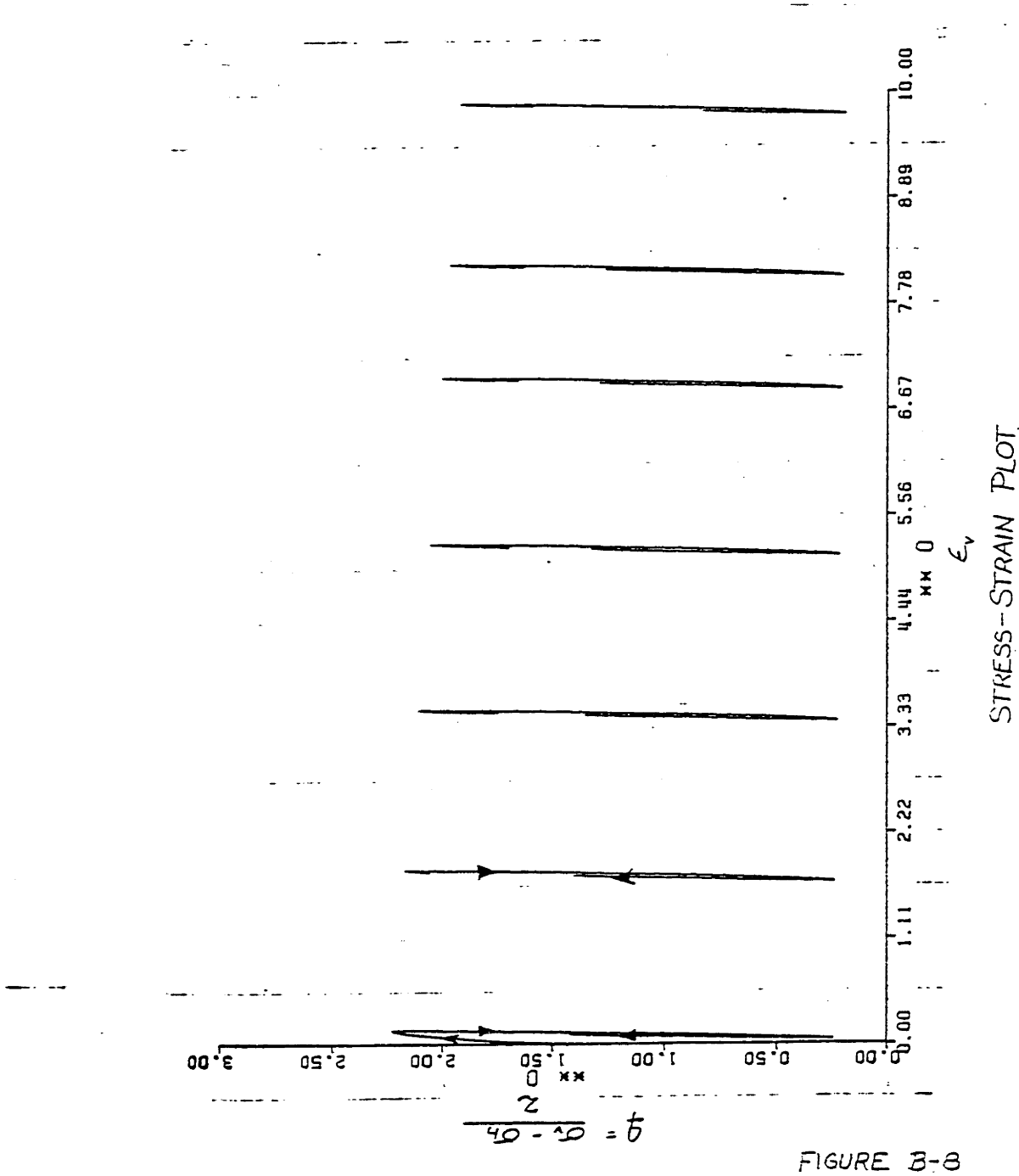

STRESS-STRAIN PLOT

FIGURE B-8

① Brass base plate
② Drainage channels
③ Drainage tube
④ Screws to attach collar
⑤ Rubber gasket
⑥ Porous stone
⑦ K_o - Ring, steel
⑧ Brass top cap
⑨ Soil sample
⑩ Steel pressure rings
⑪ Teflon membrane
⑫ Deaired oil (Vacuum filled)

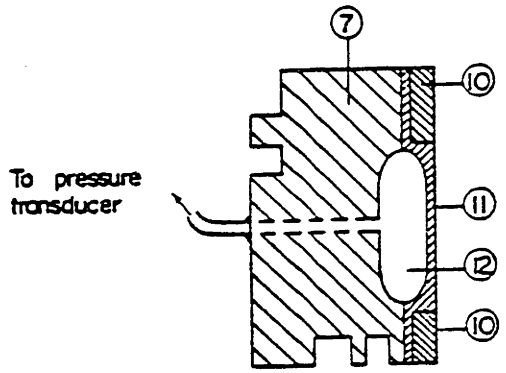

CROSS - SECTION K_o - RING
SCALE 2:1
(Membranethickness unknown)

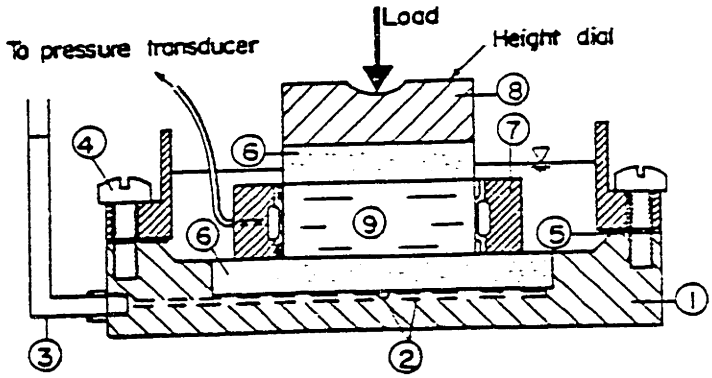

CROSS - SECTION OF OEDOMETER
SCALE 1:2

M.I.T. K_o APPARATUS (SAXENA ET AL., 1974).

FIGURE B-9

CYCLIC STRESS-STRAIN BEHAVIOR OF SAND IN OFFSHORE ENVIRONMENT

by

JAN HEDBERG

Dipl.-Ing., Technische Hochschule Darmstadt
(1972)

S.M., Massachusetts Institute of Technology
(1975)

SUBMITTED IN PARTIAL FULFILLMENT

OF THE REQUIREMENTS FOR THE

DEGREE OF

DOCTOR OF PHILOSOPHY

at the

MASSACHUSETTS INSTITUTE OF TECHNOLOGY

October, 1977

Signature of Author.....
Department of Civil Engineering, October 3, 1977

Certified by.....
Thesis Supervisor

Accepted by.....
Chairman, Department Committee

APPENDIX C

Triaxial Test Discussion

C.1 Deformation During Consolidation

All triaxial samples tested were reconstituted by vertical tamping in a cylindrical split mold. This leads to anisotropic specimen, which can be demonstrated by observations of horizontal and vertical strain during isotropic consolidation (El-Sohby and Andrawes, 1973). Arthur and Menzies (1972) reported strength and stress-strain anisotropy in cubical sand samples poured through air. That cannot be demonstrated in axially tamped cylindrical samples without changing the stress path of the sample at the same time. Therefore, the observations of anisotropy is limited to strain measurements under an isotropic consolidation stress. Ladd et al. (1977) describes anisotropy in further detail.

Table C.1a, b and c list vertical, horizontal and volumetric strain in all isotropically consolidated static and cyclic triaxial tests. Horizontal strain was not measured, but calculated from volumetric and axial strain. In Figure C.1 the difference between horizontal and vertical strain during consolidation of isotropic samples is plotted versus consolidation stress. All but 2 of the 93 tests showed a larger horizontal than vertical strain, clearly indicating anisotropy in the deformation characteristics of the samples, since for isotropic material $\varepsilon_h - \varepsilon_v = 0$. An average curve drawn through

the points show a non-linear increase of strain difference with increasing consolidation stress.

Due to this anisotropy in deformational behavior, the samples consolidated under an anisotropic state of stress can not readily be utilized to find K_o for the sand. However, if all measured values of horizontal strain are "corrected" by subtracting an amount equal to the "excess" strain due to sample anisotropy given by the curve in Figure C.1, an estimate of K_o can be obtained. The "corrected" horizontal strain ($= \varepsilon_{hcorr}$) is then representative for the horizontal strain of the samples with isotropic deformation characteristics. If the corrected strain is normalized by the vertical consolidation stress and plotted versus the consolidation stress ratio ($K_c = \bar{\sigma}_{hc}/\bar{\sigma}_{vc}$), the value of K_c producing zero horizontal strain ($= K_o$), can be found. From Figure C.2, the value of K_o appears to be 0.44.

Notable is also the approximate linear shape of the curve between $K_c = 0.5$ and $K_c = 1.5$. Smaller and larger values of the consolidation stress ratio implies an increased proximity to the failure lines, and accelerate horizontal extension and compression strain respectively. Strain values for 75 anisotropically consolidated samples are given in Table C.2a, b, and c.

C.2 Deformation During Shear

In undrained triaxial tests, only total vertical deformation is normally recorded. In drained tests, volume change

is also monitored. In about twenty of the cyclic triaxial tests performed in this investigation, a square grid with 10 mm spacing was drawn on the main membrane before sample compaction. Photos were taken of those samples at the test start, 5 - 6 times during the test, and at the end of the test. Due to the curvature of the cylindrical plexiglass chamber surrounding the sample, radial deformations could not be measured on the photos. Vertical deformation of each soil layer between horizontal lines on the sample could however be measured. At the end of the test when the plexiglass cylinder was removed, the radial deformations of each layer in the sample were measured with a caliper. The vertical deformations were measured with ruler on slides blown up on a screen to about 70 times the true sample size.

Figure C.3 shows pictures of a cyclic isotropic test sample at two stages during the test (top pictures) and a cyclic extension test at the beginning and end (lower pictures). When zero effective stress was reached, most of the strains occurred at the top of the isotropic sample. This can be seen in the first picture, taken at maximum load. Quite a few of the isotropic samples failed at the top, which also have been noted by other researchers (Castro 1969, Casagrande 1976). At maximum extension load, the sample stretches uniformly. Both a large compression strain and a large cyclic peak to peak strain resulted from that particular type of loading.

The lower part of Figure C.3 shows a cyclic extension test where the sample necked at the bottom after about 110

load cycles. Most extension test samples necked either at the top or the bottom after reaching 8 to 12% extension strain.

Figure C.4 shows two pictures of a compression cyclic triaxial test, where cyclic peak to peak strains are very small, and compressive strains just keep accumulating throughout the test. An increasing bulging of the sample is apparent from Picture 1 at the test start, to Picture 2 at the end of the test. It is also evident that the sample deforms barrelshaped, and not as a uniform cylinder. The most probable reason for this non-uniform deformation is radial shear stresses induced by the friction at the end caps.

The lower pictures in Figure C.4 show a triaxial sample before and after static compression loading. Note the more pronounced barreling that results from static loading, compared with the cyclic test samples above.

Figure C.5 presents comparisons of horizontal strain along the sample length. "Measured" strain denotes horizontal strain values based upon measured radial deformations at the end of a test. "Computed" strain is found by measuring vertical deformations of each layer, and computing horizontal strain by assuming the volume of each layer remains constant.

The isotropically consolidated test sample LC123 in Figure C.5 deforms relatively uniformly, and the measured and calculated strains compare well. Test sample LC139 contracted substantially in radial direction at the top, based on strain measurements. Radial strains calculated from vertical strain measurements and assumed constant volume of each layer are

however, essentially equal to zero. That would mean the sample top had contracted substantially and should be quite dense. Observations during the test contradicted that. The sample top underwent most deformations, and seemed quite loose. It is therefore more likely that the contact can be lost between the sand sample and the membrane in isotropic tests at zero effective stress, so that the sand can settle within the membrane and the layers do not remain at constant volume. The large absolute distance between the two strain curves in these isotropic tests is caused by the substantial consolidation strain at the postshear drainage.

Figure C.6 shows measured and calculated radial strains from cyclic compression tests. The final vertical strain exceeded 10% in both tests. The radial strains computed from radial deformation measurements show a larger value in the middle of the sample, and smaller values at the sample ends than what was computed from vertical measurements and assumed constant volume of each sample layer. This indicates that the individual layers did <u>not</u> remain at constant volume; rather, the layers at the sample ends contracted while the middle of the sample dilated. The overall sample remained, of course, undrained and at constant volume. Since the effective confining stresses on the sample never reach zero in cyclic compression tests, a good contact between sample and membrane is always ensured. Relative movements should therefore not cause the above effect.

Figure C.7 shows measured and calculated radial strains from compression cyclic tests terminated at vertical strains less than 5%. Here the strain patterns found by the two methods correspond much closer, suggesting that the non-uniform volumetric strains only become significant at vertical strains larger than 5%. Bjerrum (1973) concluded that "even in undrained tests, zones of the sample will expand, whereas others will consolidate, the bulk volume remaining unchanged." Castro (1969) and Casagrande (1971) point out, when a medium dense or dense sand is subjected to shear reversals leading to strains exceeding 1 - 2%, the sand will have a tendency to develop a redistribution of its water content. It can, therefore, be concluded that void redistribution in cyclic triaxial tests does <u>not</u> occur at vertical strains below 1 percent, but <u>can</u> occur between 1 and 5 percent strain, and certainly <u>does</u> occur at accumulated strains around 10 percent.

Figure C.8 shows two cyclic test samples, where the cyclic loading was terminated after less than 0.5 percent vertical strain, and the samples subsequently loaded in compression under static load control. The dilation of the sample center and the contraction of the ends is even more pronounced in these static tests than in the cyclic tests in Figure C.6. The same was found by comparing the pictures of static and cyclic samples in Figure C.4. Also from sample measurements to estimate an area correction factor (see Figure B.4), static test samples were found to barrel more

than cyclic test samples.

C.3 Membrane and Area Correction

A change of membrane correction factor of ± 20% around the experimentally found value has a very insignificant influence, and changes the value of maximum obliquity ($= \bar{\sigma}_v/\bar{\sigma}_h$) less than 0.2%. Use of the cylindrical area correction rather than the experimentally found area correction (see Appendix B.1, Figure B.4) changes the maximum obliquity about 1 - 1.5% and the friction angle 0.2 - 0.3 degrees. The absolute values of the shear and normal stress, however, increase from 1 to 10% with the cylindrical area correction, the larger values occurring towards the end of the test.

The pore pressure measurements in the cyclic tests were found not to be affected by membrane penetration based on data from Lade and Hernandez (1977). The reasons for that is the fine sand utilized (D_{50} = .17 mm) with associated pores on the sample surface that are very small compared to the 0.32 mm thick rubber membrane. The change in effective stress level is also relatively small, as most samples developed pore pressures from 1 to 1.5 kg/cm^2, and the maximum value was 5 kg/cm^2.

The confining stress from the membrane on the sample was found to range from 0.005 kg/cm^2 (undeformed sample) to 0.04 kg/cm^2 dependent on the magnitude of radial deformation (10% vertical strain would be associated with a membrane confinement of about 0.035 kg/cm^2). These values were

measured on an airfilled membrane. This confinement is insignificant in comparison to the effective confining stress under which triaxial tests normally are performed. However, isotropic cyclic tests reaching cyclic mobility ($\Delta u = \bar{p}_o$), are clearly influenced in their deformational behavior by the membrane confinement at zero effective stress. All triaxial tests at small effective stress ($< 1\ kg/cm^2$), unloading tests, and cyclic tests on contractive samples can be influenced. Figure C.9 presents membrane confining stress as a function of sample diameter.

C.4 Repeatability and Test Quality

Figure C.10 and C.11 present a $\bar{p}$ - q plot and shear stress, obliquity and volumetric strain versus vertical strain for two identical static tests, LS76 and LS86. The correspondence between the two tests is remarkable.

Tables in Appendix F give stresses and strains for four pairs of identical cyclic tests: in the cyclic compression tests LC80 and 120, and LC89 and 97, the number of cycles to reach 5% vertical strain varied 17% and 14% respectively (corrected for porosity differences). In the isotropic cyclic tests LC61 and 63, the number of cycles to reach 5% peak to peak strain varied 12%. In the cyclic extension tests LC136 and 147, the number of cycles to reach 5% extension strain varied only 3%. Note that these percentages, ranging from 3 to 17 percent, are <u>not</u> based upon cyclic strength, but on the much more sensitive indication; the number of load cycles to failure. The absolute number of cycles in these test

pairs vary from 25 to 2000.

The pore pressure response of soils during cyclic loading is one factor that has been of concern to researchers, especially when dealing with fine-grained soils (NGI, 1975b). The following tests shed some light on that issue concerning the Oosterschelde Fine Sand: Test LC106 loaded at 3.6 sec. period, test LC89 and 97 loaded at 8 sec. period and test LC91 loaded at 42 sec. period are tabulated below in terms of θ, the average inclination of the effective stress path of an individual load cycle to the p axis. θ is given for the first cycle, for the cycles when the pore pressure ratio (= M = $\Delta u/u_f$) is 0.5 and 1.0, and for the cycle in which a vertical

Period T, Sec.	Test # LC	Effective Stress Path Inclination, θ Cycle 1	At M=.5	At M-1	At ε_v = 5%
3.6	106	51.5	51.7	48.7	48.3
8	89	52.3	52.4	48.6	44.9
8	97	51.0	51.4	47.6	46.2
42	91	51.8	52.0	48.9	47.3

strain of 5% is reached. The magnitude of θ is apparently not influenced by the load period, indicating that full pore pressure response is achieved when the cyclic load period is 3.6 seconds as well as 42 seconds. θ was found to be 45.0° in drained tests (LC126 and 127).

C.5 Air and Water Leakage

Poulos (1964) treated air and water leakage in triaxial tests in great detail. His experimentally found rate of water leakage through the membrane under the test conditions in this

investigation (2 membranes, salt pore water fluid, natural rubber membranes and good o-ring seal). He found a leakage of 9.5 mm^3/day at $\bar{p}_o$ = 1 kg/cm^2, and 11.0 mm^3/day at $\bar{p}_o$ = 6 kg/cm^2. From the cyclic oedometer tests (Appendix F), the swelling ratio for unloading of the Oosterschedle Fine Sand was found to be approximately 0.0075. The leakage rate to produce a 2% reduction in effective stresses for the sand is then 13 mm^3/day. Tests exceeding about 13,000 cycles before reaching the K_f-line can thus be affected by leakage. Only tests LC68, LC133 and LC134 could be so affected. Using salt cell water in long-term tests might therefore be warranted, as the rate of leakage is reduced by about a factor of ten.

No measurements have been found for air leakage through triaxial membranes, but can theoretically be calculated by formulas given in Poulos (1964). For no mixing of the initially deaired cell water and under the conditions in this research effort, the rate of leakage into a sample would be about 0.4 cm^3/day. The estimated allowable leakage rate is half that much to keep the change in effective stress below 2 percent. Thus tests exceeding 5000 cycles before the failure line is reached may be influenced by air leakage. However, since an air cushion was maintained inside the cell during cyclic testing in this investigation, and mixing of the cell water can occur, it is possible that tests exceeding 500-1000 cycles can be somewhat influenced by air leakage. That would include about 20 percent of the performed cyclic tests.

Test # LS	$\bar{\sigma}_{hc}$ kg/cm^2	K_c	$\frac{\Delta V_{cons}}{V_1}$ %	ε_{vcons} %	ε_{hcons} %	ISOTROP $\varepsilon_h - \varepsilon_v$ %	ε_{hcorr} %	$\bar{\sigma}_{vc}$ kg/cm^2	$\frac{\varepsilon_{hcorr}}{\bar{\sigma}_{vc}}$ %/kg/cm^2
58	1.00	1.0	.080	.158	.078	.076	.397	1.00	.0760
59	1.00	1.0	.053	.091	.037	.009	.235	1.00	.0090
60	1.00	1.0	.050	.126	.076	.044	.303	1.00	.0440
62	1.00	1.0	.067	.138	.071	.056	.344	1.00	.0560
63	2.00	1.0	.165	.371	.207	.223	.908	2.00	.1115
64	5.00	1.0	.246	.454	.207	.175	1.153	5.00	.0350
65	2.00	1.0	.192	.298	.106	.150	.788	2.00	.0750
66	2.00	1.0	.195	.297	.102	.149	.790	2.00	.0745
67	2.00	1.0	.229	.366	.137	.218	.961	2.00	.1090
68	5.00	1.0	.290	.567	.277	.288	1.423	5.00	.0576
69	0.21	1.0	.054	.049	-.055	.029	.053	0.21	.1381
70	1.00	1.0	.068	.146	.079	.064	.360	1.00	.0640
72	3.00	1.0	.150	.320	.170	.126	.791	3.00	.0420
73	0.50	1.0	.020	.076	.056	.031	.173	0.50	.0620
74	1.00	1.0	.051	.141	.090	.059	.332	1.00	.0590
75	1.00	1.0	.041	.114	.073	.032	.269	1.00	.0320
76	1.00	1.0*	.041	.172	.131	.090	.384	1.00	.0900
76 OC	5.00	1.0	.206	.479	.273	.200	1.165	5.00	.0400
77	2.00	1.0	.250	.337	.087	.189	.924	2.00	.0945
79	2.00	1.0	.226	.327	.101	.179	.880	2.00	.0895
85	2.00	1.0	.155	.262	.107	.114	.680	2.00	.0570
86	1.00	1.0*	.051	.150	.098	.068	.350	1.00	.0680
86 OC	5.00	1.0	.181	.449	.268	.170	1.078	5.00	.0340
87	1.00	1.0*	.115	.196	.081	.114	.506	1.00	.1140
87 OC	5.00	1.0	.348	.385	.037	.106	1.119	5.00	.0212
88	2.00	1.0	.193	.323	.131	.175	.839	2.00	.0875
91	1.00	1.0*	.071	.180	.109	.098	.430	1.00	.0980

*over consolidated

Isotropic Tests, Vertical and Horizontal Strains

TABLE C.1a

Test # LS	$\bar{\sigma}_{hc}$ kg/cm^2	K_c	$\frac{\Delta V_{cons}}{V_1}$ %	ε_{vcons} %	ε_{hcons} %	ISOTROP $\varepsilon_h - \varepsilon_v$ %	ε_{hcorr} %	$\bar{\sigma}_{vc}$ kg/cm^2	$\frac{\varepsilon_{hcorr}}{\bar{\sigma}_{vc}}$ %/kg/cm^2
91 OC	4.00	1.0	.223	.493	.270	.255	1.209	4.00	.0638
93	2.00	1.0	.264	.405	.142	.257	1.074	2.00	.1285
94	2.00	1.0	.126	.422	.296	.274	.971	2.00	.1370
95	1.00	1.0*	.038	.174	.137	.092	.386	1.00	.0920
95 OC	4.00	1.0	.133	.464	.331	.226	1.062	4.00	.0565
96	1.00	1.0*	.054	.201	.147	.119	.456	1.00	.1190
96 OC	5.00	1.0	.243	.562	.318	.283	1.367	5.00	.0566
97	1.00	1.0	.044	.169	.124	.087	.382	1.00	.0870
100	2.00	1.0	.247	.355	.108	.207	.956	2.00	.1035
101	2.00	1.0	.195	.377	.182	.229	.948	2.00	.1145
102	2.00	1.0	.206	.363	.157	.215	.932	2.00	.1075
103	2.00	1.0	.977	.174	.401	.227	.253	2.00	.1265
104	5.00	1.0	1.783	.402	.691	.289	.412	5.00	.0824
105	1.00	1.0	.550	.061	.244	.183	.162	1.00	.1620
106	1.00	1.0	.613	.125	.244	.119	.162	1.00	.1620
107	1.00	1.0	.471	.038	.217	.179	.135	1.00	.1350
108	5.00	1.0	1.272	.231	.521	.290	.242	5.00	.0484
109	1.00	1.0	.447	.068	.189	.121	.107	1.00	.1070
110	5.00	1.0	1.425	.287	.569	.282	.290	5.00	.0580
111	1.00	1.0	.389	.068	.160	.092	.078	1.00	.0780
112	5.00	1.0	1.351	.199	.576	.377	.297	5.00	.0594

*over consolidated

Isotropic Tests, Vertical and Horizontal Strains

TABLE C.1b

Test # LC	$\bar{\sigma}_{hc}$ kg/cm^2	K_c	$\frac{\Delta V_{cons}}{V_1}$ %	ε_{vcons} %	ε_{hcons} %	ISOTROP $\varepsilon_h - \varepsilon_v$ %	ε_{hcorr} %	$\bar{\sigma}_{vc}$ kg/cm^2	$\frac{\varepsilon_{hcorr}}{\bar{\sigma}_{vc}}$ %/kg/cm^2
47	2.15	1.00	.908	.165	.371	.207	.223	2.15	.1115
49	2.07	1.00	.315	.057	.129	.072	-.019	2.07	-.0092
50	1.00	1.00	.316	.047	.134	.087	.052	1.00	.0520
57	.98	1.00	.370	.057	.156	.099	.074	.98	.0755
52	1.05	1.00	.268	.061	.103	.042	.021	1.05	.0020
53	1.08	1.00	.345	.067	.139	.071	.057	1.08	.0528
54	1.04	1.00	.348	.048	.150	.102	.068	1.04	.0654
55	.99	1.00	.266	.051	.108	.057	.026	.99	.0263
56	1.03	1.00	.294	.048	.123	.076	.041	1.03	.0398
57	1.01	1.00	.279	.064	.107	.043	.025	1.01	.0248
58	1.00	1.02	.238	.051	.094	.043	.012	1.00	.0120
59	1.01	1.00	.172	.054	.059	.005	-.023	1.01	-.0228
60	1.00	1.00	.279	.020	.130	.109	.048	1.00	.0480
61	1.01	1.00	.332	.081	.125	.044	.043	1.01	.0426
62	.99	1.00	.215	.038	.089	.051	.007	.99	.0071
63	.99	1.00	.269	.048	.110	.063	.028	.99	.0283
67	1.00	1.00	.282	.055	.114	.059	.032	1.00	.0320
69	1.01	1.00	.331	.054	.138	.084	.056	1.00	.0560
72	1.04	1.04	.172	.027	.072	.045	-.010	1.04	-.0096
73	3.00	1.00	.861	.148	.356	.028	.162	3.00	.0540
78	.51	1.00	.159	.030	.065	.034	.020	.51	.0392
83	3.01	1.00	.778	.123	.328	.205	.134	3.01	.0447
84	2.00	1.00	.565	.085	.240	.154	.092	2.00	.0460
85	1.01	1.00	.333	.037	.148	.111	.066	1.01	.0660
85 OC	5.00	1.00	1.251	.159	.546	.387	.267	5.00	.0534
95	3.00	1.00	.158	-.020	.089	.109	-.105	3.00	-.0350
98	2.00	1.00	.680	.155	.262	.107	.114	2.00	.0570
99	1.00	1.00	.318	.081	.119	.038	.0370	1.00	.0370
100	5.00	1.00	1.009	.201	.404	.203	.1250	5.00	.0250
101	5.00	1.00	1.265	.341	.462	.121	.1830	5.00	.0366
103	1.00	1.00	.371	.064	.154	.089	.007	1.00	.0070
119	3.00	1.00	.820	.150	.335	.184	.141	3.00	.0470
123	1.00	1.00	.230	.027	.101	.074	.019	1.00	.0190
127	5.00	1.00	1.099	.171	.464	.293	.185	5.00	.0370
128	1.50	1.00	.590	.222	.184	-.038	.067	1.50	.0447
138	1.00	1.00	.217	.044	.086	.042	.004	1.00	.0040
139	2.00	1.00	.589	.108	.241	.133	.093	2.00	.0465
144	2.50	1.00	.633	.135	.249	.114	.079	2.50	.0316
146	5.00	1.00	1.196	.209	.493	.284	. 14	5.00	.0428

Isotropic Tests
Vertical and
Horizontal Strains

TABLE C.1c

TABLE C.2a

Test # LC-	$\bar{\sigma}_{hc}$ kg/cm^2	K_c	$\frac{\Delta V_{cons}}{V_1}$ %	ε_{vcons} %	ε_{hcons} %	ISOTROP $\varepsilon_h - \varepsilon_v$ %	ε_{hcorr} %	$\bar{\sigma}_{vc_2}$ kg/cm^2	$\frac{\varepsilon_{hcorr}}{\bar{\sigma}_{vc}}$ %/kg/cm^2
61	2.00	2.0	-.127	.392	-	.255	.656	1.00	.2550
71	.50	.5	.096	.033	-	-.007	.162	1.00	-.0070
78	1.50	.55	.219	.119	-	.002	.457	2.75	.0007
89	1.50	.60	.174	.118	-	.001	.410	2.50	.0004
90	1.50	.60	.150	.181	-	.064	.511	2.50	.0256
98	2.00	2.0	-.149	.534	-	.386	.920	1.00	.3860
99	1.50	.6	.179	.160	-	.043	.498	2.50	.0172

STATIC TESTS

Test # LC-	$\bar{\sigma}_{hc}$ kg/cm^2	K_c	$\frac{\Delta V_{cons}}{V_1}$ %	ε_{vcons} %	ε_{hcons} %	ISOTROP $\varepsilon_h - \varepsilon_v$ %	ε_{hcorr} %	σ_{vc} kg/cm^2	$\frac{\varepsilon_{hcorr}}{\sigma_{vc}}$ %/kg/cm^2
64	.49	.33	.176	.253	-.039	-	-.084	1.50	-.0560
65	.51	.30	.186	.392	-.103	-	-.148	1.50	-.0987
66	.50	.50	.172	.068	.52	-	.007	1.00	.0070
68	2.50	.83	.740	.147	.296	-	.126	3.00	.0420
70	1.50	.50	.454	.259	.097	-	-.020	3.00	-.0067
71	1.30	1.30	.410	.014	.198	-	.093	1.00	.0930
74	1.50	1.50	.409	-.010	.210	-	.093	1.00	.0930
75	.70	.70	.188	.092	.048	-	-.015	1.00	-.0150
76	1.51	.50	.479	.220	.130	-	.013	3.00	.0043
77	2.01	.67	.511	.181	.165	-	.017	3.00	.0057
79	1.81	1.81	.511	-.024	.267	-	.131	1.00	.131
80	1.01	.50	.346	.182	.082	-	.000	2.00	.000
81	.50	.50	.215	.092	.062	-	.017	1.00	.0170
82	1.51	.50	.491	.250	.121	-	.004	3.00	.0013
86	4.50	1.50	1.181	.065	.558	-	.298	3.00	.0993
87	1.50	.43	.599	.267	.166	-	.049	3.50	.0140
88	1.50	.50	.589	.222	.184	-	.067	3.00	.0223
89	1.50	.60	.518	.172	.173	-	.056	2.50	.0224
90	1.50	.60	.613	.233	.190	-	.073	2.50	.0292
91	1.50	.60	.499	.140	.179	-	.062	2.50	.0248
92	1.50	.60	.493	.203	.145	-	.028	2.50	.0112
93	1.50	.60	.783	.482	.151	-	.034	2.50	.0136
94	1.50	.60	.394	.151	.122	-	.005	2.50	.0020
97	1.50	.60	.510	.164	.173	-	.056	2.50	.0224
102	1.50	1.50	.404	.034	.185	-	.068	1.00	.0680
104	1.50	.60	.557	.208	.174	-	.057	2.50	.0228
105	1.50	.60	.368	.126	.121	-	.004	2.50	.0016
106	1.50	.60	.508	.203	.153	-	.036	2.50	.0144
116	1.50	1.50	.390	.034	.178	-	.061	1.00	.0610
117	1.50	.60	.478	.167	.155	-	.038	2.50	.0152
118	1.50	.60	.594	.247	.174	-	.057	2.50	.0228
120	1.00	.50	.390	.213	.089	-	.007	2.00	.0035
121	1.50	.60	.464	.188	.138	-	.021	2.50	.0084

Anisotropic Tests, Corrected Strains

TABLE C.2b

Test # LC-	$\bar{\sigma}_{hc}$ kg/cm^2	K_c	$\frac{\Delta V_{cons}}{V_1}$ %	ε_{vcons} %	ε_{hcons} %	ISOTROP $\varepsilon_h - \varepsilon_v$ %	ε_{hcorr} %	$\bar{\sigma}_{vc_2}$ kg/cm^2	$\frac{\varepsilon_{hcorr}}{\bar{\sigma}_{vc}}$ %/kg/cm^2
122	1.50	.60	.540	.291	.125	-	.008	2.50	.0032
124	1.50	.60	.470	.152	.159	-	.042	2.50	.0168
125	1.50	.60	.490	.147	.171	-	.054	2.50	.0216
125 OC	4.80	.60	1.047	.362	.343	-	.071	8.00	.0089
126	1.50	.60	.759	.547	.106	-	-.011	2.50	-.0044
129	1.50	.60	.588	.247	.170	-	.053	2.50	.0212
130	1.50	.60	.587	.216	.186	-	.069	2.50	.0276
131	1.50	.60	.542	.199	.171	-	.054	2.50	.0216
132	1.50	.50	.475	.167	.154	-	.037	3.00	.0123
133	1.50	.50	.468	.197	.135	-	.018	3.00	.0060
134	1.50	.60	.511	.150	.181	-	.064	2.50	.0256
135	2.00	.67	.634	.202	.216	-	.068	3.00	.0227
136	4.50	1.50	.943	.094	.424	-	.164	3.00	.0547
137	1.50	.43	.540	.260	.140	-	.023	3.50	.0066
140	.50	.50	.188	.091	.049	-	.004	1.00	.0040
141	1.50	.60	.564	.250	.157	-	.040	2.50	.0160
142	1.50	.60	.404	.143	.130	-	.013	2.50	.0052
143	1.50	.60	.612	.230	.191	-	.074	2.50	.0296
145	3.00	1.50	.652	.021	.316	-	.122	2.00	.0610
147	4.50	1.50	.950	.095	.428	-	.168	3.00	.0560
148	.30	.50	.184	.068	.058	-	.013	1.00	.0130
149	2.50	.50	.841	.318	.262	-	.092	5.00	.0184
150	2.50	.71	.772	.189	.292	-	.122	3.50	.0349
151	2.50	.71	.719	.186	.266	-	.096	3.50	.0274
152	1.50	.50	.549	.201	.174	-	.057	3.00	.0190
153	2.50	.83	1.187	.386	.401	-	.231	3.00	.0770
154	2.50	.83	1.132	.338	.397	-	.227	3.00	.0757
155	2.50	.71	1.591	.863	.364	-	.194	3.50	.0554
156	2.50	.71	1.133	.451	.341	-	.171	3.50	.0489
157	1.25	.33	.582	.479	.052	-	-.050	3.75	-.0133
158	3.50	.50	1.069	.404	.332	-	.117	7.00	.0167
159	3.00	.68	.809	.116	.347	-	.153	4.40	.0348
160	3.00	.75	.674	.146	.264	-	.070	4.00	.0175
161	3.80	.55	.895	.205	.345	-	.115	6.90	.0167
162	2.90	.71	.902	.174	.364	-	.174	4.10	.0424

Anisotropic Tests, Corrected Strains

TABLE C.2c

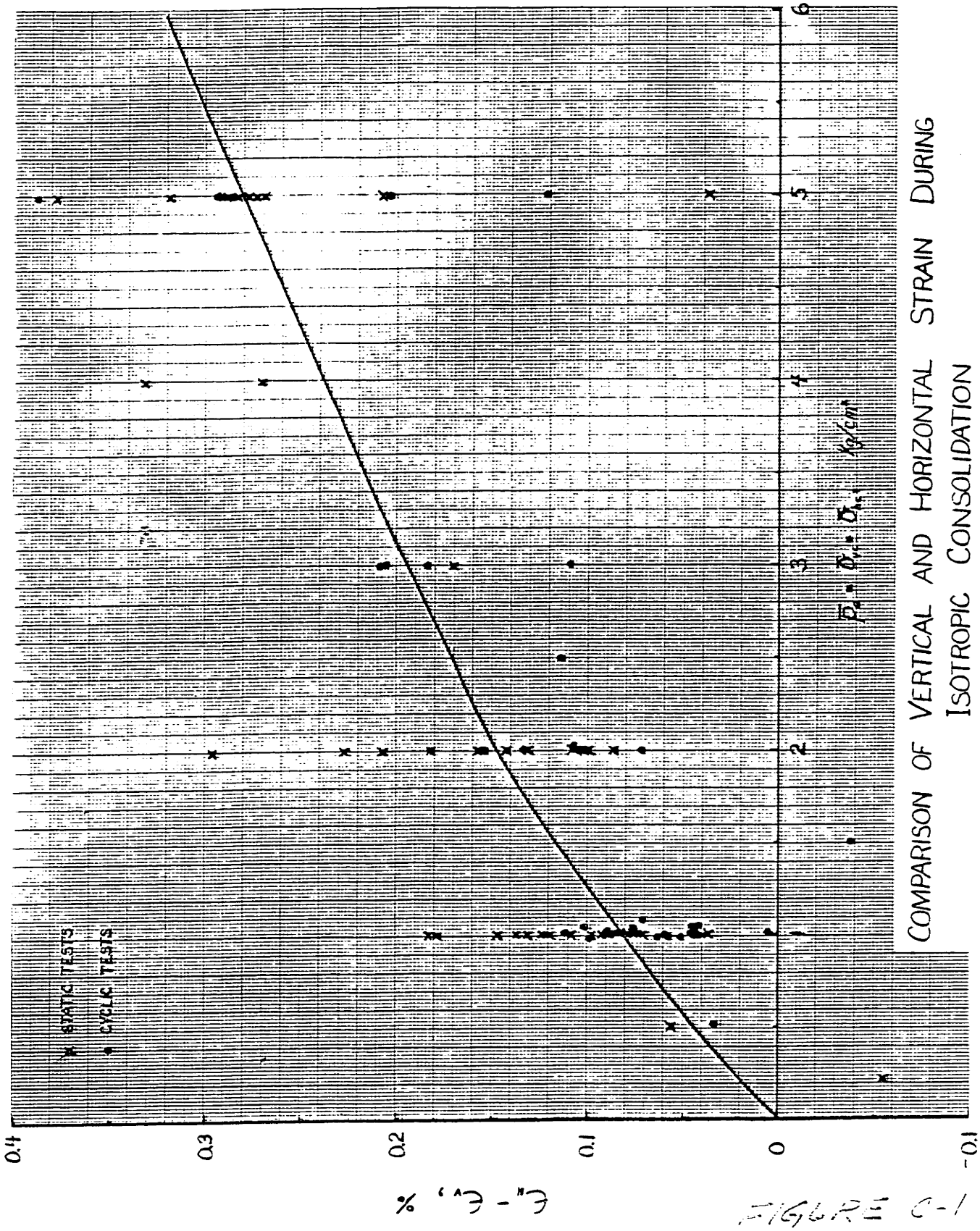

COMPARISON OF VERTICAL AND HORIZONTAL STRAIN DURING ISOTROPIC CONSOLIDATION

FIGURE C-1

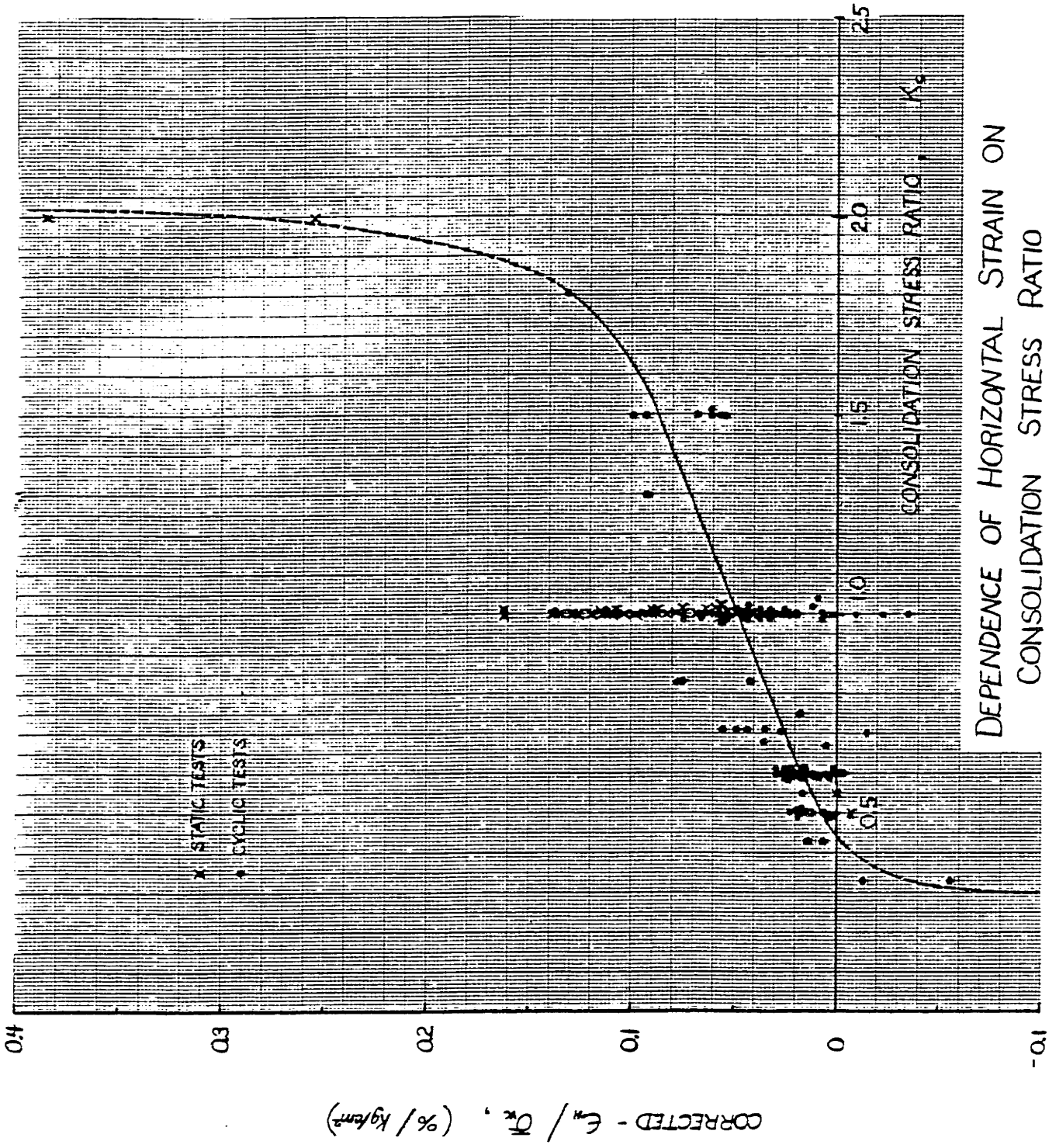
DEPENDENCE OF HORIZONTAL STRAIN ON CONSOLIDATION STRESS RATIO
CONSOLIDATION STRESS RATIO, K_c
0.5
1.0
1.5
2.0
2.5
CORRECTED - $\varepsilon_H / \bar{\sigma}_x$, (% / kg/cm²)
0.4
0.3
0.2
0.1
0
-0.1
STATIC TESTS
CYCLIC TESTS

FIGURE C-2

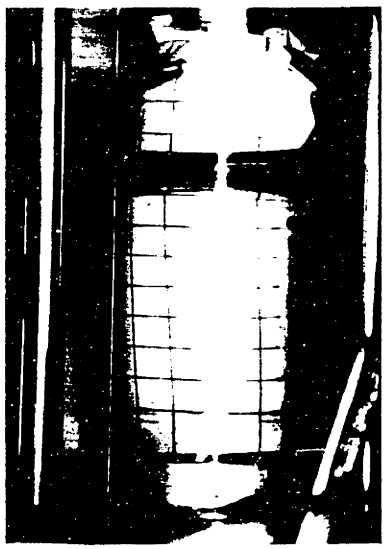

COMPRESSION LOAD
LC143, CYCLE #20

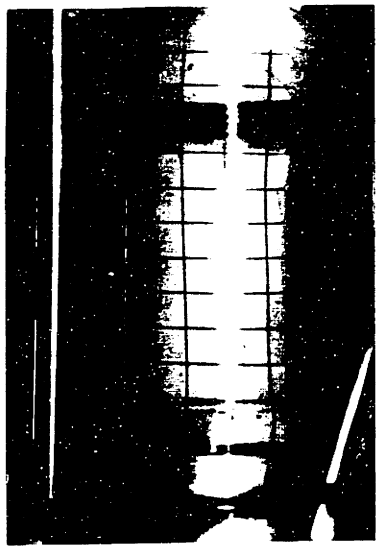

EXTENSION LOAD
LC143, CYCLE #20

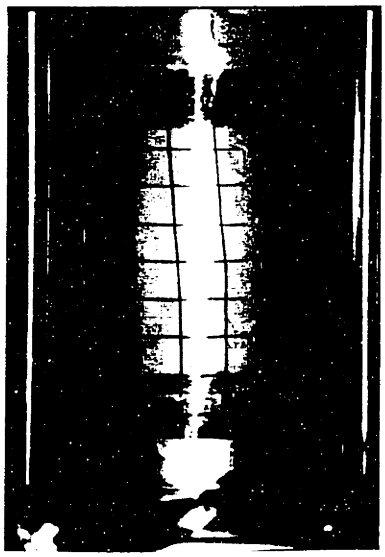

TEST START, LC136

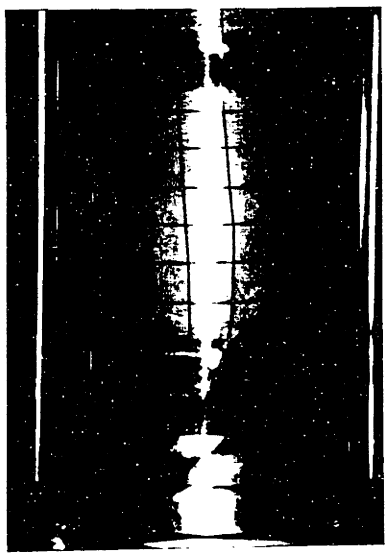

TEST END, LC136

PHOTOS OF CYCLIC COMPRESSION TEST SAMPLE WITH SHEAR STRESS REVERSAL (TOP), AND CYCLIC EXTENSION TEST SAMPLE NECKING AT THE BOTTOM.

FIGURE C.3

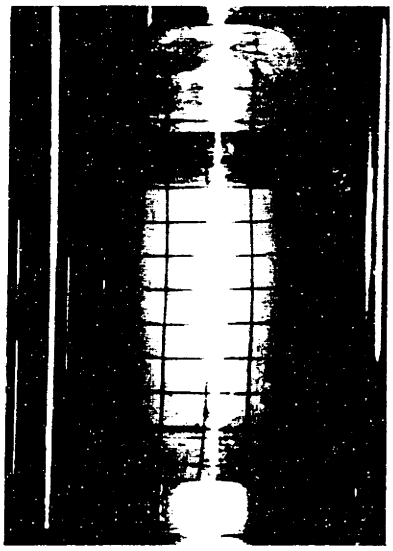

TEST START

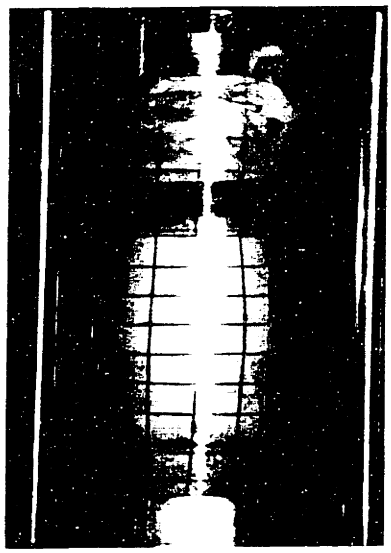

TEST END

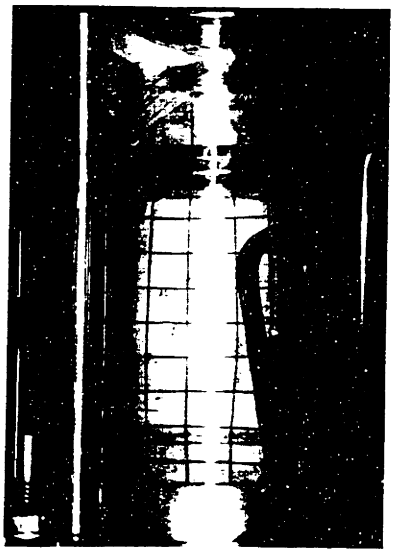

TEST START

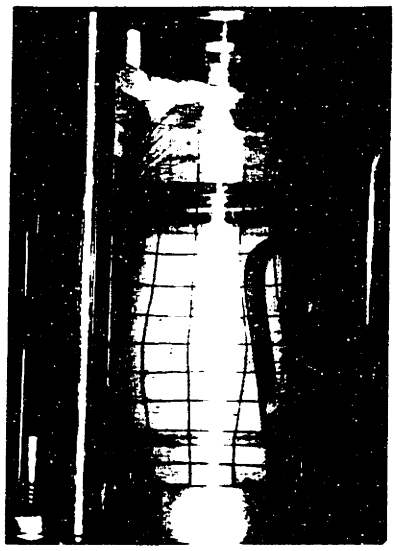

TEST END

PHOTOS OF CYCLIC COMPRESSION TEST SAMPLE (TOP) AND STATIC TEST SAMPLE (BOTTOM) AT BEGINING AND END OF TEST.

FIGURE C.4

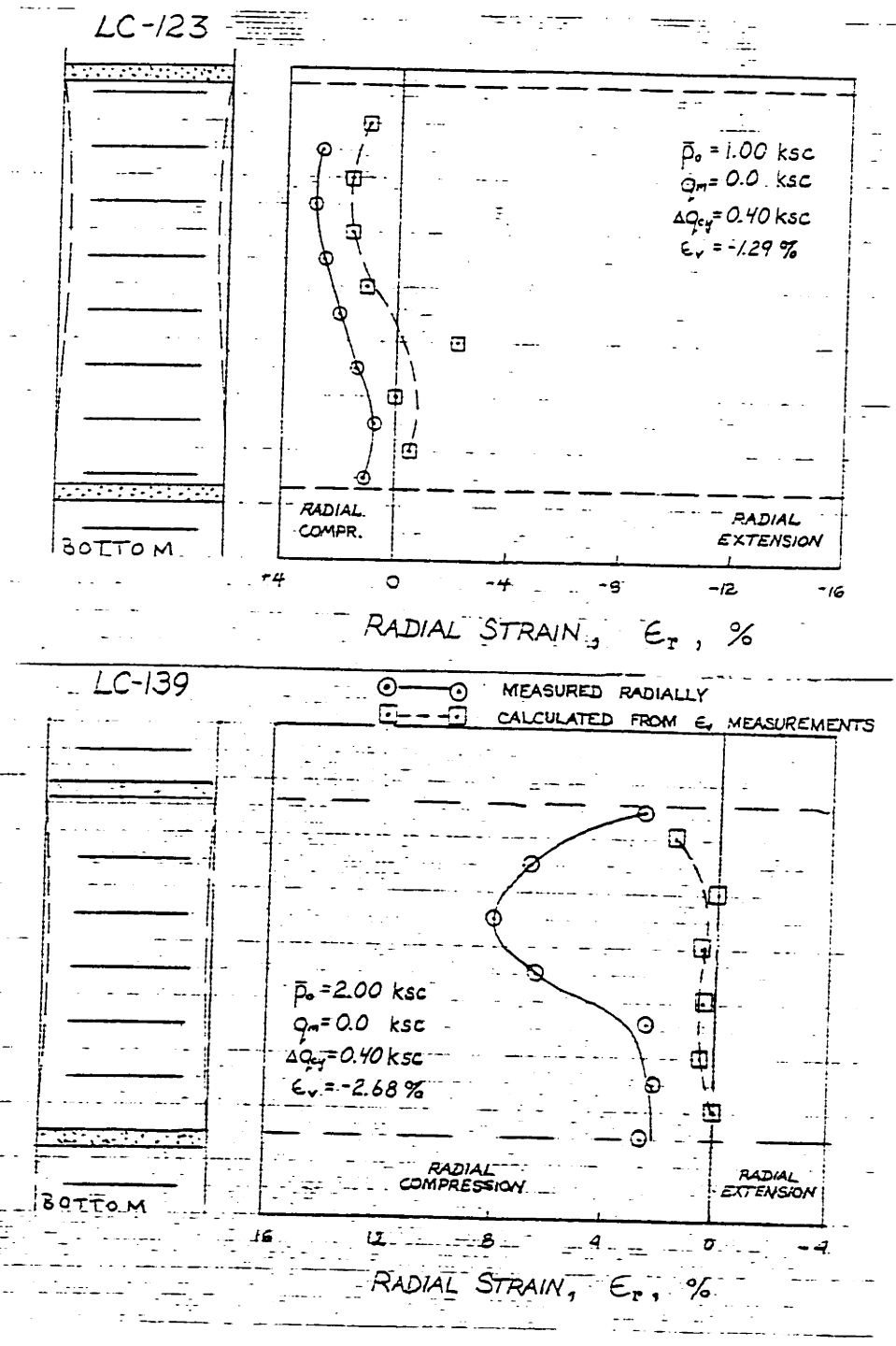

COMPARISON OF CALCULATED AND MEASURED RADIAL STRAINS IN ISOTROPIC CYCLIC TRIAXIAL TEST SAMPLES

FIGURE C-5

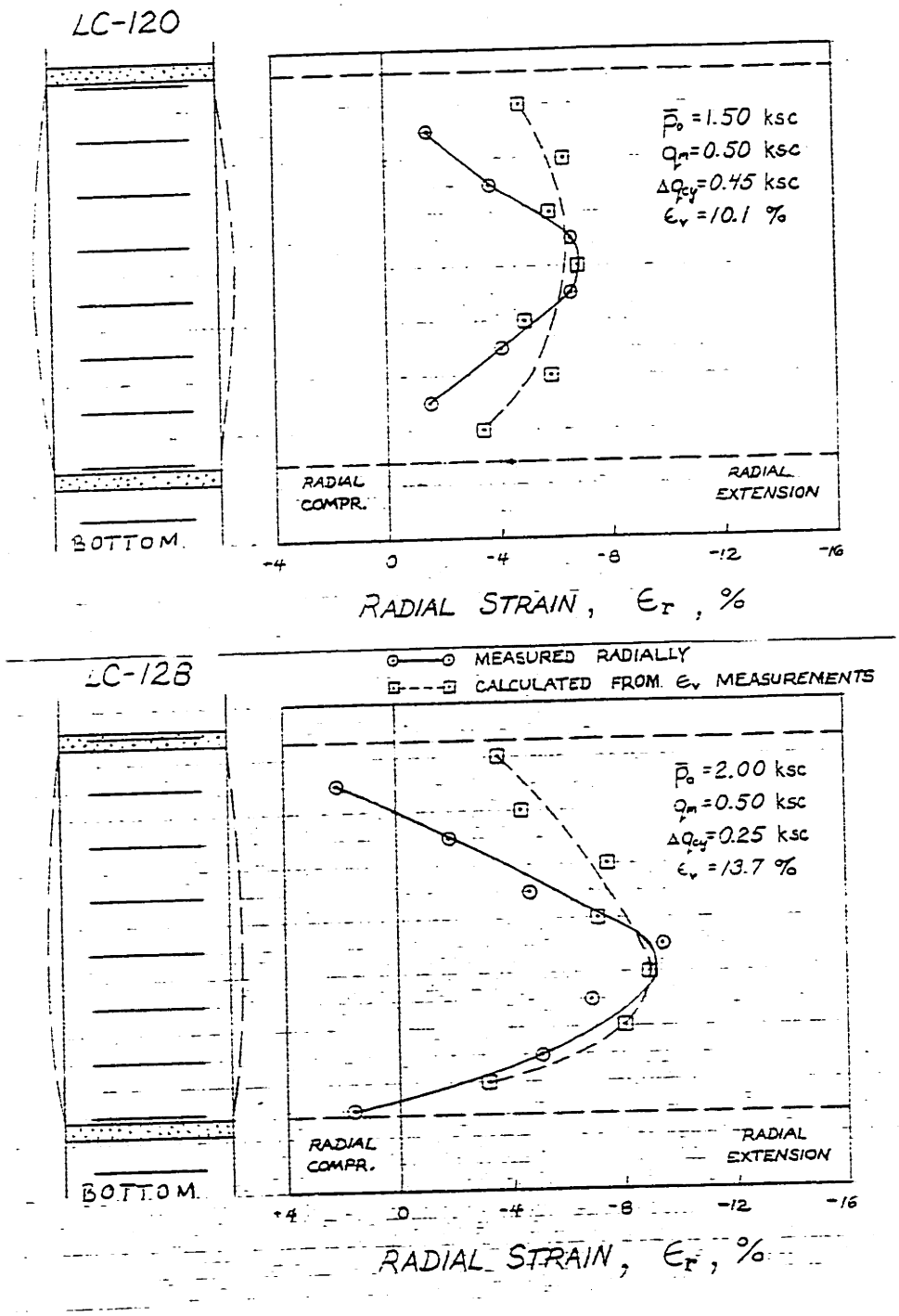

COMPARISON OF CALCULATED AND MEASURED RADIAL STRAINS IN COMPRESSION CYCLIC TRIAXIAL TEST SAMPLES

FIGURE C-6

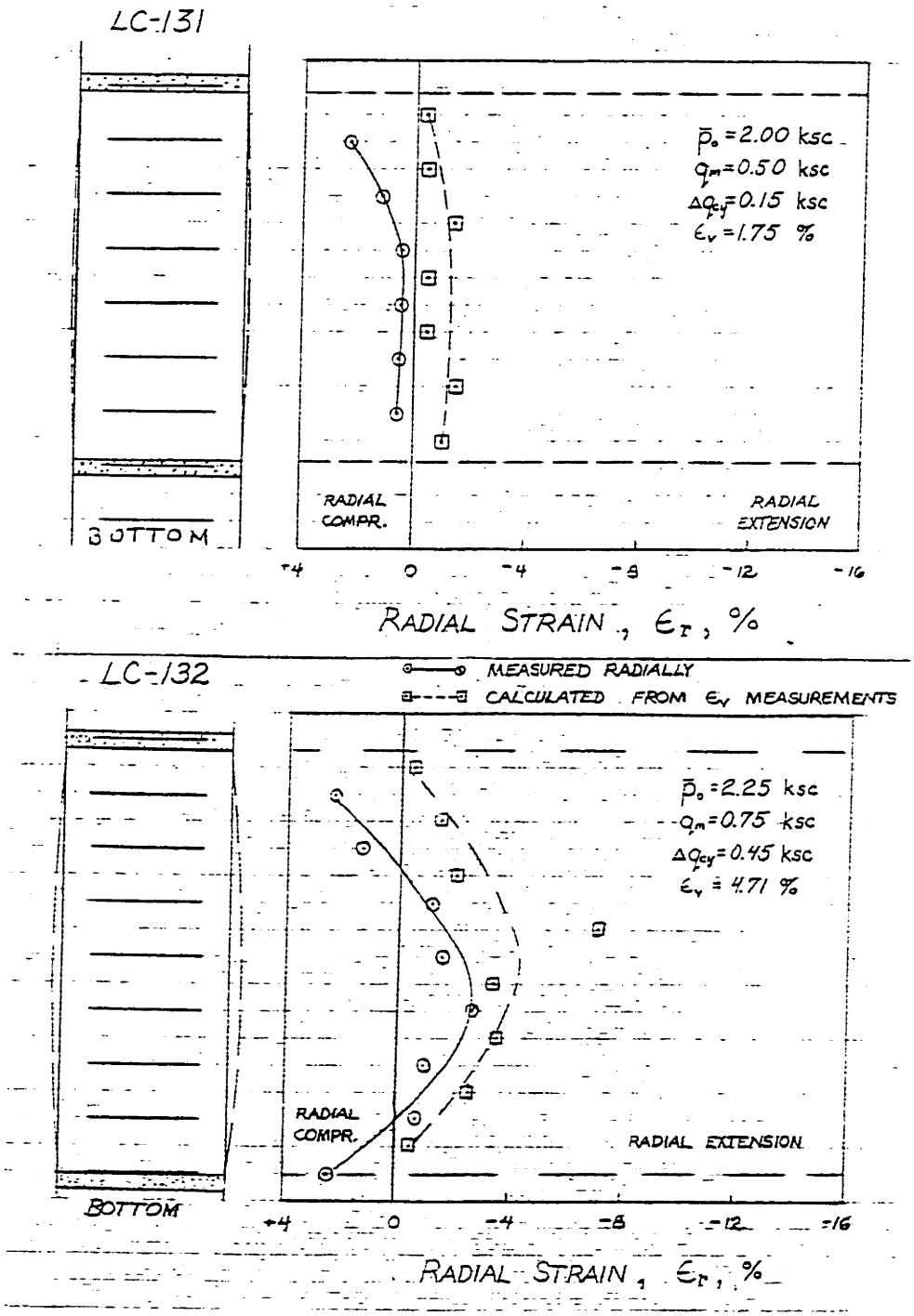

COMPARISON OF CALCULATED AND MEASURED RADIAL STRAINS IN COMPRESSION CYCLIC TRIAXIAL TEST SAMPLES

FIGURE C-7

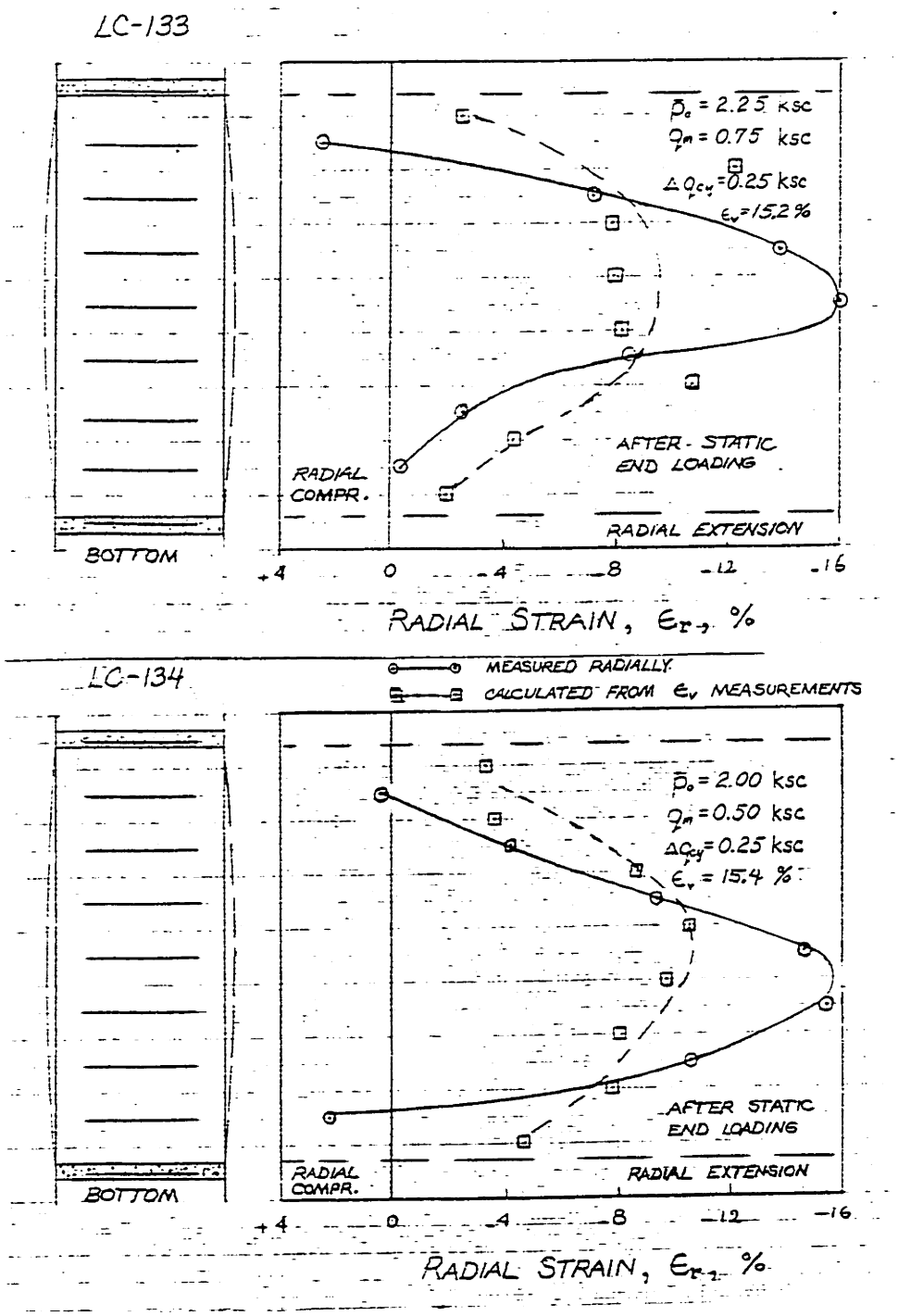

COMPARISON OF CALCULATED AND MEASURED RADIAL STRAINS IN COMPRESSION STATIC TRIAXIAL TEST SAMPLES

FIGURE C-8

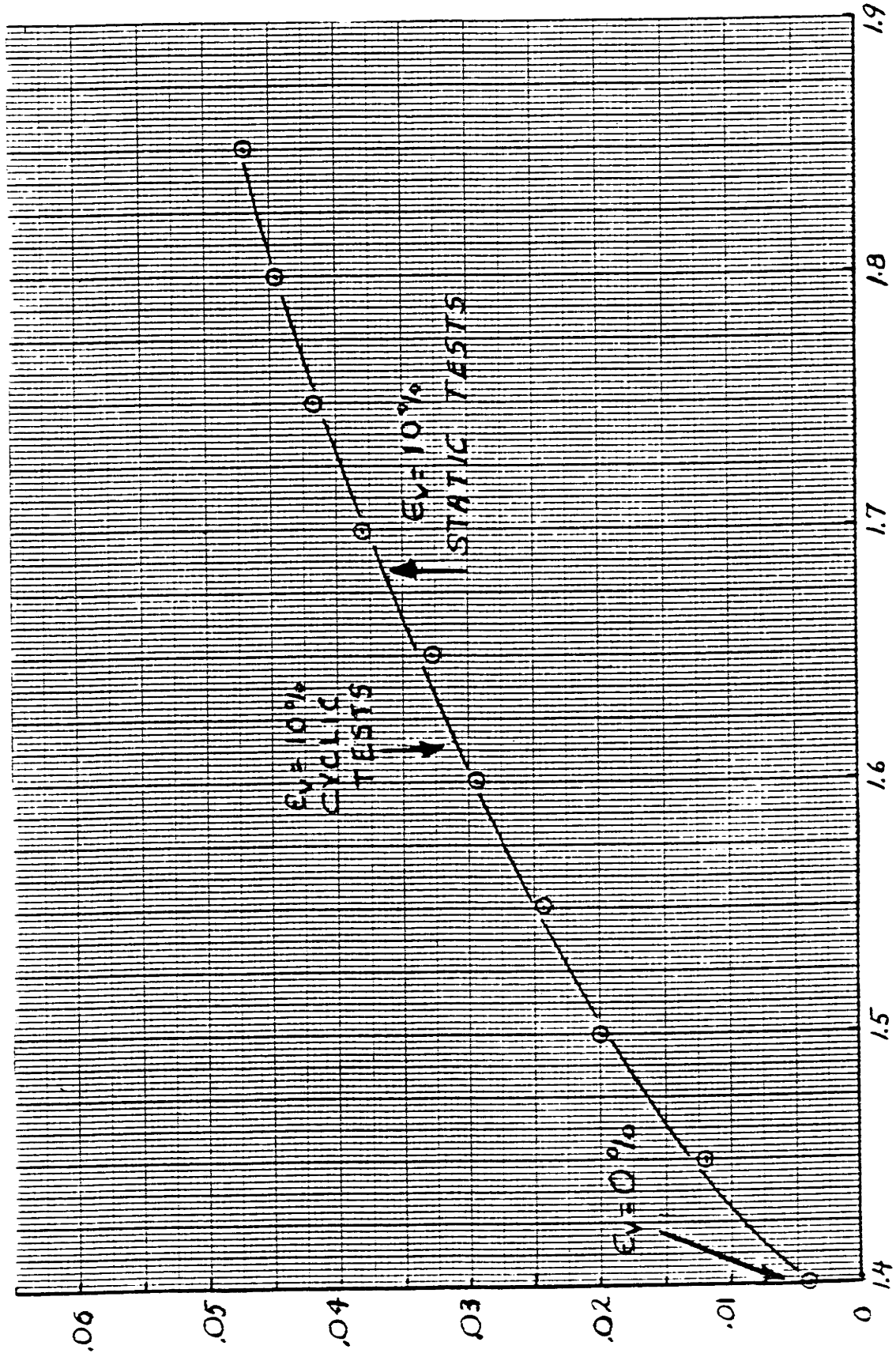

RADIAL MEMBRANE CONFINEMENT

FIGURE C-9

OOSTERSCHELDE FINE SAND

$\bar{\sigma}_{vc}$ = 1.00 Kg/cm², $\bar{\sigma}_{hc}$ = 1.00 Kg/cm², OCR = 5

	n_c %	$\bar{\phi}$ °
LS-76	41.3	36.9
LS-86	41.1	37.0

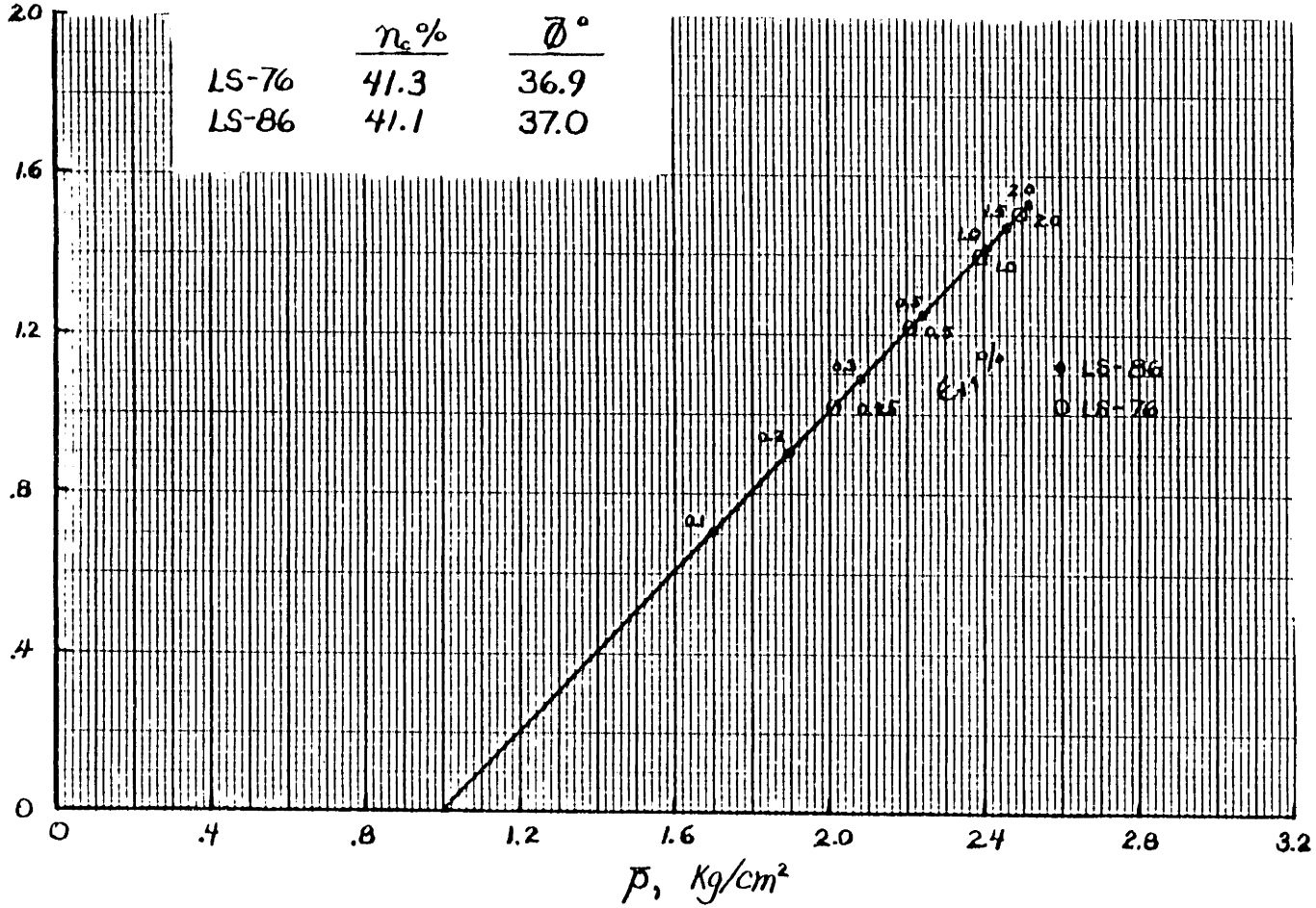

FIGURE C-10

EFFECTIVE STRESS PATHS FOR TWO IDENTICAL TESTS

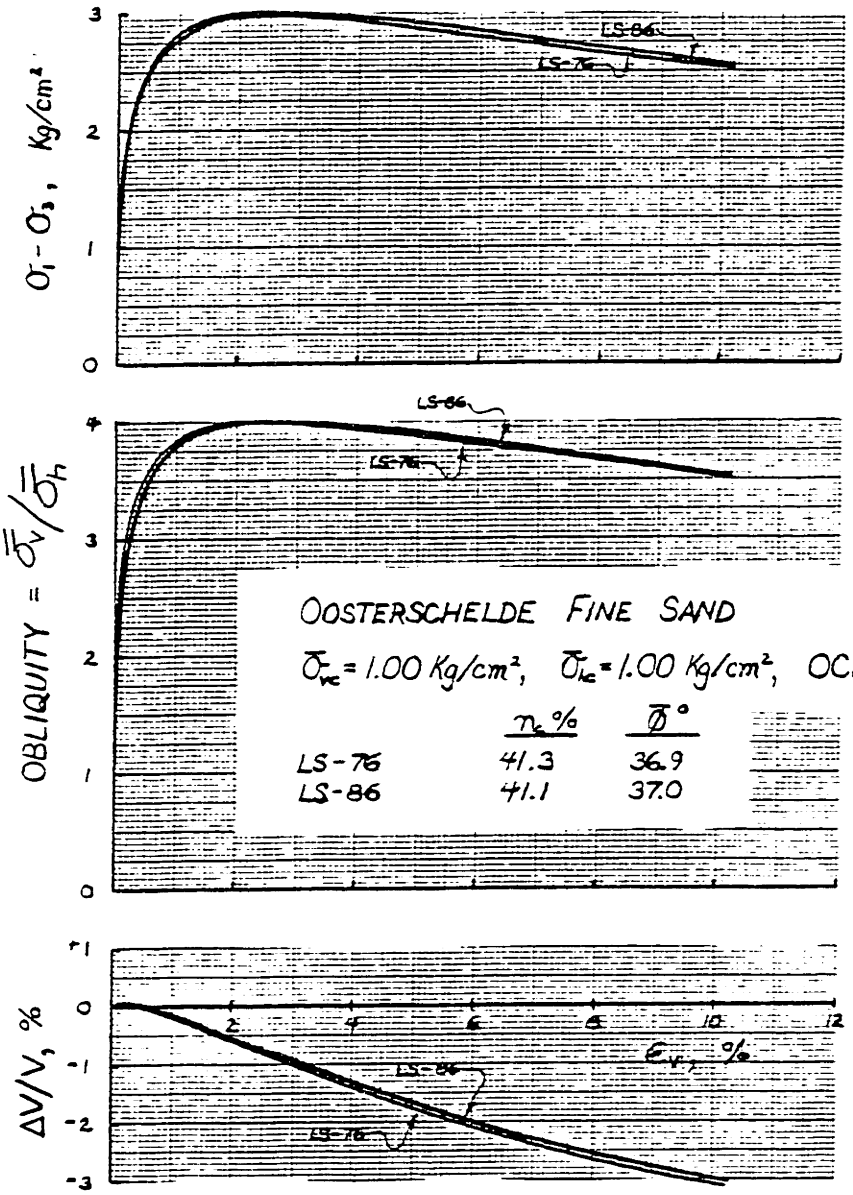

SHEAR STRESS, OBLIQUITY, AND VOLUMETRIC STRAIN FOR TWO IDENTICAL TESTS

FIGURE C-11

APPENDIX D

Static Triaxial Test Results

D.1 Dilation, Contraction and Liquefaction

A total of 34 undrained static triaxial tests were run on loose and very loose specimens. The primary objective of those tests was to investigate what Casagrande (1936) and Castro (1969) refer to as critical void ratio or critical state. Table D.1 lists stresses, strains, moduli, etc. for all 34 tests. The following abbreviations are used in the remarks column: F.S. = Fine Oosterschelde Sand, M.S. = Medium Oosterschelde Sand, Liq. = Liquefaction at the failure line, Dil. = dilation at the failure line and S.C. = Stress Control. The friction angles were measured at maximum shear stress for samples that liquefied, and at maximum obliquity for samples that dilated. The effective stress paths for the loose samples are presented in Figure D.1 to Figure D.10, organized after sand type, loading type and consolidation stress level. The sample behavior is very sensitive with respect to friction angle and sample preparation, so scatter in the results can be expected, as is the case in Figures D.3 and D.5.

Figures D.1 to 6 present stress-controlled tests, where D.1 to 3 contain results on Oosterschelde Fine Sand, D.4 to 6 on medium sand. The plots are organized with respect to magnitude of consolidation stress. Based on the effective stress path each sample follows can be decided whether the sample

liquefies or dilates when reaching the failure line, or behaves somewhere in between. In Figure D.2, the stress controlled, fine sand sample LS79 dilates, the samples LS77, 93, 100 and 103 liquefy, and LS101 approaches an intermediate behavior as the sample reaches 3 percent vertical strain before dilation starts. All the test samples, however, contract initially, and develop positive pore pressures. The medium sand sample LS111 in Figure D.4 liquefied after reaching some shear stress level, but dilated as the K_f-line was reached. That is a very good example of intermediate behavior between liquefaction and dilation in a stress-controlled test.

The stress paths in Figures D.7 to D.10 are all from strain-controlled tests. Here liquefaction is characterized by the effective stress path going down along the K_f-line (see e.g., tests LS36, 37, 38 and 39 in Figure D.8). Test LS40 in Figure D.8 dilates while test LS42 shows intermediate behavior. After reaching 8 - 10 percent vertical strain, all strain-controlled samples were reconsolidated, and then reloaded in compression, again undrained. During reloading, the samples were much stiffer and less contractive, and liquefaction did not occur. From the porosities after reconsolidation (tabulated on the figures) is evident that the samples were appreciably denser after reconsolidation. This was also the case in the reconsolidated cyclic tests that suffered cyclic mobility failure, however, they failed immediately upon reloading, which lends support to the assumption of non-uniform samples

after cyclic mobility failure.

The information from all these loose, undrained tests is synthesized in Figures D.11 and D.12. The load controlled tests on Oosterschelde Fine Sand in Figure D.11 reveal the sand is very dilatant. The open squares signify isotropically consolidated samples that liquefied, the closed squares samples that dilated, and the half-closed squares samples that showed intermediate behavior. The borderline between samples that dilate and samples that liquefy is called the critical void ratio line (Casagrande, 1936). Note that the critical void ratio line lies above the consolidation line from a one-dimensional oedometer test. The cyclic tests LC154 and 155 do not seem to follow the critical void ratio line for the static test. Although starting at higher consolidation stress, LC154 reaches the K_f-line at much smaller effective stress than LC155. It can, therefore, be that not only consolidation stress, but also failure stress influences the location of the critical void ratio line.

Figure D.12 summarized both strain control and stress control tests on Medium Oosterschelde Sand. Squares signify stress-controlled tests, and circles strain-controlled tests. The critical void ratio line for stress-controlled tests falls below the line for strain-controlled tests, indicating the effect of constant stress on the sand response: When the stress cannot be reduced by deformation, the sand is more susceptible to liquefaction. Castro (1969) and Casagrande

(1976) pointed out that load-controlled tests model the field loading correctly. The borderline between liquefaction and dilation found in strain-controlled tests, lies at about 3/4 percent higher porosity than the critical void ratio line for stress controlled tests. Both lines for medium sand are well below the one-dimensional compression curve.

Comparing the load-controlled test results on the fine and medium sand, the critical void ratio line for the fine sand is found to be about 2.5 percent porosity higher than the critical void ratio line for the medium sand (a void ratio difference of 0.08). That means the fine sand is quite a bit more dilative. From the sand description in Appendix A, the following information can be extracted:

	Fine Sand	Medium Sand
Mean grain diameter	0.17 mm	0.28 mm
Porosity at minimum relative density	46%	45%
Roundness	Subrounded	Rounded
Acid soluble (carbonates)	5%	3.3%

The mineral composition is approximately the same for both sands, with about 65% quartz and the rest mainly feldspars and carbonates. The 1% difference in porosity at minimum relative density of course contributes towards the 2.5% difference in porosity between the two critical void ratio lines. If the average number of sand grains per square centimeter

of the two sands is computed by dividing the difference between the sample and void area by the mean grain area, the fine sand is found to have 3 times as many grains per cm^2 (3000 versus 880). Knowing that a rounded, loose sand has an average of 4.4 contacts per grain (Borowicka, 1976), larger contact stresses are possible for the medium sand and thus less dilatant behavior can result.

Figure D.13 presents a comparison of a stress-controlled (LC) and a strain-controlled test (SC). The difference in effective stress path and stress-strain behavior of the two samples is relatively minor. Note, however, that the porosity of the strain-controlled sample is 0.8 percent higher than that of the stress-controlled sample. The maximum shear stress is reached at less than 1 percent vertical strain.

To summarize the observations in Figures D.1 to D.13: If loose sand samples are loaded undrained in triaxial compression tests, the samples always contract and develop positive pore pressures during the first stages of the test. When an internal friction angle of 20 to 25° is reached (effective shear stress ratio of 0.33 to 0.42), the sample may suddenly lose strength, collapse and develop large strains under the monotonic load. That is denoted <u>liquefaction</u>. Another possibility is a further increase in friction angle to about 30° at approximately constant shear stress, then an increase in shear stress as excess pore pressure decreases (the effective stress path goes up along the K_f-line). That is denoted <u>dilation</u>.

D.2 Drainage

In addition to the 34 undrained tests on loose samples to investigate critical density, 32 further tests, mostly drained and at medium density, were performed. The objectives of these tests were to examine the effects of drainage, density, stress path and stress history on the sand behavior. Most tests were performed under strain control at 1/3 percent strain per minute. A tabulation of the 32 tests is presented in Table D.2. The following abbreviations are used in the remarks column: FS = Fine Oosterschelde Sand, MS = Medium Oosterschelde Sand, Incr. pp = pore pressure increase, OCR = Overconsolidation Ratio, and e.g., (2 x I) = the number of overconsolidation cycles (2) and whether they were at isotropic stress (I) or anisotropic stress (K_c).

Figure D.14 presents two undrained and one drained test on Oosterschelde Medium Sand, all strain controlled. One of the undrained tests dilated (UC), whereas the other liquefied (UL). The difference in friction angle at maximum obliquity was less than one degree; 30.9° for the liquefying sample and 31.8° for the dilating sample. The drained triaxial sample contracted throughout the test, as can be seen from the volumetric strain curve in Figure D.14. Although reaching a higher strength than the looser undrained samples, the 31° friction angle of the drained sample is about one degree lower than that of the contractive undrained sample, despite the porosity decrease of the drained sample to 42.6%. However, the effective

stress level is much higher in the drained sample at failure.

Figure D.15 presents one drained and one undrained test on medium dense samples of Fine Sand. Initially, the drained sample is stiffer, but only as long as the effective mean normal stress is higher in the drained sample than in the undrained sample. Once dilatancy has built up enough negative pore pressure after the initial positive pore pressure, the undrained sample is much stiffer than the drained one. Similar to the initial contraction in the undrained test, the volumetric strain in the drained test shows contraction until almost the same obliquity value (3.5 vs. 3.7). The friction angle measured in the drained test was about 1 degree higher than in the undrained test, which is opposite from what was found comparing the loose samples of Oosterschelde Medium Sand. The medium dense drained sample, however, dilated at maximum obliquity with an accompanying small increase in porosity. Also, the effective stress level is smaller in the medium dense drained sample than in the undrained at failure. A plot of friction angle versus effective mean normal stress will be given at the end of this appendix.

D.3 Porosity

Figure D.16 presents three drained tests on Oosterschelde Fine Sand, performed on samples ranging in porosity from 37 to 44 percent. The smaller the porosity is, the greater the density and the soil stiffness. The maximum shear stress

increases with density. The vertical strain at maximum she stress decreases with density. At all densities the sand be haves contractive until about 80 percent of the maximum shea stress is reached.

Figure D.17 presents a plot of friction angle versus sand porosity at maximum obliquity ($= \bar{\sigma}_v/\bar{\sigma}_h$). Drained behav of the fine and medium sand are profoundly influenced by the porosity. The fine sand spans over friction angles from 43° at 37 percent porosity to 33° at 44 percent porosity, or abo 10 degrees for a 7 percent porosity change. The friction an for medium sand changes 8° over 7 percent porosity differenc Tests LS23 and 44 were run at consolidation stresses differe from 1 kg/cm^2, and are corrected to 1 kg/cm^2 based on result in Section D.4 of this appendix.

Poisson's Ratio

Figure D.18 presents a plot of Poisson's Ratio versus vertical strain for drained tests on fine sand at different porosities. Poisson's Ratio ($= \mu = - \varepsilon_h/\varepsilon_v$) is based on total strain. At vertical strains smaller than 1/4 percent, the values are erratic because the burettes with which volume change is measured are not sensitive enough and thus the calculated horizontal strains are uncertain. At strains larger than 1/4 percent, the value of Poisson's Ratio increases rapi to level off at values ranging from 0.5 at 44 percent porosit to 0,85 at 37 percent porosity. The maximum value of Poisson

Ratio is found to occur at lower vertical strain for lower sample porosities.

D.4 Influence of Stress Path on Sand Behavior in Static Triaxial Tests

Loading and Unloading

Figure D.19 presents plots of a drained loading test (L), a drained unloading test (U) and an undrained unloading test (UU), all tests performed on strain-controlled medium dense samples of Oosterschelde Medium Sand. Both unloaded samples dilate from the very beginning of the test, the drained sample having a very limited load carrying capability, whereas the undrained sample is quite strong due to development of large negative pore pressures. Both effective stress path and stress strain behavior of the undrained unloading sample (medium sand) is much like the undrained loading sample of fine sand (Figure D.20), although not as stiff. The maximum friction angle of 33.6° compares well with the friction angle of 34.1° from the undrained loading test LS28 on medium sand. Note that the curved effective stress path of the drained unloading test is caused by the increased sample area during shear, and thus decreased vertical stress by constant vertical load. The friction angle of the drained unloading test is 39.7°, and substantially larger than that of the undrained unloading test. This high value is probably influenced by the low effective stress and possibly membrane confinement as discussed in Appendix C.

Consolidation Stress Level

Figure D.21 presents a plot of drained triaxial loading tests at 1/2, 1 and 3 kg/cm^2 consolidation stress on medium dense Oosterschelde Fine Sand. The tests are plotted normalized by the vertical consolidation stress. It is clearly evident that the lower the consolidation stress, the higher the stiffness and the more pronounced the dilation. Figure D.22 presents normalized tests on Oosterschelde Medium Sand at different consolidation stresses. The results are very similar to the plots in Figure D.21 on the fine sand.

The friction angles mobilized at maximum obliquity in the drained triaxial tests at various consolidation stress levels, are plotted in Figure D.23. A change in consolidation stress from 0.5 to 3 kg/cm^2 means a decrease in friction angle from 39 to 35 degrees for the fine sand, and 38 to 31 degrees for the medium sand. Note that the measured values have been adjusted to a porosity of 41.2% based on Figure D.17. Ladd et al. (1977) treat the effect of consolidation stress in greater detail.

Consolidation Stress Ratio

The consolidation stress ratio (K_c) is defined as the ratio of horizontal to vertical stress at consolidation. For an offshore soil element, the vertical effective stress is often approximately known, whereas the horizontal stress may range within wide bounds, and is generally not known. It

is therefore conceivable that at a vertical effective stress of 1 kg/cm^2, the horizontal stress can be 0.5 as well as 2 kg/cm^2. Figure D.24 presents 3 drained triaxial tests on Oosterschelde Fine Sand at a vertical consolidation stress of 1.0 kg/cm^2, and horizontal consolidation stresses of 0.5, 1.0 and 2.0 kg/cm^2. Both stress-strain and volume change behavior of the three tests vary widely. The sample at 2.0 kg/cm^2 horizontal stress is stronger than the one at 1 kg/cm^2, which in turn is stronger than the sample consolidated to 0.5 kg/cm^2. Whereas both the sample at 0.5 and 1/0 kg/cm^2 horizontal stress contracted before dilation, the sample at 2.0 kg/cm^2 horizontal stress dilated from the very beginning of the test. Figure D.25 presents the same test types on Oosterschelde Medium Sand. The plots are very similar to the ones in Figure D.24.

Figure D.26 shows variations in mobilized friction angle at maximum obliquity for the drained triaxial tests performed at different consolidation stress ratios. All values are corrected to a mean normal consolidation stress ($\bar{p}_o$) of 1.0 kg/cm^2 (by Figure D.23), and to a porosity of 41.2 percent (by Figure D.17). The friction angles vary less than 2 degrees for different K_c-values and otherwise comparable conditions.

Overconsolidation Ratio

Figure D.27 presents three drained triaxial tests on Oosterschelde Fine Sand at overconsolidation ratios (OCR) of

1, 5 and 10. The overconsolidation ratio is the ratio of past maximum effective stress to present effective stress. Both stress-strain and volume change behavior seem to be little influenced by the overconsolidation ratio. Figure D.28 shows the mobilized friction angles at maximum obliquity (corrected to a porosity of 41.2 percent). Whereas the fine sand only increases its friction angle by about one degree at an OCR of 5, the medium sand shows an increase of 1 to 4 degrees.

Cyclic Loading Prior to Shear

One static triaxial test, LS99, was loaded undrained under load control, then unloaded and subjected to 250 load cycles, finally to be loaded statically again; all undrained. The friction angle at maximum obliquity increased thereby from 35.9° prior to cyclic loading to 37.3° thereafter. The undrained test LS90 was run on the sample of cyclic test LC-134 (ε_v = 0.38% in 20.000 load cycles), and yielded a friction angle of 39.2°. Both porosity and stress condition was the same as LS99 suggesting that the strength of sand increases after cyclic compression tests.

D.5 Summary of Static Test Findings

The main reason for performing static tests along with the investigation of cyclic sand behavior, is to establish general sand behavior believed to be common for both static and cyclic loading. The following conclusions can be made:

1. Undrained sand samples loaded statically may respond by liquefaction or dilation. These two types of response are also found in cyclic tests.
2. Decreasing sand porosity leads to a stronger sand, which is also found to hold for cyclic tests. Figure D.29 presents a plot of all static tests reported, giving maximum friction angle versus porosity. Regardless of drainage, stress condition and overconsolidation, there is a clear trend of decreasing friction angle with increasing porosity. From 37 to 47% porosity, the friction angle drops from 43 to about 20 degrees.
3. Increasing normal effective stress increases the stiffness and decreases the friction angle of statically loaded sand. Not only consolidation stress seems to be important, but also effective stress at failure. Figure D.30 presents a plot of a maximum friction angle versus mean effective failure stress for normally consolidated samples around 41% porosity. Whether increasing pore pressure (effective stress path horizontal to the left), unloaded, undrained or anisotropic, most samples plot with decreasing friction angle at

increasing failure stress.

4. Overconsolidation increases the strength of sand under both static and cyclic loading slightly.

Test # LS	Test Type	$\bar{\sigma}_{vo}$ kg/cm^2	$\bar{\sigma}_{hb}$ kg/cm^2	$\bar{\phi}$°	n_{setup} %	n_c %	ε_v At max $\bar{\sigma}_1/\bar{\sigma}_3$ %	$E^{50}_{sec.}$ kg/cm^2	K_c –	B %	$\frac{q_{max}}{q_{hc}}$	A –	At max. q ε_v %	At max. q $\bar{\phi}$ °	$\frac{q_{max}}{\bar{\sigma}_{hc}}$	ε_v At 1/2 Max. q %	ε_{vend} %	REMARKS
36	$\overline{CIU}$	.65	.65	31.1	46.48	46.06	1.47	505	1.00	91	1.09	5.26	.63	30.4	.48	.06	9.92	Liq, MS
37	$\overline{CIU}$	.65	.65	28.4	45.95	45.55	1.65	440	1.00	93	.98	14.7	.39	21.9	.34	.05	10.86	Liq, MS
38	$\overline{CIU}$	.65	.65	26.5	45.47	45.05	2.07	400	1.00	97	.94	12.6	.47	21.8	.31	.05	11.19	Liq, MS
39	$\overline{CIU}$	.64	.65	26.0	44.97	44.47	1.42	420	1.02	93	.92	15.7	.50	22.4	.32	.05	10.88	Liq, MS
40	$\overline{CIU}$	.64	.65	29.8	44.44	44.03	2.28	470	1.02	93	.48	.46	.52	24.9	.45	.06	11.21	Dil, MS
41	$\overline{CIU}$	1.99	2.00	30.7	44.46	43.41	9.55	750	1.00	99	.55	.60	2.09	28.0	.45	.12	10.57	Dil, MS
42	$\overline{CIU}$	.65	.65	29.7	44.66	44.22	2.07	550	1.00	92	.60	.71	1.90	29.7	.51	.06	11.50	MS, Dil./Liq.
43	$\overline{CIU}$	2.00	2.00	30.9	44.97	44.21	10.27	960	1.00	97	.70	1.11	.95	24.9	.38	.08	11.11	Liq, MS
45	$\overline{CIU}$	2.00	2.00	31.2	44.66	44.25	4.30	950	1.00	92	.42	.37	2.11	29.6	.57	.12	11.04	Dil, MS
46	$\overline{CIU}$	2.00	2.00	31.8	44.66	43.65	8.79	930	1.00	91	.50	.47	2.00	29.9	.51	.11	10.83	Dil, MS
47	$\overline{CIU}$	2.01	2.00	31.7	44.66	43.89	7.02	1030	1.00	94	.58	.65	.78	26.9	.46	.09	11.58	MS, Liq./Dil.
48	$\overline{CIU}$	5.00	5.00	32.0	44.66	43.53	9.85	1550	1.00	92	.67	64.7	1.03	25.2	.40	.13	11.20	MS, Liq
49	$\overline{CIU}$	.31	.30	33.6	44.66	44.37	9.84	252	1.00	100	1.00	3.70	.99	33.6	.60	.07	11.52	MS, Liq
50	$\overline{CIU}$	5.00	5.00	31.8	44.26	43.36	10.02	1640	1.00	100	.46	.40	2.06	30.5	.56	.17	11.04	DIL, MS
51	$\overline{CIU}$	.31	.30	32.6	44.66	44.49	10.38	275	1.00	95	.93	2.95	1.31	31.7	.57	.06	11.73	Liq, MS
65	$\overline{CAU}$	1.41	1.99	30.1	44.46	44.35	1.57	725	1.41	99	.45	.37	1.72	29.9	.62	.17	1.80	FS, Dil, S.C.
66	$\overline{CIU}$	1.99	2.00	31.0	44.97	44.68	1.39	1140	1.00	100	.42	.42	1.39	31.0	.63	.11	16.67	FS, Dil, S.C.
67	$\overline{CIU}$	1.99	2.00	34.1	45.47	45.13	5.58	1370	1.00	97	.62	.72	4.00	33.9	.48	.07	11.78	FS, Dil, S.C.
68	$\overline{CIU}$	5.00	5.00	30.4	45.97	45.48	3.84	1205	1.00	100	.47	.47	3.84	30.4	.58	.24	13.67	FS, Dil, S.C.
77	$\overline{CIU}$	2.00	2.00	21.7	47.49	46.62	.60	680	1.00	100	1.01	-1.11	.60	21.7	.24	.07	13.65	S.C., FS, Liq.
79	$\overline{CIU}$	2.00	2.00	31.1	46.48	45.85	5.17	390	1.00	100	.62	.94	2.98	30.5	.48	.25	10.98	S.C., Dil. FS
88	$\overline{CIU}$	2.00	2.00	19.8	44.60	44.13	.476	680	1.00	100	.45	—	.476	19.8	.28	.07	12.91	S.C., MS Liq.
92	$\overline{CIU}$	2.20	2.00	26.5	43.64	43.07	.65	1020	.90	100	.45	.58	.65	26.5	.44	.07	13.34	S.C., Liq. MS
93	$\overline{CIU}$	2.00	2.00	21.7	46.90	46.33	.55	750	1.00	100	.46	1.04	.55	21.7	.28	.07	14.09	FS, S.C., Liq.
94	$\overline{CIU}$	2.00	2.00	25.3	43.94	43.39	.77	870	1.00	99	.51	.71	.77	25.3	.37	.080	14.17	S.C., Liq. MS
100	$\overline{CIU}$	2.00	2.00	22.7	46.38	45.86	.50	705	1.00	99	.52	.90	.50	22.7	.30	.080	13.54	FS, S.C., Liq.
101	$\overline{CIU}$	2.00	2.00	26.2	46.15	45.64	5.76	680	1.00	100	.555	.84	.80	26.23	.35	.090	10.05	FS, Interm. S.C.
102	$\overline{CIU}$	2.00	2.00	30.9	43.61	43.08	5.86	750	1.00	100	.62	.81	1.33	28.7	.43	.11	9.66	Liq/Dil., S.C., MS
103	$\overline{CIU}$	2.00	2.00	20.9	46.71	46.18	.42	800	1.00	99	.445	.78	.42	20.9	.31	.07	11.55	Liq., FS, S.C.
104	$\overline{CIU}$	5.00	5.00	31.0	46.19	45.21	4.29	1320	1.00	99	.68	1.02	8.20	31.0	1.80	.13	8.45	FS, S.C., Liq./Dil.
105	$\overline{CIU}$	1.00	1.00	31.3	46.54	46.24	6.25	500	1.00	100	.58	.65	9.64	31.1	.47	.100	9.74	S.C., FS, Liq./Dil.
106	$\overline{CIU}$	1.00	1.00	30.9	43.94	43.59	3.61	235	1.00	99	.48	.46	9.95	30.1	.88	.75	9.95	S.C., MS, Dil.
110	$\overline{CIU}$	5.00	5.00	26.0	43.40	42.58	1.19	1880	1.00	101	.58	.86	.76	23.8	.34	.09	14.04	MS, Liq., S.C.
111	$\overline{CIU}$	1.00	1.00	30.8	43.65	43.43	5.13	3400	1.00	101	.66	.59	9.56	30.4	1.58	6.14	9.56	MS, Liq./Dil., S.C.

UNDRAINED STATIC TRIAXIAL TESTS ON LOOSE SAND

TABLE D.1

TABLE D.2

Test # LS	Test Type	$\bar{\sigma}_{vo}$ kg/cm^2	$\bar{\sigma}_{no}$ kg/cm^2	$\bar{\phi}$°	n_{setup} %	n_c %	ε_v At max $\bar{\sigma}_1/\bar{\sigma}_3$ %	$E^{50}_{sec_2}$ kg/cm^2	K_c –	B %	u_{max} kg/cm^2	A –	At max. q ε_v %	At max. q $\bar{\phi}$ °	Max. q kg/cm^2	ε_v At 1/2 Max. q %	ε_{vend} %	REMARKS
1	CID	3.24	3.06	33.1	41.37	40.92	6.54	1140	.94	–	–	–	4.45	32.9	3.64	.32	12.79	MS
12	CID	0.53	0.51	38.2	41.37	41.25	3.04	550	.96	94	–	–	3.04	38.1	.82	.15	7.96	MS
20	CAD	0.96	2.00	34.9	41.37	40.82	5.23	285	2.08	100	—	—	5.23	34.8	2.67	.67	10.24	MS
23	CID	0.62	0.65	42.6	37.31	37.15	.64	680	1.05	100	–	–	1.64	42.6	1.36	.20	1.64	MS
27	CID	1.00	1.00	38.3	41.37	40.95	1.37	1000	1.00	91	–	–	1.37	38.3	1.63	.18	9.04	MS, OCR=5(2xI)
28	$\overline{CAU}$	1.10	1.00	34.1	41.16	40.68	2.12	370	.91	95	.20	.15	2.05	34.1	2.05	.55	8.75	MS
29	CID	1.01	1.00	35.9	41.37	40.94	3.24	710	1.00	95	–	–	3.24	35.9	1.42	.20	10.0	MS
31	CAD	1.00	.50	37.3	41.22	40.87	1.67	350	.50	92	–	–	1.67	37.3	.52	.15	9.93	MS
32	CAD	1.00	.50	41.0	41.22	41.10	2.23	1450	.50	76	–	–	2.23	41.0	.96	.035	8.79	MS, OCR= 5(2xK$_c$)
33	$\overline{CAD}$pp	2.10	1.05	40.9	41.22	40.83	8.80	–	.50	90	–	–	–	–	–	–	9.01	MS, Incr. pp
34	CID-u	.99	1.00	39.7	41.43	41.12	12.51	3700	1.01	75	–	–	2.59	39.7	.37	.01	12.51	MS, unloading
35	CAD	.97	.50	37.7	41.22	41.12	1.74	850	.52	93	–	–	1.74	37.7	.79	.045	8.78	MS, OCR=5(2xI)
44	CID	2.01	2.00	31.0	44.26	43.39	5.58	500	1.00	98	–	–	3.7	31.0	1.90	.38	9.97	MS
58	CID	1.00	1.00	33.1	44.46	43.82	8.35	355	1.00	100	–	–	3.59	32.7	1.17	.33	11.37	FS
59	CID	1.02	1.00	43.3	38.00	37.85	2.97	1560	.99	100	–	–	2.97	43.3	2.18	.14	9.98	FS
60	CID	.90	1.00	37.8	41.23	40.87	1.74	1250	1.11	100	–	–	1.74.	37.8	1.58	.14	3.73	FS, OCR=10(20xI)
61	CAD	1.00	2.00	38.8	41.23	40.84	3.77	1070	2.00	100	–	–	3.94	38.8	3.86	.36	9.48	FS
62	CID	1.18	1.18	38.8	41.30	41.10	2.62	1300	1.00	100	–	–	2.62	38.8	1.98	.15	9.97	FS, OCR=10(1xI)
70	CID	1.00	1.02	36.6	41.43	41.05	2.92	1050	1.02	100	–	–	2.92	36.6	1.48	.14	10.19	FS
71	CAD	1.00	.50	38.2	41.33	41.13	1.80	430	.50	98	–	–	1.80	38.2	.56	.13	10.35	FS
72	CID	3.00	3.00	34.9	41.73	41.41	3.53	1340	1.00	99	–	–	3.53	34.9	4.01	.30	10.20	FS
73	CID	.52	.52	39.5	41.33	41.16	2.52	730	1.00	98	–	–	2.52	39.5	.87	.12	10.14	FS
74	$\overline{CIU}$	1.00	1.02	35.0	41.43	41.35	1.50	550	1.02	99	.27	.18	1.27	34.6	1.98	.36	3.45	FS
75	CID	1.00	1.00	43.1	37.39	37.24	1.71	1660	1.00	98	–	–	1.71	43.1	2.16	.13	10.25	FS
76	CID	1.00	1.00	36.9	41.63	41.25	2.72	1235	1.00	100	–	–	2.72	36.9	1.50	.12	10.17	FS, OCR=5(1xI)
78	$\overline{CAD}$pp	2.86	1.51	38.4	41.53	41.18	2.01	–	.53	98	–	–	–	–	–	–	14.93	FS, Incr. p.p.
86	CID	1.00	1.00	37.0	41.45	41.14	2.52	1260	1.00	99	–	–	2.52	37.0	1.51	.12	10.22	FS, OCR=5(1xI)
87	CID	1.00	1.00	37.5	41.73	41.19	2.70	870	1.00	99	–	–	2.70	37.5	1.56	.18	10.33	FS, OCR=10(1xI)
89	$\overline{CAD}$pp	2.50	1.50	39.1	41.55	41.31	1.74	–	.60	100	–	–	–	–	–	–	13.97	FS, p.p. Incr.
90	$\overline{CAU}$	2.50	1.50	39.2	41.53	41.08	.25	920	.60	99	.06	–	10.8	33.4	17.69	2.08	15.43	FS, LC134 undr.
99I	$\overline{CAU}$	2.50	1.50	35.9	41.67	41.38	1.26	850	.60	99	.25	.15	1.42	35.8	3.19	.259	1.43	FS, load control
99II	$\overline{CAU}$	2.50	1.50	37.3	41.67	41.38	.30	–	.60	99	2.76	–	5.45	35.1	5.76	3.91	5.45	After cycling
107	$\overline{CIU}$	1.00	1.00	33.6	41.08	40.80	1.52	240	1.00	100	-.70	.22	3.42	33.0	2.36	.99	14.61	Unload. MS

Static Triaxial Tests

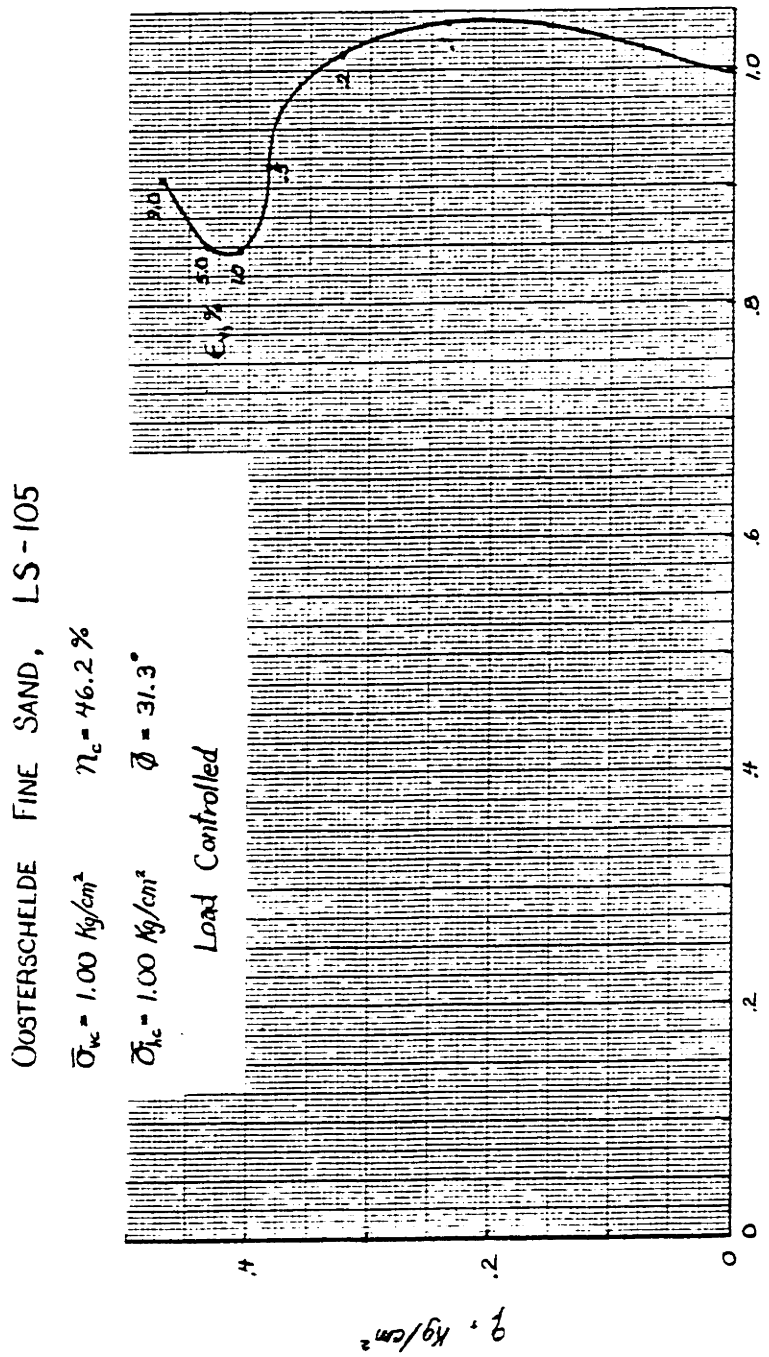

EFFECTIVE STRESS PATH OF LOOSE, FINE SAND SAMPLES TESTED UNDER STRESS CONTROL AT 1 kg/cm² CONFINING STRESS

FIGURE D-1

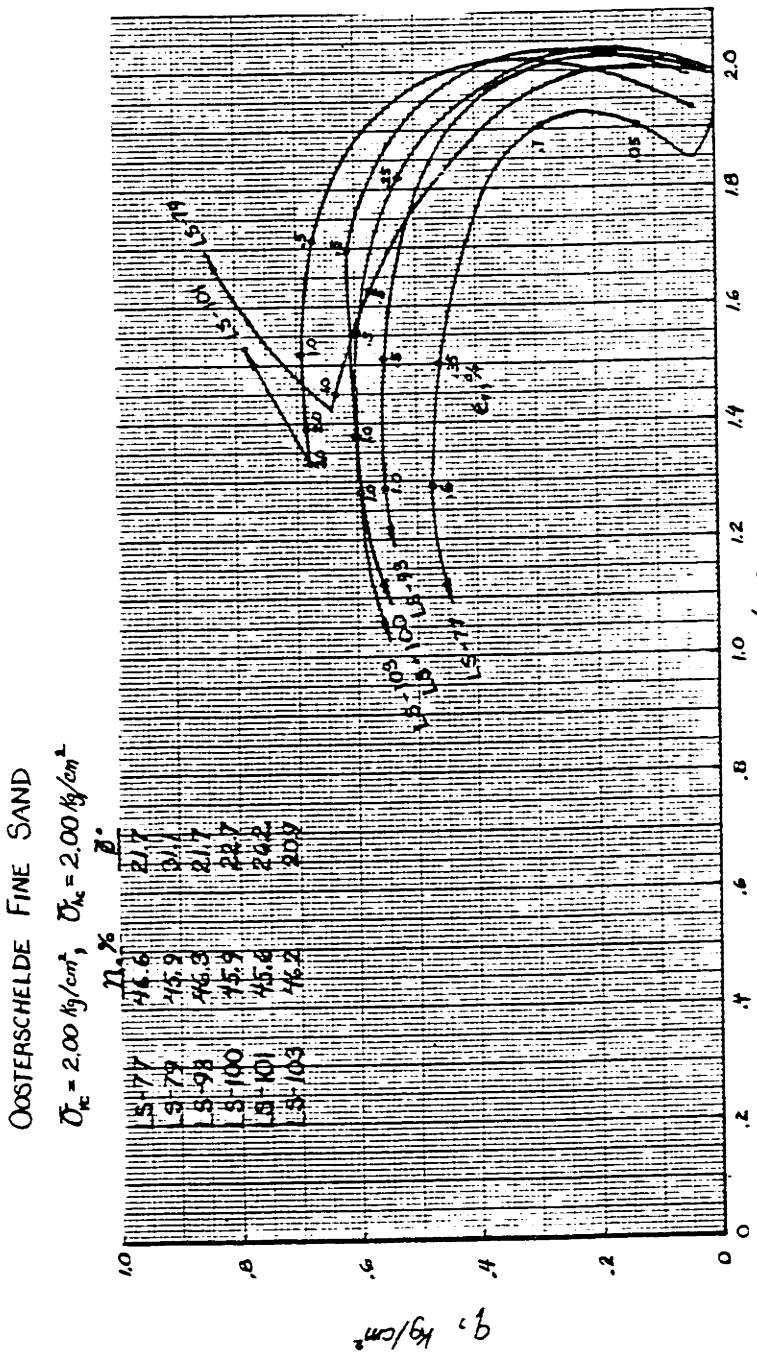

EFFECTIVE STRESS PATHS OF LOOSE, FINE SAND SAMPLES TESTED UNDER STRESS CONTROL AT 2 Kg/cm² CONFINING STRESS

FIGURE D-2

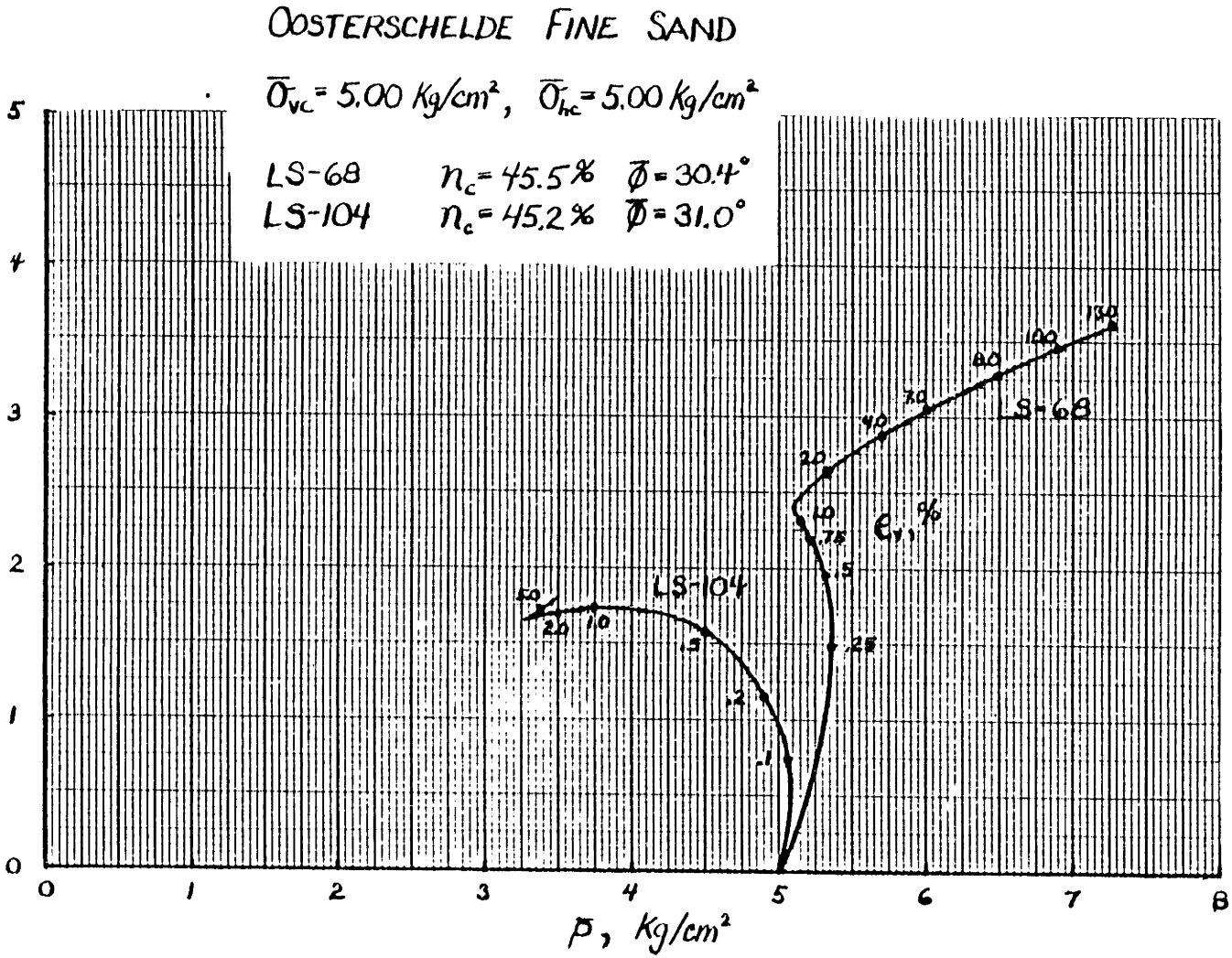

FIGURE C-3

EFFECTIVE STRESS PATHS OF LOOSE, FINE SAND SAMPLES TESTED UNDER STRESS CONTROL AT 5 Kg/cm² CONFINING STRESS

OOSTERSCHELDE MEDIUM SAND

$\bar{\sigma}_{vc}$ = 1.00 Kg/cm², $\bar{\sigma}_{hc}$ = 1.00 Kg/cm²

LS-106 n_c = 43.6% $\bar{\phi}$ = 30.9°

LS-111 n_c = 43.4% $\bar{\phi}$ = 30.8°

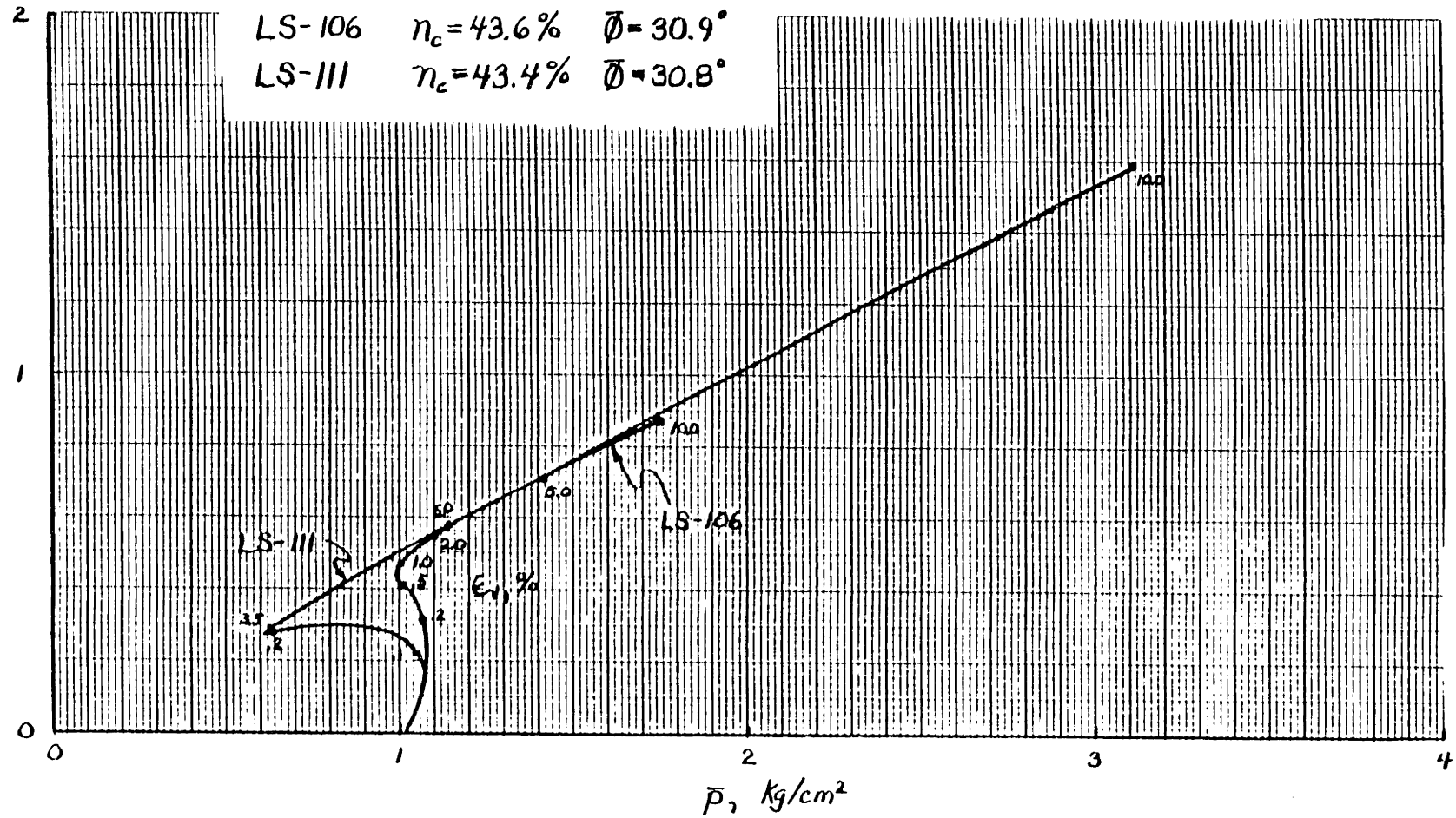

EFFECTIVE STRESS PATHS OF LOOSE, MEDIUM SAND SAMPLES TESTED UNDER STRESS CONTROL AT 1 Kg/cm² CONFINING STRESS

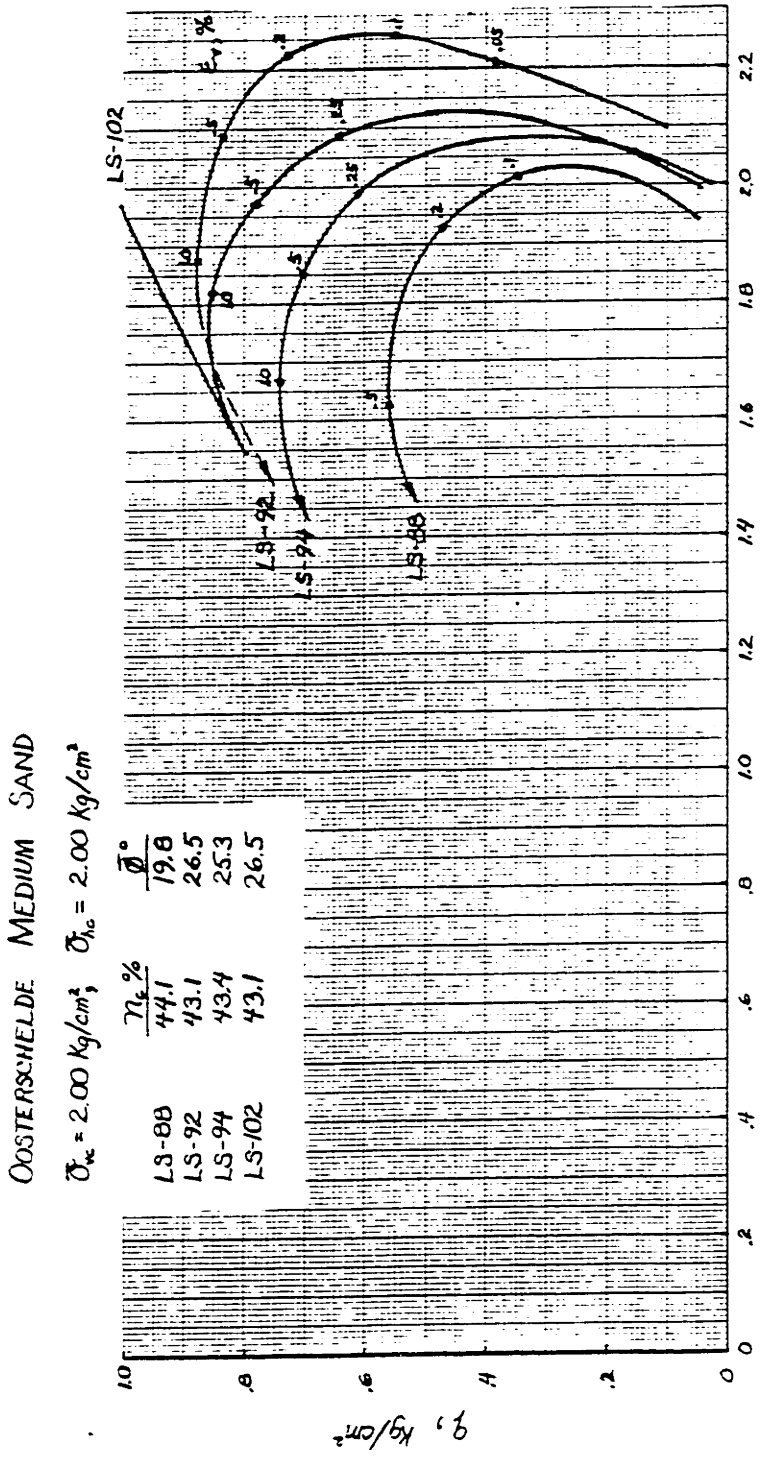

EFFECTIVE STRESS PATHS OF LOOSE, MEDIUM SAND SAMPLES TESTED UNDER STRESS CONTROL AT 2 kg/cm² CONFINING STRESS

FIGURE D-5

OOSTERSCHELDE MEDIUM SAND

$\bar{\sigma}_{vc}$ = 5.00 Kg/cm², $\bar{\sigma}_{hc}$ = 5.00 Kg/cm²

n_c = 42.6 % $\bar{\phi}$ = 26.0°

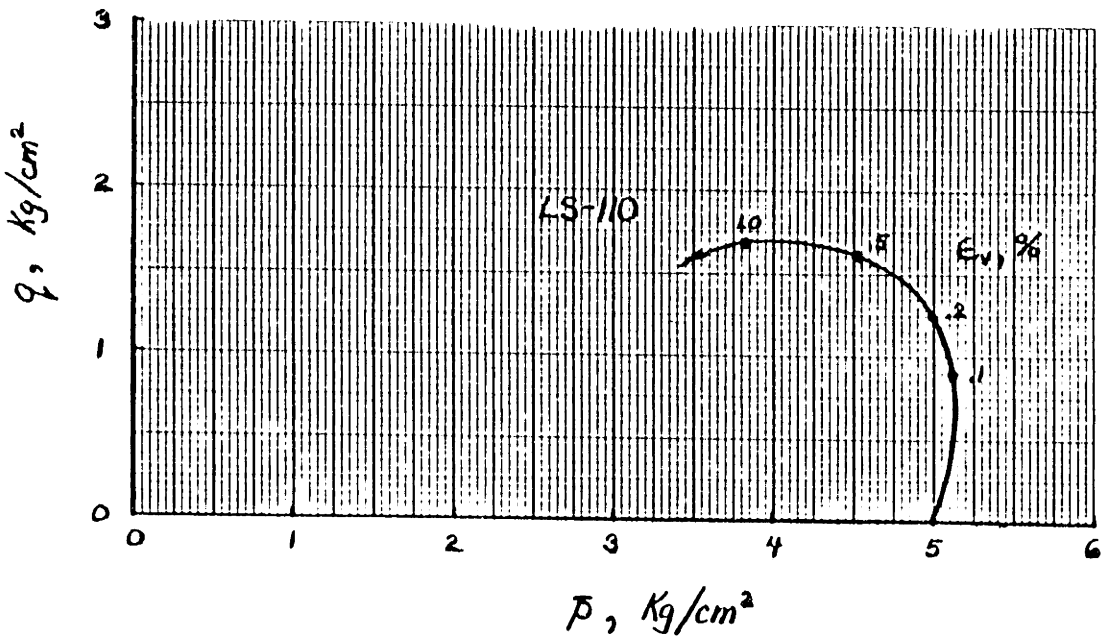

EFFECTIVE STRESS PATH OF LOOSE, FINE SAND SAMPLE TESTED UNDER STRESS CONTROL AT 5 Kg/cm² CONFINING STRESS

FIGURE 9-D

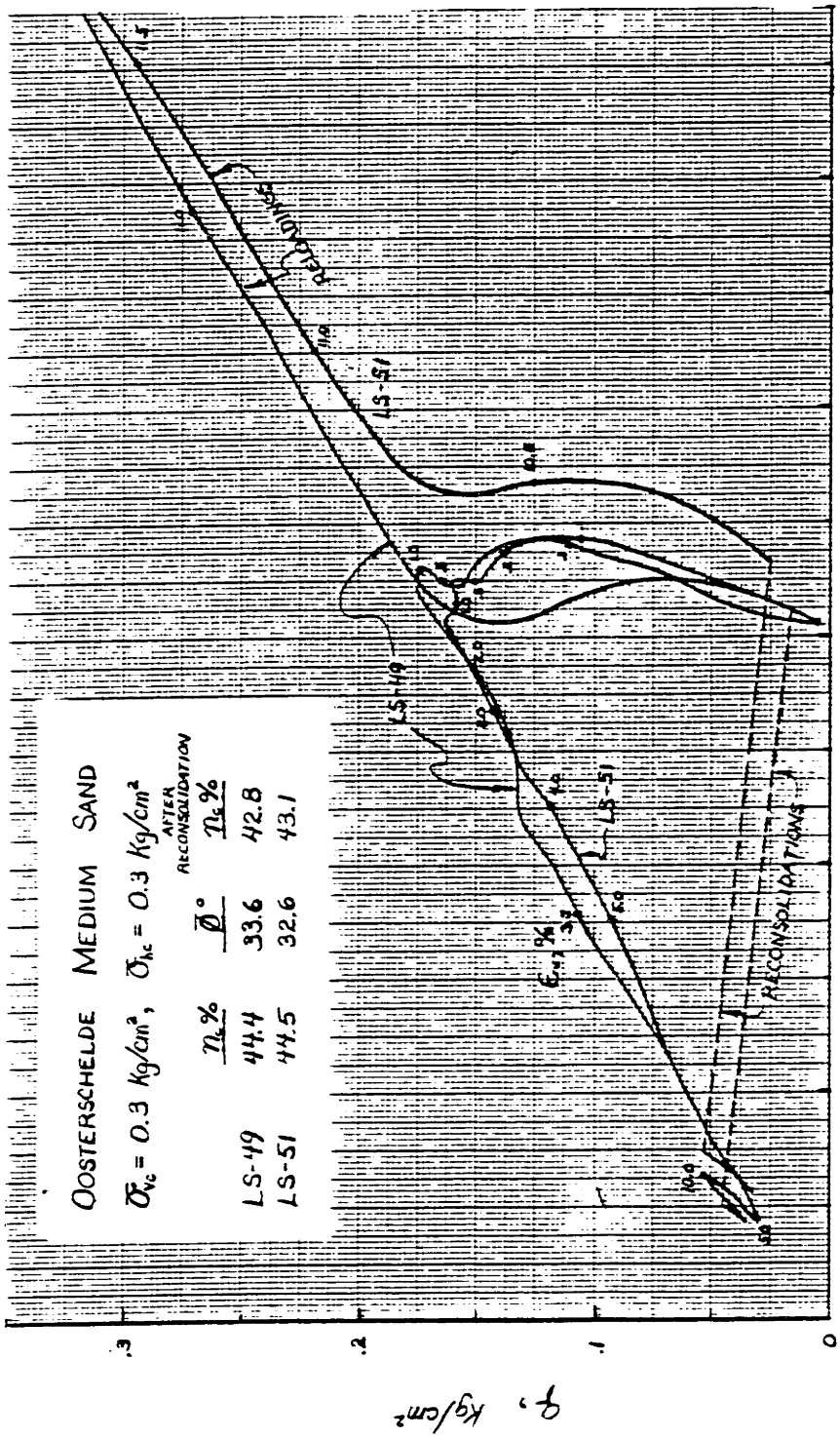

EFFECTIVE STRESS PATHS FOR LOOSE, MEDIUM SAND SAMPLES TESTED UNDER STRAIN CONTROL AT 0.3 kg/cm² CONFINING STRESS

FIGURE D-7

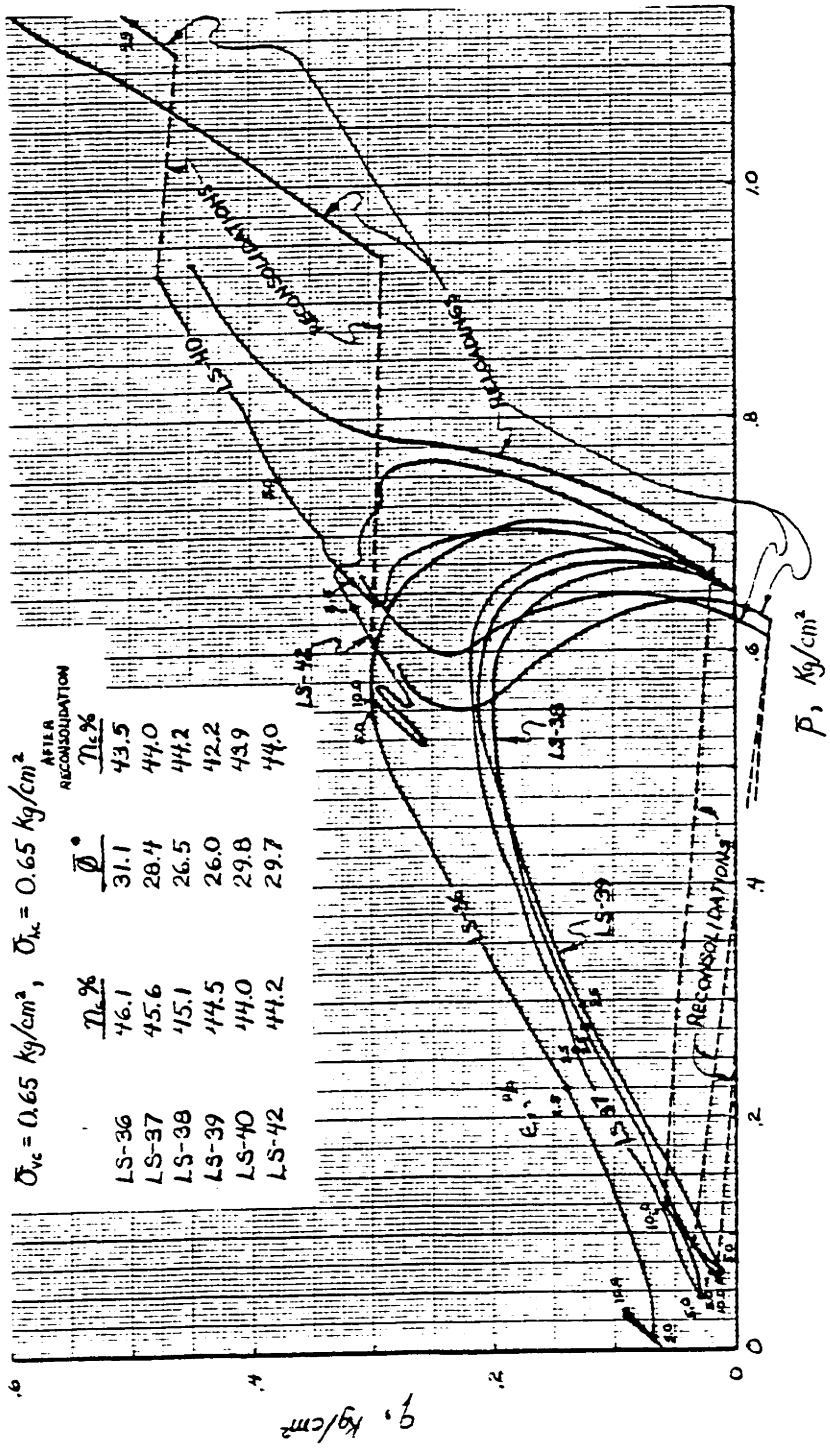

EFFECTIVE STRESS PATHS FOR LOOSE, MEDIUM SAND SAMPLES TESTED UNDER STRAIN CONTROL AT 0.65 kg/cm² CONFINING STRESS

FIGURE D-8

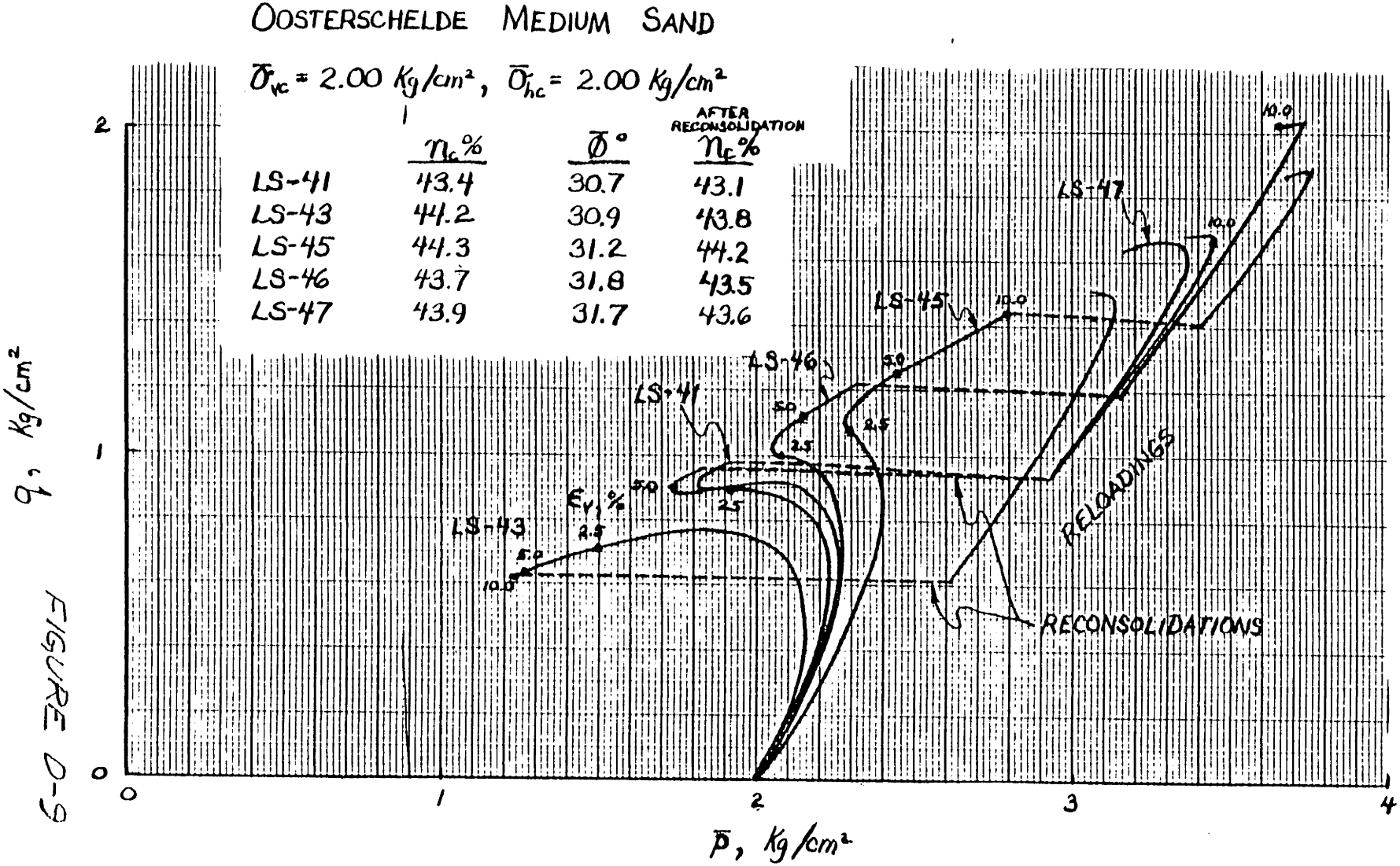

FIGURE 0-5

EFFECTIVE STRESS PATHS FOR LOOSE, MEDIUM SAND SAMPLES TESTED UNDER STRAIN CONTROL AT 2 Kg/cm² CONFINING STRESS

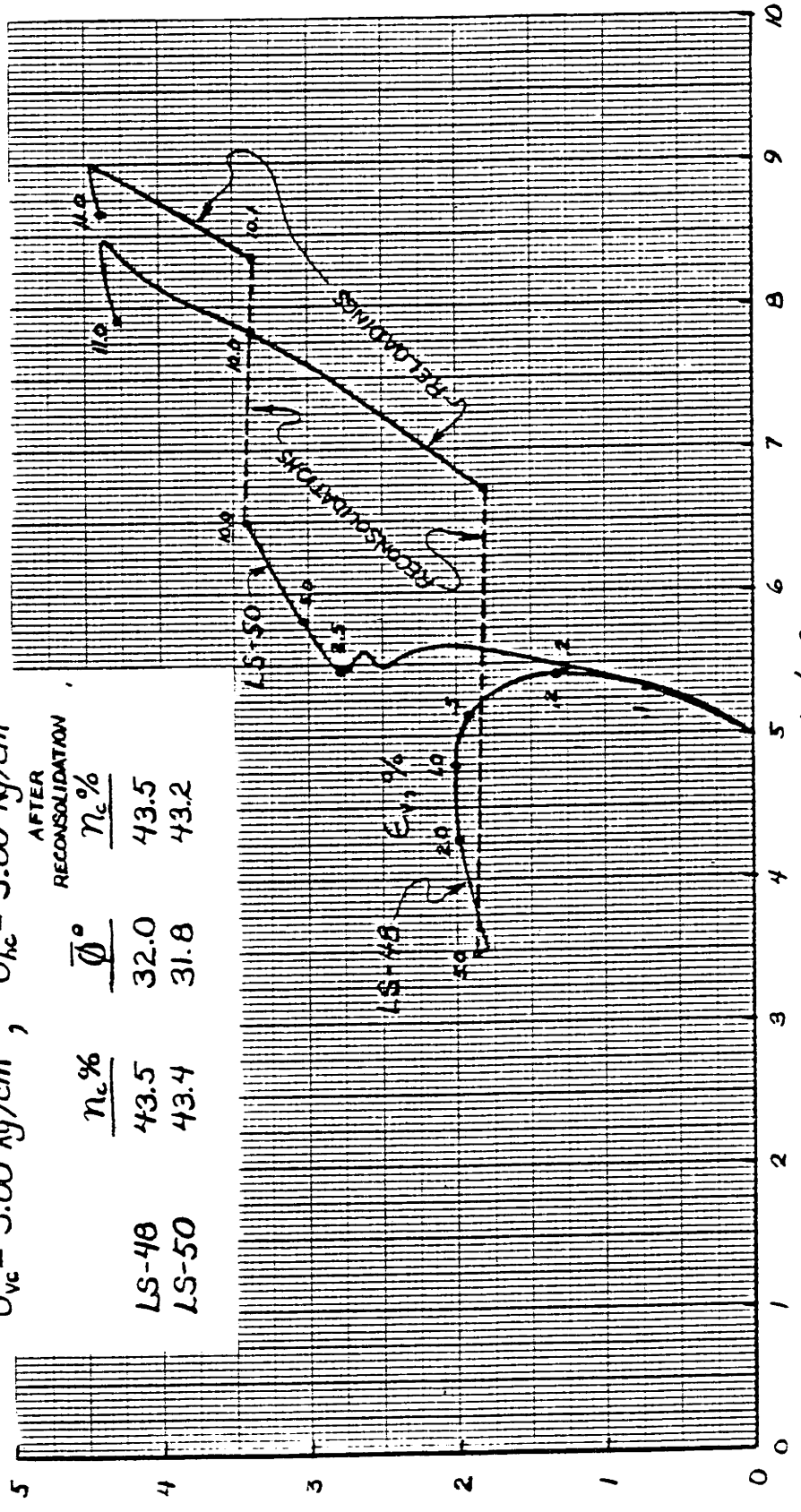

FIGURE D-10

EFFECTIVE STRESS PATHS FOR LOOSE, MEDIUM SAND SAMPLES TESTED UNDER STRAIN CONTROL AT 5 kg/cm² CONFINING STRESS

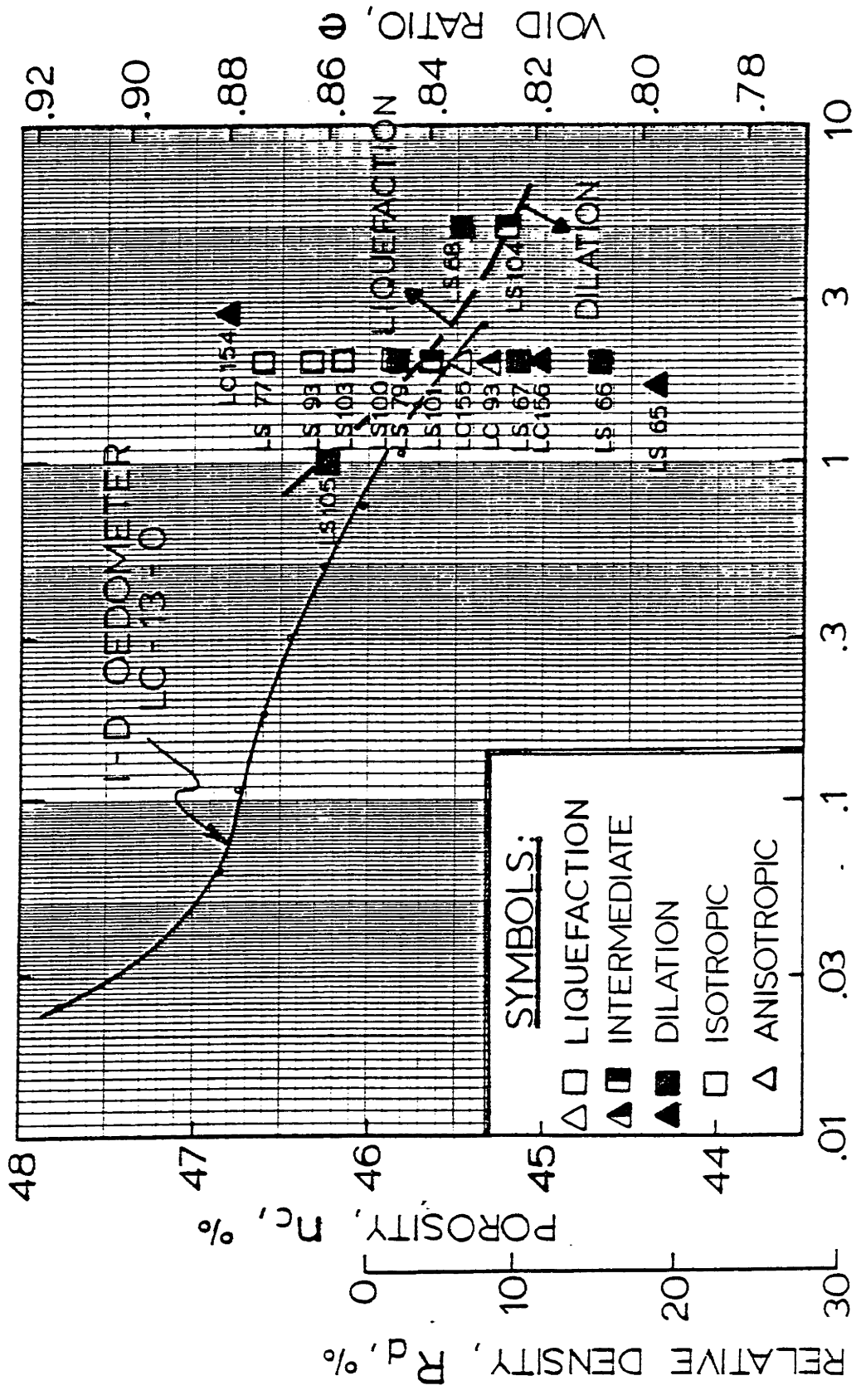

SUMMARY OF TESTS ON LOOSE, FINE SAND

FIGURE D-11

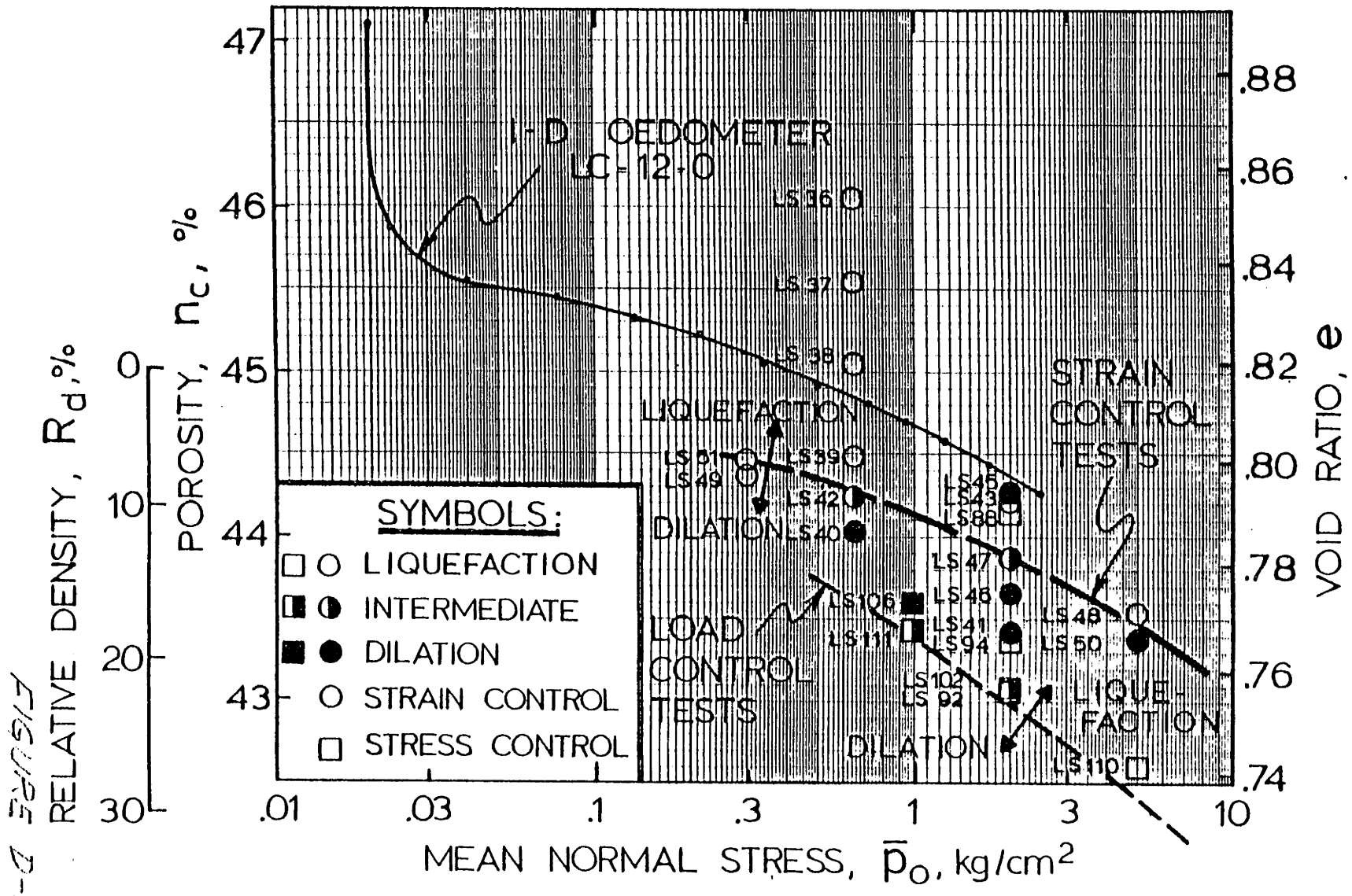

SUMMARY OF TESTS ON LOOSE, MEDIUM SAND

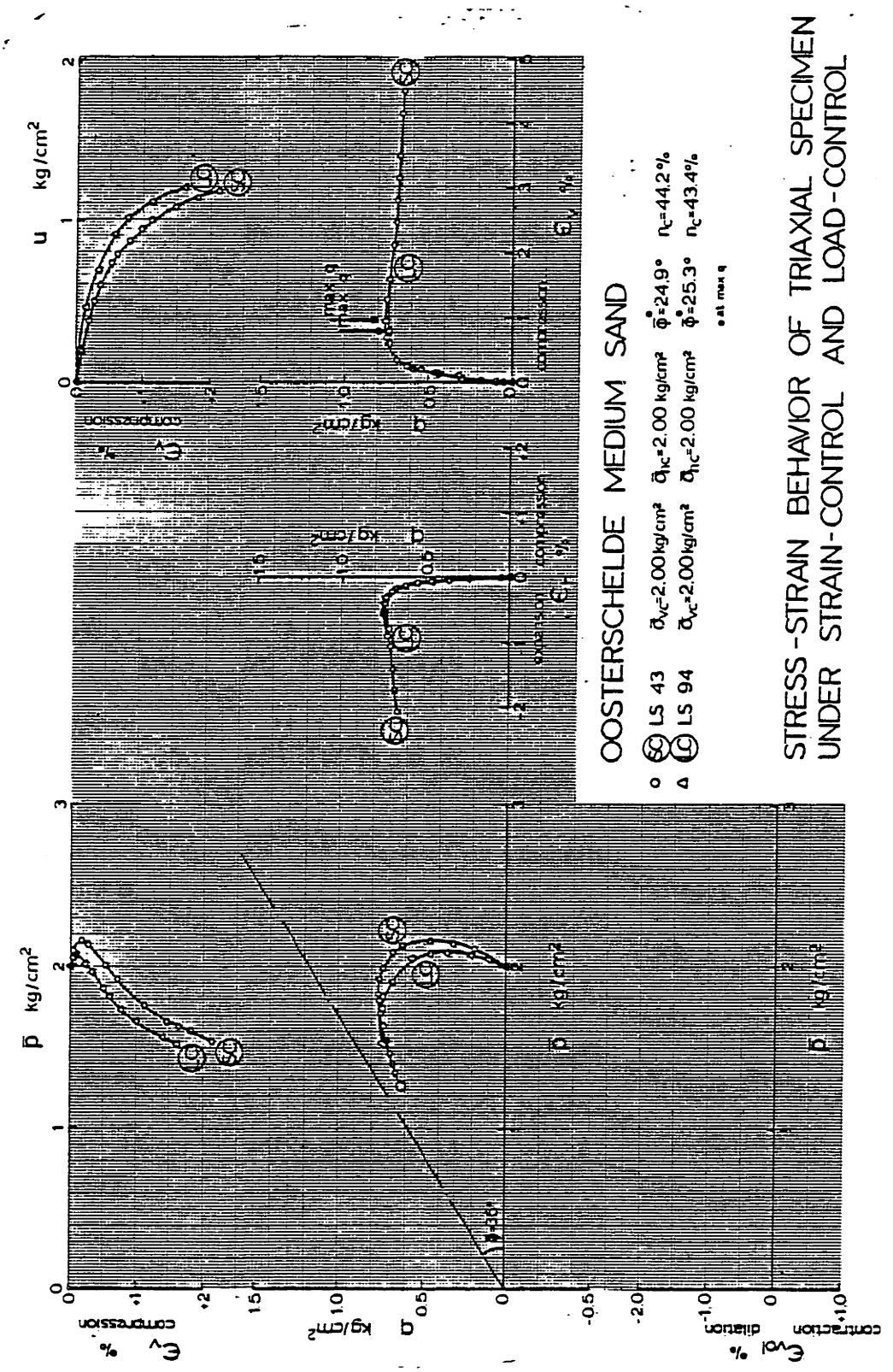
OOSTERSCHELDE MEDIUM SAND
LS 43
LS 94
STRESS-STRAIN BEHAVIOR OF TRIAXIAL SPECIMEN
UNDER STRAIN-CONTROL AND LOAD-CONTROL

FIGURE D-13

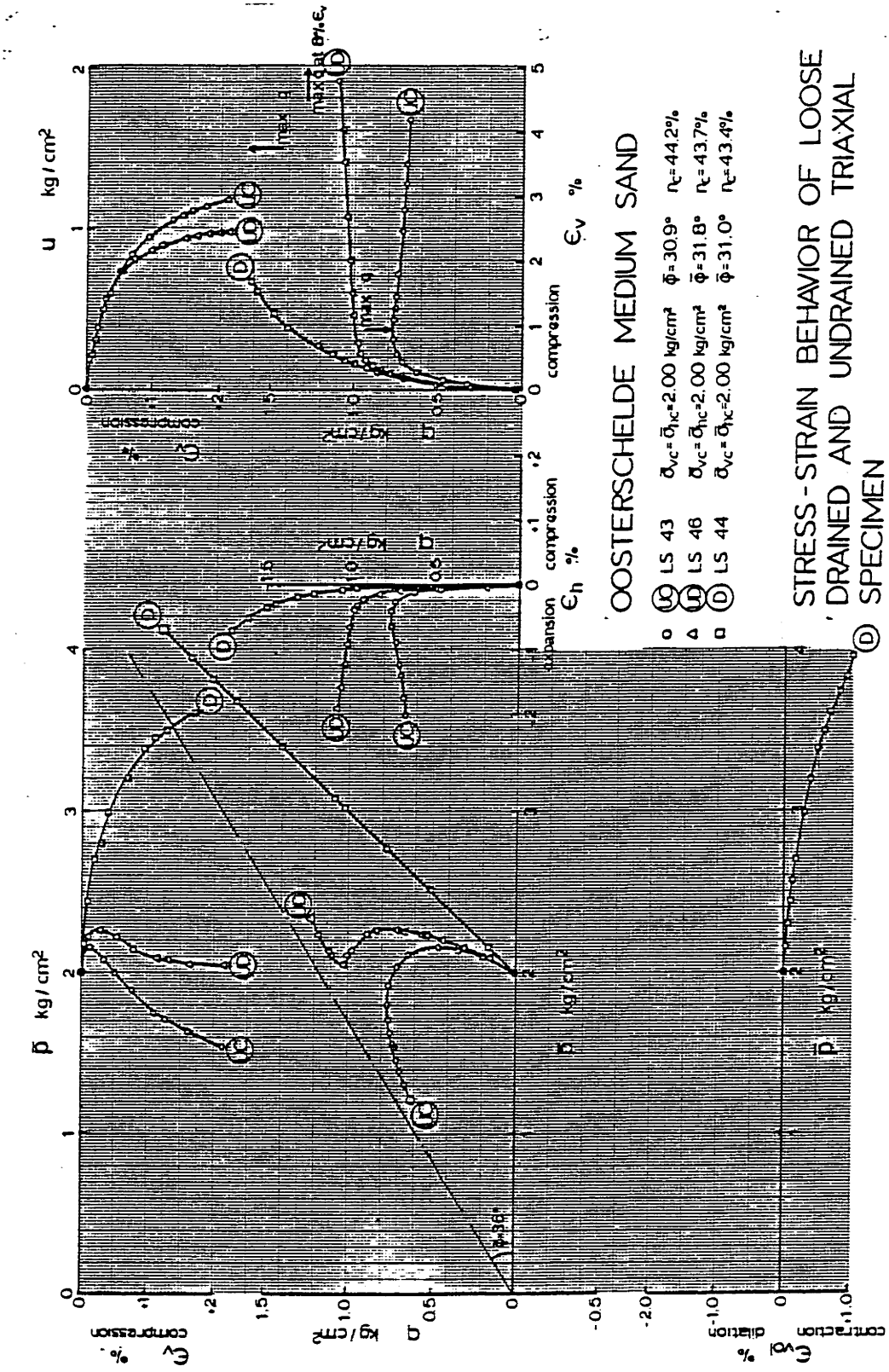
STRESS - STRAIN BEHAVIOR OF LOOSE
DRAINED AND UNDRAINED TRIAXIAL
SPECIMEN
OOSTERSCHELDE MEDIUM SAND
LS 43 $\bar{\sigma}_{1c}=\bar{\sigma}_{3c}=2.00$ kg/cm² $\bar{\phi}=30.9°$ $n_c=44.2\%$
LS 46 $\bar{\sigma}_{1c}=\bar{\sigma}_{3c}=2.00$ kg/cm² $\bar{\phi}=31.8°$ $n_c=43.7\%$
LS 44 $\bar{\sigma}_{1c}=\bar{\sigma}_{3c}=2.00$ kg/cm² $\bar{\phi}=31.0°$ $n_c=43.4\%$
$\bar{p}$ kg/cm²
ε_v %
compression
dilation
contraction
ε_h %
expansion
q kg/cm²
u kg/cm²
ε_1 %
ε_3 %
ε_{vol} %
$\bar{\phi}=36°$
max q
max ε_1

FIGURE D-14

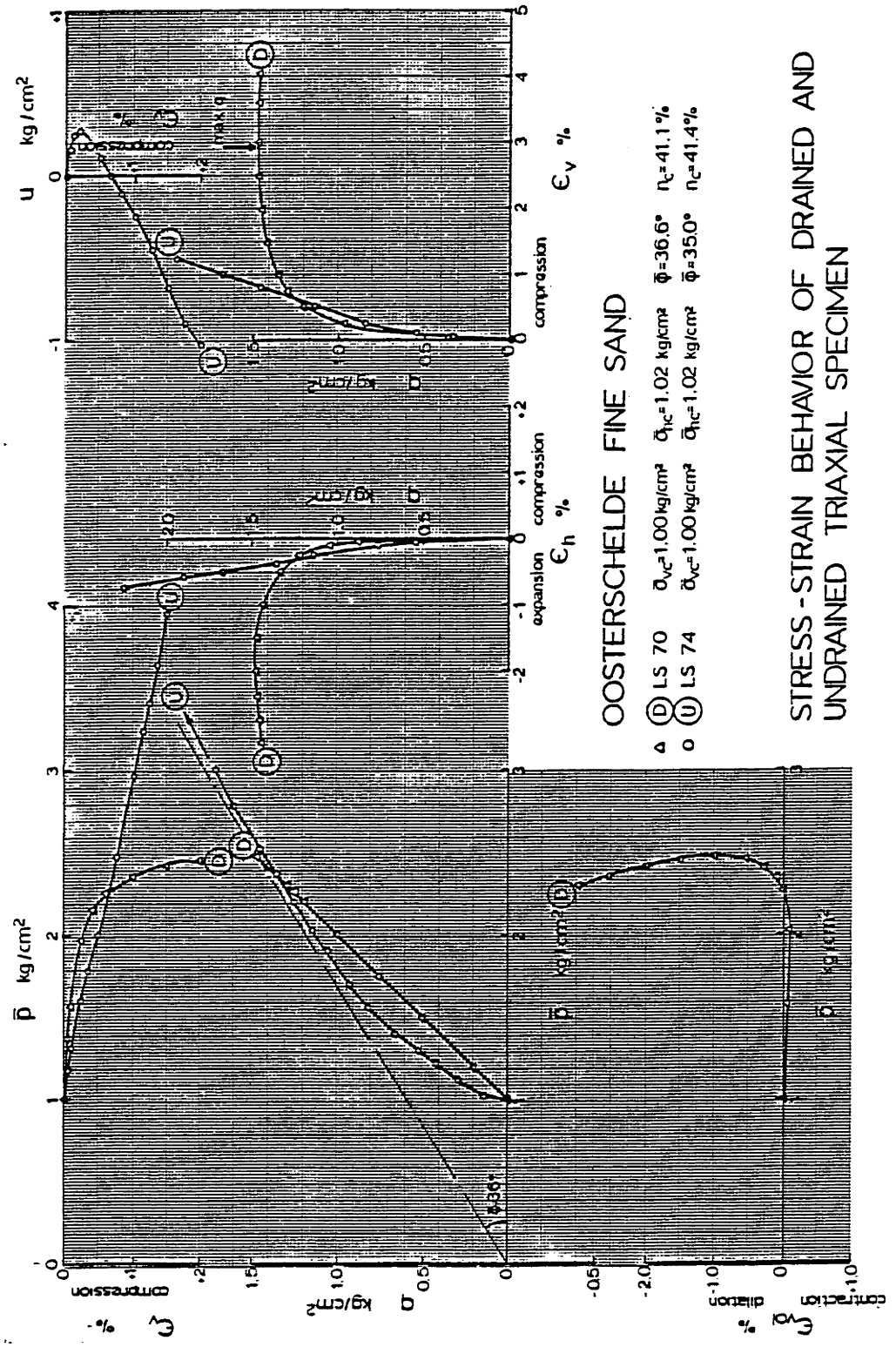
STRESS-STRAIN BEHAVIOR OF DRAINED AND UNDRAINED TRIAXIAL SPECIMEN
OOSTERSCHELDE FINE SAND
LS 70 σ̄vc=1.00 kg/cm² σ̄hc=1.02 kg/cm² φ=36.6° nc=41.1%
LS 74 σ̄vc=1.00 kg/cm² σ̄hc=1.02 kg/cm² φ=35.0° nc=41.4%
p̄ kg/cm²
u kg/cm²
q kg/cm²
εv %
εh %
εq %
compression
expansion
dilation
contraction
φ=36°

FIGURE D-15

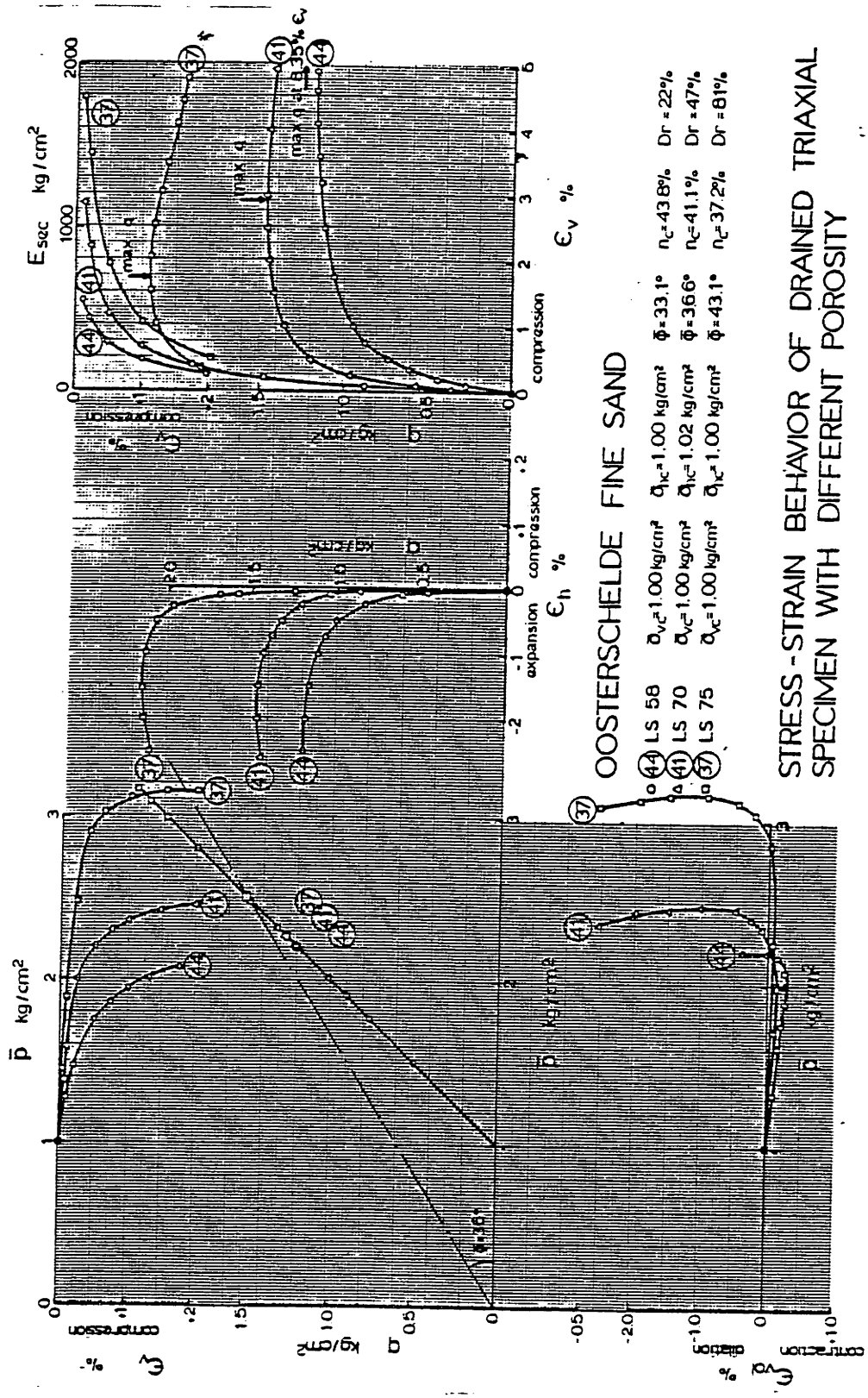
STRESS-STRAIN BEHAVIOR OF DRAINED TRIAXIAL SPECIMEN WITH DIFFERENT POROSITY
OOSTERSCHELDE FINE SAND
(44) LS 58 σ3c=1.00 kg/cm² ηc=43.8% Φ=33.1° Dr=22%
(41) LS 70 σ3c=1.02 kg/cm² ηc=41.1% Φ=36.6° Dr=47%
(37) LS 75 σ3c=1.00 kg/cm² ηc=37.2% Φ=43.1° Dr=81%
E sec kg/cm²
max q
max ε1
ε1 %
εv %
compression
expansion
p̄ kg/cm²
q kg/cm²
ω1 %
ωv %
compression
dilation

FIGURE D-16

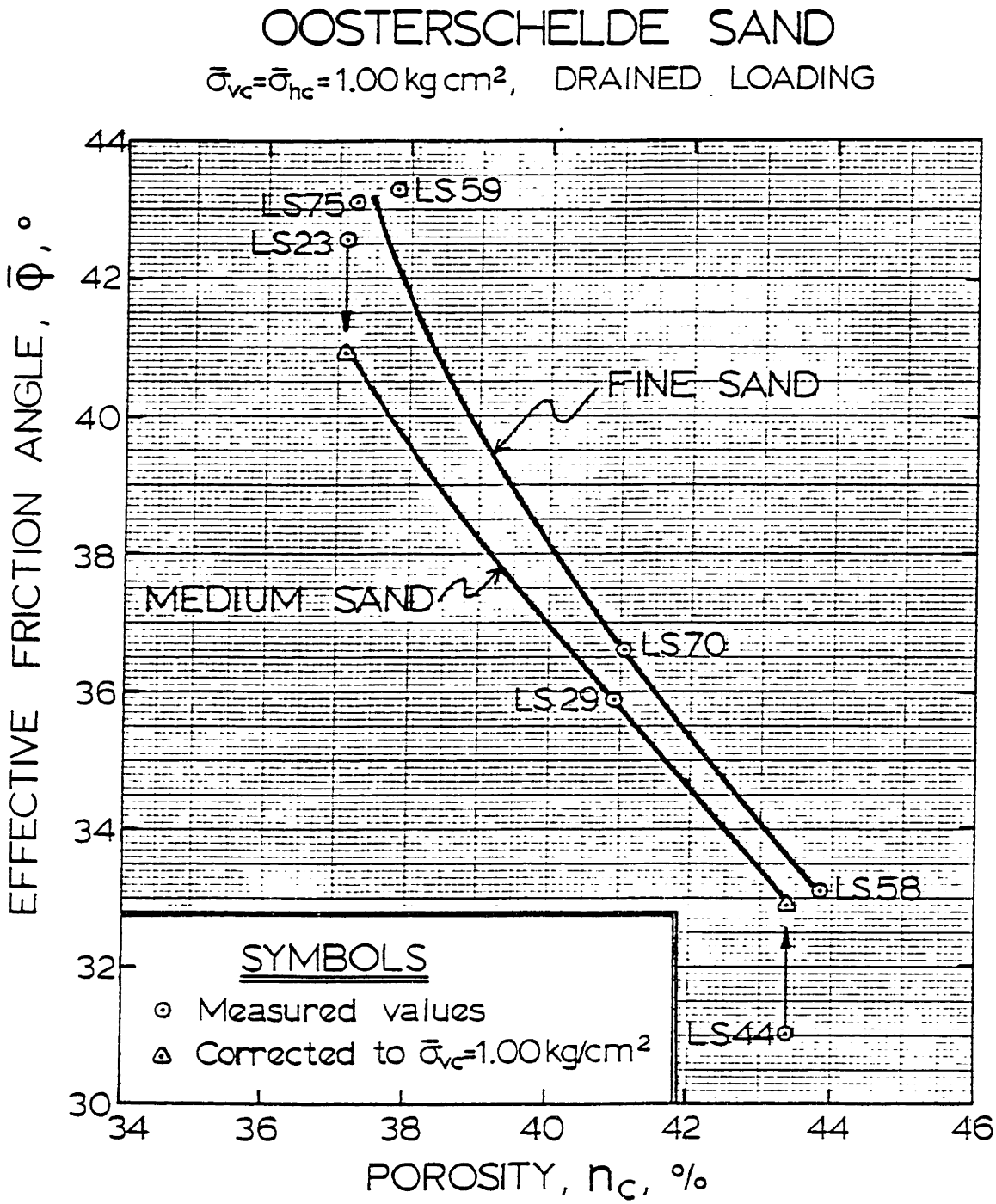

MOBILIZED FRICTION ANGLES AT MAXIMUM OBLIQUITY FOR DIFFERENT SAMPLE POROSITIES

FIGURE D-17

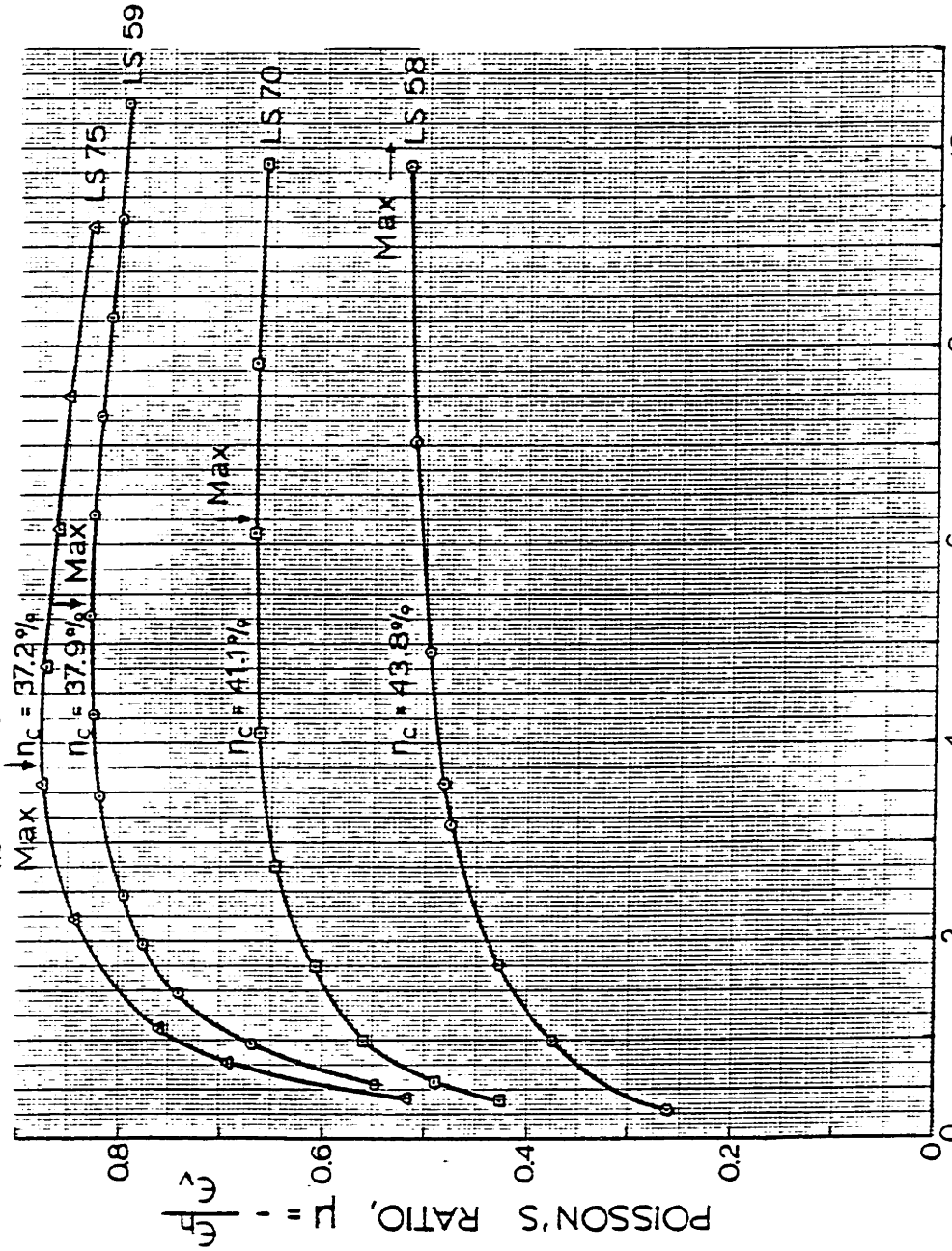

VARIATION IN POISSON'S RATIO WITH DENSITY AND STRAIN LEVEL

FIGURE D-18

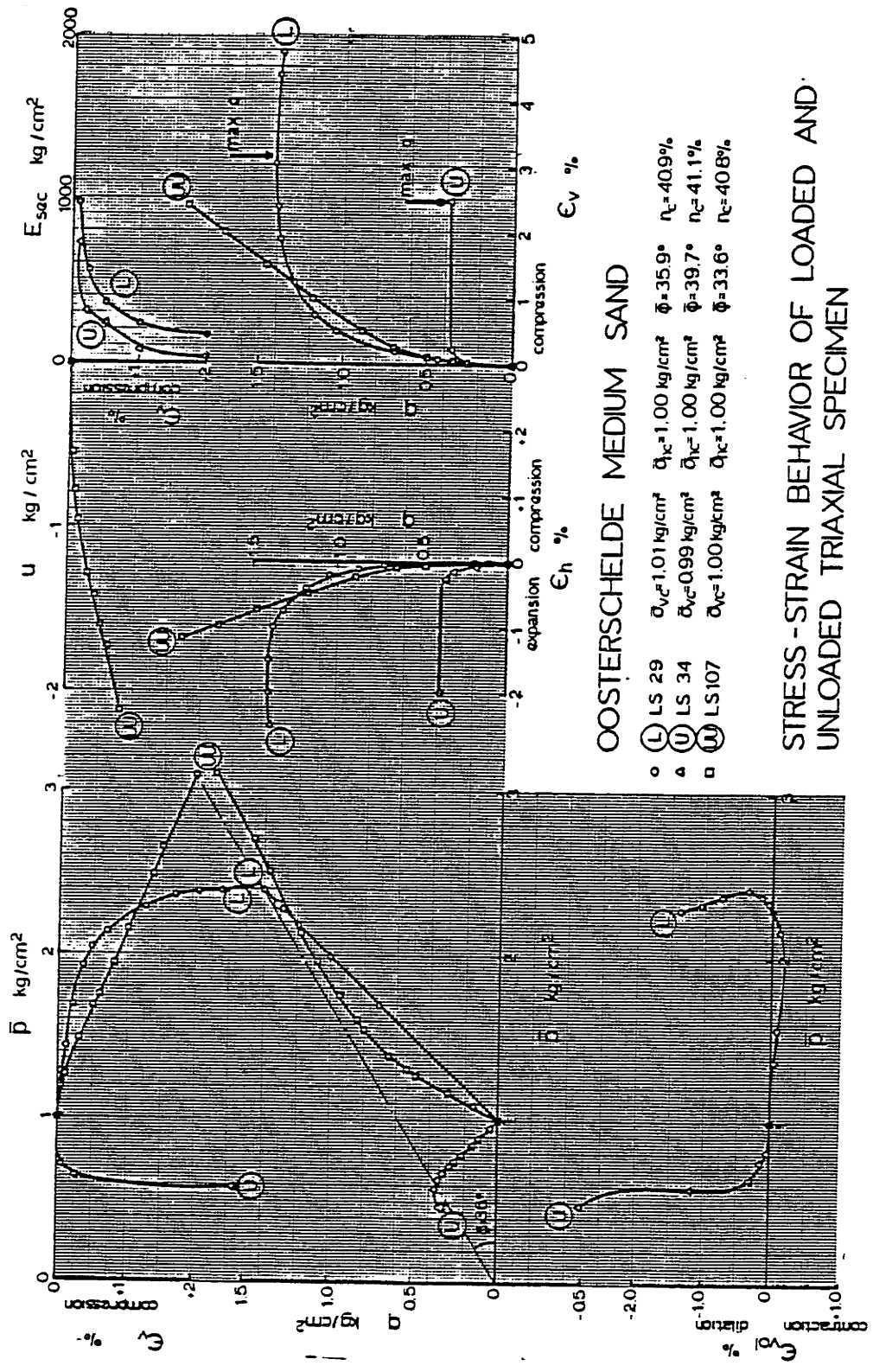
OOSTERSCHELDE MEDIUM SAND
L LS 29 σ'vc=1.01 kg/cm² σ'hc=1.00 kg/cm² φ=35.9° nc=40.9%
U LS 34 σ'vc=0.99 kg/cm² σ'hc=1.00 kg/cm² φ=39.7° nc=41.1%
U LS107 σ'vc=1.00 kg/cm² σ'hc=1.00 kg/cm² φ=33.6° nc=40.8%
STRESS-STRAIN BEHAVIOR OF LOADED AND UNLOADED TRIAXIAL SPECIMEN

FIGURE D-19

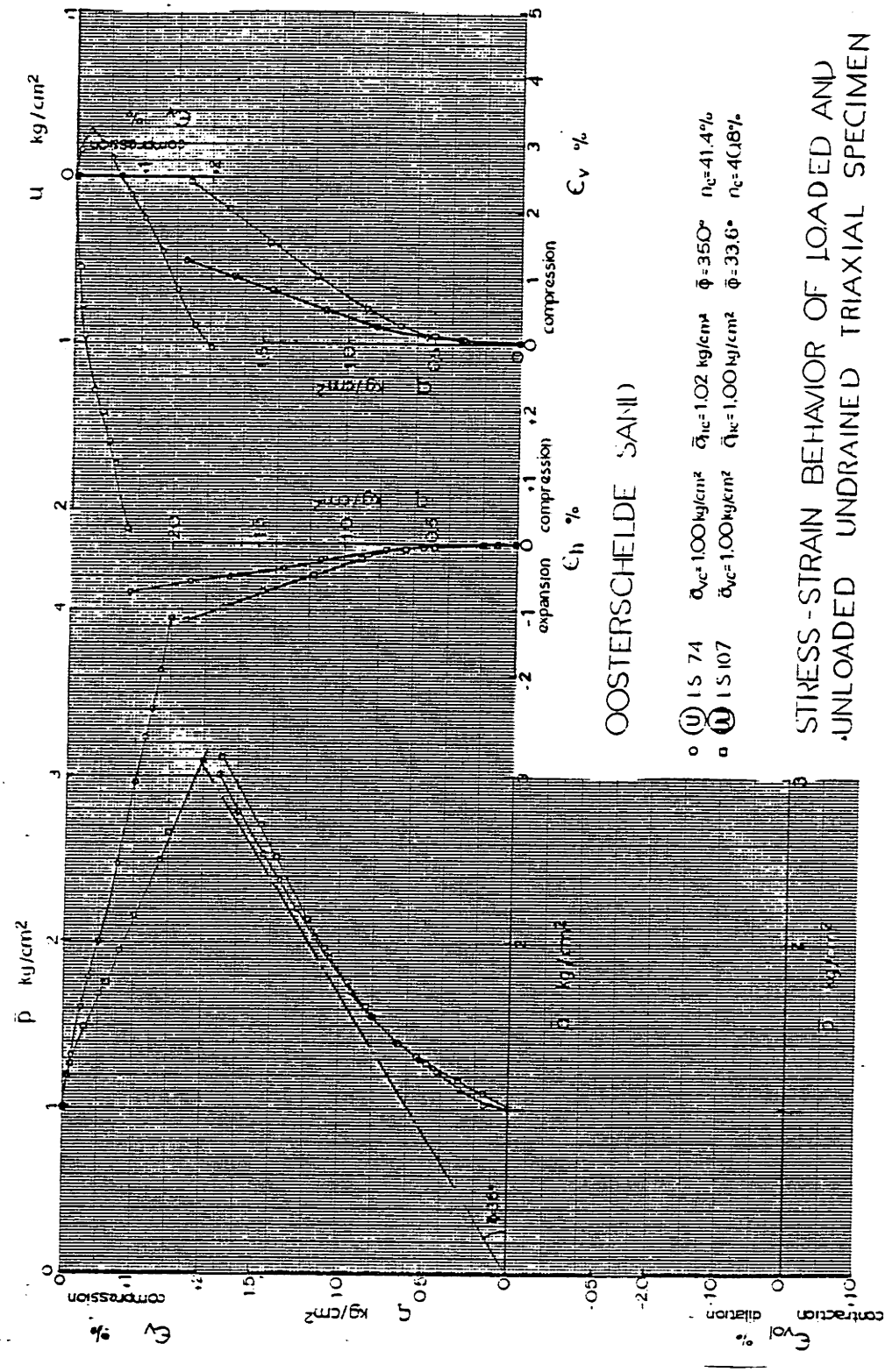
OOSTERSCHELDE SAND
STRESS-STRAIN BEHAVIOR OF LOADED AND UNLOADED UNDRAINED TRIAXIAL SPECIMEN
compression
expansion
compression
dilation
contraction

FIGURE D-20

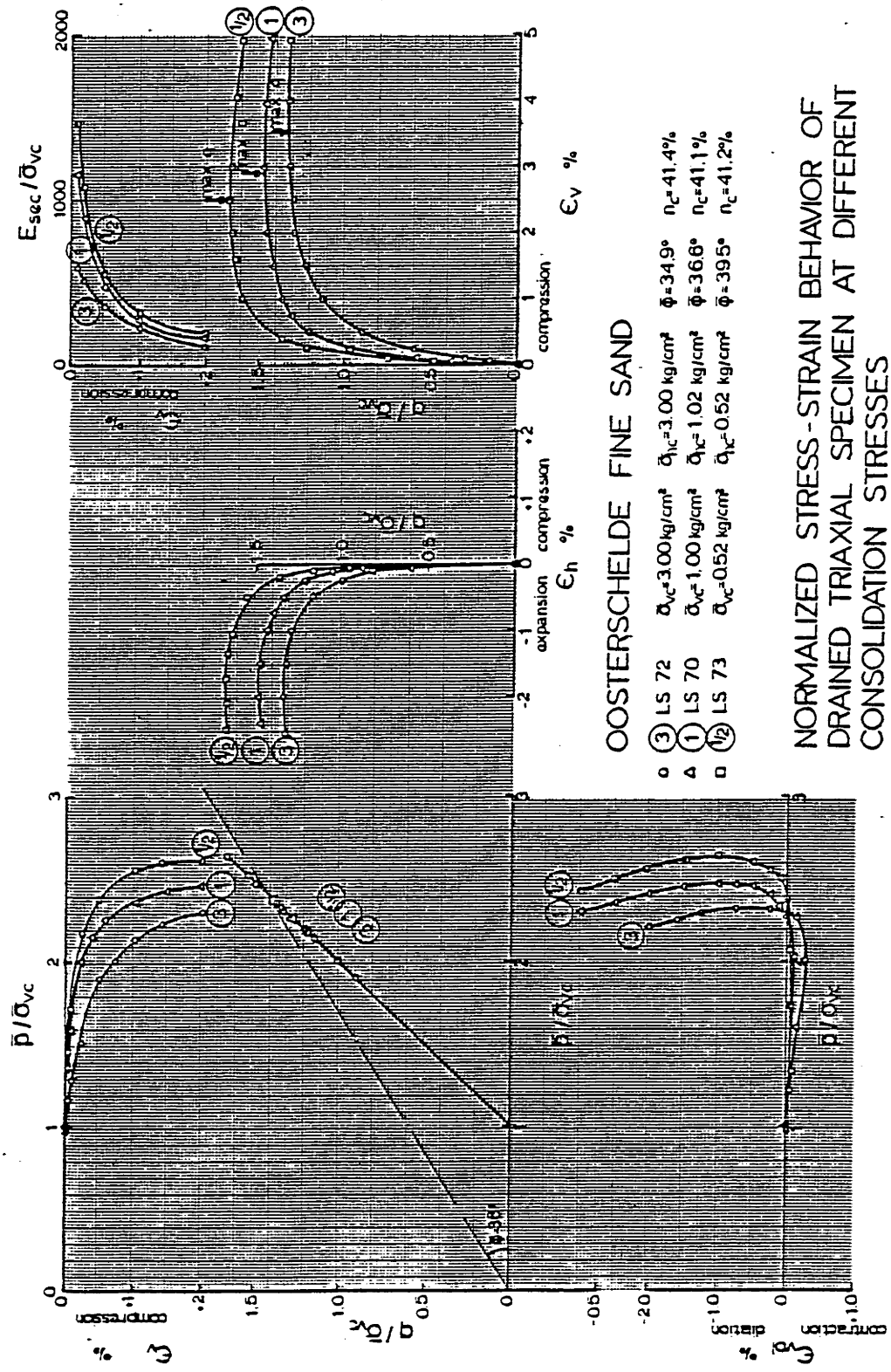
OOSTERSCHELDE FINE SAND
③ LS 72 σ̄vc=3.00 kg/cm² φ̄=34.9° nc=41.4%
① LS 70 σ̄vc=1.00 kg/cm² φ̄=36.6° nc=41.1%
½ LS 73 σ̄vc=0.52 kg/cm² φ̄=39.5° nc=41.2%
NORMALIZED STRESS-STRAIN BEHAVIOR OF DRAINED TRIAXIAL SPECIMEN AT DIFFERENT CONSOLIDATION STRESSES
Esec/σ̄vc
q/σ̄vc
p̄/σ̄vc
εv %
εh %
compression
expansion
compaction
dilation

FIGURE D-21

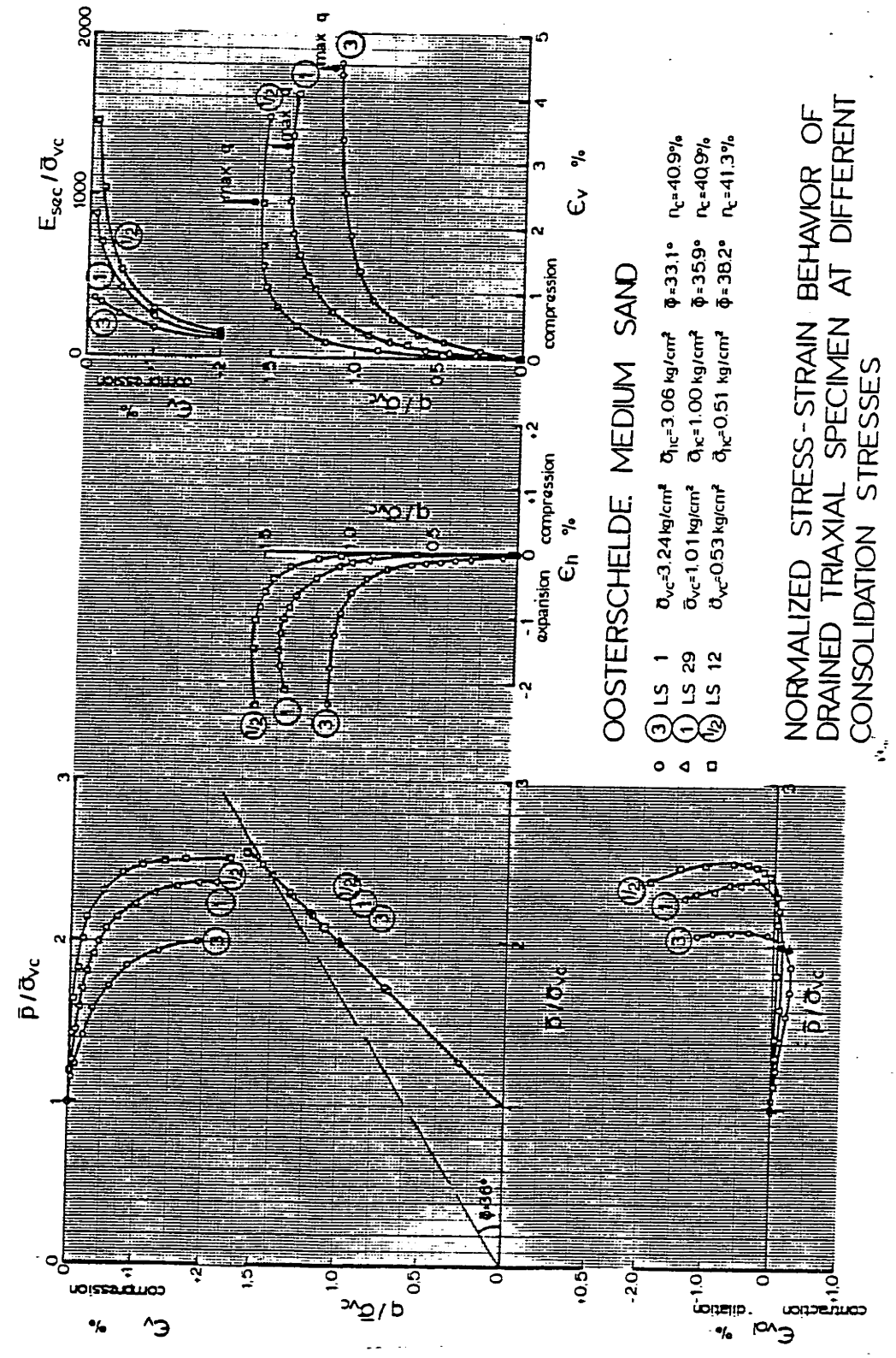
OOSTERSCHELDE MEDIUM SAND
③ LS 1 σ̄vc=3.24 kg/cm² σ̄hc=3.06 kg/cm² φ=33.1° nc=40.9%
① LS 29 σ̄vc=1.01 kg/cm² σ̄hc=1.00 kg/cm² φ=35.9° nc=40.9%
½ LS 12 σ̄vc=0.53 kg/cm² σ̄hc=0.51 kg/cm² φ=38.2° nc=41.3%
NORMALIZED STRESS-STRAIN BEHAVIOR OF DRAINED TRIAXIAL SPECIMEN AT DIFFERENT CONSOLIDATION STRESSES
compression
expansion
contraction
dilation
max q
φ=36°

FIGURE D-22

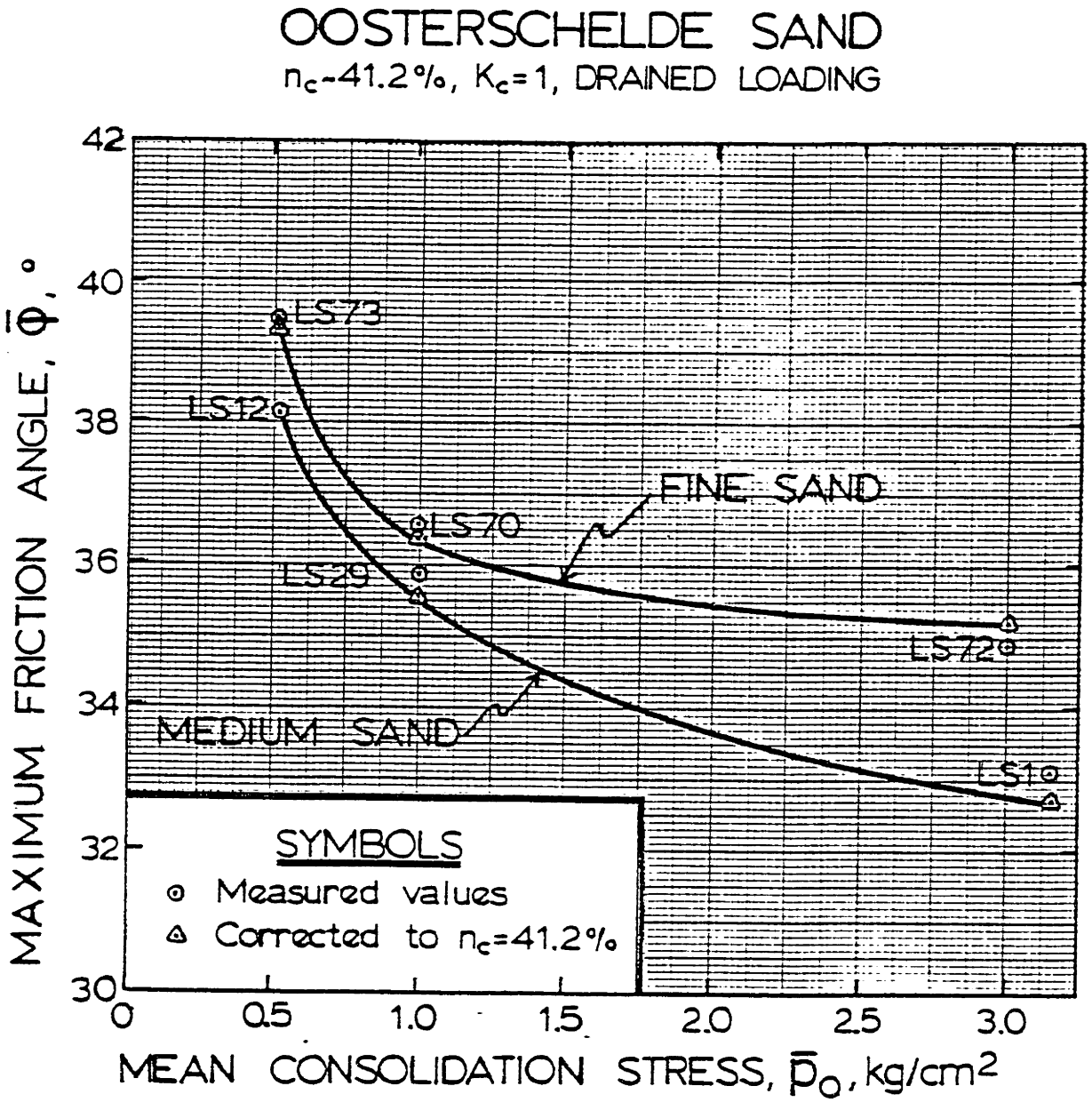

MOBILIZED FRICTION ANGLES AT MAXIMUM OBLIQUITY FOR DIFFERENT CONSOLIDATION STRESSES

FIGURE D-23

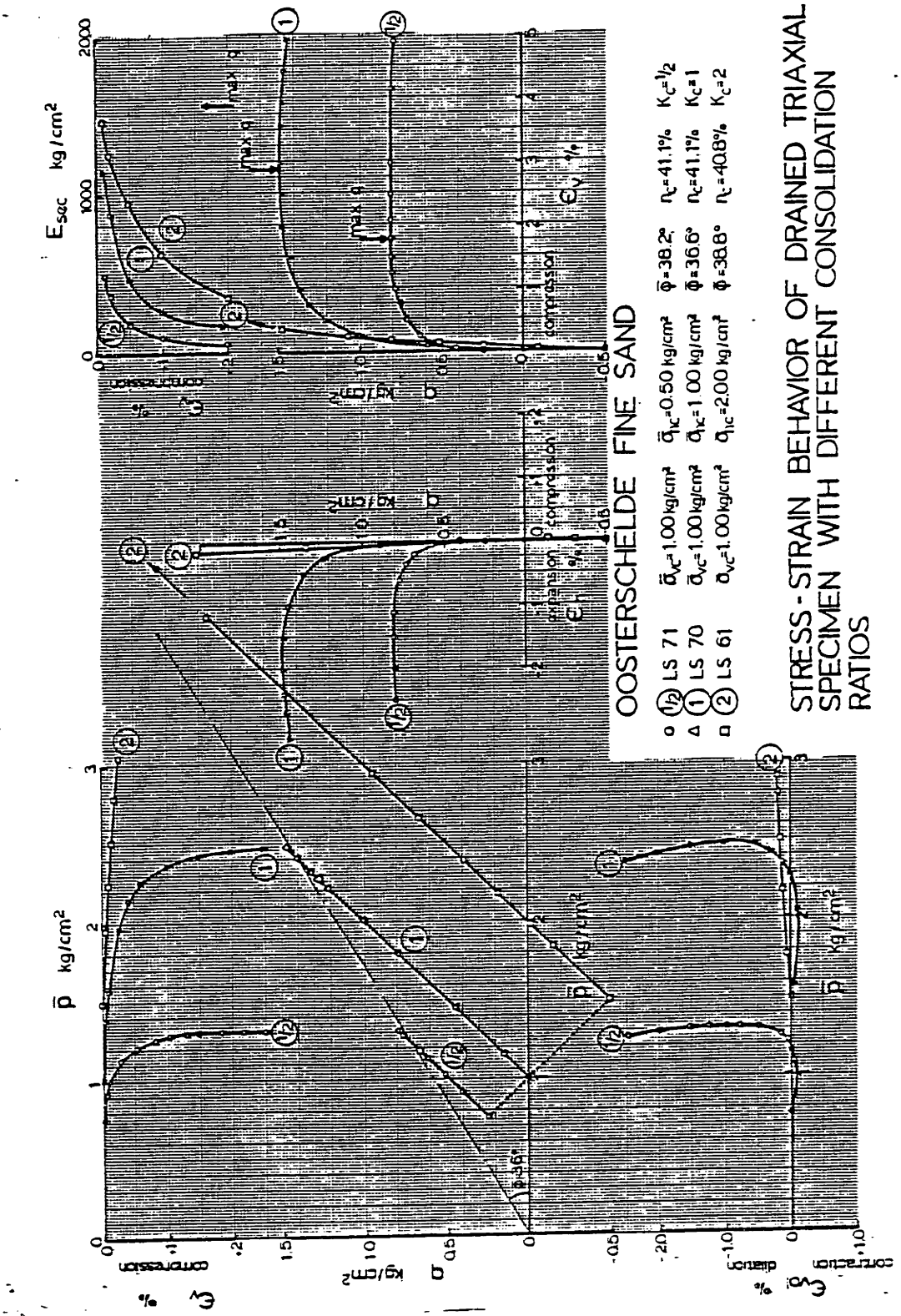
OOSTERSCHELDE FINE SAND
STRESS-STRAIN BEHAVIOR OF DRAINED TRIAXIAL SPECIMEN WITH DIFFERENT CONSOLIDATION RATIOS
LS 71
LS 70
LS 61
compression
dilatation
expansion

FIGURE D-24

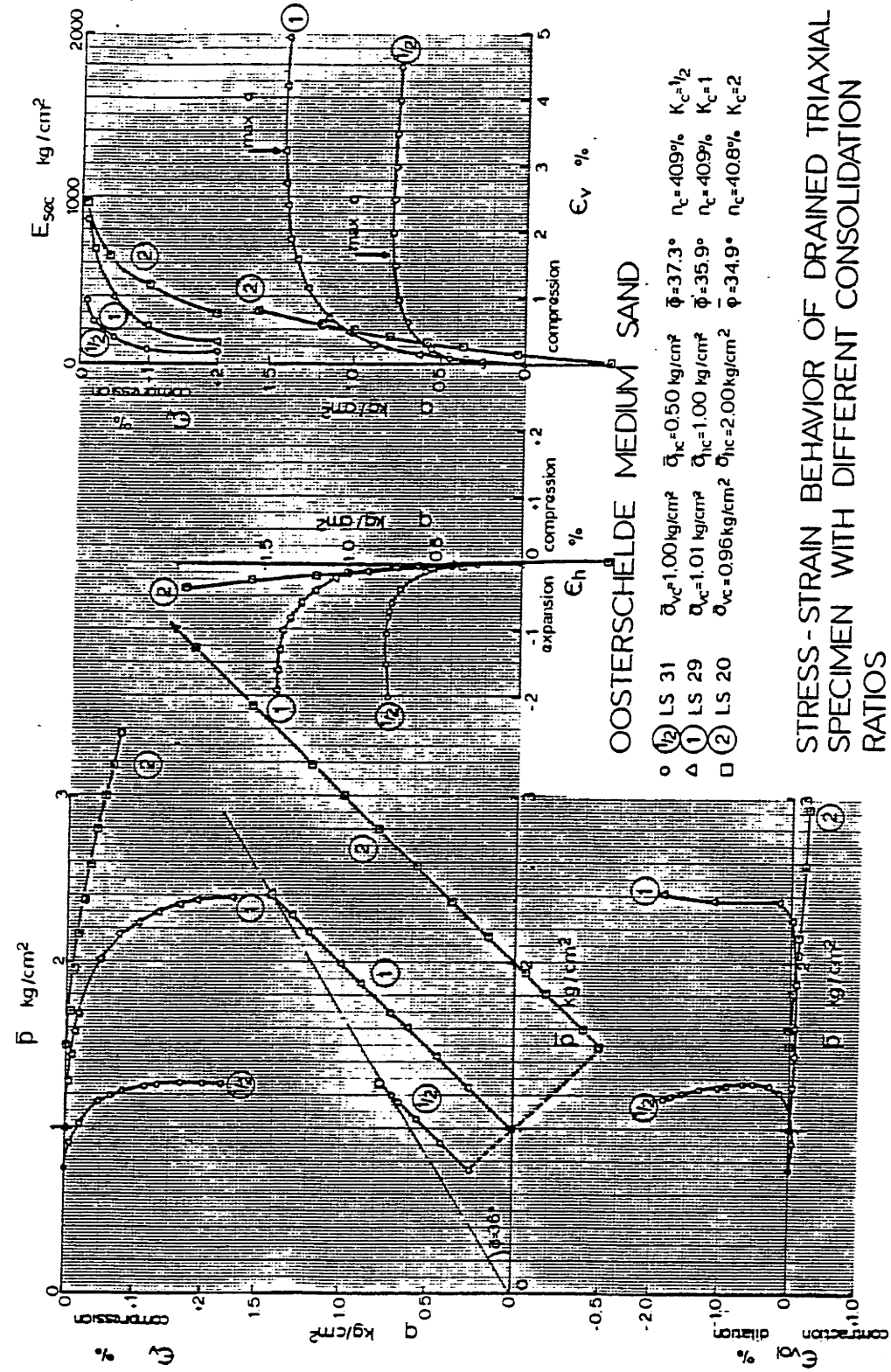
OOSTERSCHELDE MEDIUM SAND
STRESS-STRAIN BEHAVIOR OF DRAINED TRIAXIAL SPECIMEN WITH DIFFERENT CONSOLIDATION RATIOS
LS 31
LS 29
LS 20
compression
expansion
dilatancy
contraction
kg/cm²

FIGURE D-25

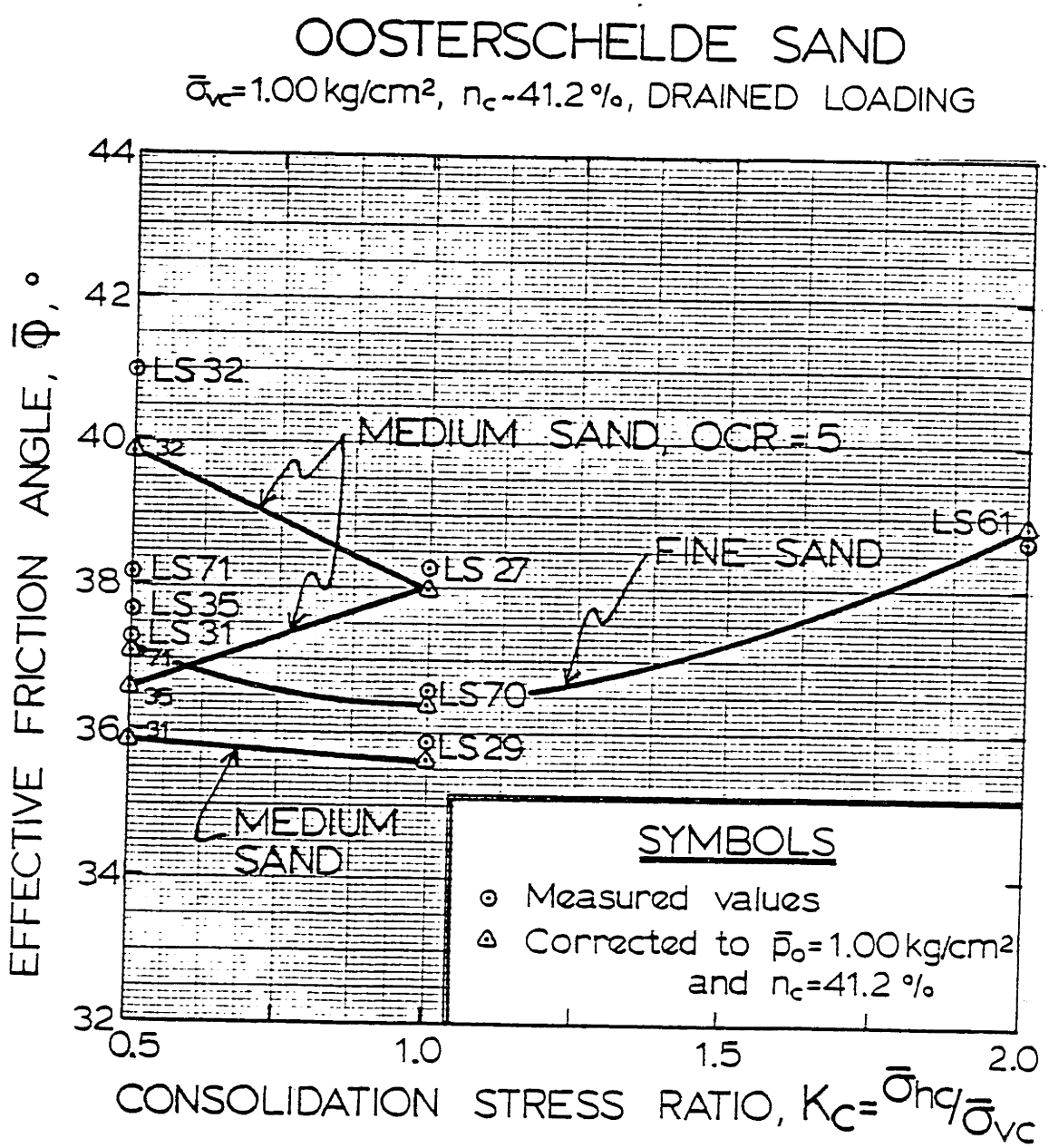

MOBILIZED FRICTION ANGLES AT MAXIMUM OBLIQUITY FOR DIFFERENT CONSOLIDATION STRESS RATIOS

FIGURE 3-26

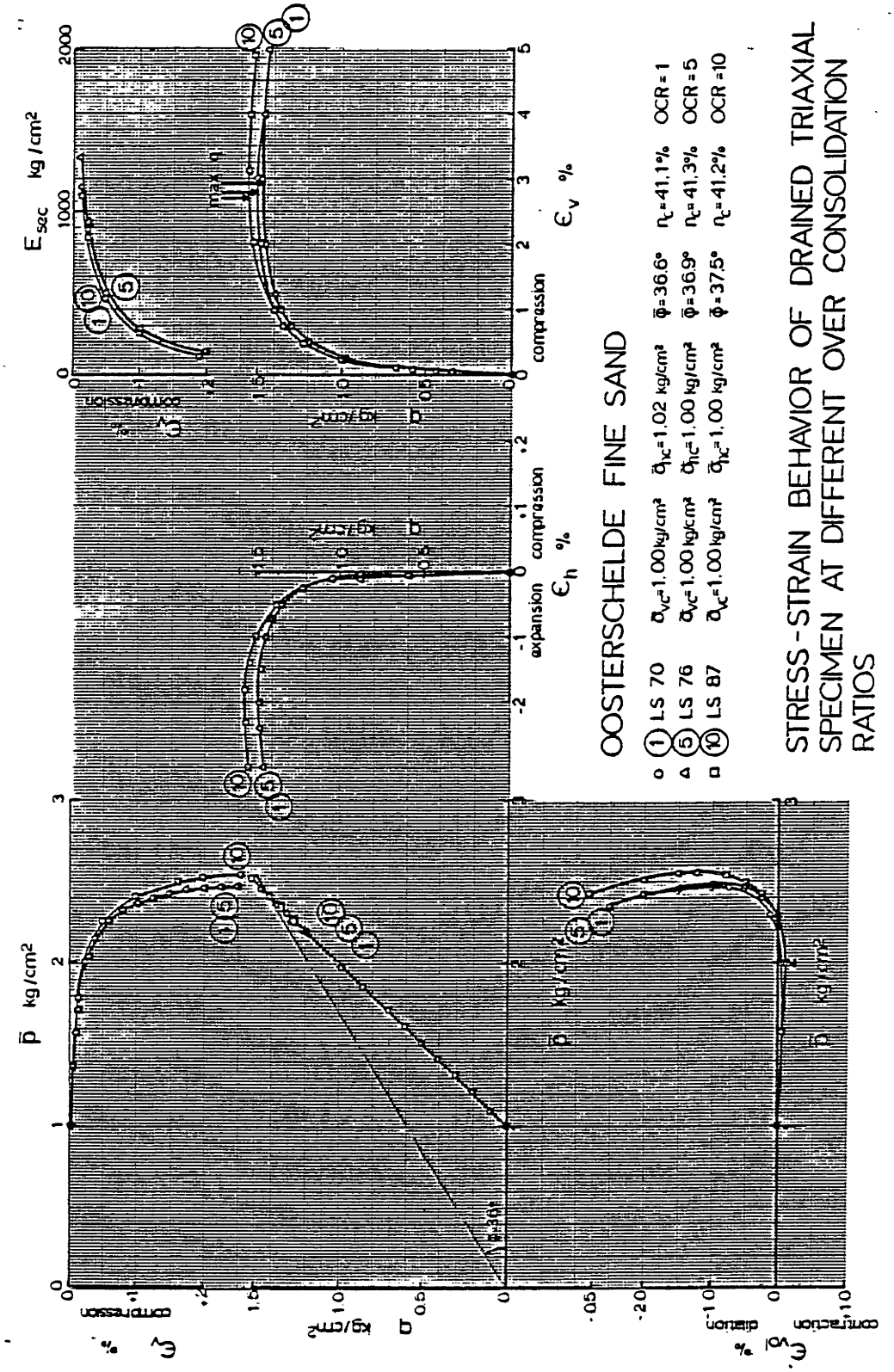
OOSTERSCHELDE FINE SAND
① LS 70 σ'vc=1.00 kg/cm² σ'hc=1.02 kg/cm² φ̄=36.6° nc=41.1% OCR=1
⑤ LS 76 σ'vc=1.00 kg/cm² σ'hc=1.00 kg/cm² φ̄=36.9° nc=41.3% OCR=5
⑩ LS 87 σ'vc=1.00 kg/cm² σ'hc=1.00 kg/cm² φ̄=37.5° nc=41.2% OCR=10
STRESS-STRAIN BEHAVIOR OF DRAINED TRIAXIAL SPECIMEN AT DIFFERENT OVER CONSOLIDATION RATIOS
E sec kg/cm²
max q
compression
expansion
kg/cm²
p̄ kg/cm²
dilation
contraction

FIGURE D-27

OOSTERSCHELDE SAND

$\bar{\sigma}_{vc}$=1.00 kg/cm², $\bar{\sigma}_{hc}$ =0.50 or 1.00 kg/cm², n_c ~ 41.2%, DRAINED LOADING

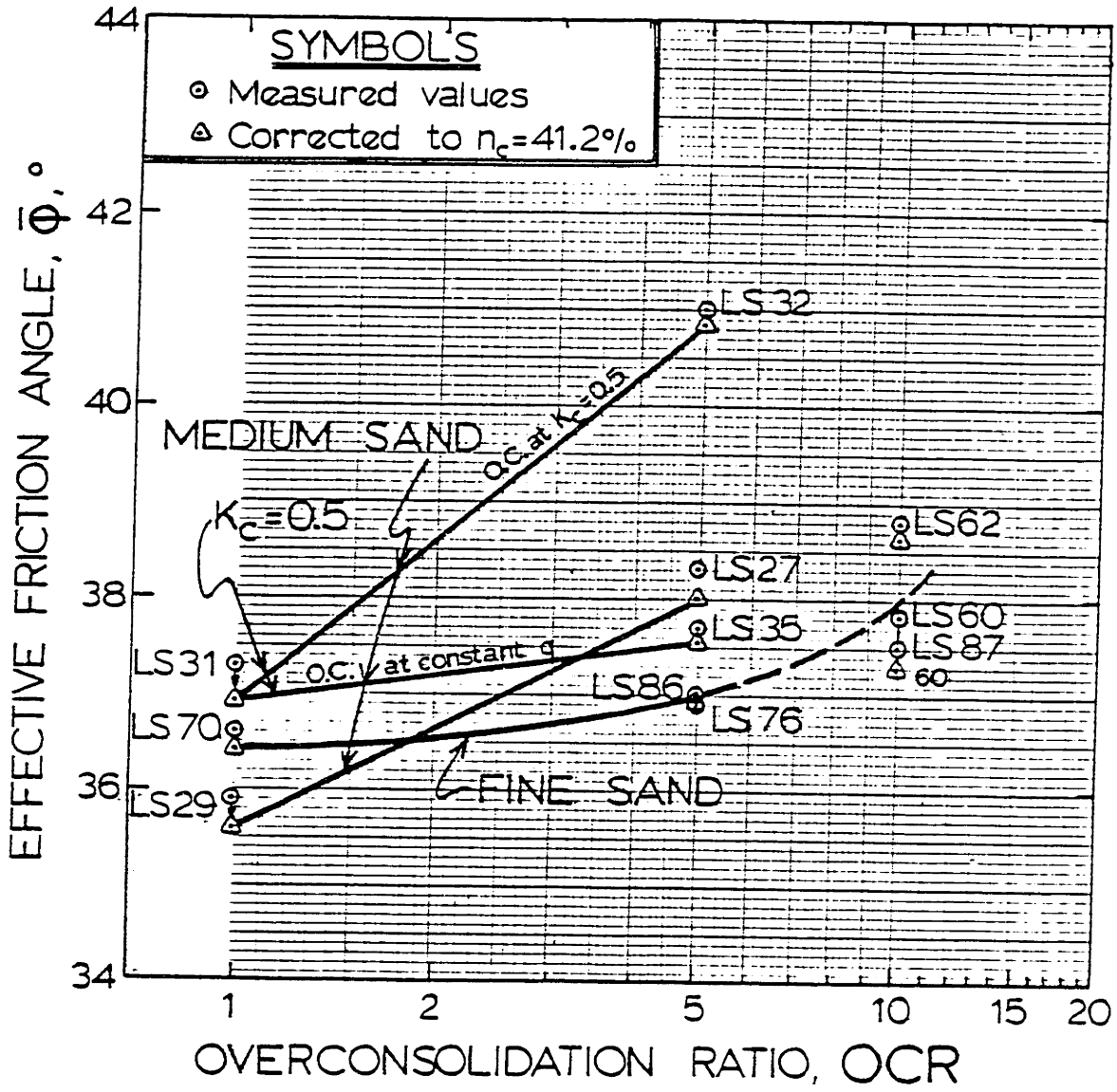

MOBILIZED FRICTION ANGLES AT MAXIMUM OBLIQUITY FOR DIFFERENT OVERCONSOLIDATION RATIOS

FIGURE D-28

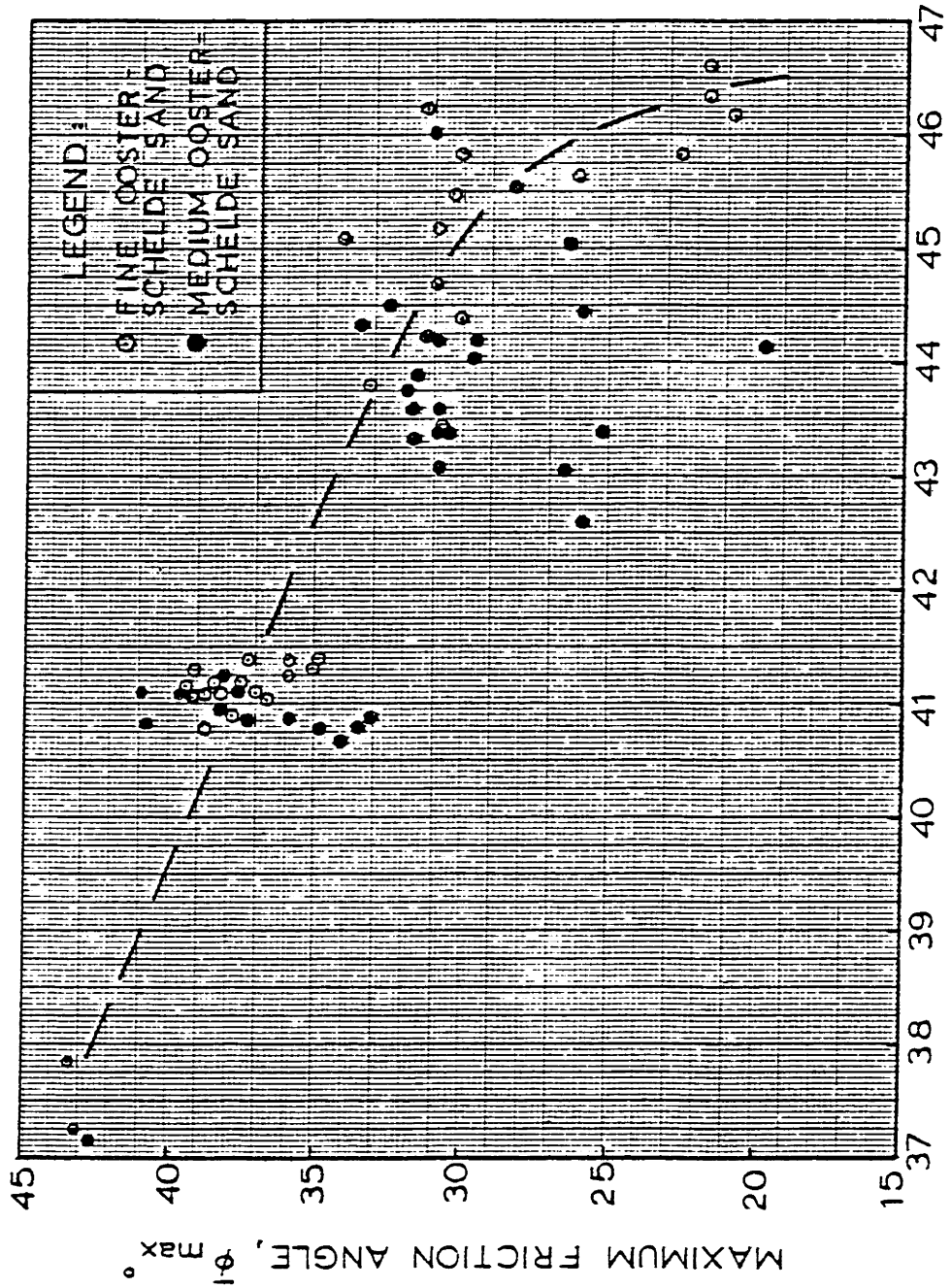

VARIATIONS IN MAXIMUM FRICTION ANGLE WITH PORSITY

FIGURE D-29

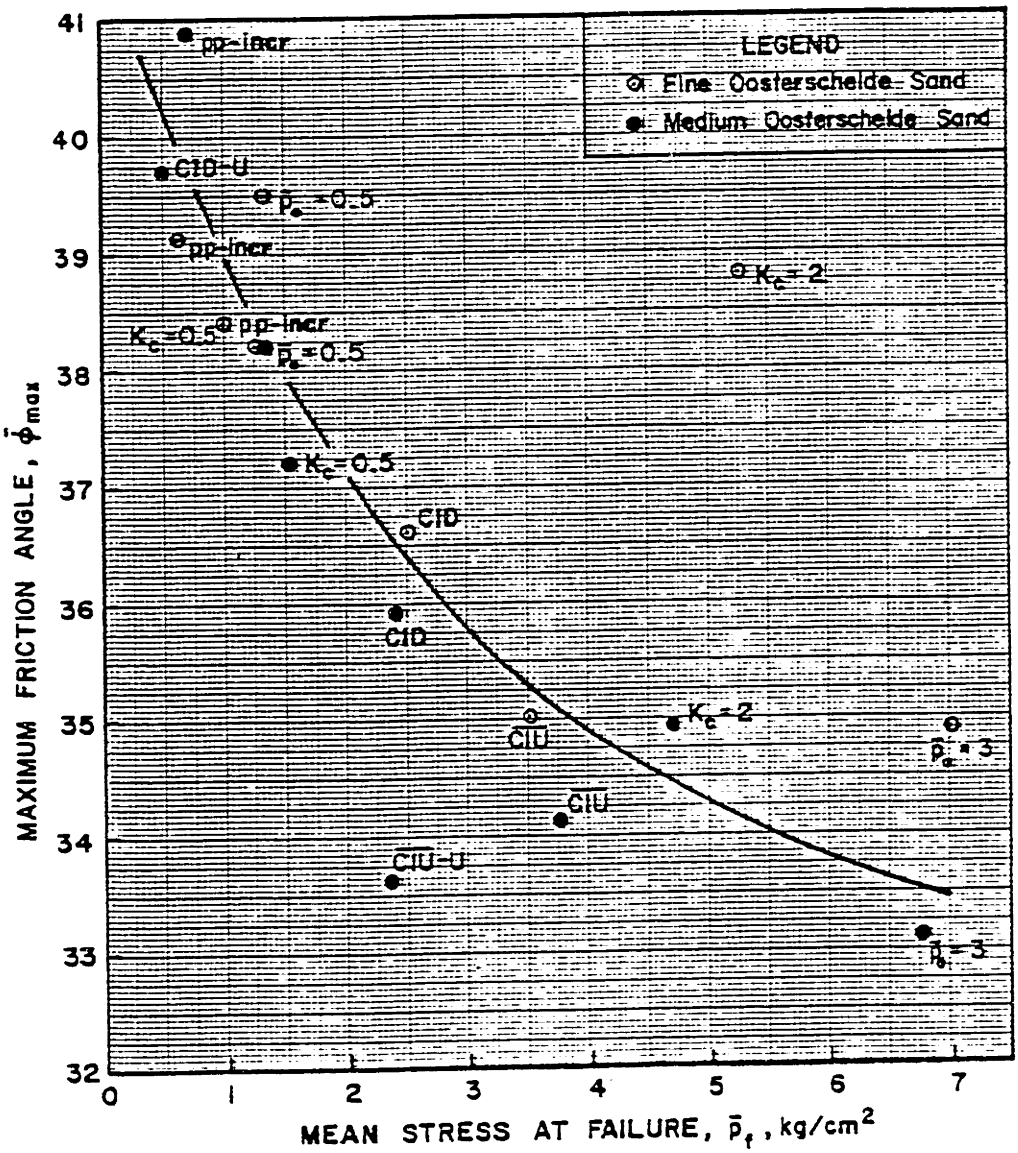

VARIATIONS IN FRICTION ANGLE WITH MEAN EFFECTIVE STRESS AT FAILURE FOR NORMALLY CONSOLIDATED SAMPLES AT 41 % POROSITY

FIGURE D-30

APPENDIX E

Summary Plots From Cyclic Triaxial Tests

This appendix gives plots of total stress path, pore pressure contours and strain contours for all test series that have been performed and not reported in Chapter IV. Summary plots of equivalent number of cycles versus strain are also presented in this appendix, as well as plots of strain amplitude. Detailed cyclic triaxial test results for individual tests are given in Appendix F.

E.1 Strain and Pore Pressure Contours for the Prediction Procedure

Porosity

The contour plots are only briefly described here; Chapter IV gives a thorough description and discussion. Figures E.1 to E.3 present total stress paths for cyclic test series on sand samples at different porosities. Both extension, compression and isotropic cyclic test series have been performed. Strain and pore pressure contours for the test series are given in Figures E.4 to E.12. The contour plots for the isotropic tests in Figure E.3 are given in Figures IV.11 and IV.12 in Chapter IV. No pore pressure contours exist for the extension test series LC86, 147 and 136, since 1% strain was already reached after the first cycle. The slope of these contours are plotted in Figures IV.8 and IV.9 in Chapter IV.

Cyclic Shear Stress Ratio

Figures E.13 to E.15 present total stress paths for isotropic and compression cyclic test series with varying cyclic shear stress ratio. Strain and pore pressure contours for the test series are given in Figures E.16 to E.21. The contour slopes are plotted in Figures IV.19 and IV.20.

Mean Consolidation Stress

Figures E.22 and E.23 present total stress paths for cyclic test series with varying mean consolidation stress at constant shear stress ratio. Strain and pore pressure contours are given in Figures E.24 to E.28. No pore pressure contours exist for the cyclic extension test series, since test LC86 reached 1% strain during the first cycle. The contour slopes are plotted in Figures IV.32, IV.33 and IV.39 for respectively compression test strain contours, compression test pore pressure contours and isotropic test pore pressure contours.

Mean Shear Stress Ratio

Figure E.29 presents the total stress path for one test series with varying mean shear stress ratio. Strain and pore pressure contours are given respectively in Figures E.30 and E.31.

E.2 Additional Strain and Pore Pressure Contours

In addition to the test series performed to obtain necessary data for the prediction procedure, several additional test series were performed to investigate the influence of parameters not explicitly examined in the prediction procedure. The result of that investigation is reported below.

Consolidation Stress Ratio

The influence of consolidation stress ratio ($K_c=\bar{\sigma}_{hc}/\bar{\sigma}_{vc}$) on strain and pore pressure is for practical problems rather interesting since the vertical stress in the foundation below an offshore gravity structure can be relatively reliably established, whereas the magnitude of horizontal stress may be associated with a large uncertainty. Test series as the ones Figures E.32 to E.35 give total stress paths for, all have a constant vertical stress, and a varying horizontal stress. For a given vertical stress, porosity and cyclic shear stress, the influence of variations in horizontal stress on strain and pore pressure development can be directly assessed. Figure E.36 compares all four test series at ($\pm$) 1% vertical strain (1% for compression tests, $\pm$1% for isotropic tests). The magnitude of K_c has a major influence on the number of load cycles required to reach 1% vertical strain. Analogous to the findings in Chapter II, the tests with $K_c > 1$ (extension cyclic tests) require fewer cycles than isotropic cyclic tests

(K_c = 1) to reach 1% strain. Tests with K_c < 1 (compression cyclic tests) require generally more cycles than isotropic cyclic tests to reach 1% strain. Strain and pore pressure in Figures E.37 to E.44 are quite non-linear, and not as orderly and consistent as Figure E.36 indicates.

Mean Normal Stress

Figures E.45 to E.47 present total stress paths for cyclic test series with varying mean normal stress, where the mean and cyclic shear stress rather than the mean and cyclic shear stress ratio is constant. Contours for 1% vertical strain for three of the test series and 0.03% vertical strain for the fourth are plotted in Figure E.48. The lines are reasonably parallel and log-linear, supporting the independence of mean normal stress from other test parameters. However, the strain contours in Figures E.49 to E.52 are not as near to parallel as those for constant mean and cyclic shear stress ratio. This is one of the reasons why tests at constant mean and cyclic shear stress ratio were utilized for the prediction procedure.

Another way to vary mean normal stress is to keep the cyclic shear stress and the mean shear stress ratio constant, as shown in Figure E.53. Strain and pore pressure contours for that case are given in Figures E.54 and E.55, and are close to parallel.

Vertical Consolidation Stress

Figures E.56 and E.57 present total stress paths for tests with constant horizontal consolidation stress and cyclic shear stress, but varying vertical consolidation stress. Figure E.58 gives contours for 0.11% and 1% vertical strain for the test series. Strain and pore pressure contours are given in Figures E.59 to E.62. The contours are clearly non-linear. Evidently any variations in mean shear stress will lead to non-linear strain and pore pressure contours.

E.3 Equivalent Load Cycle Plots

The prediction plots in Chapter IV are all derived by taking mean values of the available tests at each mean shear stress ratio. Figure E.63 presents equivalent load cycle plots of all cyclic compression tests at $q_m/\bar{p}_o = 0.25$ versus vertical strain. Figure E.64 gives equivalent load cycles for various mean shear stress ratios versus strain. The results in Figure E.63 scatter by a factor of 2 at 10 cycles, a factor of 2 at 100 cycles, a factor of 5 at 1000 cycles, and a factor of 2 at 5000 cycles.

Figures E.65 to E.67 present equivalent load cycles for all available cyclic compression tests versus pore pressure ratio. These plots are the basis for Figure V.7 in Chapter V. The results in Figure E.65 show a scatter in pore pressure ratio of a factor of 3 at 10 cycles, a factor of about 1.6 at

100 cycles, and a factor of 2.1 at 500 cycles. The results in Figure E.66 scatter by a factor of 1.6 at 10 cycles, 2 at 100 cycles and 2 at 1000 cycles.

Figure E.67 presents the equivalent load cycles versus pore pressure ratio for all isotropic tests at cyclic shear stress ratios of 0.15 to 0.40. The five tests run at $\Delta q_{cy}/\bar{p}_o = 0.20$, scatter by a factor of 1.5 at 10 cycles, 1.7 at 50 cycles and 1.7 at 100 cycles. The limited number of tests is certainly a factor in keeping the scatter low. The prediction plot in Figure V.11 is based on the average values from Figure E.68.

E.4 Strain Amplitude

Figures E.69 to E.72 present plots of the cyclic strain amplitude versus number of load cycles required to reach 1% vertical strain for various test series. The cyclic strain amplitude is measured at a pore pressure ratio of 0.5, and defined as the difference between the maximum and the minimum strain reading within one load cycle. Figure E.69 presents two test series with varying mean normal stress. The number of load cycles required to reach 1% vertical strain clearly decreases with increasing cyclic strain amplitude. Figure E.70 shows three test series with varying horizontal stress. The same observations as above are made. For the tests at varying mean consolidation stress in Figure E.71, as well as

the tests with varying mean shear stress in Figure E.72, the number of load cycles to 1% vertical strain again decreases with an increasing cyclic strain amplitude.

E.5 Cyclic Modulus

A plot of "cyclic" modulus E_c (2 x maximum shear stress divided by accumulated vertical strain) versus pore pressure ratio for all compression tests is given in Figure E.73. The modulus variation with pore pressure is almost log-linear, and the best fit given by $E_c = 7000 \cdot 10^{-\frac{M}{0.7}}$ kg/cm^2. The maximum scatter in the data points is a factor of 3 at all plotted pore pressure ratios.

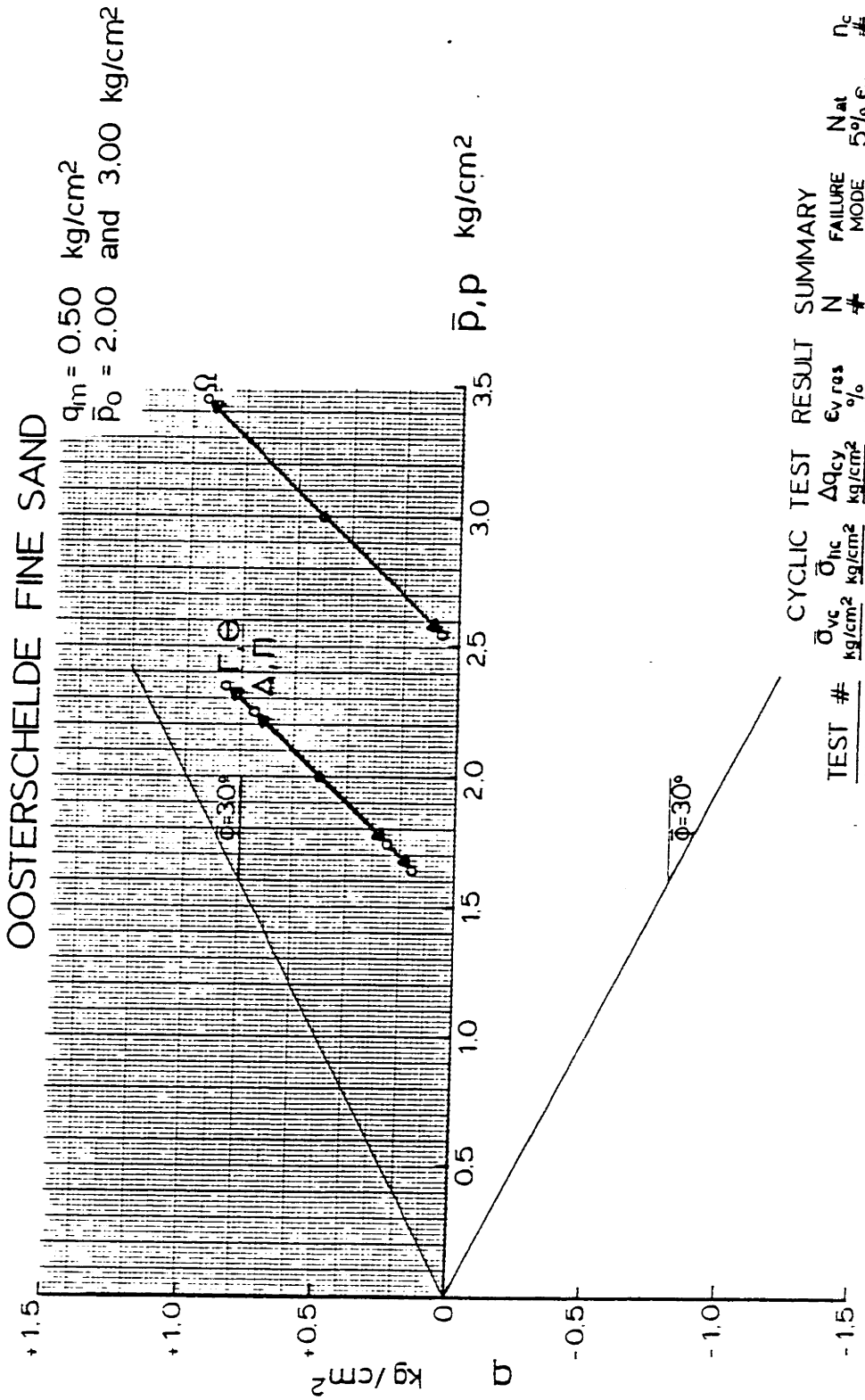

CYCLIC TEST RESULT SUMMARY

TEST #	$\bar{\sigma}_{vc}$ kg/cm²	$\bar{\sigma}_{hc}$ kg/cm²	Δq_{cy} kg/cm²	$\epsilon_{v\,res}$ %	N #	FAILURE MODE	N_{at} 5% ϵ_v	n_c #
Δ LC 129	2.50	1.50	0.25	13.50	3600	COMPR.	1400	43.5
Π LC 134	2.50	1.50	0.25	0.38	20000	COMPR.	—	43.7
Γ LC 130	2.50	1.50	0.35	10.20	1000	COMPR.	546	43.2
Θ LC 142	2.50	1.50	0.35	8.39	9000	COMPR.	4700	41.7
Ω LC 156	3.50	2.50	0.45	10.84	32	COMPR.	32	45.0
Ω LC 151	3.50	2.50	0.45	10.34	6650	COMPR.	5140	41.4

TOTAL STRESS PATHS (TSP-u_B) FOR CYCLIC TRIAXIAL TESTS WITH DIFFERENT POROSITY, n_c

FIGURE E-1

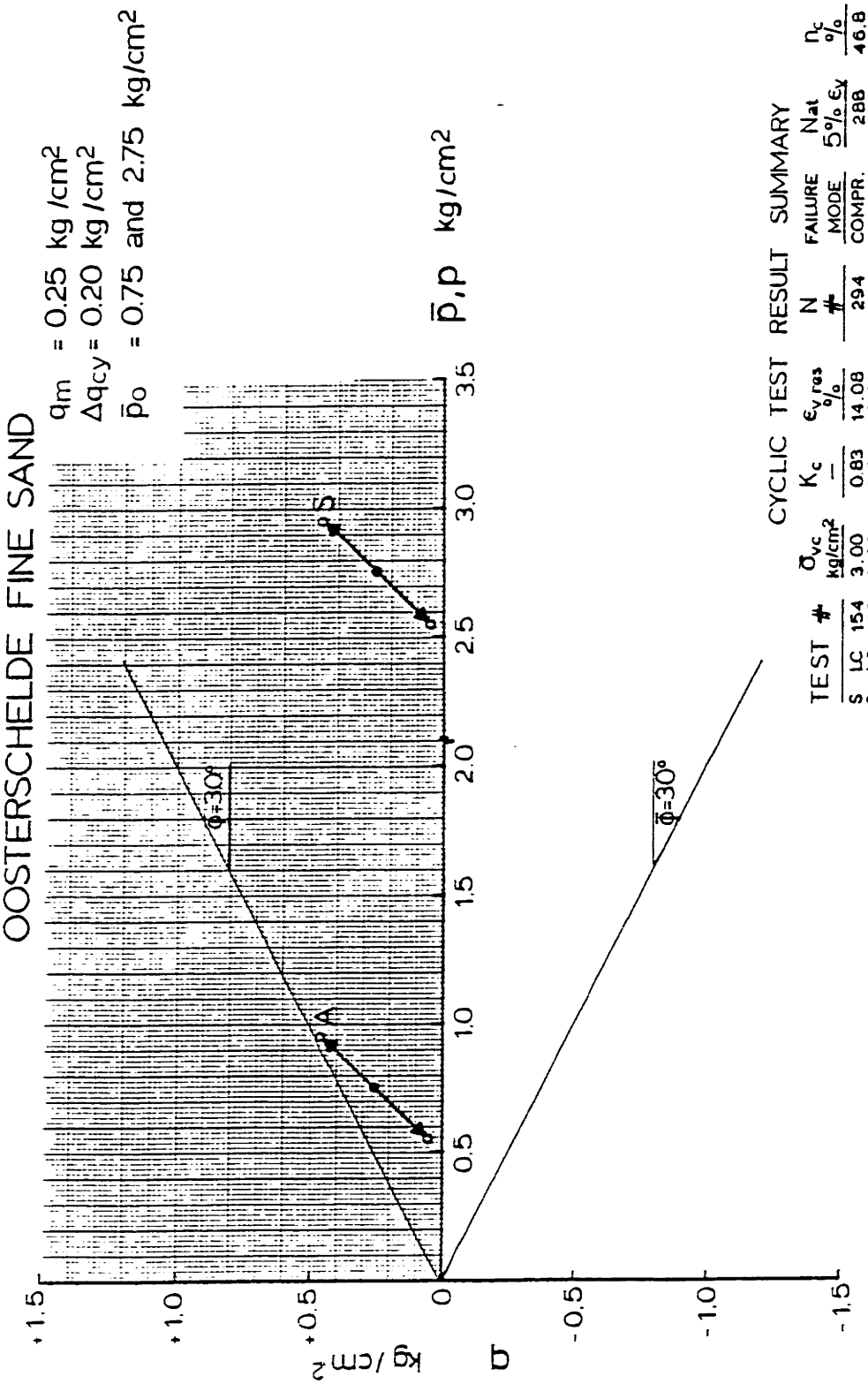

CYCLIC TEST RESULT SUMMARY

TEST	#	$\bar{\sigma}_{vc}$ kg/cm²	K_c —	$\epsilon_{v\,res}$ %	N #	FAILURE MODE	Nat 5% ϵ_v	n_c %
S LC	154	3.00	0.83	14.08	294	COMPR.	288	46.8
S LC	68	3.00	0.83	0.03	29460	COMPR.	—	40.9
A LC	148	1.00	0.50	10.18	12000	COMPR.	5405	41.1
A LC	66	1.00	0.50	6.30	19800	COMPR.	15150	40.4

TOTAL STRESS PATHS (TSP-u_B) FOR ANISOTROPIC CYCLIC TESTS WITH DIFFERENT POROSITY, n_c

FIGURE E-2

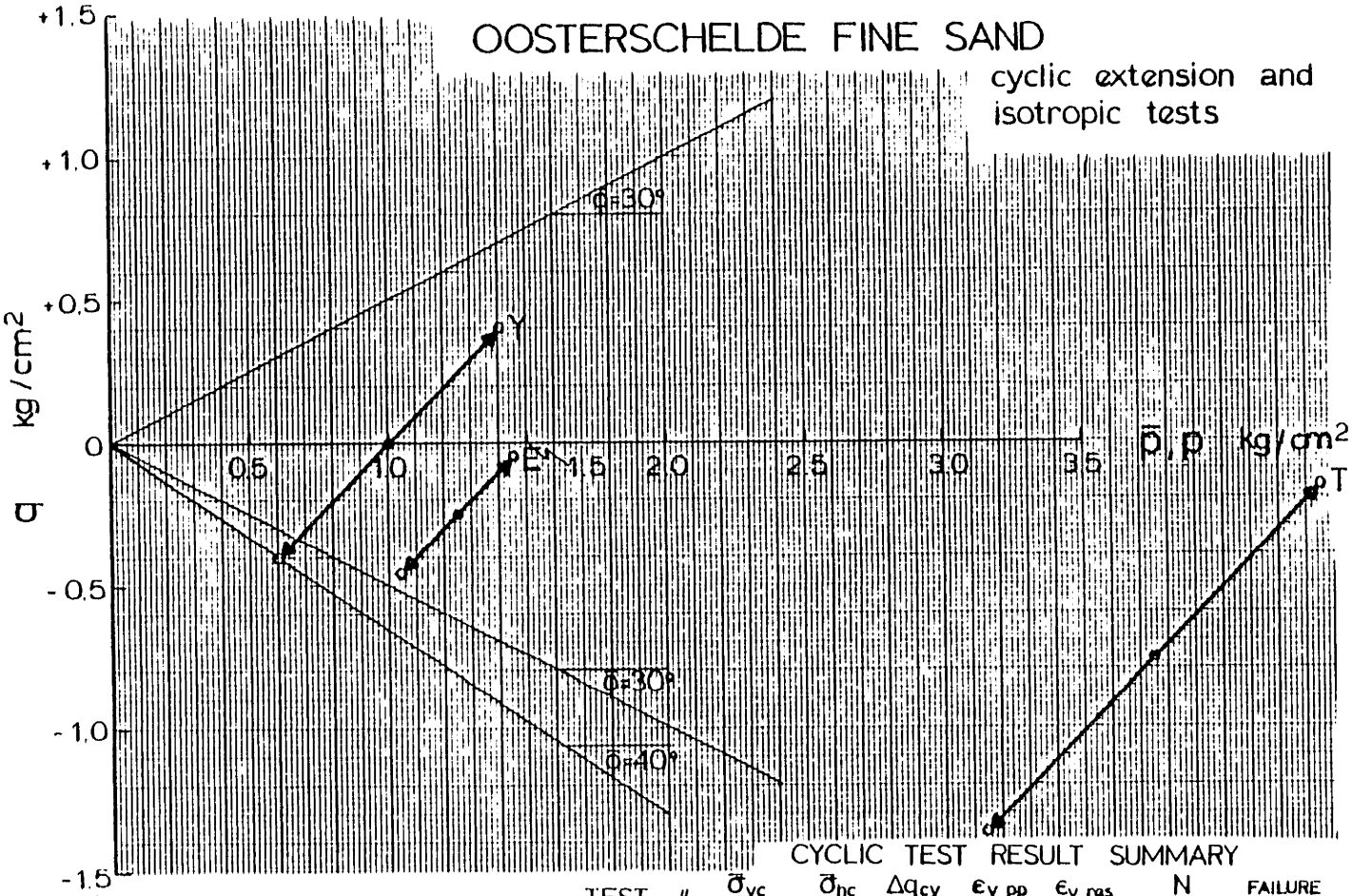

CYCLIC TEST RESULT SUMMARY

TEST	#	$\bar{\sigma}_{vc}$ kg/cm²	$\bar{\sigma}_{hc}$ kg/cm²	Δq_{cy} kg/cm²	$\epsilon_{v\ pp}$ %	$\epsilon_{v\ res}$ %	N #	FAILURE MODE	N_{at} 5% ϵ_v	n_c #
Y LC	123	1.00	1.00	0.40	11.81	-1.29	87	DEF.	71	38.6
Y LC	67	1.00	1.00	0.40	20.90	-0.20	13	DEF.	6	40.9
E LC	74	1.00	1.50	0.20	1.20	-12.70	110	EXT.	60	41.3
E LC	116	1.00	1.50	0.20	0.70	-9.68	1050	EXT.	810	40.0
T LC	86	3.00	4.50	0.60	0.58	-8.60	18	EXT.	12	41.2
T LC	147	3.00	4.50	0.60	0.52	-7.13	110	EXT.	92	40.0
T LC	136	3.00	4.50	0.60	0.82	-10.75	120	EXT.	96	39.9

FIGURE E-3

TOTAL STRESS PATHS (TSP-u_B) FOR CYCLIC TESTS WITH DIFFERENT POROSITY, n_c

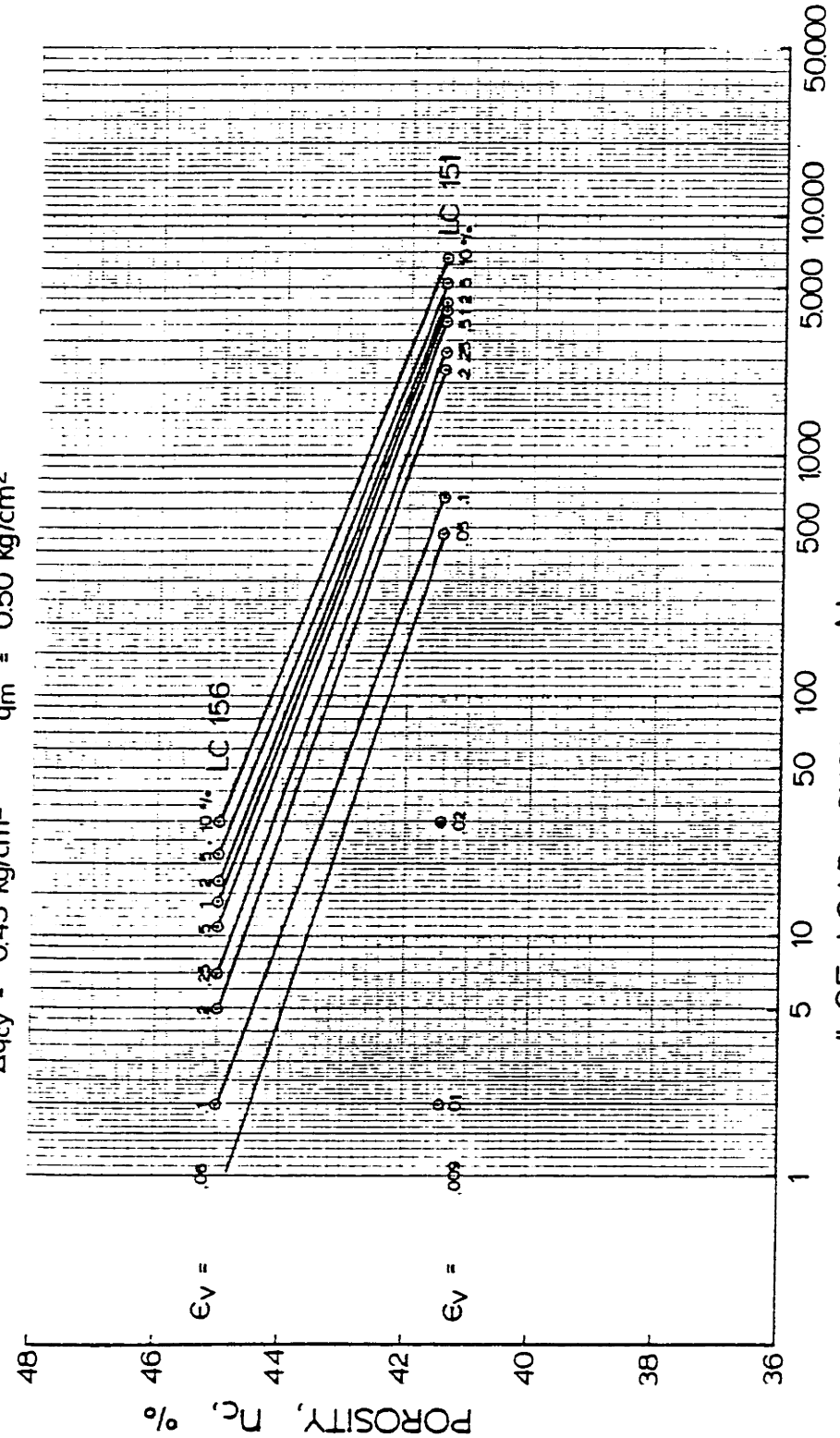

STRAIN CONTOURS FOR COMPRESSION CYCLIC TESTS ON SAMPLES AT DIFFERENT POROSITIES

FIGURE E-4

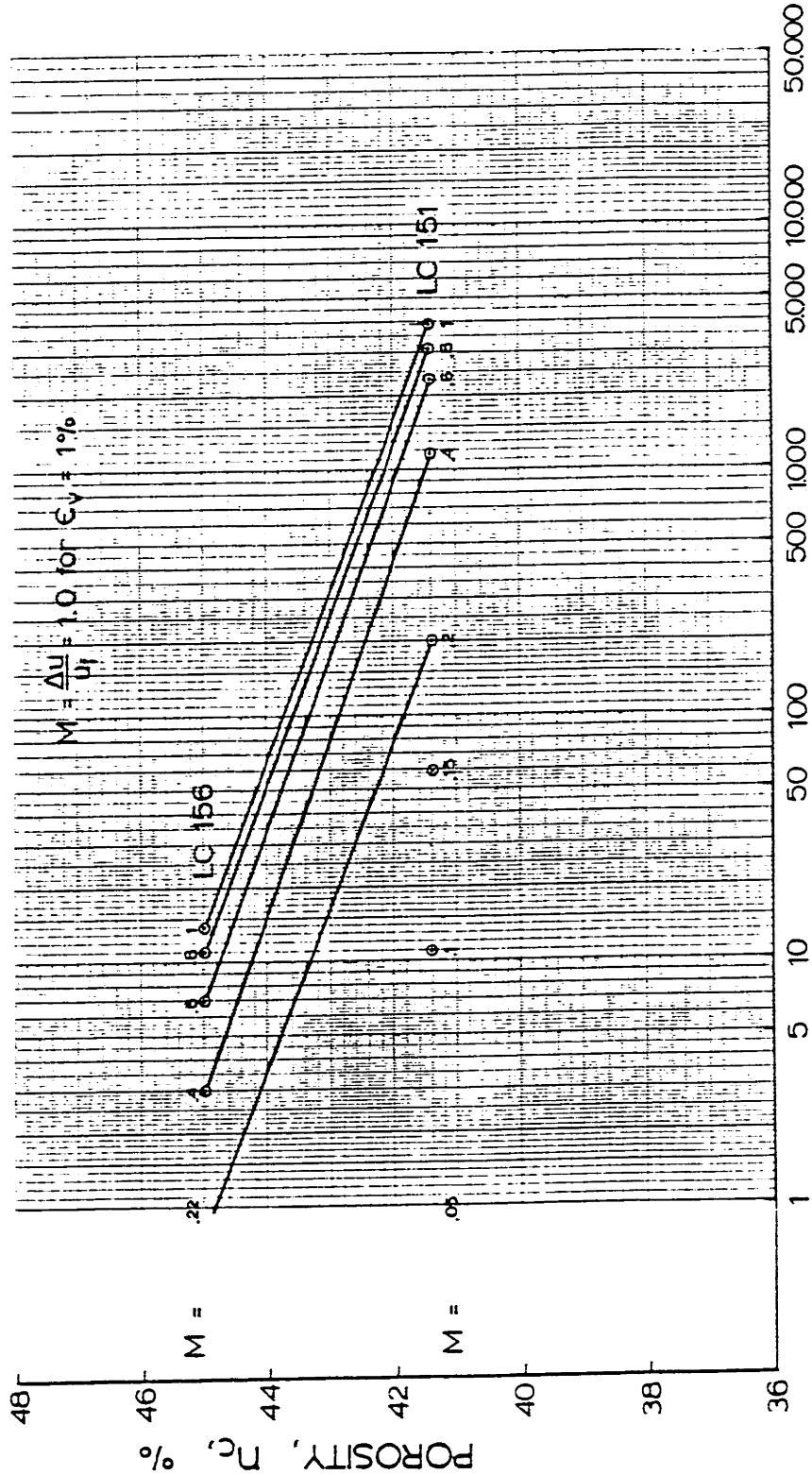

PORE PRESSURE CONTOURS FOR COMPRESSION CYCLIC TESTS ON SAMPLES AT DIFFERENT POROSITIES

FIGURE E-5

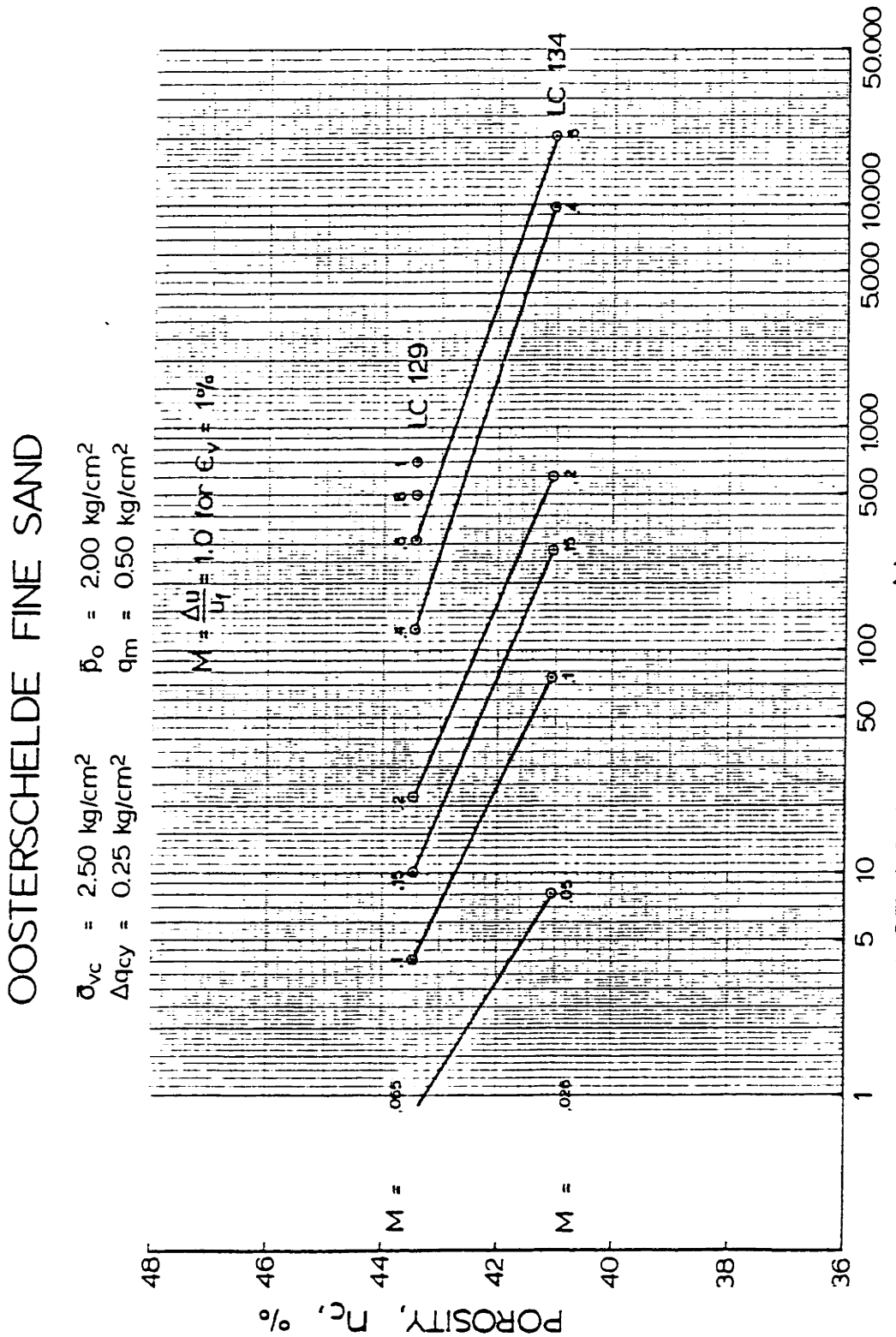

PORE PRESSURE CONTOURS FOR COMPRESSION CYCLIC TESTS ON SAMPLES AT DIFFERENT POROSITIES

FIGURE E-6

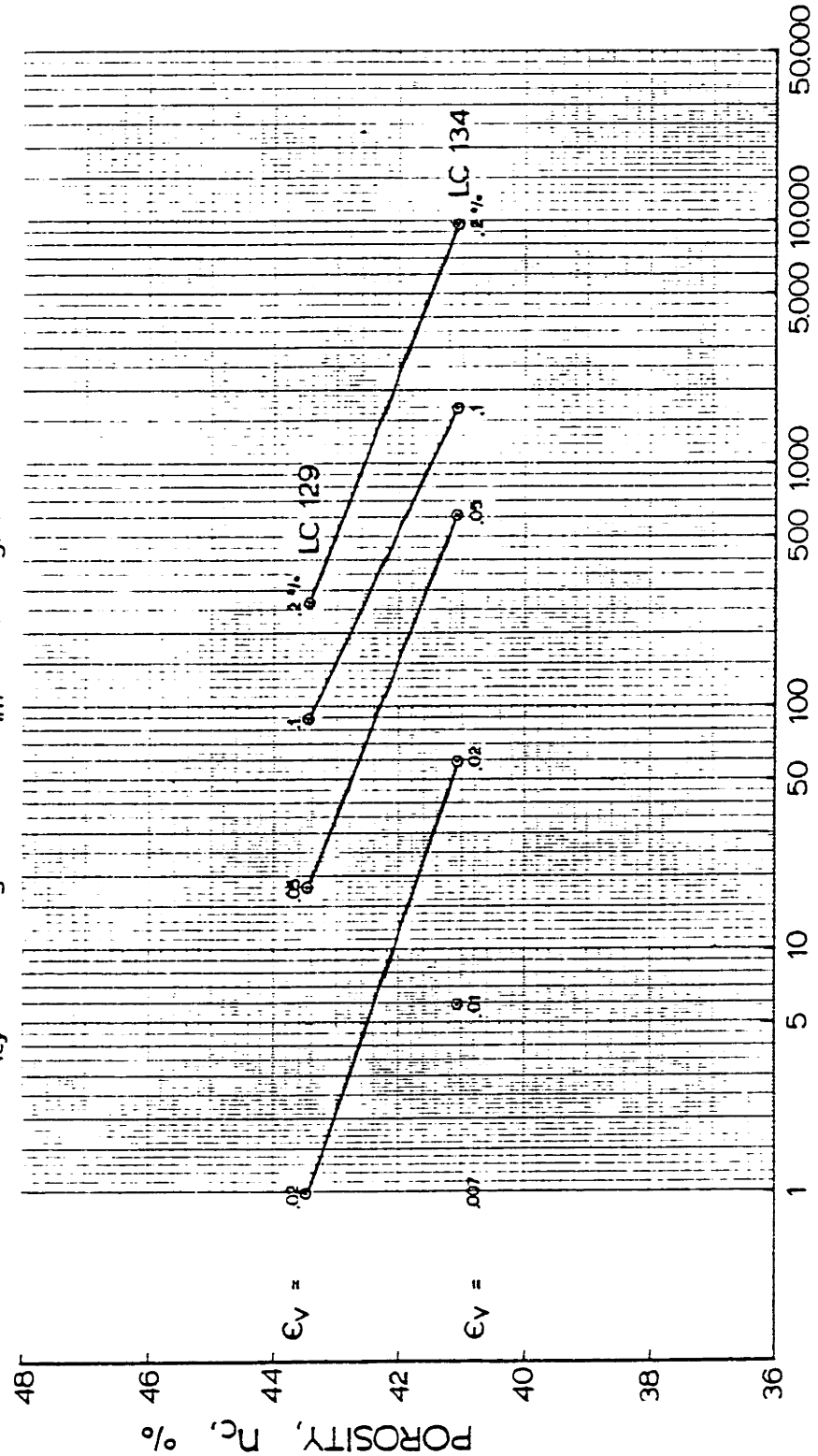

STRAIN CONTOURS FOR COMPRESSION CYCLIC TESTS ON SAMPLES AT DIFFERENT POROSITIES

FIGURE E-7

OOSTERSCHELDE FINE SAND

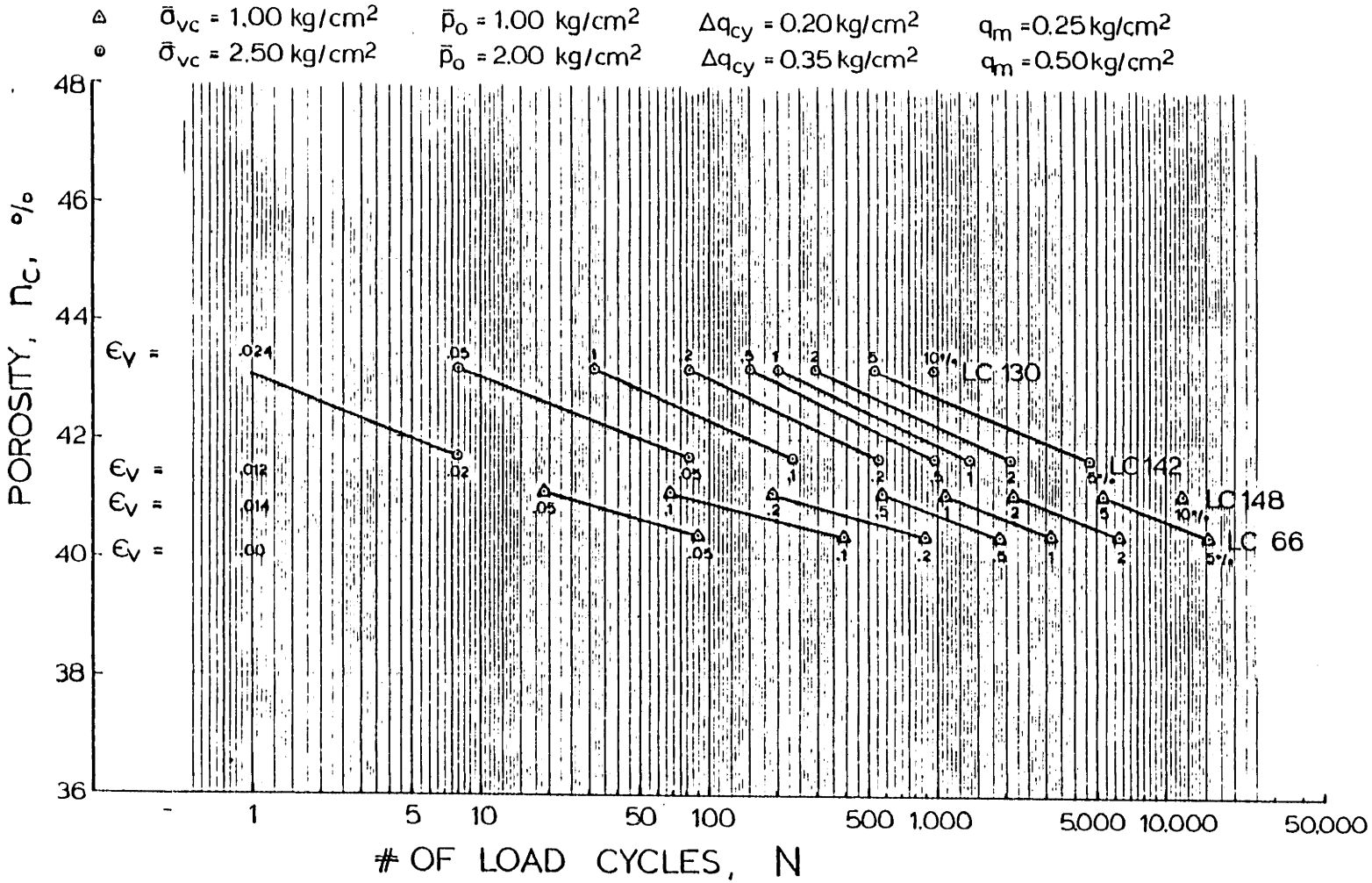

STRAIN CONTOURS FOR COMPRESSION CYCLIC TESTS ON SAMPLES AT DIFFERENT POROSITIES

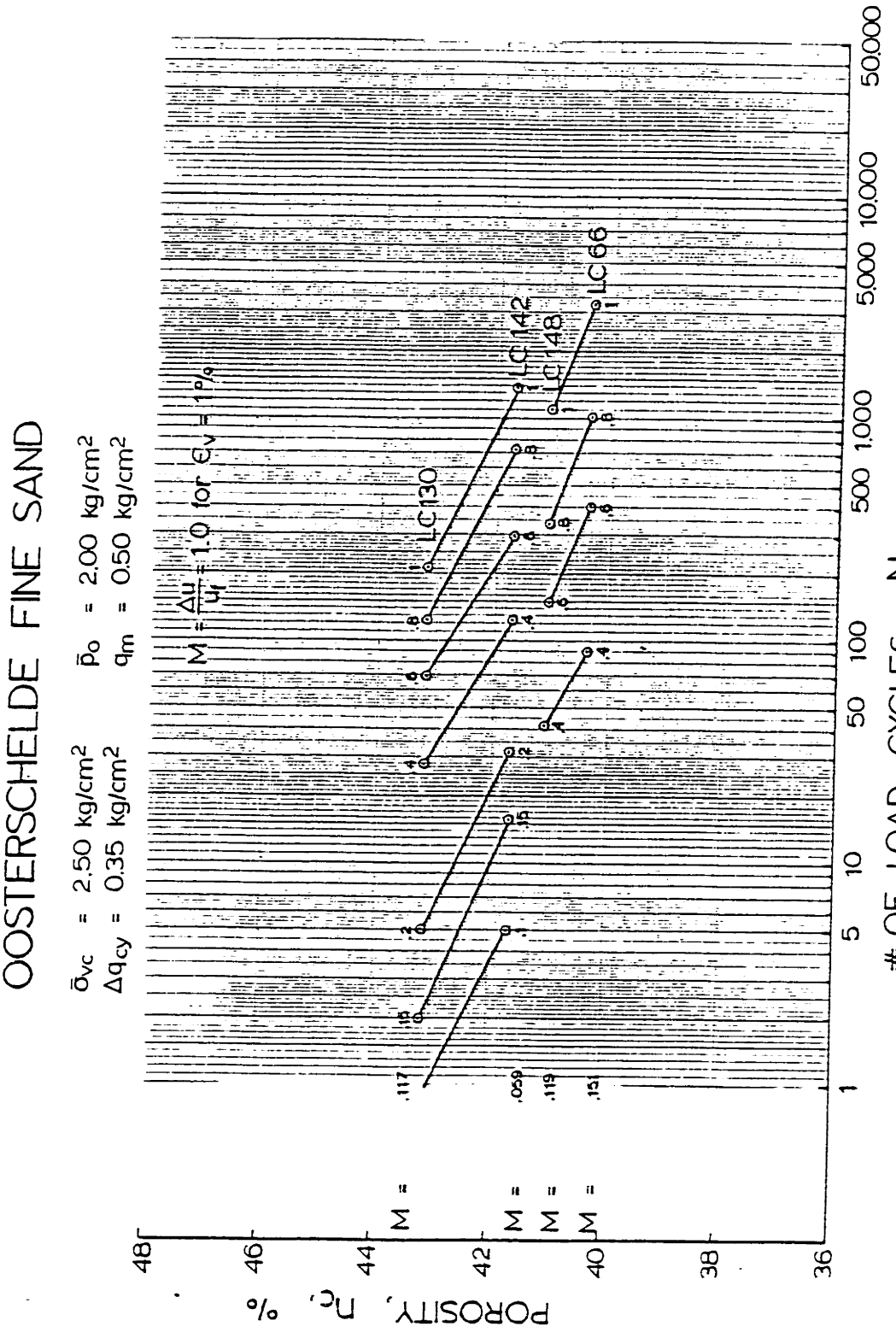

PORE PRESSURE CONTOURS FOR COMPRESSION CYCLIC TESTS ON SAMPLES AT DIFFERENT POROSITIES

FIGURE II-9

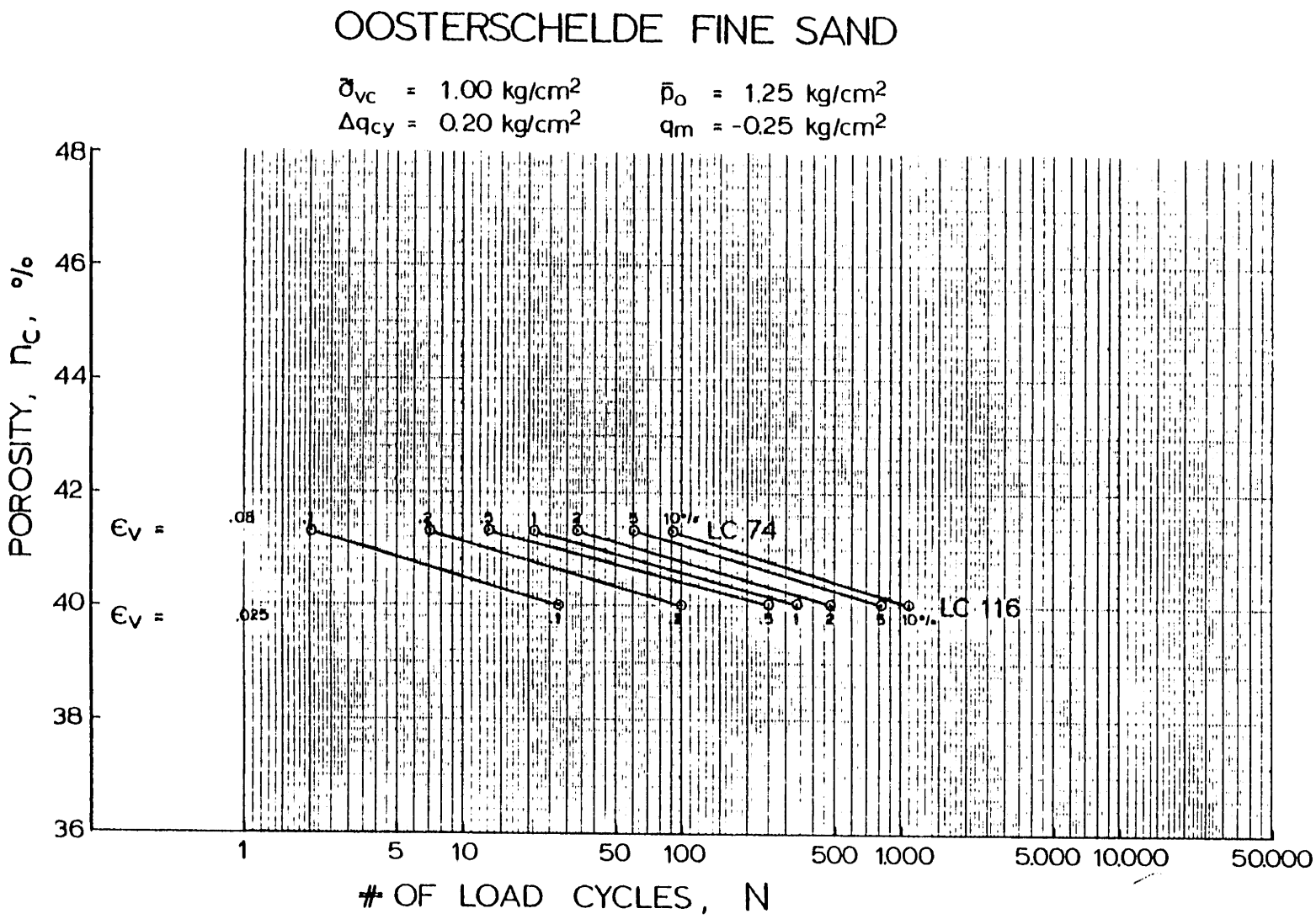

FIGURE E-10

STRAIN CONTOURS FOR EXTENSION CYCLIC TESTS ON SAMPLES AT DIFFERENT POROSITIES

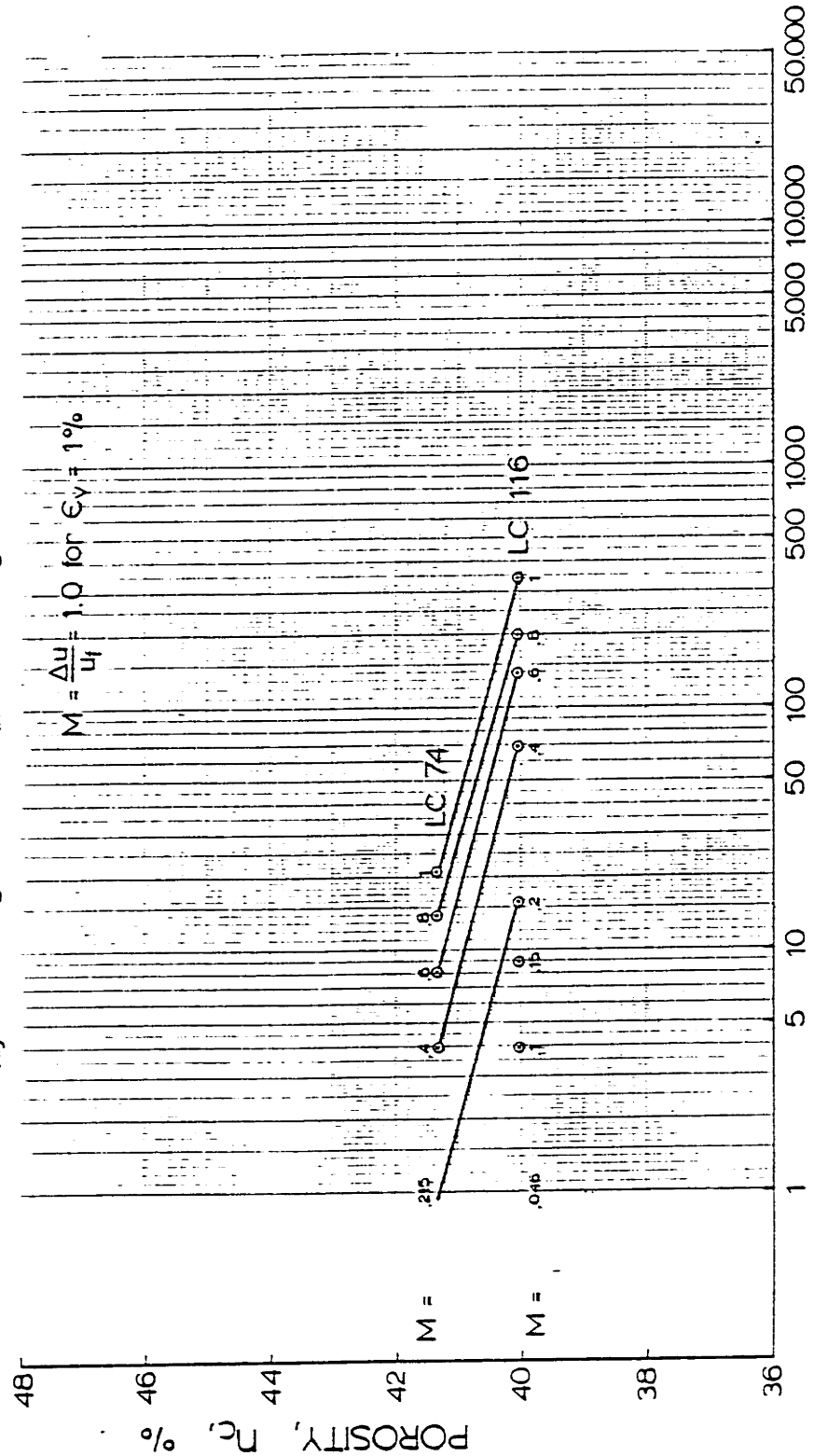

PORE PRESSURE CONTOURS FOR EXTENSION CYCLIC TESTS ON SAMPLES AT DIFFERENT POROSITIES

FIGURE II-11

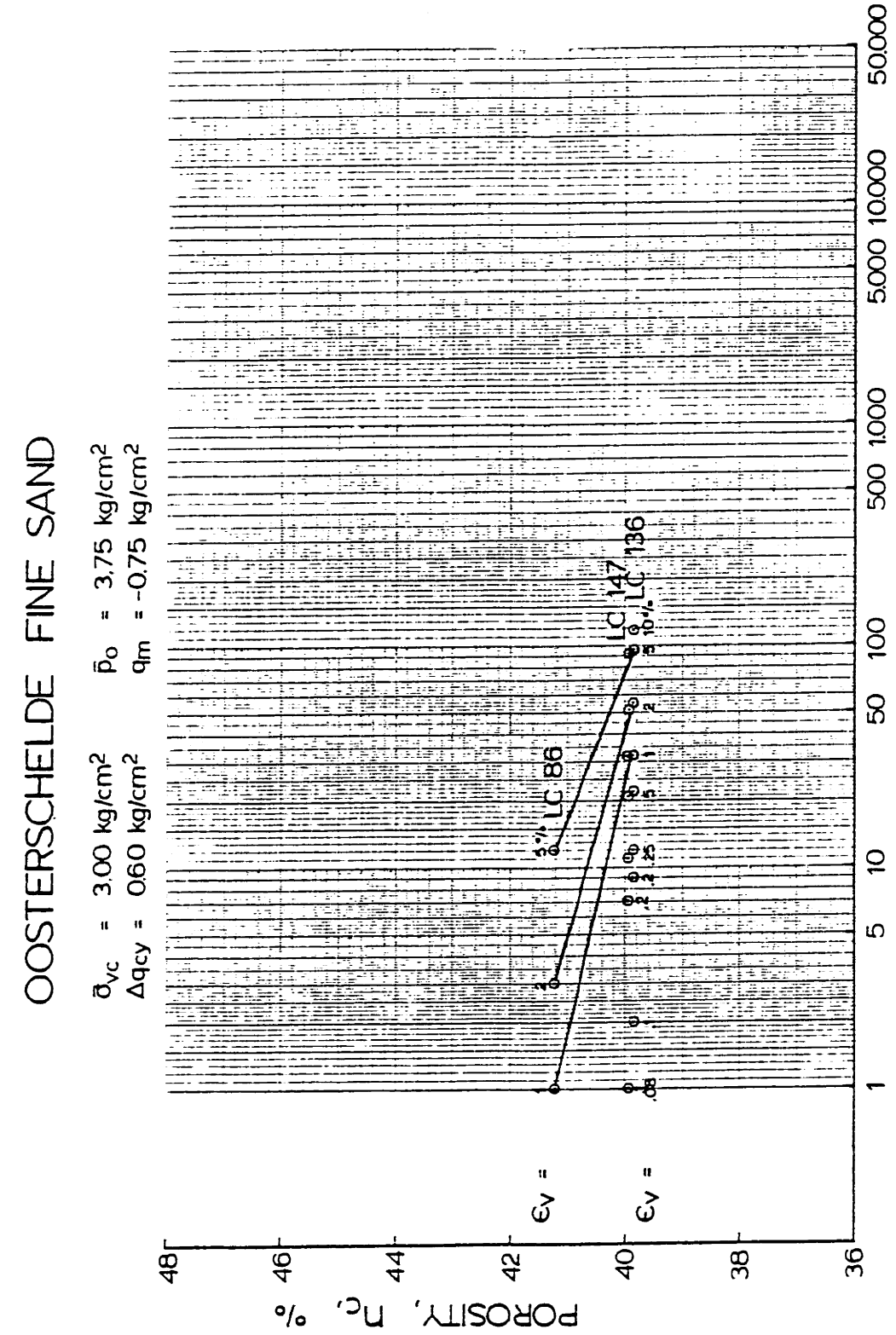

STRAIN CONTOURS FOR EXTENSION CYCLIC TESTS ON SAMPLES AT DIFFERENT POROSITIES

FIGURE E-12

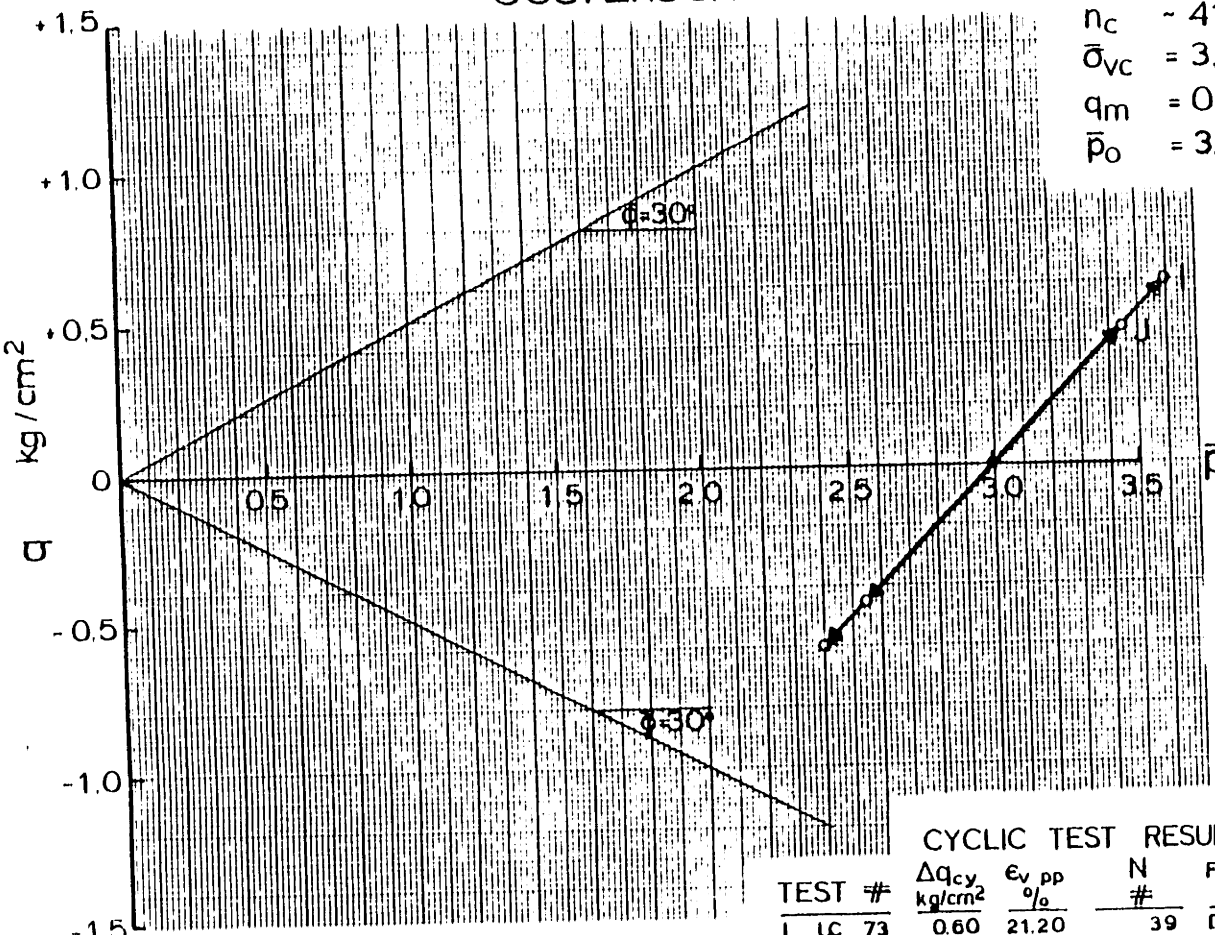

CYCLIC TEST RESULT SUMMARY

TEST #	Δq_{cy} kg/cm²	$\epsilon_{v\,pp}$ %	N #	FAILURE MODE	Nat 5% ϵ_v	Ncorr #	n_c %
I LC 73	0.60	21.20	39	DEF.	34	33	41.2
J LC 83	0.45	18.20	451	DEF.	449	534	41.4

FIGURE E-13

TOTAL STRESS PATHS (TSP-u_B) FOR ISOTROPIC CYCLIC TESTS WITH DIFFERENT CYCLIC SHEAR STRESS RATIO, $\Delta q_{cy}/\bar{p}_o$

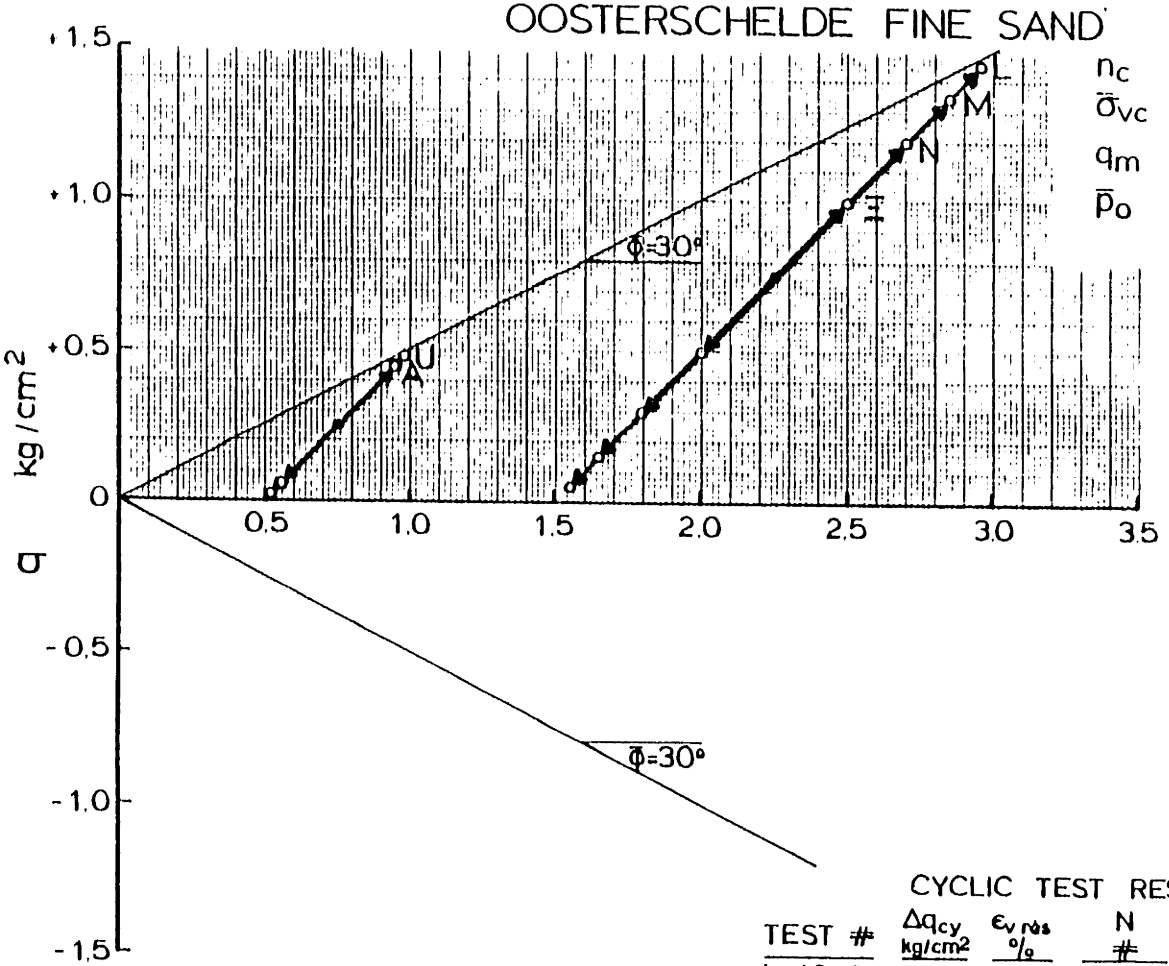

CYCLIC TEST RESULT SUMMARY

TEST #			Δq_{cy} kg/cm²	$\epsilon_{v\,res}$ %	N #	FAILURE MODE	N_{at} 5% ϵ_v	N_{corr} #	n_c %
L	LC	76	0.70	10.80	520	COMPR.	198	185	41.2
M	LC	152	0.60	13.64	3750	COMPR.	950	1342	41.4
N	LC	132	0.45	4.71	9700	COMPR.	~10500	15000	41.4
Ξ	LC	133	0.25	0.11	29790	COMPR.	–	–	41.3
U	LC	140	0.23	13.10	3100	COMPR.	1445	1200	41.1
A	LC	148	0.20	10.18	12000	COMPR.	5405	4740	41.1

TOTAL STRESS PATHS (TSP-u_B) FOR ANISOTROPIC CYCLIC TESTS WITH DIFFERENT CYCLIC SHEAR STRESS RATIO, $\Delta q_{cy}/\bar{p}_o$

FIGURE E-14

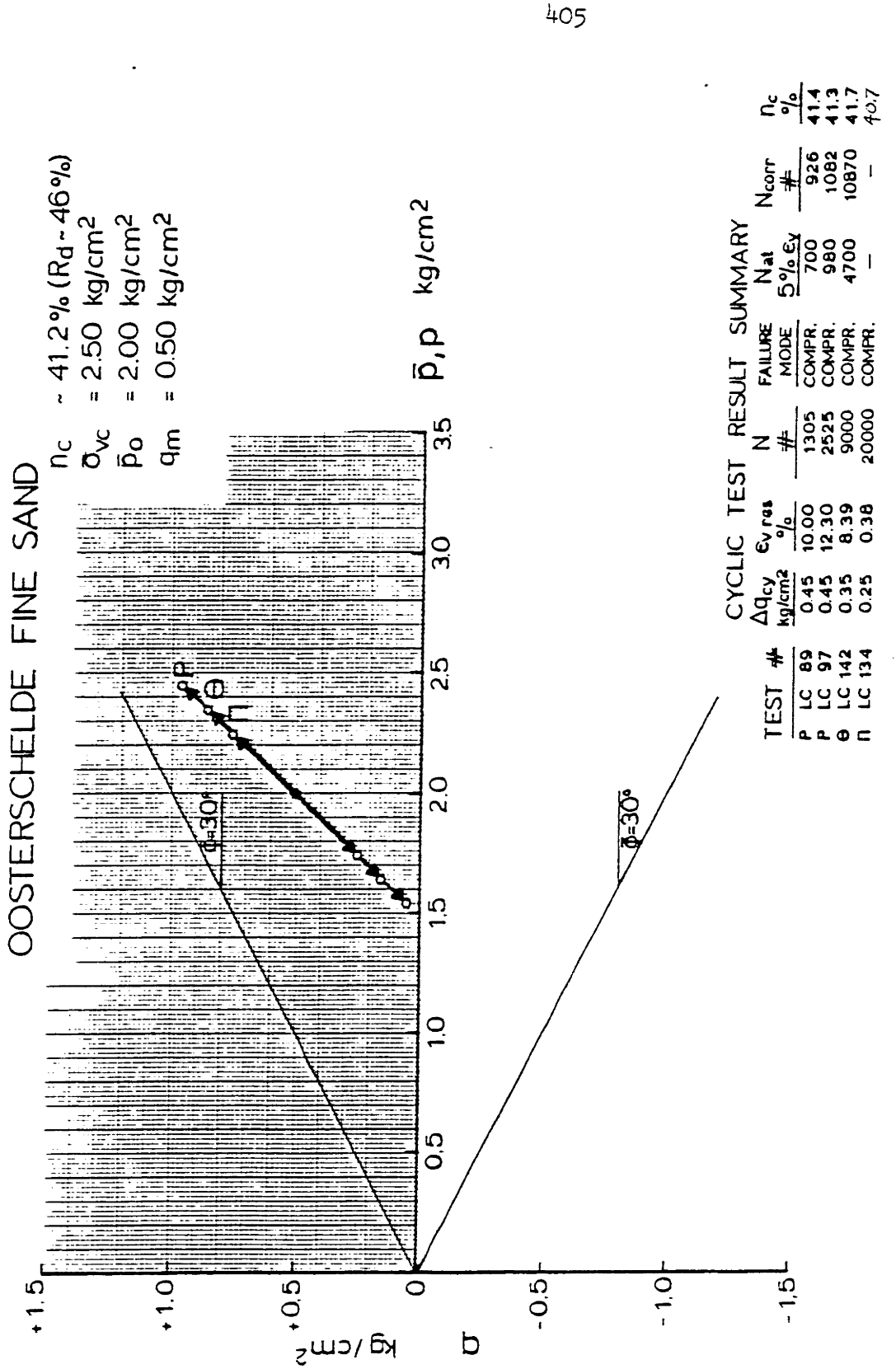

CYCLIC TEST RESULT SUMMARY

TEST #	Δq_{cy} kg/cm²	$\epsilon_{v\,res}$ %	N #	FAILURE MODE	N_{at} 5% ϵ_y	N_{corr} #	n_c %
P LC 89	0.45	10.00	1305	COMPR.	700	926	41.4
P LC 97	0.45	12.30	2525	COMPR.	980	1082	41.3
Θ LC 142	0.35	8.39	9000	COMPR.	4700	10870	41.7
Π LC 134	0.25	0.38	20000	COMPR.	—	—	40.7

TOTAL STRESS PATHS (TSP-u_B) FOR ANISOTROPIC CYCLIC TESTS WITH DIFFERENT CYCLIC SHEAR STRESS RATIO, $\Delta q_{cy}/\bar{p}_o$

FIGURE E-15

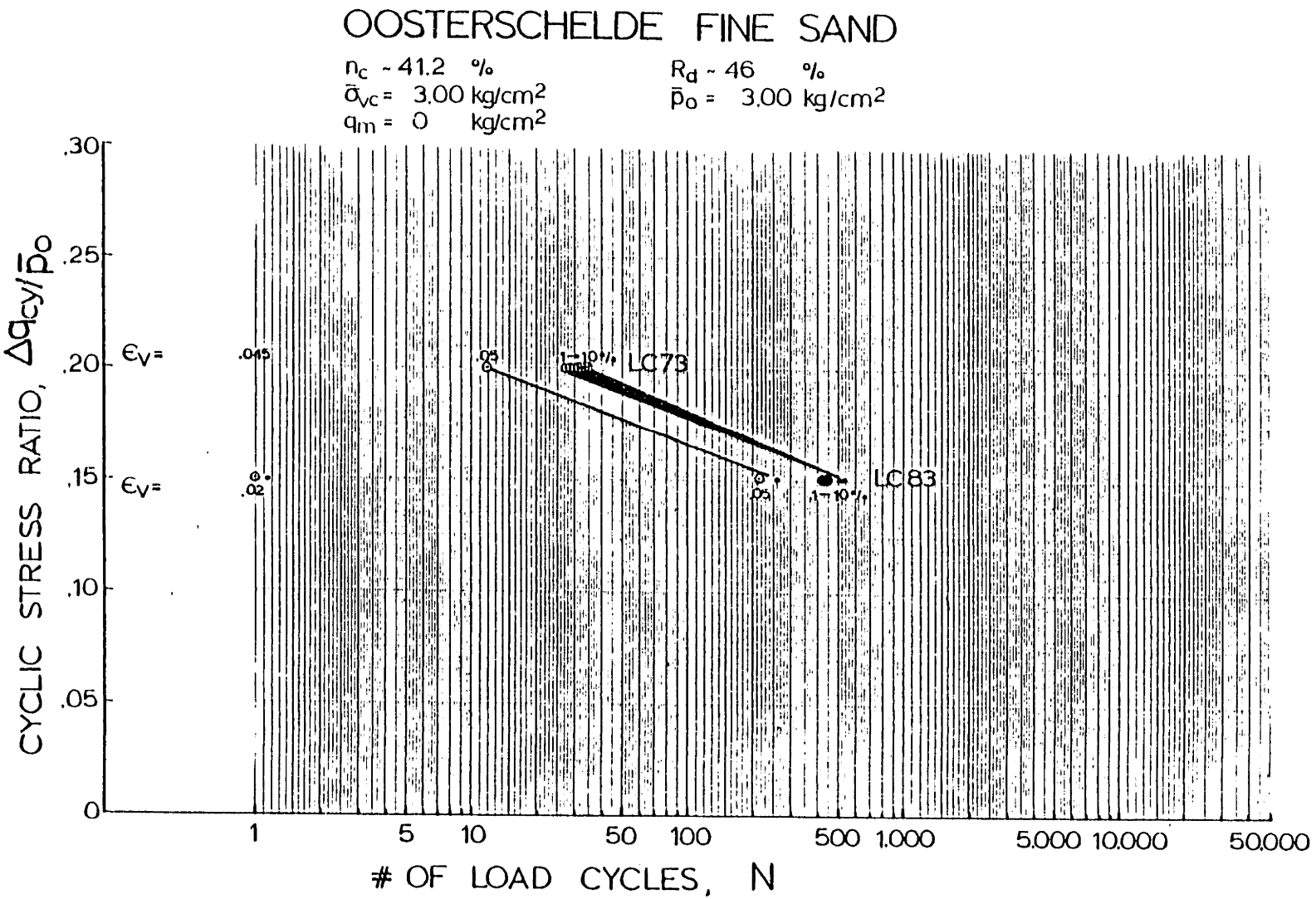

STRAIN CONTOURS FOR ISOTROPIC CYCLIC TESTS ON SAMPLES AT DIFFERENT CYCLIC SHEAR STRESS RATIOS

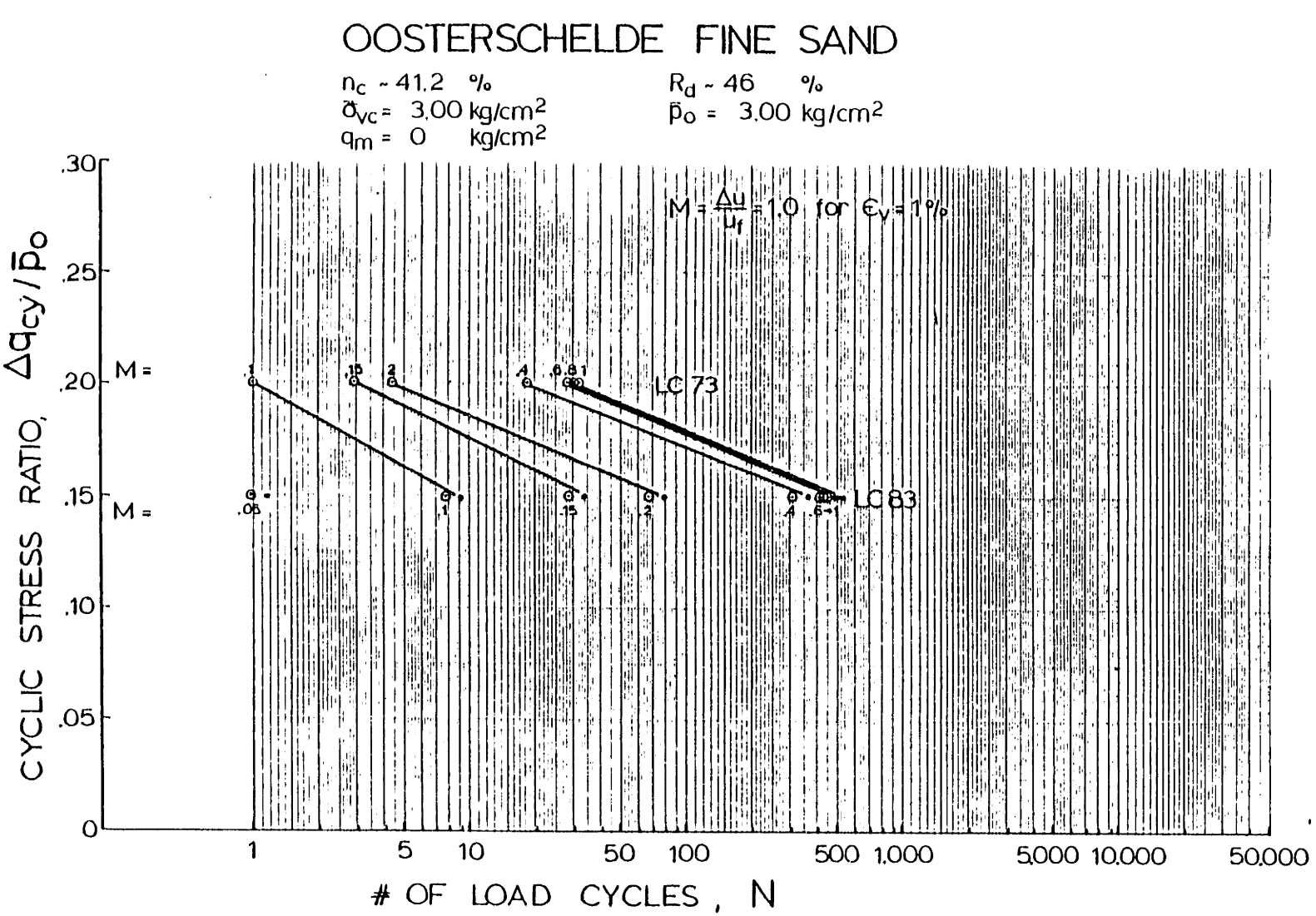

Figure 3-17

PORE PRESSURE CONTOURS FOR ISOTROPIC CYCLIC TESTS ON SAMPLES AT DIFFERENT CYCLIC SHEAR STRESS RATIOS

OOSTERSCHELDE FINE SAND

n_c ~ 41.2 % R_d ~ 46 %

$\bar{\sigma}_{vc}$ = 3.00 kg/cm² $\bar{p}_o$ = 2.25 kg/cm²

q_m = 0.75 kg/cm²

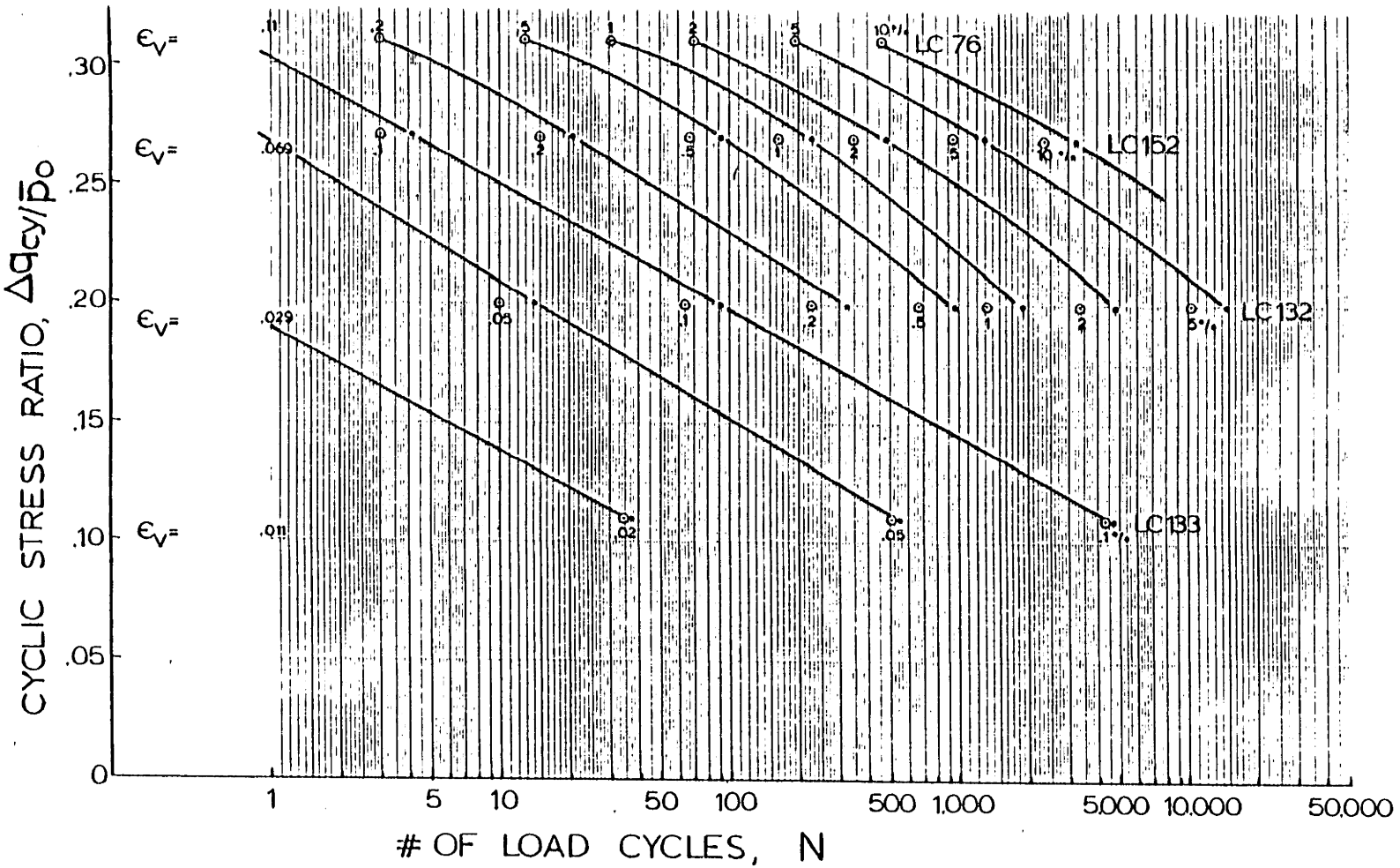

STRAIN CONTOURS FOR COMPRESSION CYCLIC TESTS ON SAMPLES AT DIFFERENT CYCLIC SHEAR STRESS RATIOS

PORE PRESSURE CONTOURS FOR COMPRESSION CYCLIC TESTS ON SAMPLES AT DIFFERENT CYCLIC SHEAR STRESS RATIOS

FIGURE II-19

OOSTERSCHELDE FINE SAND

△	n_c ~ 41.2%	R_d ~ 46%	$\bar{\sigma}_{vc}$ = 1.00 kg/cm²	$\bar{p}_o$ = 0.75 kg/cm²	q_m = 0.25 kg/cm²
⊡ ⊙	n_c ~ 41.2%	R_d ~ 46%	$\bar{\sigma}_{vc}$ = 2.50 kg/cm²	$\bar{p}_o$ = 2.00 kg/cm²	q_m = 0.50 kg/cm²

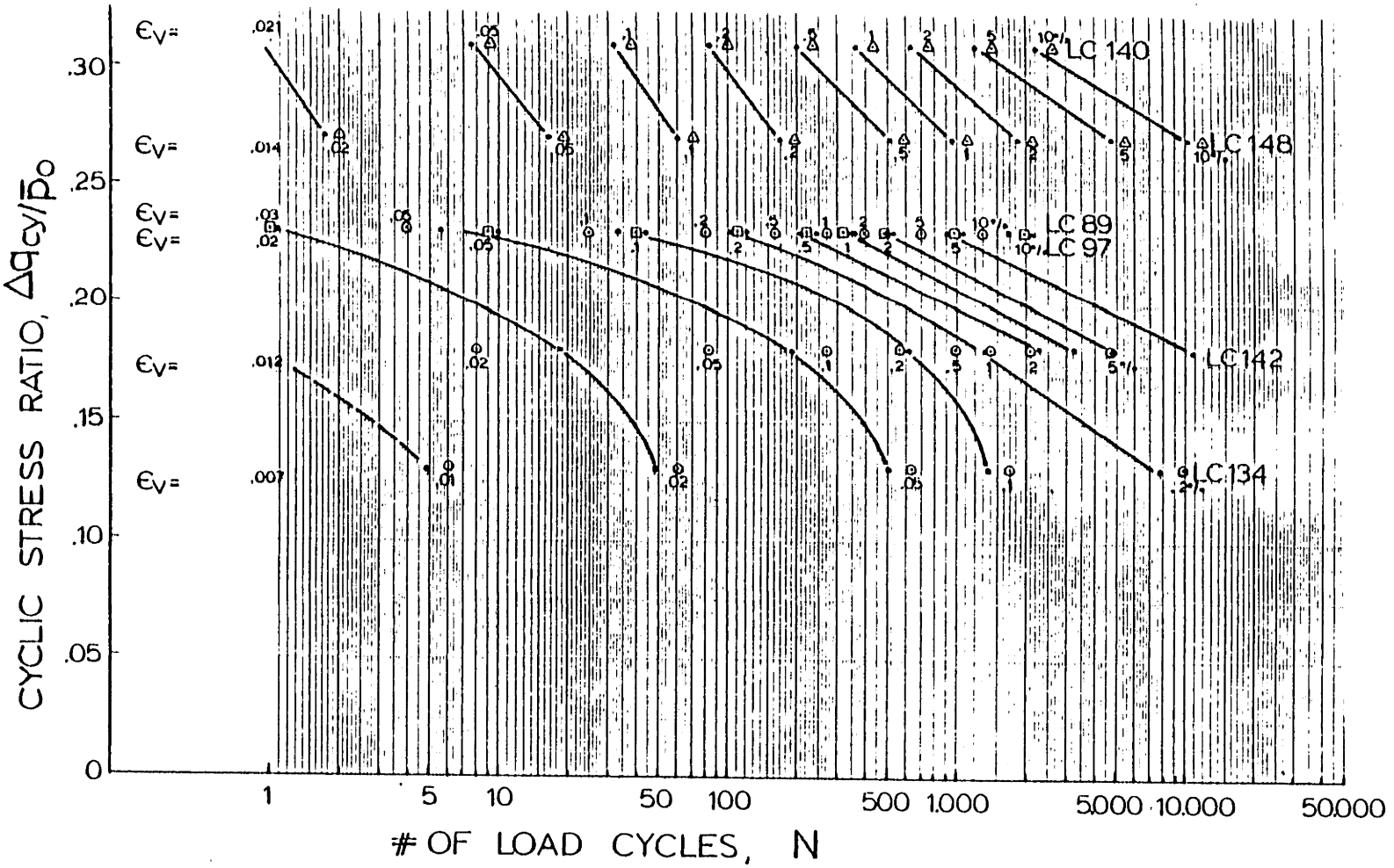

STRAIN CONTOURS FOR COMPRESSION CYCLIC TESTS ON SAMPLES AT DIFFERENT CYCLIC SHEAR STRESS RATIOS

OOSTERSCHELDE FINE SAND

△ n_c ~ 41.2 % R_d ~ 46 % $\bar{\sigma}_{vc}$ = 1.00 kg/cm² $\bar{p}_o$ = 0.75 kg/cm² q_m = 0.25 kg/cm²

⊡ ⊙ n_c ~ 41.2 % R_d ~ 46 % $\bar{\sigma}_{vc}$ = 2.50 kg/cm² $\bar{p}_o$ = 2.00 kg/cm² q_m = 0.50 kg/cm²

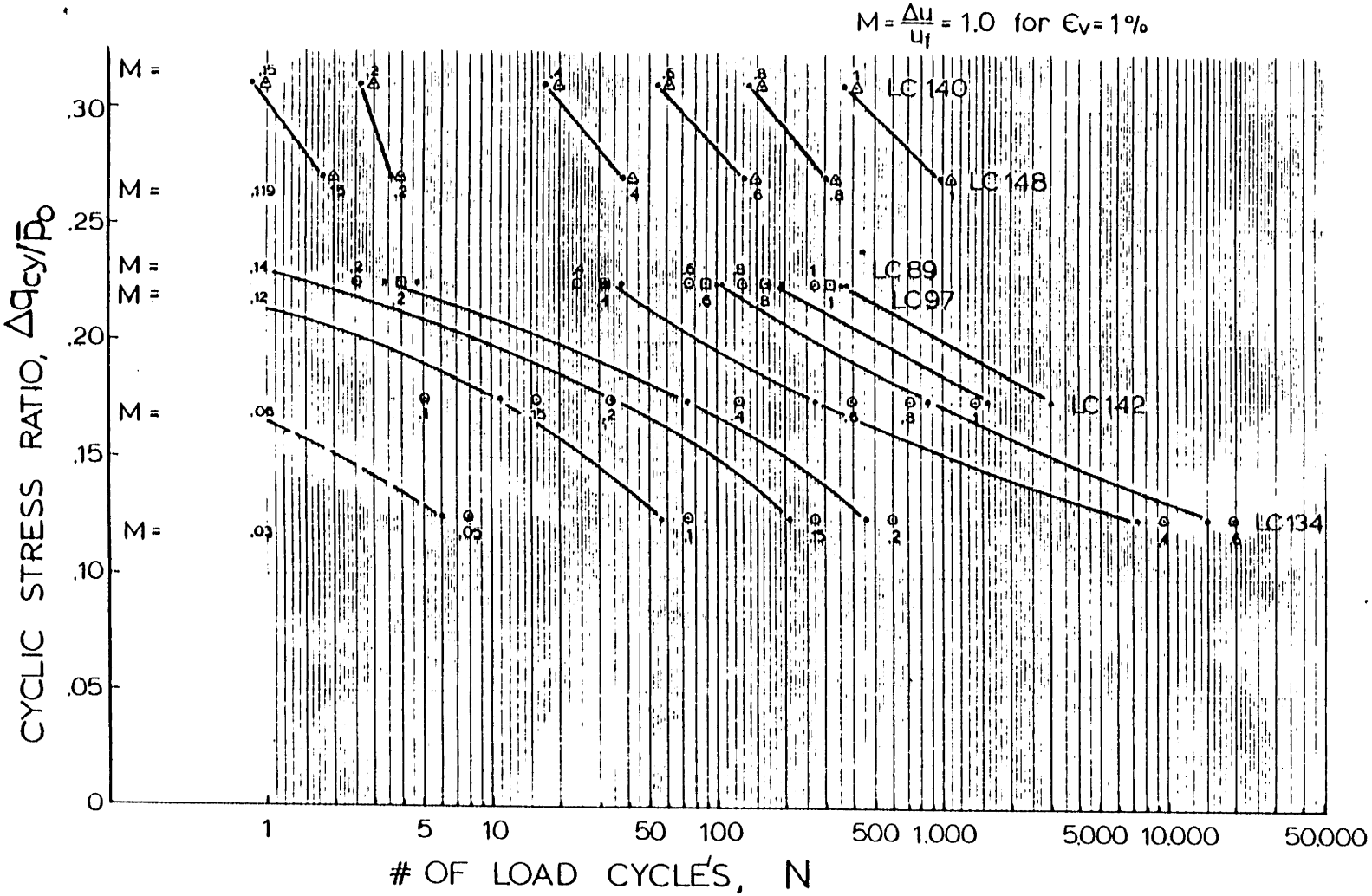

PORE PRESSURE CONTOURS FOR COMPRESSION CYCLIC TESTS ON SAMPLES AT DIFFERENT CYCLIC SHEAR STRESS RATIOS

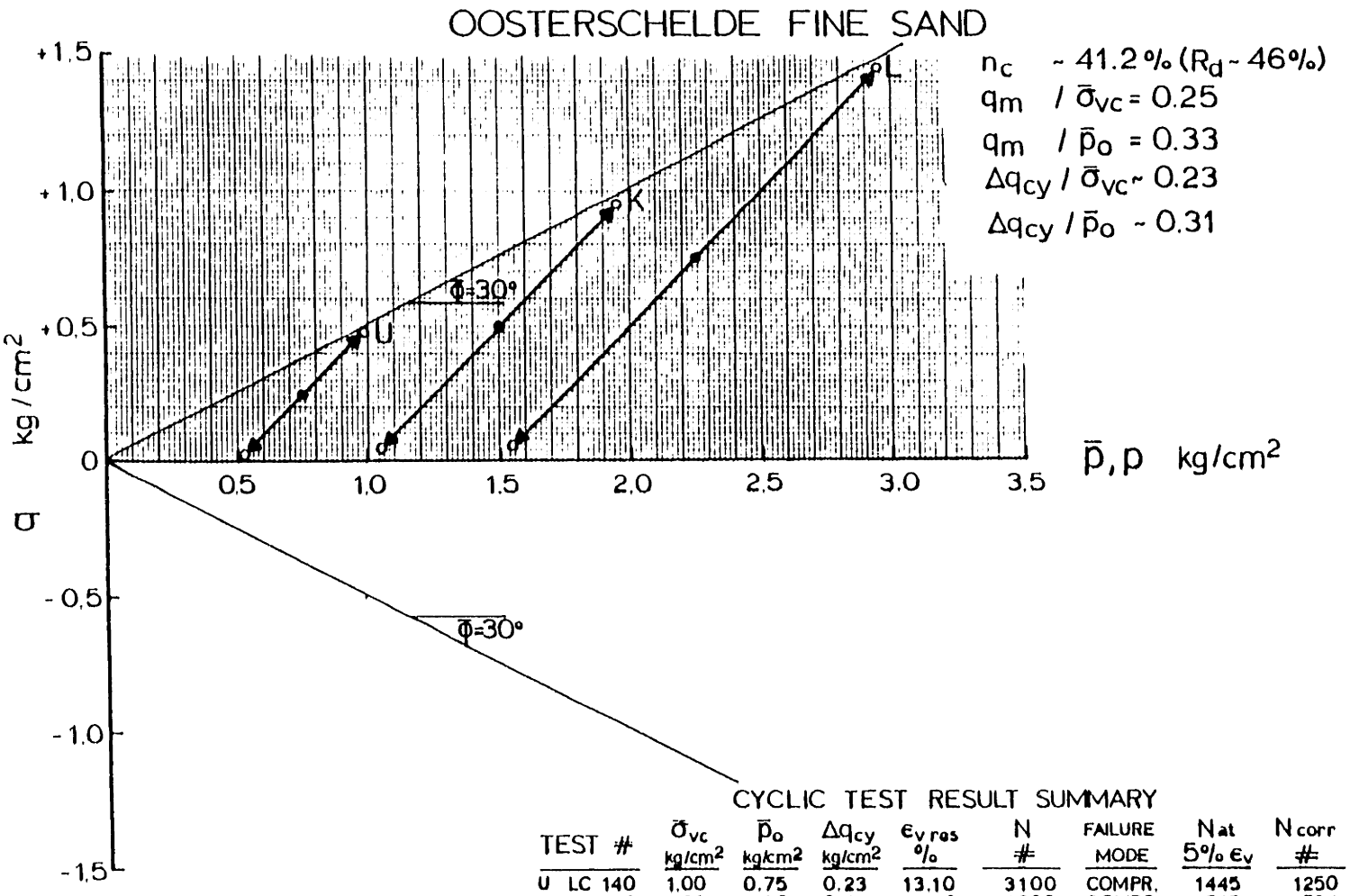

CYCLIC TEST RESULT SUMMARY

TEST #	$\bar{\sigma}_{vc}$ kg/cm²	$\bar{p}_o$ kg/cm²	Δq_{cy} kg/cm²	$\epsilon_{v\,res}$ %	N #	FAILURE MODE	N at 5% ϵ_v	N corr #	n_c %
U LC 140	1.00	0.75	0.23	13.10	3100	COMPR.	1445	1250	41.1
K LC 80	2.00	1.50	0.45	12.60	1700	COMPR.	515	524	41.2
L LC 76	3.00	2.25	0.70	10.80	520	COMPR.	198	185	41.2

TOTAL STRESS PATHS (TSP-u_B) FOR ANISOTROPIC CYCLIC TESTS WITH DIFFERENT MEAN NORMAL STRESS, $\bar{p}_o$

FIGURE E-22

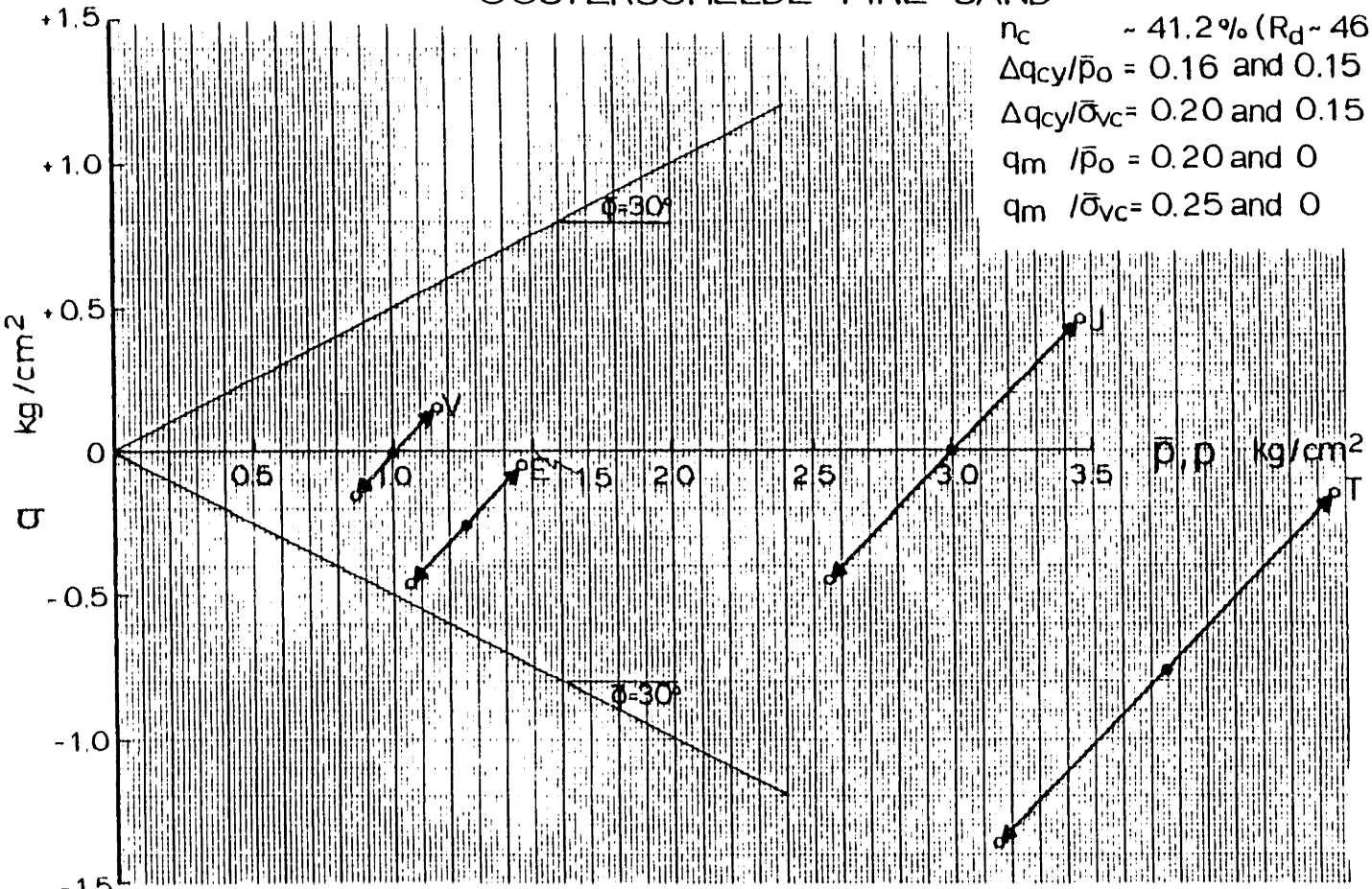

CYCLIC TEST RESULT SUMMARY

TEST	#	$\bar{\sigma}_{vc}$ kg/cm²	K_c –	$\epsilon_{v\ res}$ %	N #	FAILURE MODE	Nat 5% ϵ_v	Ncorr #	n_c %
E LC	74	1.00	1.50	-12.70	110	EXT.	60	77	41.3
T LC	86	3.00	1.50	-8.60	18	EXT.	12	12	41.2
V LC	60	1.00	1.00	12.90*	2712	DEF.	2708	4000	41.5
J LC	83	3.00	1.00	18.20*	451	DEF.	449	534	41.4

*$\epsilon_{v\ pp}$

TOTAL STRESS PATHS (TSP-u_B) FOR CYCLIC TESTS WITH DIFFERENT MEAN NORMAL STRESS, $\bar{p}_o$

FIGURE E-23

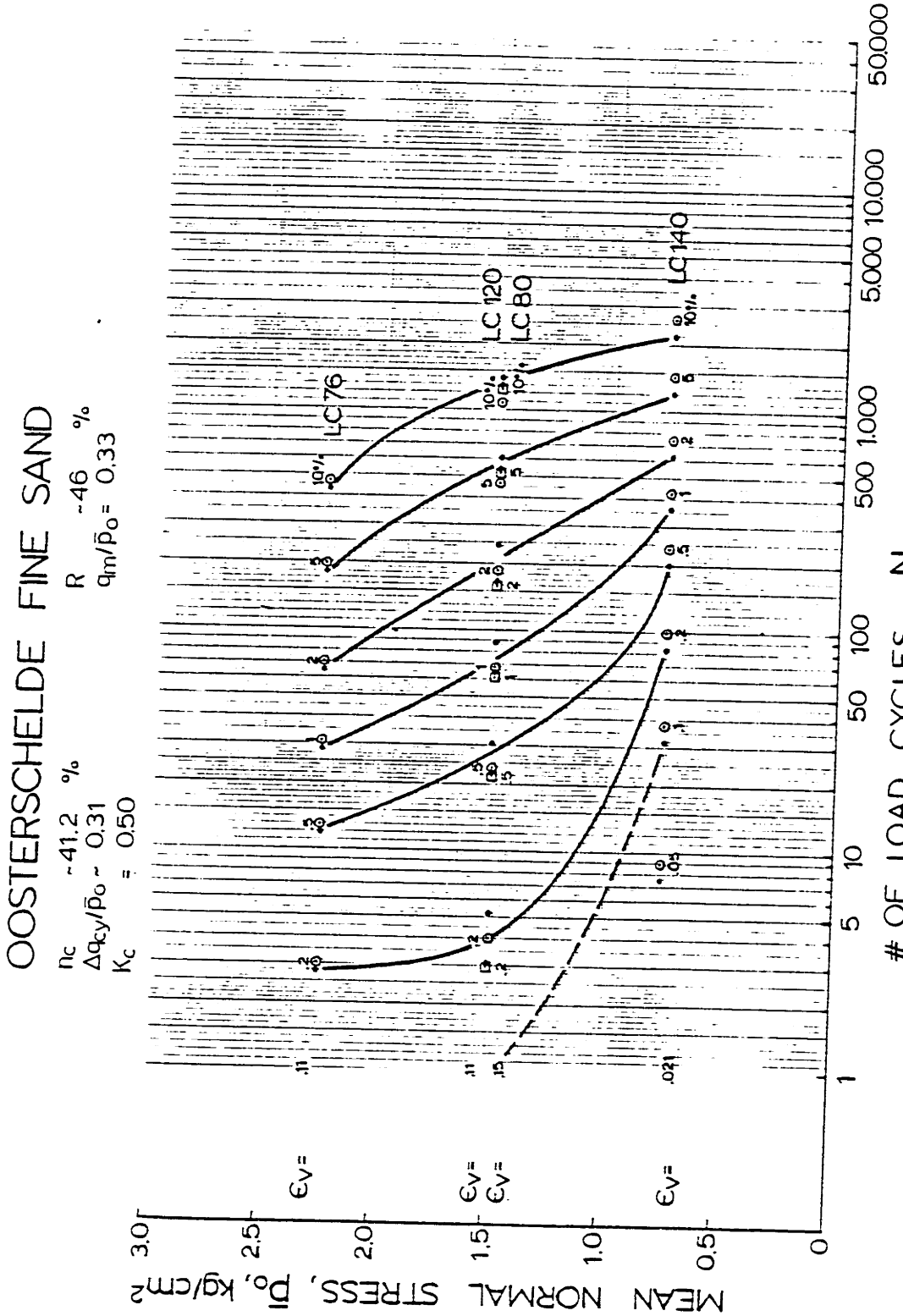

STRAIN CONTOURS FOR COMPRESSION CYCLIC TESTS ON SAMPLES AT DIFFERENT MEAN NORMAL STRESSES

Figure 5-24

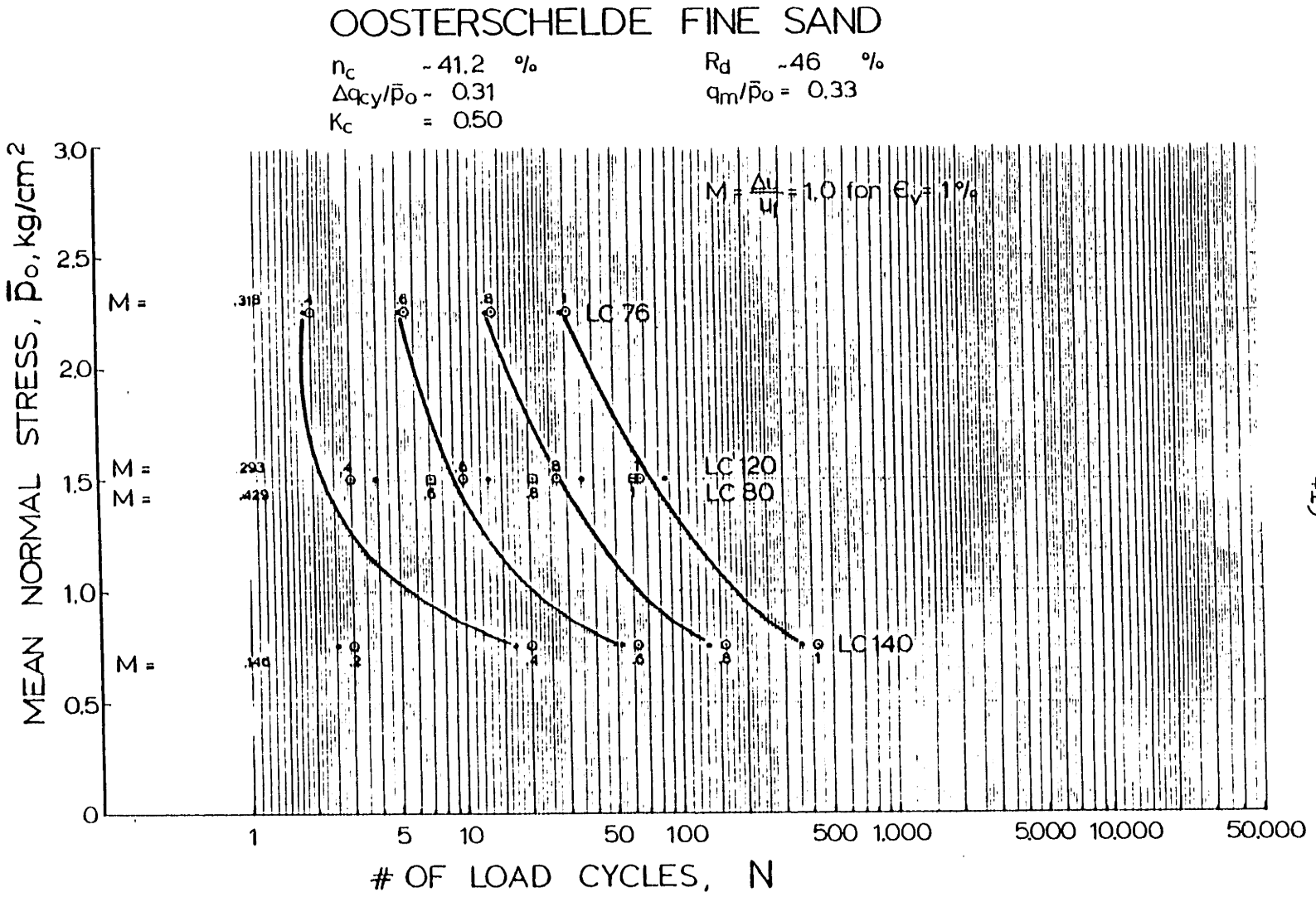

PORE PRESSURE CONTOURS FOR COMPRESSION CYCLIC TESTS ON SAMPLES AT DIFFERENT MEAN NORMAL STRESSES

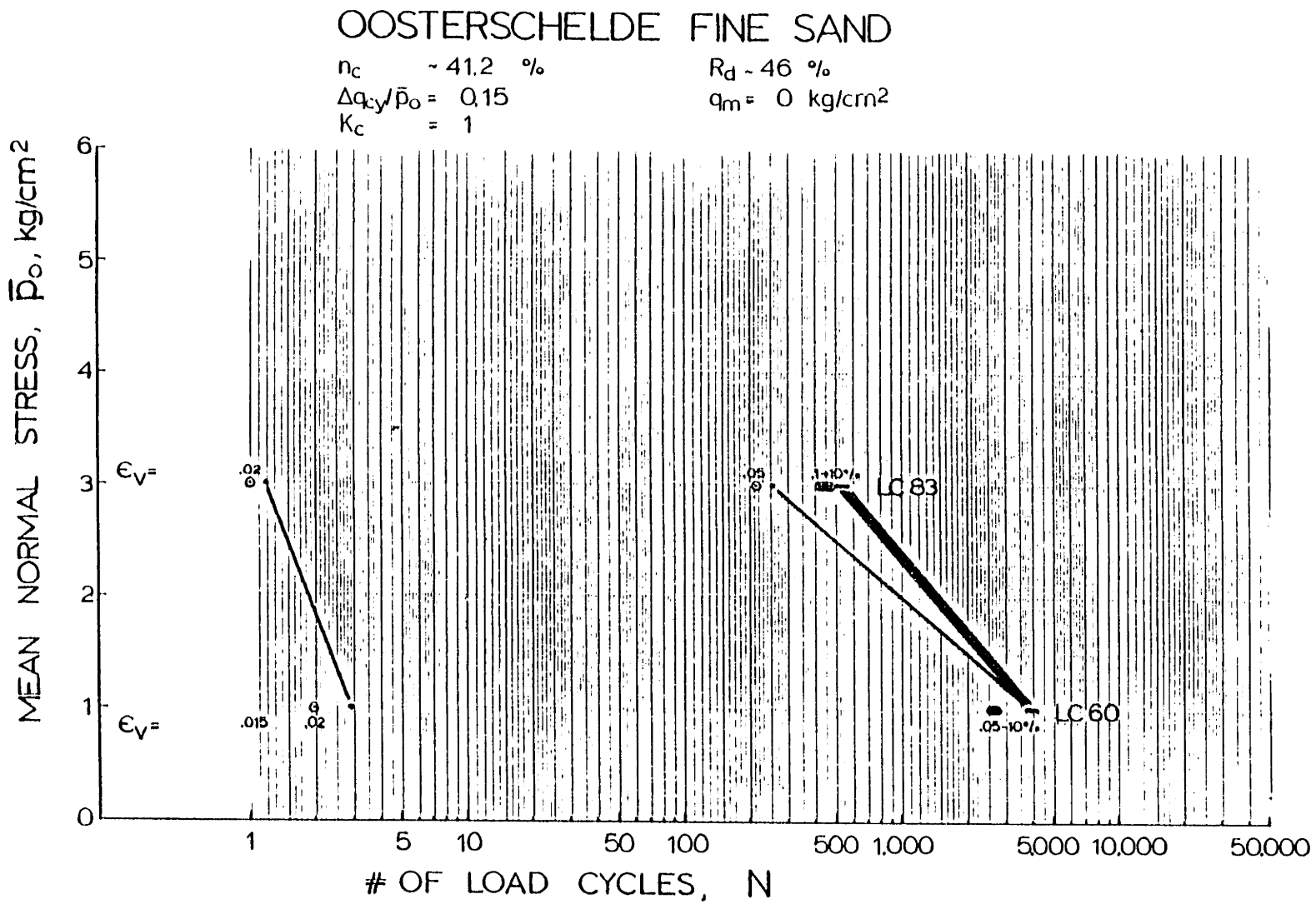

STRAIN CONTOURS FOR ISOTROPIC CYCLIC TESTS ON SAMPLES AT DIFFERENT MEAN NORMAL STRESSES

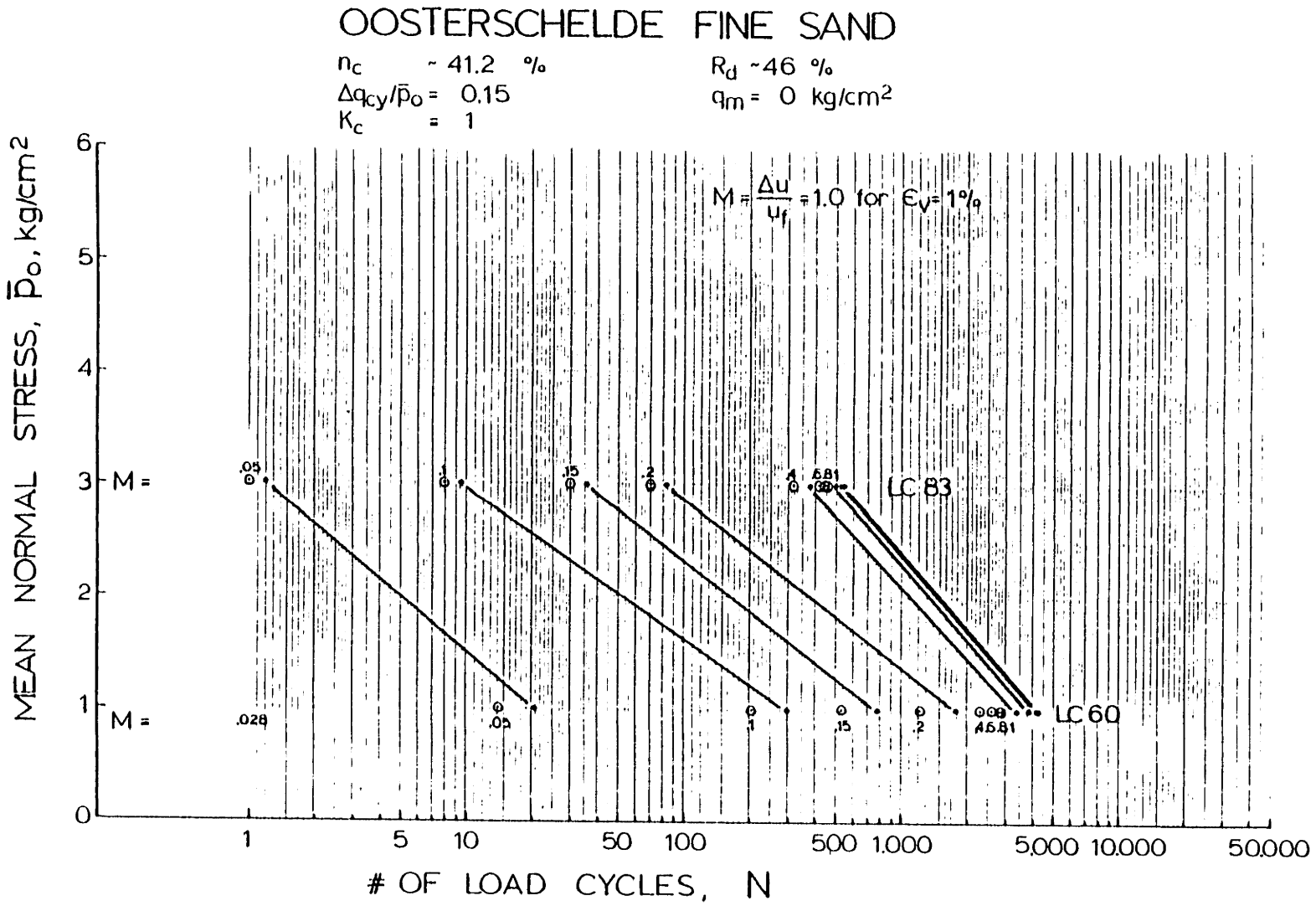

PORE PRESSURE CONTOURS FOR ISOTROPIC CYCLIC TESTS ON SAMPLES AT DIFFERENT MEAN NORMAL STRESSES

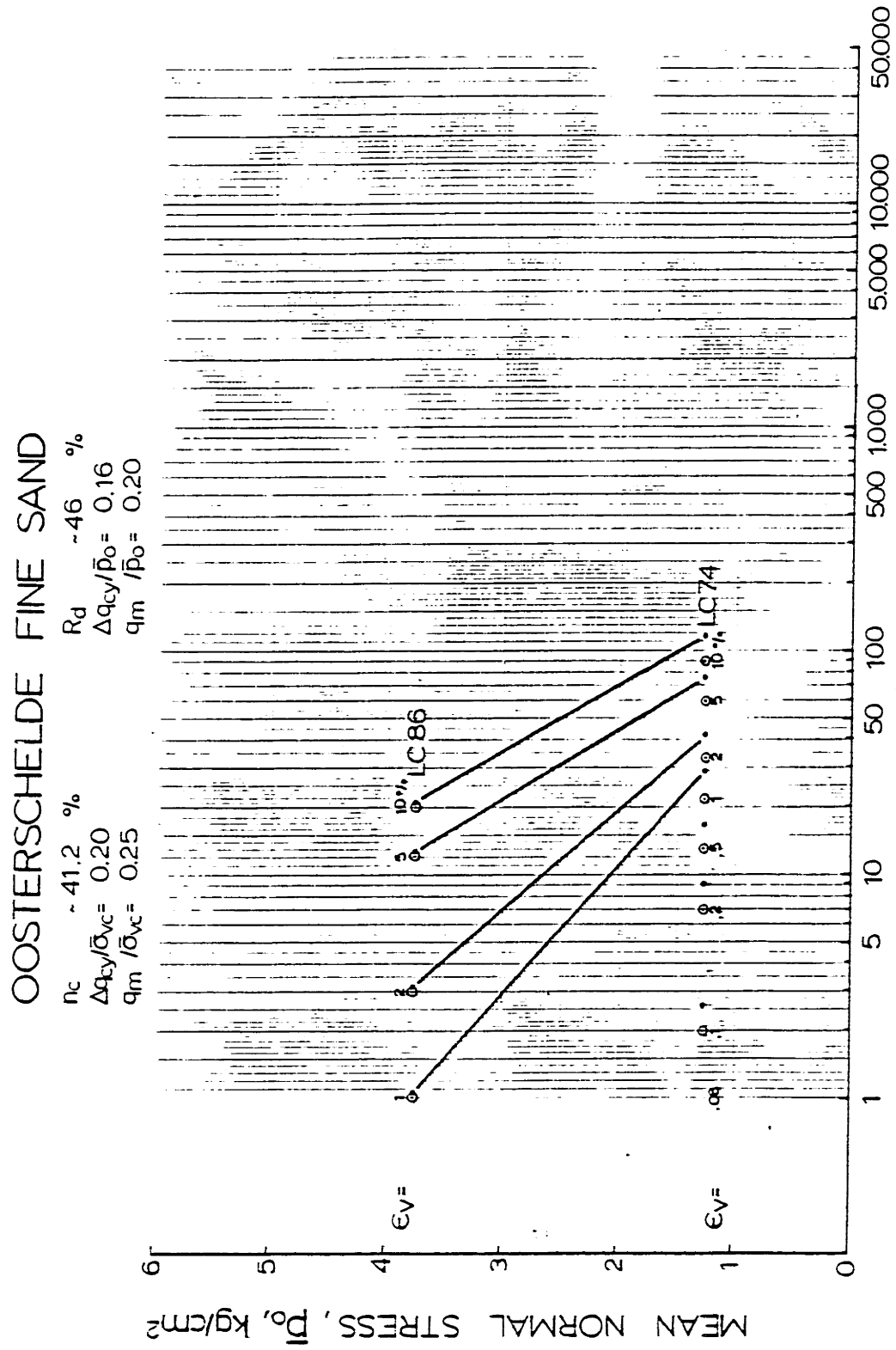

STRAIN CONTOURS FOR EXTENSION CYCLIC TESTS ON SAMPLES AT DIFFERENT MEAN NORMAL STRESSES

FIGURE E-28

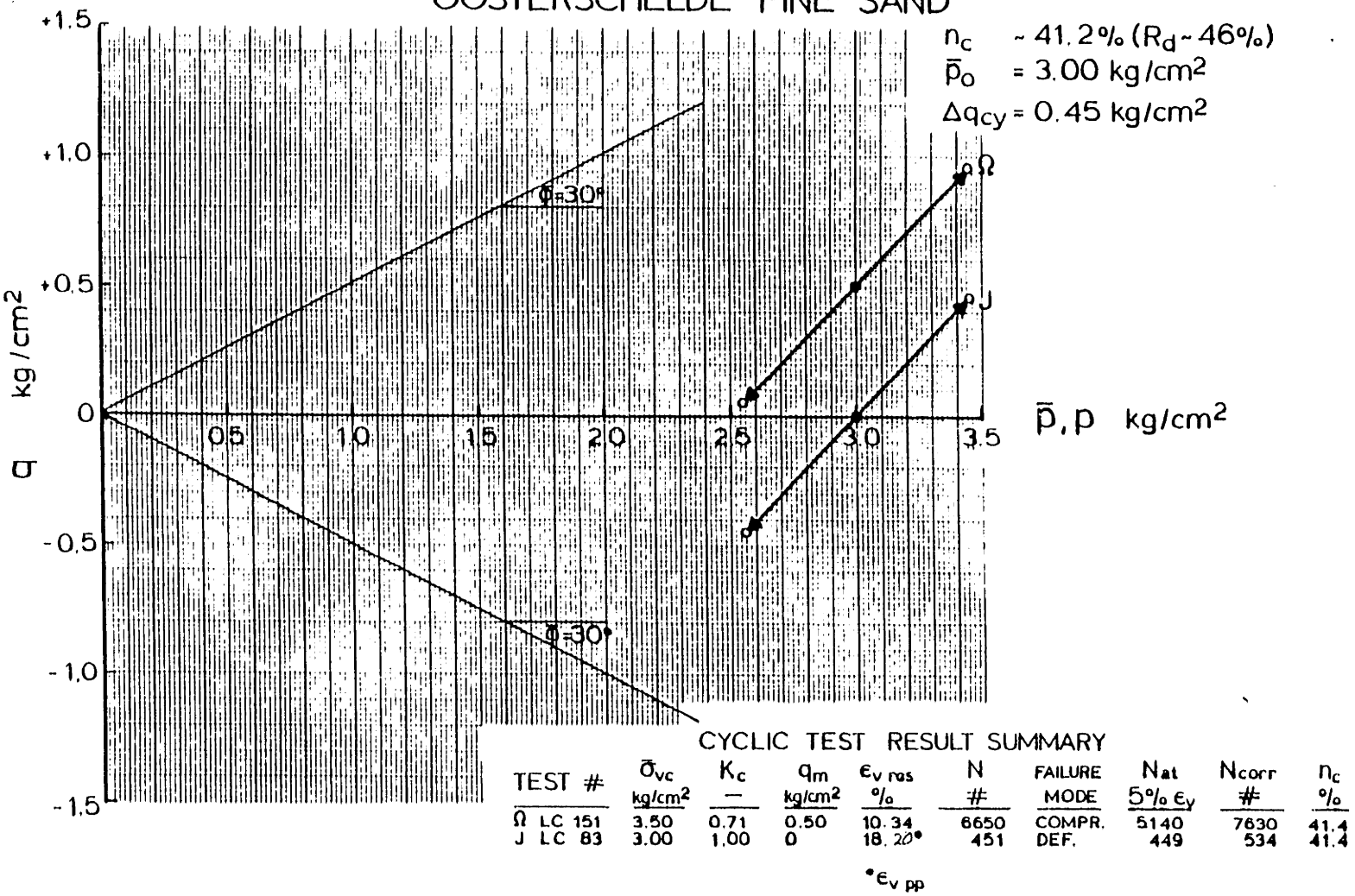

CYCLIC TEST RESULT SUMMARY

TEST #	$\bar{\sigma}_{vc}$ kg/cm²	K_c —	q_m kg/cm²	$\epsilon_{v\ res}$ %	N #	FAILURE MODE	N_{at} 5% ϵ_y	N_{corr} #	n_c %
Ω LC 151	3.50	0.71	0.50	10.34	6650	COMPR.	5140	7630	41.4
J LC 83	3.00	1.00	0	18.20*	451	DEF.	449	534	41.4

*$\epsilon_{v\ pp}$

TOTAL STRESS PATHS (TSP-u_B) FOR CYCLIC TESTS WITH DIFFERENT MEAN SHEAR STRESS, $q_m / \bar{p}_o$

FIGURE E-29

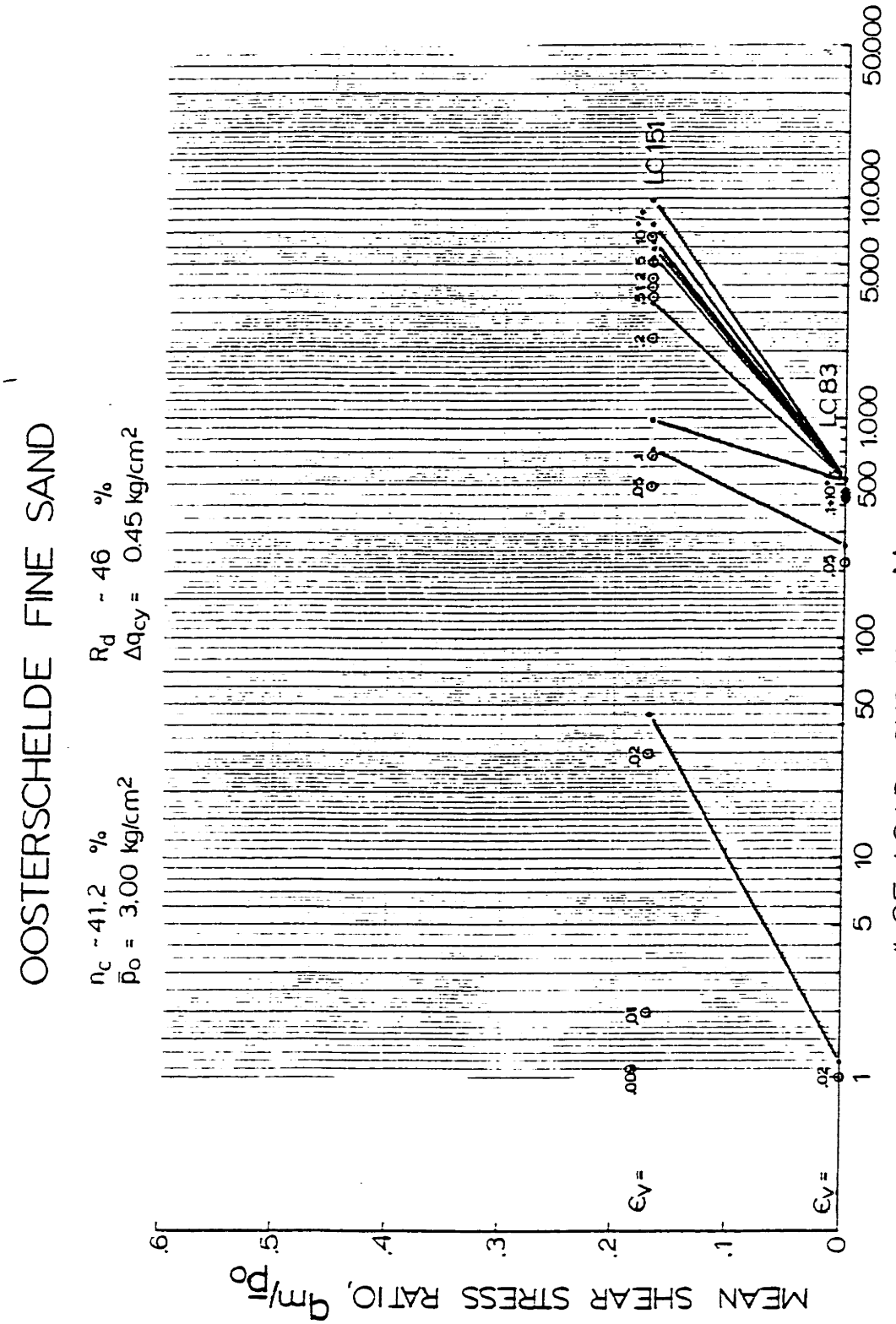

STRAIN CONTOURS FOR CYCLIC TESTS ON SAMPLES AT DIFFERENT MEAN SHEAR STRESS RATIOS

FIGURE II-30

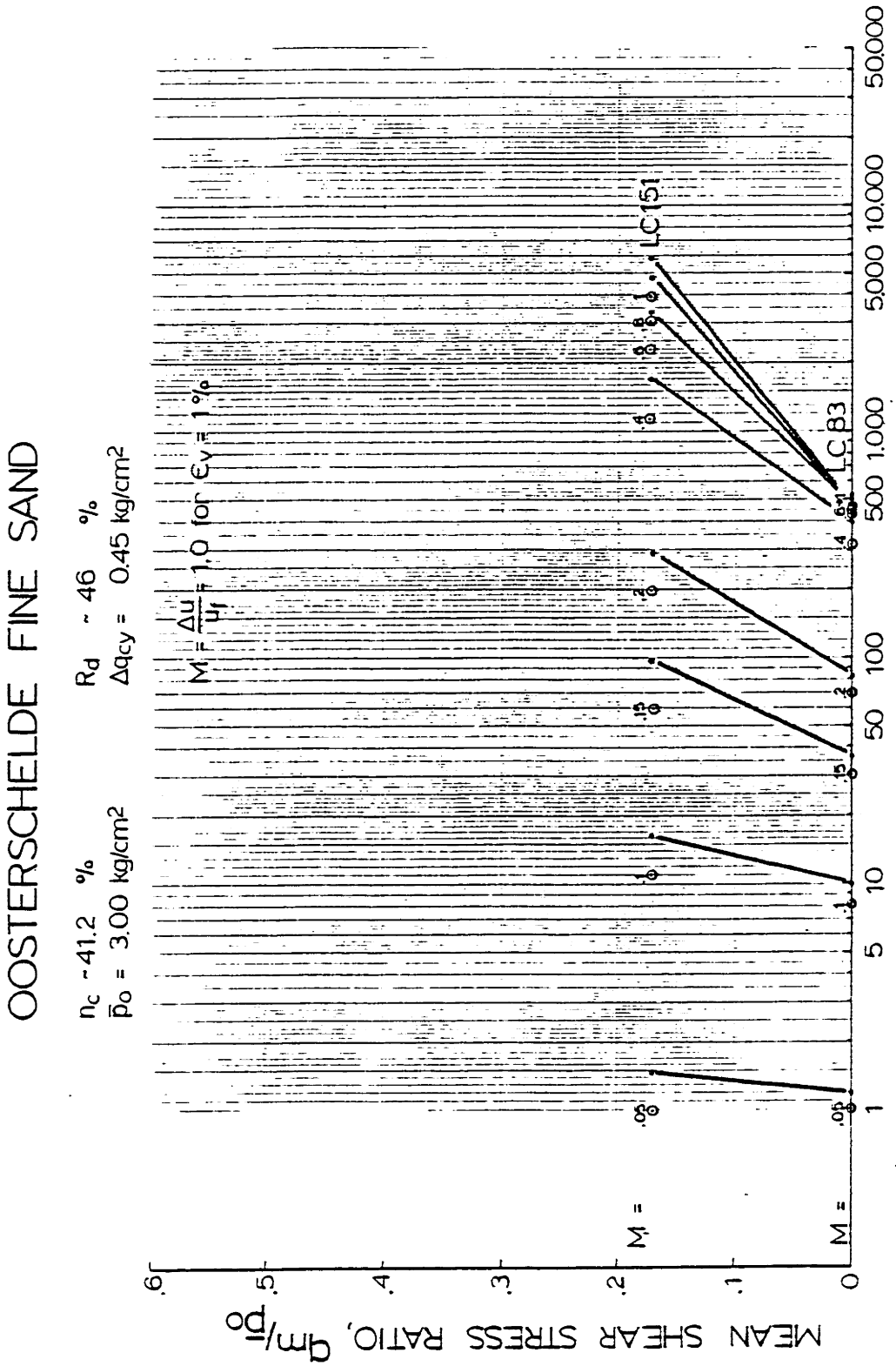

PORE PRESSURE CONTOURS FOR CYCLIC TESTS ON SAMPLES AT DIFFERENT MEAN SHEAR STRESS RATIOS

Figure II-31

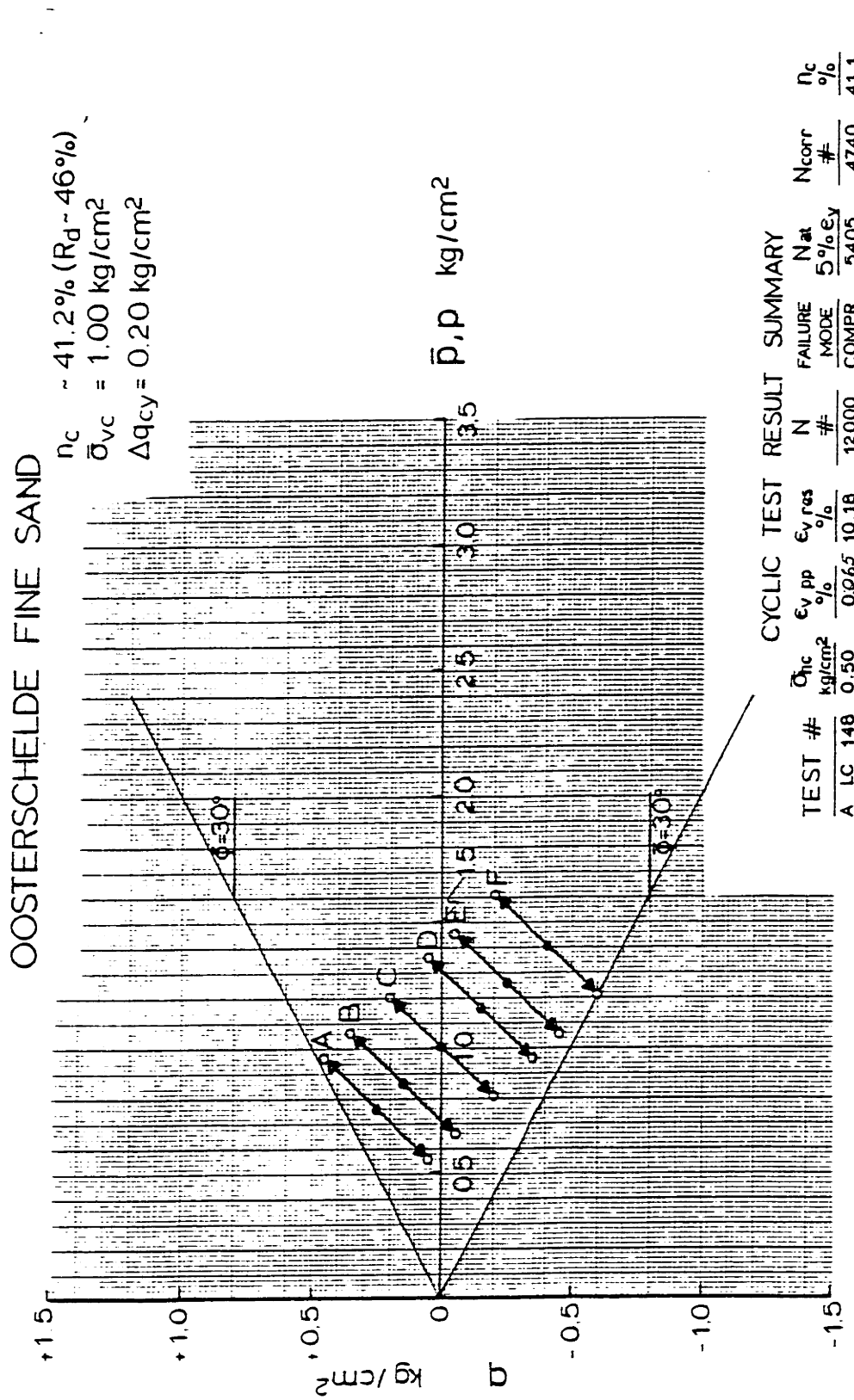

CYCLIC TEST RESULT SUMMARY

TEST #	$\bar{\sigma}_{hc}$ kg/cm²	$\epsilon_{v\,pp}$ %	$\epsilon_{v\,res}$ %	N #	FAILURE MODE	N_{at} 5% ϵ_y	N_{corr} #	n_c %
A LC 148	0.50	0.065	10.18	12000	COMPR.	5405	4740	41.1
B LC 75	0.70	12.60	0.85	421	DEF.	419	256	40.9
C LC 138	1.00	14.14	-1.35	260	DEF.	259	334	41.4
D LC 71	1.30	17.00	-3.03	86	DEF.	83	89	41.2
E LC 74	1.50	1.20	-12.70	110	EXT.	60	77	41.3
F LC 79	1.80	0.21	-8.40	160	EXT.	92	95	41.2

TOTAL STRESS PATHS (TSP-u_B) FOR CYCLIC TESTS WITH DIFFERENT CONSOLIDATION STRESS RATIO, $K_c = \bar{\sigma}_{hc}/\bar{\sigma}_{vc}$

FIGURE E-32

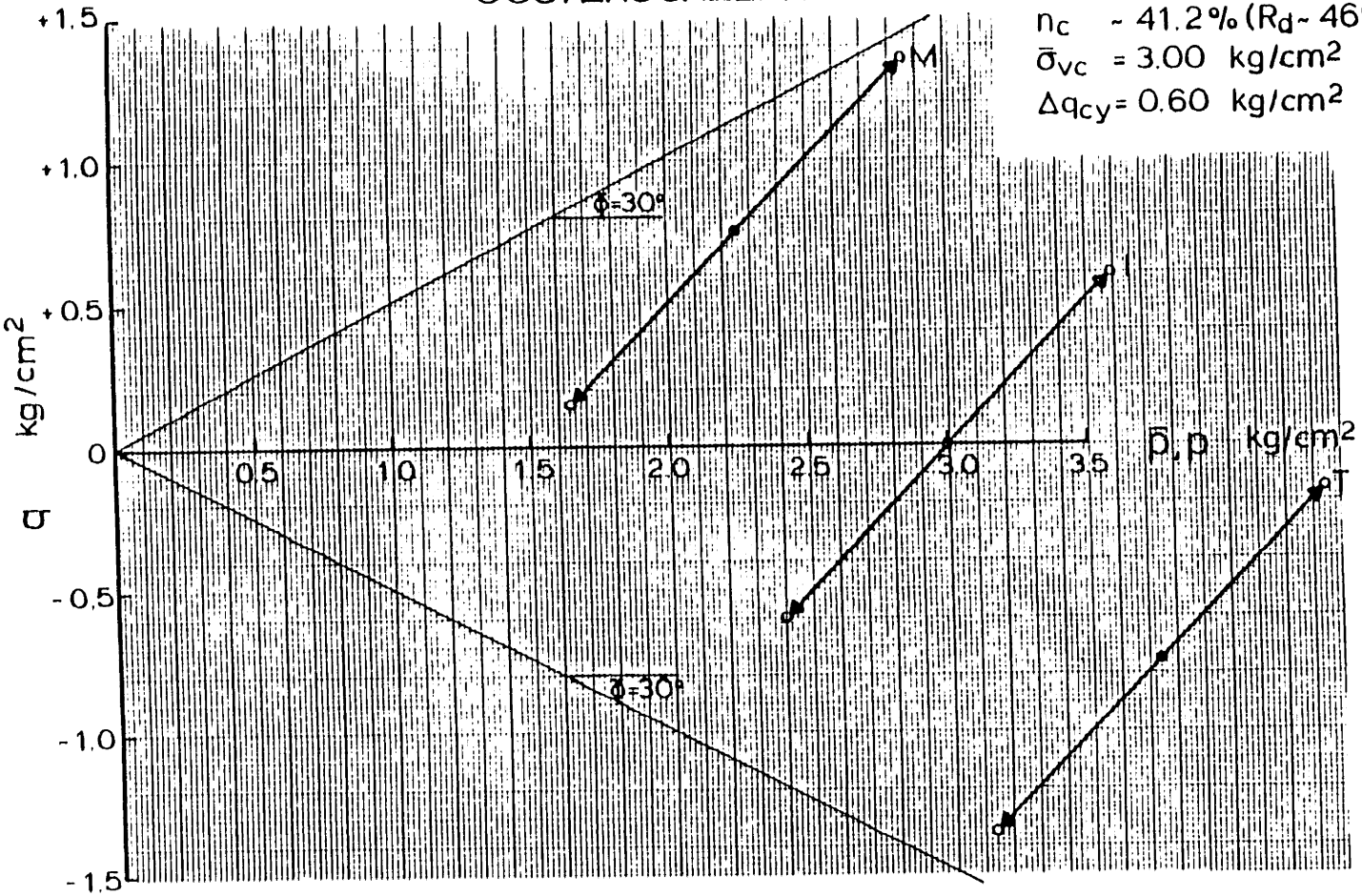

CYCLIC TEST RESULT SUMMARY

TEST #	K_c –	$\varepsilon_{v\,pp}^{cgs}$ %	N #	FAILURE MODE	N_{at} 5% ε_v	N_{corr} #	n_c %
M LC 152	0.50	13.64	3750	COMPR.	950	1342	41.4
I LC 73	1.00	21.20	39	DEF.	34	33	41.2
T LC 86	1.50	-8.60	18	EXT.	12	12	41.2

TOTAL STRESS PATHS (TSP-u_B) FOR CYCLIC TESTS WITH DIFFERENT CONSOLIDATION STRESS RATIO, $K_c = \bar{\sigma}_{hc}/\bar{\sigma}_{vc}$

FIGURE E-32

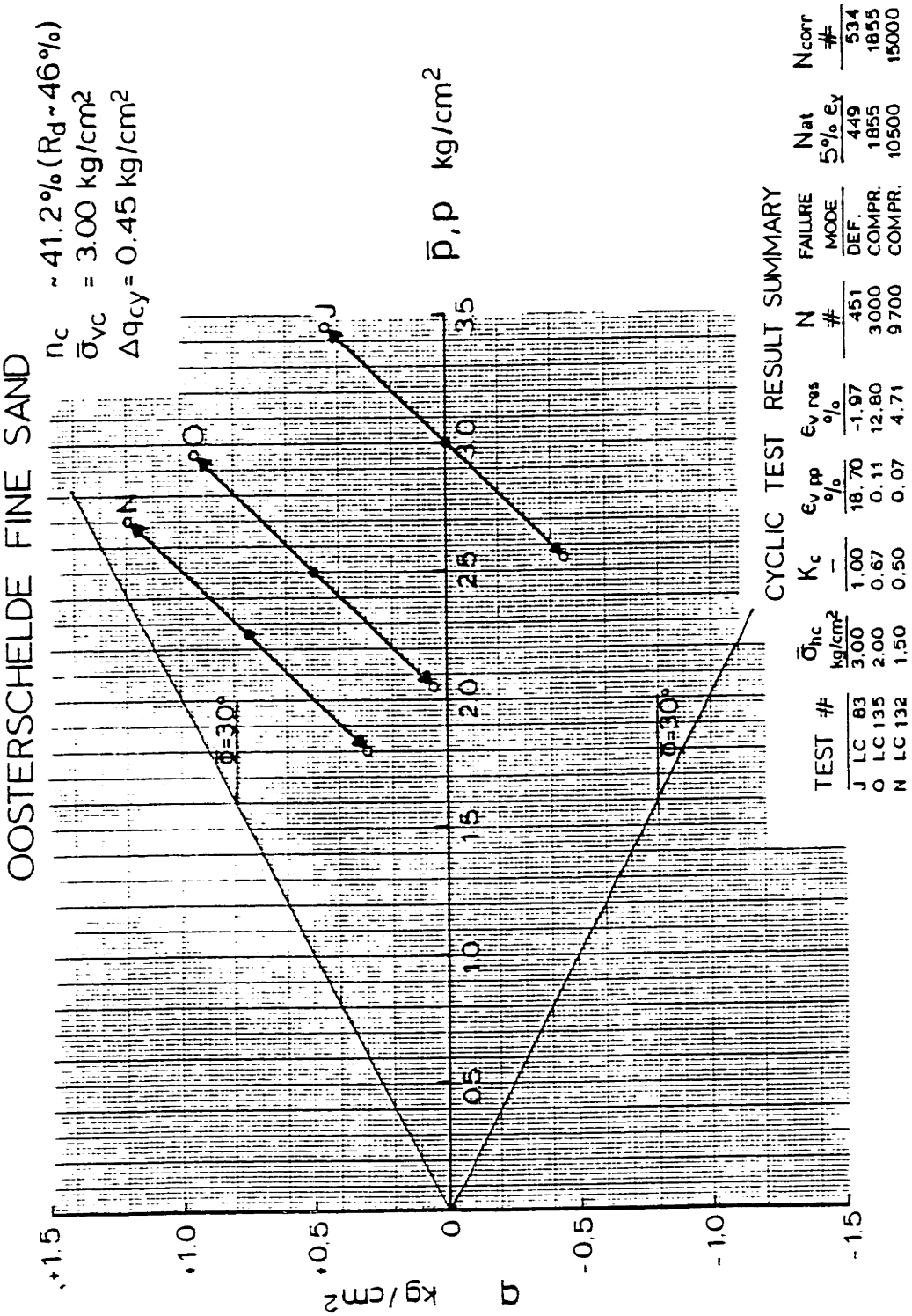

CYCLIC TEST RESULT SUMMARY

TEST #	$\bar{\sigma}_{hc}$ kg/cm²	K_c –	$\epsilon_{v\,pp}$ %	$\epsilon_{v\,res}$ %	N #	FAILURE MODE	Nat 5% ϵ_y	N_{corr} #	n_c %
J LC 83	3.00	1.00	18.70	-1.97	451	DEF.	449	534	41.4
O LC 135	2.00	0.67	0.11	12.80	3000	COMPR.	1855	1855	41.2
N LC 132	1.50	0.50	0.07	4.71	9700	COMPR.	10500	15000	41.4

TOTAL STRESS PATHS (TSP-u_B) FOR CYCLIC TESTS
WITH DIFFERENT CONSOLIDATION STRESS RATIO, $K_c = \bar{\sigma}_{hc}/\bar{\sigma}_{vc}$

FIGURE E-34

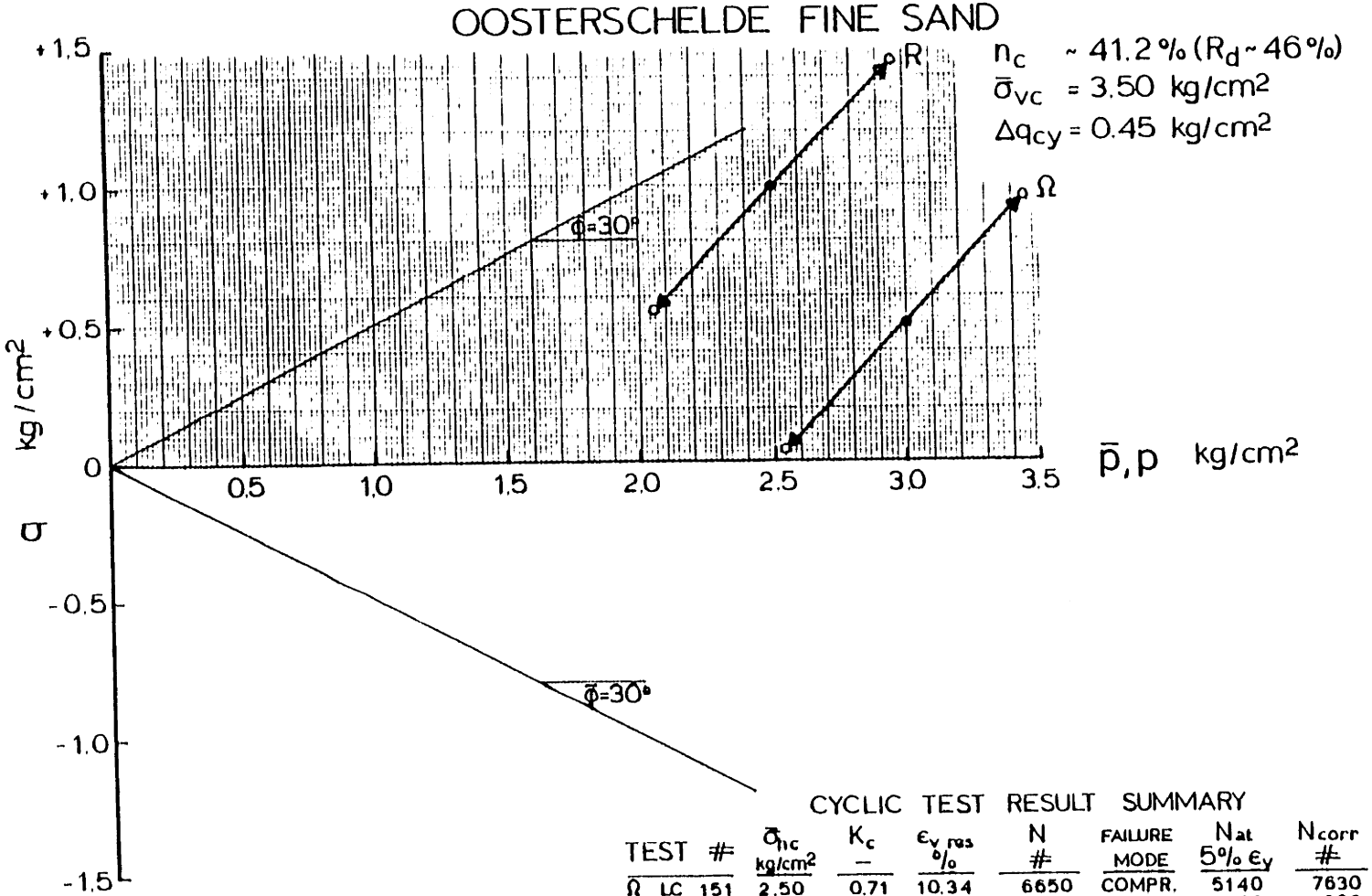

CYCLIC TEST RESULT SUMMARY

TEST #	$\bar{\sigma}_{hc}$ kg/cm²	K_c —	$\epsilon_{v\,res}$ %	N #	FAILURE MODE	N_{at} 5% ϵ_y	N_{corr} #	n_c %
Ω LC 151	2.50	0.71	10.34	6650	COMPR.	5140	7630	41.4
R LC 137	1.50	0.43	4.33	29120	COMPR.	~36500	43000	41.3

FIGURE E-35

TOTAL STRESS PATHS (TSP-u_B) FOR ANISOTROPIC CYCLIC TESTS WITH DIFFERENT CONSOLIDATION STRESS RATIO, $K_c = \bar{\sigma}_{hc}/\bar{\sigma}_{vc}$

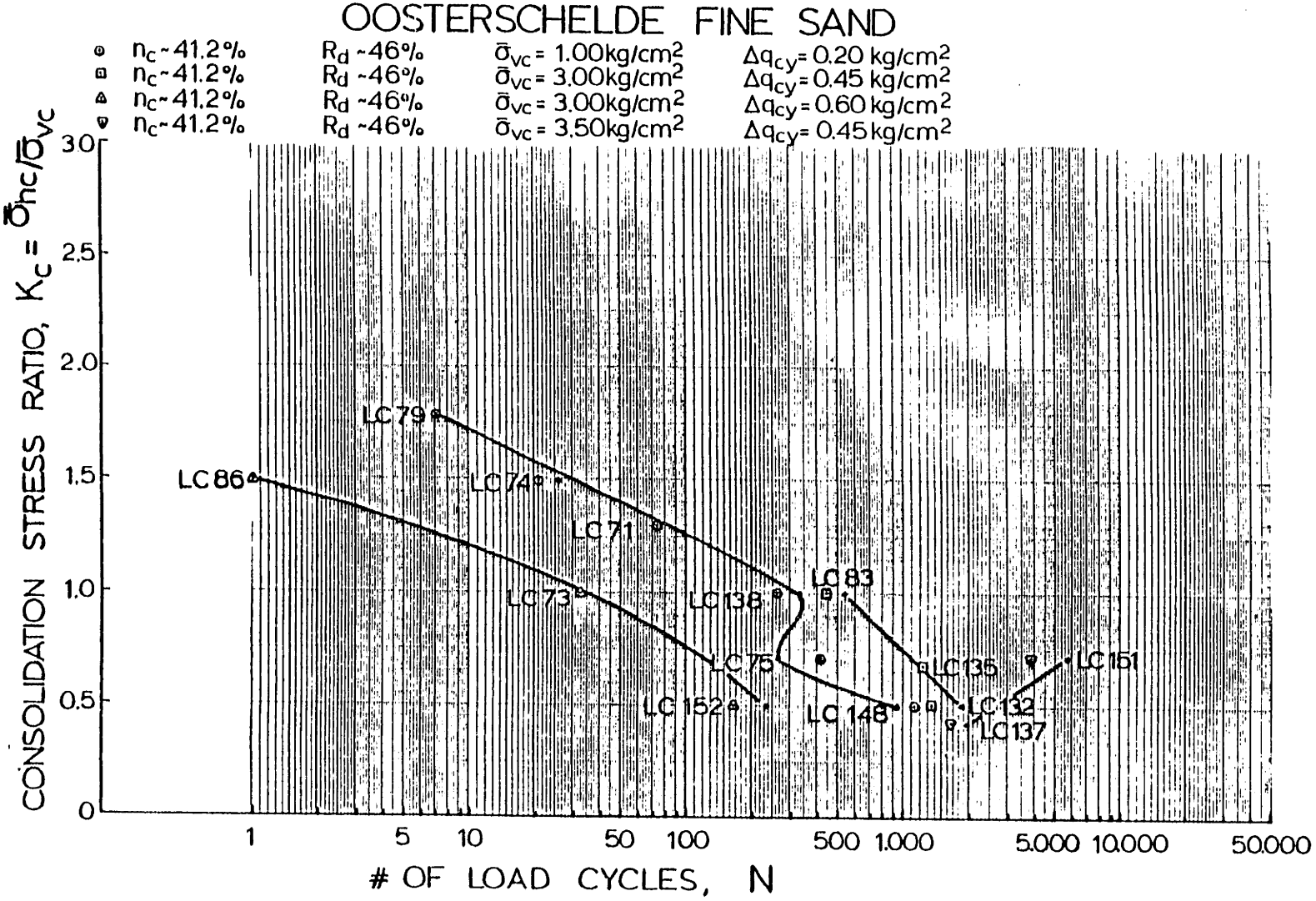

INFLUENCE OF CONSOLIDATION STRESS RATIO ON NUMBER OF LOAD CYCLES TO REACH 1% VERTICAL STRAIN IN CYCLIC TRIAXIAL TESTS WITH CONSTANT VERTICAL CONSOLIDATION STRESSES

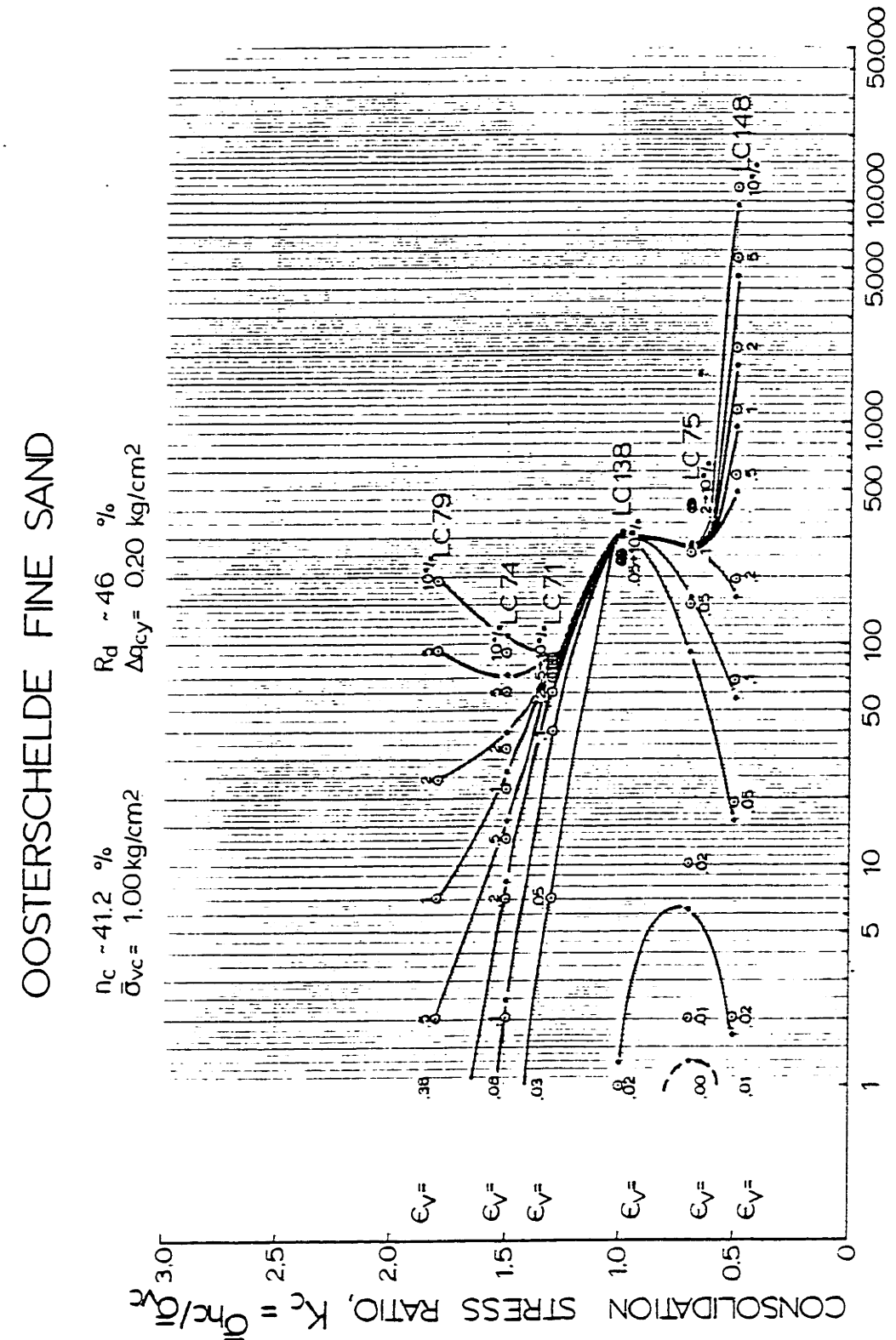

STRAIN CONTOURS FOR CYCLIC TESTS ON SAMPLES AT DIFFERENT CONSOLIDATION STRESS RATIOS

FIGURE II-37

OOSTERSCHELDE FINE SAND

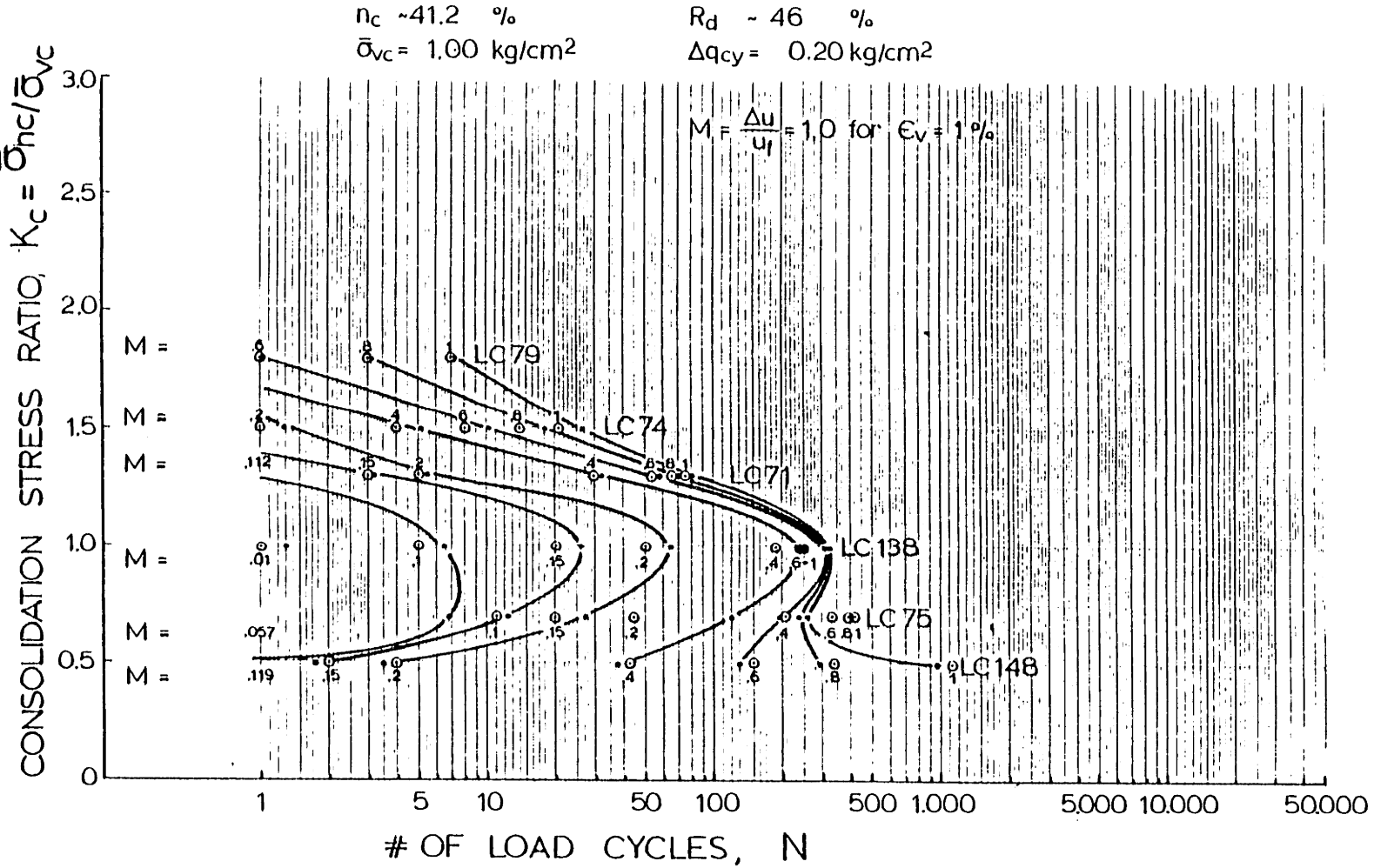

PORE PRESSURE CONTOURS FOR CYCLIC TESTS ON SAMPLES AT DIFFERENT CONSOLIDATION STRESS RATIOS

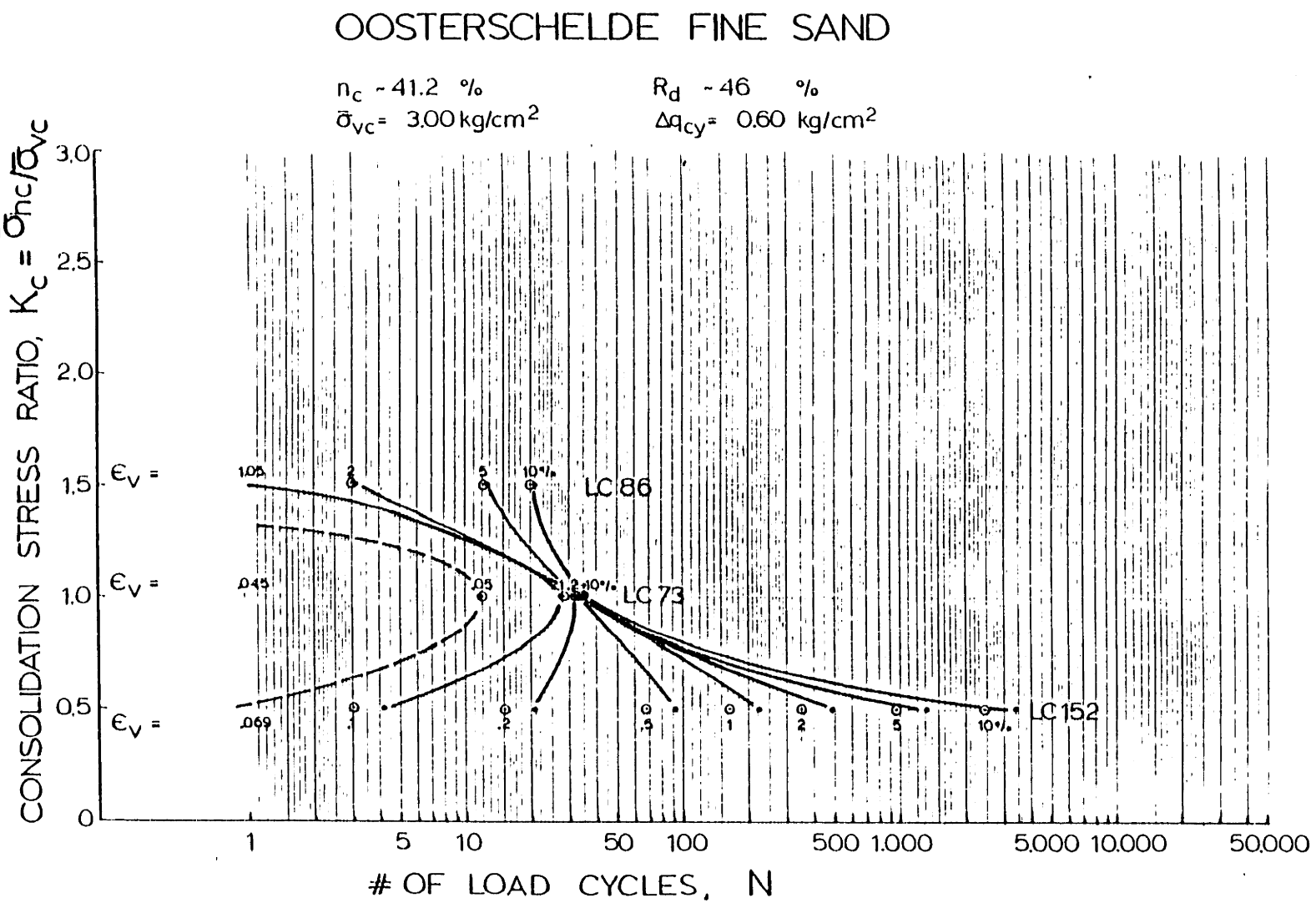

STRAIN CONTOURS FOR CYCLIC TESTS ON SAMPLES AT DIFFERENT CONSOLIDATION STRESS RATIOS

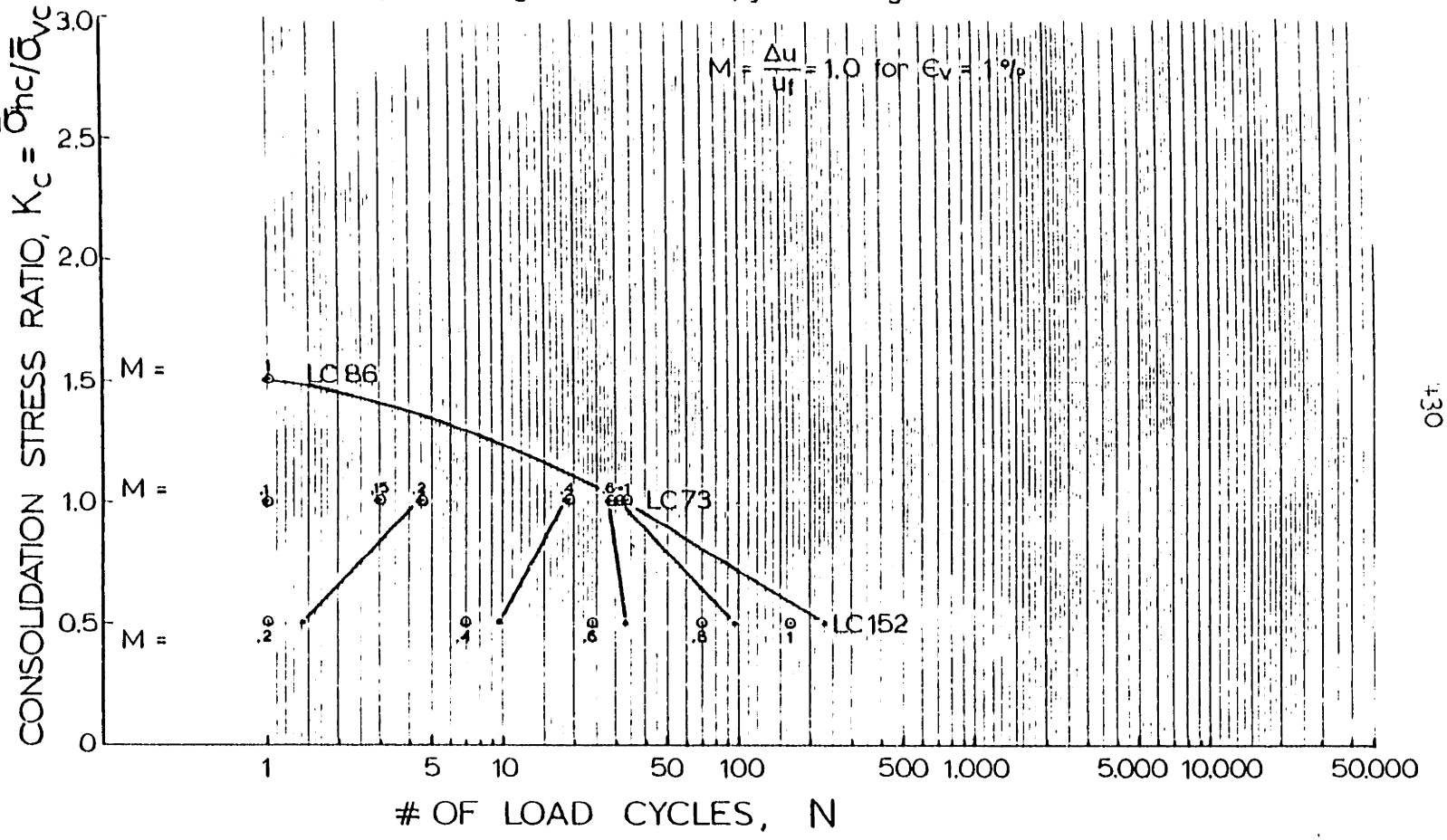

PORE PRESSURE CONTOURS FOR CYCLIC TESTS ON SAMPLES AT DIFFERENT CONSOLIDATION STRESS RATIOS

FIGURE II - 40

OOSTERSCHELDE FINE SAND

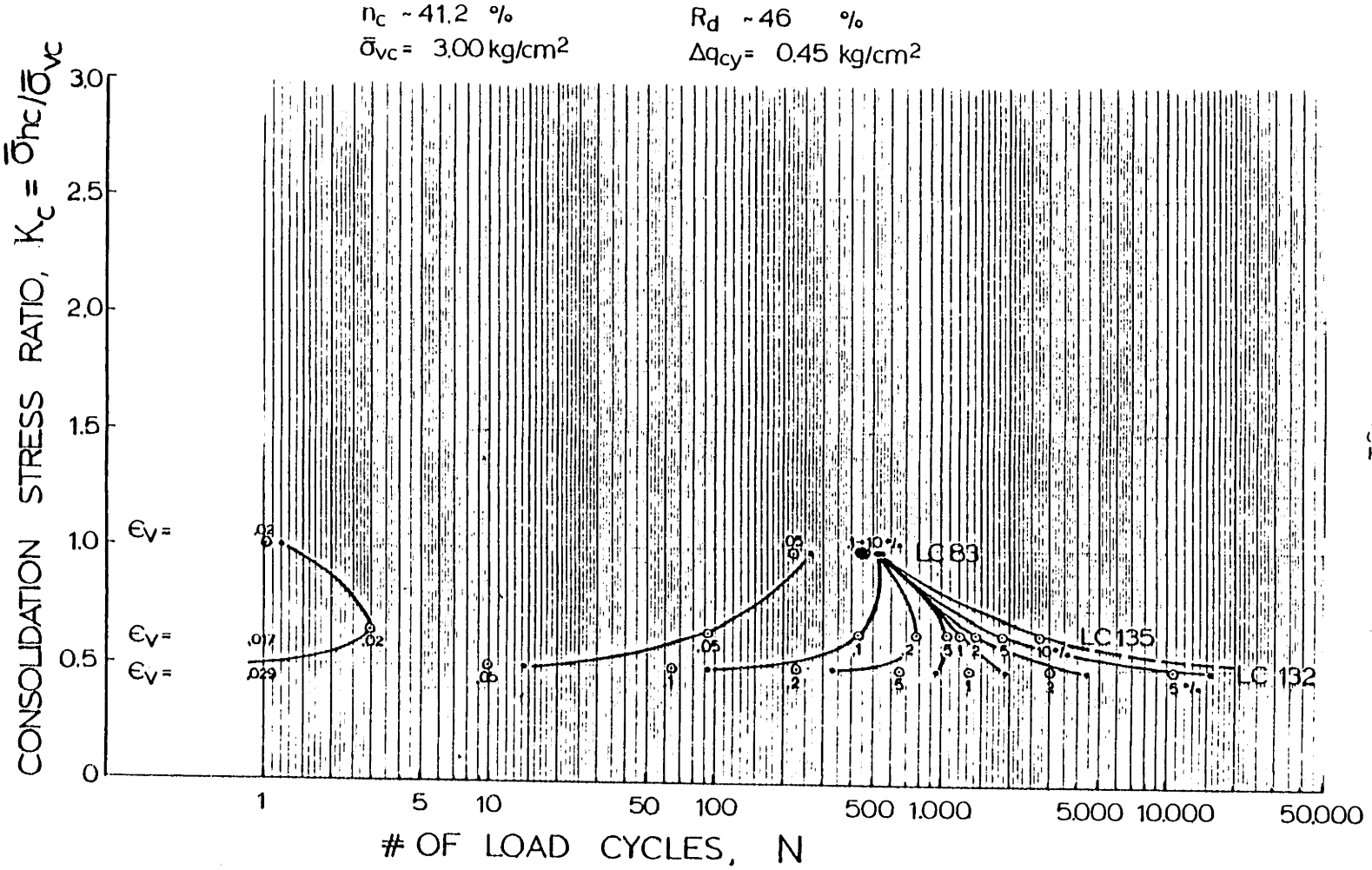

STRAIN CONTOURS FOR CYCLIC TESTS ON SAMPLES AT DIFFERENT CONSOLIDATION STRESS RATIOS

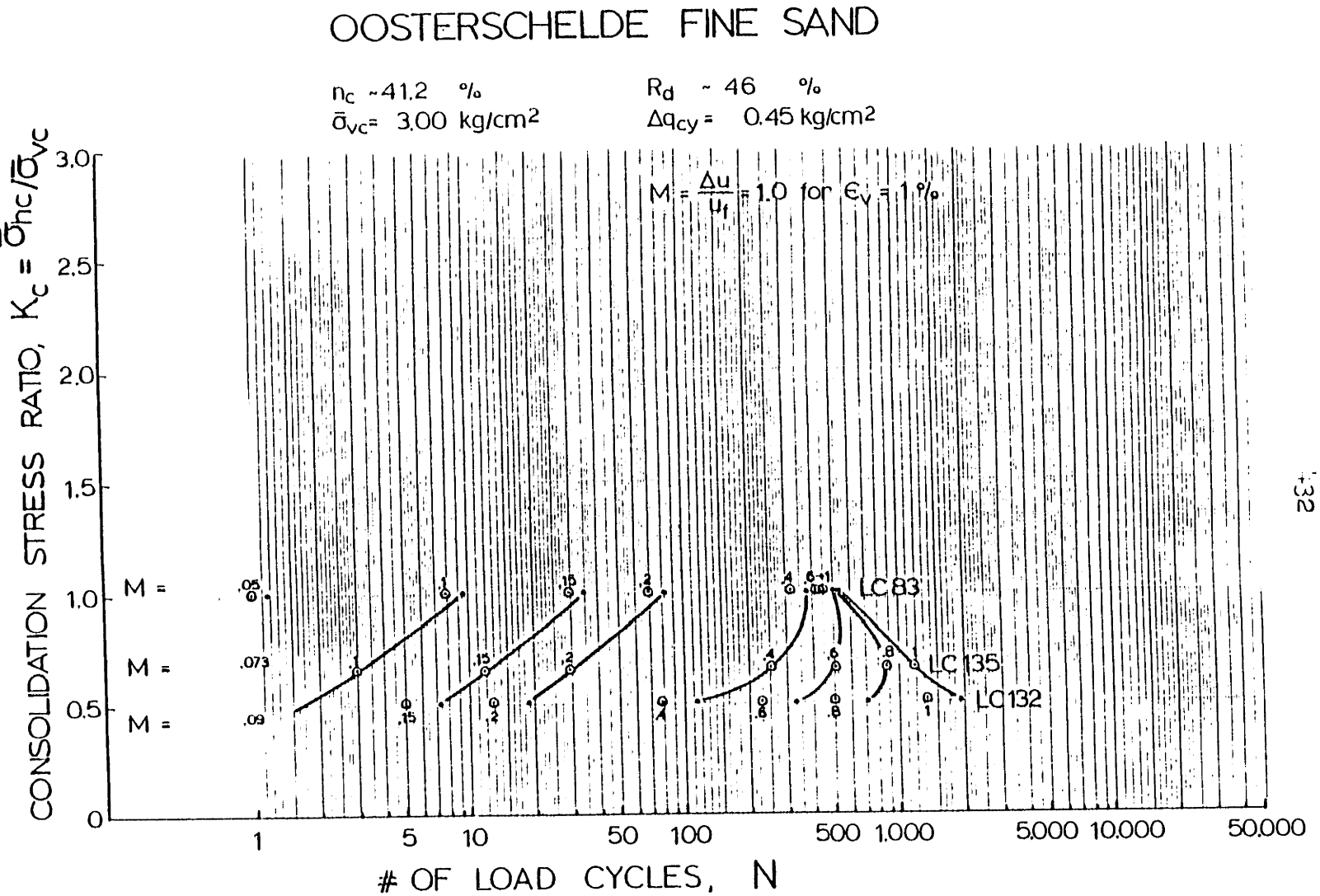

PORE PRESSURE CONTOURS FOR CYCLIC TESTS ON SAMPLES AT DIFFERENT CONSOLIDATION STRESS RATIOS

OOSTERSCHELDE FINE SAND

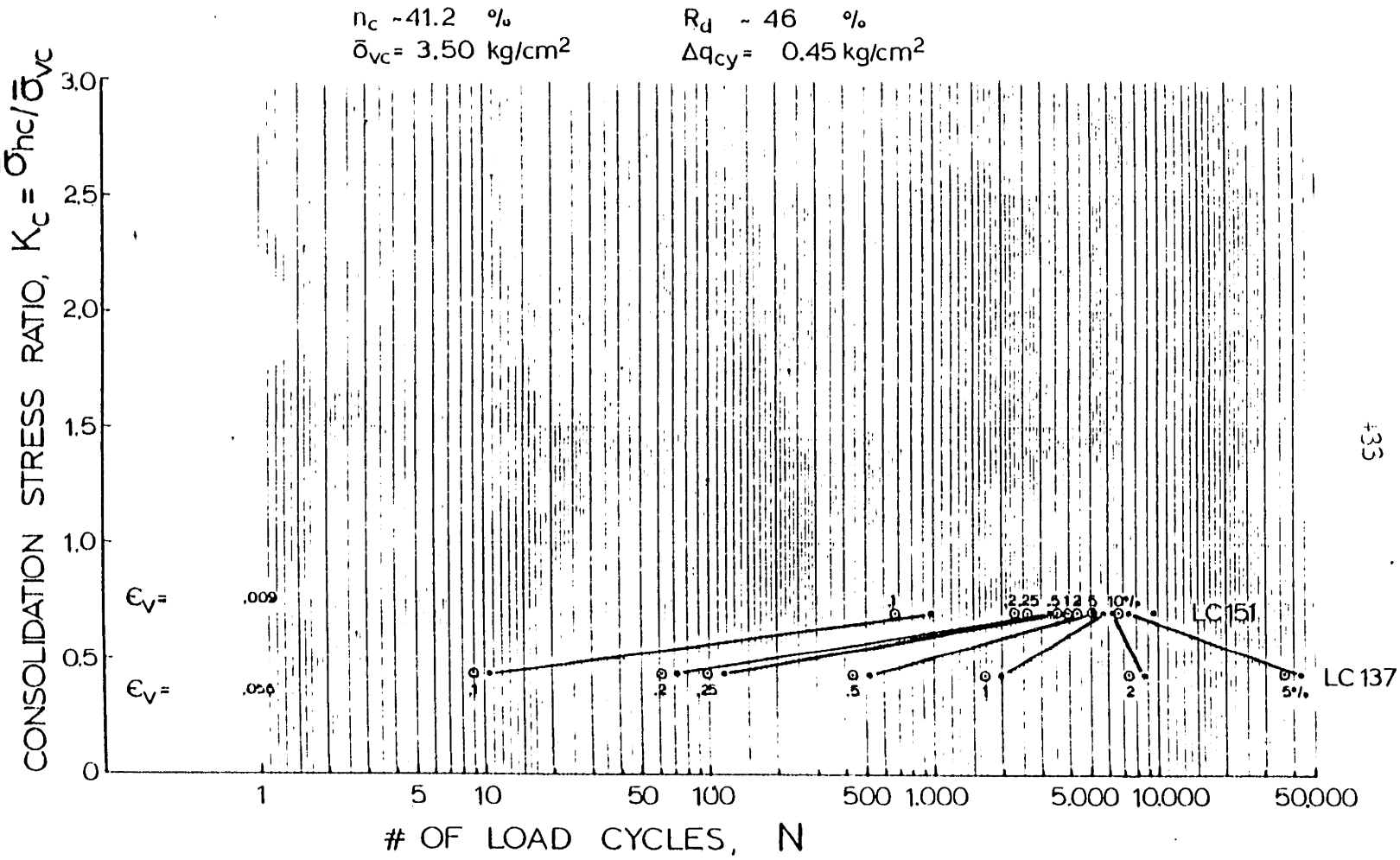

STRAIN CONTOURS FOR COMPRESSION CYCLIC TESTS
ON SAMPLES AT DIFFERENT CONSOLIDATION STRESS RATIOS

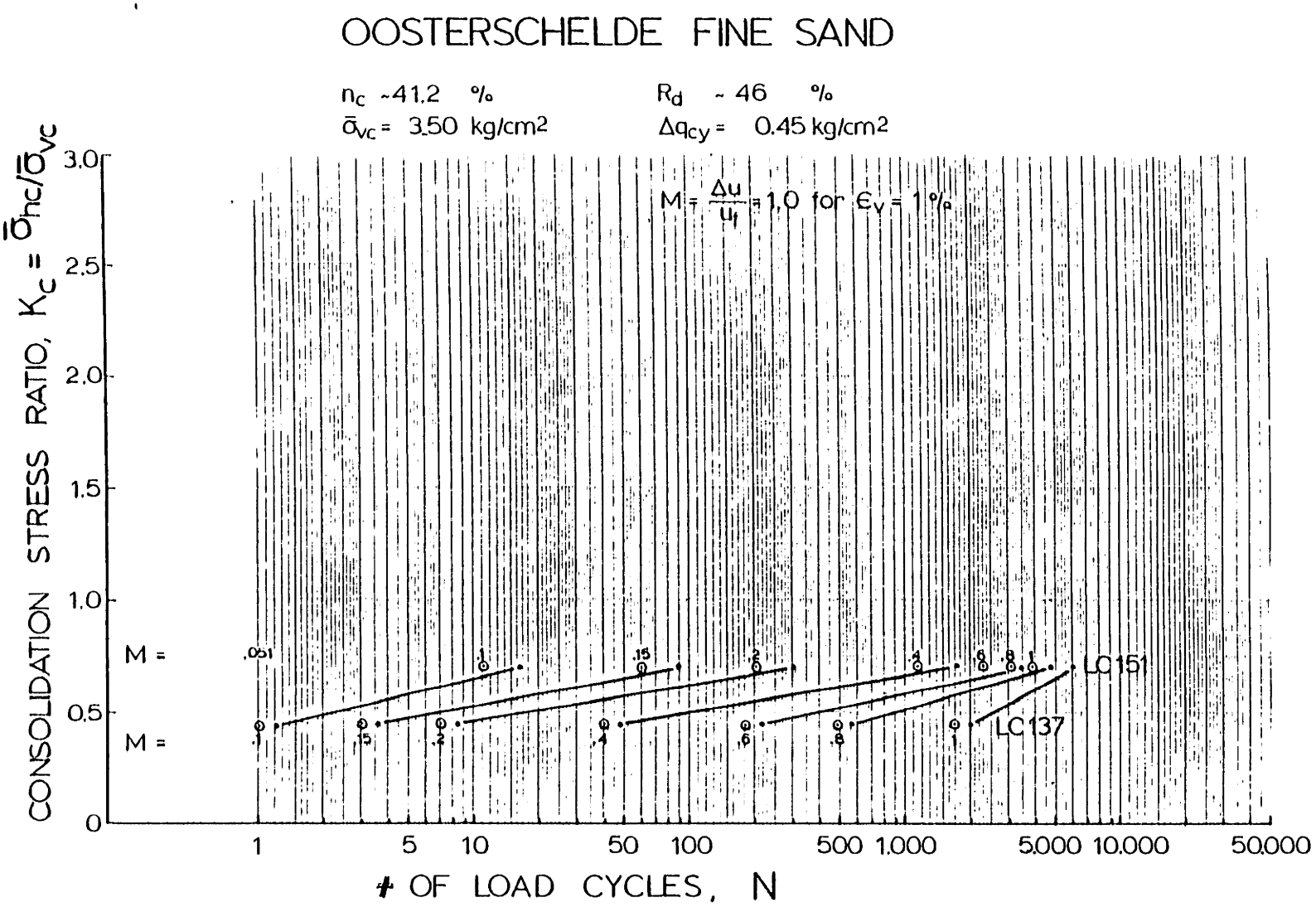

PORE PRESSURE CONTOURS FOR COMPRESSION CYCLIC TESTS ON SAMPLES AT DIFFERENT CONSOLIDATION STRESS RATIOS

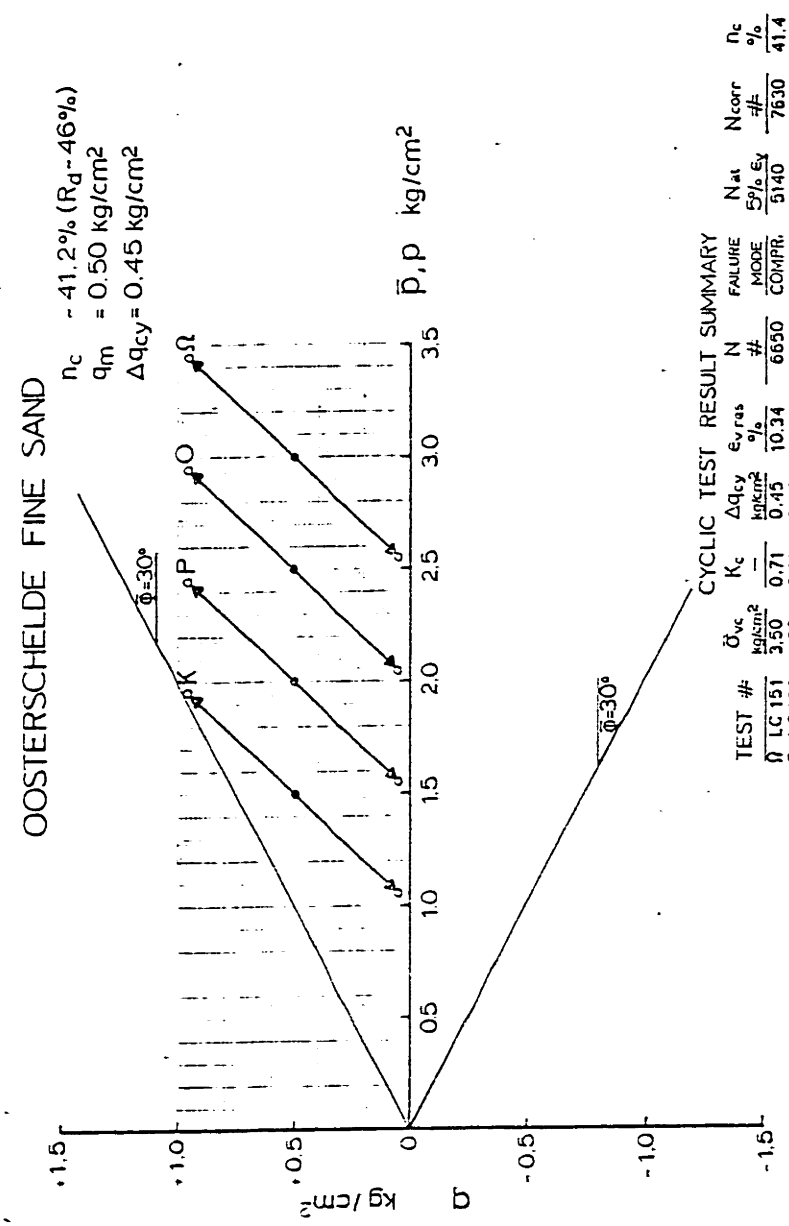

CYCLIC TEST RESULT SUMMARY

TEST #	$\bar{\sigma}_{vc}$ kg/cm²	K_c –	Δq_{cy} kg/cm²	$\varepsilon_{v\,ras}$ %	N #	FAILURE MODE	N_{at} 5% ε_y	N_{corr} #	n_c %
Ω LC 151	3.50	0.71	0.45	10.34	6650	COMPR.	5140	7630	41.4
O LC 135	3.00	0.67	0.45	12.80	3000	COMPR.	1855	1855	41.2
P LC 89	2.50	0.60	0.45	10.00	1305	COMPR.	700	926	41.4
P LC 97	2.50	0.60	0.45	12.30	2525	COMPR	980	1082	41.3
K LC 80	2.00	0.53	0.45	12.60	1700	COMPR.	515	524	41.2
K LC 120	2.00	0.50	0.45	10.10	1100	COMPR.	464	614	41.4

TOTAL STRESS PATHS (TSP-u_B) FOR ANISOTROPIC CYCLIC TESTS WITH DIFFERENT MEAN NORMAL STRESS, $\bar{p}_o$

FIGURE E-45

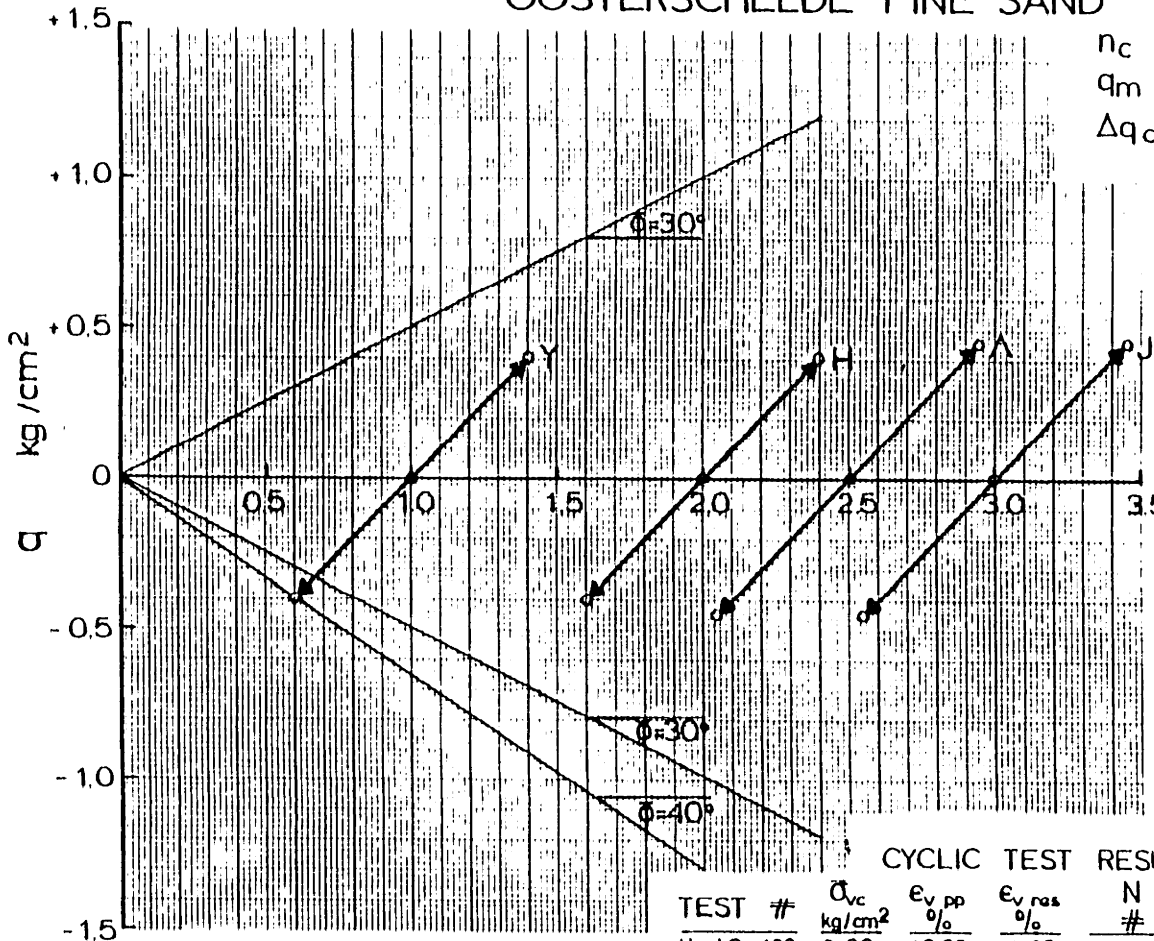

CYCLIC TEST RESULT SUMMARY

TEST #	$\bar{\sigma}_{vc}$ kg/cm²	$\epsilon_{v\,pp}$ %	$\epsilon_{v\,res}$ %	N #	FAILURE MODE	N_{at} 5% ϵ_v	N_{corr} #	n_c %
H LC 139	2.00	10.99	-2.68	70	DEF.	69	97	41.5
Y LC 67	1.00	20.90	-0.20	13	DEF.	6	5	40.9
J LC 83	3.00	18.17	-1.97	451	DEF.	449	534	41.4
Λ LC 144	2.50	10.00	-2.49	206	DEF.	205	258	41.4

TOTAL STRESS PATHS (TSP-u_B) FOR ISOTROPIC CYCLIC TESTS WITH DIFFERENT MEAN NORMAL STRESS, $\bar{p}_o$

FIGURE E-40

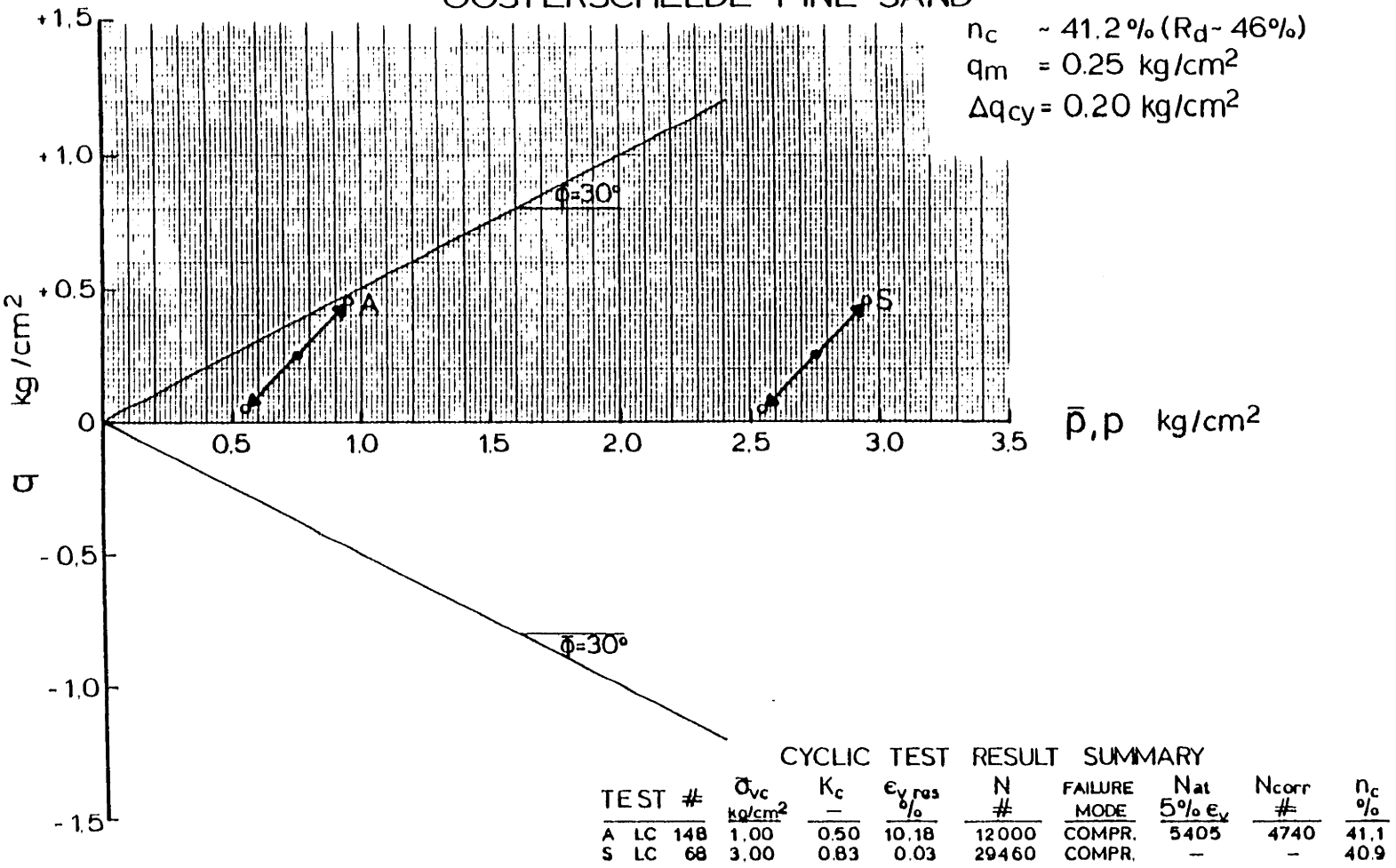

CYCLIC TEST RESULT SUMMARY

TEST #	$\bar{\sigma}_{vc}$ kg/cm²	K_c —	$\epsilon_{v\,res}$ %	N #	FAILURE MODE	Nat 5% ϵ_v	Ncorr #	n_c %
A LC 148	1.00	0.50	10.18	12000	COMPR.	5405	4740	41.1
S LC 68	3.00	0.83	0.03	29460	COMPR.	—	—	40.9

FIGURE E-47

TOTAL STRESS PATHS (TSP-u_B) FOR ANISOTROPIC CYCLIC TESTS WITH DIFFERENT MEAN NORMAL STRESS, $\bar{p}_o$

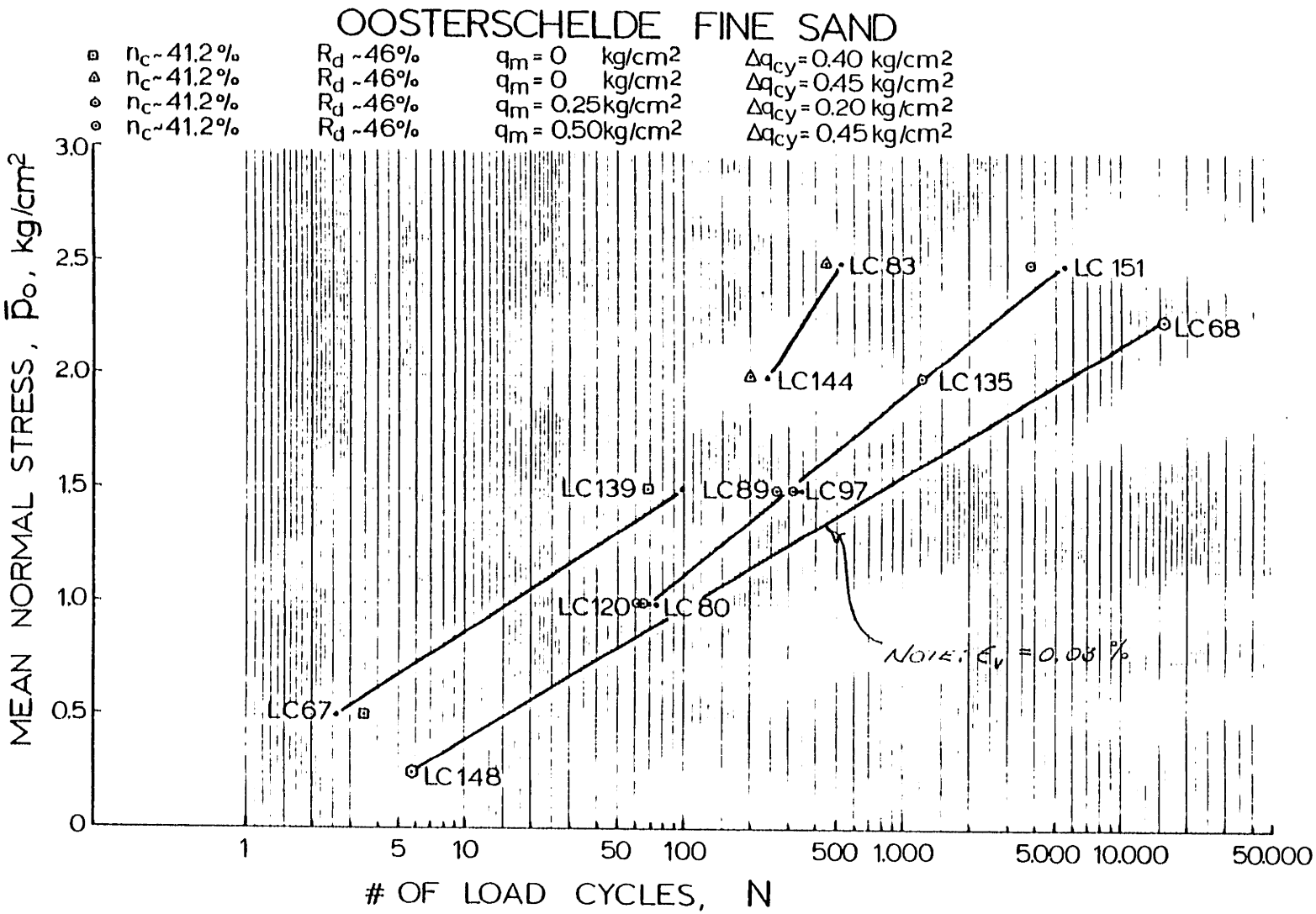

INFLUENCE OF MEAN NORMAL STRESS ON NUMBER OF LOAD CYCLES TO REACH 1% VERTICAL STRAIN IN CYCLIC TRIAXIAL TESTS WITH CONSTANT MEAN SHEAR STRESS

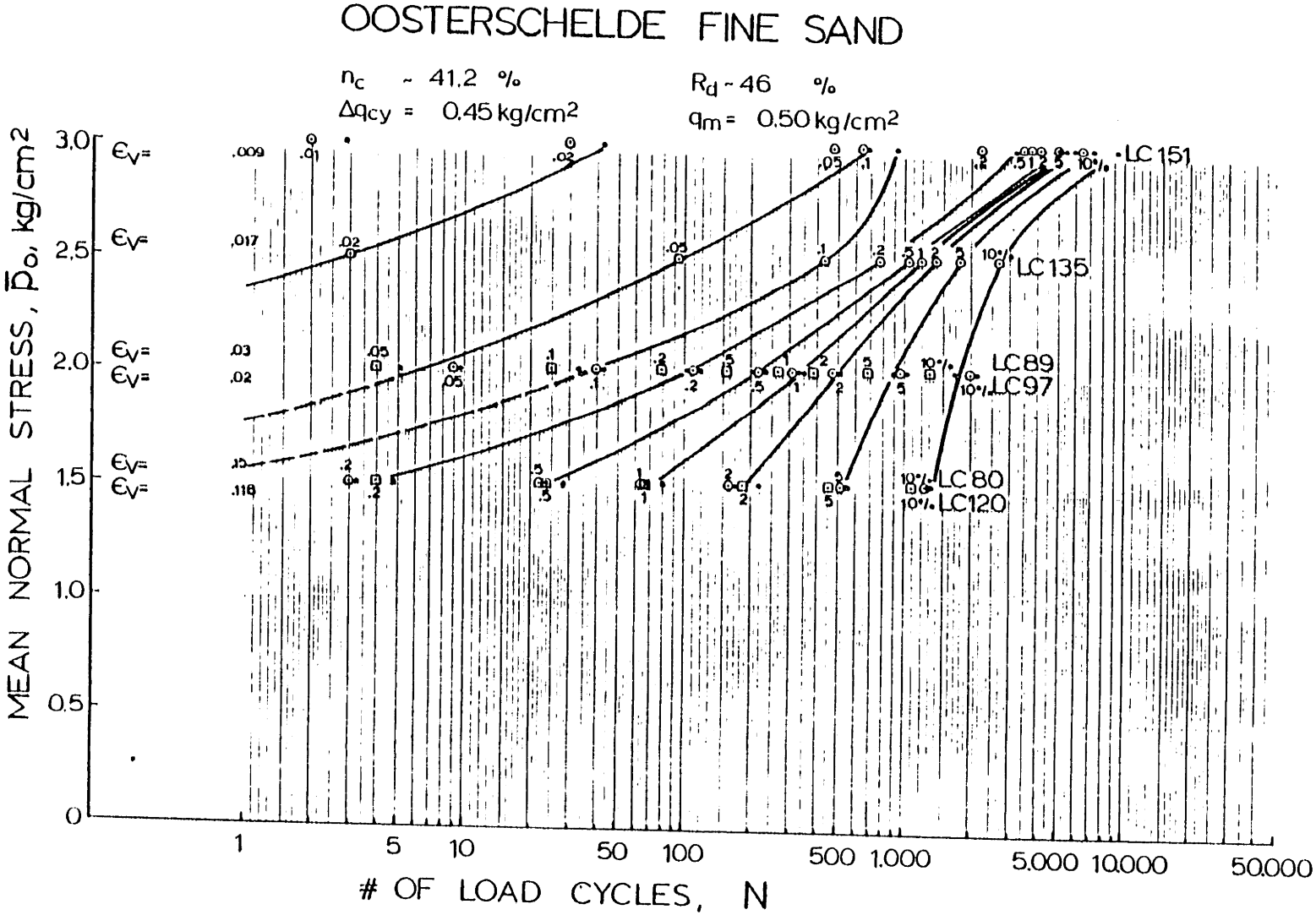

FIGURE 5-49

STRAIN CONTOURS FOR COMPRESSION CYCLIC TESTS ON SAMPLES AT DIFFERENT MEAN NORMAL STRESSES

OOSTERSCHELDE FINE SAND

n_c ~ 41.2 % R_d ~ 46 %

Δq_{cy} = 0.45 kg/cm² q_m = 0.50 kg/cm²

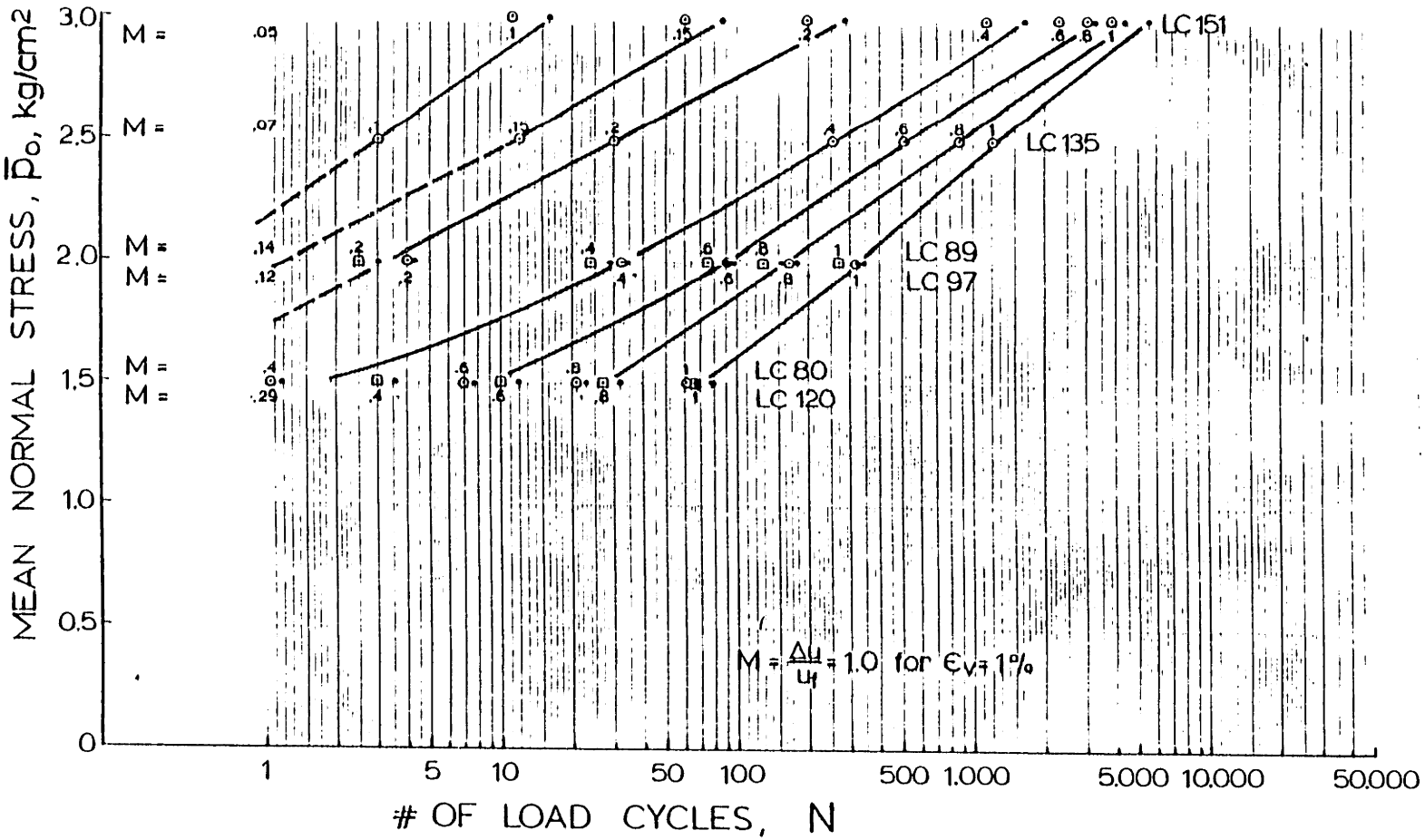

Figure 5.5

PORE PRESSURE CONTOURS FOR COMPRESSION CYCLIC TESTS ON SAMPLES AT DIFFERENT MEAN NORMAL STRESSES

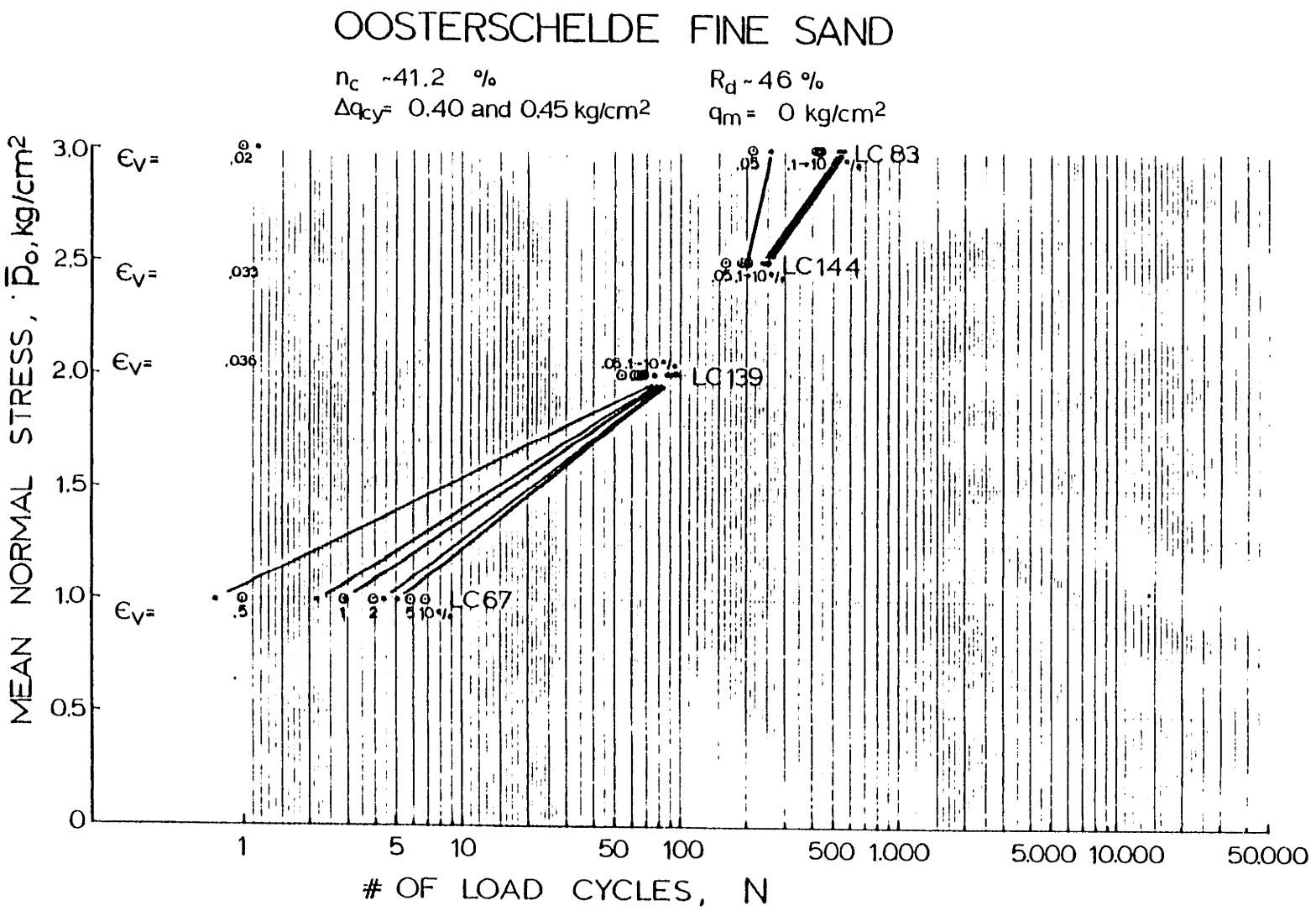

STRAIN CONTOURS FOR ISOTROPIC CYCLIC TESTS ON SAMPLES AT DIFFERENT MEAN NORMAL STRESSES

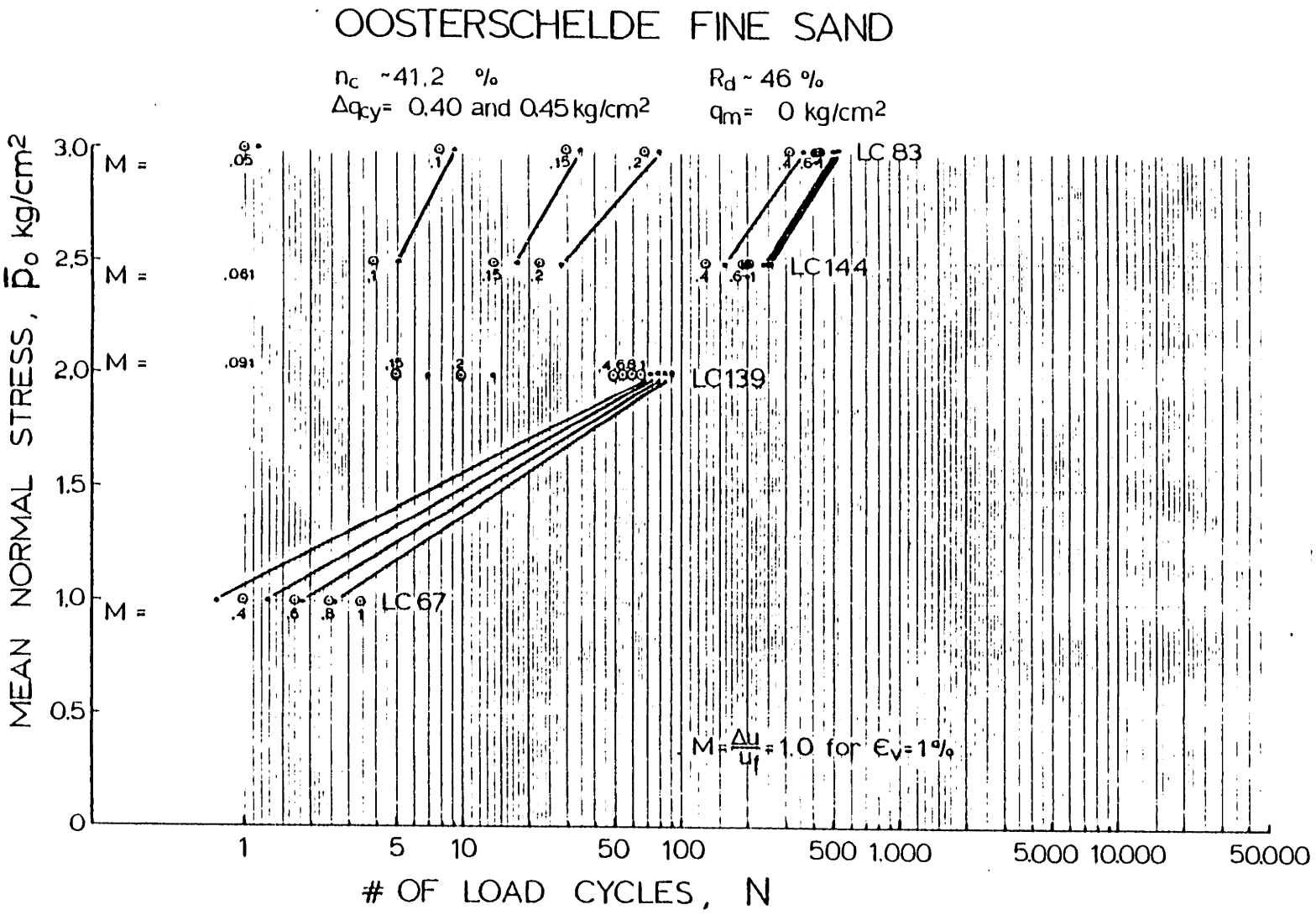

PORE PRESSURE CONTOURS FOR ISOTROPIC CYCLIC TESTS ON SAMPLES AT DIFFERENT MEAN NORMAL STRESSES

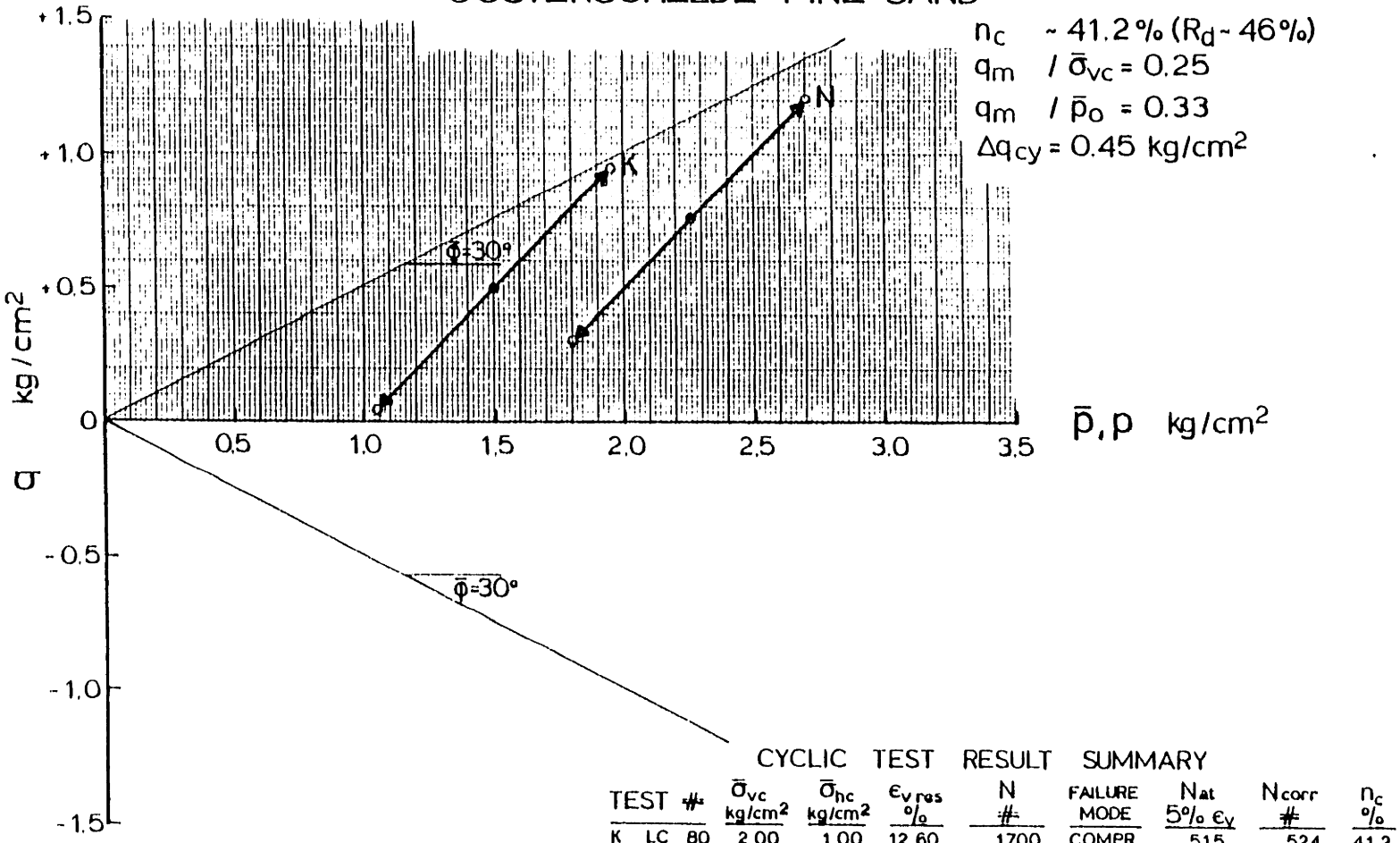

CYCLIC TEST RESULT SUMMARY

TEST #	$\bar{\sigma}_{vc}$ kg/cm²	$\bar{\sigma}_{hc}$ kg/cm²	$\epsilon_{v\,res}$ %	N #	FAILURE MODE	N_{at} 5% ϵ_v	N_{corr} #	n_c %
K LC 80	2.00	1.00	12.60	1700	COMPR.	515	524	41.2
K LC 120	2.00	1.00	10.10	1100	COMPR.	464	614	41.4
N LC 132	3.00	1.50	4.71	9700	COMPR.	10500	15000	41.4

FIGURE E-52

TOTAL STRESS PATHS (TSP-u_B) FOR ANISOTROPIC CYCLIC TESTS WITH DIFFERENT MEAN NORMAL STRESS, $\bar{p}_o$

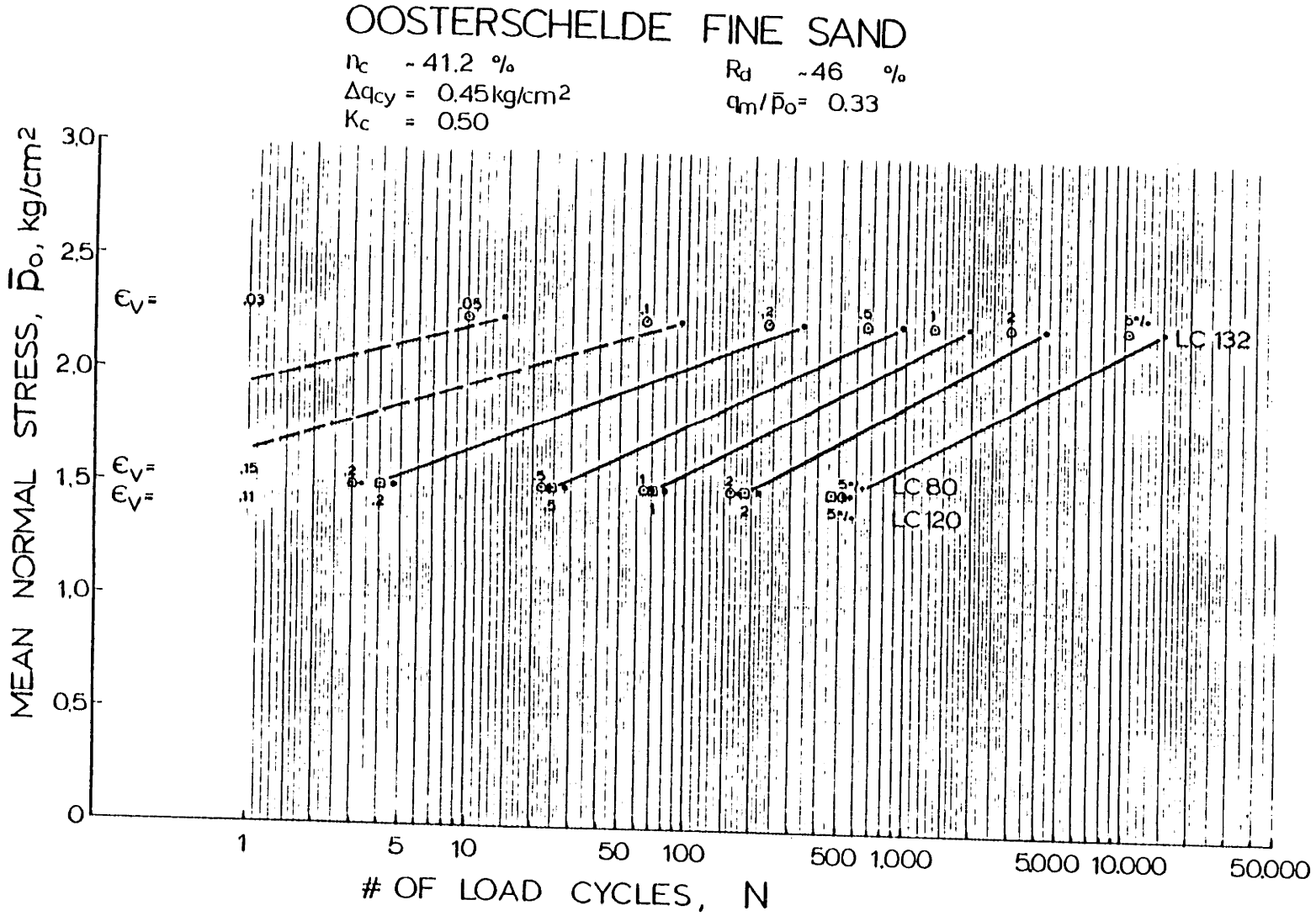

STRAIN CONTOURS FOR COMPRESSION CYCLIC TESTS ON SAMPLES AT DIFFERENT MEAN NORMAL STRESSES

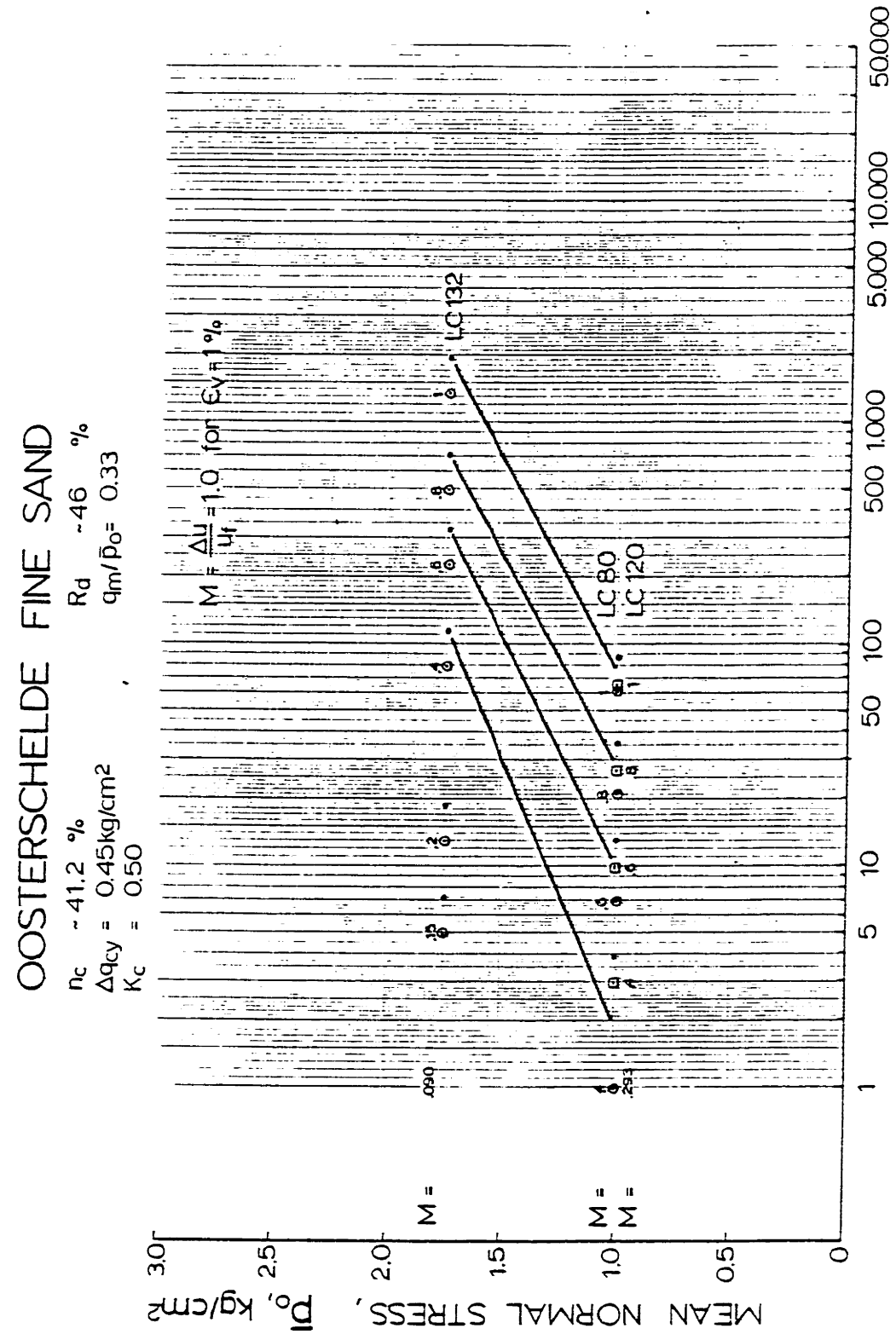

PORE PRESSURE CONTOURS FOR COMPRESSION CYCLIC TESTS ON SAMPLES AT DIFFERENT MEAN NORMAL STRESSES

FIGURE II-55

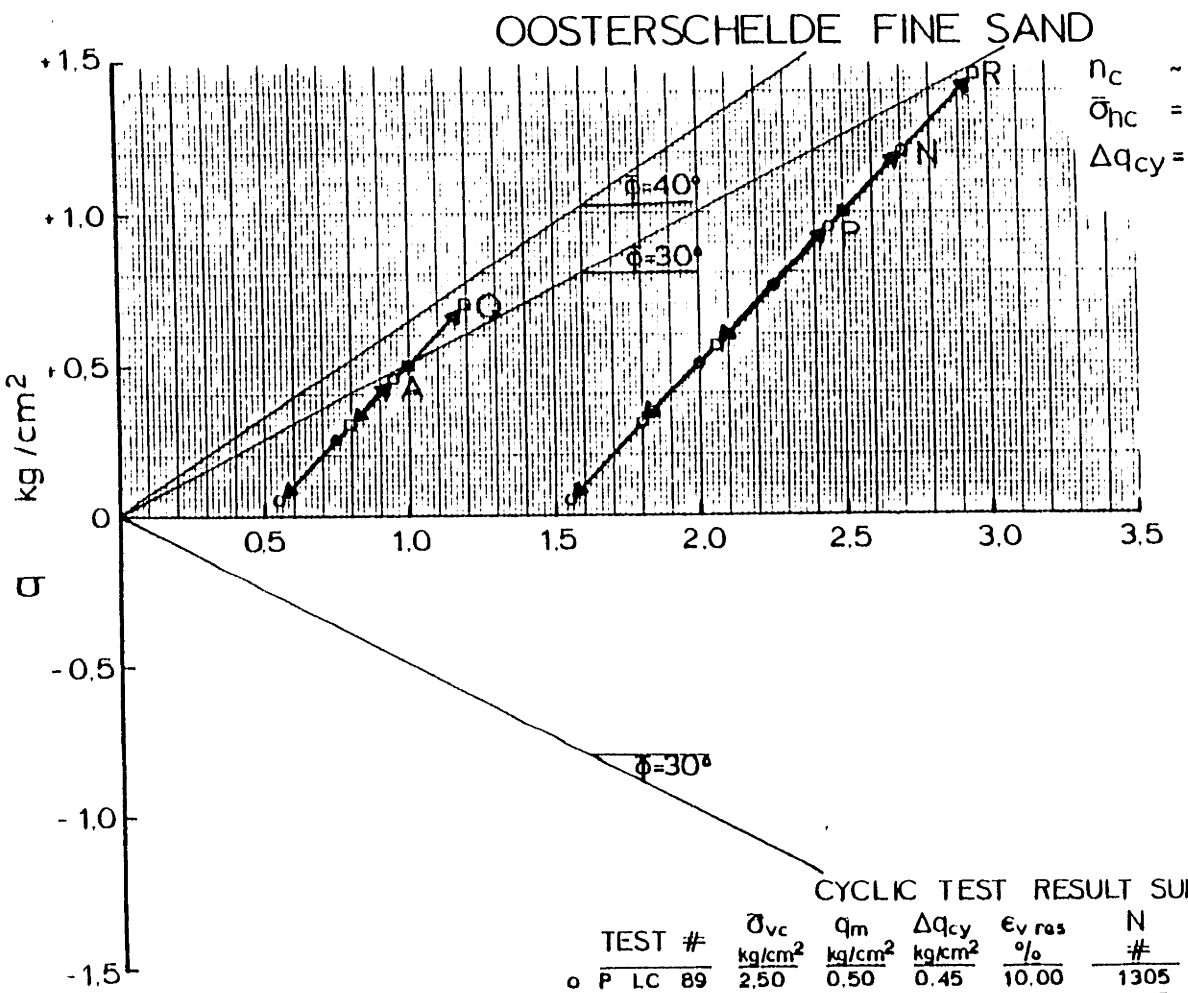

CYCLIC TEST RESULT SUMMARY

	TEST #	$\bar{\sigma}_{vc}$ kg/cm²	q_m kg/cm²	Δq_{cy} kg/cm²	$\epsilon_{v\ res}$ %	N #	FAILURE MODE	N_{at} 5% ϵ	N_{corr} #	n_c %
o	P LC 89	2.50	0.50	0.45	10.00	1305	COMPR.	700	926	41.4
o	P LC 97	2.50	0.50	0.45	12.30	2525	COMPR.	980	1082	41.3
o	N LC 132	3.00	0.75	0.45	4.71	9700	COMPR.	10500	15000	41.4
□	R LC 137	3.50	1.00	0.45	4.33	29120	COMPR.	36500	43000	41.3
o	A LC 148	1.00	0.25	0.20	10.18	12000	COMPR.	5405	4740	41.1
□	Q LC 65	1.50	0.50	0.20	4.80	117000	COMPR.	130000	180000	41.4

TOTAL STRESS PATHS (TSP-u_B) FOR ANISOTROPIC CYCLIC TESTS WITH DIFFERENT VERTICAL CONSOLIDATION STRESS, $\bar{\sigma}_{vc}$

FIGURE E-52

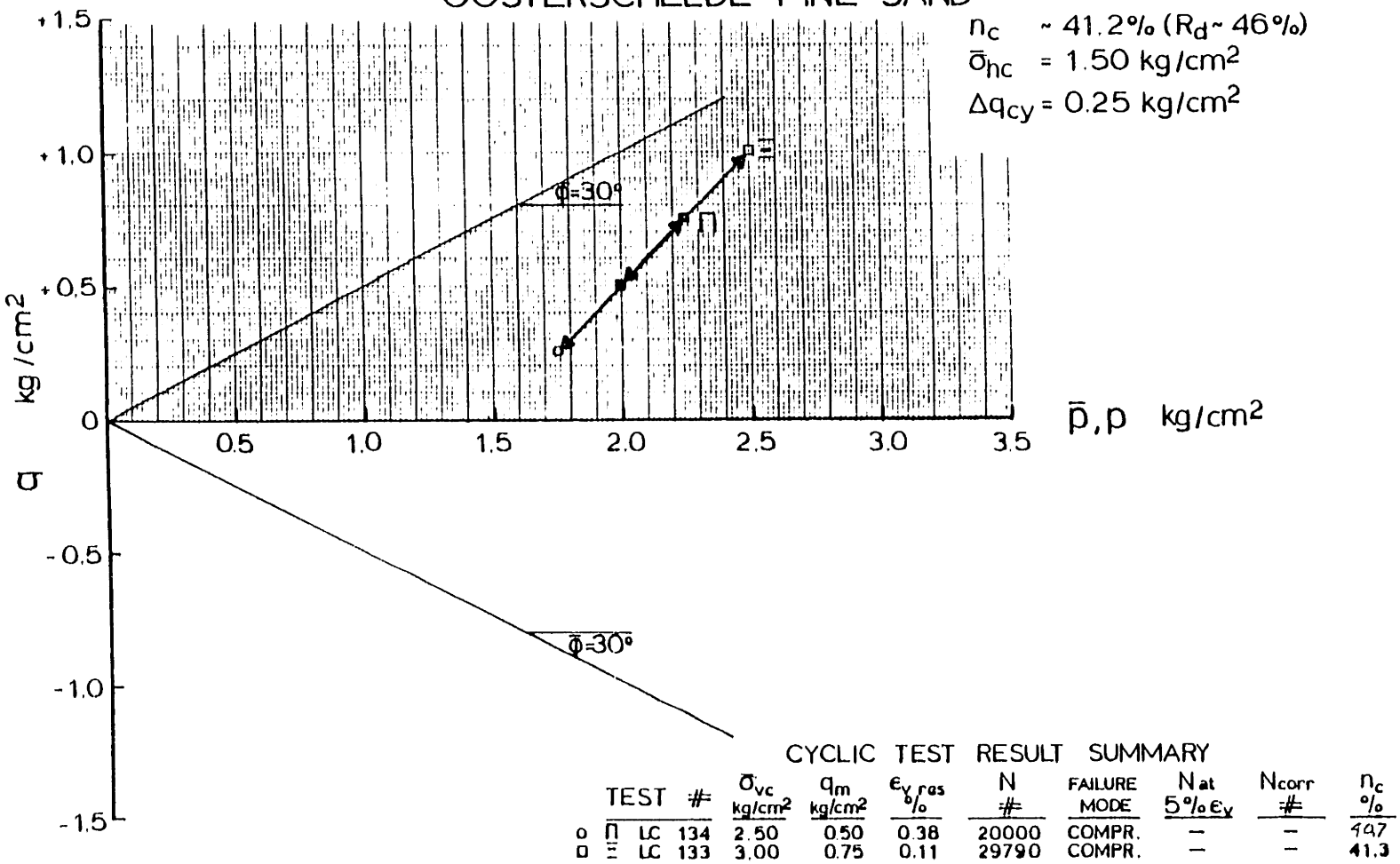

CYCLIC TEST RESULT SUMMARY

	TEST	#	$\bar{\sigma}_{vc}$ kg/cm²	q_m kg/cm²	$\epsilon_{v\,res}$ %	N #	FAILURE MODE	N at 5% ϵ_v	N_{corr} #	n_c %
o	Π	LC 134	2.50	0.50	0.38	20000	COMPR.	–	–	41.7
□	Ξ	LC 133	3.00	0.75	0.11	29790	COMPR.	–	–	41.3

FIGURE E-57

TOTAL STRESS PATHS (TSP-u_B) FOR ANISOTROPIC CYCLIC TESTS WITH DIFFERENT VERTICAL CONSOLIDATION STRESS, $\bar{\sigma}_{vc}$

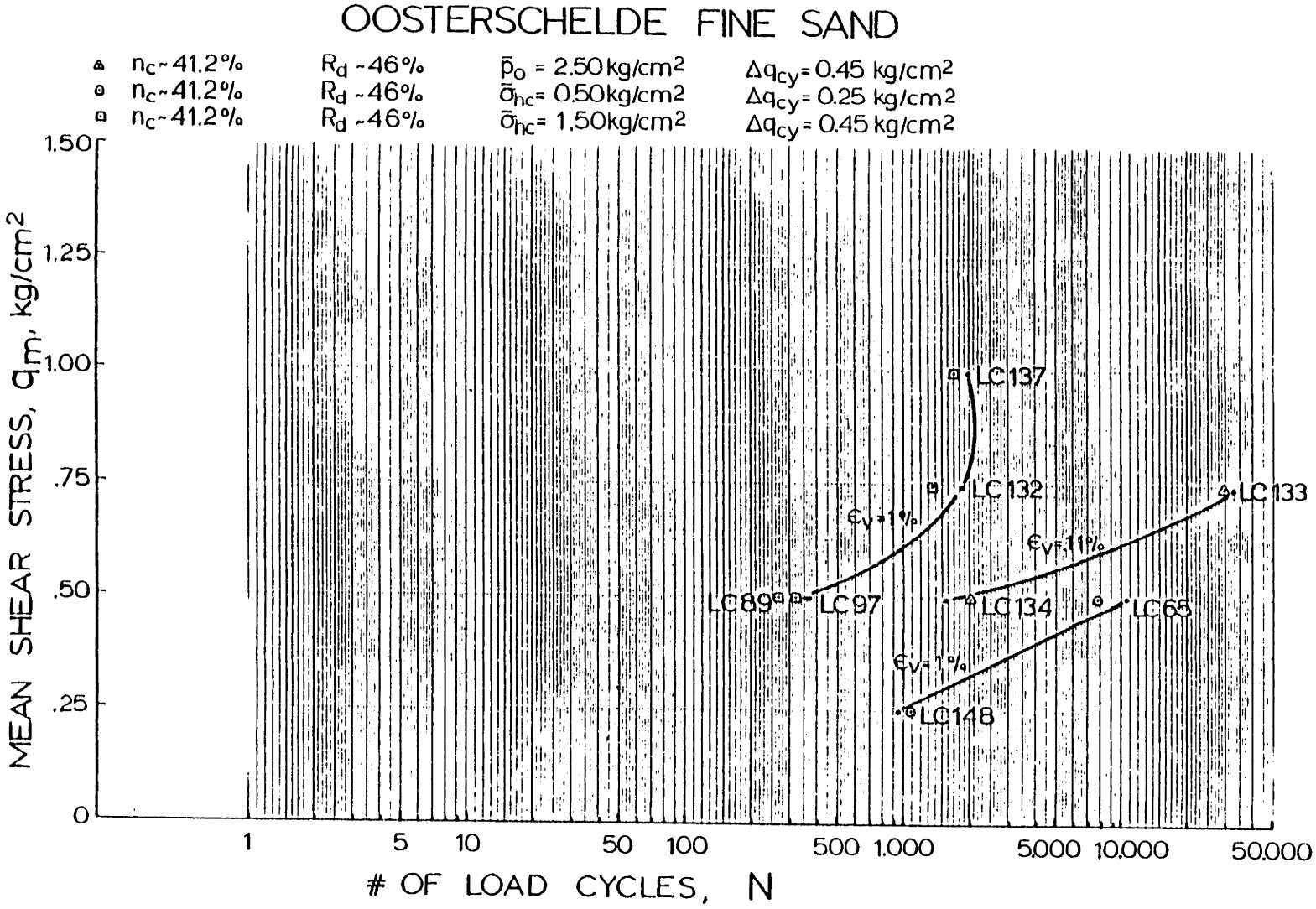

INFLUENCE OF MEAN SHEAR STRESS ON NUMBER OF LOAD CYCLES TO REACH SOME VERTICAL STRAIN IN CYCLIC COMPRESSION TESTS WITH CONSTANT HORIZONTAL STRESS

OOSTERSCHELDE FINE SAND

n_c ~ 41.2 % R_d ~ 46 %

$\bar{\sigma}_{hc}$ = 1.50 kg/cm² Δq_{cy} = 0.45 kg/cm²

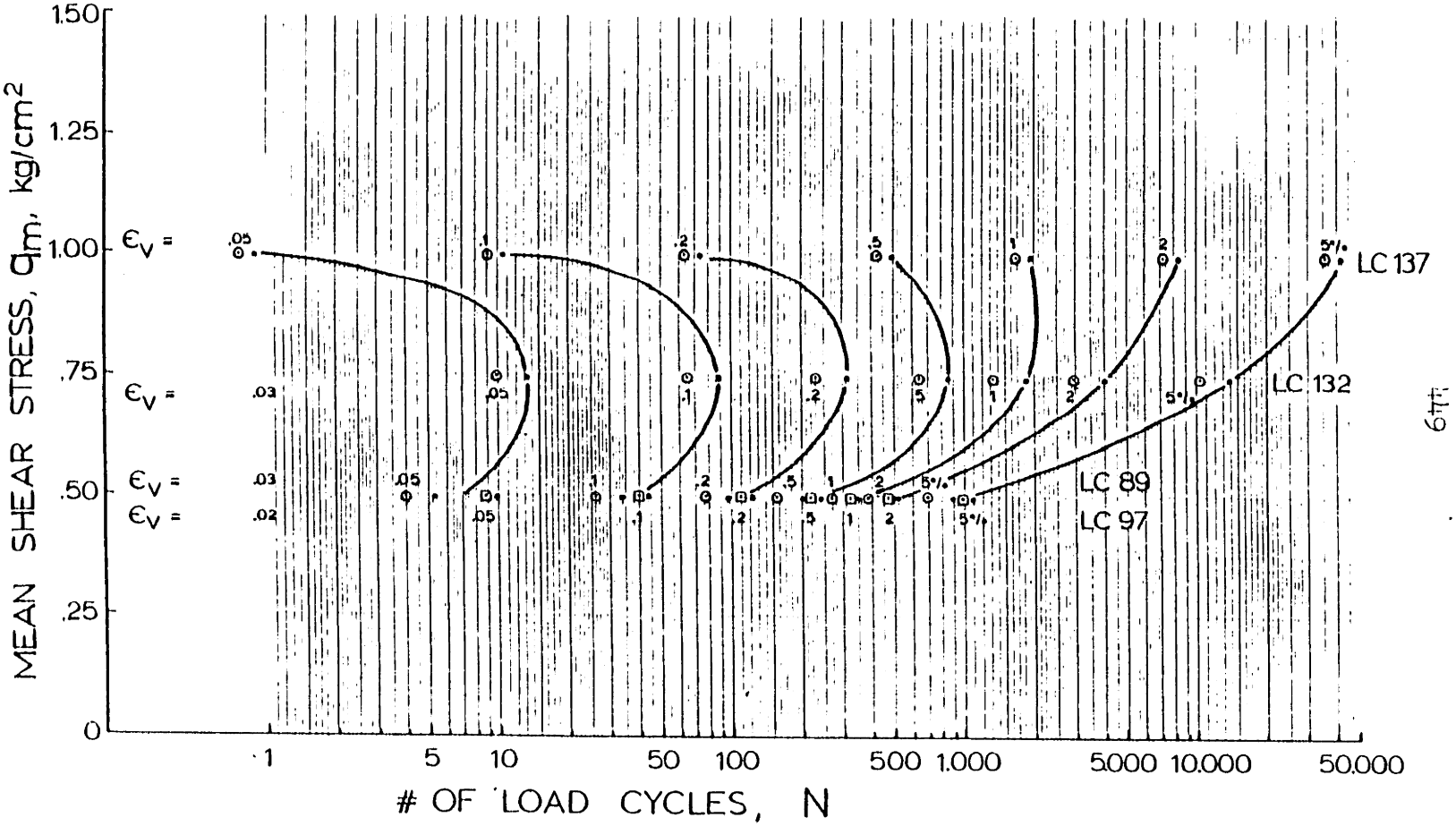

STRAIN CONTOURS FOR COMPRESSION CYCLIC TESTS ON SAMPLES AT DIFFERENT MEAN SHEAR STRESSES

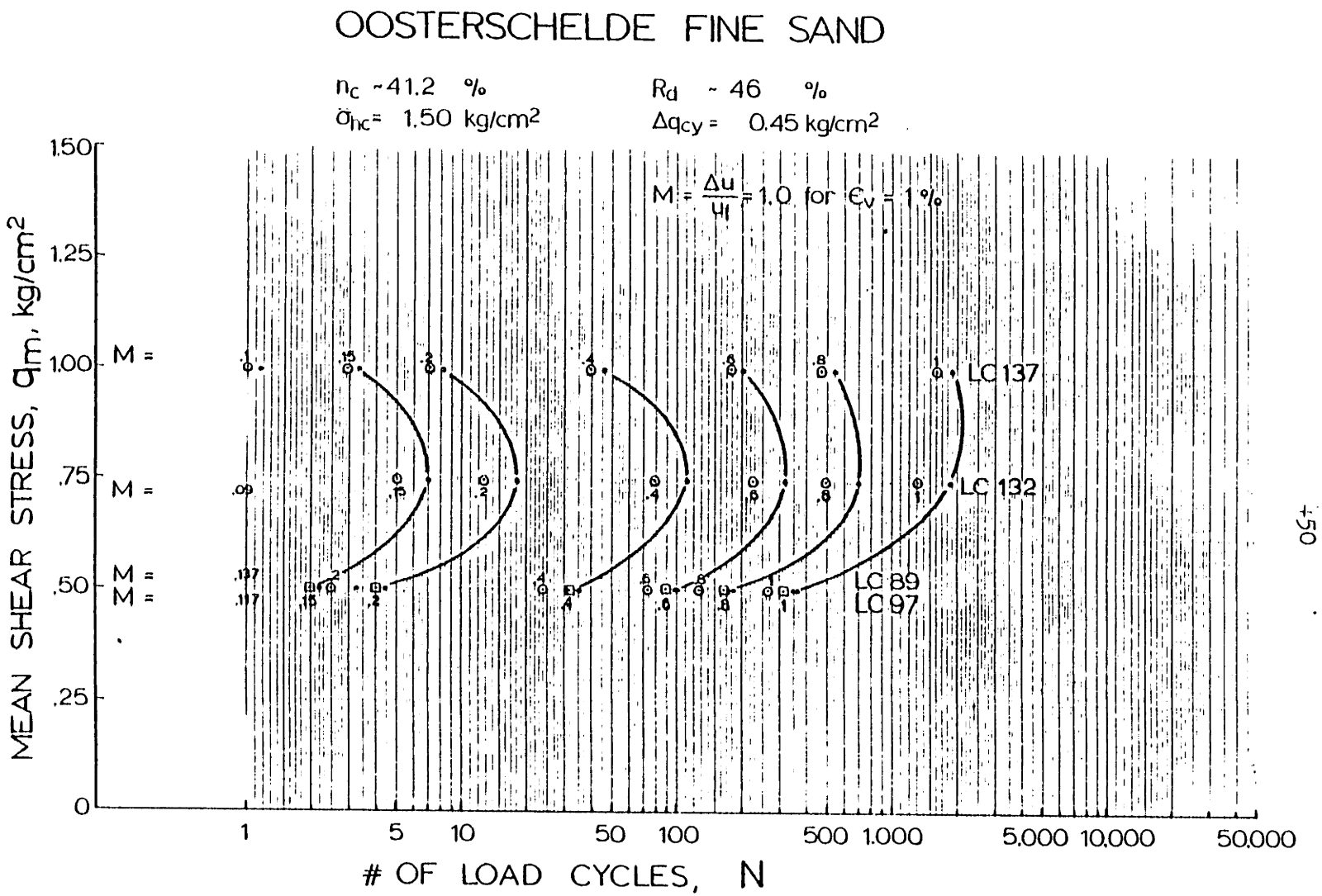

PORE PRESSURE CONTOURS FOR COMPRESSION CYCLIC TESTS ON SAMPLES AT DIFFERENT MEAN SHEAR STRESSES

OOSTERSCHELDE FINE SAND

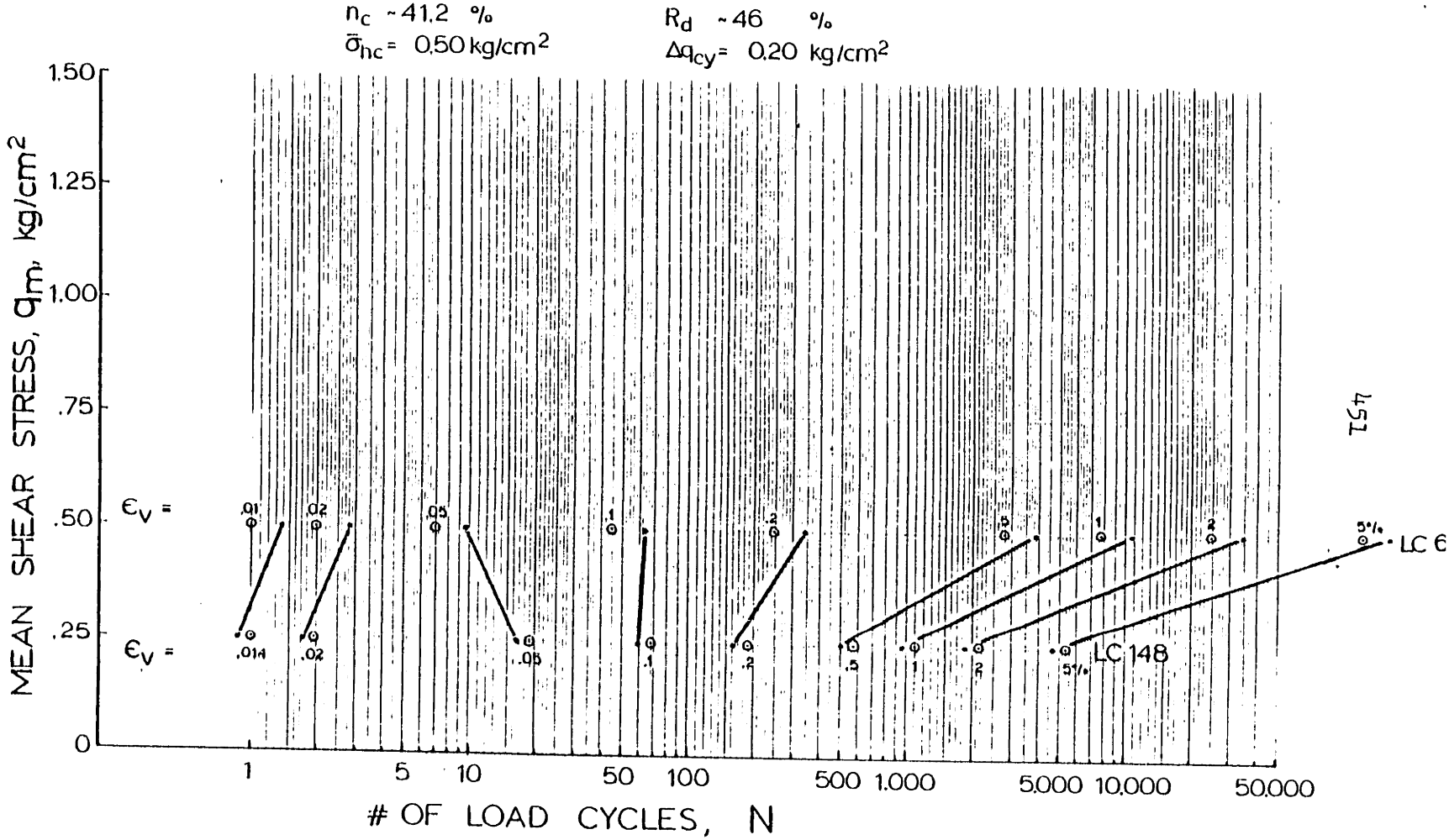

STRAIN CONTOURS FOR COMPRESSION CYCLIC TESTS ON SAMPLES AT DIFFERENT MEAN SHEAR STRESSES

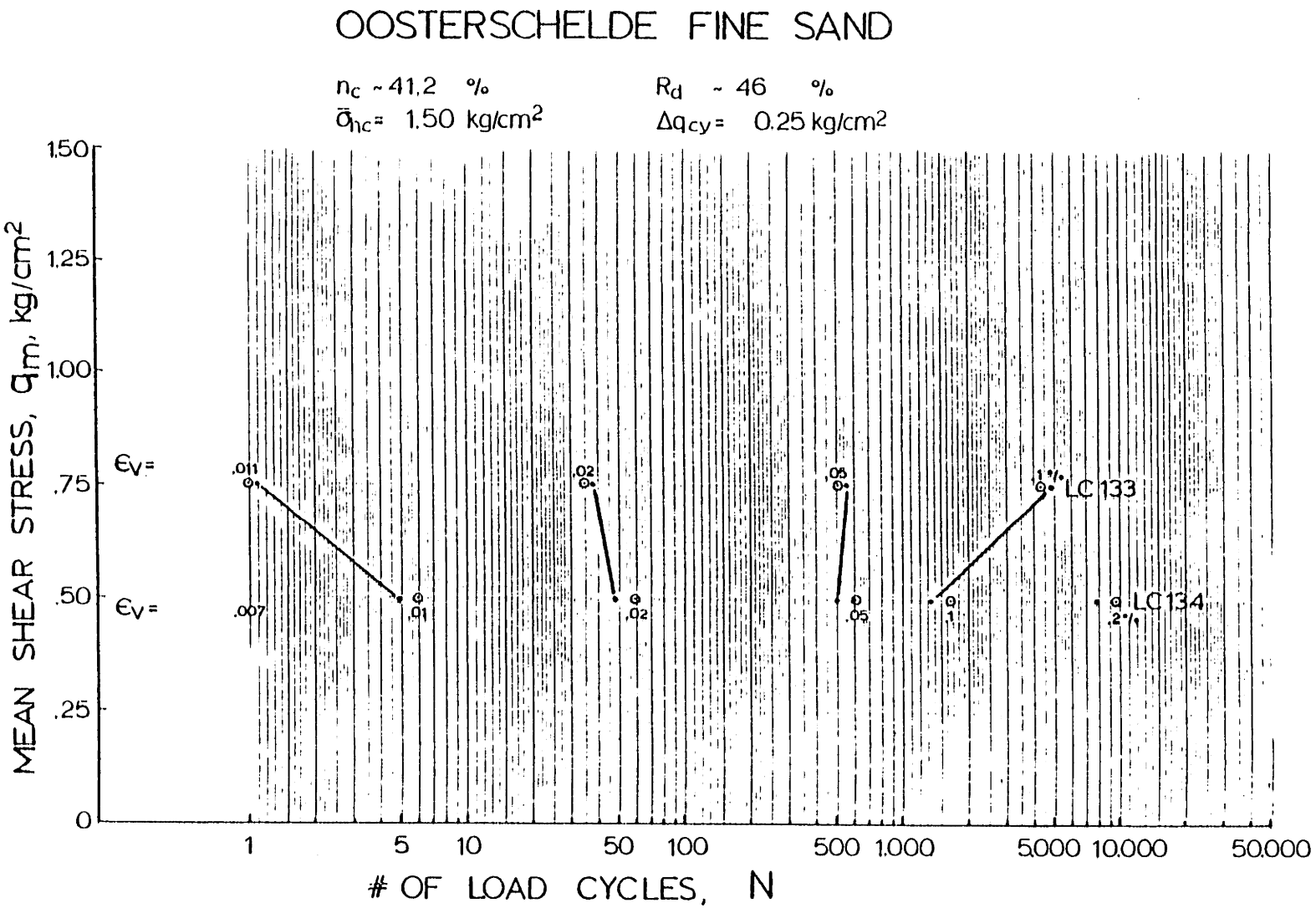

STRAIN CONTOURS FOR COMPRESSION CYCLIC TESTS ON SAMPLES AT DIFFERENT MEAN SHEAR STRESSES

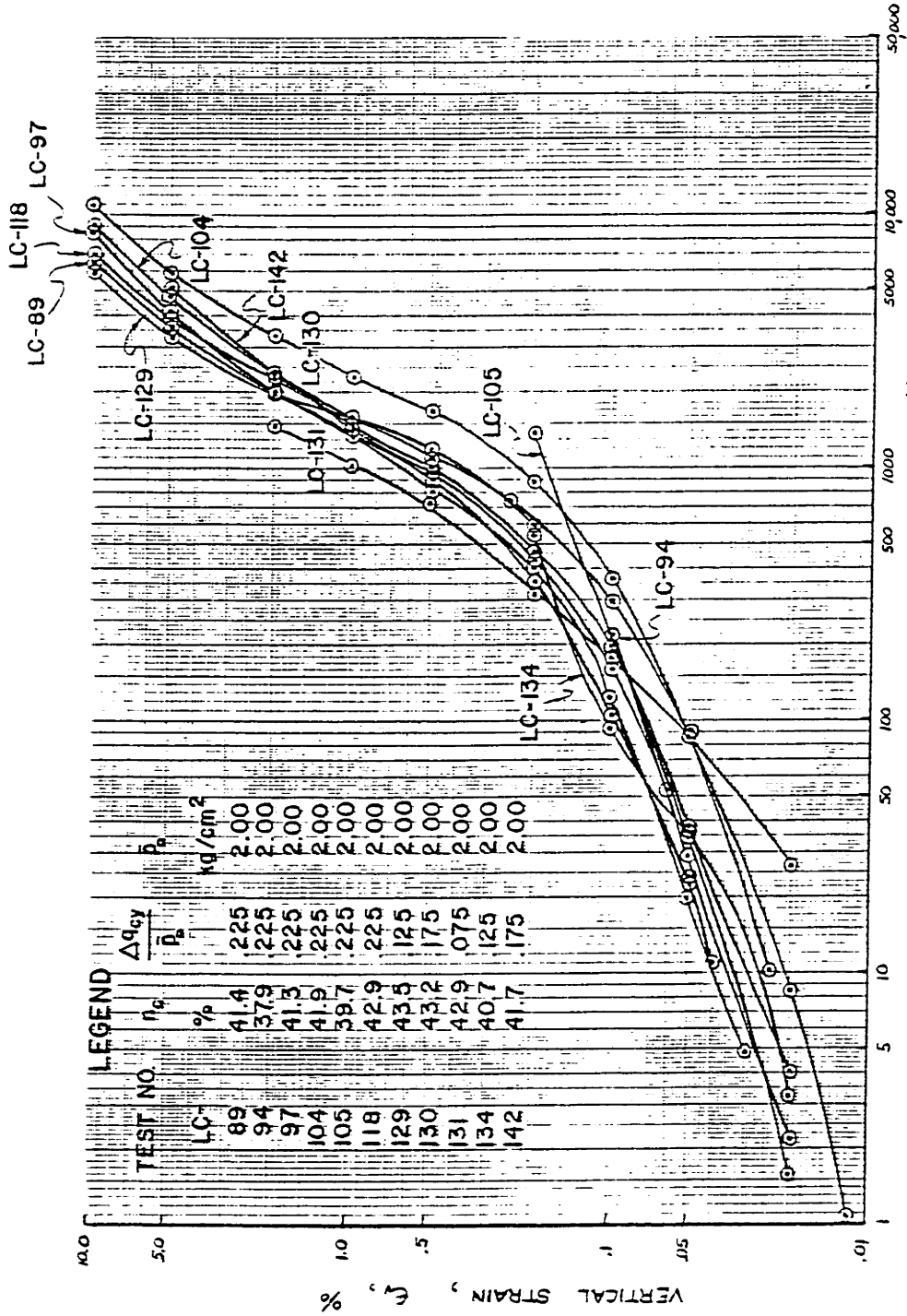

STRAIN VERSUS NUMBER OF NORMALIZED LOAD CYCLES IN TESTS WITH $q_m/p_o = .25$

FIGURE E-63

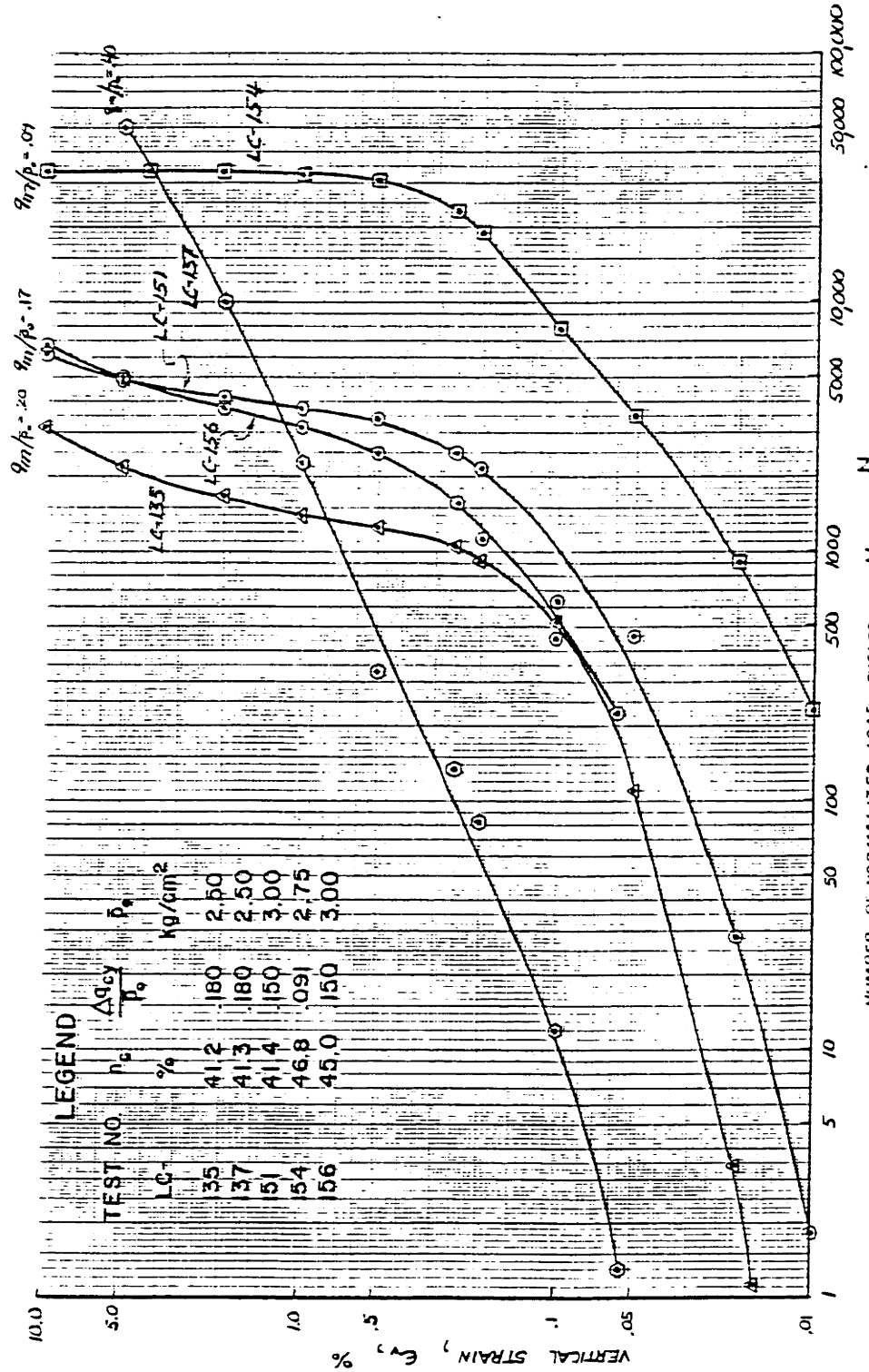

STRAIN VERSUS NUMBER OF NORMALIZED LOAD CYCLES IN COMPRESSION TESTS

FIGURE E-64

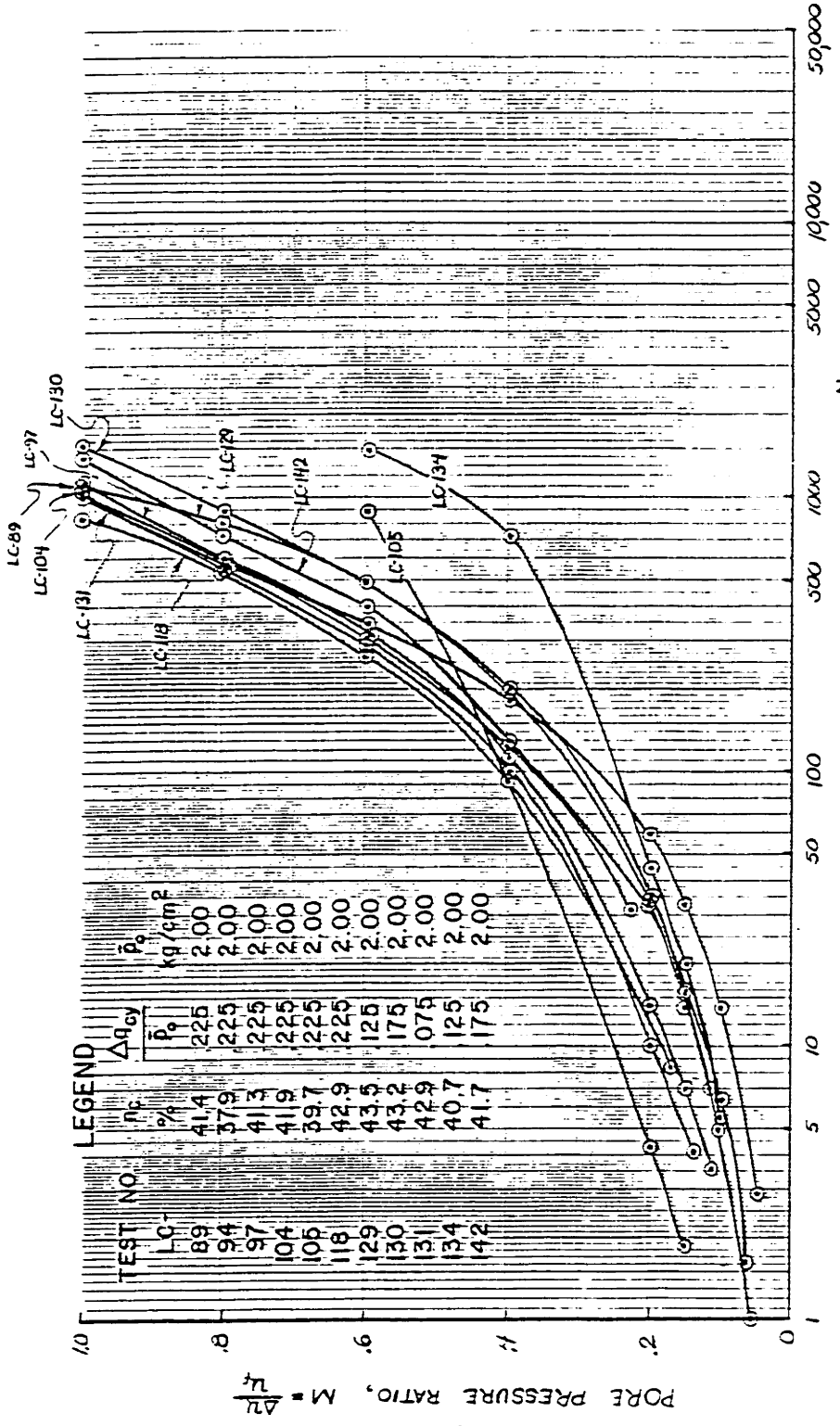

PORE PRESSURE RATIO VERSUS NUMBER OF NORMALIZED LOAD CYCLES IN TESTS WITH $\bar{p}_i/\bar{p}_o = .25$

FIGURE E-65

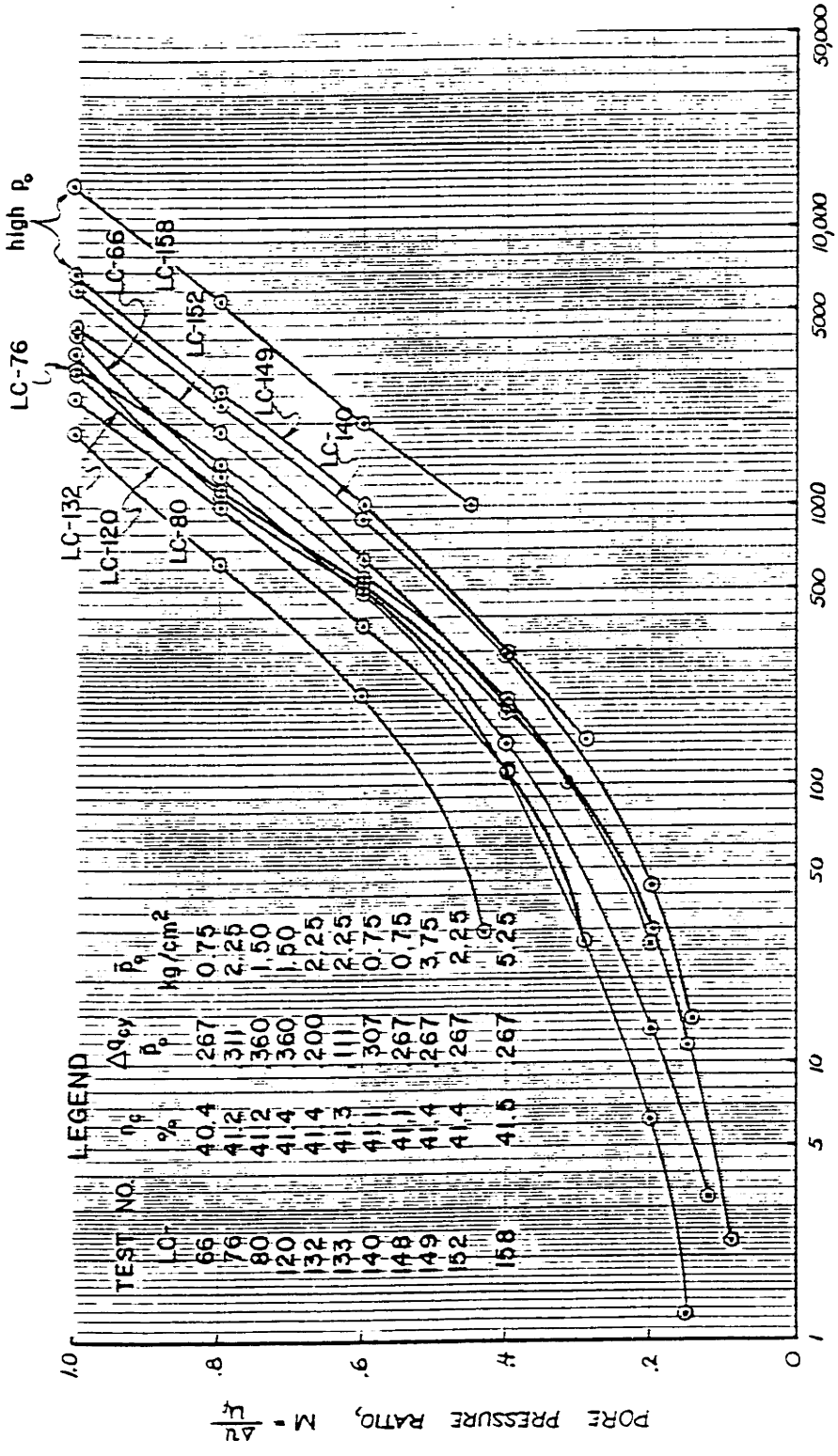

PORE PRESSURE RATIO VERSUS NUMBER OF NORMALIZED LOAD CYCLES IN TESTS WITH $\bar{\sigma}_m / \bar{p}_o = .33$

FIGURE E-66

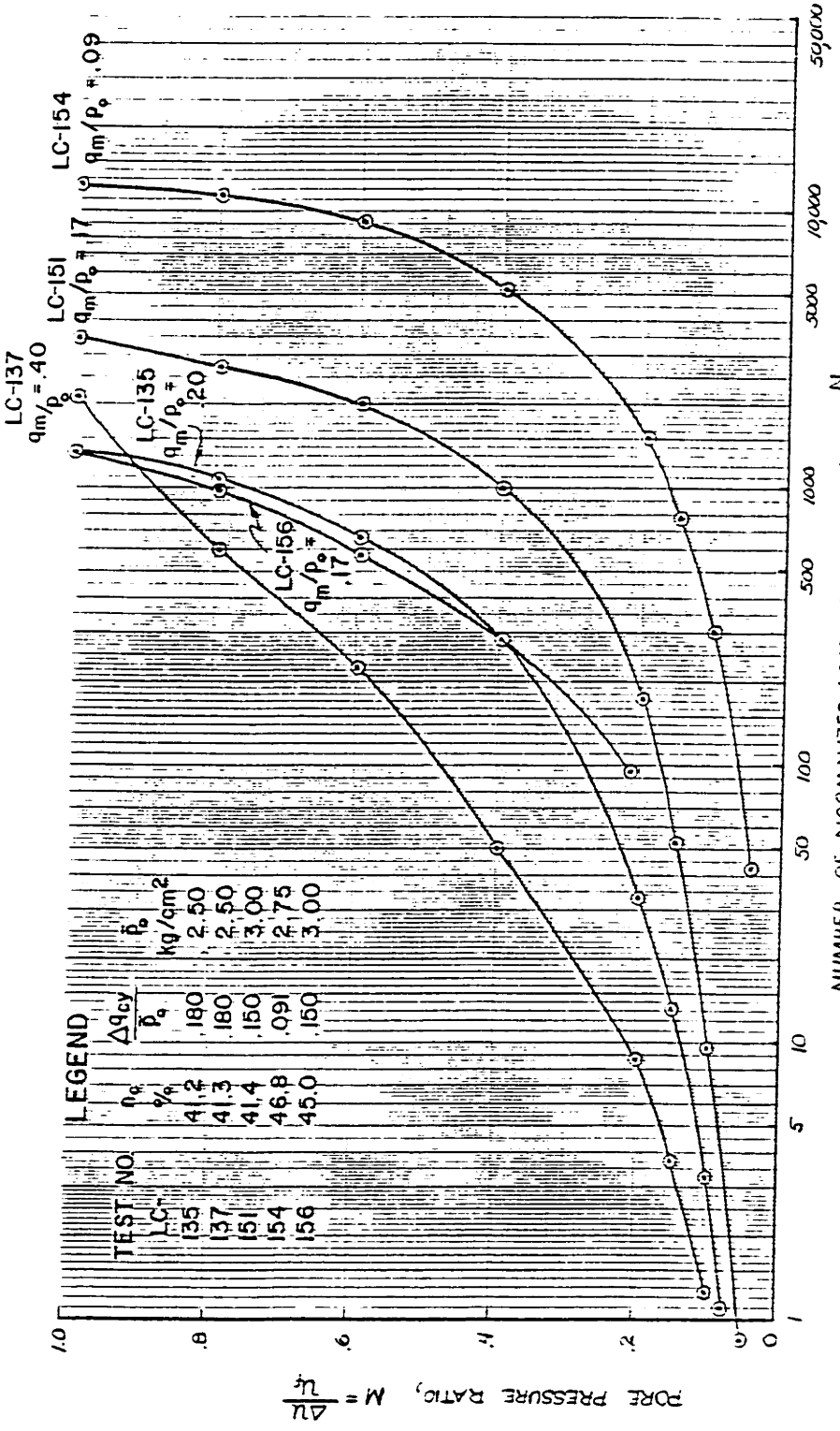

PORE PRESSURE RATIO VERSUS NUMBER OF NORMALIZED LOAD CYCLES IN COMPRESSION TESTS

FIGURE E-67

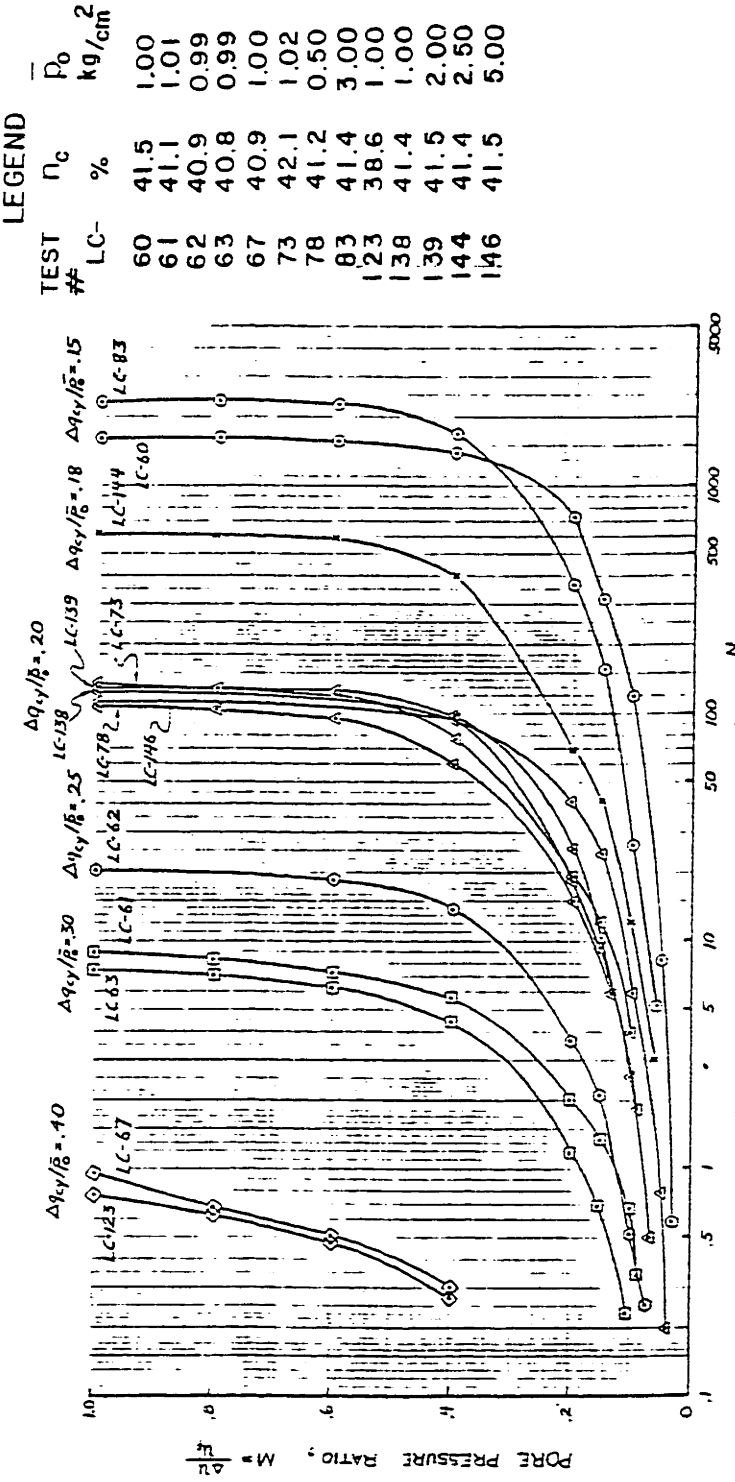

PORE PRESSURE RATIO VERSUS NUMBER OF NORMALIZED LOAD CYCLES IN ISOTROPIC TESTS

FIGURE E-68

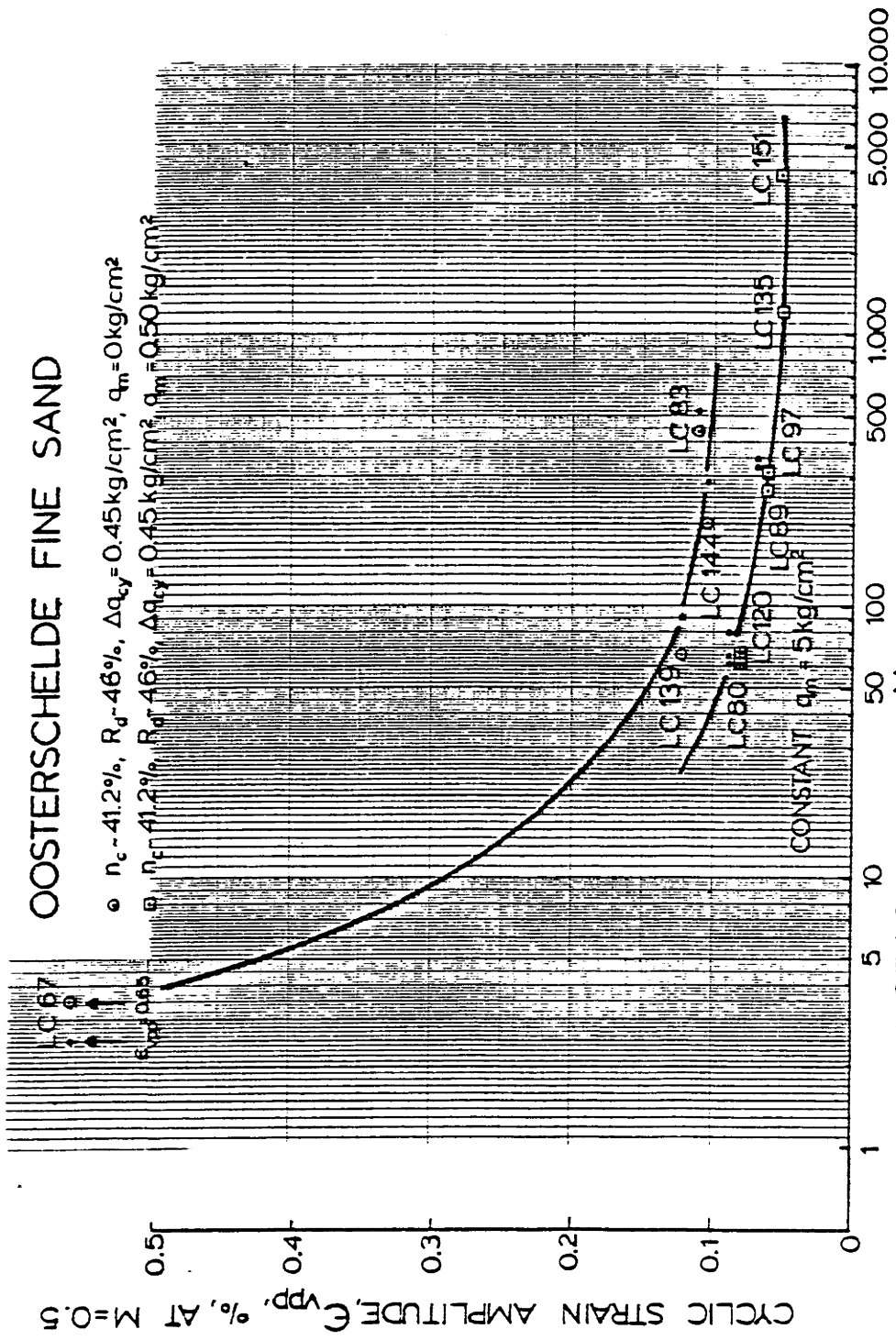

INFLUENCE OF CYCLIC STRAIN AMPLITUDE ON THE NUMBER OF LOAD CYCLES TO REACH 1% VERTICAL STRAIN IN CYCLIC TESTS WITH CONSTANT MEAN SHEAR STRESSES

FIGURE E-69

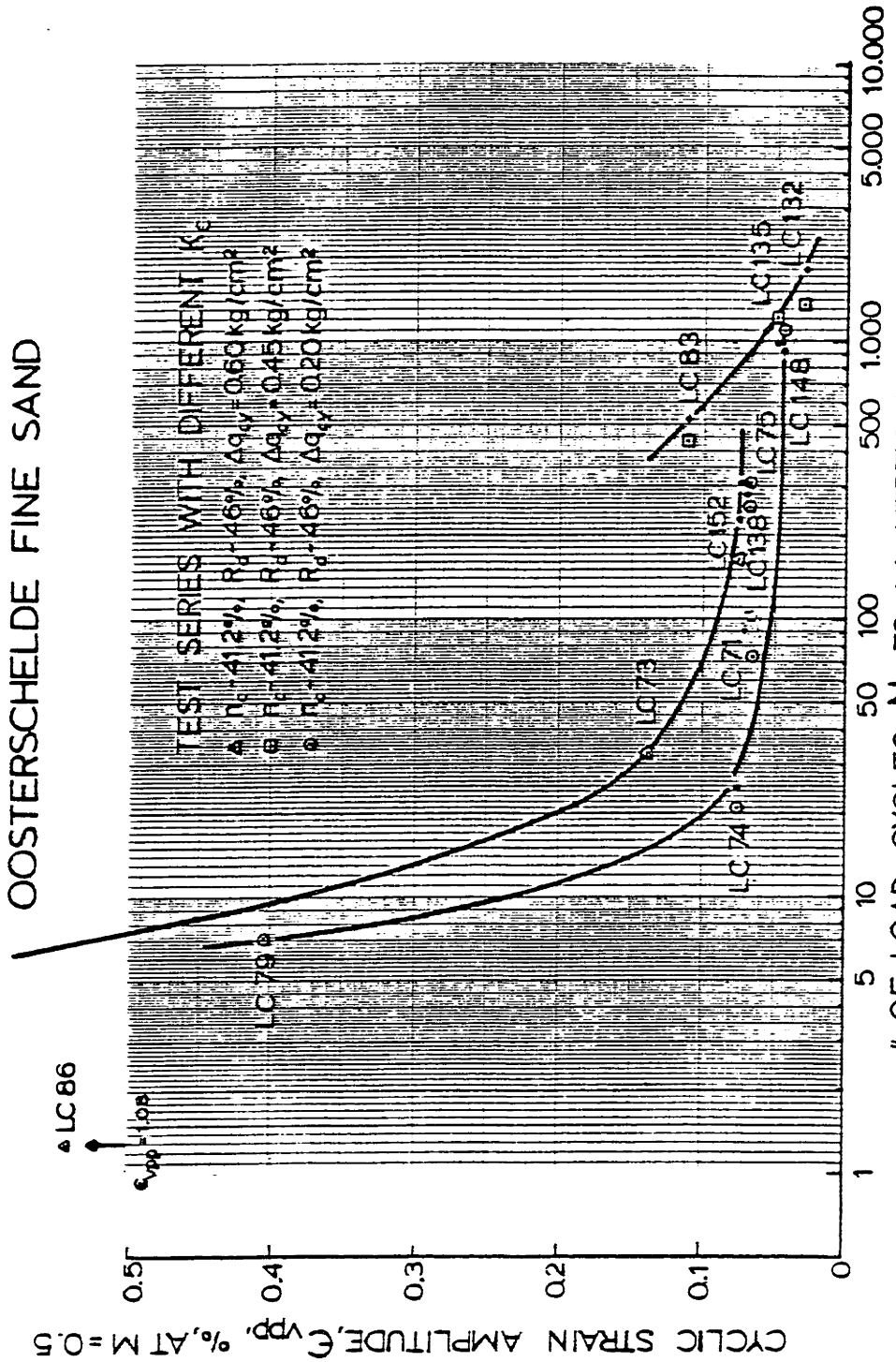

INFLUENCE OF CYCLIC STRAIN AMPLITUDE ON THE NUMBER OF LOAD CYCLES TO REACH 1% VERTICAL STRAIN IN CYCLIC TESTS WITH CONSTANT CYCLIC SHEAR STRESSES

FIGURE E·70

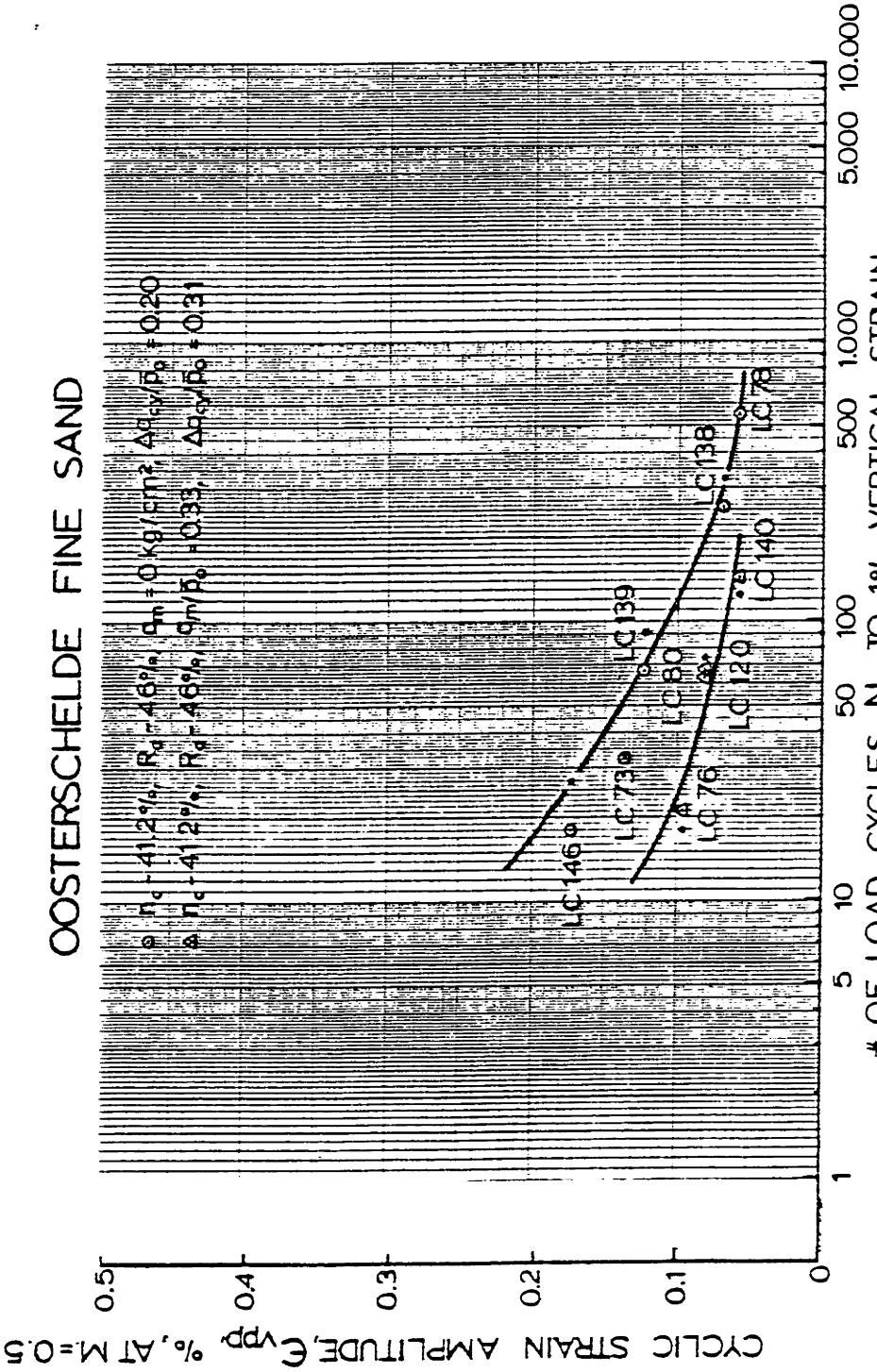

INFLUENCE OF CYCLIC STRAIN AMPLITUDE ON THE NUMBER OF LOAD CYCLES TO REACH 1% VERTICAL STRAIN IN CYCLIC TESTS WITH CONSTANT CYCLIC STRESS RATIOS

FIGURE E-71

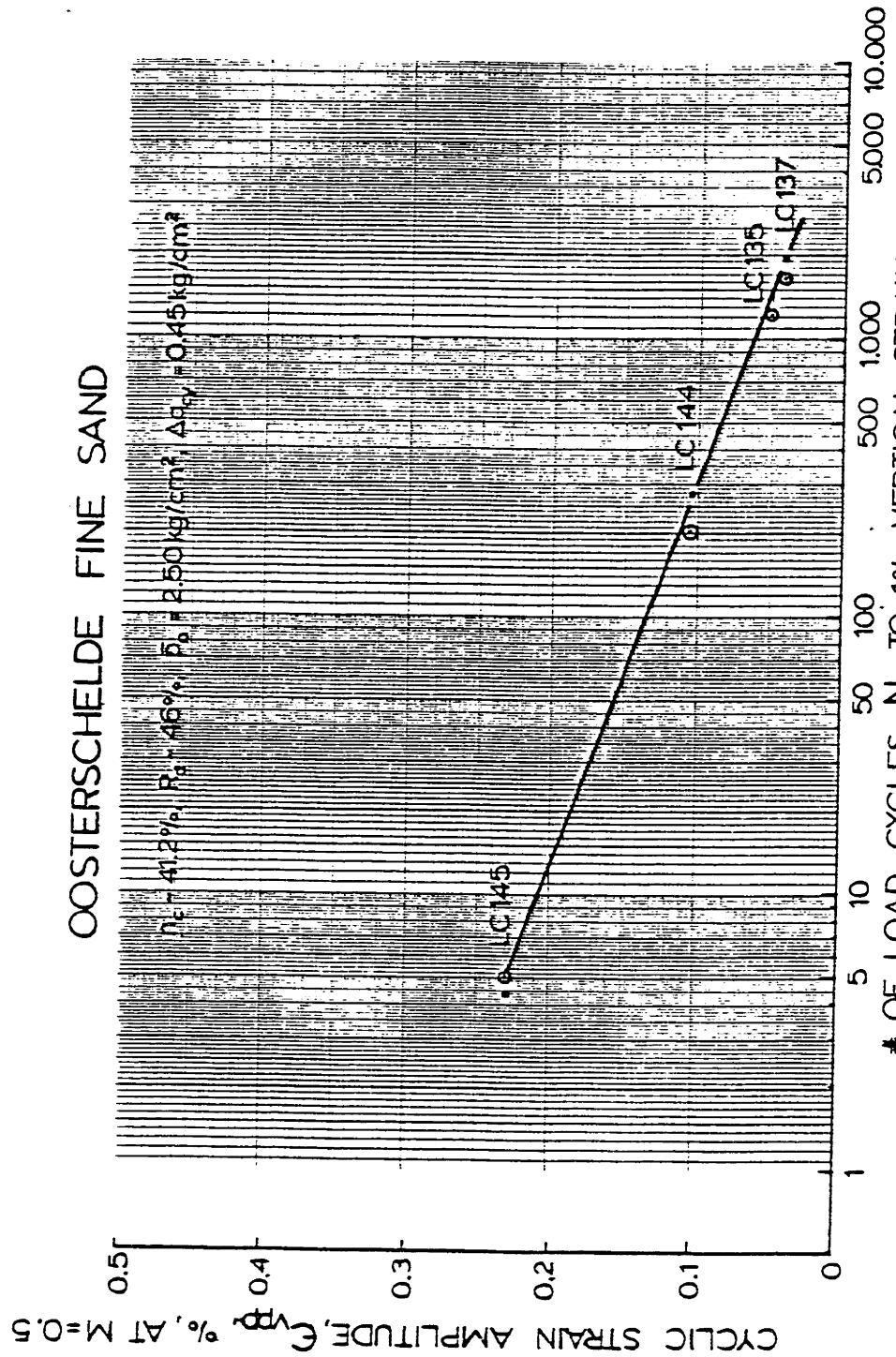

INFLUENCE OF CYCLIC STRAIN AMPLITUDE ON THE NUMBER OF LOAD CYCLES TO REACH 1% VERTICAL STRAIN IN CYCLIC TESTS WITH DIFFERENT MEAN SHEAR STRESSES

FIGURE E-72

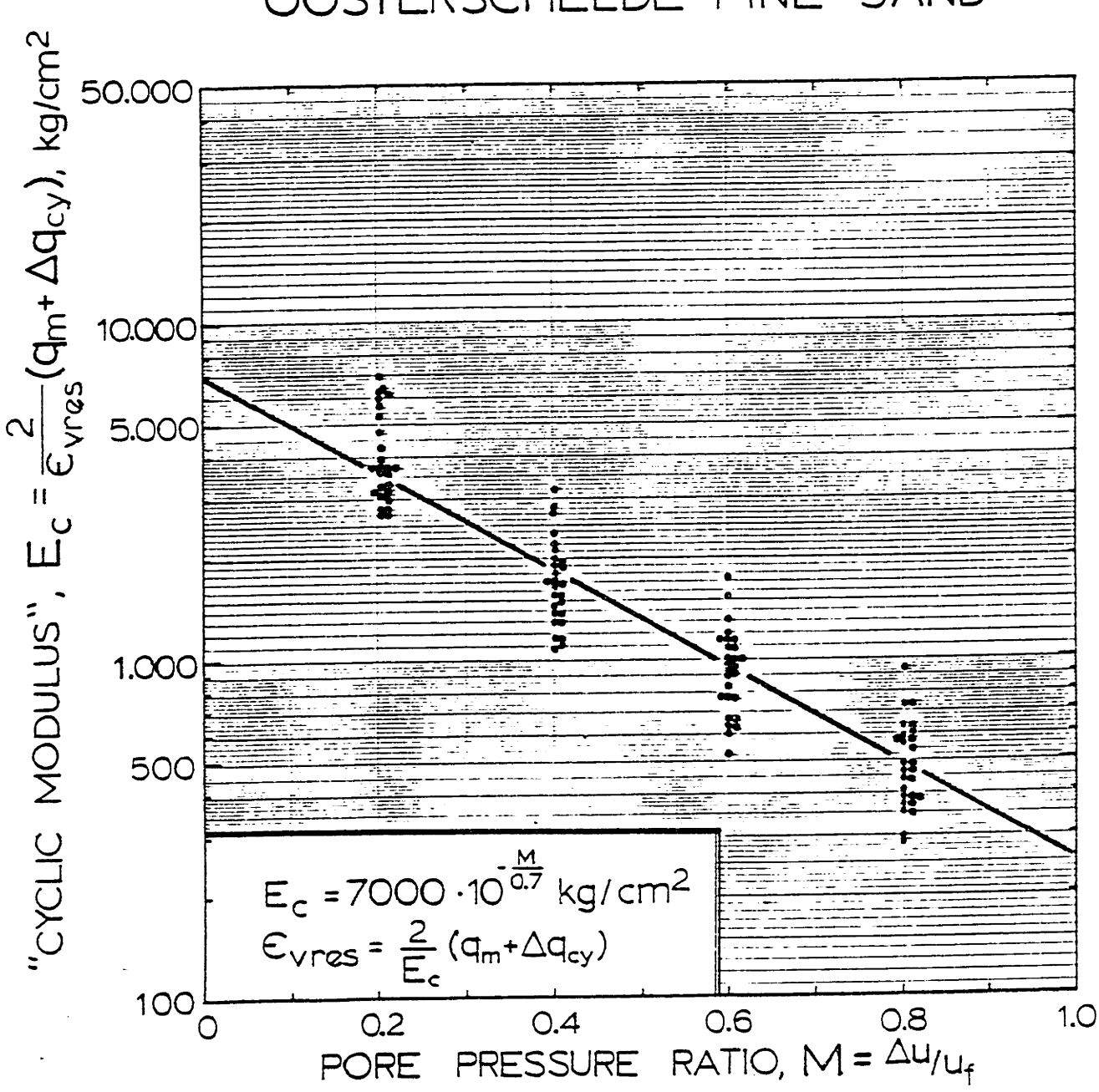

CYCLIC MODULUS FOR COMPRESSION TESTS

FIGURE E-73

APPENDIX F

Cyclic Triaxial Test Results

This appendix gives a tabulation of the cyclic triaxial tests utilized for the prediction procedure described in this report, and the tests performed to investigate the effects of stress history and drainage. For easy reference, tables are provided and organized according to test type: Tables F.1a, b, and c contain cyclic isotropic tests and cyclic extension tests; Tables F.2a, b, and c contain cyclic compression tests, and Tables F.3a, b, and c contain "special" cyclic tests to examine dilation and liquefaction, drainage and stress history. The tables, besides giving stresses, porosities and friction angles (a), give the development of strain (b), and pore pressure throughout the cyclic tests (c). These strain and pore pressure values are plotted for test series where porosity or stress path is varied, to give strain and pore pressure contours for the prediction procedure (Chapter IV and Appendix E).

F.1 Test Tabulations and Plots

The cyclic triaxial tests performed during this investigation are reported in detail below. The tests are for easy reference organized according to type: cyclic isotropic tests, cyclic compression tests, cyclic extension test and

"special" cyclic test, containing tests with stress history, drained tests and tests that contracted or liquefied. Plots from a representative selection of tests are given.

Cyclic Isotropic Tests

The 14 cyclic isotropic tests are tabulated in Table F.1a, b and c. These tables contain in addition 8 cyclic extension tests. Figure F.1 shows the effective stress path and the stress-strain curve for selected cycles in test LC123. Lines signifying a friction angle of $\bar{\phi}$ = 36 degrees are drawn on the effective stress path plot. All cycles are numbered. Figure F.2 presents the maximum, mean and minimum values of shear stress acting on the sample in each load cycle (top plot). The corresponding values of vertical strain, pore pressure and mean effective stress are plotted in the three following plots (Chapter II gives detailed descriptions). All tests are presented in this form. Figures F.3 and F.4 present test LC138. This test was reconsolidated after the cyclic mobility failure, and subjected to further cyclic loading, presented in Figures F.5 and F.6. The sample then failed during the first load cycle. Figures F.7 to F.12 present test LC139 with two reconsolidations, as Figures F.15 to F.24 for test LC146 with four reconsolidations.

Cyclic Compression Tests

Figures F.25 and F.26 present test LC75, a cyclic compression test with slight stress reversal. The test suffered a failure in cyclic mobility. Figures F.27 to F.68 give further compression test plots. Test LC143 (Figures F.55 and F.56) is another test with slight stress reversal. All test results are tabulated in Tables F.2a, b and c.

Cyclic Extension Tests

Figures F.69 and F.70 present a cyclic extension test with slight stress reversal. After accumulating some extension strains, the sample fails by cyclic mobility. Further extension tests are presented in Figures F.71 to F.78. The test results are tabulated in Tables F.1a, b and c.

Special Cyclic Tests

Tables F.3a, b and c present the test results from all test deviations from standard undrained test procedure, or responding with dilation or liquefaction rather than contraction. Figures F.79 and F.80 present a cyclic compression test run with a period of 42 sec. Figures F.81 and F.82 show a test on loose sand that liquefied during the first loading and strained 8%, but dilated at the failure line. Note that the effective stress paths follow the inclination of the failure line ($\sim$ 31°), rather than being inclined 46 - 47 degrees.

Figures F.83 and F.84 present the cyclic compression test LC94 that dilated, after initially contracting. LC95 is the isotropic reconsolidated sample of test LC94, and did also dilate after an initial contraction (Figures F.85 and F.86). Test LC100 in Figures F.87 and F.88 was reconsolidated after reaching a pore pressure ratio of 0.44 in 25 load cycles. Test LC102 in Figures F.89 and F.90 had a loose middle layer. Test LC103 in Figures F.91 and F.92 was reconsolidated after reaching a pore pressure ratio of 0.45 in 99 cycles. LC106 was run with a loading period of 3.6 sec. Test LC117 in Figures F.95 and F.96 was reconsolidated after reaching a pore pressure ratio of 0.69 in 140 cycles. Test LC119 reached M = 0.54 in 24 cycles. The first stage of test LC121 (200 cycles) was run at a cyclic shear stress of 0.45 kg/cm^2, the last 8600 cycles with Δq_{cy} = 0.35 kg/cm^2. Test LC122 was the other way around, first came 1500 load cycles with Δq_{cy} = 0.35 kg/cm^2, then 1550 cycles with Δq_{cy} = 0.45 kg/cm^2. The load change can clearly be seen in both of the summary plots.

Test LC124I was drained off 10% of the generated pore pressure each 50th cycle for the first 900 cycles. The summary plot in figure F.104 shows a curve of volumetric strain instead of pore pressure. After the 900 partially drained load cycles, the sample was reconsolidated, and loaded cyclically undrained (Figures F.105 and F.106). Test LC125 (Figures F.107 and F.108) had an over consolidation ratio of

Cyclic Compression Tests

Figures F.25 and F.26 present test LC75, a cyclic compression test with slight stress reversal. The test suffered a failure in cyclic mobility. Figures F.27 to F.68 give further compression test plots. Test LC143 (Figures F.55 and F.56) is another test with slight stress reversal. All test results are tabulated in Tables F.2a, b and c.

Cyclic Extension Tests

Figures F.69 and F.70 present a cyclic extension test with slight stress reversal. After accumulating some extension strains, the sample fails by cyclic mobility. Further extension tests are presented in Figures F.71 to F.78. The test results are tabulated in Tables F.1a, b and c.

Special Cyclic Tests

Tables F.3a, b and c present the test results from all test deviations from standard undrained test procedure, or responding with dilation or liquefaction rather than contraction. Figures F.79 and F.80 present a cyclic compression test run with a period of 42 sec. Figures F.81 and F.82 show a test on loose sand that liquefied during the first loading and strained 8%, but dilated at the failure line. Note that the effective stress paths follow the inclination of the failure line ($\sim 31°$), rather than being inclined 46 - 47 degrees.

Figures F.83 and F.84 present the cyclic compression test LC94 that dilated, after initially contracting. LC95 is the isotropic reconsolidated sample of test LC94, and did also dilate after an initial contraction (Figures F.85 and F.86). Test LC100 in Figures F.87 and F.88 was reconsolidated after reaching a pore pressure ratio of 0.44 in 25 load cycles. Test LC102 in Figures F.89 and F.90 had a loose middle layer. Test LC103 in Figures F.91 and F.92 was reconsolidated after reaching a pore pressure ratio of 0.45 in 99 cycles. LC106 was run with a loading period of 3.6 sec. Test LC117 in Figures F.95 and F.96 was reconsolidated after reaching a pore pressure ratio of 0.69 in 140 cycles. Test LC119 reached M = 0.54 in 24 cycles. The first stage of test LC121 (200 cycles) was run at a cyclic shear stress of 0.45 kg/cm^2, the last 8600 cycles with Δq_{cy} = 0.35 kg/cm^2. Test LC122 was the other way around, first came 1500 load cycles with Δq_{cy} = 0.35 kg/cm^2, then 1550 cycles with Δq_{cy} = 0.45 kg/cm^2. The load change can clearly be seen in both of the summary plots.

Test LC124I was drained off 10% of the generated pore pressure each 50th cycle for the first 900 cycles. The summary plot in figure F.104 shows a curve of volumetric strain instead of pore pressure. After the 900 partially drained load cycles, the sample was reconsolidated, and loaded cyclically undrained (Figures F.105 and F.106). Test LC125 (Figures F.107 and F.108) had an over consolidation ratio of

10. Tests LC126 and LC127 were drained, and have volumetric strain plotted instead of pore pressure in Figures F.110 and F.112. Test LC128I was again a partially drained sample, with 10% of Δu drained off every 50 cycles for 1000 cycles. Figures F.115 and F.116 present the undrained cyclic loading of Test LC128 after partial drainage and consolidation. Test LC133 dilated from the very beginning of the test (Figures F.117 and F.118). Test LC141 was a drained test with a porosity of 43%. Test LC155 (Figure F.121) liquefied during the first load cycle. The dotted line and circles in Figure F.121 signifies measured values at the end of travel for the piston in the triaxial cell. Test LC156 is identical to LC155 that liquefied, but has 0.4% less porosity, and did not liquefy. However, the effective stress path followed the K_f-line rather than being inclined the usual 46-47 degrees.

F.2 Influence of Stress and Strain History

Table F.4 presents 12 cyclic isotropic tests where the triaxial sample was brought to cyclic mobility failure and reconsolidated several times. Whatever number of load cycles were required to cause cyclic mobility the first time, 1 or 2 load cycles were enough to bring about cyclic mobility after the first and second reconsolidation, although the average sample porosity then was much lower. Static tests that liquefied, did not reliquefy after reconsolidation, suggesting

that the repeated cyclic mobility failures in cyclic tests can be caused by redistribution of voids occurring when the sample is sheared back and forth at zero effective stress.

Test LC54 was subjected to 50 drained load cycles before starting undrained cyclic loading. The sample required 249 cycles to reach cyclic mobility, whereas the identical test LC62 without the drained preloading required only 59 cycles. Test sample LC58 was subjected to zero effective stress for a very short period of time, and without straining more than 0.3%. The subsequent undrained cyclic loading brought about cyclic mobility in 10 cycles, whereas an interpolation on Figure IV.24 for a cyclic shear stress of 0.255 kg/cm^2 gives 115 cycles to failure.

Test LC121 strained 0.5% in 200 load cycles at a cyclic shear stress of 0.45 kg/cm^2. After decreasing the cyclic shear stress to 0.35 kg/cm^2 (but no consolidation), 6800 load cycles were required to produce an additional 1.8% vertical strain accumulation. Tests LC122 and LC142 at a cyclic shear stress of 0.35 kg/cm^2 but with no precycling, required respectively 1320 and 1420 load cycles to accumulate 1.8% strain between the same two strain values (0.5 and 2.3% ε_v). Test LC122 accumulated 2.2% vertical strain in 1500 load cycles of 0.35 kg/cm^2 cyclic shear stress. An additional 2% vertical strain was accumulated in 490 load cycles with 0.45 kg/cm^2 cyclic shear stress. Comparable tests at Δq_{cy} =

0.45 kg/cm^2 and no precycling required 205 (LC89) and 360 (LC97) cycles to accumulate the same 2% ε_v.

Test LC124, where 10% of the accumulated pore pressure were drained off every 50 cycles, required 900 cycles to reach 0.23% vertical strain. The comparable tests LC89 and LC97 required respectively 130 and 170 cycles. Test LC128 required 1000 load cycles to reach 0.15% vertical strain with 10% pore pressure being drained off each 50 cycles. LC129 reached the same strain in 180 undrained cycles. In undrained loading after the partially drained preloading and reconsolidation, both tests required about 4 times as many load cycles to reach 1% strain as tests with no preloading (2800 versus 700 and 1130 versus 270/320).

The drained cyclic compression test LC126 required 28,000 load cycles to reach 1.2% vertical strain, comparable undrained tests 400 and 470 cycles (LC89 and LC97). The drained compression test LC141 reached 1% vertical strain in 2600 cycles, the undrained counterpart LC118 required only 22 cycles to 1% ε_v. The drained cyclic isotropic test LC127 reached 0.1% peak-to-peak strain in 2000 cycles, the undrained test LC146 the same in 12 cycles. Figure F.124 presents a plot of vertical strain versus log number of cycles for the three drained tests.

Cyclic tests that were reconsolidated after reaching a pore pressure ratio of about 0.5 and then reloaded, showed the

following number of load cycles to reach the pore pressure ratio the first and second loading:

Test #	M	$\Delta V/V_c$ %	# of Load Cycles 1st Time	2nd Time
LC100	.44	.24	25	130
LC103	.45	.12	99	625
LC117	.69	.11	140	610
LC119	.54	.25	24	265

Test LC102 had one loose layer and strained 5% in 110 load cycles. The identical test, LC116, with the same uniform porosity, required 810 load cycles to strain 5%.

The results of all the special tests discussed above are synthesized in Figures III.7 and III.8 in Chapter III.

Test # LC	Type	$\bar{\sigma}_{vo}$ kg/cm^2	$\bar{\sigma}_{ho}$ kg/cm^2	$\bar{p}_o$ kg/cm^2	K_c -	Δq_{cy} kg/cm^2	q_m kg/cm^2	B %	$\frac{\Delta V_{cons}}{V_i}$ %	n_c %	$\bar{\varphi}_{cycl}$ °	ε_{vres} %	ε_{vpp} %	Δu kg/cm^2	N -	$\frac{\Delta V_{end}}{V_c}$ %	$\bar{\varphi}_{stat}$ °	REMARKS
60	CIU	1.00	1.00	1.00	1.0	.15	0	100	.28	41.5	40.3	-1.65	12.9	1.00	2712	3.04	-	Isotropic
61	CIU	1.01	1.01	1.01	1.0	.30	0	100	.31	41.1	37.3	-2.20	9.3	1.03	30	3.58	34.7**	Isotropic
62	CIU	.99	.99	.99	1.0	.25	0	99	.22	40.9	36.9	-1.40	17.0	1.01	86	3.43	38.1	Isotropic
63	CIU	.99	.99	.99	1.0	.30	0	99	.27	40.8	38.3	-1.80	15.0	1.02	40	3.02	38.2	Isotropic
67	CIU	1.00	1.00	1.00	1.0	.40	0	99	.28	40.9	39.5	-.20	20.9	1.01	13	3.16	-	Isotropic
72	CIU	1.00	1.04	1.02	1.04	.44	0	98	.17	41.4	36.3*	-.45	23.5	1.00	11	2.83	-	Isotropic
73	CIU	3.00	3.00	3.0	1.0	.60	0	98	.86	41.2	38.7	-1.43	21.2	3.02	39	3.77	-	Isotropic
78	CIU	.50	.51	.50	1.0	.10	0	100	.16	41.2	35.4*	1.43	17.65	.54	540	4.01	-	Isotropic
83	CIU	3.00	3.01	3.00	1.0	.45	0	99	.97	41.4	39.1	-1.97	18.17	3.02	451	4.15	33.8	Isotropic
123	CIU	1.00	1.00	1.00	1.0	.40	0	100	.23	38.6	38.7	-1.29	11.81	1.0	87	2.51	-	Isotropic
138	CIU	1.00	1.0	1.00	1.0	.20	0	100	.22	41.4	36.2	-1.35	14.14	1.01	260	3.23	-	Isotropic
139	CIU	2.00	2.00	2.00	1.0	.40	0	99	.59	41.5	40.4	-2.68	10.99	2.06	70	3.29	-	Isotropic
144	CIU	2.50	2.50	2.50	1.0	.45	0	99	.63	41.4	36.7	-2.49	10.03	2.55	206	3.19	-	Isotropic
146	CIU	5.00	5.00	5.00	1.0	1.0	0	99	1.19	41.5	36.5	-3.15	13.25	5.05	21	2.86	-	Isotropic
71	CAU	1.00	1.30	1.15	1.30	.20	-.15	98	.41	41.2	41.9	-3.03	17.0	1.16	86	1.46	-	Extension
74	CAU	1.0	1.50	1.25	1.5	.20	-.25	100	.18	41.3	38.0	-12.7	1.2	1.41	110	1.02	-	Extension
79	CAU	1.0	1.81	1.40	1.81	.20	-.40	98	.51	41.2	36.4	-8.40	.21	.28	160	.07	-	Extension
86	CAU	3.0	4.50	3.75	1.5	.60	-.75	99	1.18	41.2	36.8	-8.59	.58	1.45	18	.77	27.3	Extension
116	CAU	1.0	1.50	1.25	1.50	.20	-.25	100	.39	40.0	38.5	-9.68	.70	1.13	1050	.66	38.9	Extension
136	CAU	3.0	4.50	3.75	1.50	.60	-.75	99	.94	39.9	37.2*	-10.75	.82	.77	120	.19	-	Extension
145	CAU	2.0	3.0	2.50	1.50	.45	-.50	98	.66	41.1	36.6*	-8.00	1.94	.66	20	.82	-	Extension
147	CAU	3.0	4.5	3.75	1.5	.60	-.75	99	.95	40.0	39.8	-7.13	.52	1.04	110	.16	-	Extension

*different criterion

**undrained

SUMMARY TABLE OF CYCLIC ISOTROPIC AND EXTENSION TESTS

TABLE F.10

Test # LC	Type	At N=1 ϵ_v%	NUMBER OF CYCLES AT FOLLOWING STRAINS, ϵ_v or ϵ_{vpp},%											A at 1st max. q	ESP INCLINATION θ,°			
			.005	.01	.02	.05	.1	.2	.5	1.0	2.0	5.0	10.0		Cy. 1	At .5M	At M-1	At ϵ_v-5%
60	$\overline{CIU}$	.015	-	-	-	-	-		2702	2704	2706	2708	2710	.24	59.1	65.2	-	-
61	$\overline{CIU}$	.045	-	-	-	13	20	22	23	25	27	29	31	.23	58.8	67.6	-	-
62	$\overline{CIU}$	.02	-	-	1	62	70	71	75	77	78	81	83	.23	58.3	69.6	-	-
63	$\overline{CIU}$	.045	-	-	-	11	24	28	29	31	33	36	38	.26	58.0	69.3	-	-
67	$\overline{CIU}$	.25	-	-	-	-	-	-	1	3	4	6	7	.19	57.7	~80.0	-	-
72	$\overline{CIU}$	.30	-	-	-	-	-	-	1	2	3	5	6.5	.21	61.1	61.1	-	-
73	$\overline{CIU}$	.045	-	-	-	12	28	30	31	32	33	34	36	.28	55.4	62.3	-	-
78	$\overline{CIU}$	.015	-	-	300	500	500	501	530	532	534	536	538	.14	56.2	-	-	-
83	$\overline{CIU}$	.02	-	-	1	220	437	444	445	446	447	449	450	.23	55.1	60.9	-	-
123	$\overline{CIU}$	.069	-	-	-	-	24	39	42	52	60	71	81	.19	56.4	74.0	-	-
138	$\overline{CIU}$	.021	-	-	-	241	248	250	254	256	257	259	260	.21	54.4	-	-	-
139	$\overline{CIU}$	.036	-	-	-	-	-	-	65	67	68	69	70	.18	54.5	60.7	-	-
144	$\overline{CIU}$	.033	-	-	-	-	-	-	200	202	203	205	206	.23	54.2	60.1	-	-
146	$\overline{CIU}$	.066	-	-	-	-	-	-	17	18	19	20	22	.29	54.0	61.5	86.5	-
71	$\overline{CAU}$	.03	-	-	-	7	40	60	70	73	80	83	84	.23	57.4	66.8	87.6	-
74	$\overline{CAU}$	.08	-	-	-	-	2	7	13	22	33	60	90	.25	57.1	70.2	93.3	125.0
79	$\overline{CAU}$	.38	-	-	-	-	-	-	2	7	24	92	~190	.30	54.7	54.7	95.4	106.1
86	$\overline{CAU}$	1.05	-	-	-	-	-	-	1	1	3	12	>20	.28	41.3	-	-	124.2
116	$\overline{CAU}$	.024	-	-	-	27	98	171	250	333	480	810	~1080	.34	63.2	69.3	89.0	101.8
136	$\overline{CAU}$	.079	-	-	-	-	2	9	22	32	55	96	119	.32	57.3	70.2	89.2	112.6
145	$\overline{CAU}$	.215	-	-	-	-	-	-	3	5	9	16	22	.25	51.7	-	96.8	132.6
147	$\overline{CAU}$	.095	-	-	-	-	1	7	21	32.5	51	92	-	.29	55.2	69.6	86.6	118.0

TABLE E.1b

STRAIN DEVELOPMENT IN CYCLIC ISOTROPIC AND EXTENSION TESTS

Test # LC	Type	u at N=1 kg/cm²	M at N=1	M = .05 N	M = .05 ε_v %	M = .1 N	M = .1 ε_v %	M = .15 N	M = .15 ε_v %	M = .20 N	M = .20 ε_v %	M = .40 N	M = .40 ε_v %	M = .60 N	M = .60 ε_v %	M = .80 N	M = .80 ε_v %	M=1.0 N	u_f kg/cm²	At M=1 $\bar{\varphi}_{max}$ °	At M=.5 ε_{vpp} %
60	$\overline{CIU}$	.027	.028	14	.02	202	.02	532	.00	1220	.03	2340	.04	2630	.08	2700	.13	2706	.97	38.3	.06
61	$\overline{CIU}$	.081	.85	-	-	2	.04	4	.04	5	.04	17	.07	22	.23	25	.47	27	.95	36.5	.28
62	$\overline{CIU}$	.066	.072	-	-	2	.02	8	.02	14	.02	52	.03	70	.08	-	-	78	.92	≈37	.12
63	$\overline{CIU}$	.101	.106	-	-	-	-	3	.04	4	.04	19	.06	27	.16	31	.53	33	.96	37.5	.19
67	$\overline{CIU}$	.314	.345	-	-	-	-	-	-	-	-	-	-	-	-	-	-	3.5	.91	≈34	.67
72	$\overline{CIU}$	.302	.487	-	-	-	-	-	-	-	-	-	-	1	.34	2	.50	3	.62	33.1	.68
73	$\overline{CIU}$	.267	.094	-	-	1	.05	3	.05	4.5	.04	19	.06	29	.14	31	.39	32.5	2.85	≈34	.15
78	$\overline{CIU}$	.020	.040	4	.015	30	.015	120	.015	200	.015	450	.02	-	-	-	-	534	≈.50	-	.06
83	$\overline{CIU}$	.145	.050	1	.03	8	.03	30	.03	70	.03	322	.05	429	.08	445	.34	447	2.93	33.8	.12
123	$\overline{CIU}$	.109	.118	-	-	-	-	2	.060	3	.06	23	.09	39	.20	48	.38	60	.92	37.9	.29
138	$\overline{CIU}$	.063	.07	-	-	5	.02	20	.02	50	.02	190	.03	242	.09	>250	-	256	.95	-	.073
139	$\overline{CIU}$	.178	.091	-	-	1	.035	5	.031	10	.03	50	.05	-	-	-	-	67	1.95	35.7	.131
144	$\overline{CIU}$	.148	.061	-	-	4	.031	14	.031	23	.03	134	.035	193	.08	201	.41	203	2.41	35.1	.113
146	$\overline{CIU}$	.586	.133	-	-	-	-	1	.066	2	.057	10	.07	16	.15	18	.61	19	4.40	32.3	.190
71	$\overline{CAU}$	.069	.112	-	-	-	-	3	-.04	5	-.04	30	-.08	54	-.16	65	-.38	73	.62	≈37.0	.07
74	$\overline{CAU}$	.103	.215	-	-	-	-	-	-	1	-.07	4	-.14	8	-.24	14	-.44	21	.48	33.9	.08
79	$\overline{CAU}$	.207	.591	-	-	-	-	-	-	-	-	-	-	1	-.36	3	-.56	7	.35	33.5	.41
86	$\overline{CAU}$	-	-	-	-	-	-	-	-	--	-	-	-	-	-	-	-	1	1.29	30.7	1.08
116	$\overline{CAU}$	.025	.046	1	-.017	4	-.024	9	-.030	16	-.03	70	-.07	140	-.14	200	-.29	335	.55	38.6	.048
136	$\overline{CAU}$	.357	.244	-	-	-	-	-	-	1	-.08	4	-.12	10	-.21	20	-.46	32	1.46	35.8	.09
145	$\overline{CAU}$	.442	.496	-	-	-	-	-	-	-	-	3/4	-.18	2	-.36	3	-.58	5	.89	34.5	.239
147	$\overline{CAU}$	.391	.244	-	-	-	-	-	-	3/4	-.08	4	-.15	13	-.30	21	-.50	33	1.60	36.7	.091

PORE PRESSURE DEVELOPMENT IN CYCLIC ISOTROPIC AND EXTENSION TESTS

TABLE F.1c

Test # LC	Type	$\bar{\sigma}_{vo}$ kg/cm^2	$\bar{\sigma}_{ho}$ kg/cm^2	$\bar{P}_o$ kg/cm^2	K_c -	Δq_{cy} kg/cm^2	q_m kg/cm^2	B %	$\frac{\Delta V_{cons}}{V_i}$ %	n_c %	$\bar{\varphi}_{cycl}$ °	ε_{vres} %	ε_{vpp} %	Δu kg/cm^2	N -	$\frac{\Delta V_{end}}{V_c}$ %	$\bar{\varphi}_{stat}$ °	REMARKS
66	CAU	1.00	.50	.75	.50	.20	.25	99	.17	40.39	39.1	6.30	.06	.27	19800	.12	-	Compression
68I	CAU	3.00	2.50	2.75	.83	.20	.25	100	.74	40.86	-	.03	.02	.31	29460	.03	-	Compression
75	CAU	1.00	.70	.85	.70	.20	.15	98	.19	40.90	38.8*	.85	12.6	.65	421	1.28	-	Compression
76	CAU	3.00	1.51	2.25	.50	.70	.75	99	.48	41.16	39.0	10.8	.14	.92	520	.17	38.2	Compression
80	CAU	2.00	1.01	1.50	.50	.45	.50	100	.35	41.21	38.1	12.55	.10	.58	1700	.17	-	Compression
89	CAU	2.50	1.50	2.00	.60	.45	.50	100	.52	41.37	38.8	10.0	.12	1.09	1305	.31	37.3	Compression
97	CAU	2.50	1.50	2.00	.60	.45	.50	99	.51	41.26	37.7	12.3	.10	1.07	2525	.30	36.4	Compression
104	CAU	2.50	1.50	2.00	.60	.45	.50	99	.56	41.93	37.4	8.37	.11	1.04	650	.30	36.7	Compression
105	CAU	2.50	1.50	2.00	.60	.45	.50	100	.37	39.73	32.8*	.36	.08	.66	9500	.10	38.5	Compression
118	CAU	2.50	1.50	2.00	.60	.45	.50	100	.60	42.93	37.2	11.03	.21	1.22	130	.42	-	Compression
120	CAU	2.00	1.00	1.50	.50	.45	.50	99	.39	41.37	38.7	10.09	.11	.58	1100	.24	-	Compression
129	CAU	2.50	1.50	2.00	.60	.25	.50	99	.59	43.48	34.2	13.52	.05	1.10	3600	.38	-	Compression
130	CAU	2.50	1.50	2.00	.60	.35	.50	100	.59	43.19	36.1	10.15	.084	1.06	1000	.31	-	Compression
131	CAU	2.50	1.50	2.00	.60	.15	.50	100	.54	42.92	32.9	1.75	.033	.96	10700	.29	-	Compression
132	CAU	3.00	1.50	2.25	.50	.45	.75	100	.48	41.42	36.2	4.71	.07	.72	9700	.15	-	Compression
134	CAU	2.50	1.50	2.00	.60	.25	.50	99	.52	40.68	-	.38	.042	.56	20000	-	39.2	Compression
135	CAU	3.00	2.00	2.50	.67	.45	.50	99	.63	41.20	38.5	12.82	.114	1.64	3000	.31	-	Compression
137	CAU	3.50	1.50	2.50	.43	.45	1.00	100	.54	41.30	35.2	4.33	.062	.51	29120	.08	-	Compression
140	CAU	1.00	.50	.75	.50	.23	.25	99	.19	41.11	40.2	13.10	.115	.34	3100	-	-	Compression
142	CAU	2.50	1.50	2.00	.60	.35	.50	100	.40	41.71	36.4	8.39	.071	1.02	9000	.24	-	Compression
143	CAU	2.50	1.50	2.00	.60	.55	.50	100	.62	43.17	36.9	14.13	7.52	1.51	19	3.70	-	Compression
148	CAU	1.00	.50	.75	.50	.20	.25	100	.19	41.12	36.2	10.18	.065	.26	12000	.11	-	Compression
149	CAU	5.00	2.50	3.75	.50	1.0	1.25	100	.84	41.38	36.7	9.83	.121	1.24	1220	.20	-	Compression
151	CAU	3.50	2.50	3.00	.71	.45	.50	99	.72	41.44	38.5	10.34	.107	2.01	6650	.34	-	Compression
152	CAU	3.00	1.50	2.25	.50	.60	.75	99	.73	41.41	37.7	13.64	.097	.82	3750	.14	-	Compression
154	CAU	3.00	2.50	2.75	.83	.20	.25	100	1.13	46.80	29.3	14.08	.308	2.38	294	1.77	-	Compression
158	CAU	7.00	3.50	5.25	.50	1.40	1.75	99	1.08	41.53	35.0	10.07	.14	1.80	450	.22	-	Compression

*Different criterion

SUMMARY TABLE OF CYCLIC COMPRESSION TESTS

TABLE F.22

Test # LC	Type	At N=1 ε_v%	# OF CYCLES AT FOLLOWING STRAINS; ε_u%											At 1st max. q	ESP INCLINATION ϕ^o			
			.005	.01	.02	.05	.1	.2	.5	1.0	2.0	5.0	10.0		Cy 1	At .5%	At M=1	At ε_v=5%
66	CAU	.00	–	–	2	90	400	900	1900	3270	6400	15150	>20000	.12	50.8	50.8	48.5	47.5
68I	CAU	.00	3303	5355	9660		–	–	–	–	–	–	–		57.1	–	–	–
75	CAU	.00	–	2	10	150	283	358	410	413	416	419	421	.19	53.3	53.0	38.9	34.9
76	CAU	.11	–	–	–	–	–	3	13	31	71	198	470	.10	48.9	49.0	47.0	44.8
80	CAU	.15	–	–	–	–	–	3	22	62	160	515	1258	.18	49.0	48.9	47.5	46.1
89	CAU	.03	–	–	–	4	25	80	160	270	390	700	1305	.19	52.3	52.4	48.6	44.9
97	CAU	.02	–	–	–	9	40	110	220	320	480	980	2000	.16	51.0	51.4	47.6	46.2
104	CAU	.04	–	–	–	2	9	30	80	125	200	410	~770	.20	50.6	50.9	47.2	44.9
105	CAU	.01	–	1	4	90	500	3400	>9500	–	–	–	–	.8	52.5	–	–	–
118	CAU	.061	–	–	–	–	3	8	18	26	41	72	121	.27	50.3	50.3	45.0	39.5
120	CAU	.110	–	–	–	–	–	4	24	66	187	464	1088	.12	48.5	49.0	47.6	46.0
129	CAU	.020	–	–	1	18	90	271	550	703	895	1440	2600	.18	50.6	50.8	48.2	47.1
130	CAU	.024	–	–	–	8	34	84	155	213	306	546	985	.22	51.9	51.7	47.5	45.5
131	CAU	.003	7	45	217	717	1471	3371	5950	8200	11500	–	–	.16	52.4	51.6	47.9	–
132	CAU	.029	–	–	–	10	65	232	670	1350	3040	10500	–	.19	50.9	50.4	48.2	47.5
134	CAU	.007	–	6	60	17	1675	9733	20000	–	–	–	–	.16	52.4	–	–	–
135	CAU	.017	–	–	3	95	439	790	1060	1210	1405	1855	2705	.22	53.5	53.4	48.6	46.5
137	CAU	.056	–	–	–	–	9	62	440	1680	~7350	~36500	–	.08	49.3	49.7	49.3	47.4
140	CAU	.021	–	–	–	9	38	99	240	435	745	1445	2600	.12	50.6	50.4	48.2	46.8
142	CAU	.012	–	–	8	83	270	563	990	1400	2120	4700	–	.16	52.0	51.9	48.2	47.2
143	CAU	.10	–	–	–	–	–	3	7	11	15	17	18	.28	49.0	48.7	41.0	–
148	CAU	.014	–	–	2	19	68	193	575	1105	2140	5405	11765	.09	49.7	50.2	48.2	47.2
149	CAU	.107	–	–	–	–	–	4	19	47	117	424	1254	.12	48.4	49.3	48.8	47.1
151	CAU	.009	–	2	30	482	671	2272	3570	3910	4300	5140	6600	.22	53.7	54.8	49.2	47.5
152	CAU	.069	–	–	–	–	3	15	68	165	350	950	2400	.11	49.3	49.6	48.2	47.0
154	CAU	.007	–	2	8	30	67	165	267	282	285	288	291	.37	53.8	55.2	44.9	33.7
158	CAU	.21	–	–	–	–	–	–	5	14	38	139	396	.18	48.3	48.3	47.4	48.3

TABLE E.26

STRAIN DEVELOPMENT IN CYCLIC COMPRESSION TESTS

Test # I.C	Type	u at N=1 kg/cm²	M at N=1	M = .05 N	M = .05 ε_v %	M = .1 N	M = .1 ε_v %	M = .15 N	M = .15 ε_v %	M = .20 N	M = .20 ε_v %	M = .40 N	M = .40 ε_v %	M = .60 N	M = .60 ε_v %	M = .80 N	M = .80 ε_v %	M=1.0 N	u_f kg/cm²	At M=1 $\bar{\varphi}_{max}$	At M=.5 ε_{vpp} %
66	CAU	.032	.151	-	-	-	-	-	-	5	.02	90	.05	400	.10	1020	.23	3270	.215	37.2	.05
681	CAU	-	-	-	-	-	-	-	-	-	-	-	-	-	-	-	-	-	-	-	-
75	CAU	.034	.057	-	-	11	.02	20	.02	45	.03	205	.06	335	.15	390	.34	415	.60	38.8	.07
76	CAU	.185	.318	-	-	-	-	-	-	.5	~.08	2	.16	5	.28	14	.50	31	.58	35.9	.11
80	CAU	.163	.429	-	-	-	-	-	-	-	-	1	.16	7	.29	21	.48	62	.38	35.8	.09
89	CAU	.115	.137	-	-	-	-	1	.04	2.5	.04	24	.10	75	.19	130	.35	270	.84	36	.07
97	CAU	.098	.117	-	-	-	-	2	.03	4	.03	32	.08	90	.16	168	.33	320	.84	35.9	.07
104	CAU	.134	.170	-	-	-	-	-	-	2	.05	11	.10	31	.20	64	.40	125	.79	34.8	.08
105	CAU	.086	.096	-	-	1	.01	4	.02	9	.02	200	.06	1900	.16	-	-	-	.90*	38.6*	.07
118	CAU	.193	.221	-	-	-	-	-	-	.7	.06	4	.12	10	.24	17	.51	26	.87	33.7	.082
120	CAU	.106	.293	-	-	-	-	-	-	1	.07	3	.17	10	.30	27	.54	66	.36	36.1	.090
129	CAU	.055	.065	-	-	4	.029	10	.040	22	.05	125	.11	310	.22	500	.41	703	.84	31.5	.04
130	CAU	.097	.117	-	-	-	-	2	.031	5	.04	28	.10	70	.17	125	.34	213	.83	33.8	.057
131	CAU	.013	.014	24	.007	115	.015	273	.023	490	.04	1500	.10	2800	.17	4680	.31	8200	.93	32.3	.023
132	CAU	.054	.090	-	-	1	.029	5	.041	13	.04	80	.11	230	.20	500	.37	1350	.60	35	.040
134	CAU	.024	.026	8	.011	75	.018	277	.030	600	.05	9800	.20	20000	.38	-	-	-	.91*	34.6*	.036
135	CAU	.097	.073	-	-	3	.020	12	.027	30	.035	260	.07	520	.12	890	.26	1210	1.34	35.8	.060
137	CAU	.037	.099	-	-	1	.056	3	.071	7	.09	40	.17	~180	.25	480	.51	1680	.37	34.7	.050
140	CAU	.031	.146	-	-	-	-	1	.021	3	.03	20	.07	63	.14	160	.32	425	.21	38.2	.063
142	CAU	.052	.059	-	-	5	.012	16	.019	33	.03	125	.06	400	.13	720	.28	1400	.88	35.3	.051
143	CAU	.293	.308	-	-	-	-	-	-	.5	~.07	2	.14	4	.25	7	.48	11	.95	34.2	.119
148	CAU	.022	.119	-	-	-	-	2	.019	4	.025	43	.08	150	.17	340	.31	1105	.188	36.2	.048
149	CAU	.254	.292	-	-	-	-	-	-	3/4	.07	2	.14	7	.26	18	.48	47	.87	5.0	.107
151	CAU	.091	.051	-	-	11	.016	60	.024	200	.027	1150	.14	2310	.20	3100	.26	3910	1.77	35.5	.061
152	CAU	.105	.198	-	-	-	-	-	-	1	.07	7	.14	24	.25	70	.49	165	.53	35.7	.088
154	CAU	.085	.043	1	.011	7	.030	18	.046	35	.06	120	.16	210	.27	263	.46	282	1.99	25.5	.043
158	CAU	.494	.445	-	-	-	-	-	-	-	-	-	-	2	.30	5.5	.52	14	1.11	33.7	.294

PORE PRESSURE DEVELOPMENT IN CYCLIC COMPRESSION TESTS

*calculated values

TABLE E.23

Test # LC	Type	$\bar{\sigma}_{vo}$ kg/cm^2	$\bar{\sigma}_{ho}$ kg/cm^2	$\bar{p}_o$ kg/cm^2	K_c kg/cm^2	Δq_{cy} kg/cm^2	q_m kg/cm^2	B %	$\frac{\Delta V_{cons}}{V_i}$ %	n_c %	$\bar{\Phi}_{cycl}$ °	ϵ_{yres} %	ϵ_{vpp} %	u kg/cm^2	N -	$\frac{\Delta V_{end}}{V_c}$ %	$\bar{\Phi}_{stat}$ °	REMARKS
58	$\overline{CIU}$	.97	1.00	.99	1.02	.225	.0	99	.24	41.25	39.1	-1.45	19.3	1.02	15	3.24	-	$\bar{\sigma}_c$=0 shortly
65	$\overline{CAU}$	1.50	.051	1.0	.30	.20	.50	98	.19	41.4	36.7*	4.80	.04	.07	117000	.03	38.8	11 days long
85	$\overline{CIU}$	1.00	1.01	1.0	1.0	.20	.0	98	.58	41.04	37.7	-1.95	9.60	1.02	1110	3.61	37.7	OCR=10
91	$\overline{CAU}$	2.50	1.50	2.0	.60	.45	.50	99	.50	41.04	37.8	8.70	.10	.99	3610	.26	38.1	T=42 sec.
93	$\overline{CAU}$	2.50	1.50	2.0	.60	.39	.50	99	.78	45.30	31.8	16.84	2.01	1.50	6	3.78	-	Part. Liq.
94	$\overline{CAU}$	2.50	1.50	2.0	.60	.45	.50	100	.39	37.94	-	.12	.04	-.15	10000	-.01	-	Dilated
95	$\overline{CIU}$	3.00	3.00	3.0	1.0	.60	.0	100	.16	37.94	-	-.04	.05	-.43	8500	-.03		Dilated
100	$\overline{CIU}$	5.00	5.00	5.00	1.00	1.0	.0	99	1.01	41.31	42.2	-1.41	9.87	4.95	153	.24	35.3	Reconsolidated
102	$\overline{CAU}$	1.00	1.50	1.25	1.50	.20	.25	99	.40	39.78	43.2	-7.09	.50	.70	190	.26	37.8	Loose Layer
103	$\overline{CIU}$	1.00	1.00	1.00	1.00	.20	.0	99	.34	41.35	36.9	-1.13	13.03	1.03	688	.12	37.0	Reconsolidated
106	$\overline{CAU}$	2.50	1.50	2.00	.60	.45	.50	100	.51	40.89	39.1	9.35	.11	1.07	5400	.26	39.2	T=3.6 sec.
117	$\overline{CAU}$	2.50	1.50	2.00	.60	.45	.50	99	.48	41.05	38.4	10.10	.10	1.04	3660	.26	-	Reconsolidated
119	$\overline{CIU}$	3.00	3.00	3.00	1.00	.60	.0	98	.82	41.04	37.8	-5.42	16.69	2.98	288	3.35	37.0	Reconsolidated
121I	$\overline{CAU}$	2.5	1.5	2.00	.60	.45	.50	98	.46	41.04		.54	.03	-	200		36.0	Δq_{cy}=.45 kg/cm^2
121II	$\overline{CAU}$	2.5	1.5	2.00	.60	.35	.50	-	-	-	36.7*	2.15	-	.96	8600	.25	-	Δq_{cy}=.35 kg/cm^2
122I	$\overline{CAU}$	2.5	1.5	2.00	.60	.35	.50	99	.54	41.06	-	2.24	.10	1.02	1500	-	38.8	Δq_{cy}=.35 kg/cm^2
122II	$\overline{CAU}$	2.5	1.5	2.00	.60	.45	.50	-	-	-	38.9	4.05	-	-	1550	.18	-	Δq_{cy}=.45 kg/cm^2
124I	CAD Δu	2.5	1.5	2.00	.60	.45	.50	100	.47	41.00	-	.23	.07	-	900	-	-	Drained Partial
124II	$\overline{CAU}$	2.5	1.5	2.00	.60	.45	.50	100	.24	40.73	38.0	14.28	.11	1.11	8100	.46	-	Undrained
125	$\overline{CAU}$	2.5	1.5	2.00	.60	.45	.50	100	.79	41.22	38.7	13.44	.11	1.13	6300	.25	-	OCR=5
126	CAD	2.5	1.5	2.00	.60	.45	.50	98	.76	41.02	-	1.16	.07	-	28520	.68*	37.0	Drained
127	CID	5.0	5.0	5.00	1.0	1.0	.0	98	1.09	41.20	-	.176	.11	-	2300	.95*	33.2	Drained
128I	CAD Δu	2.50	1.50	2.00	.60	.25	.50	100	.60	42.97	-	.149	.034	-	1000	-	-	Drained Partial
128II	$\overline{CAU}$	2.50	1.50	2.00	.60	.25	.50	100	-	42.81	35.0	13.73	.05	1.07	16800	.27	-	Undrained
133	$\overline{CAU}$	3.00	1.50	2.25	.50	.25	.75	98	.47	41.25	-	.112	.021	-2.11	29790	-.25	37.1	Dilated
141	CAD	2.50	1.50	2.00	.60	.45	.50	100	.57	43.05	-	2.21	.080	-	30000	-	-	Drained
155	$\overline{CAU}$	3.50	2.50	3.00	.71	.45	.50	100	1.59	45.44	-	.219	-	.73	1/2	2.17	-	Liquefied
156	$\overline{CAU}$	3.50	2.50	3.00	.71	.45	.50	99	1.13	45.00	31.9	10.84	.29	2.11	32	-	-	Contracted

*different criterion

SUMMARY PLOT OF "SPECIAL" CYCLIC TESTS

TABLE F.5B

Test # LC	Type	At N=1 ε_v %	# OF CYCLES AT FOLLOWING STRAINS, ε_v% or ε_{vpp},%											At 1st max. q	ESP INCLINATION, θ°			
			.005	.01	.02	.05	.1	.2	.5	1.0	2.0	5.0	10.0		Cy 1	At .5M	At M=1	At ε_v=5%
58	$\overline{CIU}$	.12	-	-	-	-	2	4	5	6	8	10	12	-	42.4	66.1	-	-
65	$\overline{CAU}$	.01	-	1	2	7	45	250	2850	7800	25000	∿130000	-	.06	46.7	48.1	47.6	-
85	$\overline{CIU}$	.025	-	-	-	1066	1097	1101	1102	1104	1106	1109	1111	.18	59.4	61.6	-	-
91	$\overline{CAU}$	.04	-	-	-	2	30	128	340	550	900	1930	∿4200	.18	51.8	52.0	48.9	47.3
93	$\overline{CAU}$	8.58	-	-	-	-	-	-	1	1	1	1	2	1.26	32.1	-	32.1	32.1
94	$\overline{CAU}$	.02	-	-	1	900	8500	-	-	-	-	-	-	-	-	-	-	-
95	$\overline{CIU}$	.02	-	-	1	4500	-	-	-	-	-	-	-	-	-	-	-	-
100	$\overline{CIU}$	.08	-	-	-	-	137	146	147	149	150	152	153	.28	54.6	57.8	47.3	32.1
102	$\overline{CAU}$	.06	-	-	-	-	13	38	64	84	112	165	-	.25	52.6	66.2	91.0	121.0
103	$\overline{CIU}$	.025	-	-	-	649	661	662	681	682	683	685	687	.18	54.5	55.9	31.9	32.4
106	$\overline{CAU}$	.03	-	-	-	4	60	275	670	1000	1550	3050	5800	.18	51.5	51.7	48.7	48.3
117	$\overline{CAU}$	.001	4	8	60	260	460	604	782	942	1190	1950	-	.18	51.3	51.5	48.1	46.8
119	$\overline{CIU}$	.04	-	-	-	185	277	283	286	288	290	293	-	.37	59.4	62.7	38.4	31.4
121I	$\overline{CAU}$	.040	-	-	-	2	13	53	185	-	-	-	-	.21	51.0	-	-	-
121II	$\overline{CAU}$	-	-	-	-	-	-	-	1420	3110	7875	-	-	-	-	-	-	-
122I	$\overline{CAU}$	.045	-	-	-	2	10	50	80	190	500	-	-	.31	51.6	52.1	48.7	47.7
124I	CAD Δu	.016	-	-	2	50	235	795	-	-	-	-	-	.154	52.9	52.3	49.0	47.7
124II	$\overline{CAU}$	.00	100	250	460	772	1085	1371	1720	2030	2520	3710	5820	-	-	-	-	-
125	$\overline{CAU}$	.002	-	-	1	13	1218	1602	2008	2340	2780	3780	5360	.13	53.0	52.2	48.9	47.1
126	CAD	.208	-	-	-	-	-	-	100	13700	-	-	-	-	45.03	-	-	-
127	CID	.052	-	-	-	-	-	∿3000	-	-	-	-	-	-	45.04	-	-	-
128I	CAD Δu	.009	-	2	30	175	510	-	-	-	-	-	-	-	-	-	-	-
128II	$\overline{CAU}$	-.003	200	320	600	1063	1591	2410	3240	3800	4660	7280	12400	.15	52.7	51.7	48.1	46.8
133	$\overline{CAU}$	.011	-	-	35	515	4330	>29790	-	-	-	-	-	.12	50.7	-	-	-
141	CAD	.064	-	-	-	-	5	36	440	2580	19900	-	-	-	-	-	-	-
155	$\overline{CAU}$	12.7	-	-	-	-	-	-	-	-	-	-	-	-	-	-	-	-
156	$\overline{CAU}$	.059	-	-	-	-	2	5	11	14	17	22	30	.46	50.6	51.3	43.4	35.1

STRAIN DEVELOPMENT IN "SPECIAL" CYCLIC TESTS

TABLE 11.3b

Test # LC	Type	u at N=1 kg/cm²	u at N=1 -	M = .05 N -	M = .05 ϵ_v %	M = .1 N -	M = .1 ϵ_v %	M = .15 N -	M = .15 ϵ_v %	M = .20 N -	M = .20 ϵ_v %	M = .40 N -	M = .40 ϵ_v %	M = .60 N -	M = .60 ϵ_v %	M = .80 N -	M = .80 ϵ_v %	M=1.0 N -	u_f kg/cm²	M=1 $\bar{p}_{max}$	At M=.5 ϵ_{vpp} %
58	CIU	.302	.305		-	-	-	-	-	1/2	.12	2	.10	3.5	.17	5.5	.41	8	.99	.38	.22
65	CAU	-	-		-	-	-	-	-	-	-	-	-	-	-	-	-	7800	.03	35.8	.03
85	CIU	-.005	-.005	200	.03	417	.03	577	.03	680	.025	990	.035	1091	.07	1101	.20	1106	.97	36.9	.09
91	CAU	.103	.124	-	-	-	-	2	.05	4.5	.06	42	.11	135	.21	280	.40	550	.83	36.2	.07
93	CAU	-	-	-	-	-	-	-	-	-	-	-	-	-	-	-		1/2	1.14	31.8	-
94	CAU	-	-	-	-	-	-	-	-	-	-	-	-	-	-	-	-	-	-	-	.04
95	CIU	-	-	-	-	-	-	-	-	-	-	-	-	-	-	-	-	-	-	-	.05
100	CIU	.279	.072	-	-	3	.07	12	.055	27	.06	100	.07	137	.10	147	.29	149	3.86	34.5	.17
102	CAU	.103	.180	-	-	-	-	-	-	1.5	-.06	14	-.10	36	-.19	58	-.40	84	.57	40.5	.06
103	CIU	.006	.006	58	.025	157	.025	265	.025	363	.03	607	.04	665	.12	675	.23	682	.98	41.9	.085
106	CAU	.101	.117	-	-	-	-	2	.04	6	.05	55	.09	200	.16	460	.30	1000	.86	36.8	.07
117	CAU	-	-	-	-	-	-	-	-	55	.018	250	.05	460	.10	669	.28	942	.825	35.8	.074
119	CIU	-	-	-	-	11	.04	19	.04	35	.04	186	.05	270	.08	284	.23	288	2.57	37.1	.138
1211	CAU	-	-	-	-	-	-	-	-	-	-	-	-	-	-	-	-	-	-	-	.071
12111	CAU	-	-	-	-	-	-	-	-	-	-	-	-	-	-	-	-	-	-	-	-
1221	CAU	.143	.162	-	-	-	-	-	-	2	.06	20	.13	72	.25	180	.43	465	.88	36.1	.052
12211	CAU	.143	.162	-	-	-	-	-	-	-	-	-	-	-		-	-	-	-	-	-
1241	CAD Au	-	-	-	-	-	-	-	-	-	-	-	-	-	-	-	-	-	-	-	-
12411	CAU	.008	.010	23	.00	90	.004	182	.006	280	.01	660	.04	1060	.09	1440	.23	2030	.83	36.1	.074
125	CAU	.025	.029	7	.004	54	.009	158	.014	285	.02	800	.06	1290	.11	1730	.26	2340	.84	35.9	.073
126	CAD	-	-	-	-	-	-	-	-	-	-	-	-	-	-	-	-	-	-	-	.110
127	CID	-	-	-	-	-	-	-	-	-	-	-	-	-	-	-	-	-	-	-	.075
1281	CAD Au	-	-	-	-	-	-	-	-	-	-	-	-	-	-	-	-	-	-	-	-
12811	CAU	-.019	-.022	136	.002	280	.008	442	.015	620	.02	1350	.07	2070	.15	2950	.31	3800	.87	32.3	.042
133	CAU	-	-	-	-	-	-	-	-	-	-	-	-	-	-	-	-	-	-	-	.021
141	CAD	-	-	-	-	-	-	-	-	-	-	-	-	-	-	-	-	-	-	-	.082*
155	CAU	-	-	-	-	-	-	-	-	-	-	-	-	-	-	-	-	-	-	-	-
156	CAU	.376	.216	-	-	-	-	-	-	-	-	3	.14	7	.26	11	.48	14	1.74	29.8	.085

PORE PRESSURE DEVELOPMENT IN "SPECIAL" CYCLIC TESTS

		VIRGIN.			1st CONSOL.		2nd CONSOL.			3rd CONSOL.			4th CONSOL.			5th
Test # LC-	n_c %	# cycles Drained	n_c %	# cycles To ϵ_{vpp}=2%	n_c %	# cycles To ϵ_{vpp}=2%	# cycles Drained	n_c %	# cycles To ϵ_{vpp}=2%	# cycles Drained	n_c %	# cycles To ϵ_{vpp}=2%	# cycles Drained	n_c %	# cycles To ϵ_{vpp}=2%	n_c %
51	41.41	-	41.41	1925	39.24	2	20	37.92	2	-	37.49	2	-	37.49	-	-
53	41.07	-	41.07	8	39.22	1	-	37.89	1	20	36.85	40	-	36.03	-	-
54	41.22	50	41.22	247	39.80	1	-	38.20	1	-	36.92	-	-	-	-	-
55	41.06	-	41.06	111	38.77	1	-	37.23	1	-	36.72	1	2	35.58	14	35.02
56	41.19	-	41.19	168	38.83	1		38.20	1	2	36.49	2	-	35.65	-	-
57	41.01	-	41.01	79	39.83	1	-	37.56	2	-	36.13	-	-	-	-	-
58	41.25	-	41.25	8	39.60	1	-	38.12	1	-	36.32	-	-	-	-	-
59	41.26	-	41.26	545	39.14	2	-	37.77	-	-	-	-	-	-	-	-
60	41.54	-	41.54	2706	39.70	1	-	38.26	1	5	37.21	26	-	36.47	-	-
138	41.42	-	41.42	257	39.47	1	-	37.97	1	-	-	-	-	-	-	-
139	41.50	-	41.50	68	39.50	1	-	37.96	1	-	37.02	-	-	-	-	-
146	42.06	-	42.06	19	40.35	1	-	39.24	1	-	38.55	21	-	37.64	10	37.27

ISOTROPIC CYCLIC TESTS RECONSOLIDATED AND RELOADED

TABLE F.1

OOSTERSCHELDE SAND, LC-123

$\bar{\sigma}_{vc}$ = 1.00 kg/cm², $\bar{\sigma}_{hc}$ = 1.00 kg/cm², n_c = 39.6%, $\bar{e}$ = 0.77

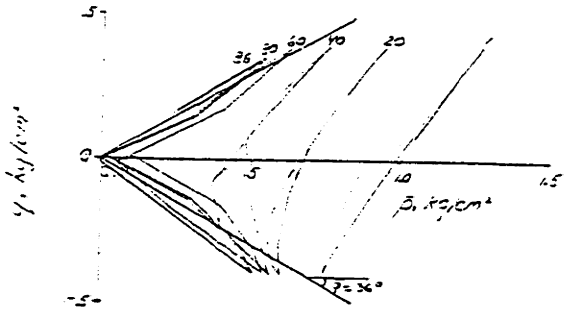

EFFECTIVE STRESS PATH

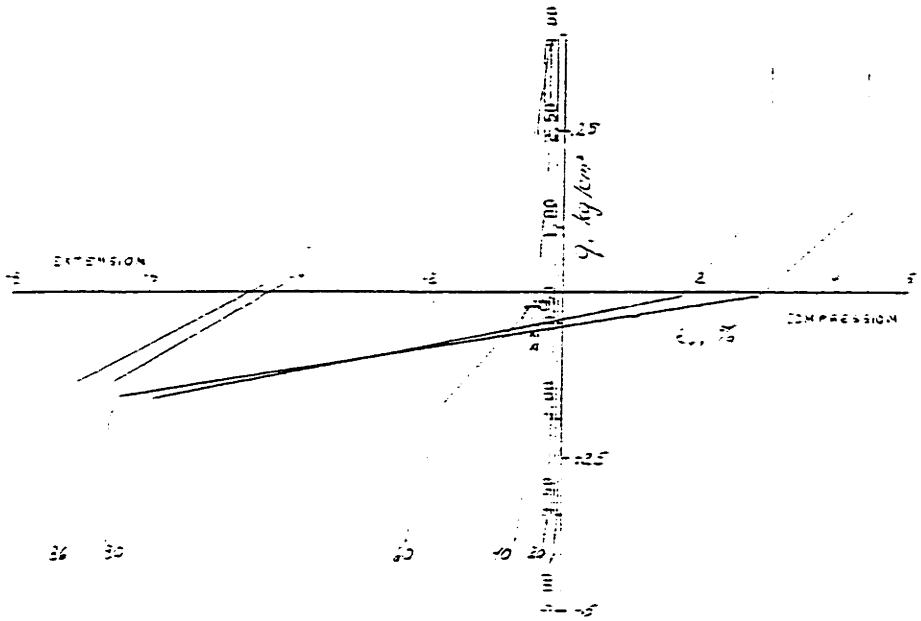

FIGURE F-1

STRESS vs. STRAIN

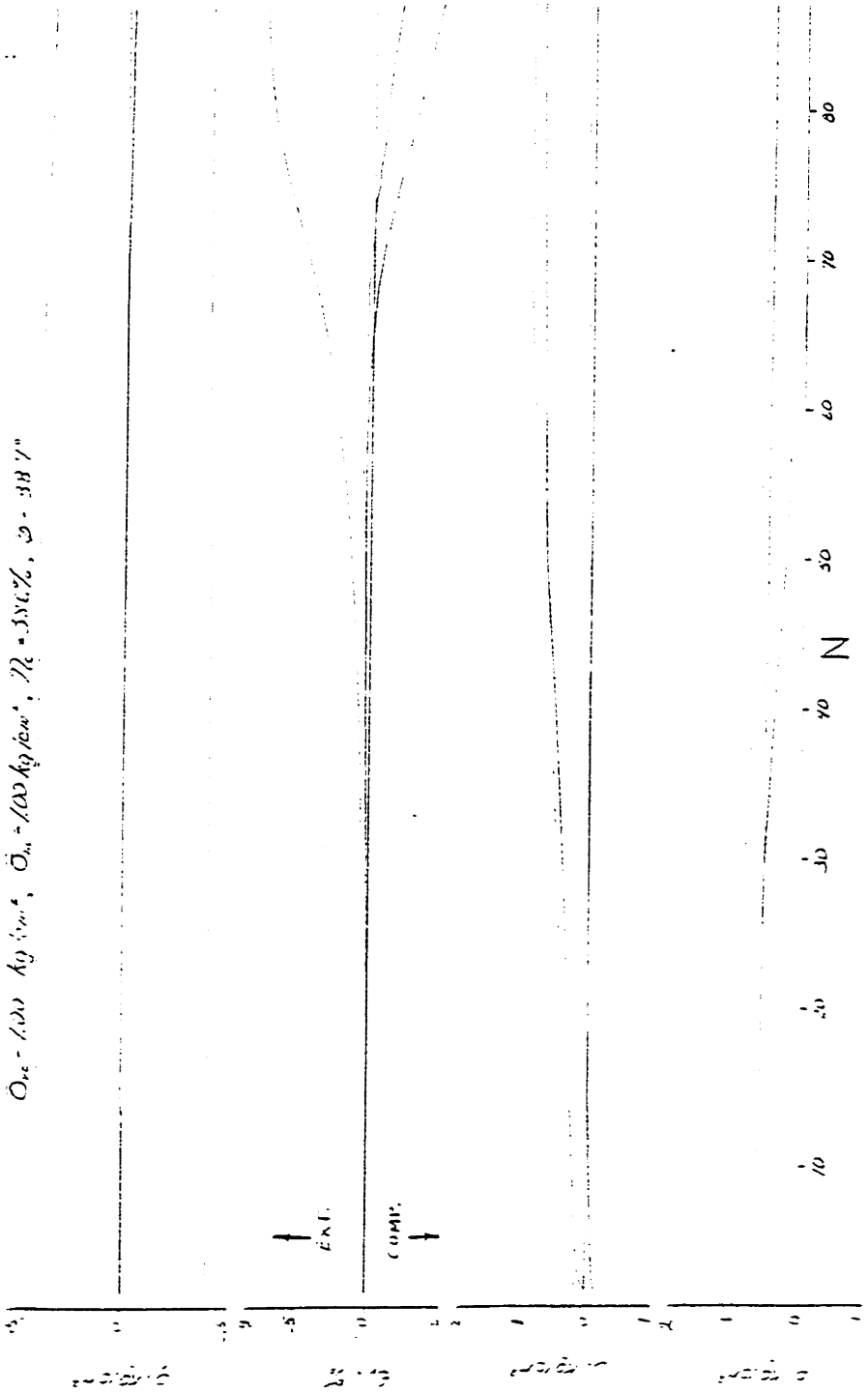

STRESS, STRAIN and PORE PRESSURE

FIGURE F-2

OOSTERSCHELDE SAND, LC-138

$\bar{\sigma}_{1c} = 1.00$ kg/cm², $\bar{\sigma}_{3c} = 1.00$ kg/cm², $n_c = 41.4\%$, $\bar{\phi} = 36.2°$

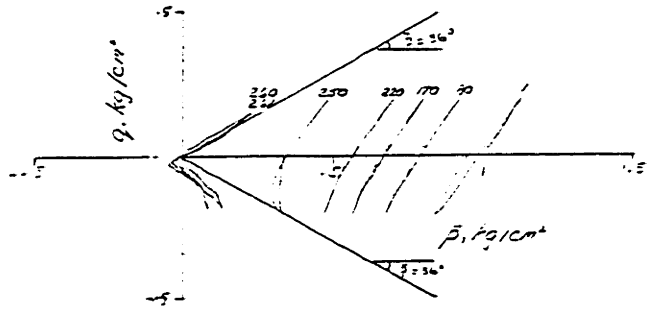

EFFECTIVE STRESS PATH

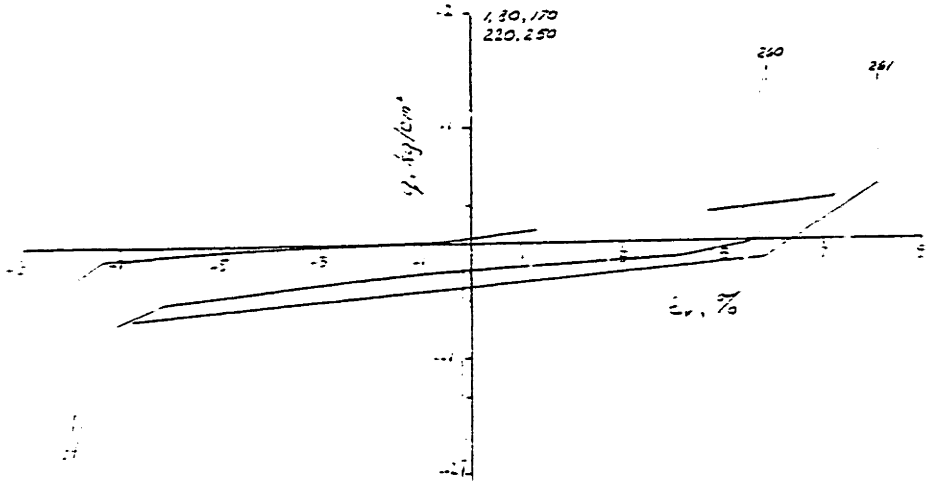

STRESS vs. STRAIN

FIGURE F-3

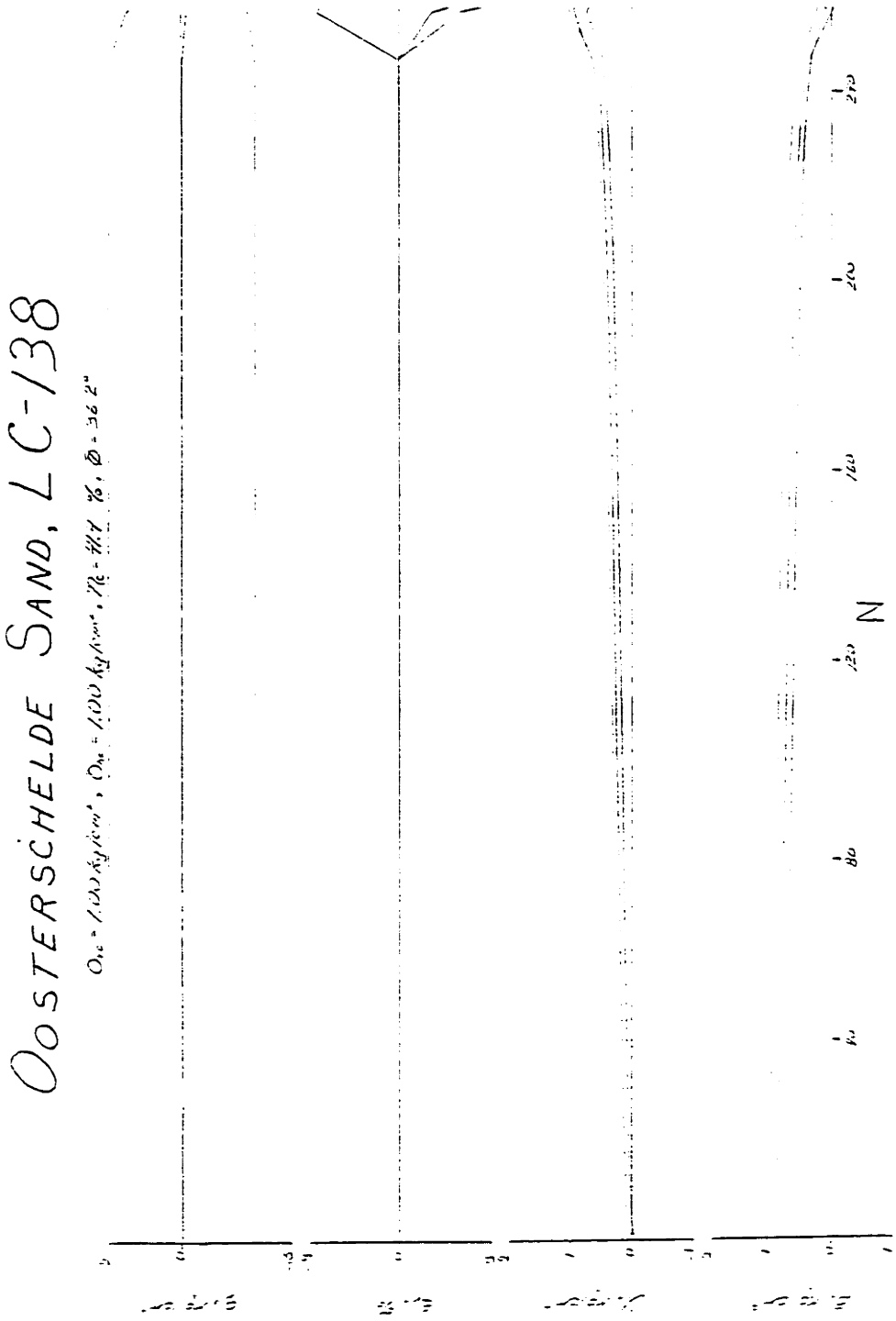

STRESS, STRAIN and PORE PRESSURE

FIGURE F-4

OOSTERSCHELDE SAND, LC-138RE

$\bar{\sigma}_{1c}$ = 1.00 kg/cm², $\bar{\sigma}_{3c}$ = 1.00 kg/cm², n_c = 39.5%

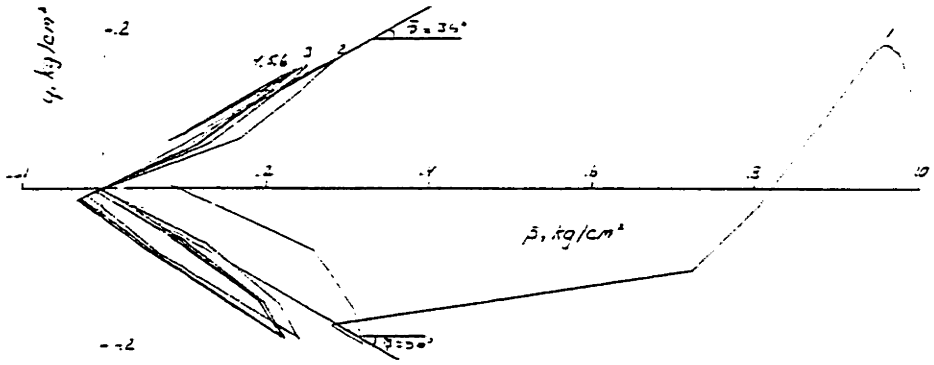

EFFECTIVE STRESS PATH

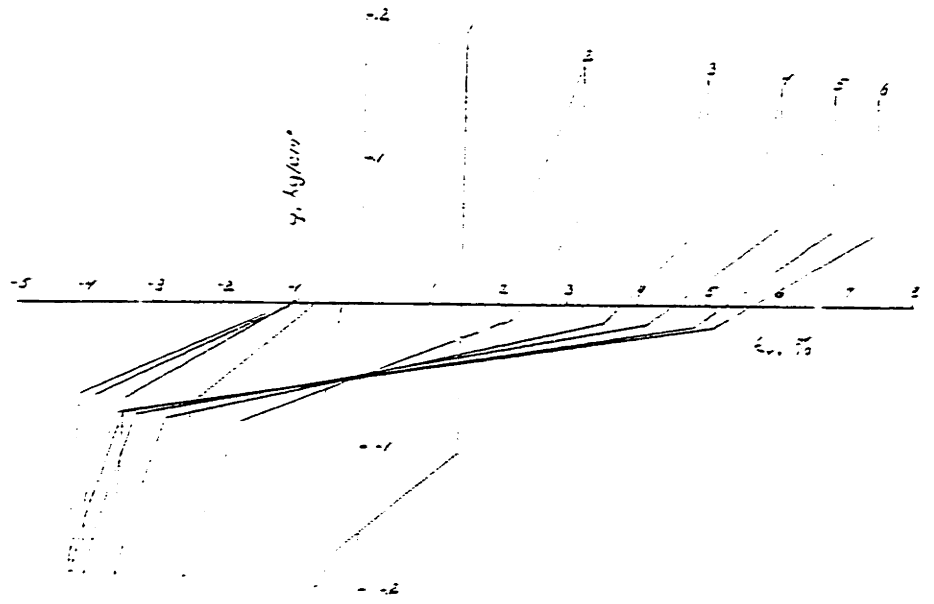

STRESS vs. STRAIN

FIGURE F-5

OOSTERSCHELDE SAND, LC-138RE
STRESS, STRAIN and PORE PRESSURE
N

FIGURE F-6

OOSTERSCHELDE SAND, LC-139

$\bar{\sigma}_{1c} = 2.50\ kg/cm^2$, $\bar{\sigma}_{3c} = 2.50\ kg/cm^2$, $\eta_c = 41.5\ \%$, $\bar{\phi} = -3.4°$

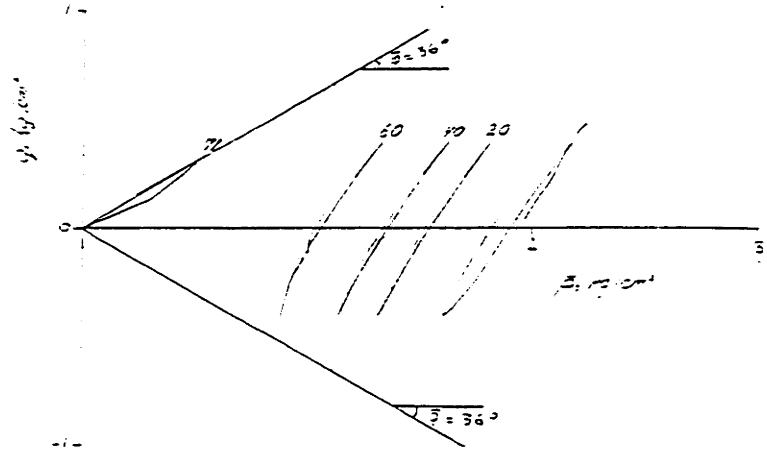

STRESS vs. STRAIN

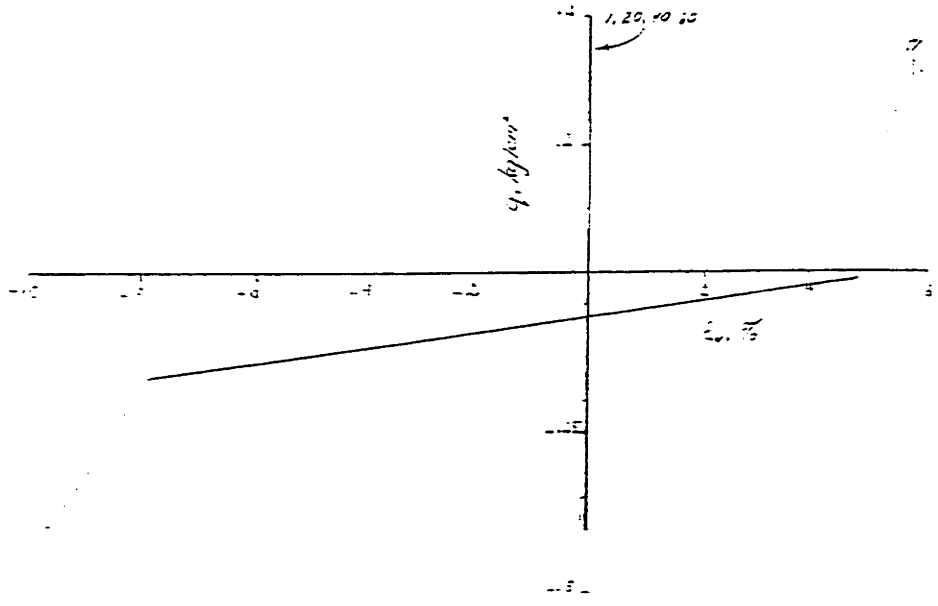

STRESS vs. STRAIN

FIGURE F-7

OOSTERSCHELDE SAND, LC-139

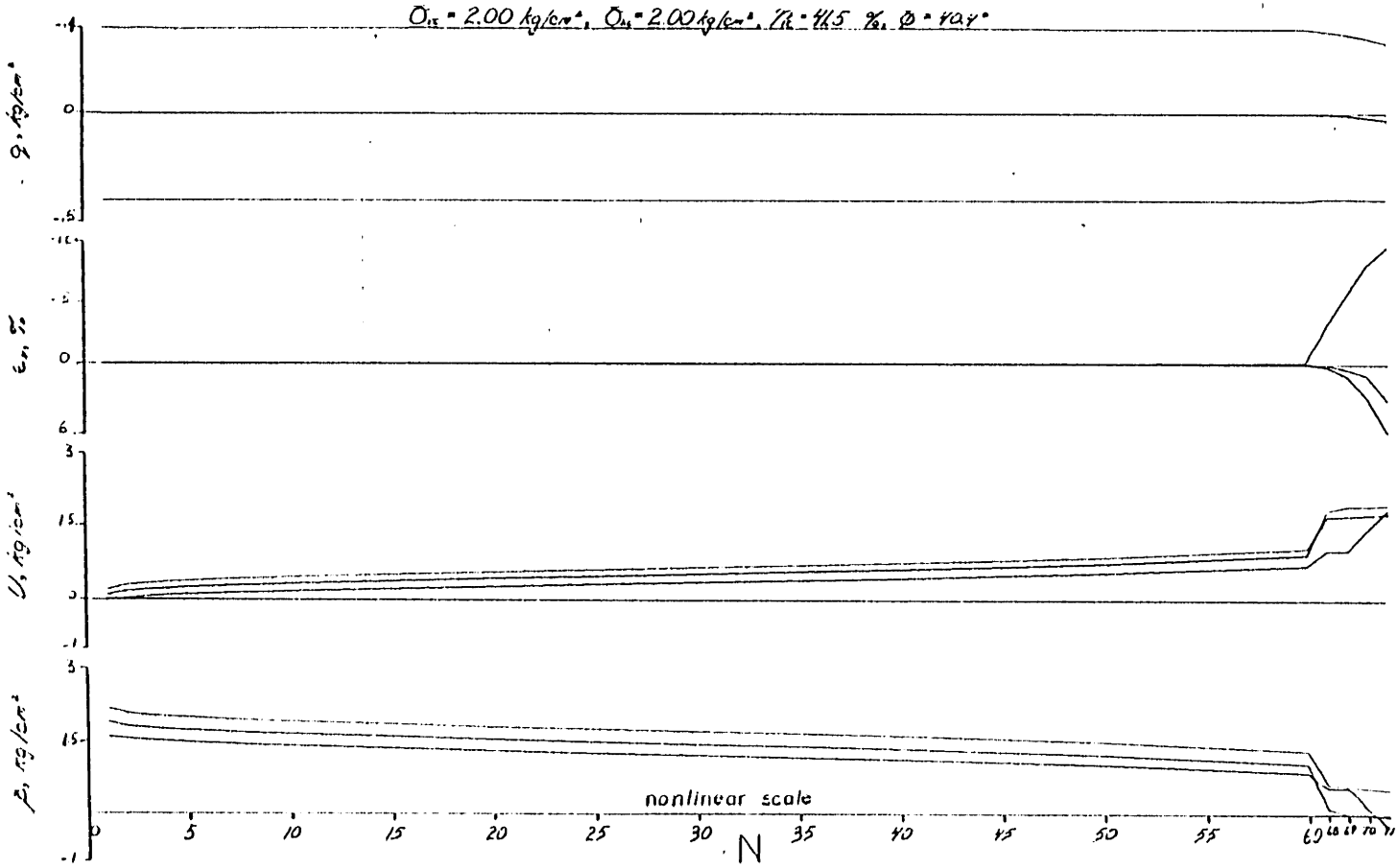

STRESS, STRAIN and PORE PRESSURE

OOSTERSCHELDE SAND, LC-139RE

$\bar{\sigma}_{vc}$ = 2.00 kg/cm², $\bar{\sigma}_{hc}$ = 2.00 kg/cm², n_c = 38.5%

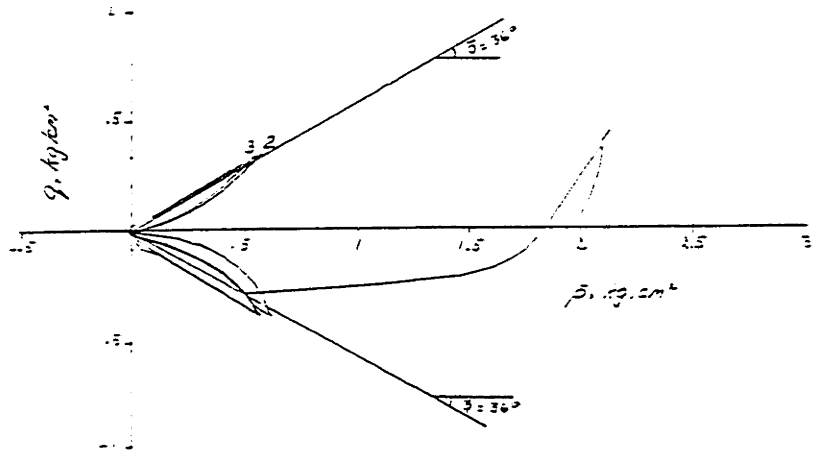

EFFECTIVE STRESS PATH

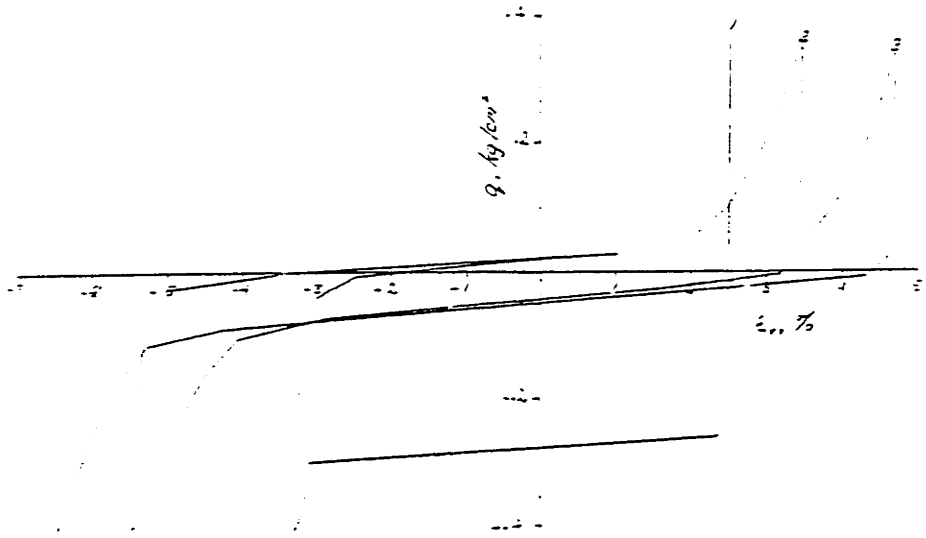

STRESS vs. STRAIN

FIGURE F-9

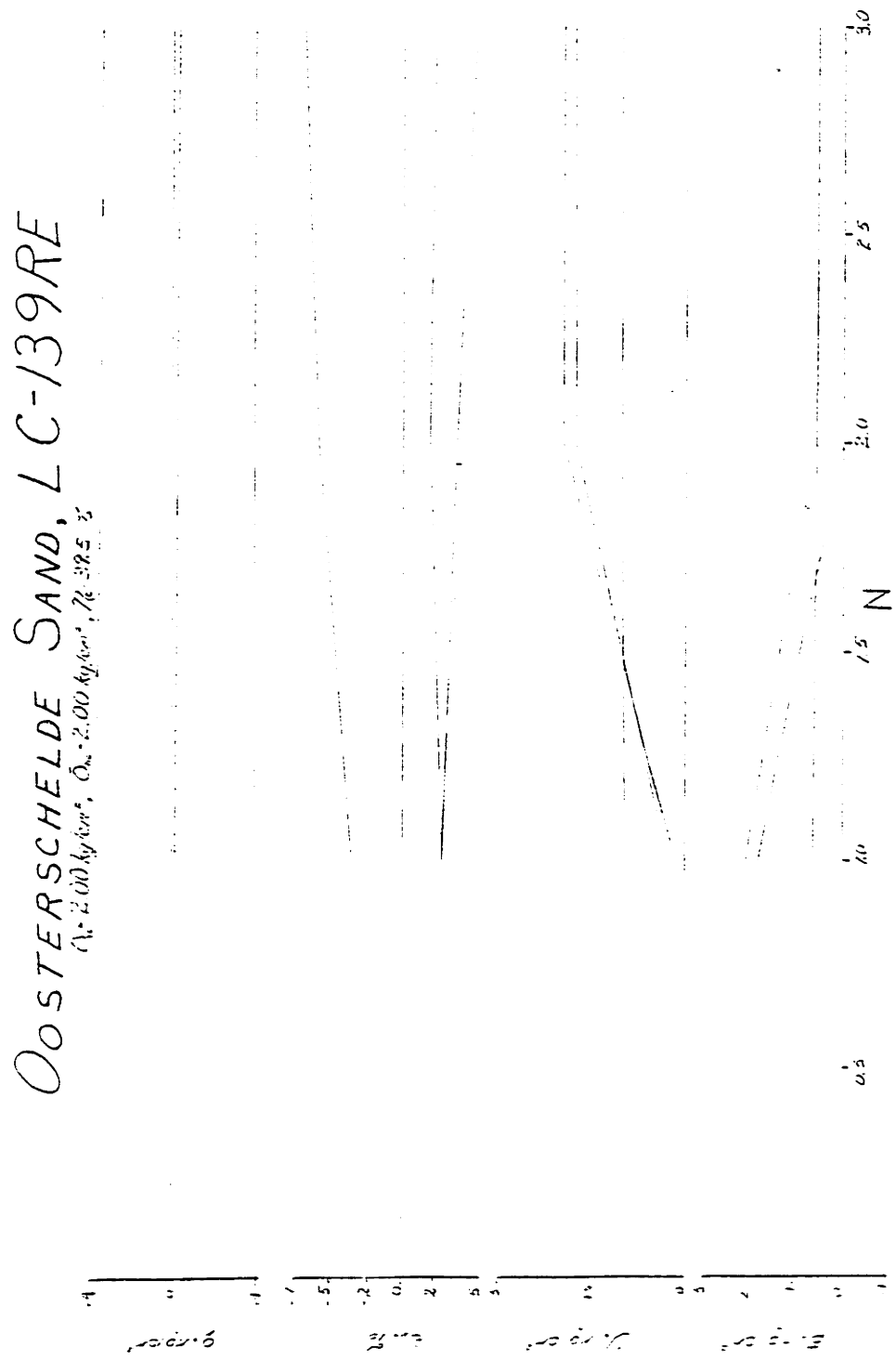
OOSTERSCHELDE SAND, LC-139RE
STRESS, STRAIN and PORE PRESSURE
N

FIGURE F-10

OOSTERSCHELDE SAND, LC-139RR

$\bar{\sigma}_{3c} = 2.00 \text{ kg/cm}^2$, $\bar{\sigma}_{3c} = 3.00 \text{ kg/cm}^2$, $n_c = 32.3\%$

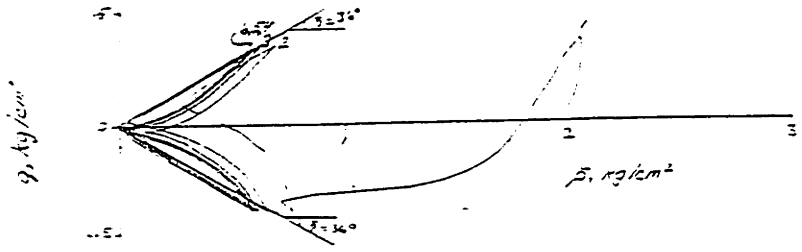

EFFECTIVE STRESS PATH

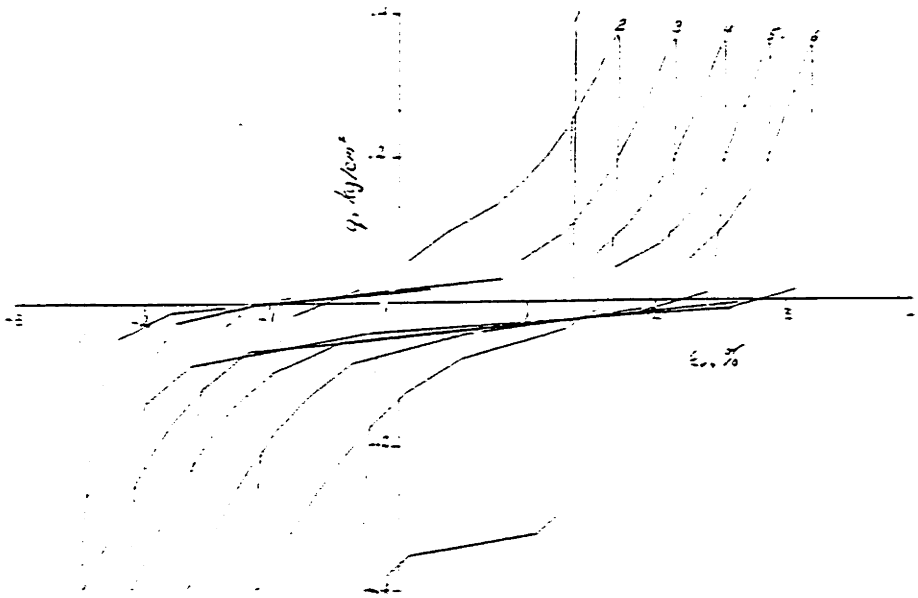

STRESS vs. STRAIN

FIGURE F-11

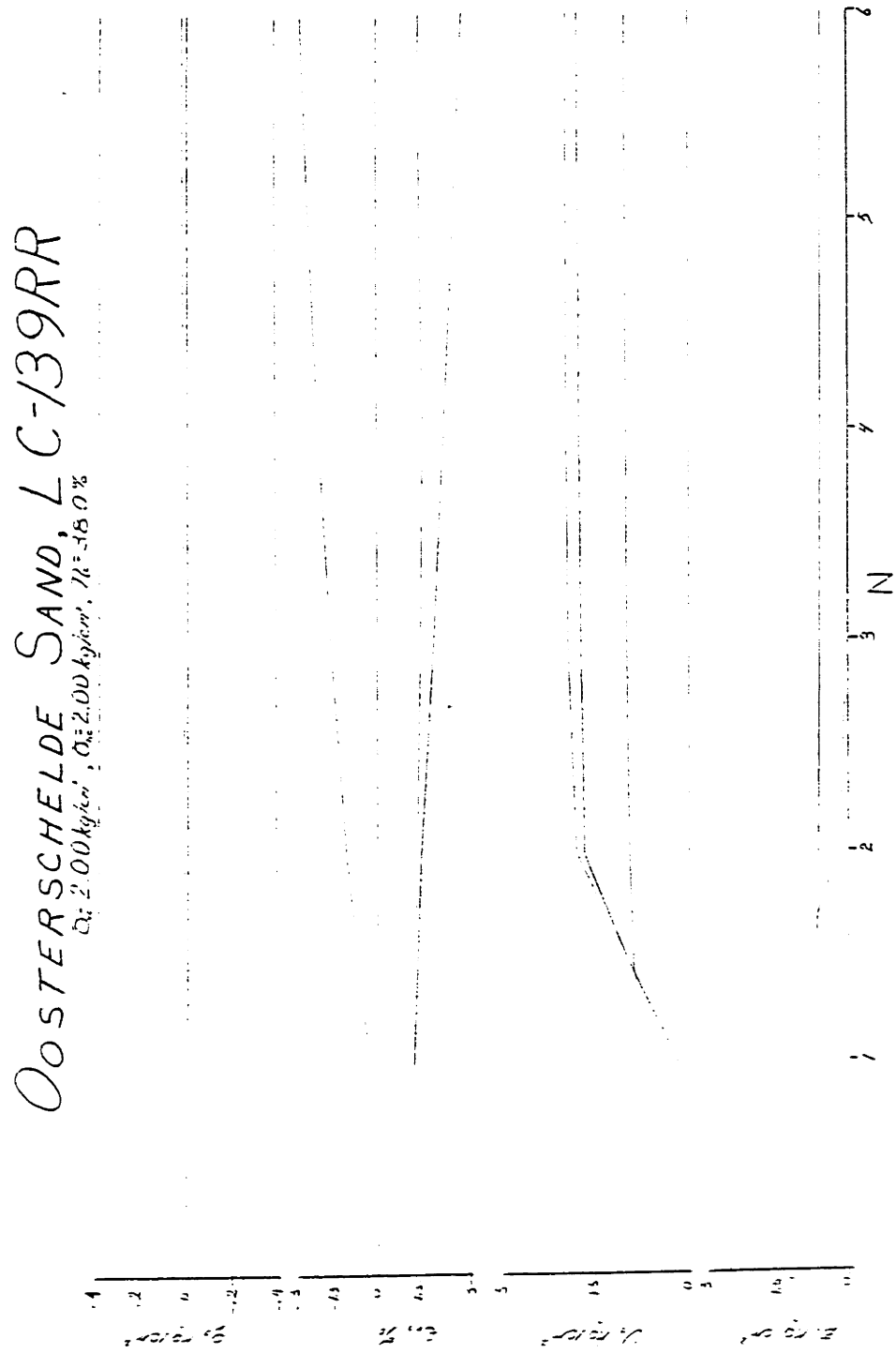
OOSTERSCHELDE SAND, LC-139RR
σ₃: 2.00 kg/cm², σ₃: 2.00 kg/cm², Dr: 38.0%
STRESS, STRAIN and PORE PRESSURE
N

FIGURE F-12

OOSTERSCHELDE SAND, LC-144

$\bar{\sigma}_{1c} = 2.50 kg/cm^2$, $\bar{\sigma}_{3c} = 2.50 kg/cm^2$, $n_c = 41.4\%$, $\phi = 36.7°$

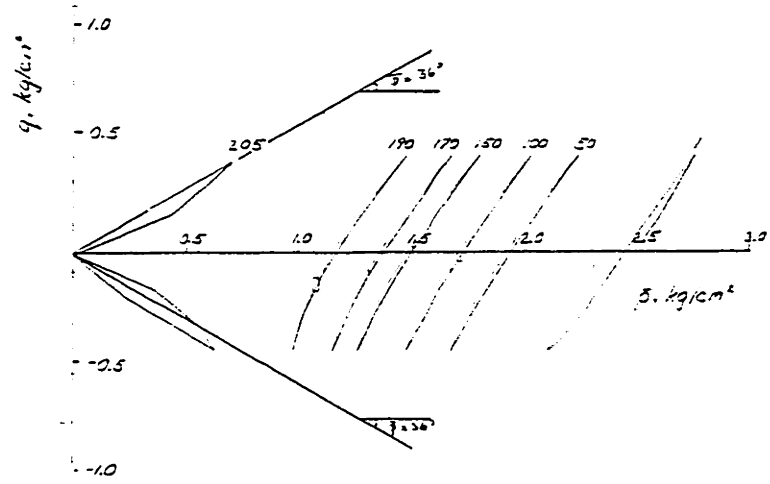

EFFECTIVE STRESS PATH

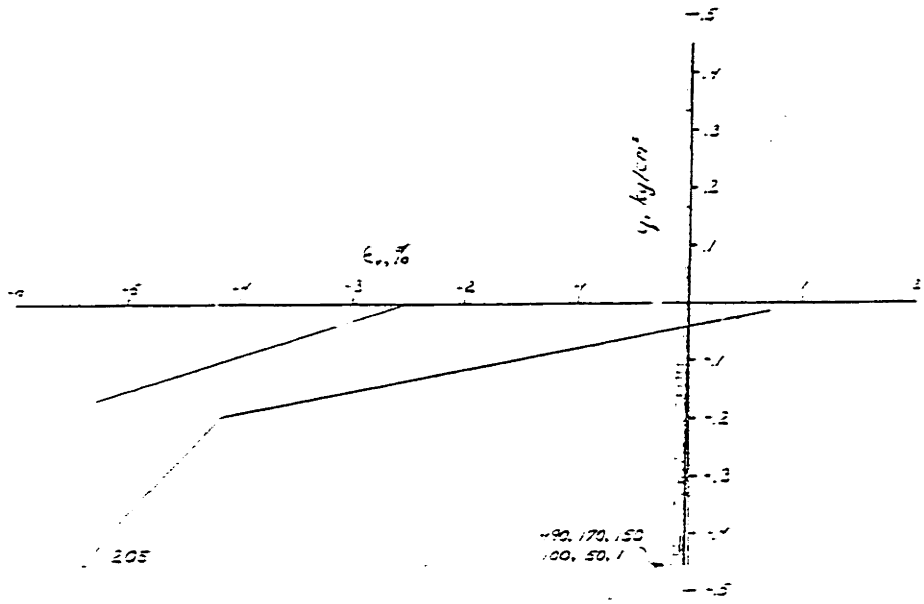

STRESS vs. STRAIN

FIGURE F-13

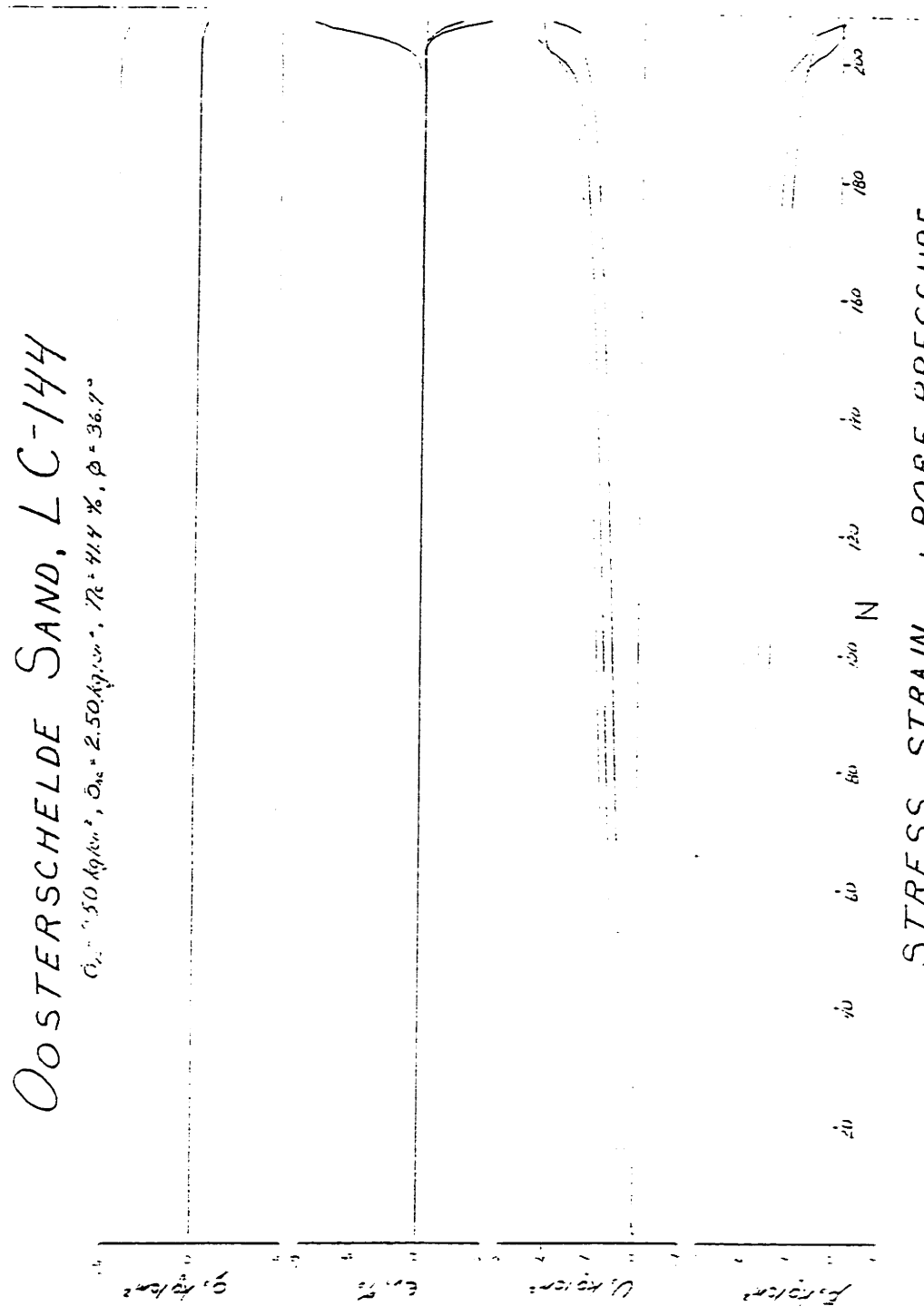
OOSTERSCHELDE SAND, LC-144
STRESS, STRAIN and PORE PRESSURE
N

FIGURE F-14

OOSTERSCHELDE SAND, LC-146

$\bar{\sigma}_{3c} = 5.00 kg/cm^2$, $\bar{\sigma}_{1c} = 5.00 kg/cm^2$, $n_c = 41.5\%$, $\bar{\phi} = 36.5°$

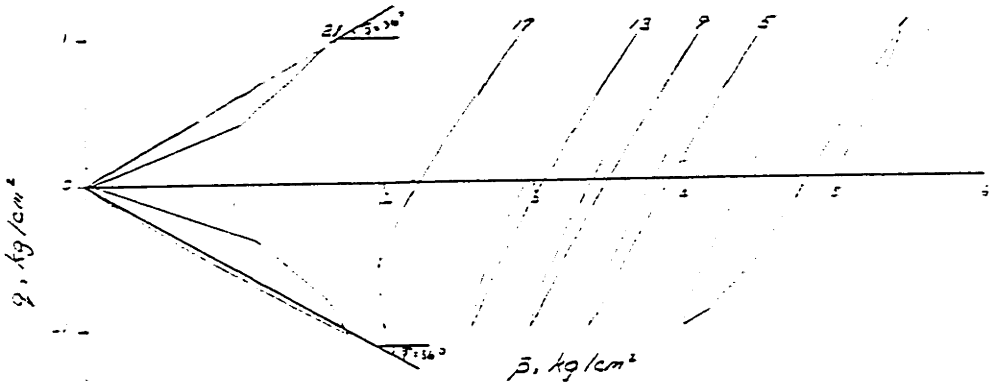

EFFECTIVE STRESS PATH

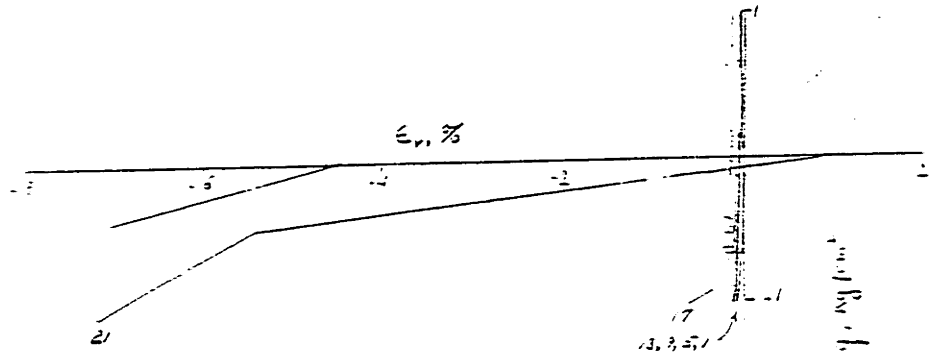

STRESS vs. STRAIN

FIGURE F-15

OOSTERSCHELDE SAND, LC-146
σ_c = 5.00 kg/cm², σ_{3c} = 5.00 kg/cm², n_c = 44.5%, ϕ = 36.5°
STRESS, STRAIN and PORE PRESSURE
N

FIGURE F-6

OOSTERSCHELDE SAND, LC-146R1

$\bar{\sigma}_{3c} = 5.00$ kg/cm², $\bar{\sigma}_{1c} = 5.00$ kg/cm², $\eta_c = 10.4$ %

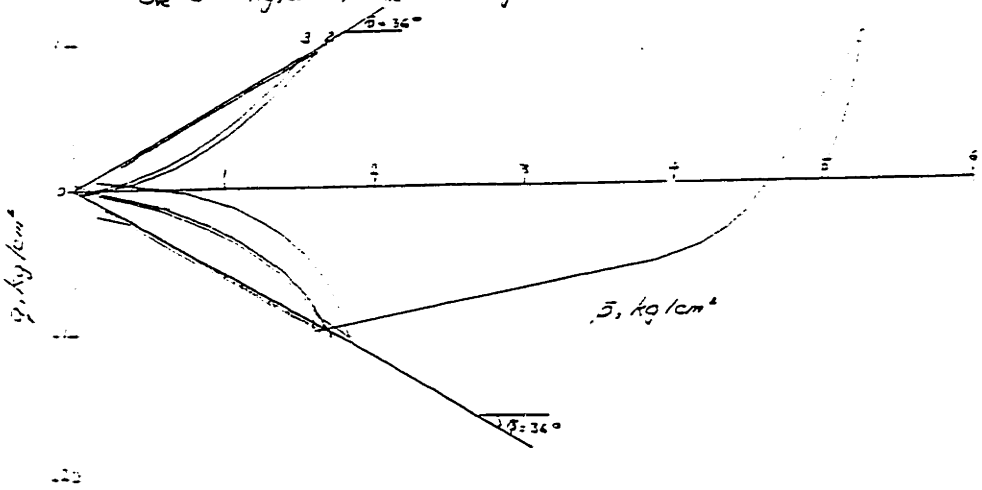

EFFECTIVE STRESS PATH

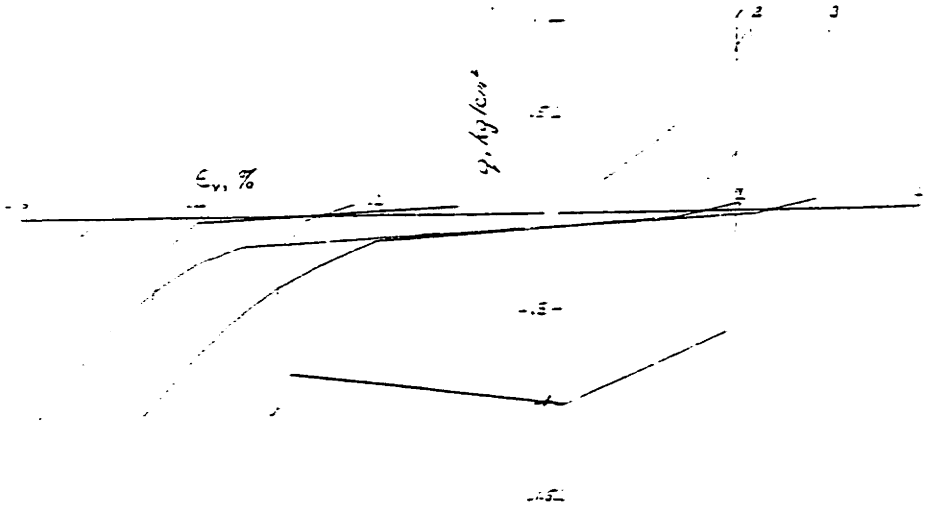

STRESS vs. STRAIN FIGURE F-17

OOSTERSCHELDE SAND, LC-146 RI
STRESS, STRAIN and PORE PRESSURE
N

FIGURE F-18

OOSTERSCHELDE SAND, LC-146R2

$\bar{\sigma}_{1c} = 5.00\ kg/cm^2$, $\bar{\sigma}_{3c} = 5.00\ kg/cm^2$, $n_c = 39.2\ \%$

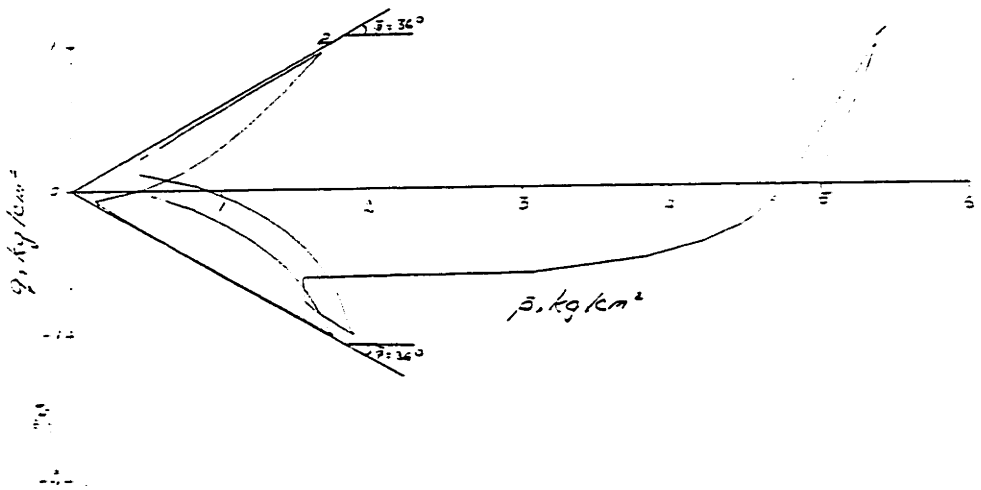

EFFECTIVE STRESS PATH

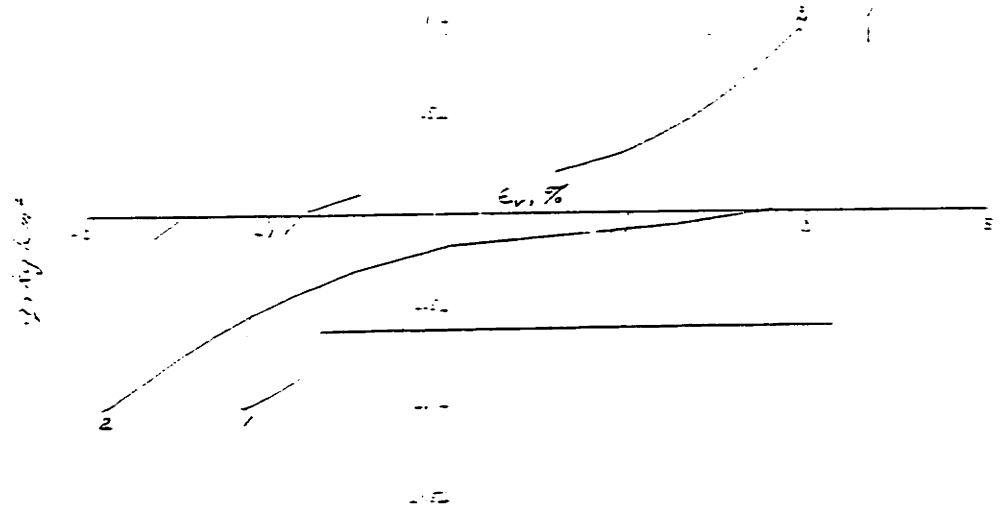

STRESS vs. STRAIN

FIGURE F-19

OOSTERSCHELDE SAND, LC-146R2
STRESS, STRAIN and PORE PRESSURE
N

FIGURE F-20

OOSTERSCHELDE SAND, LC-146R3

$\bar{\sigma}_{1c} = 5.00$ kg/cm², $\bar{\sigma}_{3c} = 5.00$ kg/cm², $\eta_c = 33.6\%$

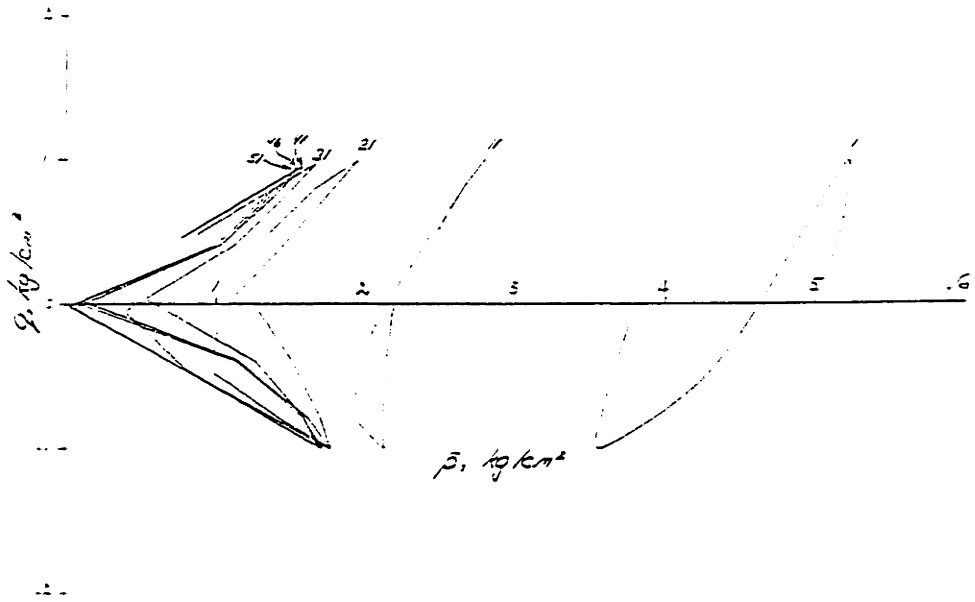

EFFECTIVE STRESS PATH

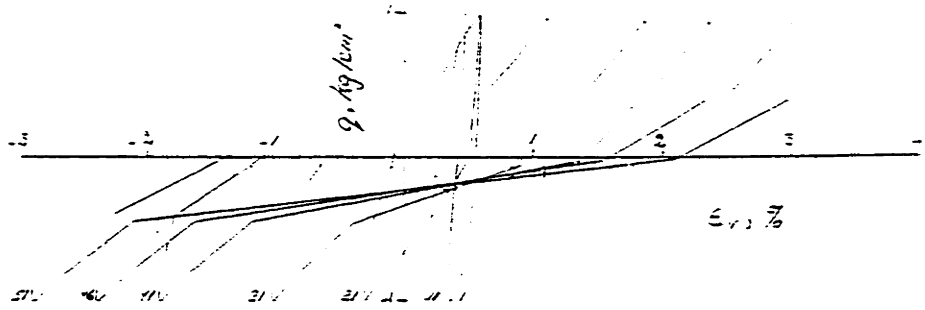

STRESS vs. STRAIN

FIGURE F-2.1

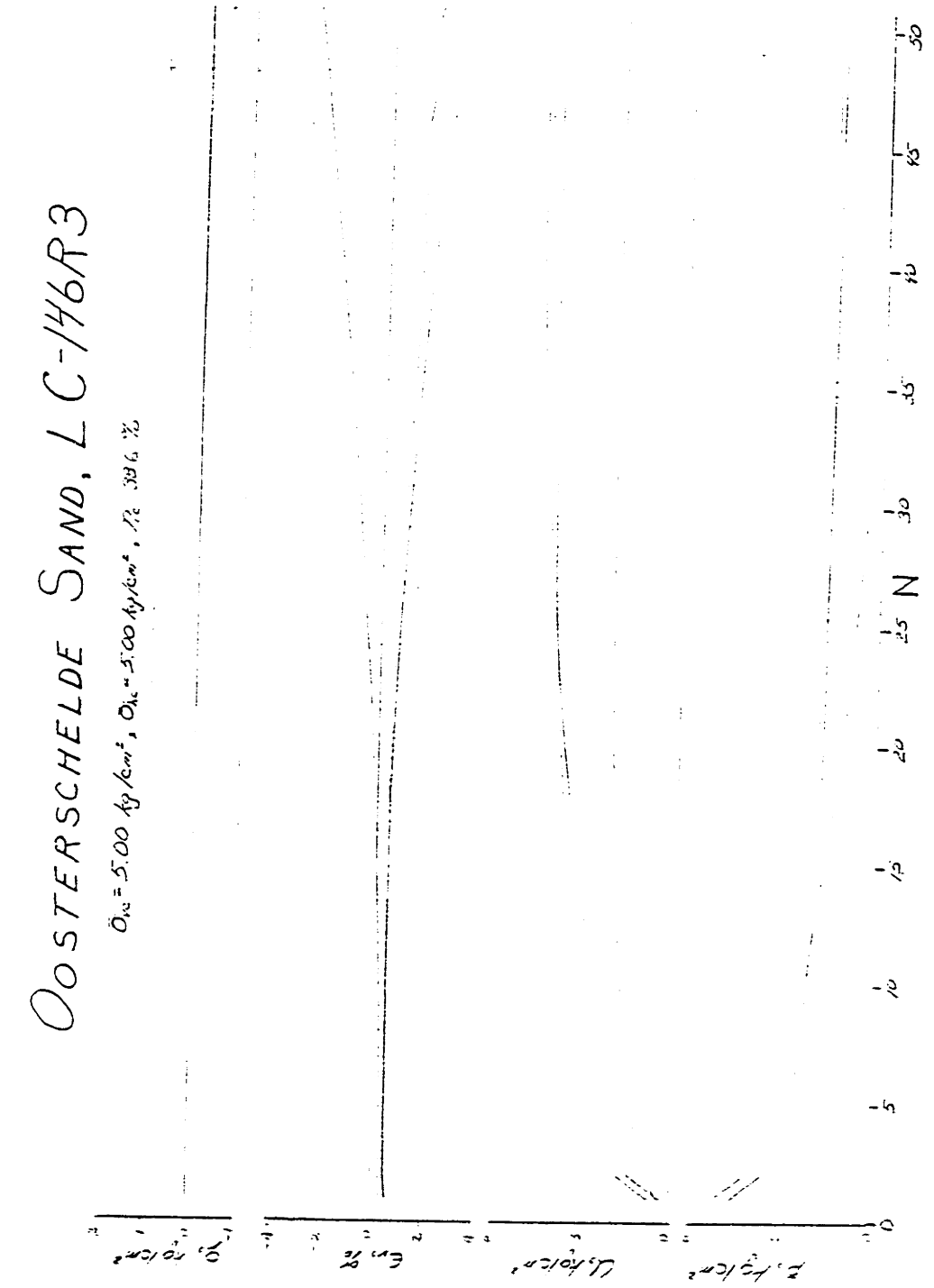
OOSTERSCHELDE SAND, LC-1/16R3
STRESS, STRAIN and PORE PRESSURE
N

FIGURE F-22

OOSTERSCHELDE SAND, LC-146R4

$\bar{\sigma}_{vc}$ = 5.00 kg/cm², $\bar{\sigma}_{hc}$ = 5.00 kg/cm², η_c = 37½ %

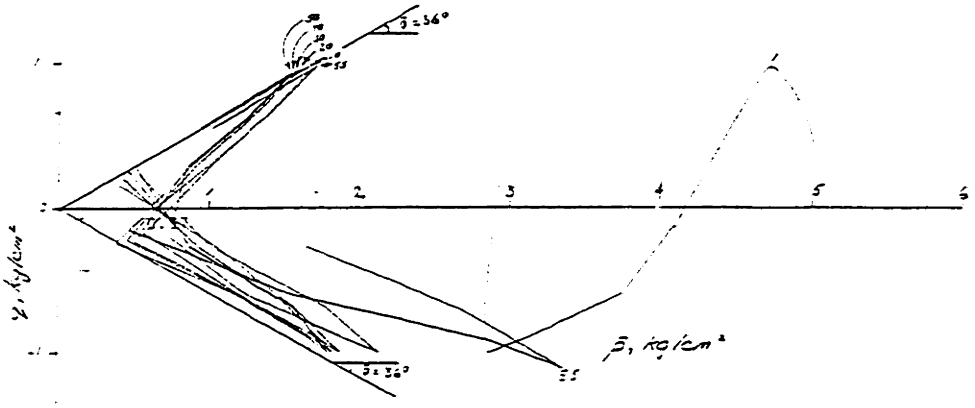

EFFECTIVE STRESS PATH

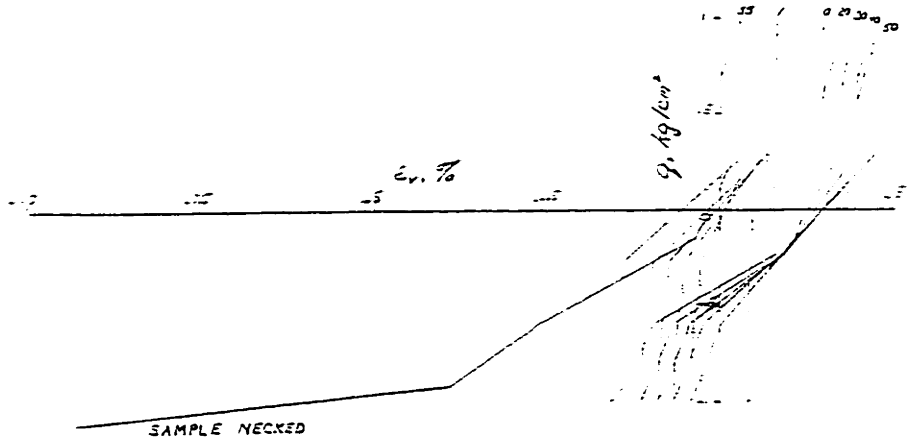

STRESS vs. STRAIN FIGURE F-23

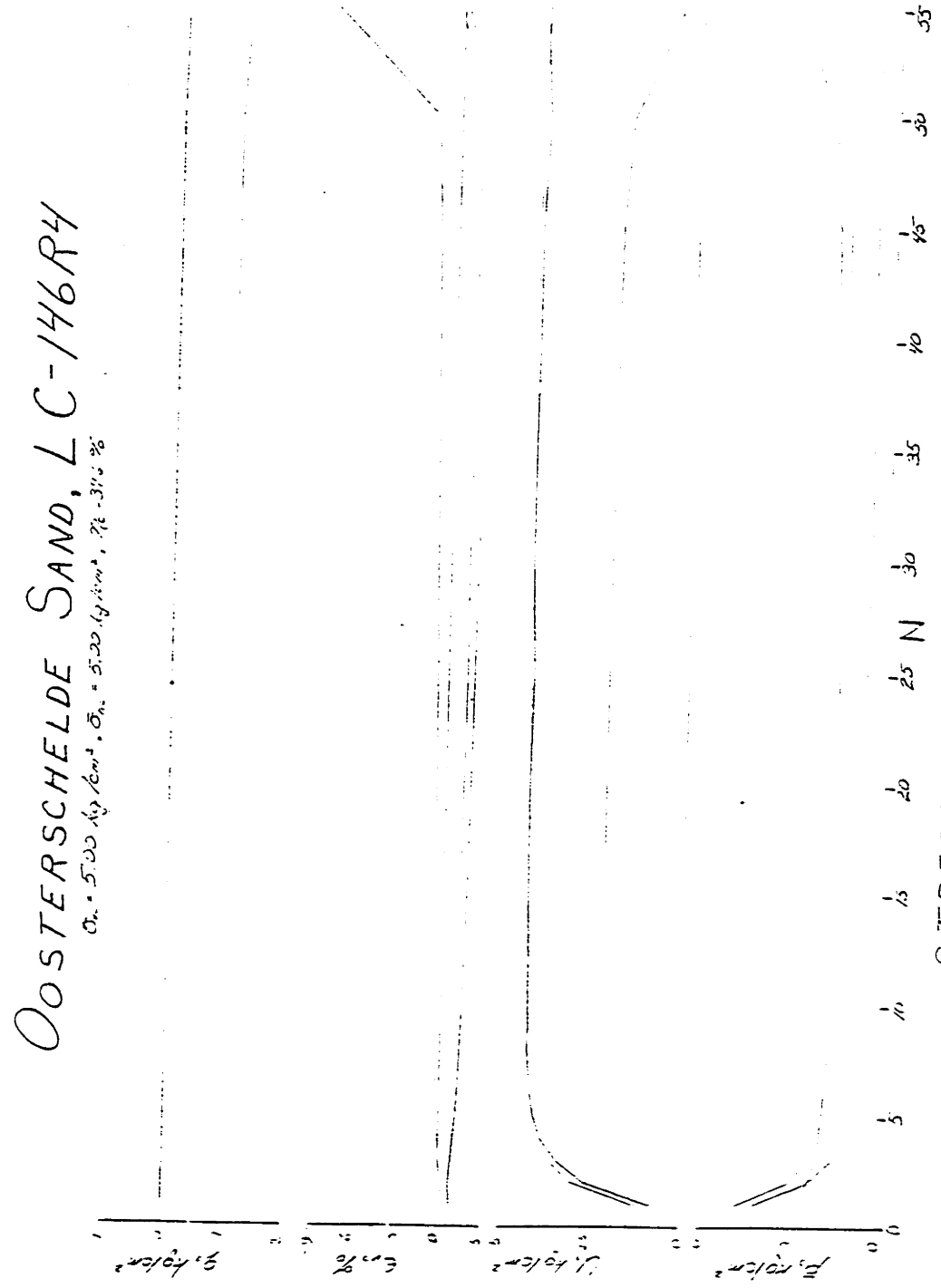
OOSTERSCHELDE SAND, LC-1146R4
STRESS, STRAIN and PORE PRESSURE
N

FIGURE F-24

OOSTERSCHELDE SAND, LC-75

$\bar{\sigma}_{ic}$ = 1.00 kg/cm², $\bar{\sigma}_{hc}$ = 0.70 kg/cm², n_c = 40.9%, ϕ = 38.8°

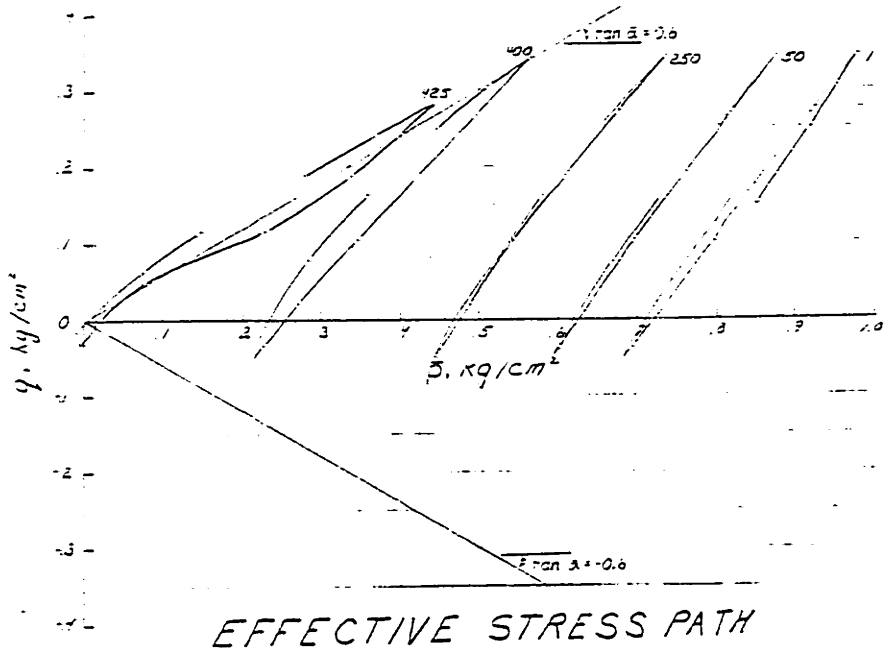

EFFECTIVE STRESS PATH

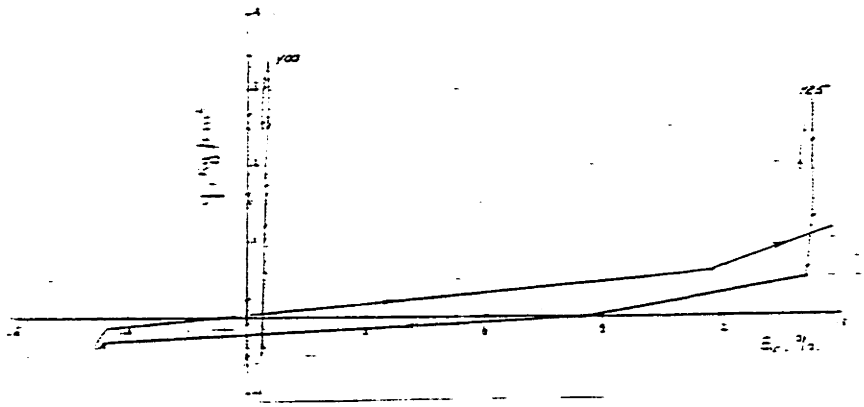

STRESS vs. STRAIN

FIGURE F-25

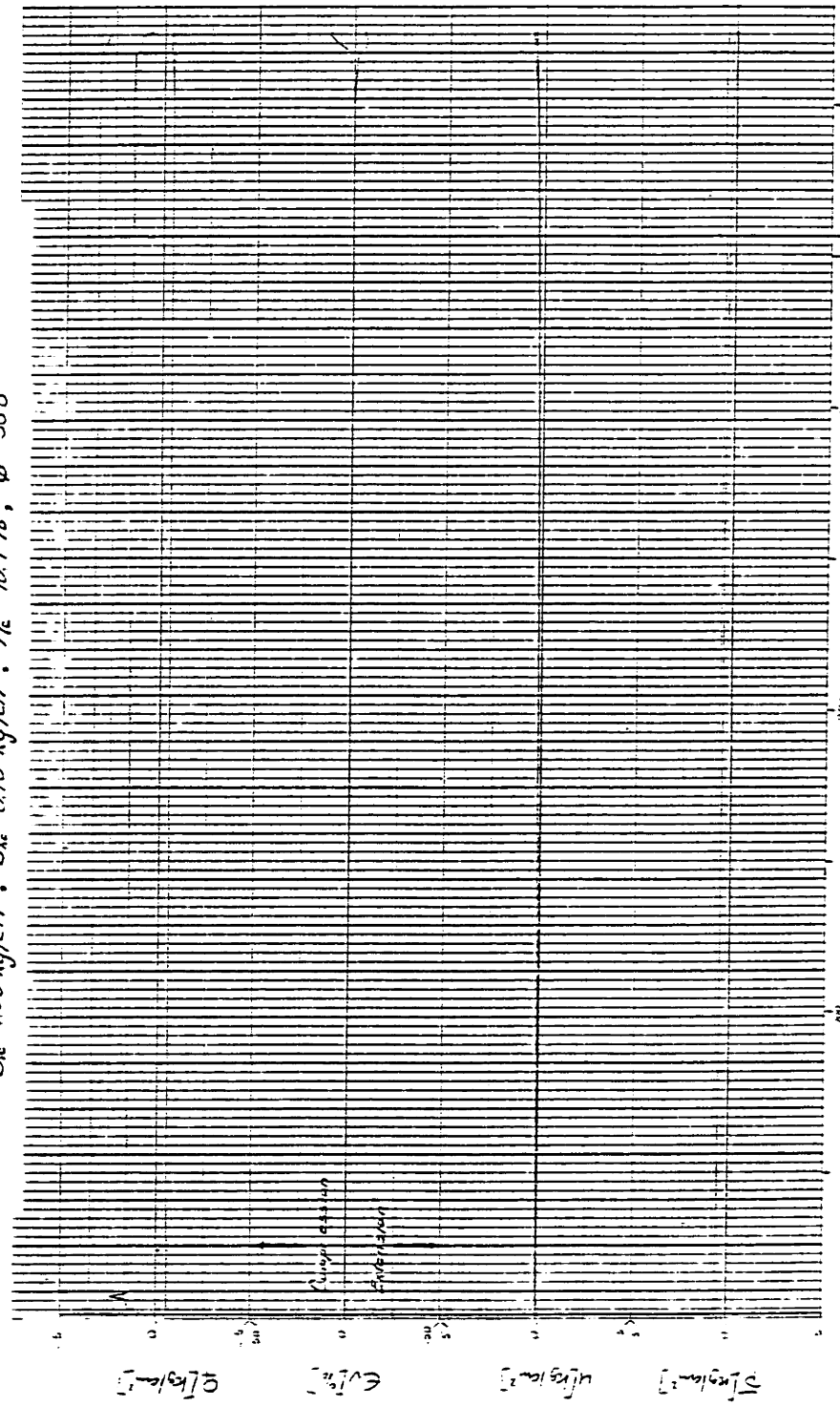

OOSTERSCHELDE SAND, LC-75

σ_{zc} = 1.00 kg/cm², σ_{xc} = 0.70 kg/cm², n_c = 40.4 %, ϕ = 38.8°

STRESS, STRAIN and PORE PRESSURE

FIGURE F-26

OOSTERSCHELDE SAND, LC-97

$\bar{\sigma}_{3c} = 2.50$ kg/cm², $\bar{\sigma}_{hc} = 1.50$ kg/cm², $n_c = 41.3\%$, $\phi = 37.7°$

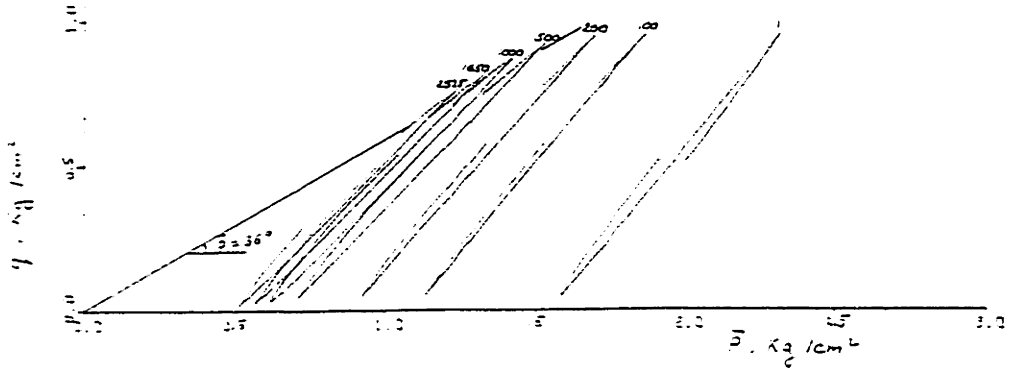

EFFECTIVE STRESS PATH

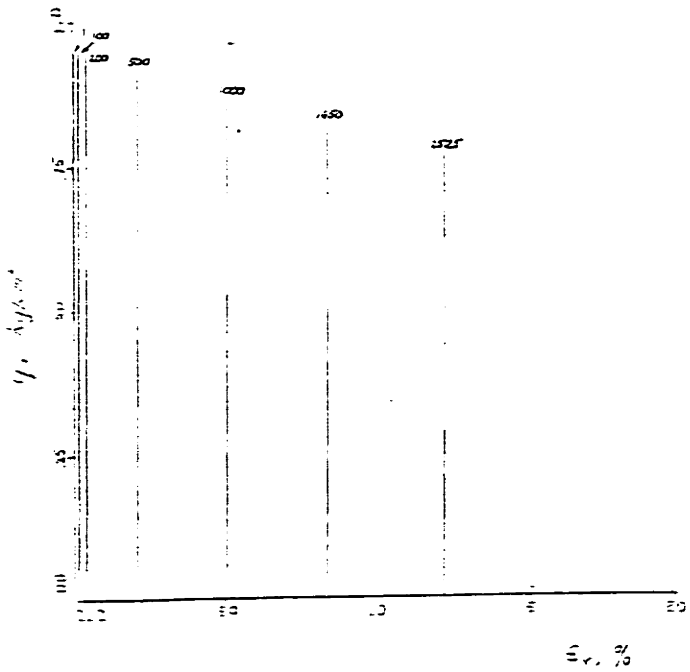

STRESS vs. STRAIN

FIGURE F-27

OOSTERSCHELDE SAND, LC-97

σ_{hc} = 2.50 kg/cm², σ_{vc} = 1.50 kg/cm², D_r = 53 %, ϕ = 32.7°

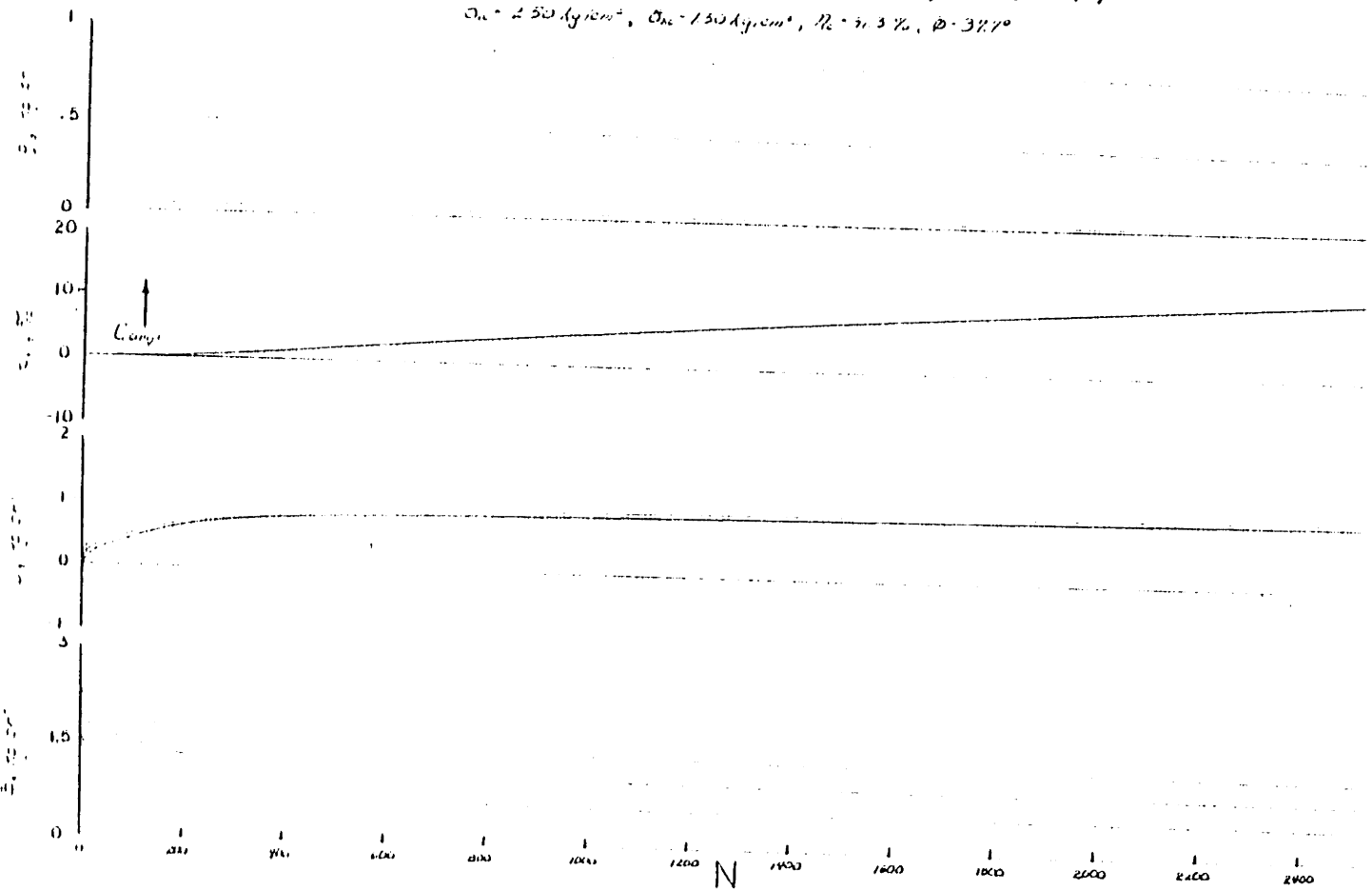

STRESS, STRAIN and PORE PRESSURE

FIGURE F-23

OOSTERSCHELDE SAND, LC-104

$\bar{\sigma}_c$ = 2.50 kg/cm², $\bar{\sigma}_{hc}$ = 1.50 kg/cm², n_c = 41.9 %, ϕ = 37.2°

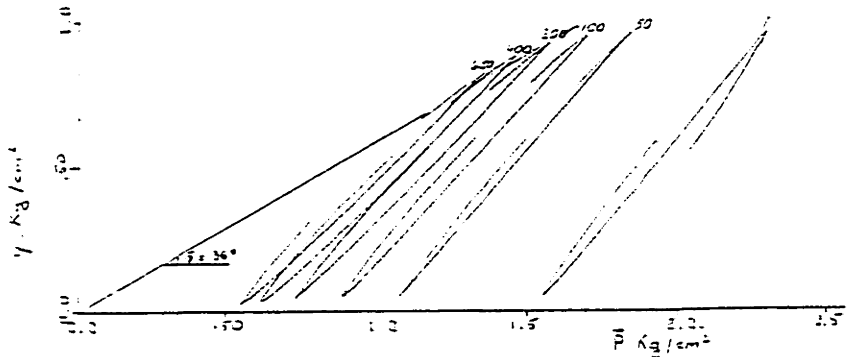

EFFECTIVE STRESS PATH

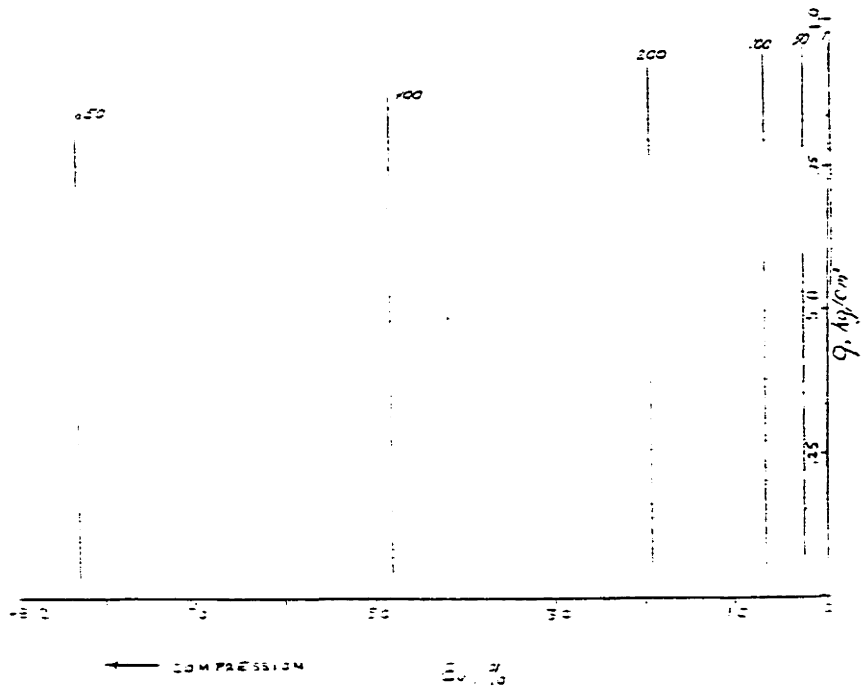

STRESS vs. STRAIN

FIGURE F-29

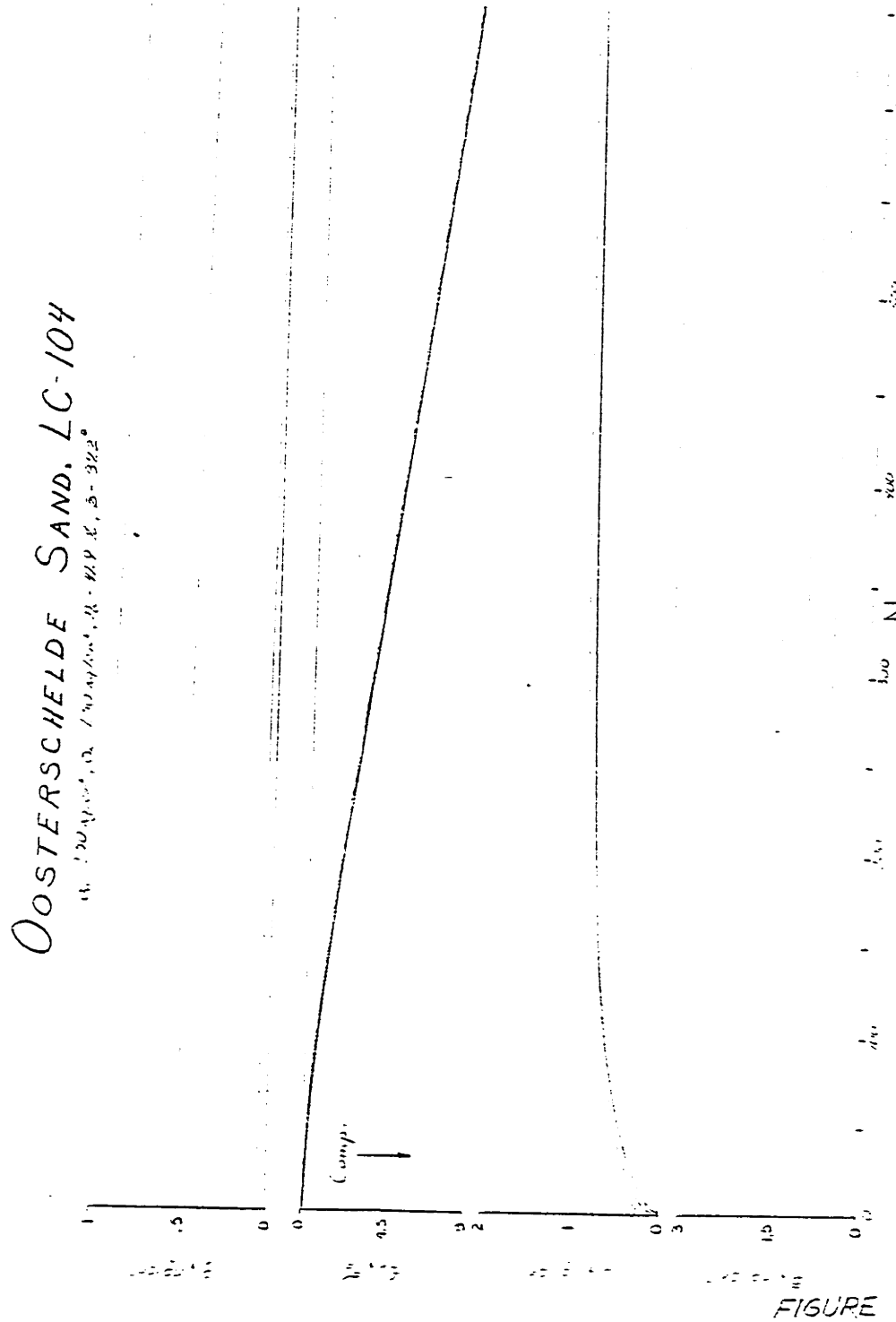

FIGURE F-30

OOSTERSCHELDE SAND, LC-105

$\bar{\sigma}_{1c} = 2.50 kg/cm^2$, $\bar{\sigma}_{3c} = 1.50 kg/cm^2$, $\eta_c = 37.1\%$, $\bar{\phi} = 32.8°$

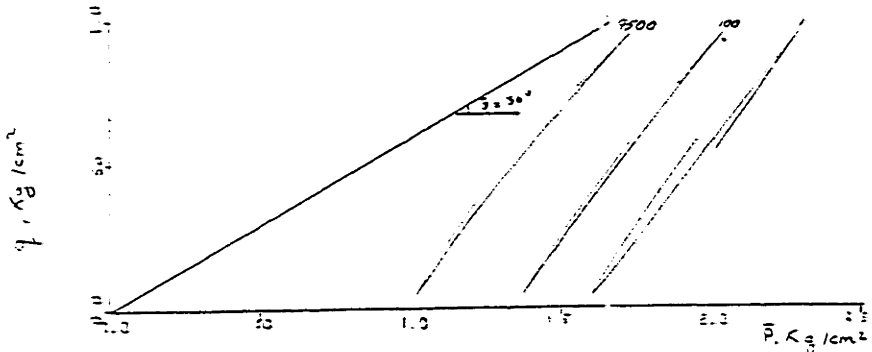

EFFECTIVE STRESS PATH

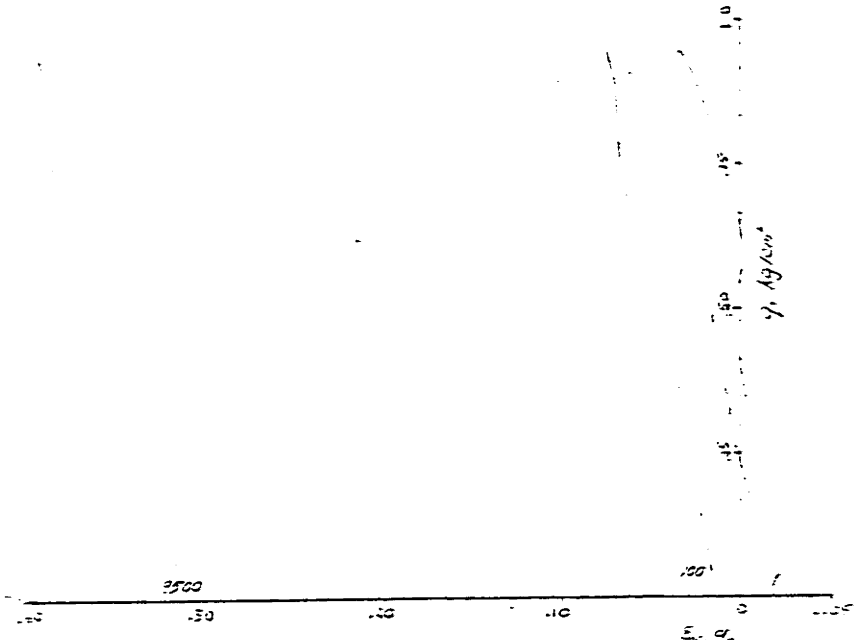

STRESS vs. STRAIN

FIGURE F-31

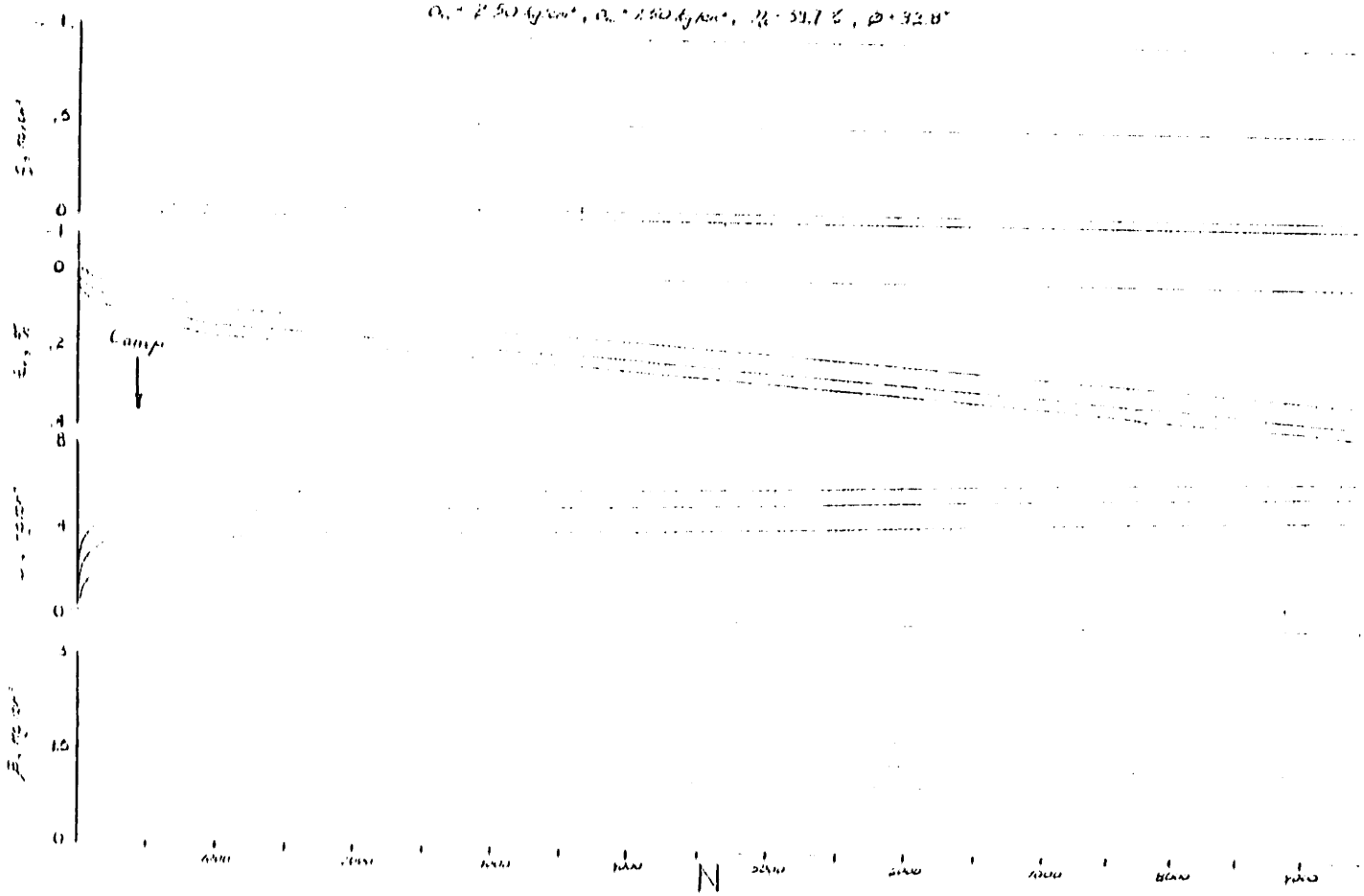

FIGURE F-32 STRESS, STRAIN and PORE PRESSURE

OOSTERSCHELDE SAND, LC-118

$\bar{\sigma}_{hc}$ = 2.50 kg/cm², $\bar{\sigma}_{hc}$ = 1.50 kg/cm², n_c = 42.9 %, ϕ = 37.2°

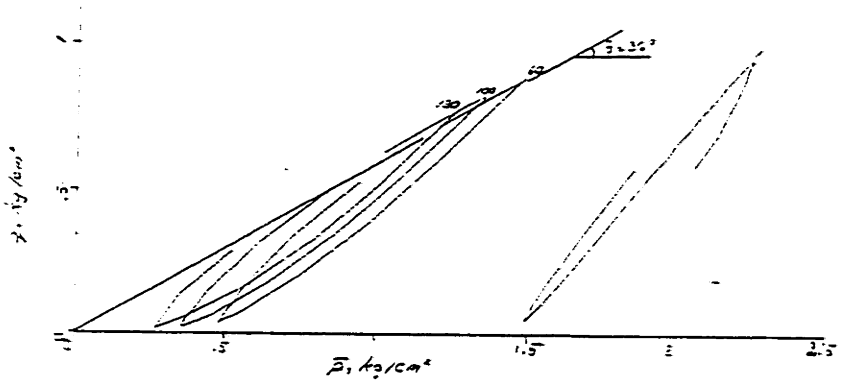

EFFECTIVE STRESS PATH

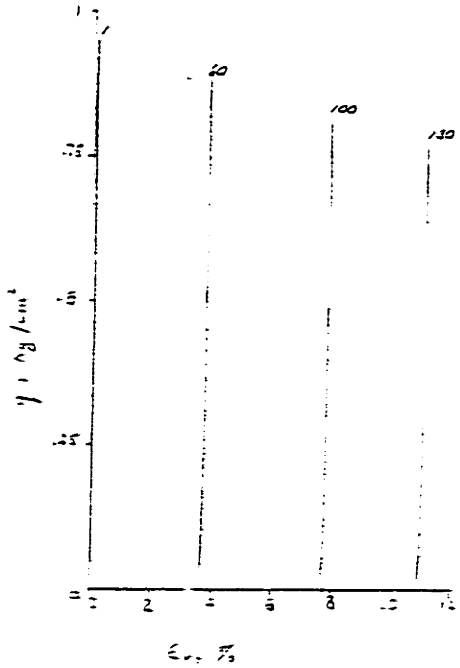

STRESS vs. STRAIN

FIGURE F-33

OOSTERSCHELDE SAND, LC-118

$\sigma_3' = 250$ kg/cm², $\sigma_c' = 250$ kg/cm², $\gamma_d = 123$ %, $\phi = .382$"

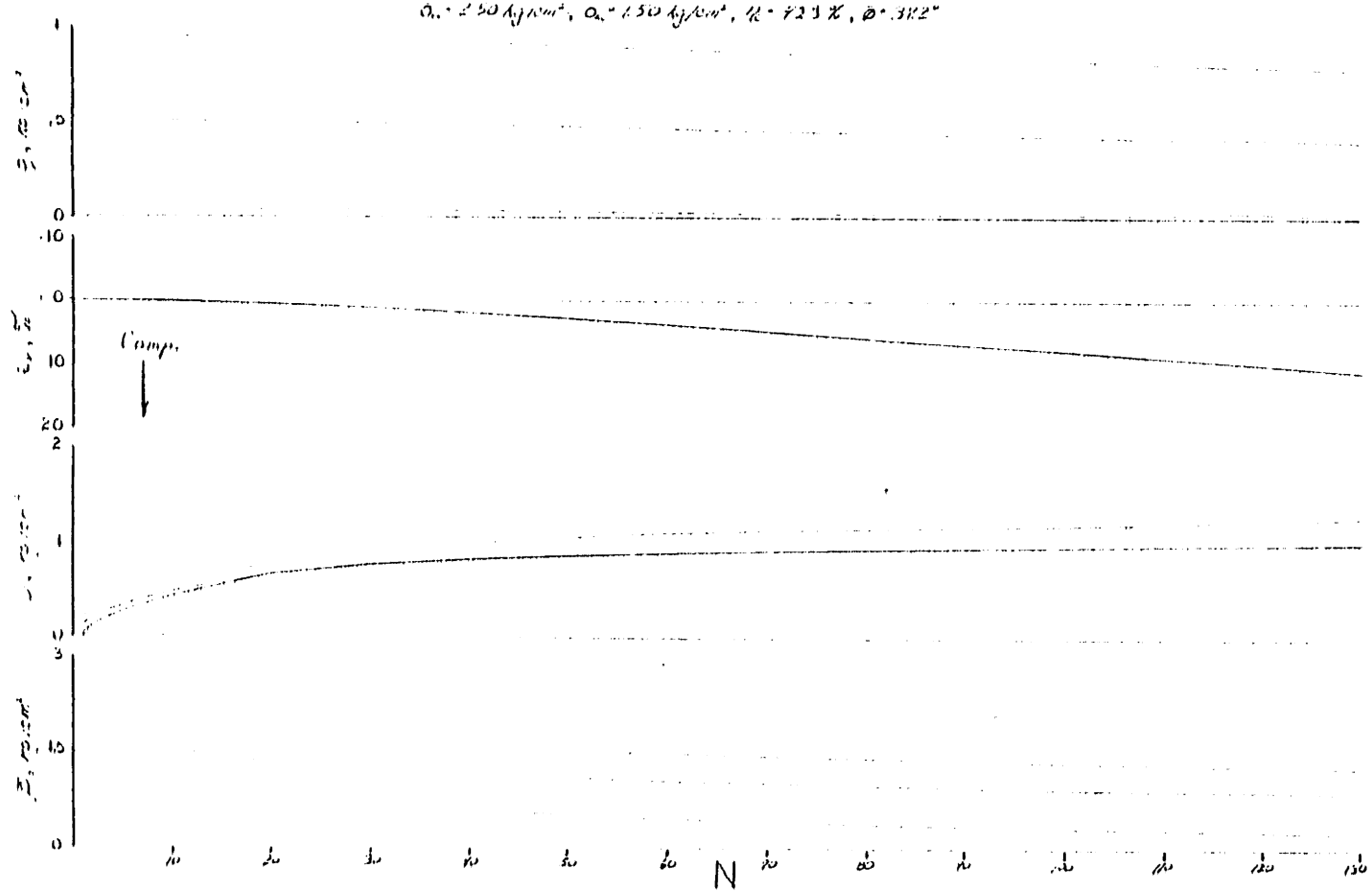

STRESS, STRAIN and PORE PRESSURE

FIGURE F-22H

OOSTERSCHELDE SAND, LC-120

$\bar{\sigma}_{3c} = 2.00 kg/cm^2$, $\bar{\sigma}_{1c} = 1.00 kg/cm^2$, $\eta_c = 41.4\%$, $\phi = 38.7°$

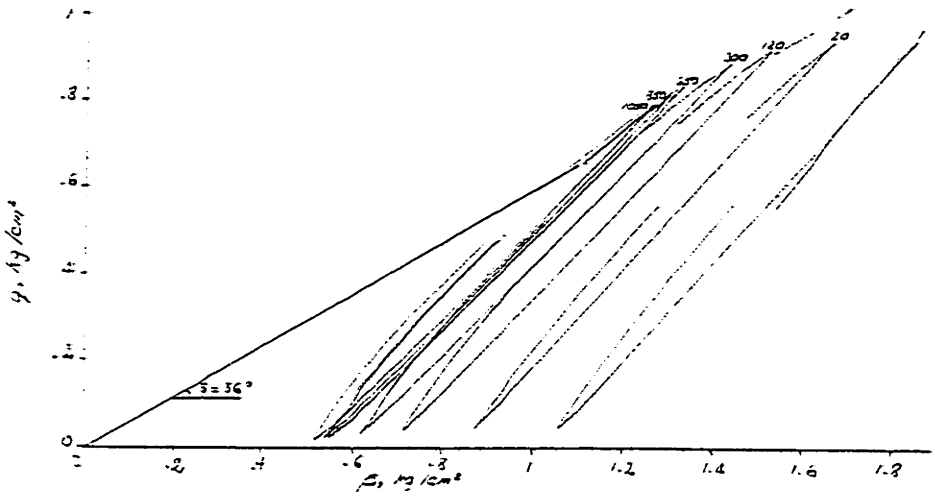

EFFECTIVE STRESS PATH

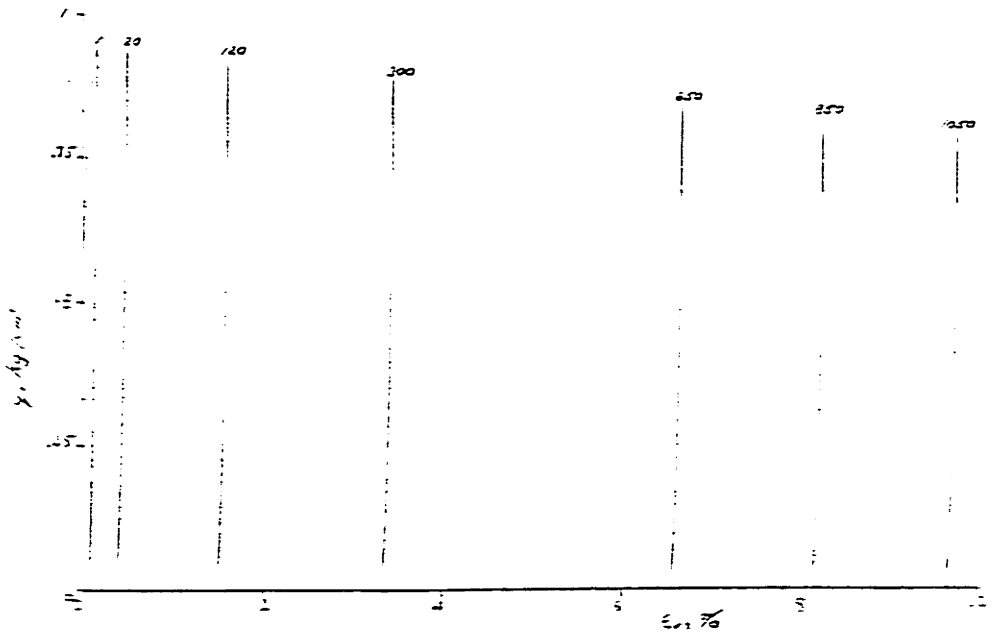

STRESS vs. STRAIN

FIGURE F-35

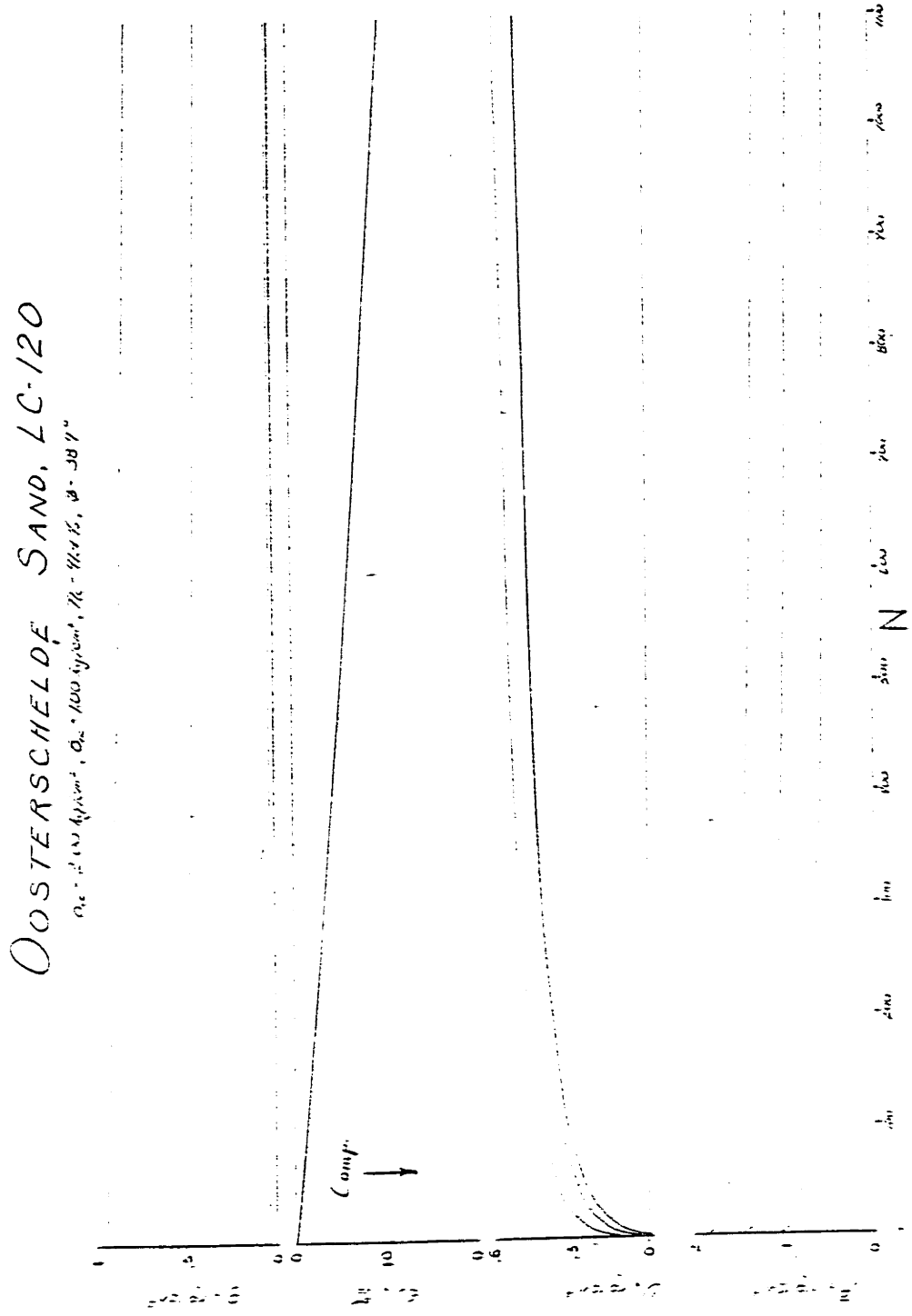
OOSTERSCHELDE SAND, LC-120
Comp.
STRESS, STRAIN and PORE PRESSURE
N

FIGURE F-36

OOSTERSCHELDE SAND, LC-129

$\bar{\sigma}_{vc} = 2.50\ kg/cm^2$, $\bar{\sigma}_{hc} = 1.50\ kg/cm^2$, $\eta_c = 1.55\%$. $\phi = 31.2°$

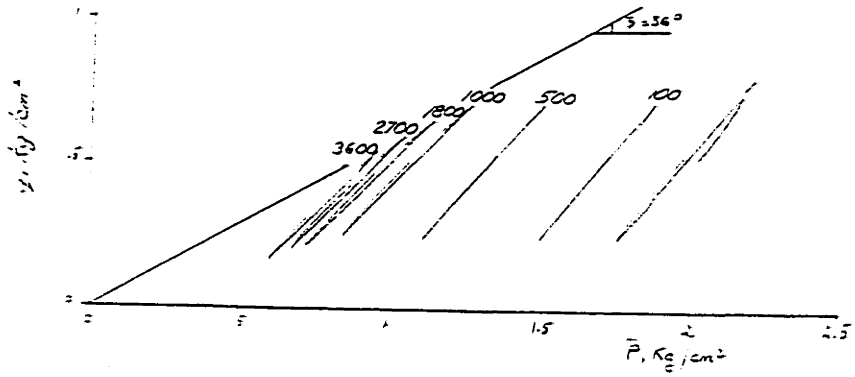

EFFECTIVE STRESS PATH

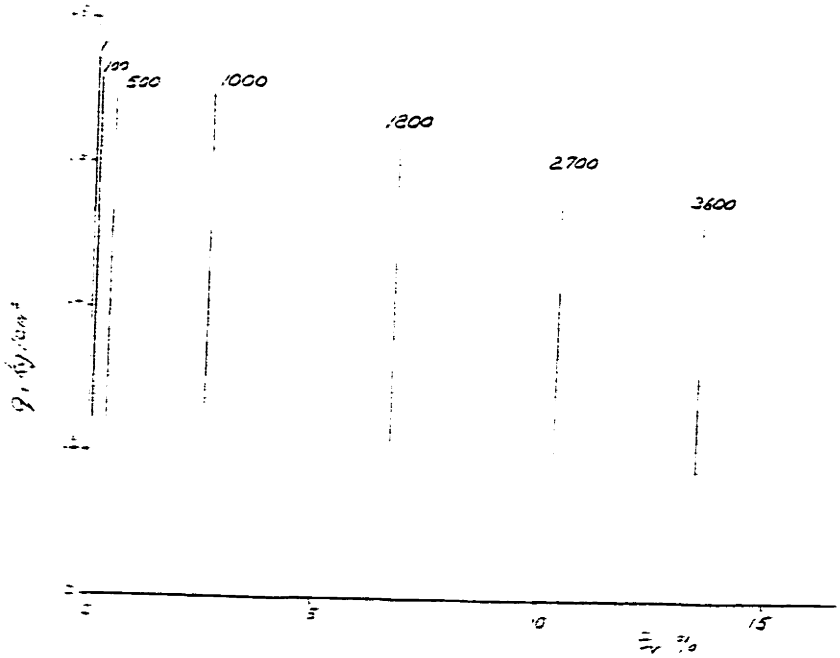

STRESS vs. STRAIN

FIGURE F-37

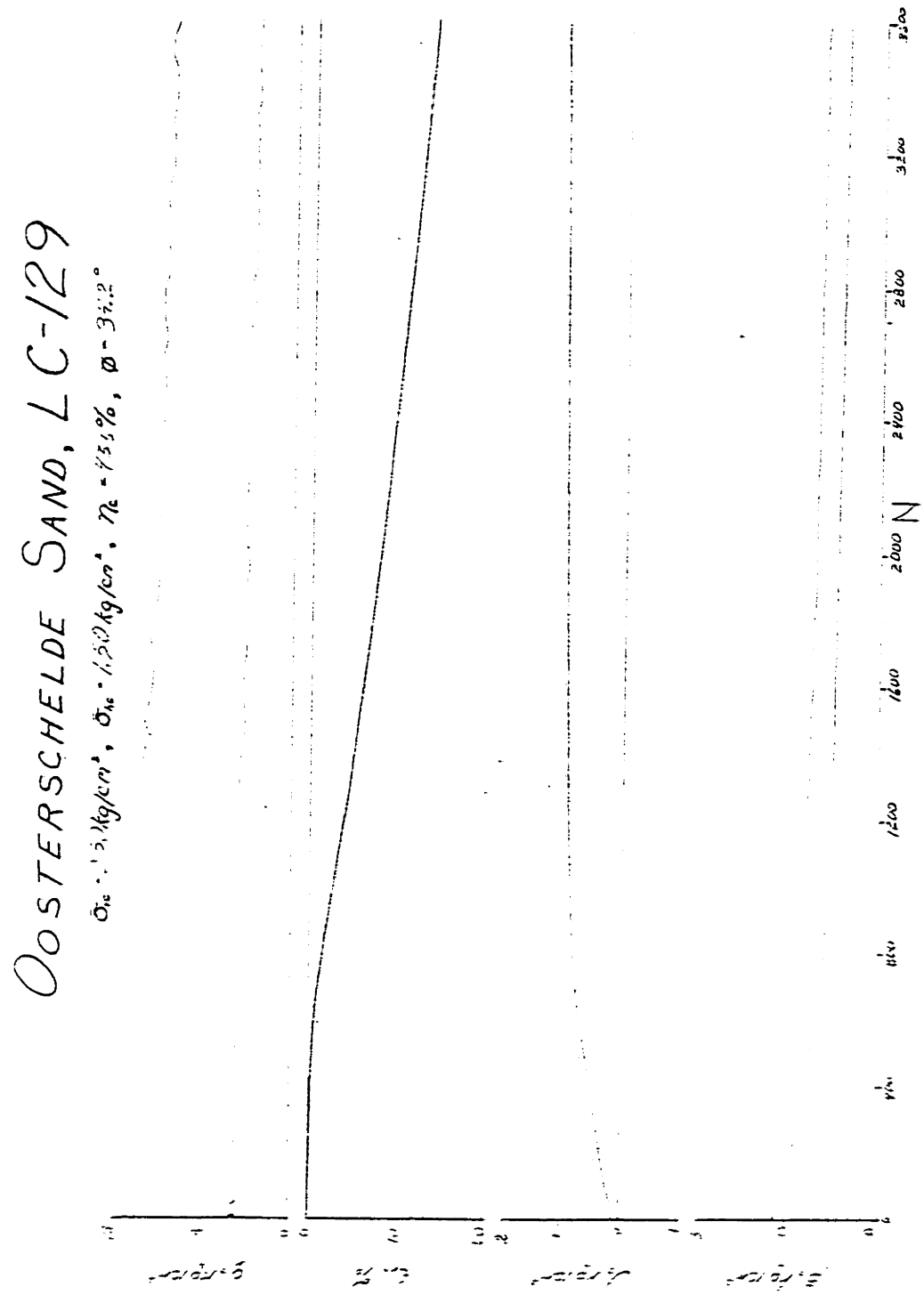
OOSTERSCHELDE SAND, LC-129
STRESS, STRAIN and PORE PRESSURE
N

FIGURE F-38

OOSTERSCHELDE SAND, LC-130

$\bar{\sigma}_{3c} = 2.50$ kg/cm², $\bar{\sigma}_{3c} = 1.50$ kg/cm², $\eta_c = 132\%$, $\bar{\phi} = 35.^\circ$

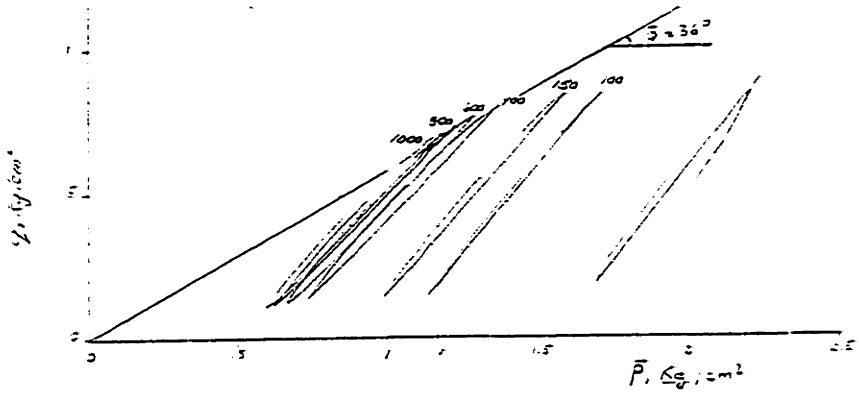

EFFECTIVE STRESS PATH

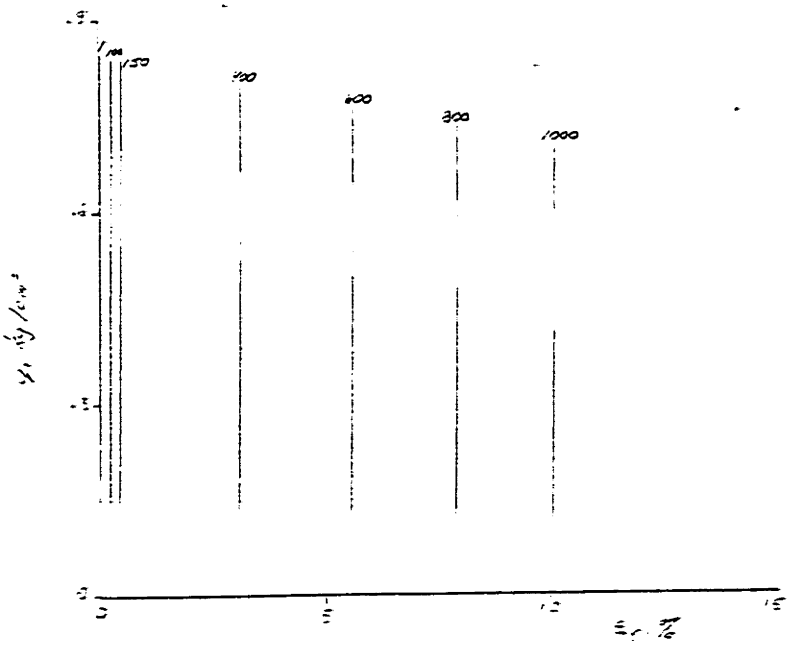

STRESS vs. STRAIN

FIGURE F-39

OOSTERSCHELDE SAND, LC-130

σ_3 = 2.50 kg/cm², σ_{vo} = 1.50 kg/cm², D_r = 43.2 %, ϕ = 36.1°

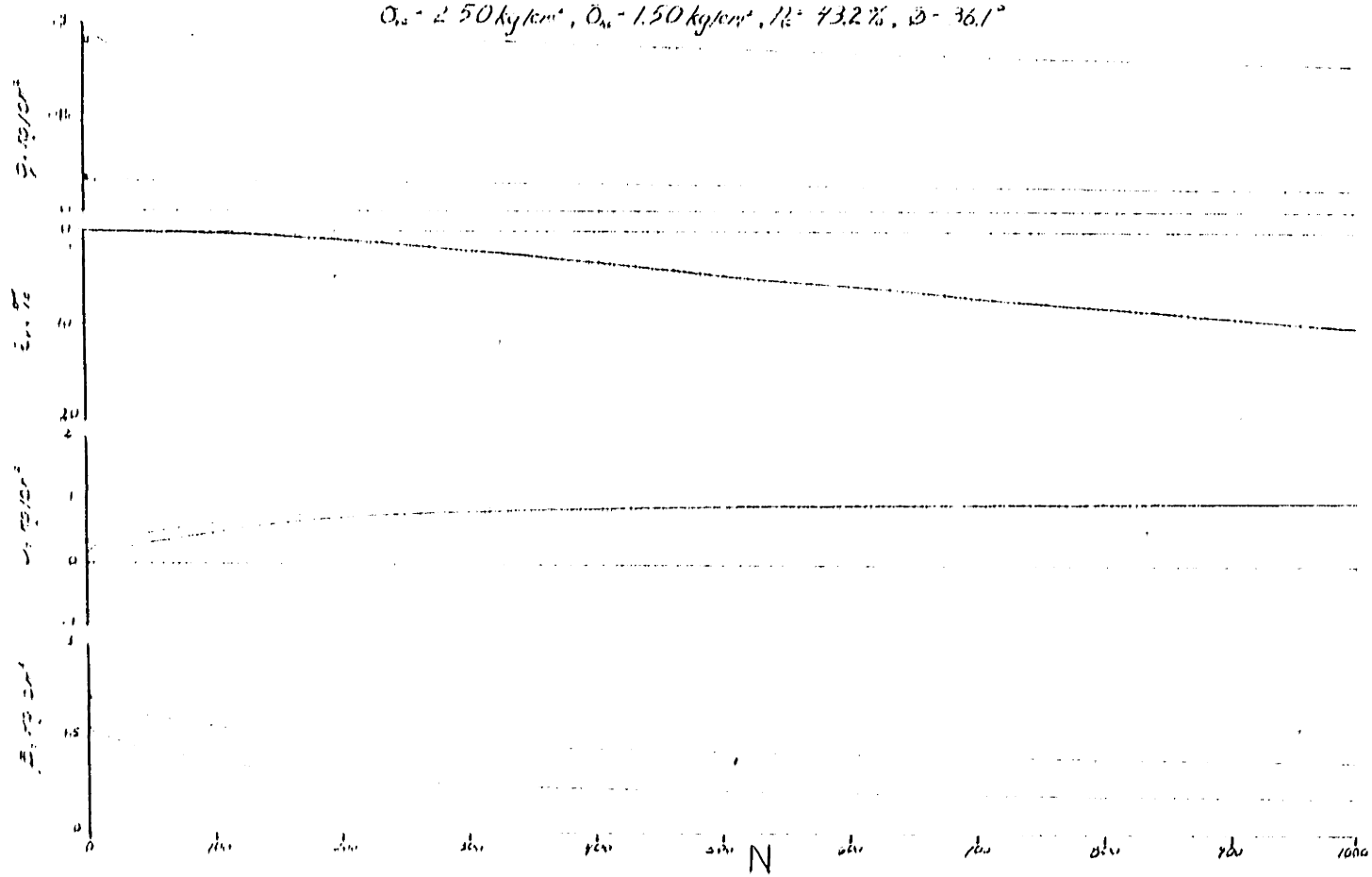

STRESS, STRAIN and PORE PRESSURE

FIGURE 5.10

OOSTERSCHELDE SAND, LC-131

$\bar{\sigma}_{3c} = 2.50\ kg/cm^2$, $\bar{\sigma}_{1c} = 1.50\ kg/cm^2$, $\eta_c = -2.3\%$, $\phi = 33.3°$

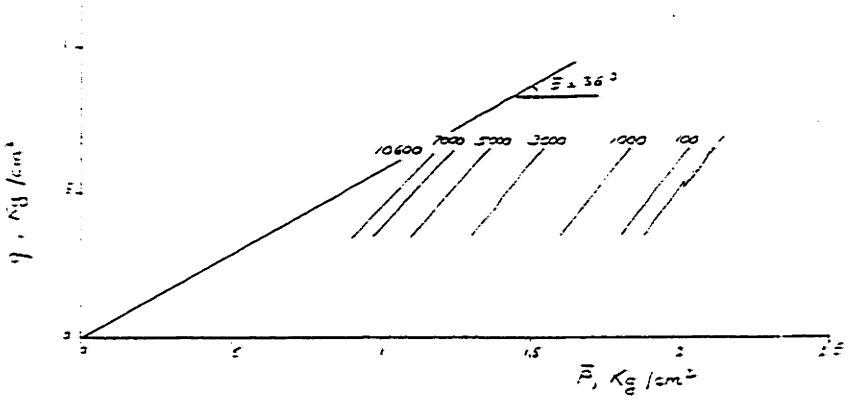

EFFECTIVE STRESS PATH

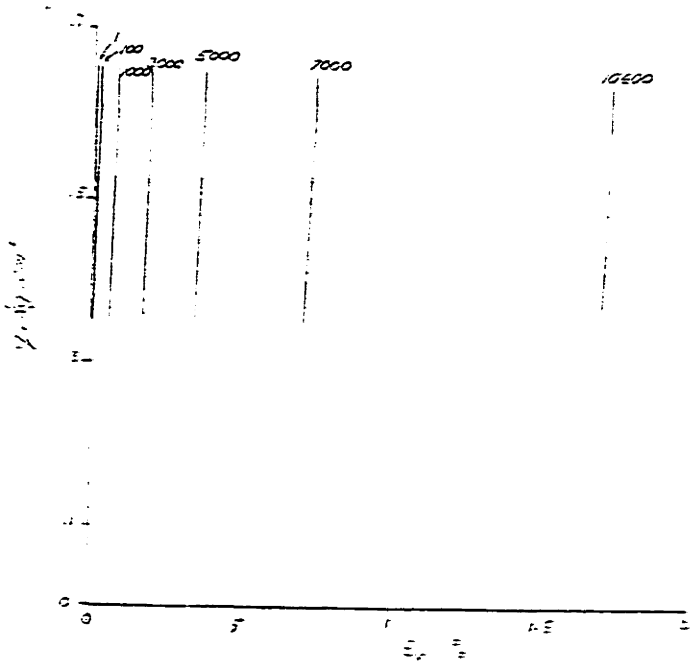

STRESS vs. STRAIN

FIGURE F-41

OOSTERSCHELDE SAND, LC-131

$\bar{\sigma}_c$ = 2.50 kg/cm², σ_m = 1.50 kg/cm², n_c = 42.9 %, $\bar{D}$ = 32.4°

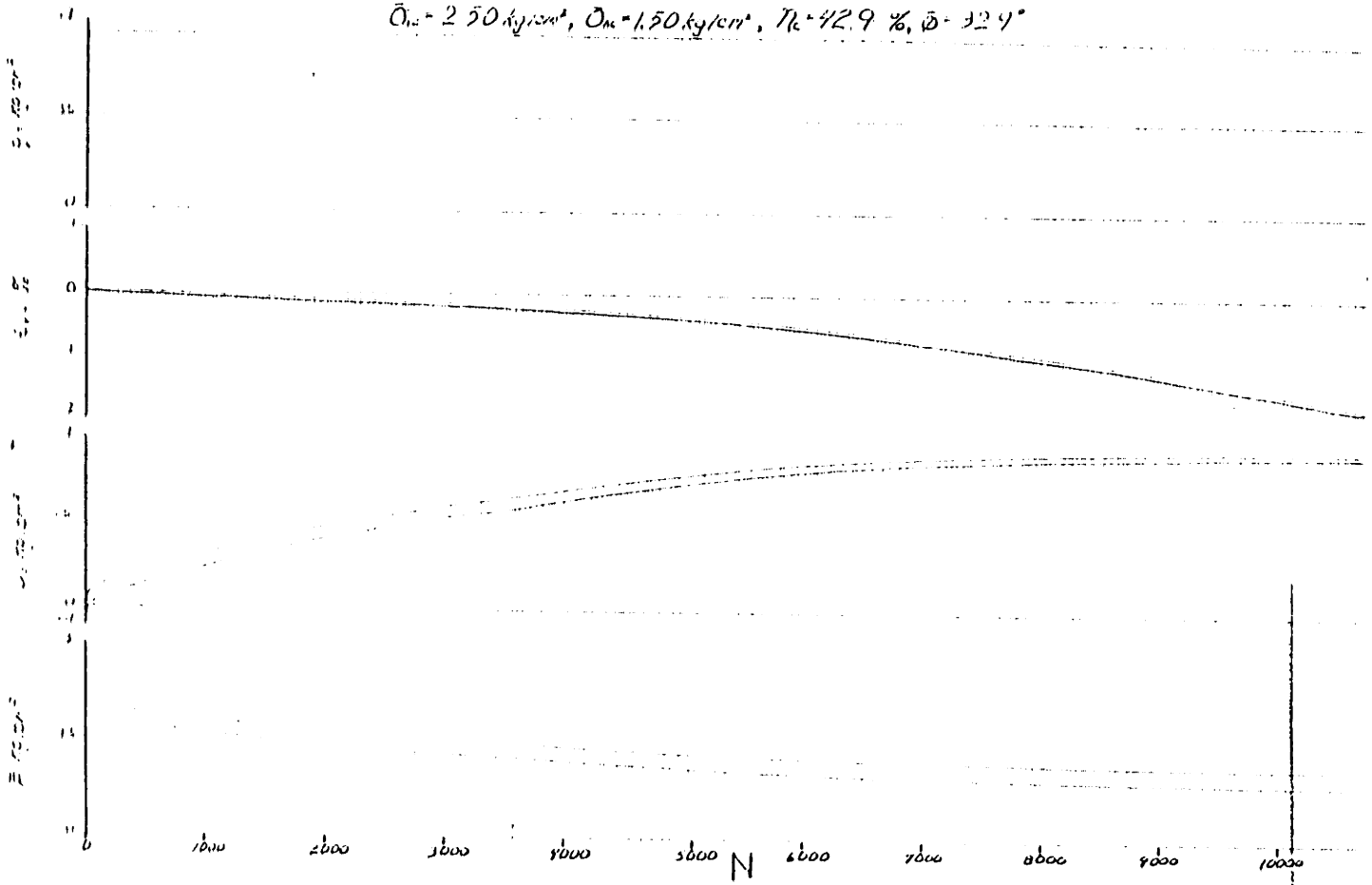

STRESS, STRAIN and PORE PRESSURE

FIGURE F-42

OOSTERSCHELDE SAND, LC-132

$\bar{\sigma}_{1c} = 3.00 kg/cm^2$, $\bar{\sigma}_{3c} = 1.50 kg/cm^2$, $\eta_c = 71.4\%$, $\phi = 36.2°$

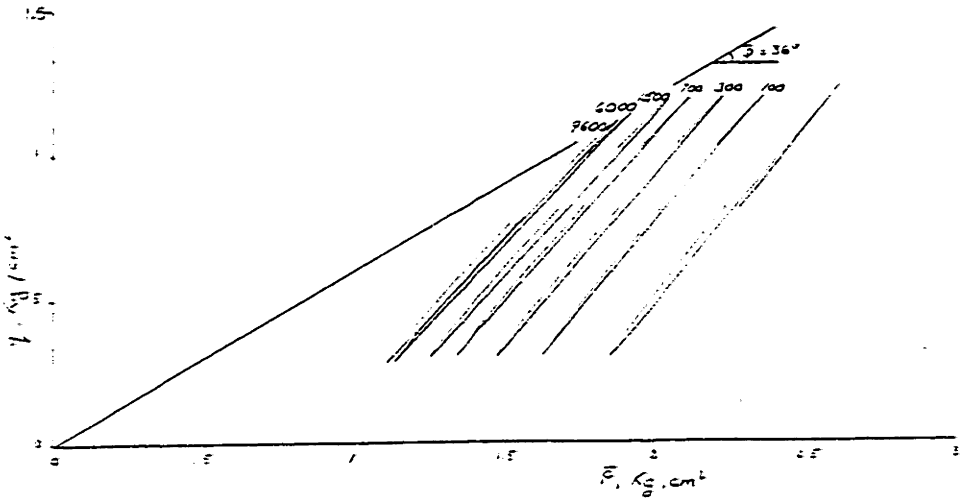

EFFECTIVE STRESS PATH

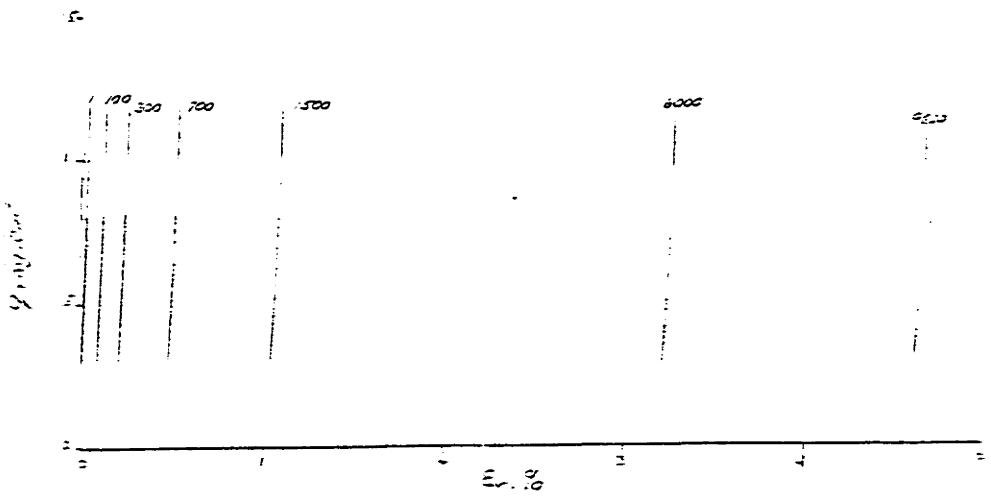

STRESS vs. STRAIN

FIGURE F-43

OOSTERSCHELDE SAND, LC-132

σ_{1c} = [illegible] kg/cm², σ_{3c} = [illegible] kg/cm², n_c = 44.4 %, ϕ = [illegible]°

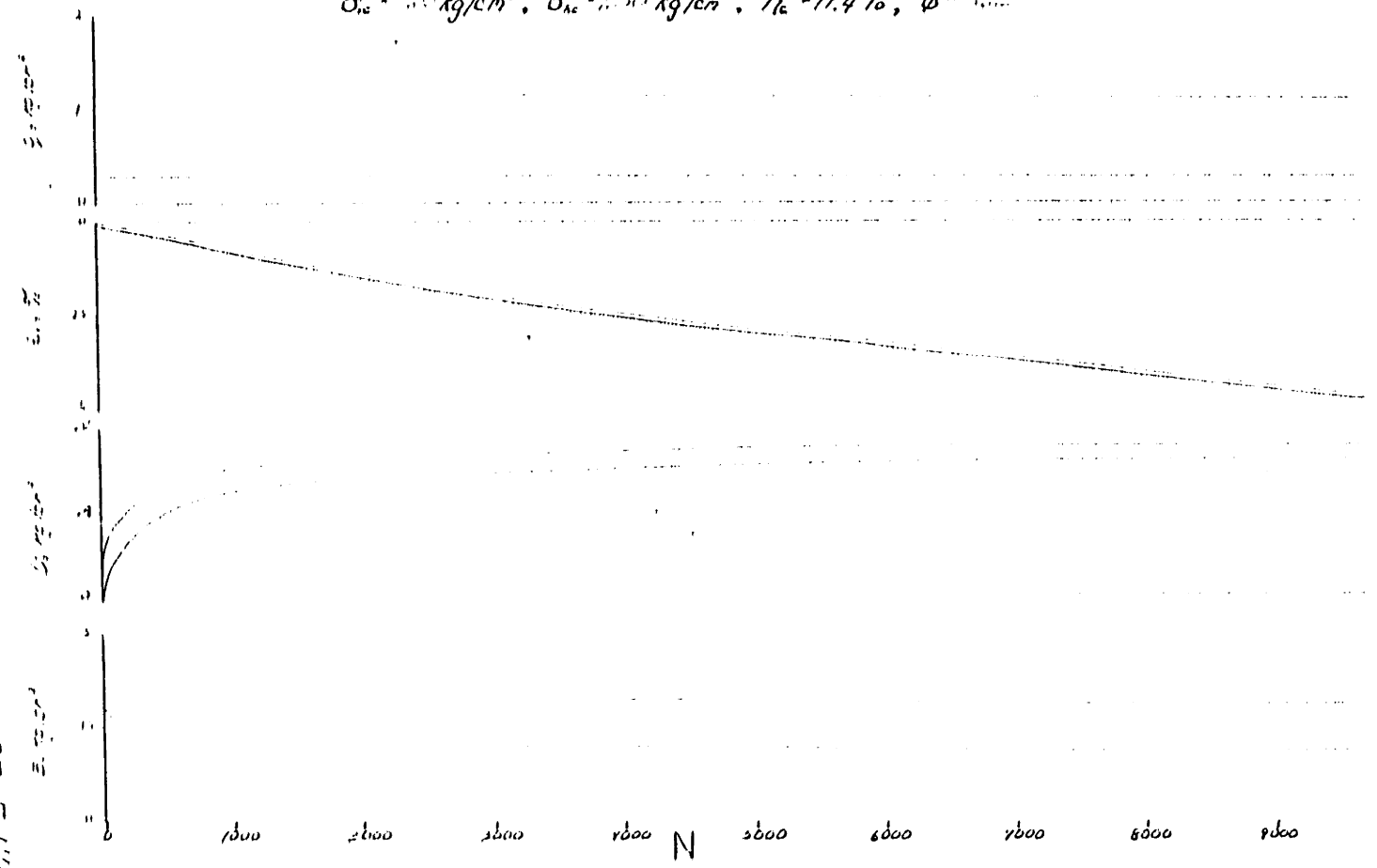

STRESS, STRAIN and PORE PRESSURE

FIGURE F-44

OOSTERSCHELDE SAND, LC-134

$\bar{\sigma}_{3c}$ = 2.50 kg/cm², $\bar{\sigma}_{1c}$ = 1.50 kg/cm², η_c = 41.1 %

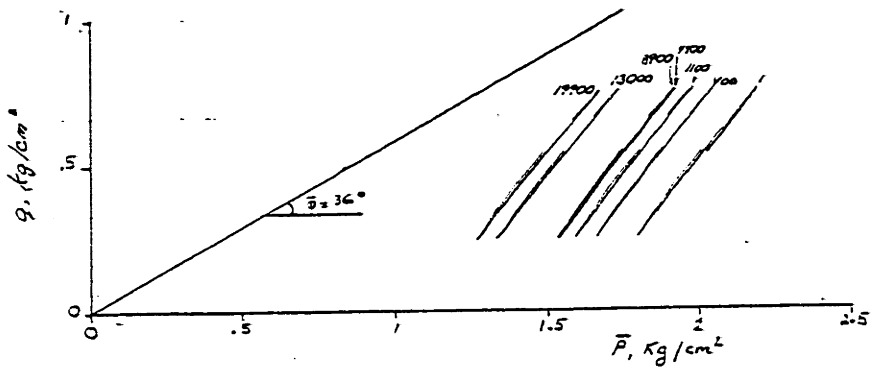

EFFECTIVE STRESS PATH

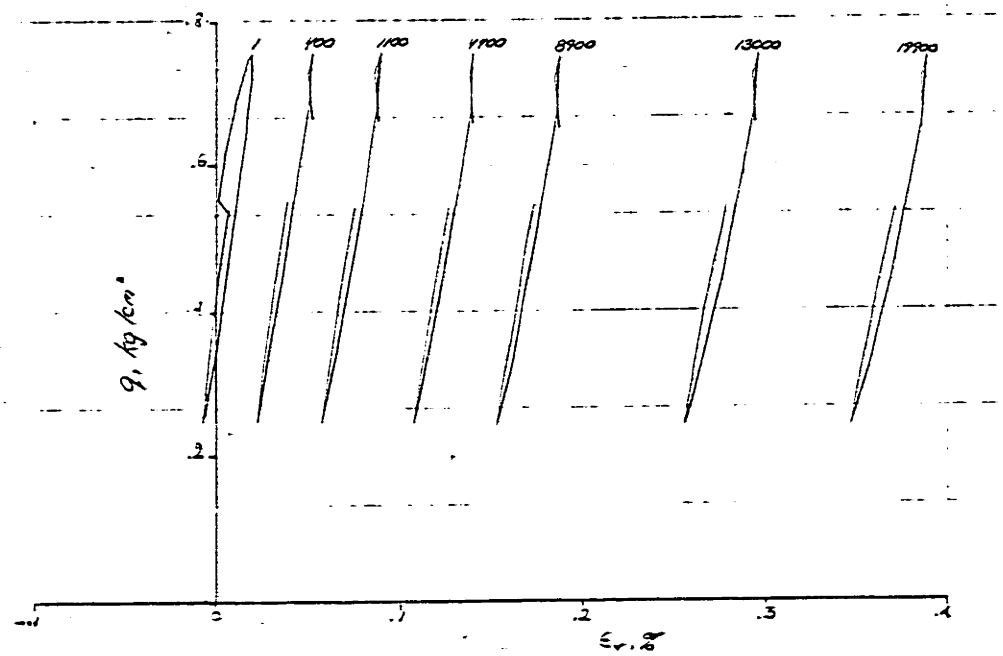

STRESS vs. STRAIN

FIGURE F-45

OOSTERSCHELDE SAND, LC-134

$\bar{\sigma}_{1c}$ = 2.50 kg/cm², $\bar{\sigma}_{3c}$ = 1.50 kg/cm², η_c = 41.1%.

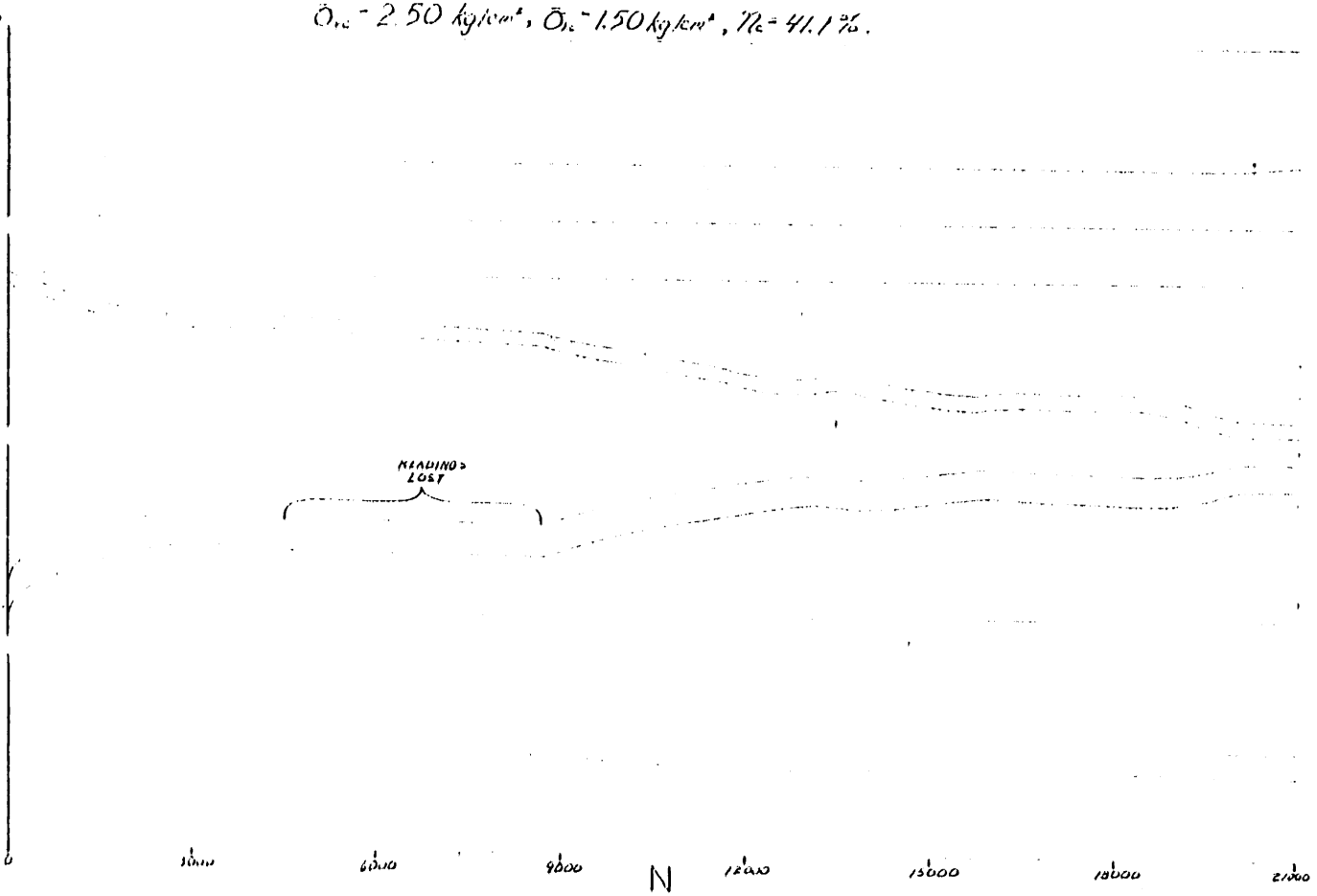

FIGURE C-116

STRESS, STRAIN and PORE PRESSURE

OOSTERSCHELDE SAND, LC-135

$\bar{\sigma}_{1c} = 3.00\ kg/cm^2$, $\bar{\sigma}_{3c} = 2.00\ kg/cm^2$, $\eta_c = 4/2.5$, $\bar{\beta} = 32.5°$

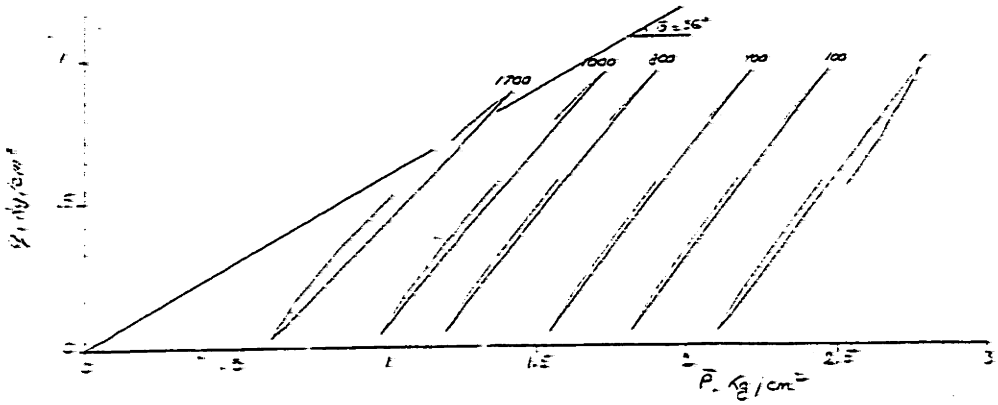

EFFECTIVE STRESS PATH

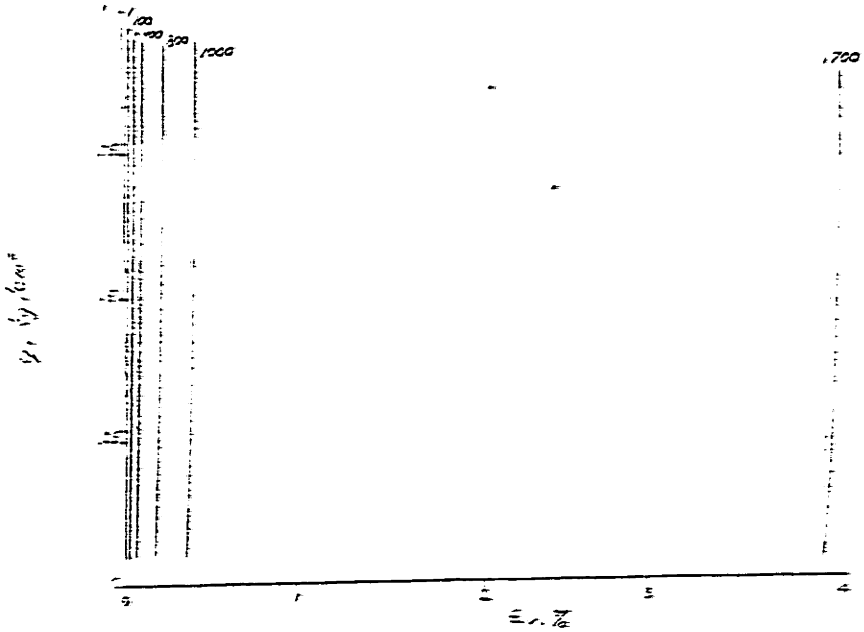

STRESS vs. STRAIN

FIGURE F-47

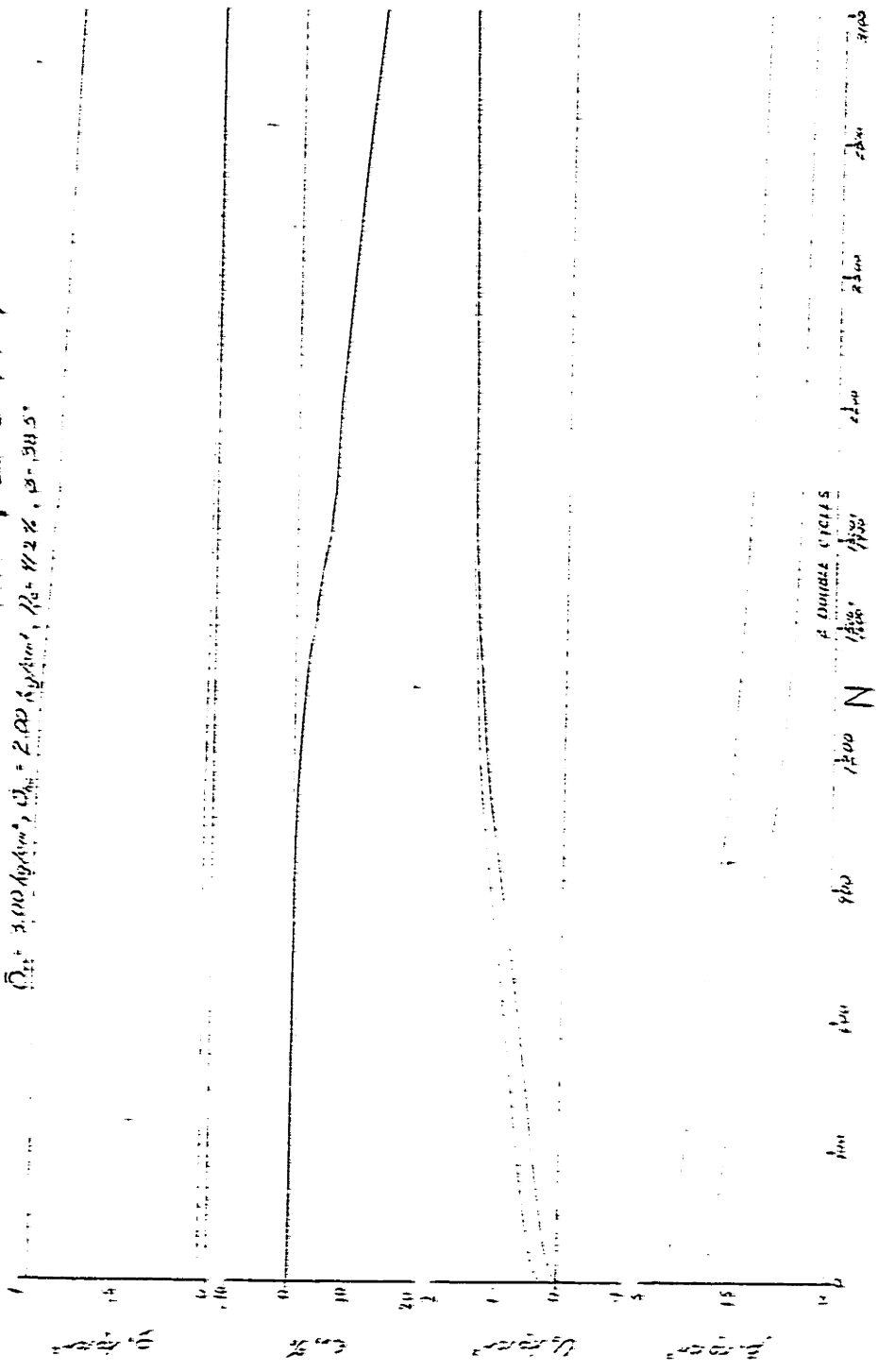

FIGURE F-43

OOSTERSCHELDE SAND, LC-137

$\sigma_{3c} = 3.50 kg/cm^2$, $\sigma_{1c} = 1.50 kg/cm^2$, $\eta_c = 41.3\%$, $\phi = 35.2°$

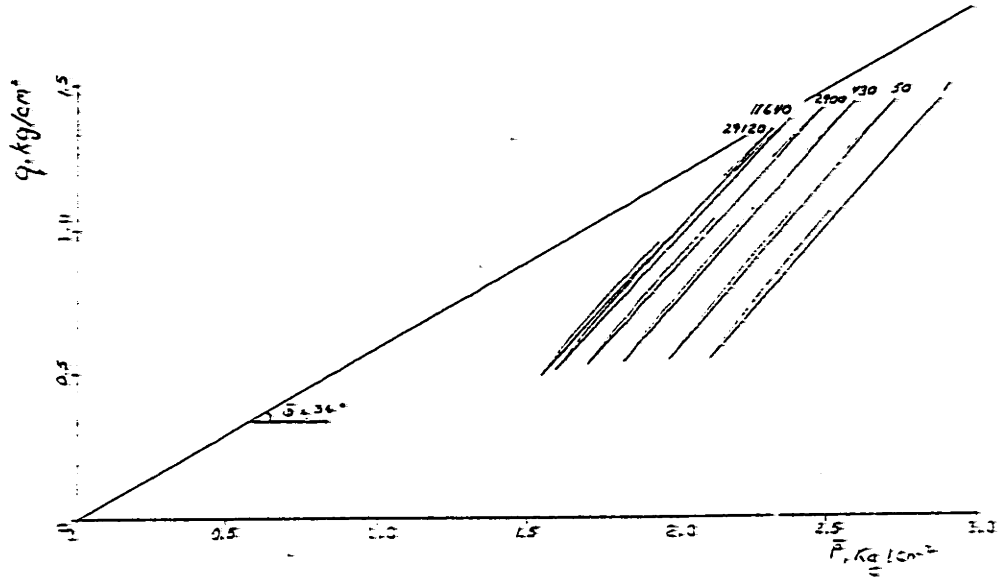

EFFECTIVE STRESS PATH

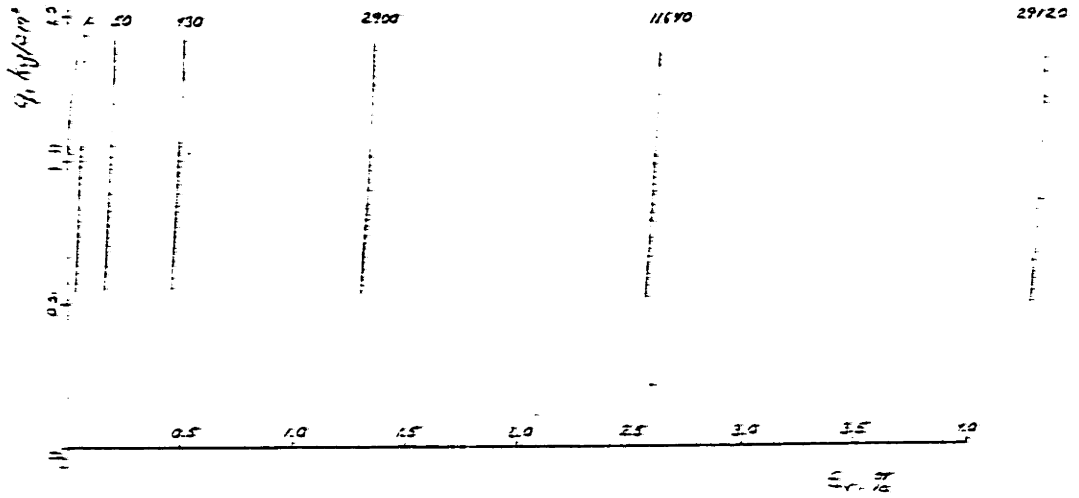

STRESS vs. STRAIN

FIGURE F-49

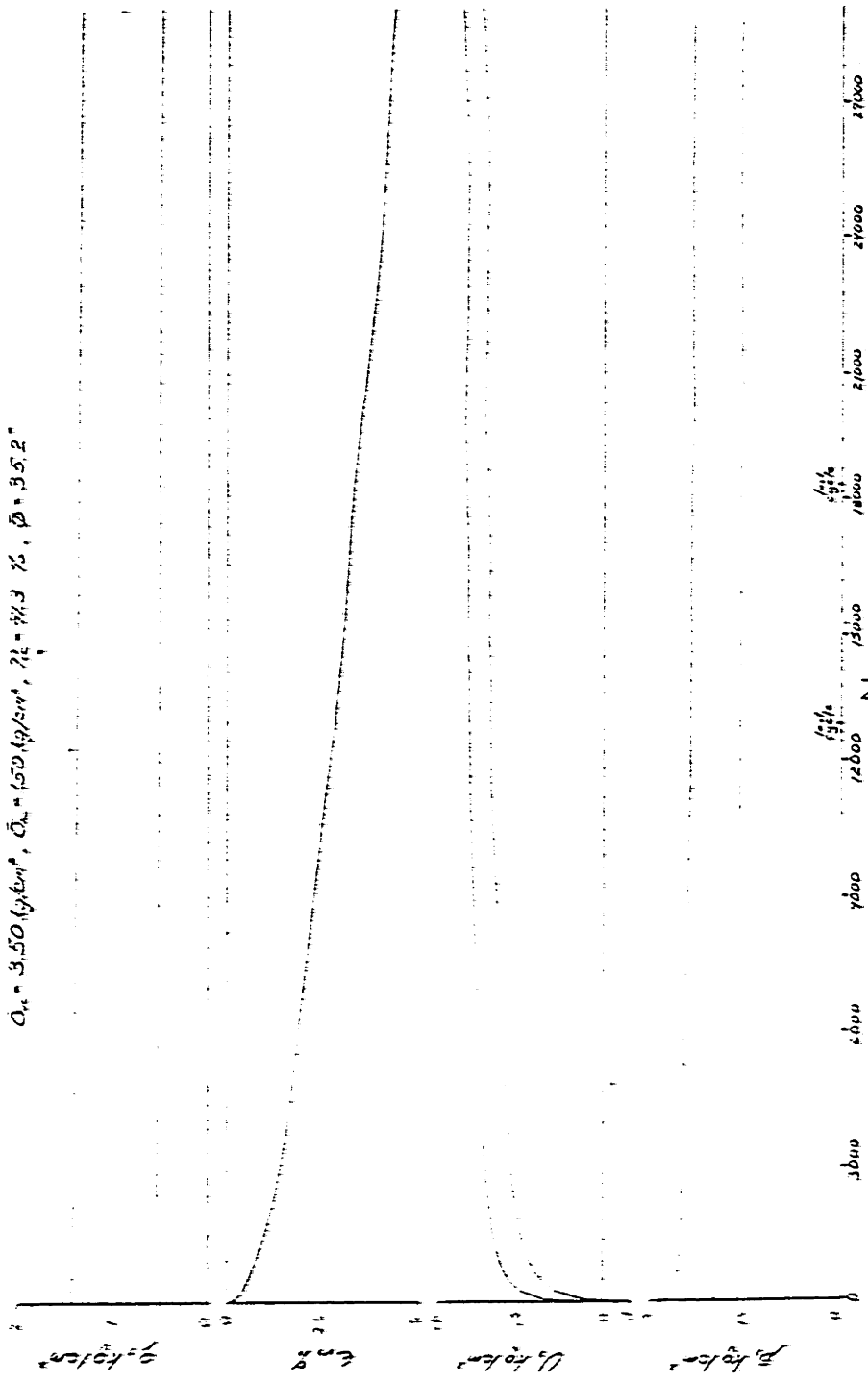
OOSTERSCHELDE SAND, LC-137
STRESS, STRAIN and PORE PRESSURE
N

FIGURE F-50

OOSTERSCHELDE SAND, LC-140

$\sigma_{1c} = 1.00 kg/cm^2$, $\sigma_{3c} = 0.50 kg/cm^2$, $\eta_c = \pm 1\%$, $\phi = \pm 0.2°$

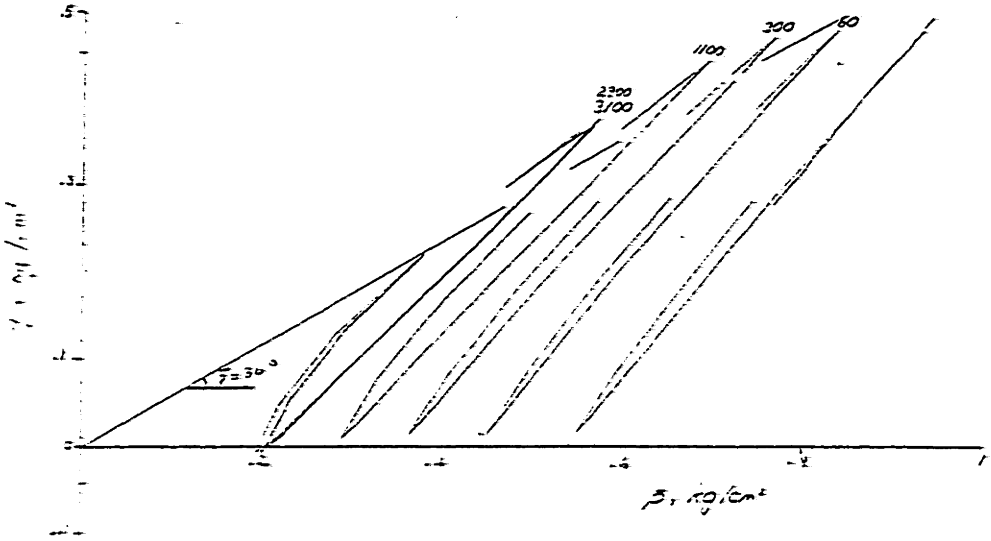

EFFECTIVE STRESS PATH

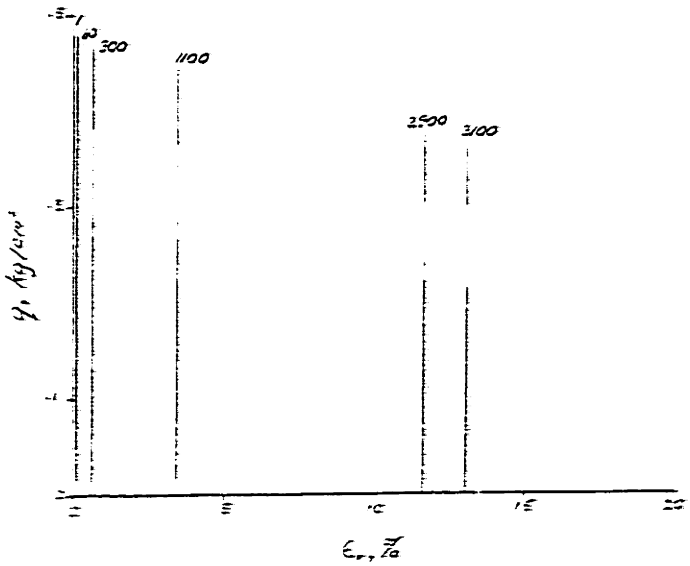

FIGURE F-51

STRESS vs. STRAIN

OOSTERSCHELDE SAND, LC-140

σ_{1c} = 1.00 kg/cm², σ_{3c} = 0.50 kg/cm², η_c = 33.1 %, ϕ = 33.3°

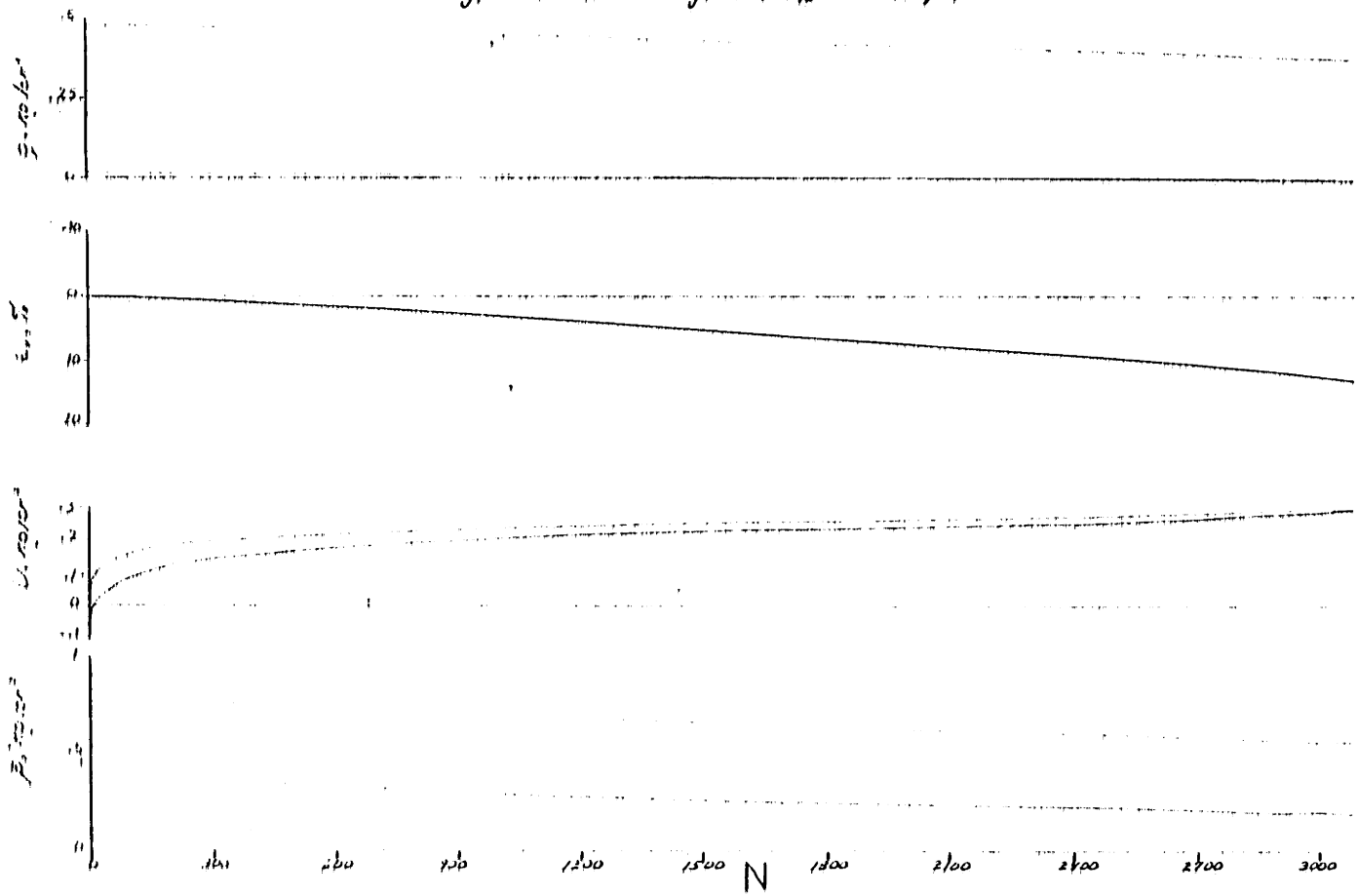

STRESS, STRAIN and PORE PRESSURE

FIGURE C-52

OOSTERSCHELDE SAND, LC-142

$\bar{\sigma}_{1c} = 2.50\ kg/cm^2$, $\bar{\sigma}_{3c} = 1.50\ kg/cm^2$, $\eta_c = 41.7\ \%$, $\bar{\phi} = 36.4°$

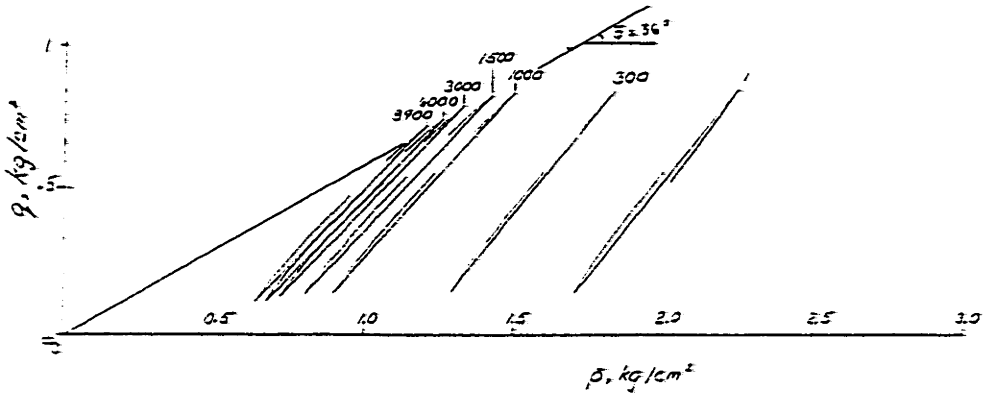

EFFECTIVE STRESS PATH

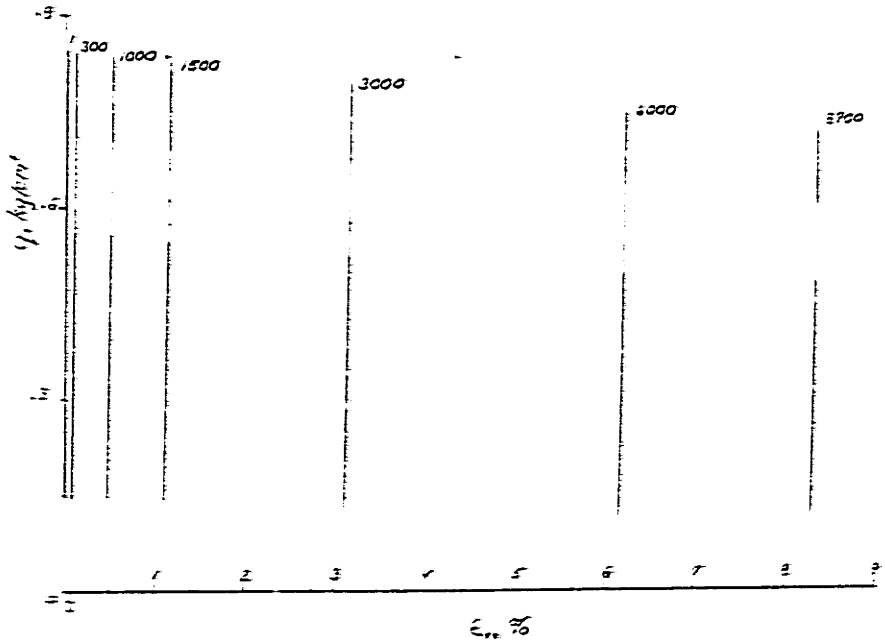

STRESS vs. STRAIN

FIGURE F-53

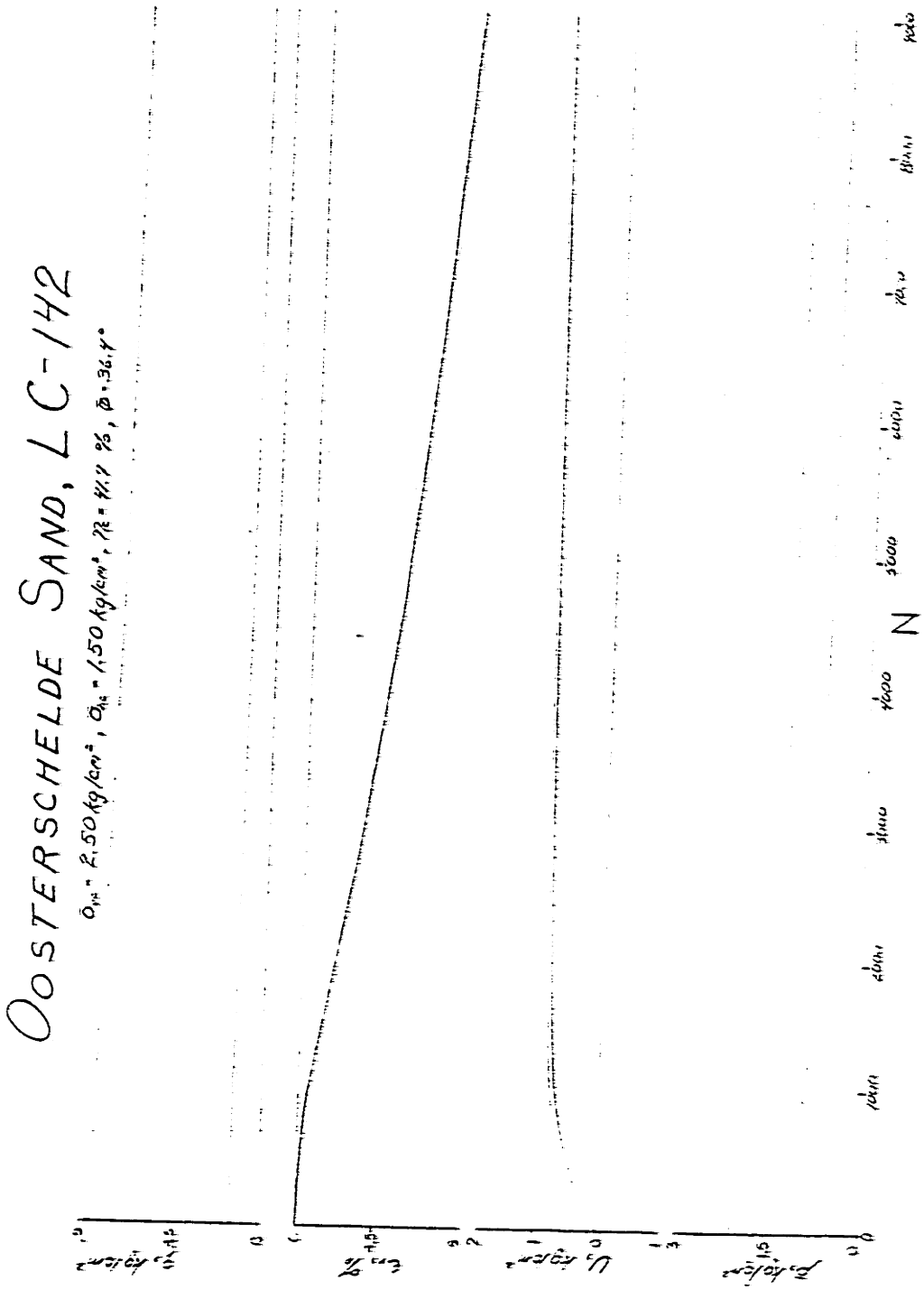
OOSTERSCHELDE SAND, LC-142
STRESS, STRAIN and PORE PRESSURE
N

FIGURE F-54

OOSTERSCHELDE SAND, LC-143

$\bar{\sigma}_{1c} = 2.50 kg/cm^2$, $\bar{\sigma}_{3c} = 1.50 kg/cm^2$, $\eta_c = 73.2\%$, $\phi = 36.3°$

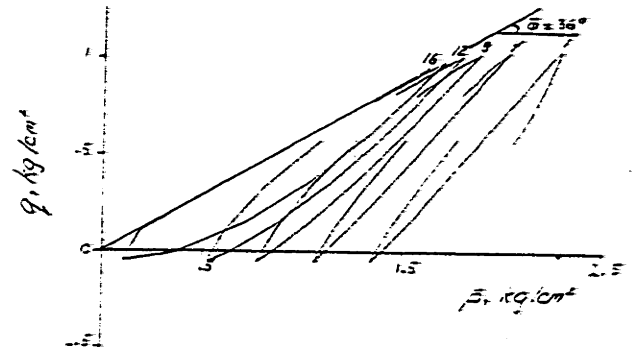

EFFECTIVE STRESS PATH

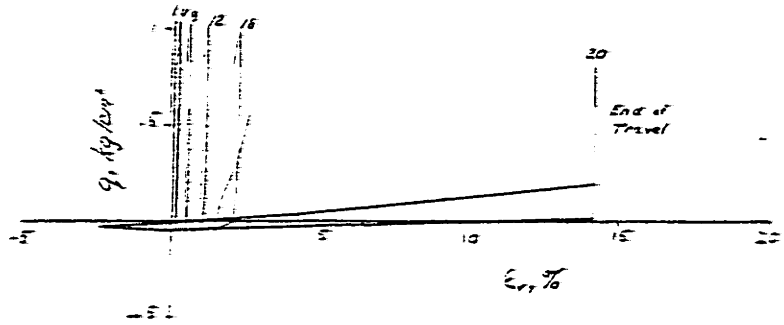

STRESS vs. STRAIN

FIGURE F-55

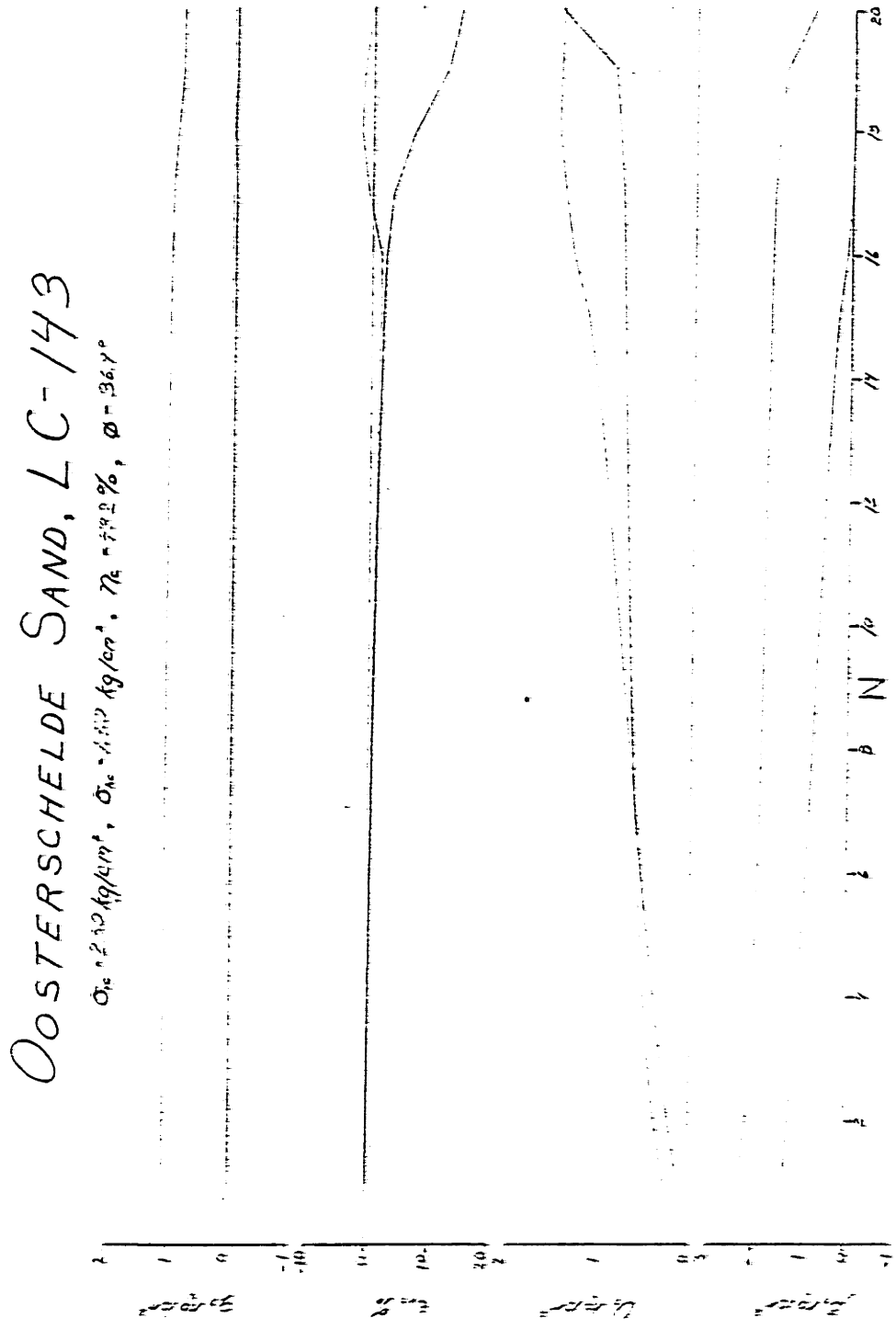

FIGURE F-56

OOSTERSCHELDE SAND, LC-148

$\bar{\sigma}_{1c} = 1.00 kg/cm^2$, $\bar{\sigma}_{3c} = 0.50 kg/cm^2$, $n_c = 41.1\%$, $\phi = 36.2°$

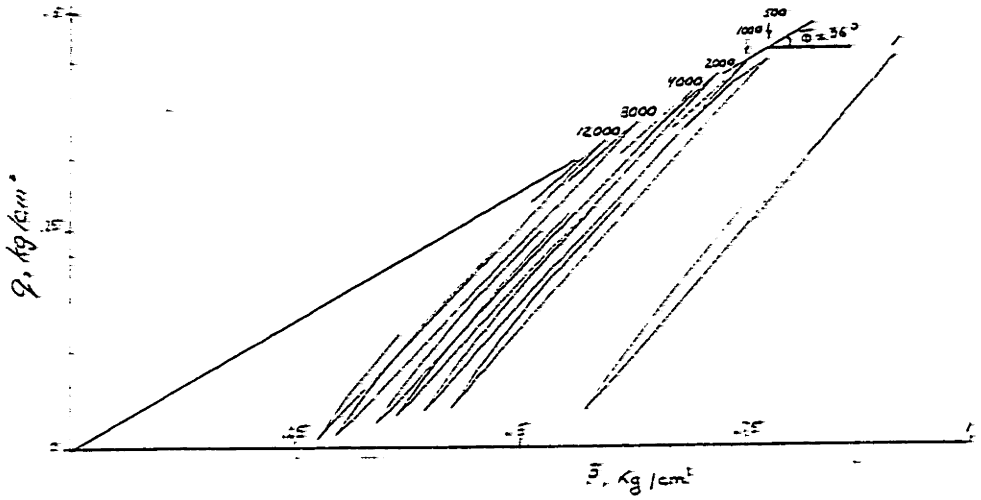

EFFECTIVE STRESS PATH

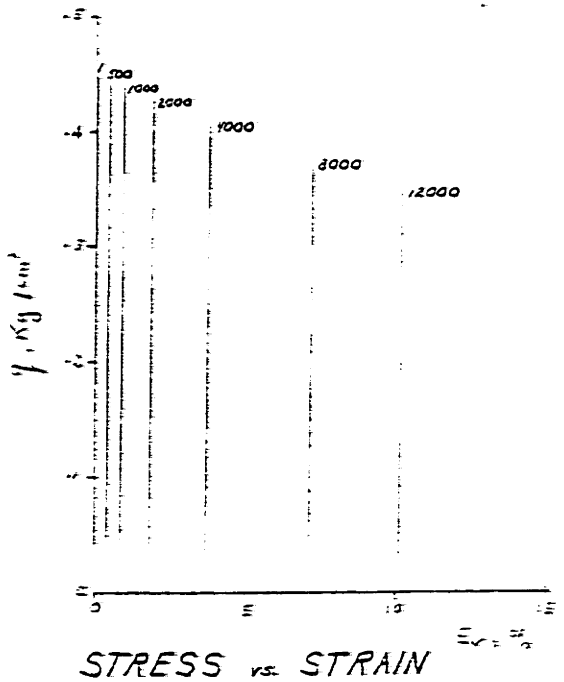

STRESS vs. STRAIN

FIGURE F-5

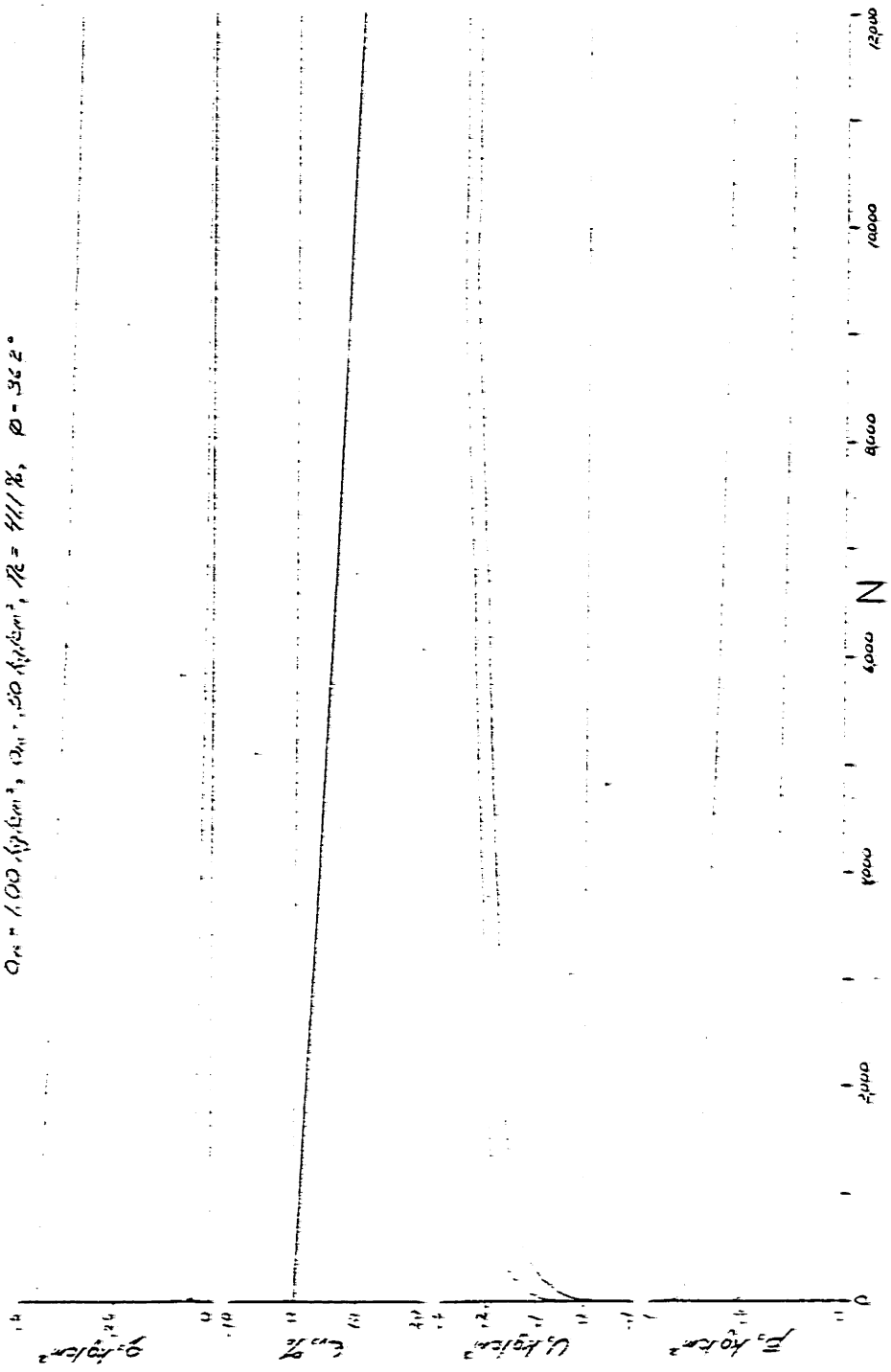
OOSTERSCHELDE SAND, LC-148
STRESS, STRAIN and PORE PRESSURE
N

FIGURE F-53

OOSTERSCHELDE SAND, LC-149

$\bar{\sigma}_{1c} = 5.00\ kg/cm^2$, $\bar{\sigma}_{3c} = 2.50\ kg/cm^2$, $\eta_c = 41.5\ \%$, $\phi = 36.7°$

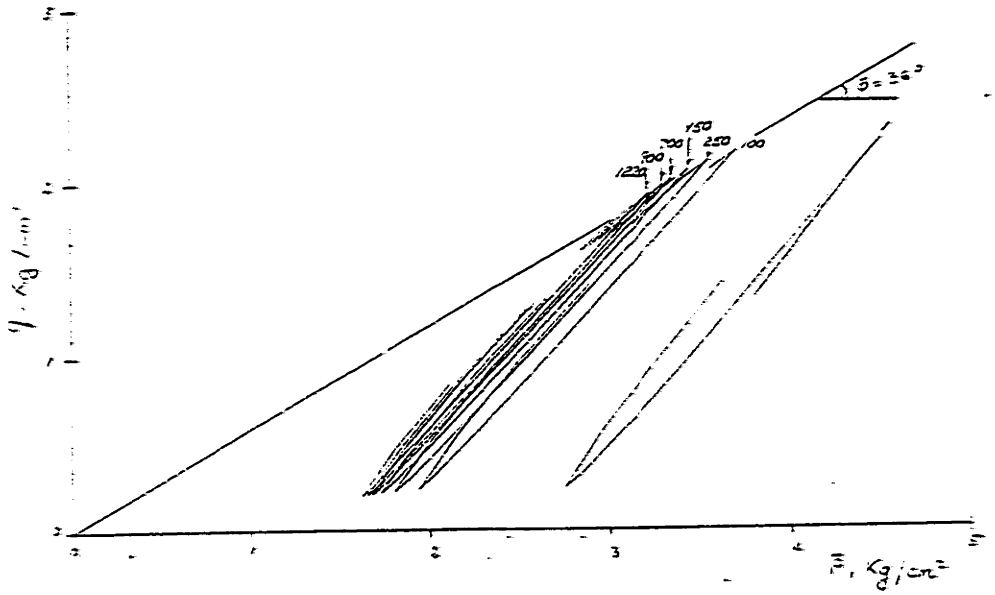

EFFECTIVE STRESS PATH

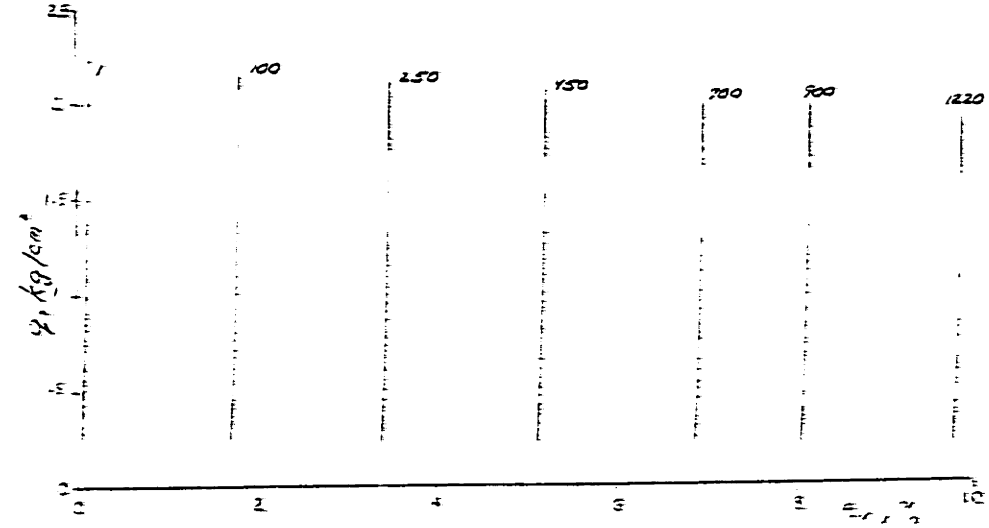

STRESS vs. STRAIN

FIGURE F-59

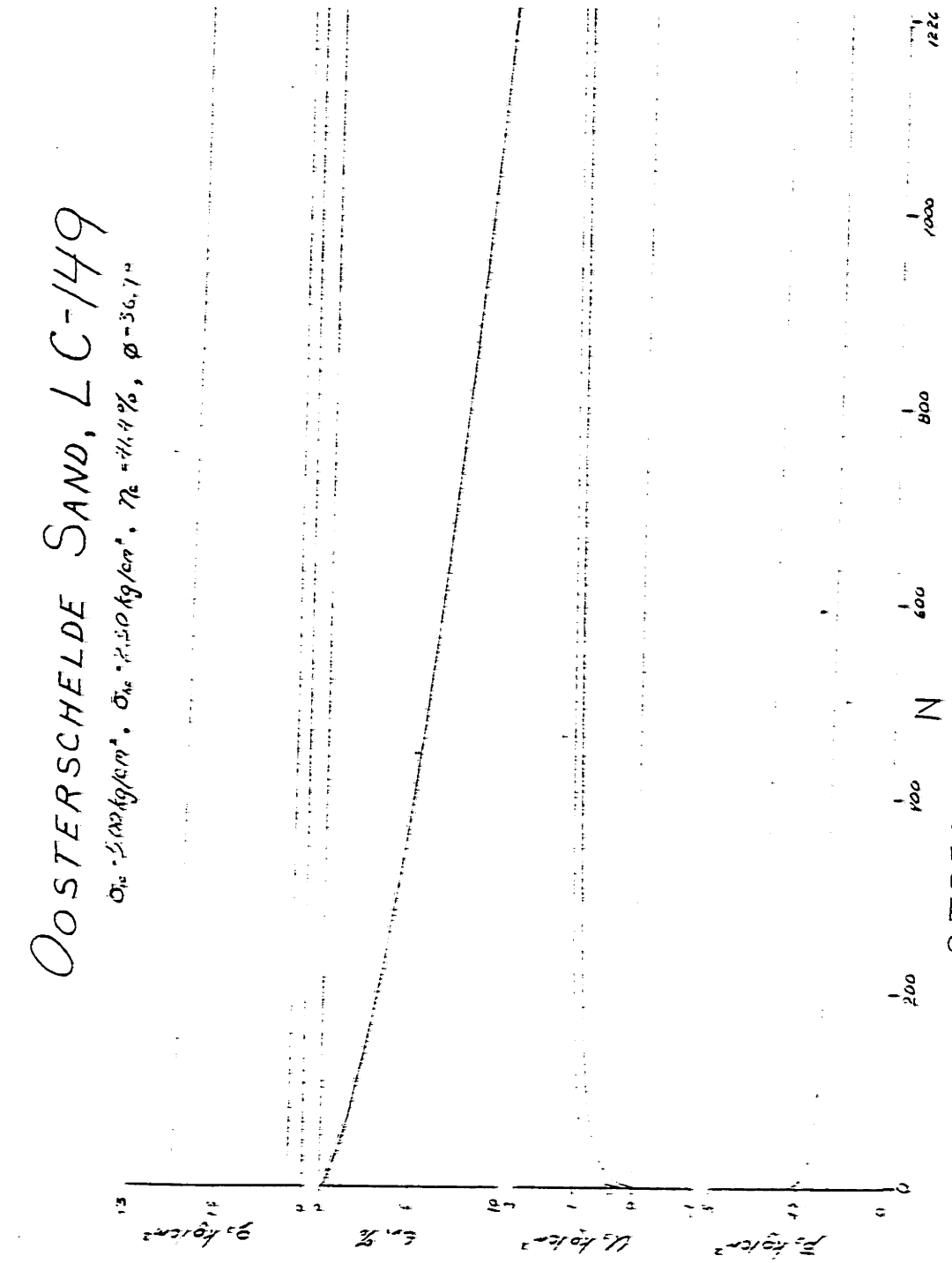
OOSTERSCHELDE SAND, LC-149
STRESS, STRAIN and PORE PRESSURE
N
200
100
600
800
1000
1226

FIGURE F-60

OOSTERSCHELDE SAND, LC-151

$\bar{\sigma}_{1c} = 3.50\ kg/cm^2$, $\bar{\sigma}_{3c} = 2.50\ kg/cm^2$, $\eta_c = 41.4\ \%$, $\phi = 33.5°$

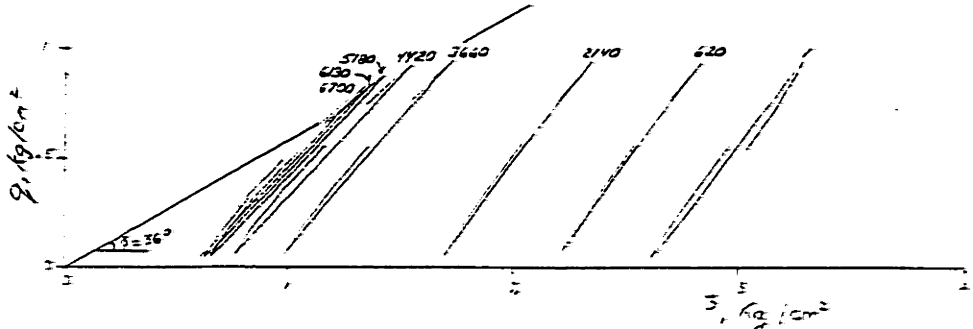

EFFECTIVE STRESS PATH

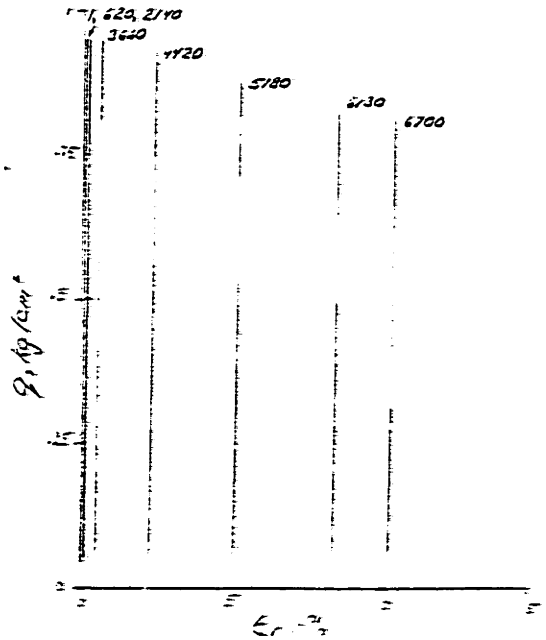

STRESS vs. STRAIN

FIGURE F-51

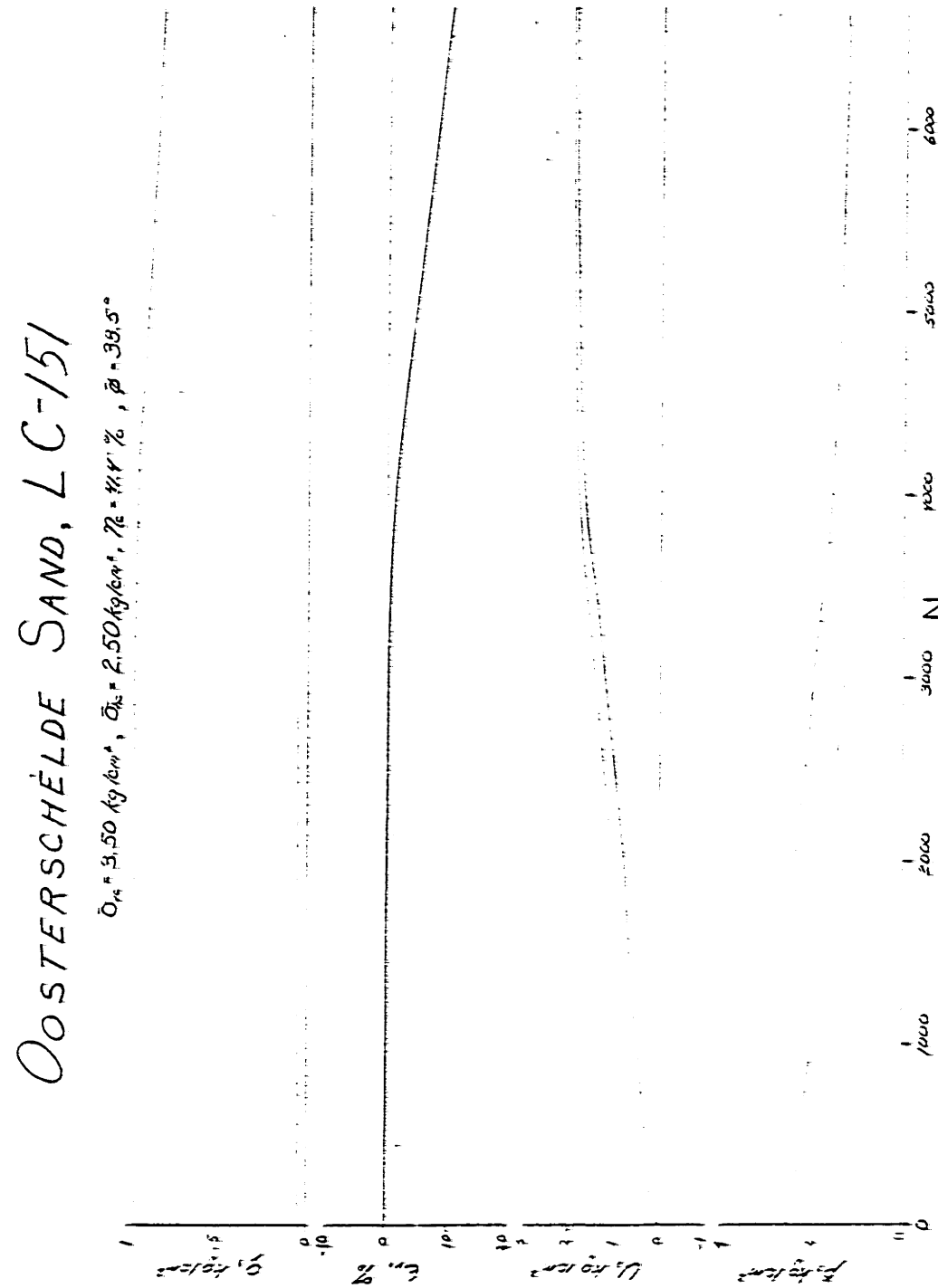
OOSTERSCHELDE SAND, LC-151
$\bar{\sigma}_{ri}$ = 3,50 kg/cm², $\bar{\sigma}_{hc}$ = 2,50 kg/cm², η_c = 44,4 %, $\bar{\phi}$ = 38,5°
STRESS, STRAIN and PORE PRESSURE
N
1000
2000
3000
4000
5000
6000
ε_1, %
u_c, kg/cm²
p_c, kg/cm²
q_c, kg/cm²

FIGURE E-62

OOSTERSCHELDE SAND, LC-152

$\bar{\sigma}_{1c} = 3.00$ kg/cm², $\bar{\sigma}_{3c} = 1.50$ kg/cm², $\eta_c = 44.4$ %, $\bar{\phi} = 32.7°$

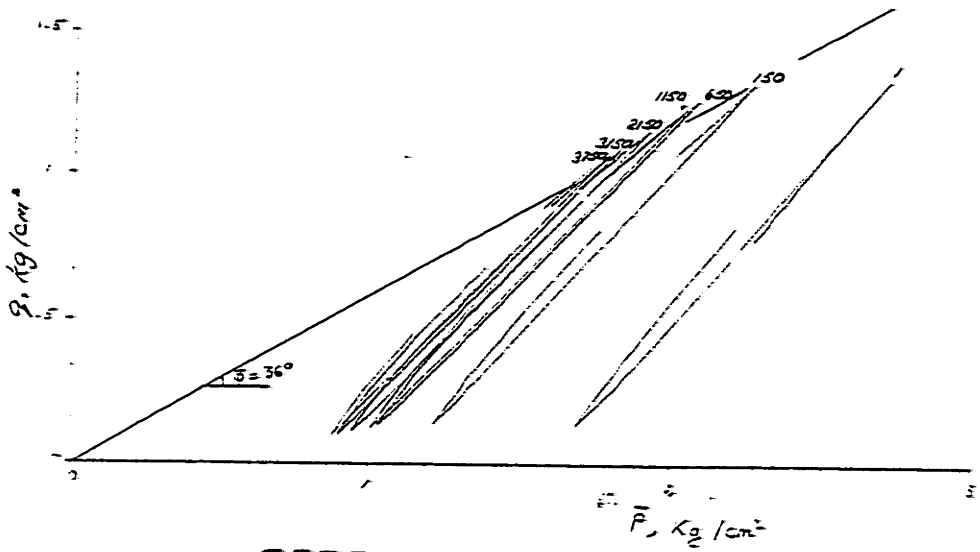

EFFECTIVE STRESS PATH

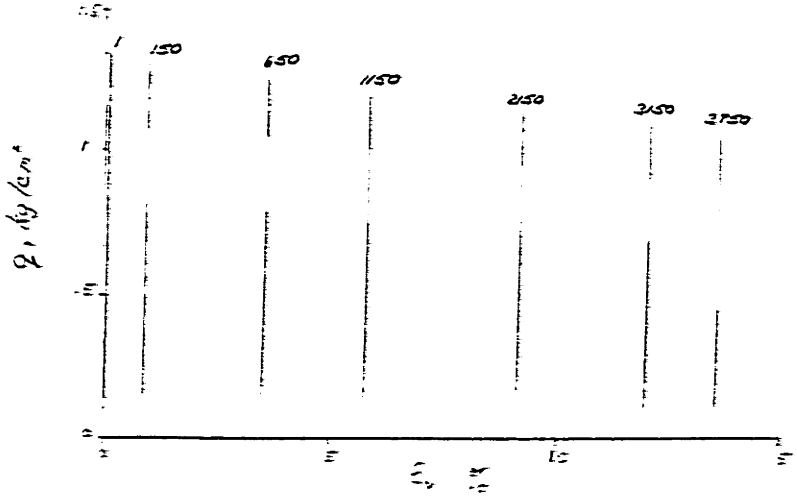

STRESS vs. STRAIN

FIGURE F-63

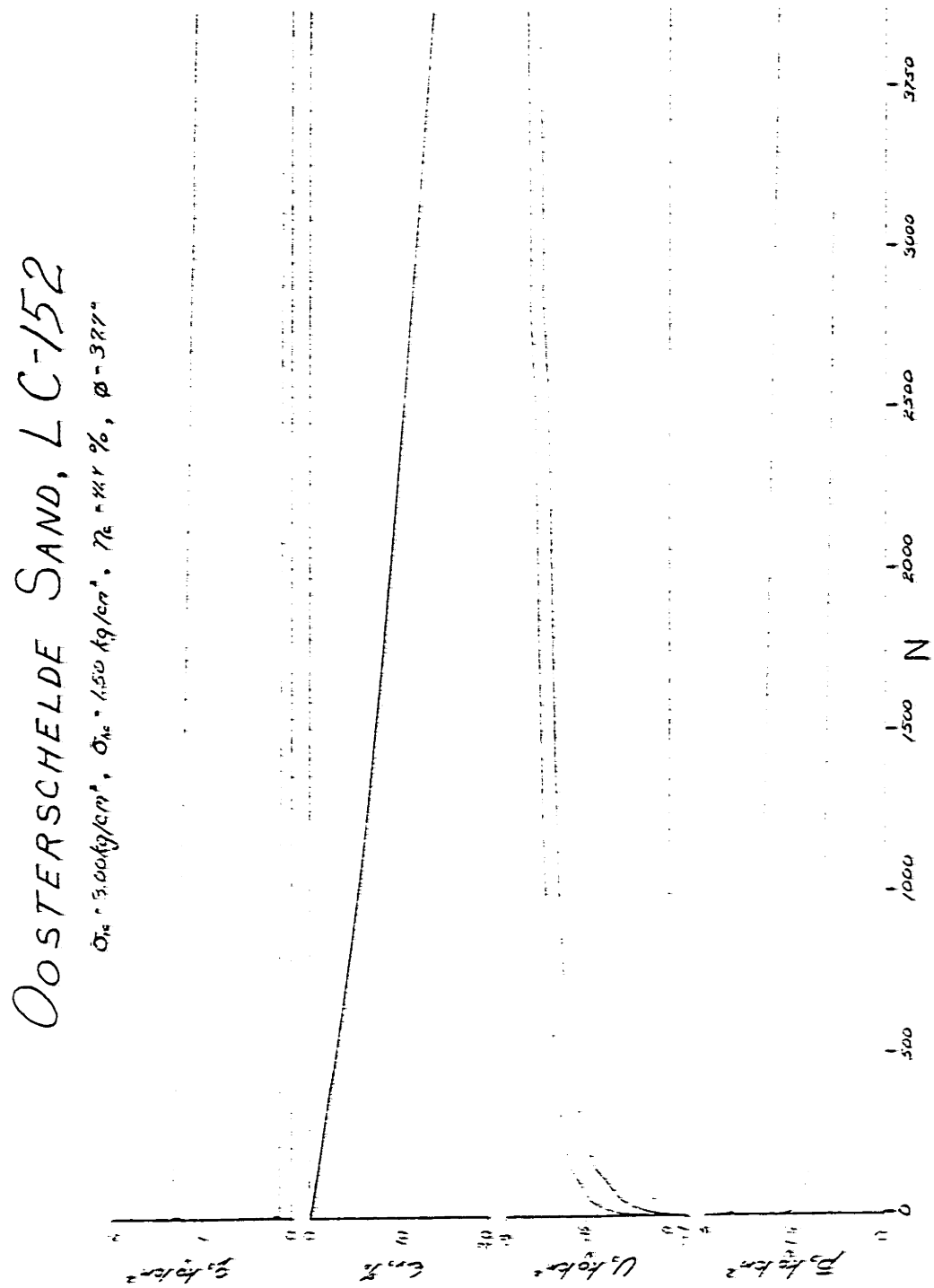
OOSTERSCHELDE SAND, LC-152
σ3c = 3.00 kg/cm², σ1c = 1.50 kg/cm², nc = xx %, ø = 37°
STRESS, STRAIN and PORE PRESSURE
N
500
1000
1500
2000
2500
3000
3750
0

FIGURE F-67

OOSTERSCHELDE SAND, LC-154

$\bar{\sigma}_{1c} = 3.00\ kg/cm^2$, $\bar{\sigma}_{3c} = 2.50\ kg/cm^2$, $\eta_c = 1.20$, $\bar{\phi} = 29.3°$

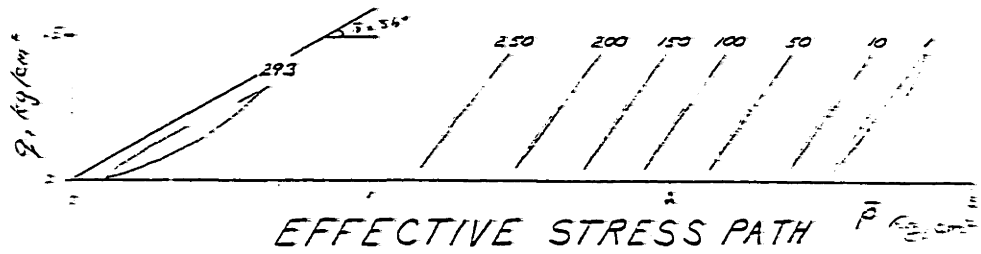

EFFECTIVE STRESS PATH

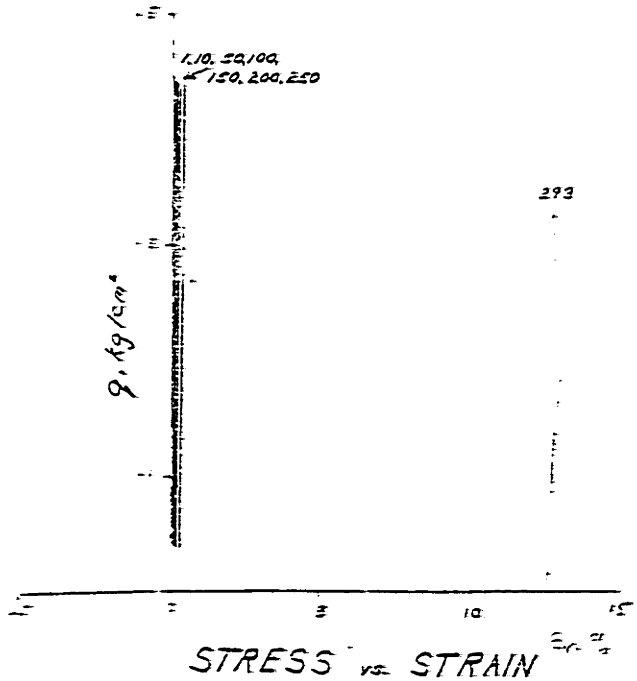

STRESS vs. STRAIN

FIGURE F-65

OOSTERSCHELDE SAND, LC-154

σ_{vc} = 3.00 kg/cm², σ_{hc} = 2.50 kg/cm², γ_d = 16.8 %, ϕ = 29.3°

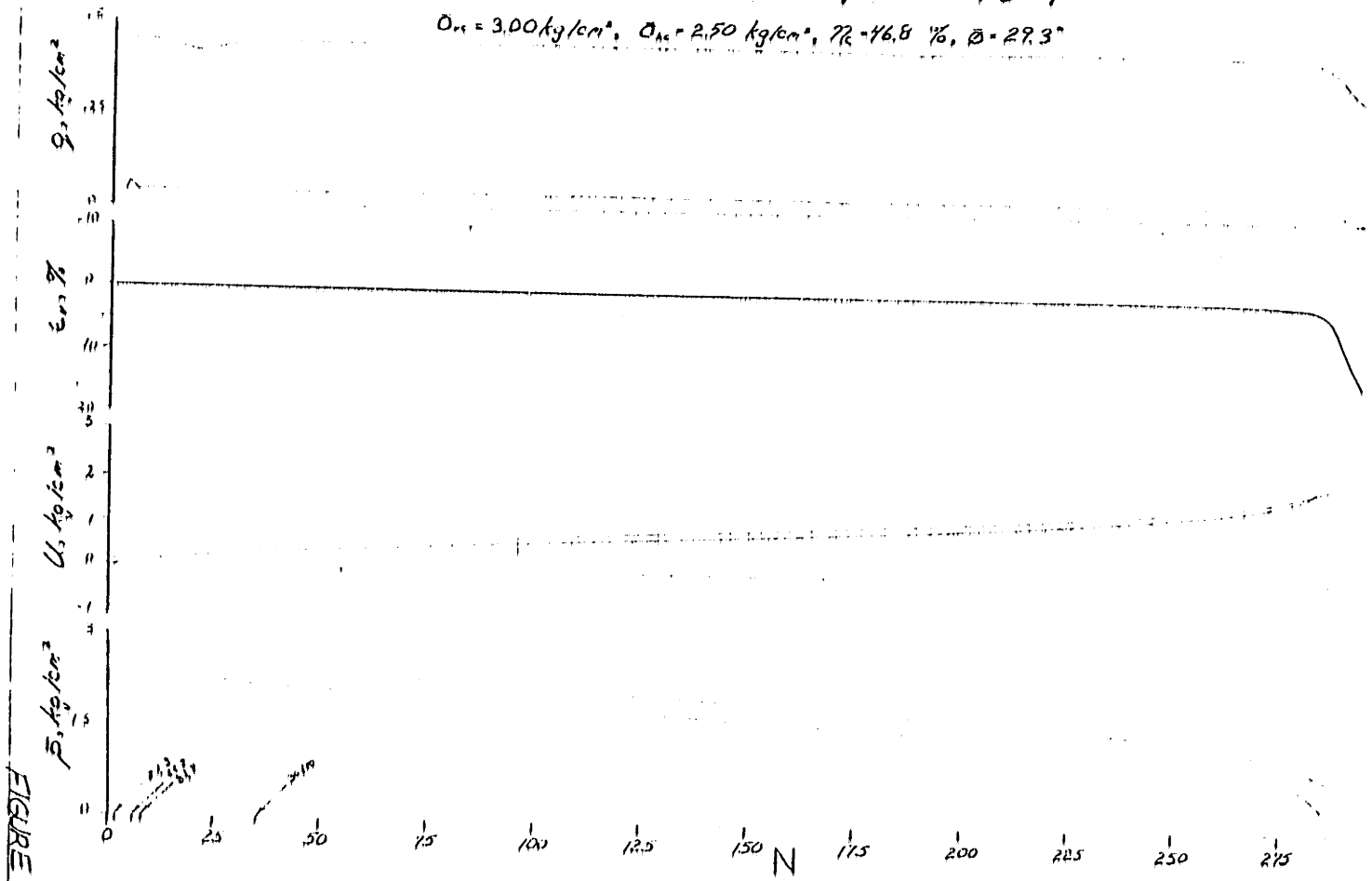

FIGURE F-156

STRESS, STRAIN and PORE PRESSURE

OOSTERSCHELDE SAND, LC-158

$\bar{\sigma}_{1c}$ = 7.00 kg/cm², $\bar{\sigma}_{3c}$ = 3.50 kg/cm², n_c = 41.5%, ϕ = 35.0°

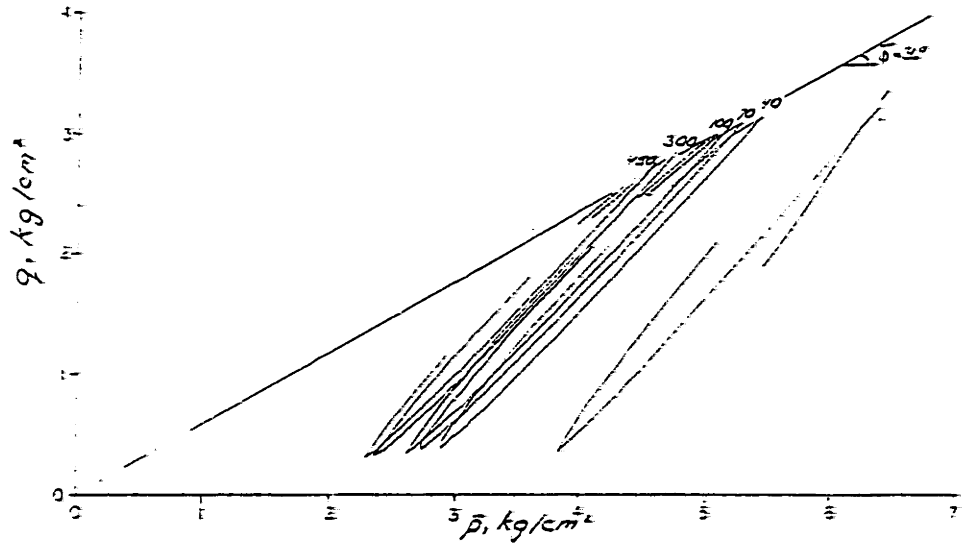

STRESS vs. STRAIN

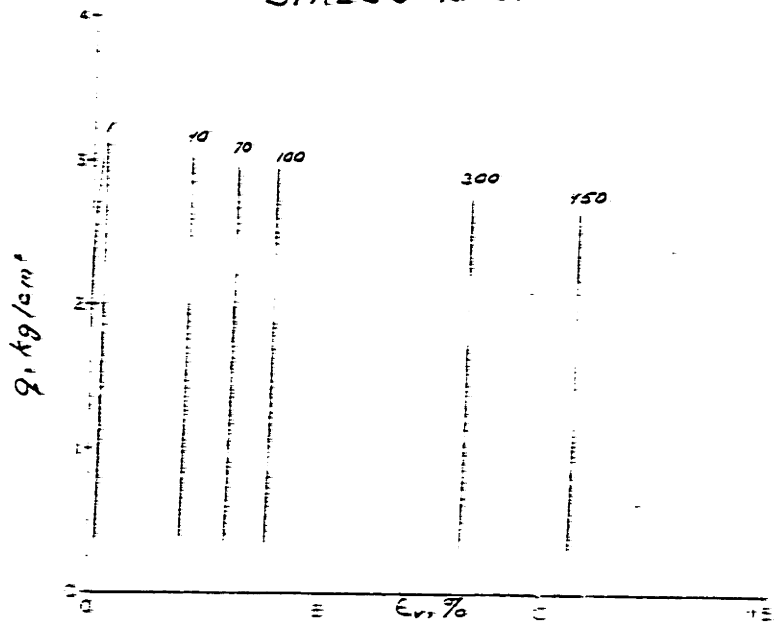

EFFECTIVE STRESS PATH

FIGURE E-67

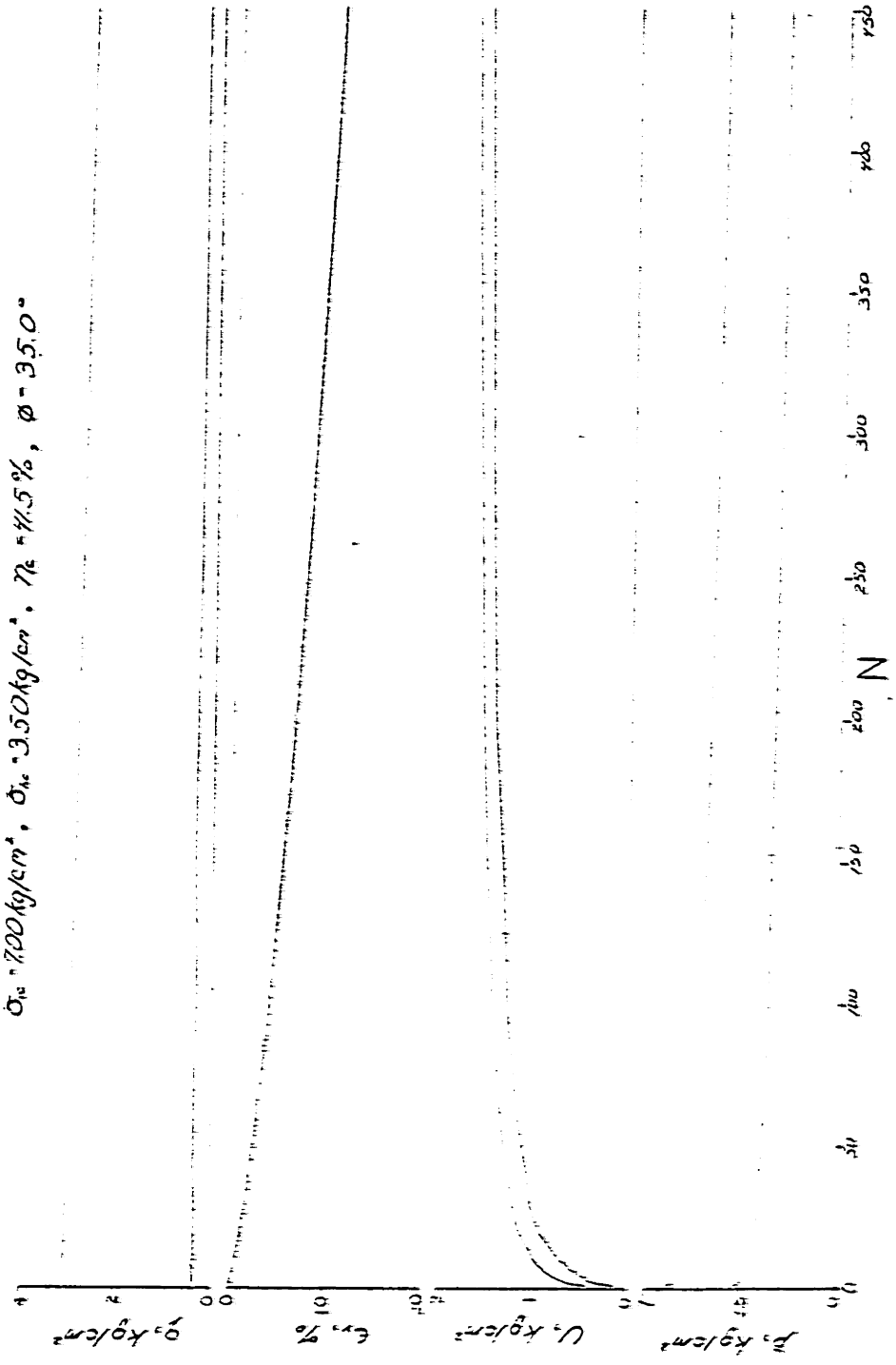
OOSTERSCHELDE SAND, LC-158
σ3c = 700 kg/cm², σ1c = 3.50 kg/cm², nc = 41.5%, φ = 35.0°
STRESS, STRAIN and PORE PRESSURE
N
p, kg/cm²
U, kg/cm²
εv, %
ρ, kg/cm²

FIGURE F-33

OOSTERSCHELDE SAND, LC-71

$\bar{\sigma}_{1c} = 1.00\ kg/cm^2$, $\bar{\sigma}_{3c} = 1.30\ kg/cm^2$, $n_c = 41.2\ \%$, $\phi = 41.9°$

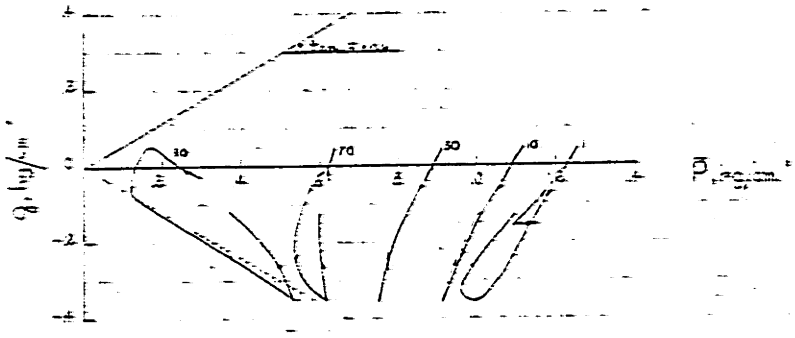

EFFECTIVE STRESS PATH

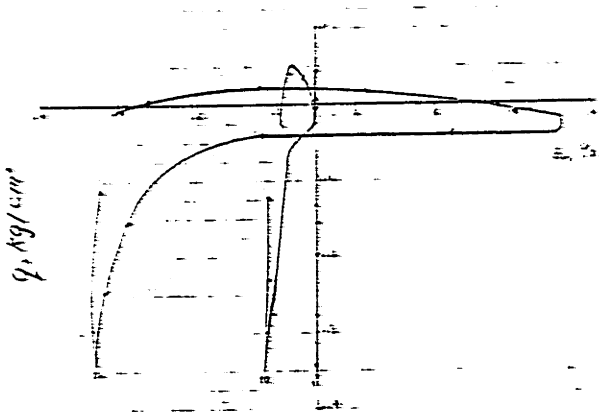

STRESS vs. STRAIN

FIGURE F-67

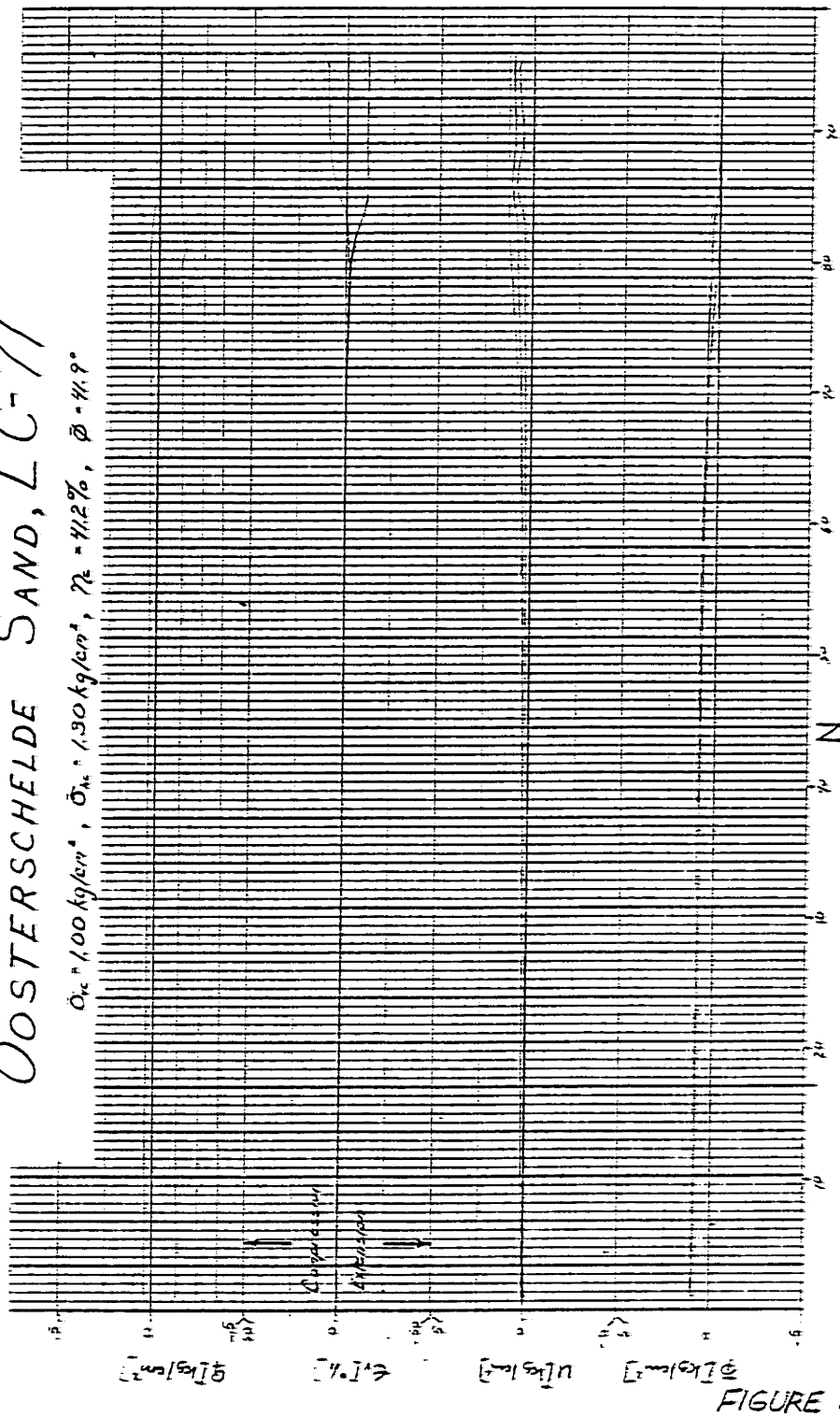

FIGURE F-70

OOSTERSCHELDE SAND, LC-116

$\bar{\sigma}_{hc}$ = 1.00 kg/cm², $\bar{\sigma}_{hc}$ = 1.50 kg/cm², n_c = 40.0 %, $\bar{\phi}$ = 38.5°

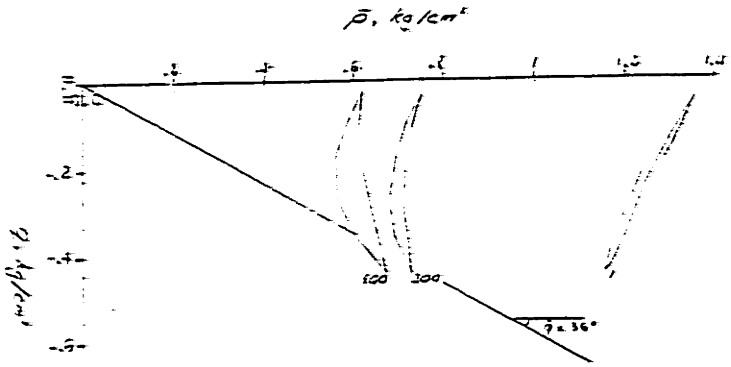

EFFECTIVE STRESS PATH

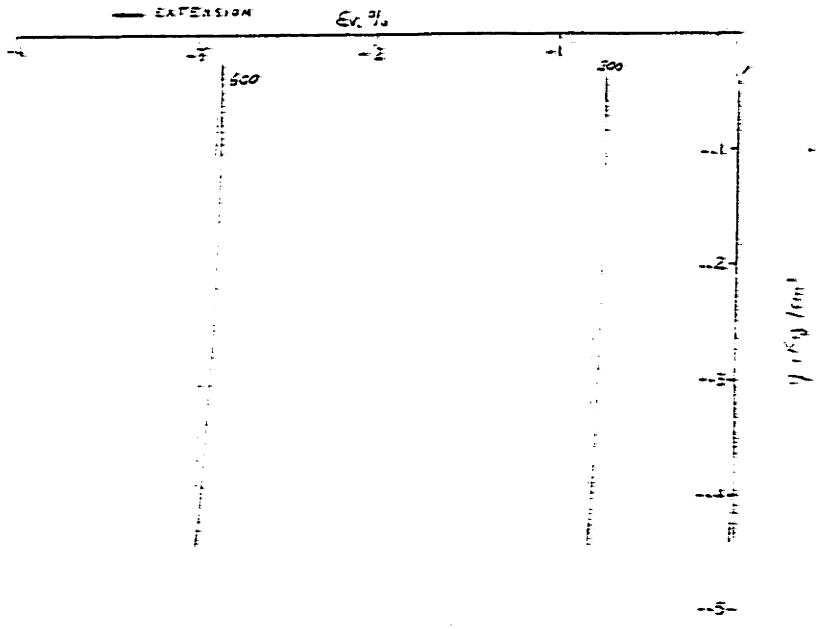

STRESS vs. STRAIN

FIGURE F-71

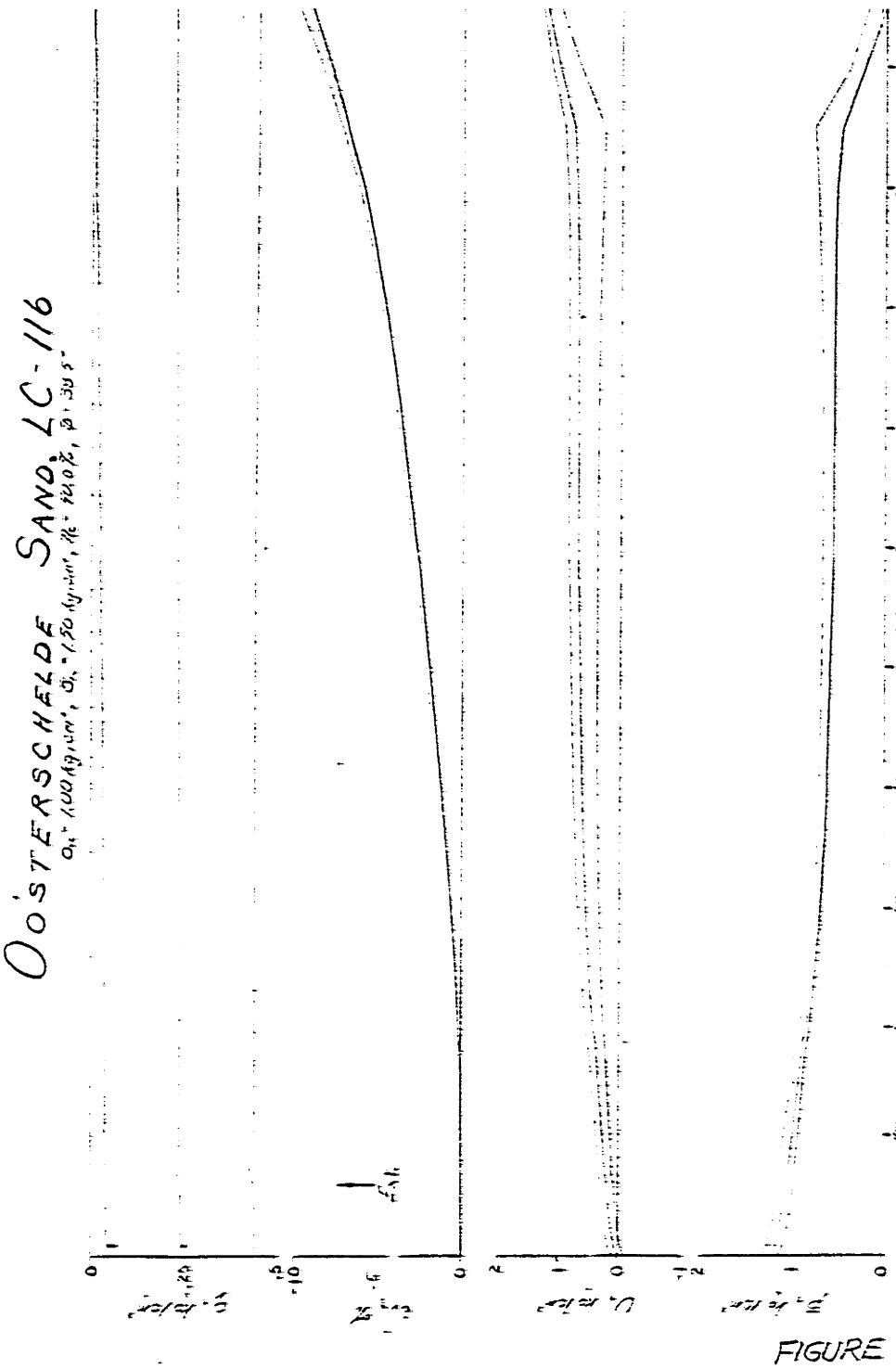
OOSTERSCHELDE SAND, LC-116
STRESS, STRAIN and PORE PRESSURE
N

FIGURE F-72

OOSTERSCHELDE SAND, LC-136

σ_{3c} = 3.00 kg/cm², $\bar{\sigma}_{vc}$ = 4.59 kg/cm², γ_d = 99.9 %, $\bar{\sigma}$ = 37.2°

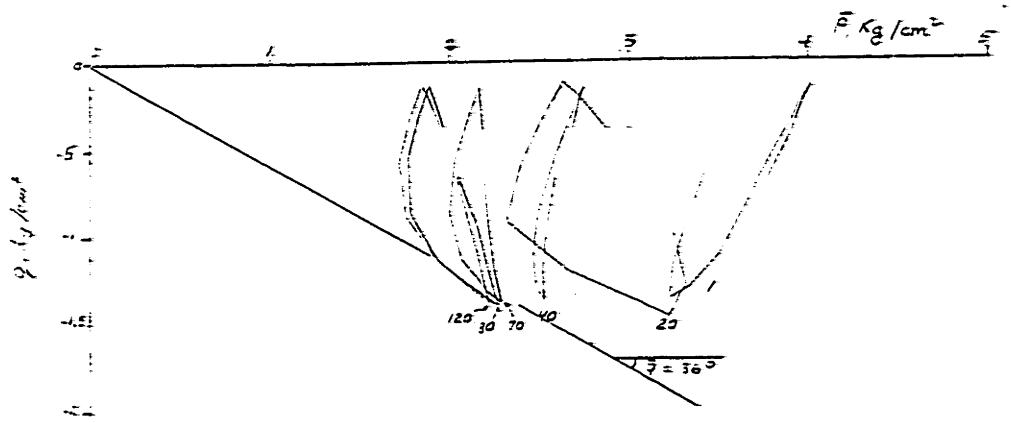

EFFECTIVE STRESS PATH

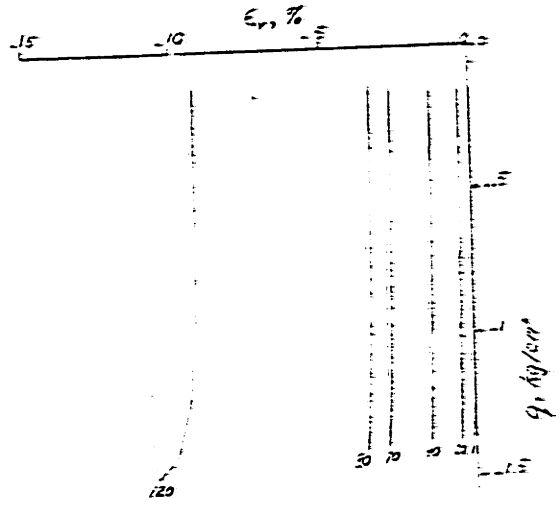

STRESS vs. STRAIN

FIGURE F-73

OOSTERSCHELDE SAND, LC-136

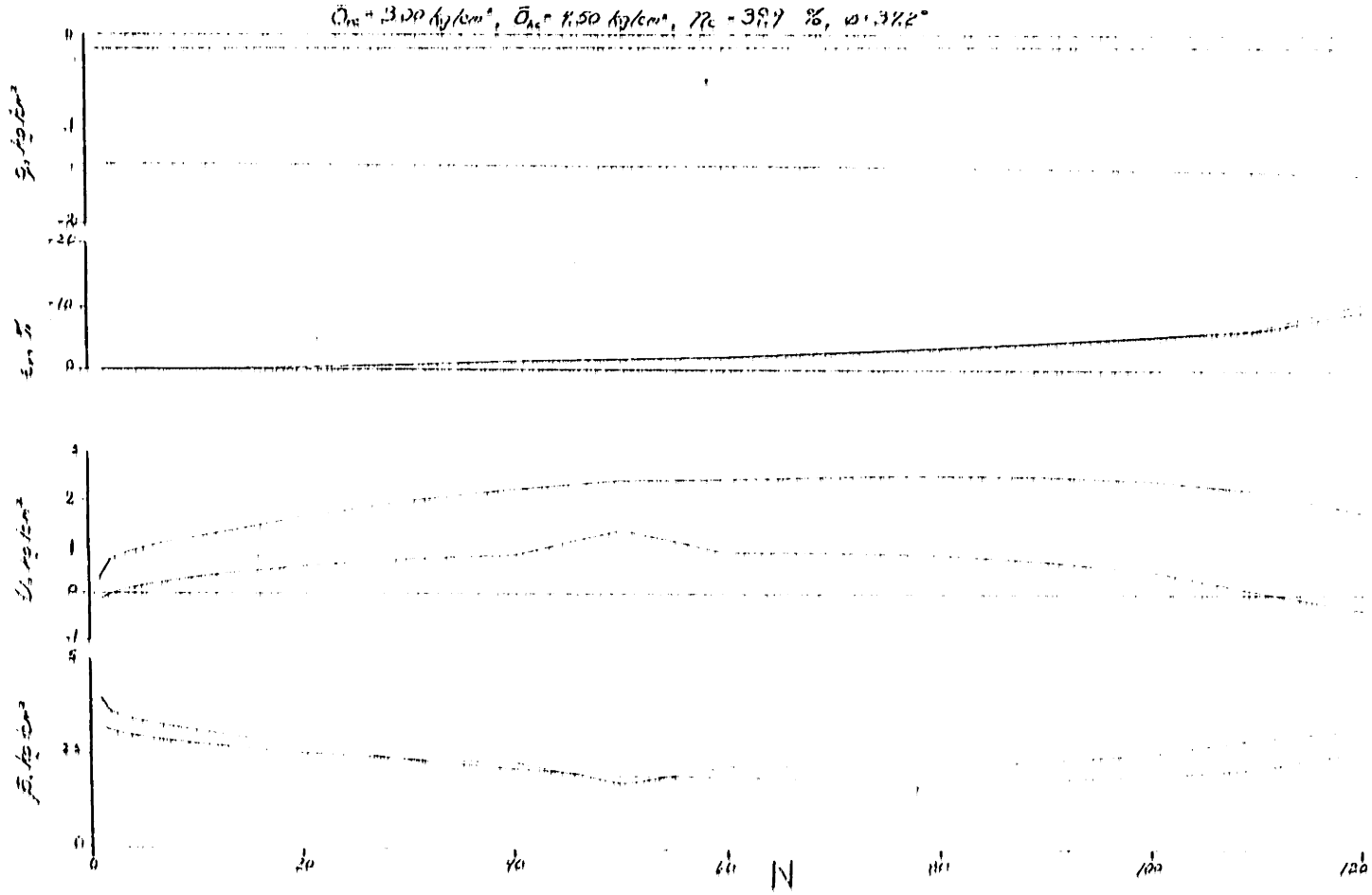

FIGURE F-74

OOSTERSCHELDE SAND, LC-145

$\bar{\sigma}_{3c} = 2.00\ kg/cm^2$, $\bar{\sigma}_{3c} = 3.00\ kg/cm^2$, $\eta_c = 41.1\ \%$, $\phi = 36.6°$

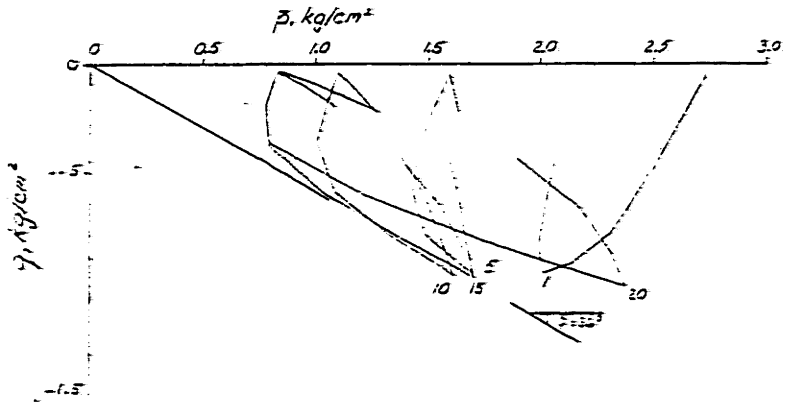

EFFECTIVE STRESS PATH

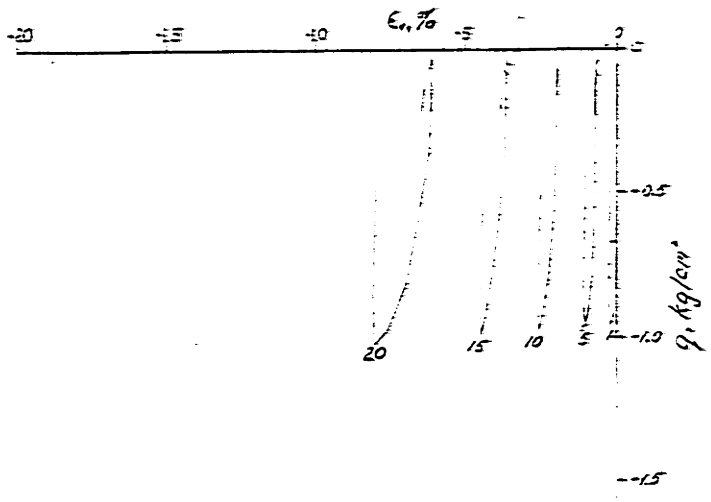

STRESS vs. STRAIN

FIGURE F-75

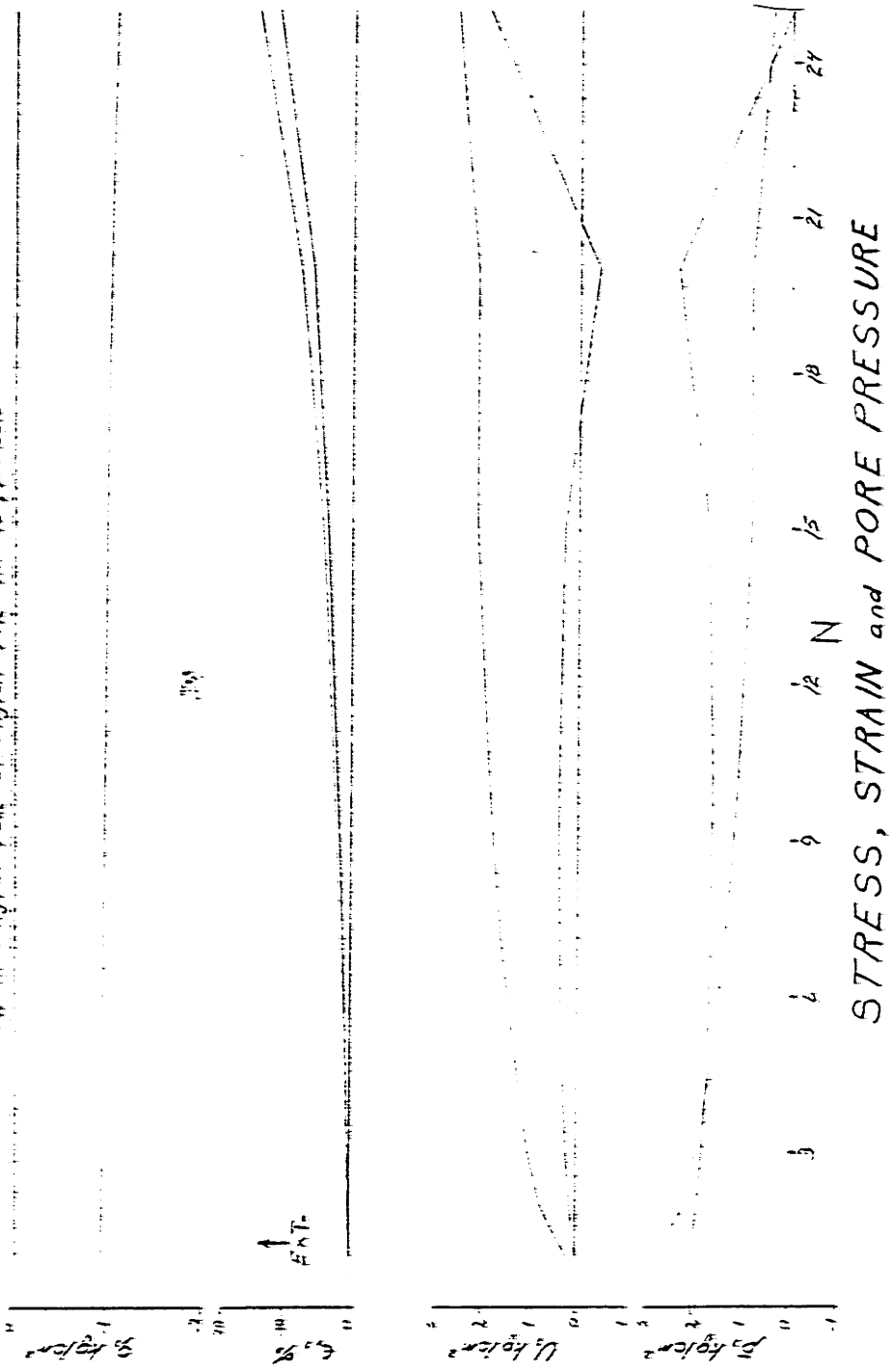
OOSTERSCHELDE SAND, LC-145
σ3 = 2,00 kg/cm², σ1c = 3,00 kg/cm², Dr = 111 %, φ = 36,5°
STRESS, STRAIN and PORE PRESSURE
N

FIGURE F-76

OOSTERSCHELDE SAND, LC-147

$\bar{\sigma}_{1c} = 3.00\ kg/cm^2$, $\bar{\sigma}_{3c} = 1.50\ kg/cm^2$, $\eta_c = 40.0\%$, $\phi = 37.3°$

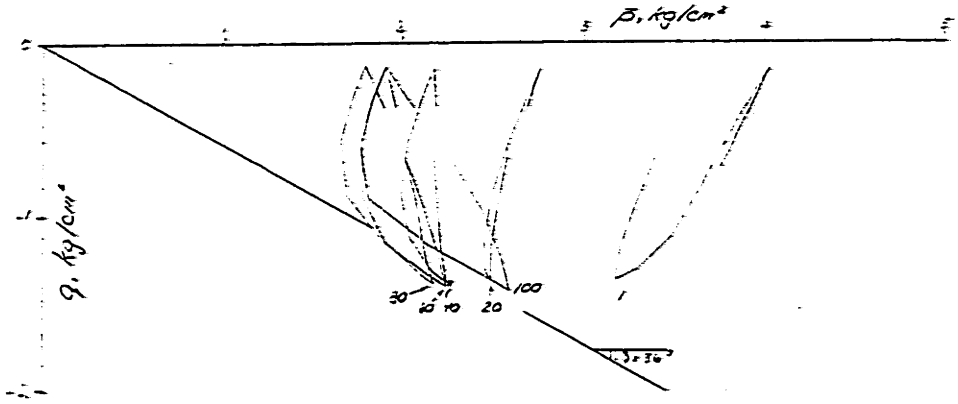

EFFECTIVE STRESS PATH

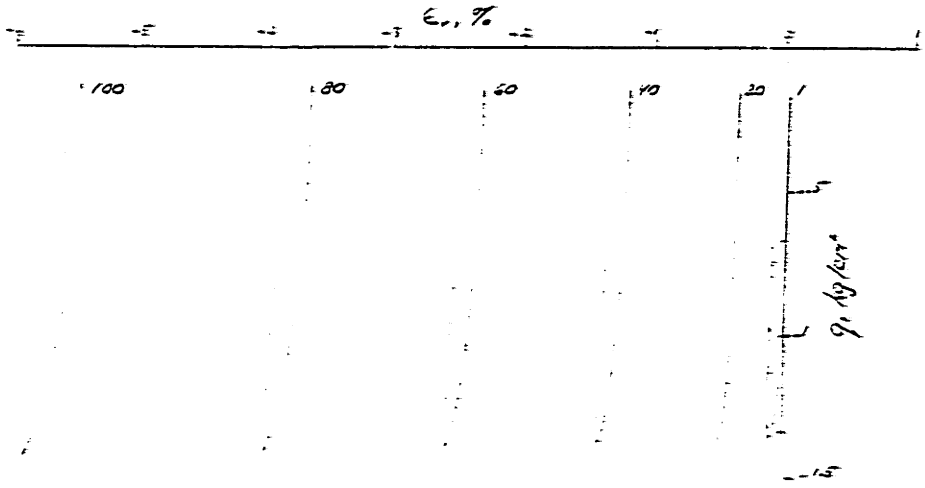

STRESS vs. STRAIN

FIGURE F-77

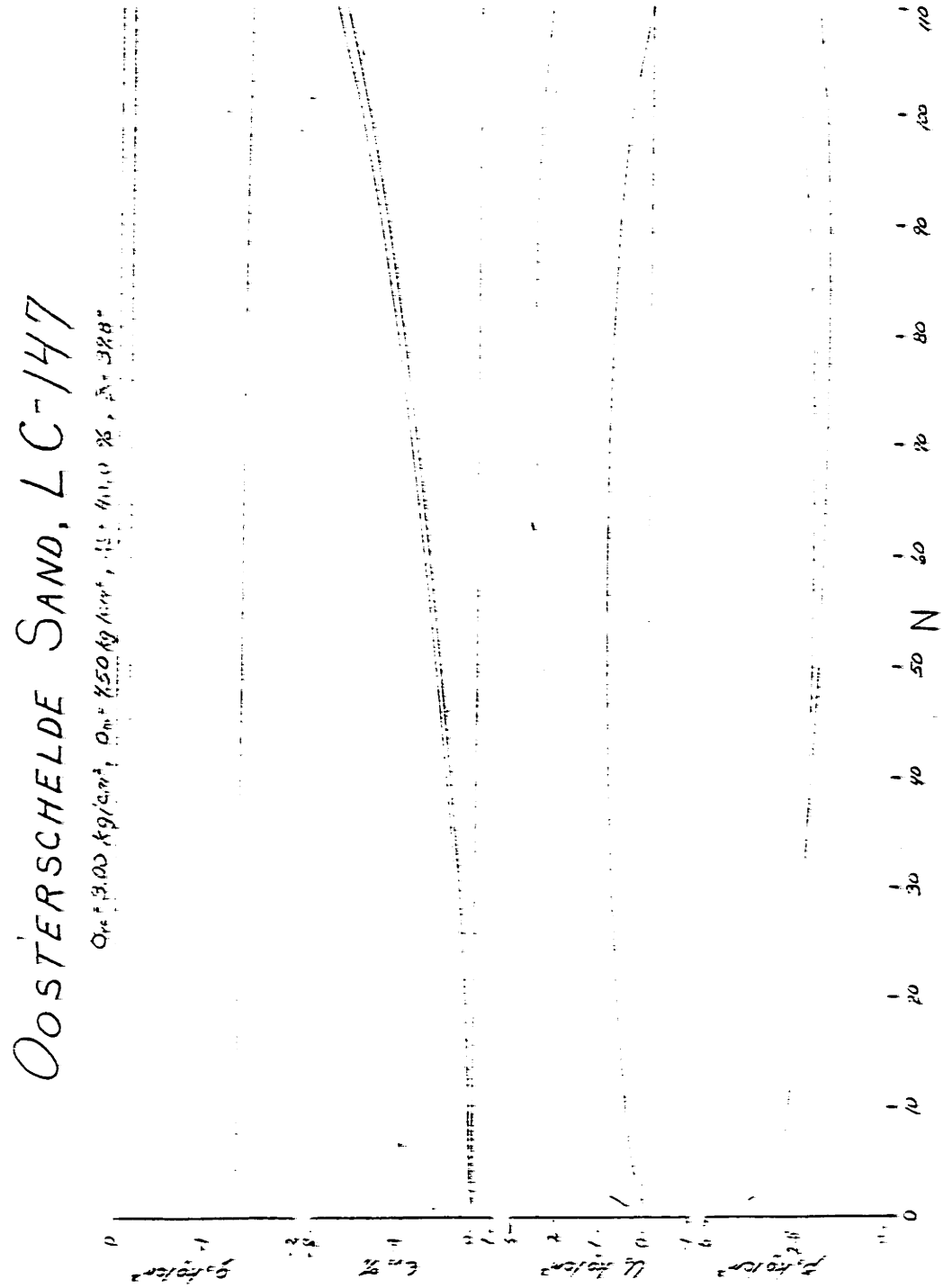
OOSTERSCHELDE SAND, LC-147
STRESS, STRAIN and PORE PRESSURE
N

FIGURE F-73

OOSTERSCHELDE SAND, LC-91

$\bar{\sigma}_{1c} = 2.50\ kg/cm^2$, $\bar{\sigma}_{3c} = 1.50\ kg/cm^2$, $\eta_c = 41.0\ \%$, $\bar{\phi} = 32.8°$

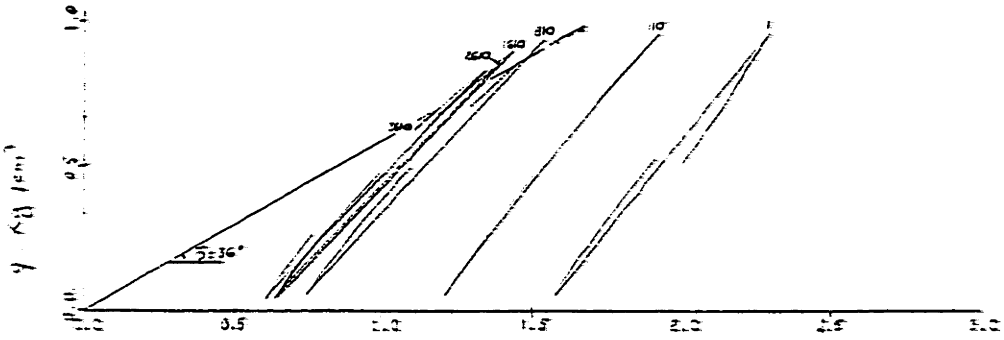

EFFECTIVE STRESS PATH

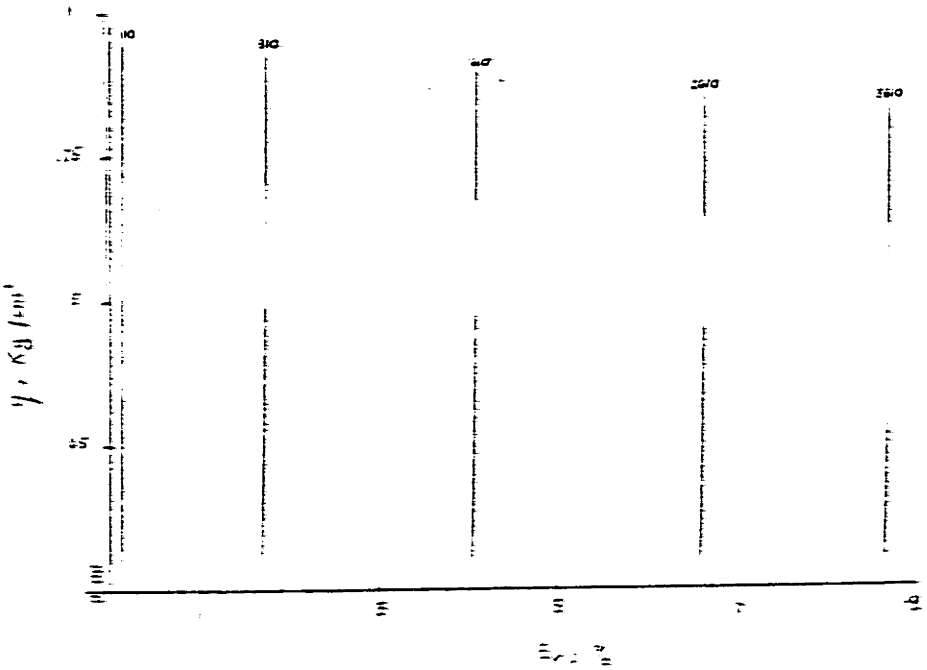

STRESS vs. STRAIN

FIGURE C-79

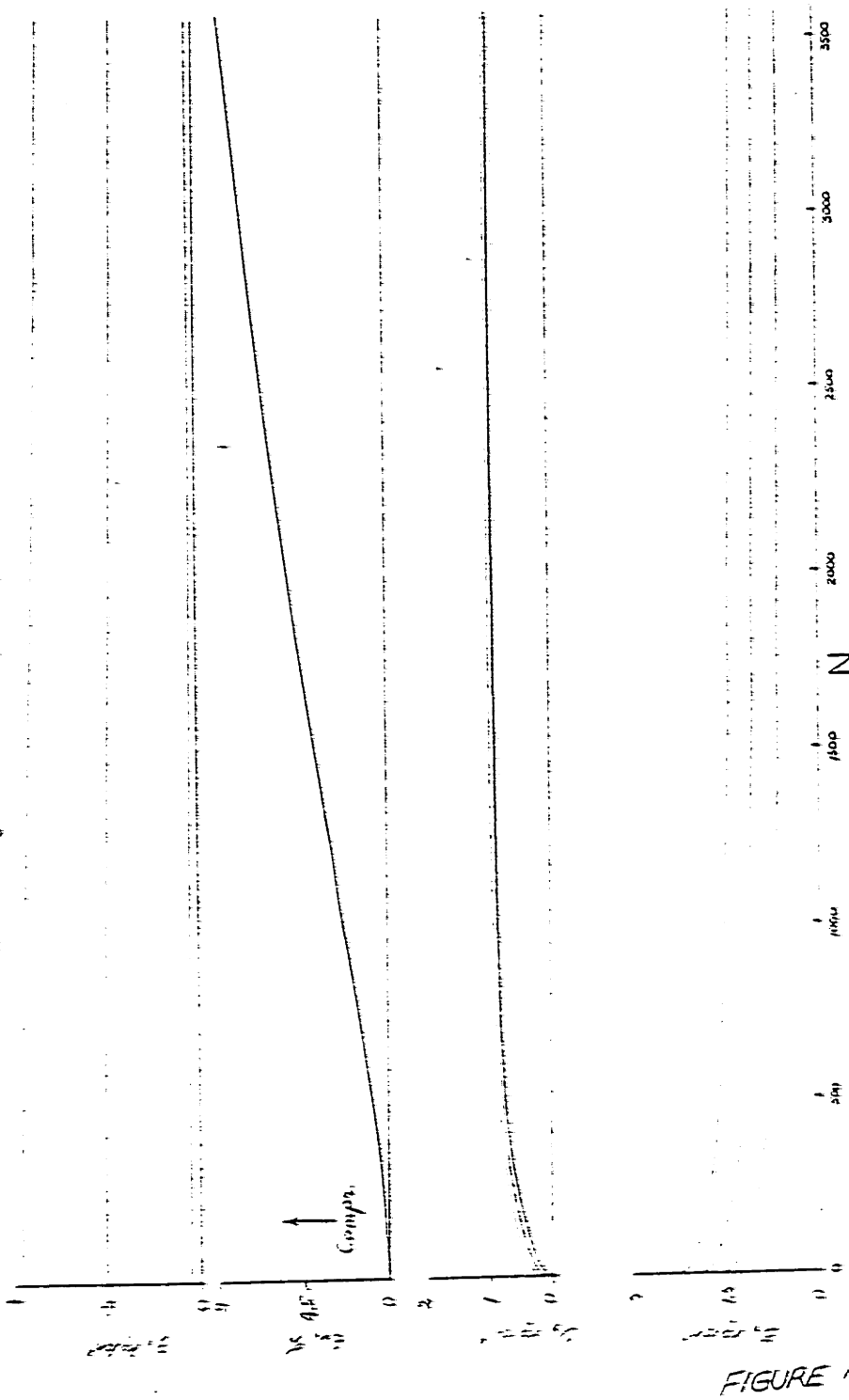

FIGURE F-30

OOSTERSCHELDE SAND, LC-93

$\bar{\sigma}_{hc}$ = 2.50 kg/cm², $\bar{\sigma}_{hc}$ = 1.50 kg/cm², n_c = 45.3%, ϕ = 31.8°

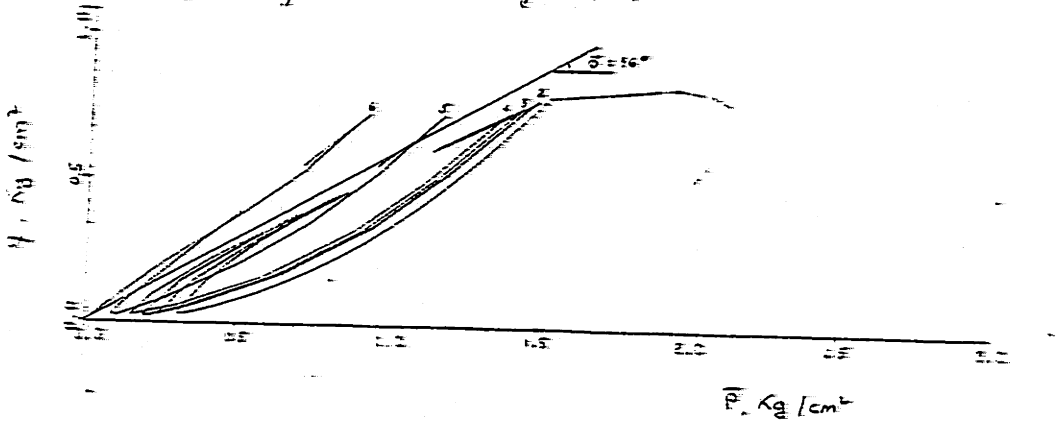

EFFECTIVE STRESS PATH

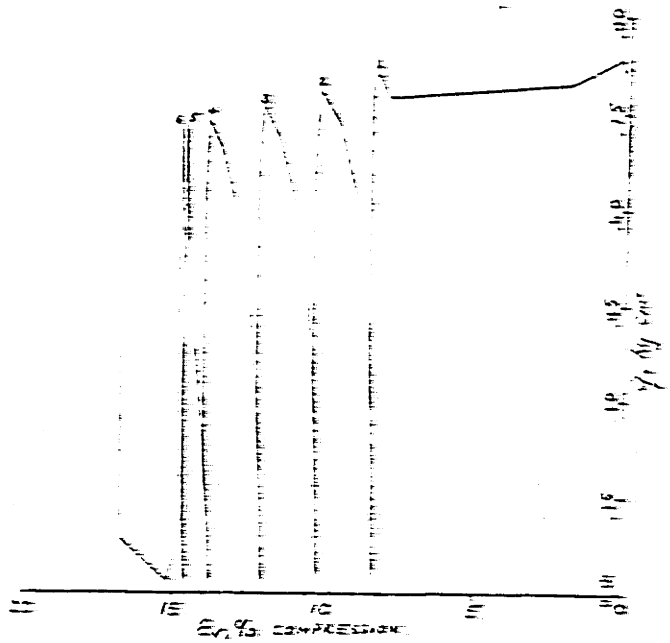

STRESS vs. STRAIN

FIGURE F-31

FIGURE F-82

OOSTERSCHELDE SAND, LC-94

$\bar{\sigma}_c = 2.50 kg/cm^2$, $\bar{\sigma}_{1c} = 1.50 kg/cm^2$, $\eta_c = 32.9\%$,

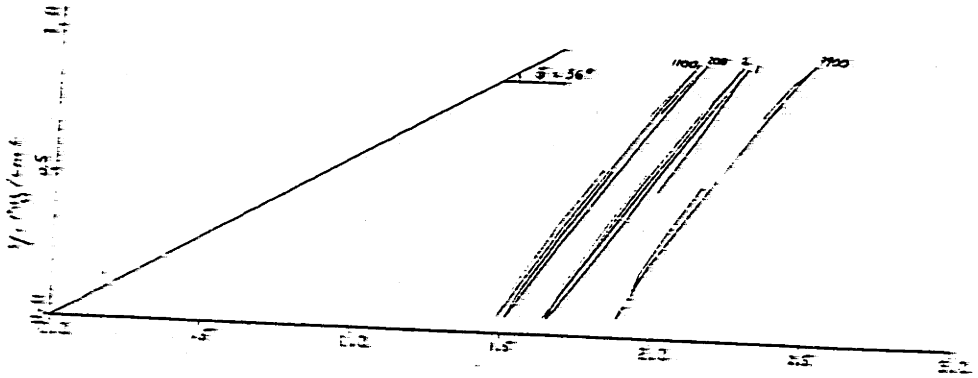

EFFECTIVE STRESS PATH

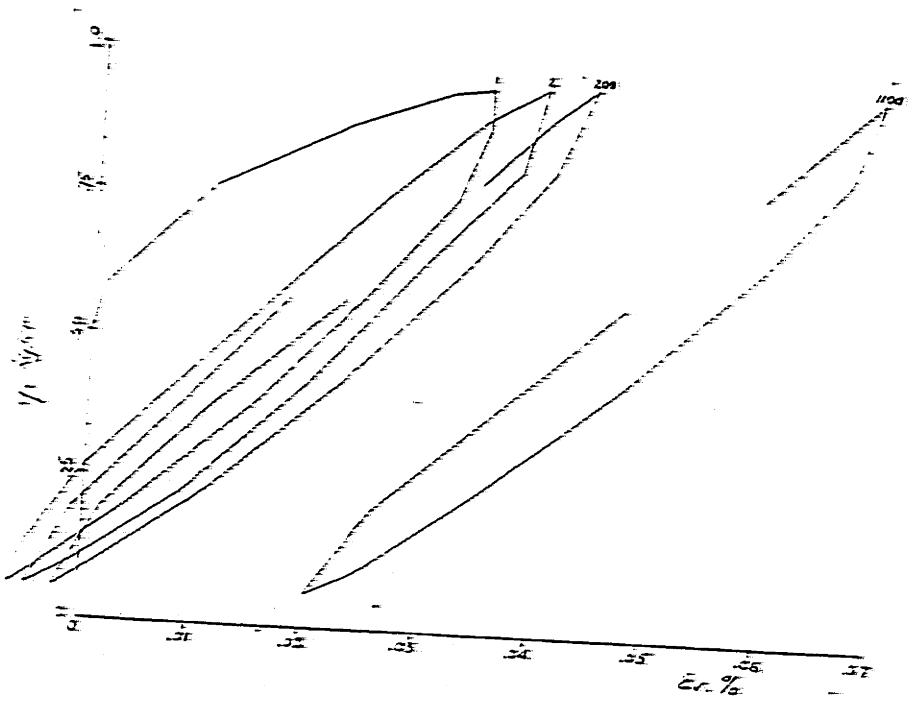

STRESS vs. STRAIN

FIGURE F-33

OOSTERSCHELDE SAND, LC-94

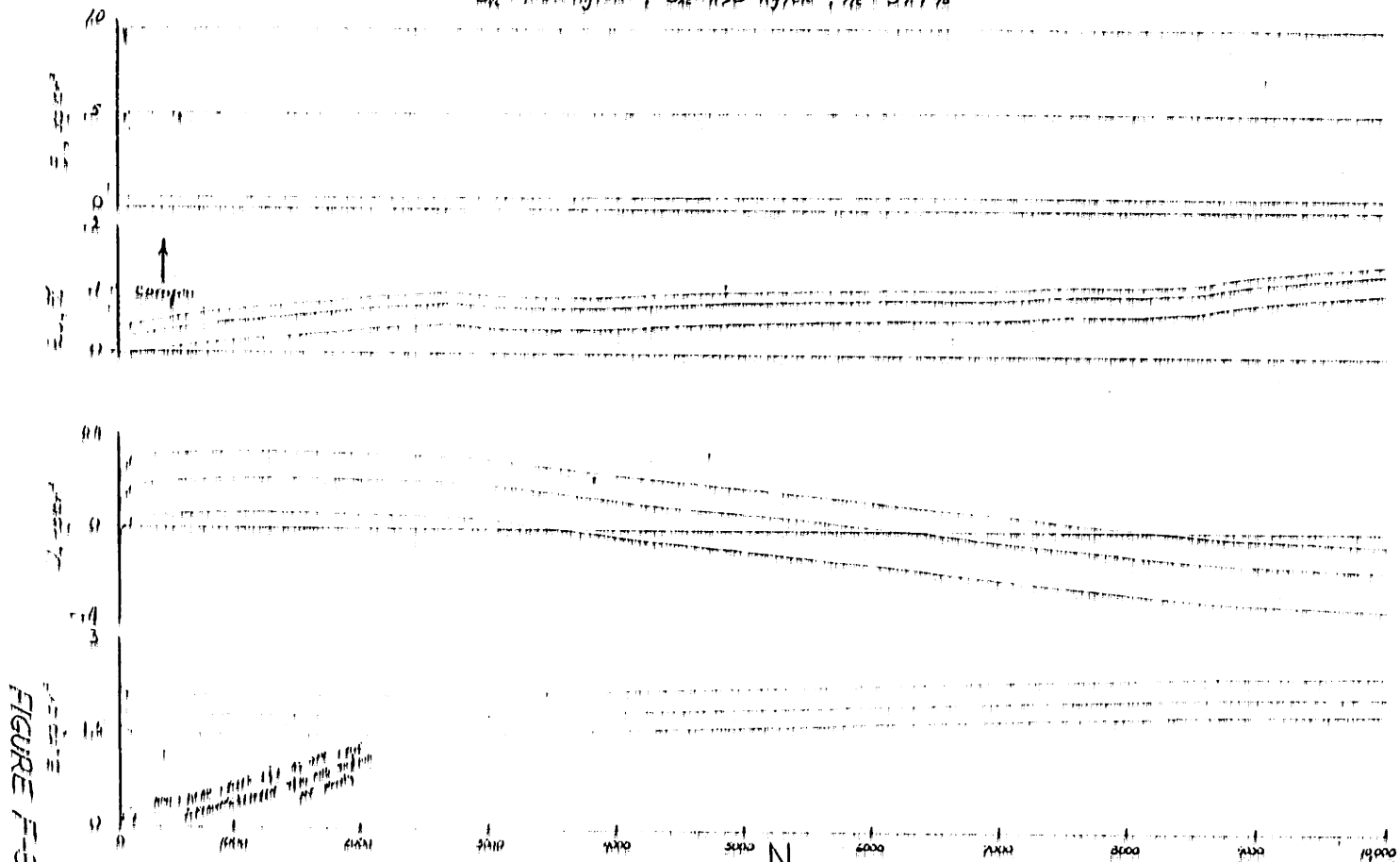

FIGURE F-24

STRESS STRAIN and PORE PRESSURE

OOSTERSCHELDE SAND, LC-95

$\sigma_{vc} = 3.00 kg/cm^2$, $\sigma_{hc} = 3.00 kg/cm^2$, $n_c = 37.9\%$

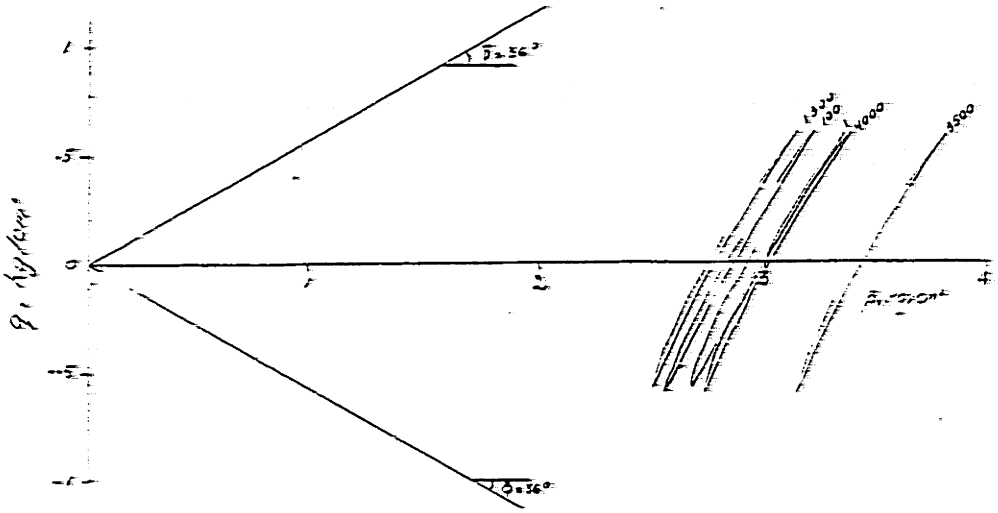

EFFECTIVE STRESS PATH

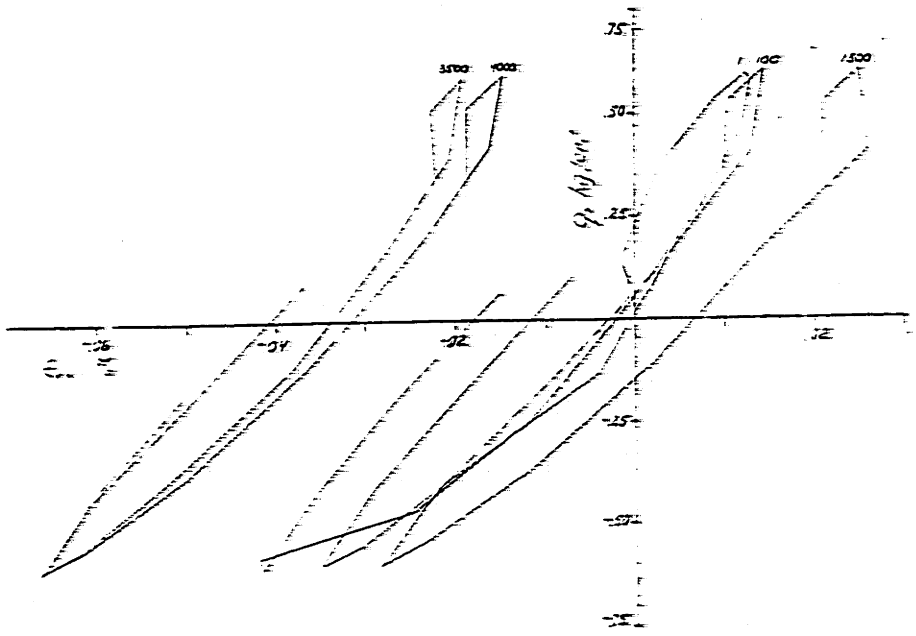

STRESS vs. STRAIN FIGURE F-85

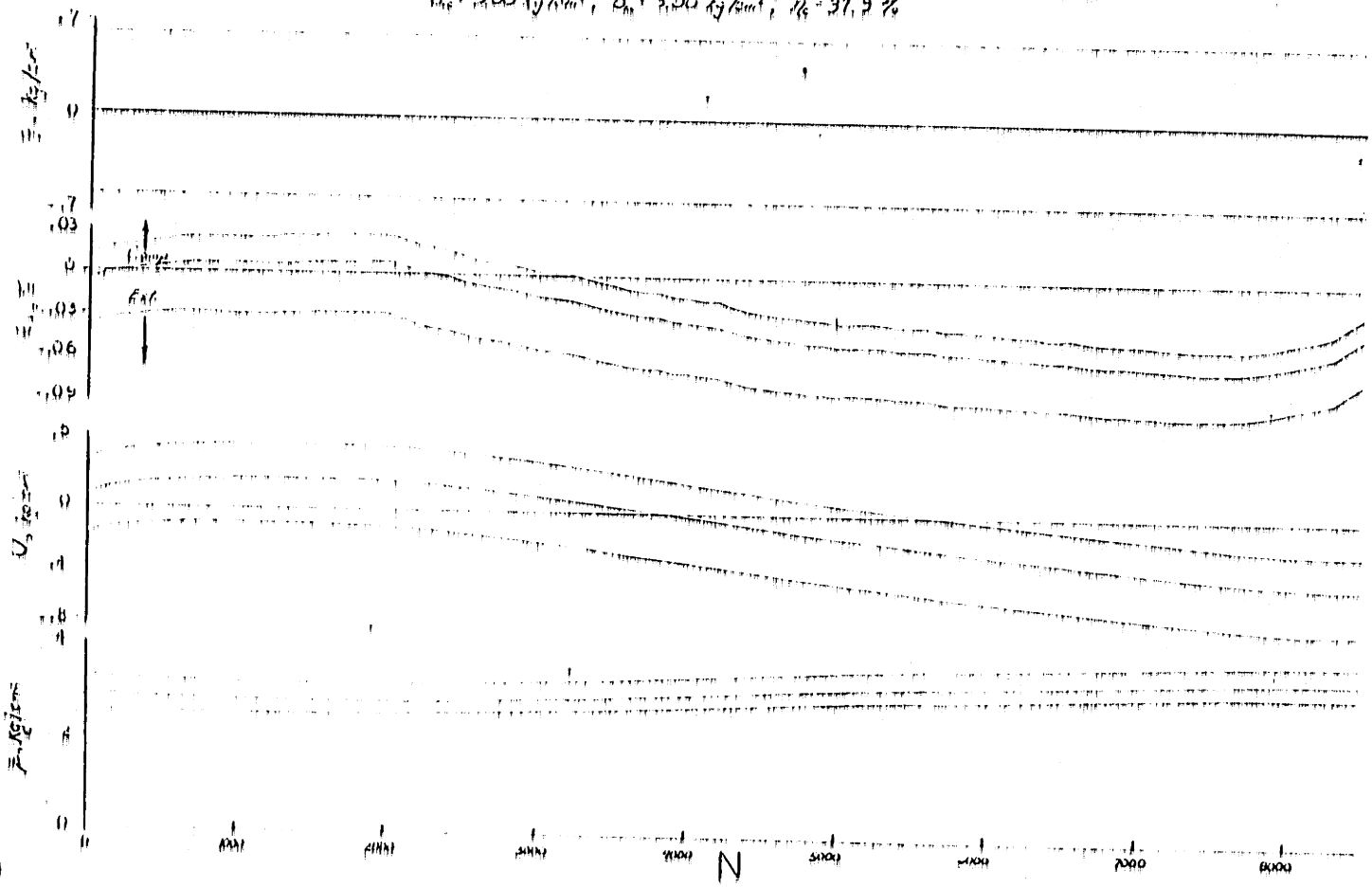

FIGURE E-83

STRESS, STRAIN and PORE PRESSURE

OOSTERSCHELDE SAND, LC-100

$\bar{\sigma}_{1c} = 5.00$ kg/cm², $\bar{\sigma}_{3c} = 5.00$ kg/cm², $n_c = 41.5\%$
RECONSOLIDATION AFTER 25 cycles to $n_{rc} = 41.3\%$ $\bar{\phi} = 42.2°$

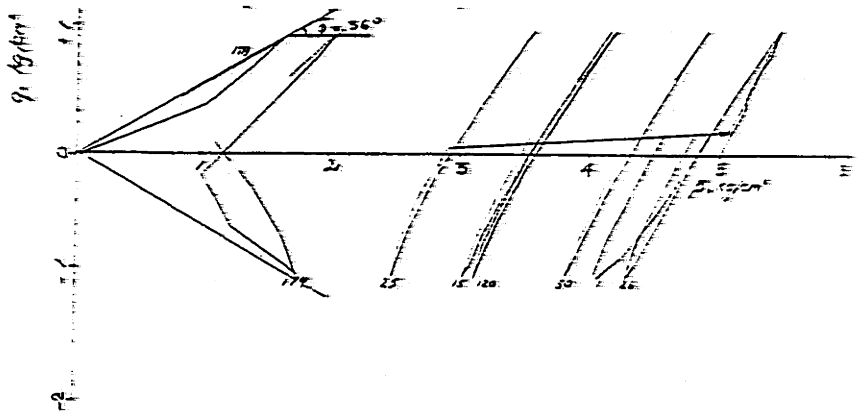

EFFECTIVE STRESS PATH

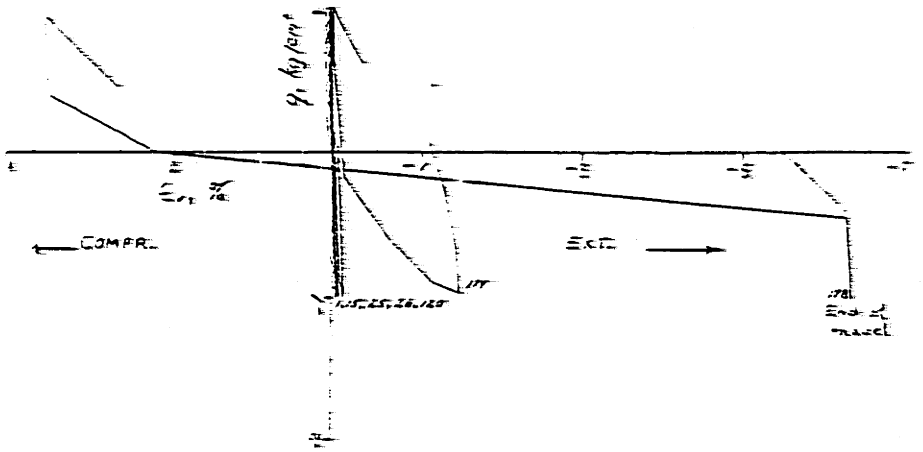

STRESS vs STRAIN

FIGURE F-57

OOSTERSCHELDE SAND, LC-100

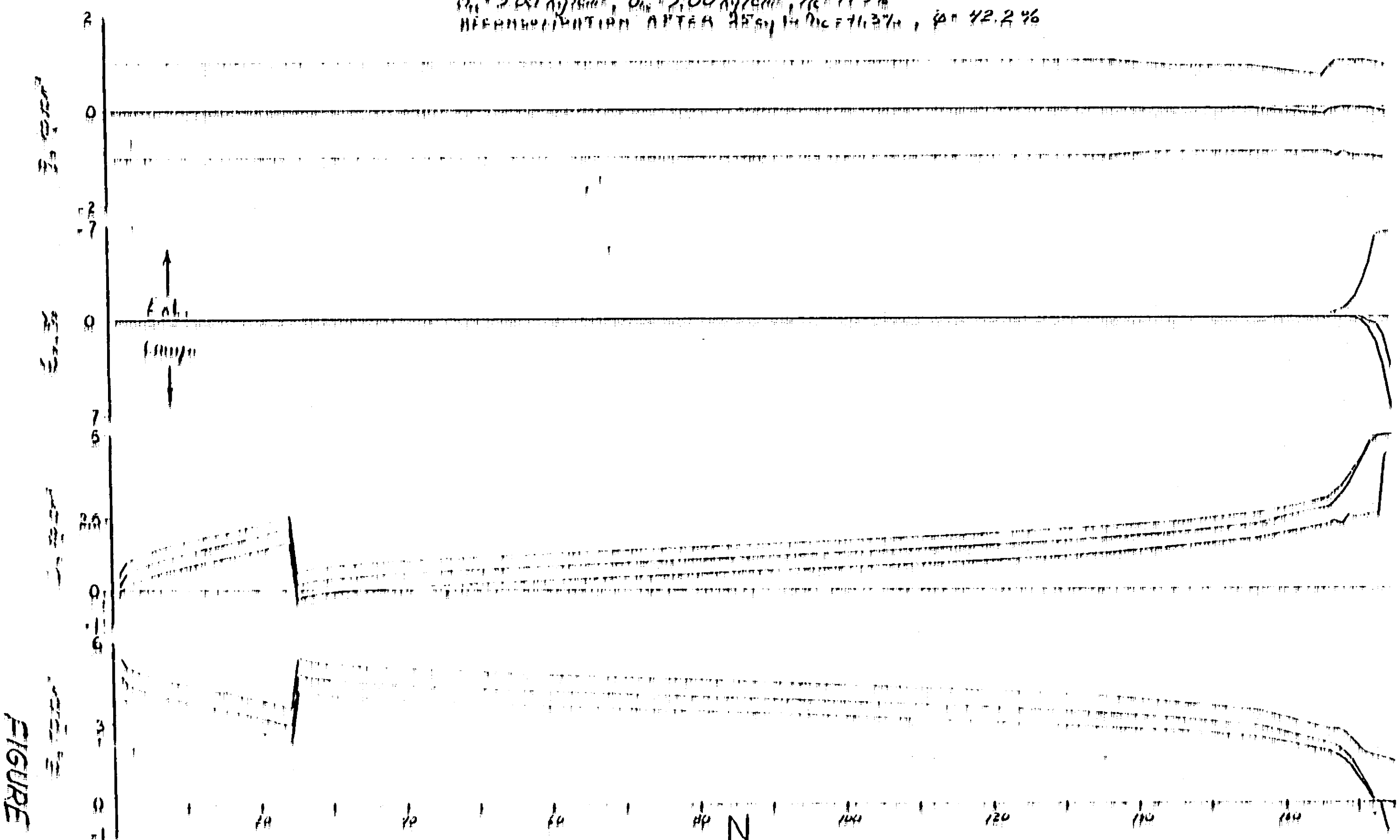

STRESS, STRAIN and PORE PRESSURE

FIGURE F-38

OOSTERSCHELDE SAND, LC-102

$\bar{\sigma}_{1c}$ = 1.00 kg/cm², $\bar{\sigma}_{3c}$ = 1.50 kg/cm², n_c = 32.8%, ϕ = 43.2°

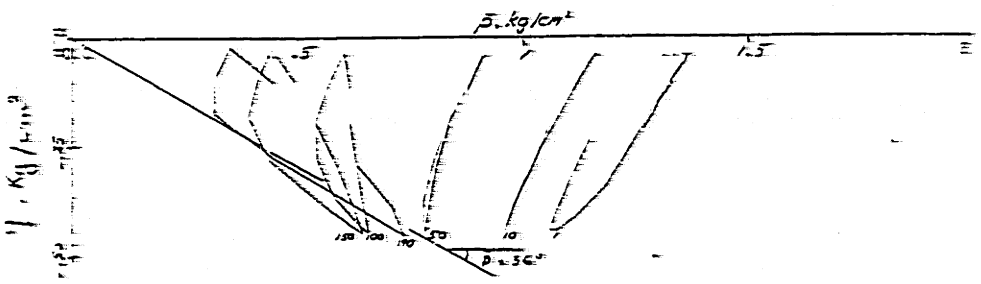

EFFECTIVE STRESS PATH

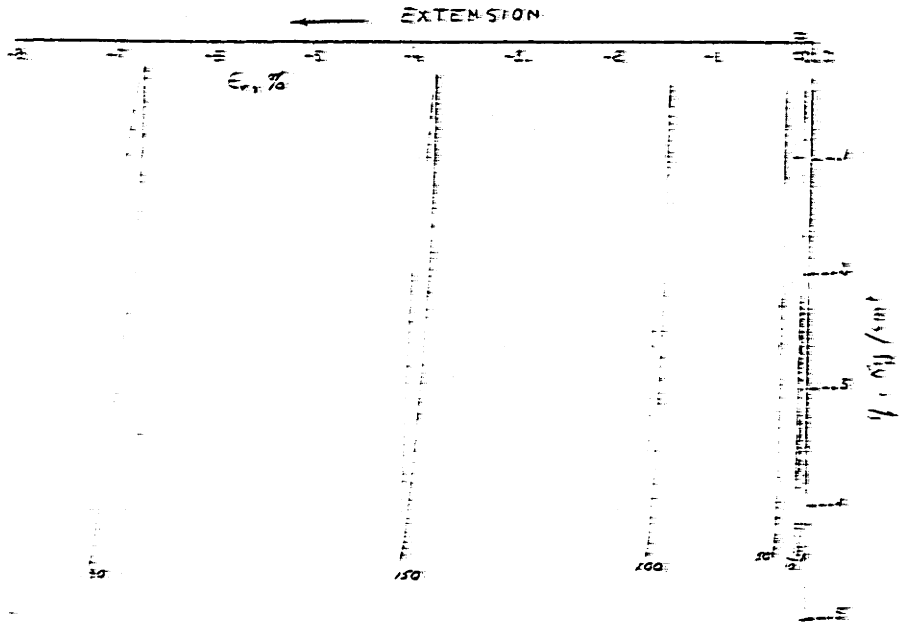

STRESS vs. STRAIN FIGURE F-32

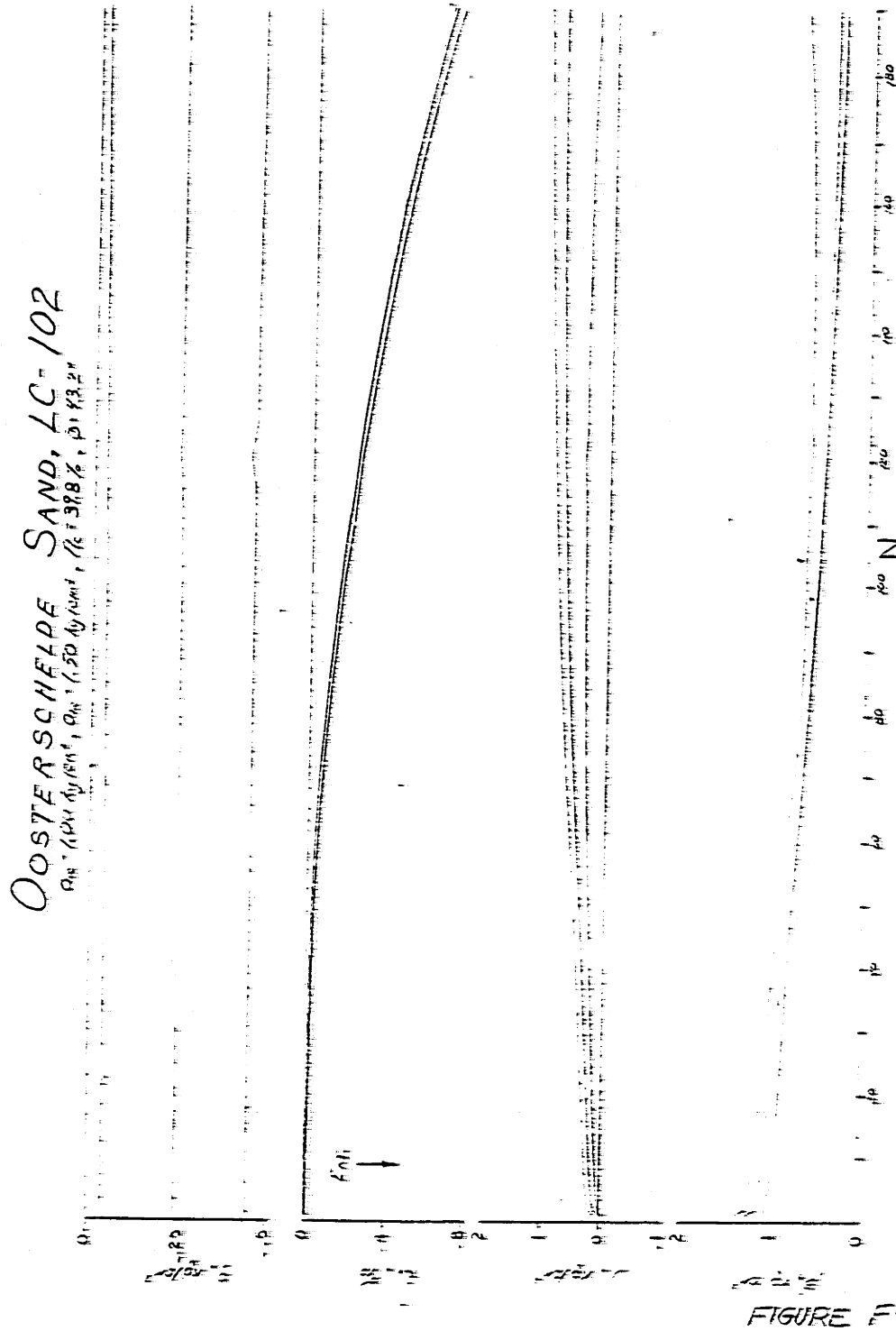

FIGURE F-20

OOSTERSCHELDE SAND, LC-103

$\bar{\sigma}_{hc}$ = 1.00 kg/cm², $\bar{\sigma}_{hc}$ = 1.00 kg/cm², n_c = 41.4 %,

RECONSOLIDATION AFTER 99 cycles, n_c = 41.3 %

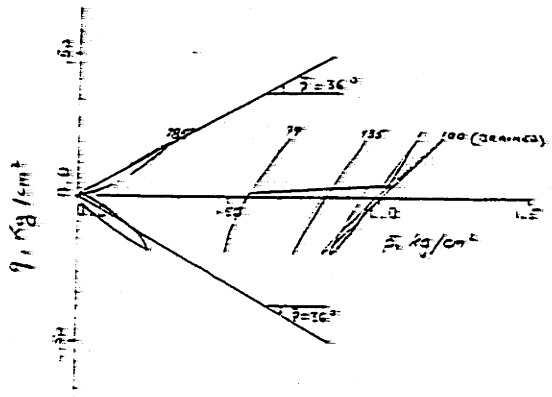

EFFECTIVE STRESS PATH

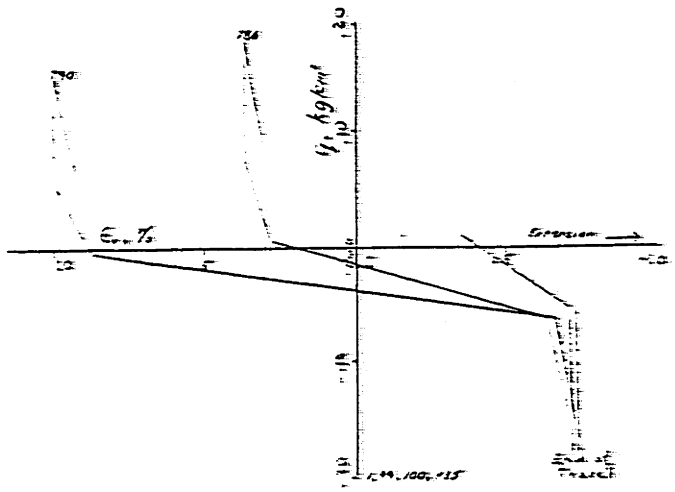

STRESS vs. STRAIN

FIGURE F-91

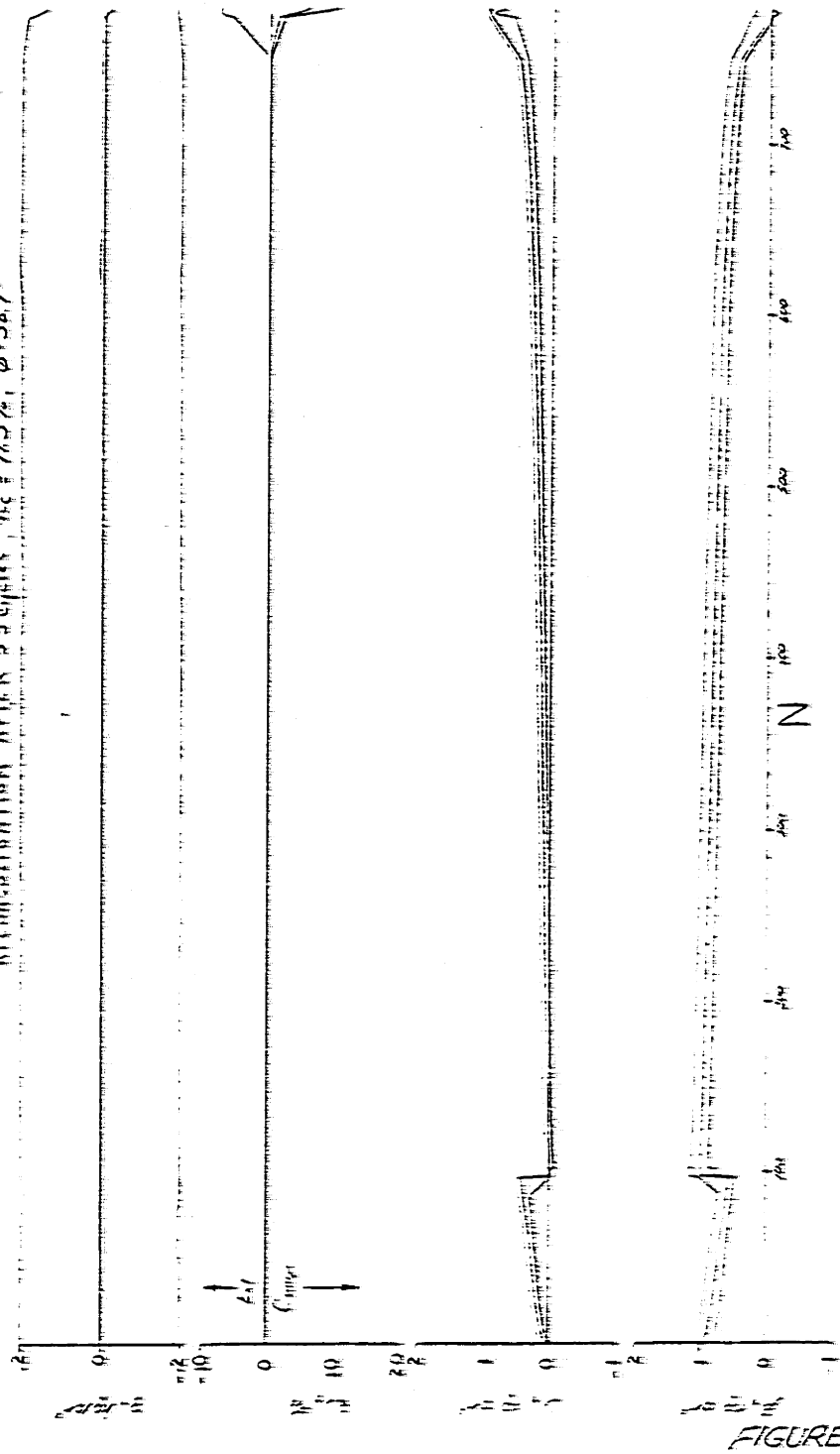
OOSTERSCHELDE SAND, LC-103
STRESS, STRAIN and PORE PRESSURE
N

FIGURE F-92

OOSTERSCHELDE SAND, LC-106

$\bar{\sigma}_{1c} = 2.50 kg/cm^2$, $\bar{\sigma}_{3c} = 1.50 kg/cm^2$, $\eta_c = 40.9\%$, $\phi = 39.1°$

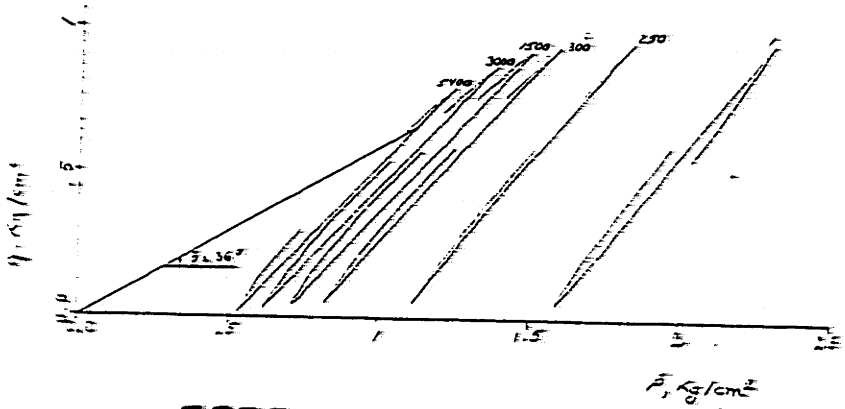

EFFECTIVE STRESS PATH

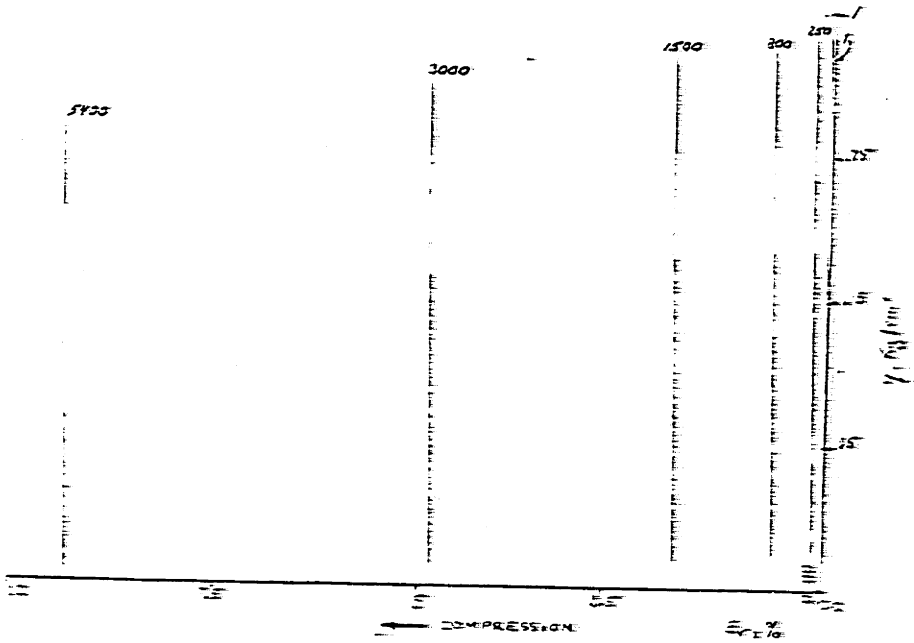

STRESS vs. STRAIN

FIGURE F-93

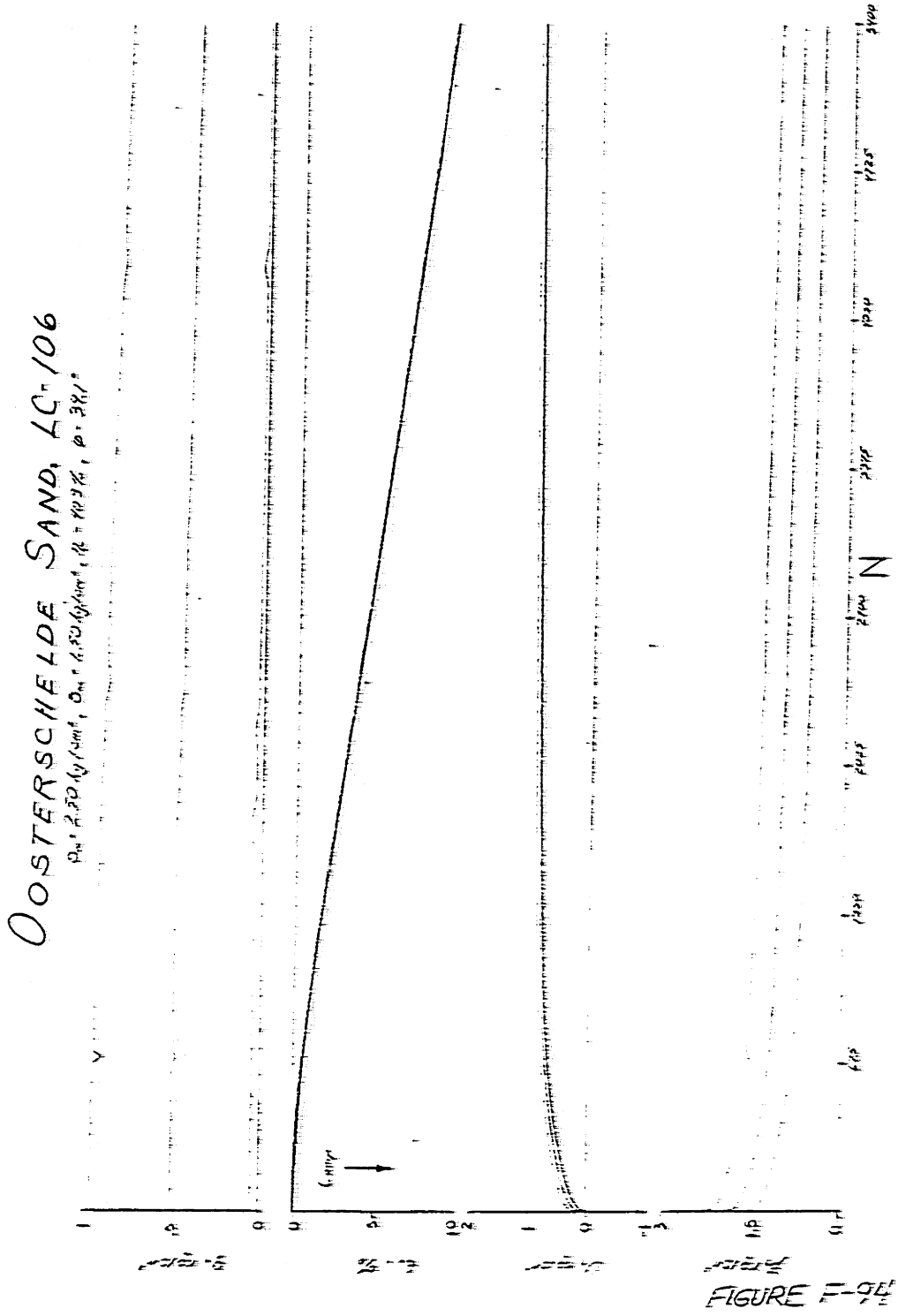

FIGURE F-94

OOSTERSCHELDE SAND, LC-117

$\bar{\sigma}_c$ = 250 kg/cm², $\bar{\sigma}_{hc}$ = 150 kg/cm², n_c = 41.1 %, ϕ = 38.4°

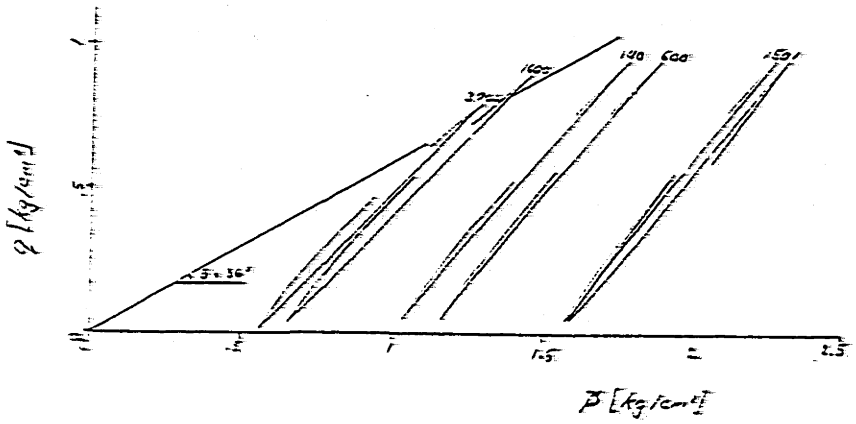

EFFECTIVE STRESS PATH

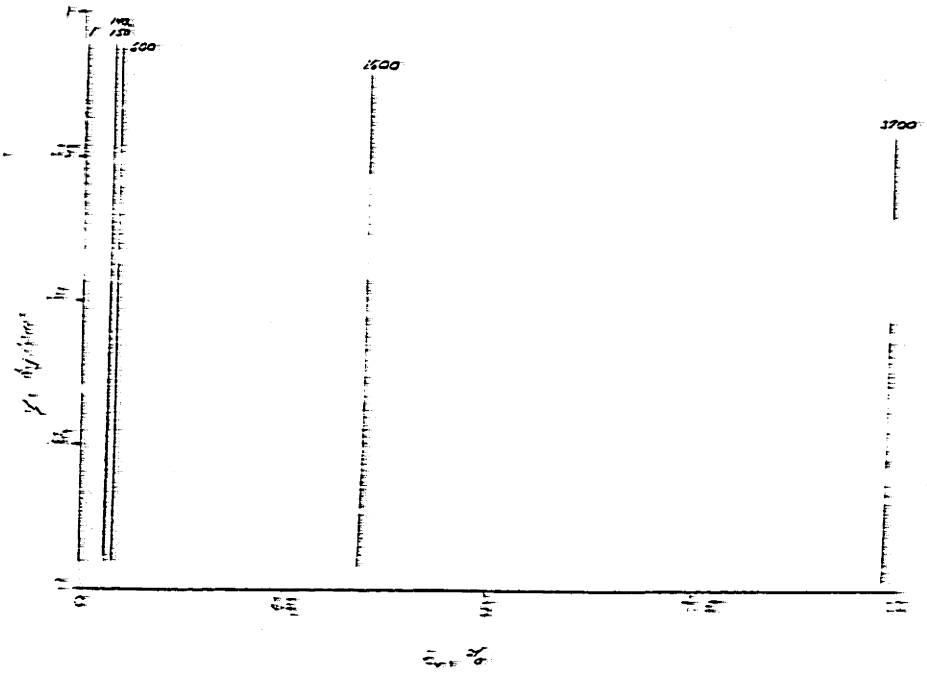

STRESS vs. STRAIN

FIGURE F-95

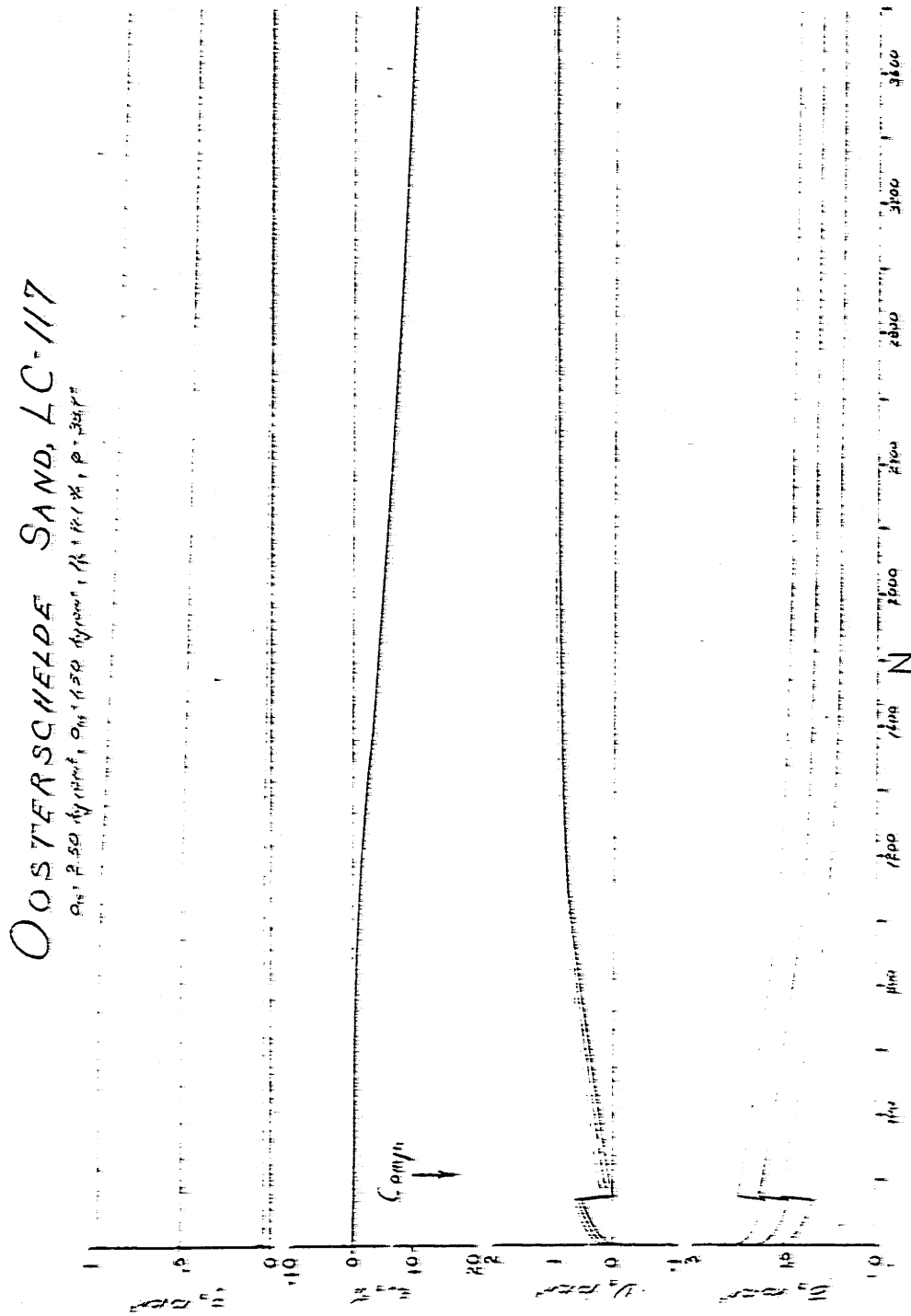
OOSTERSCHELDE SAND, LC-117
STRESS, STRAIN AND PORE PRESSURE
N

FIGURE F-96

OOSTERSCHELDE SAND, LC-119

$\bar{\sigma}_{1c} = 3.00 kg/cm^2$, $\bar{\sigma}_{3c} = 3.00 kg/cm^2$, $\eta_c = 41.0\ \%$, $\phi = 37.8°$

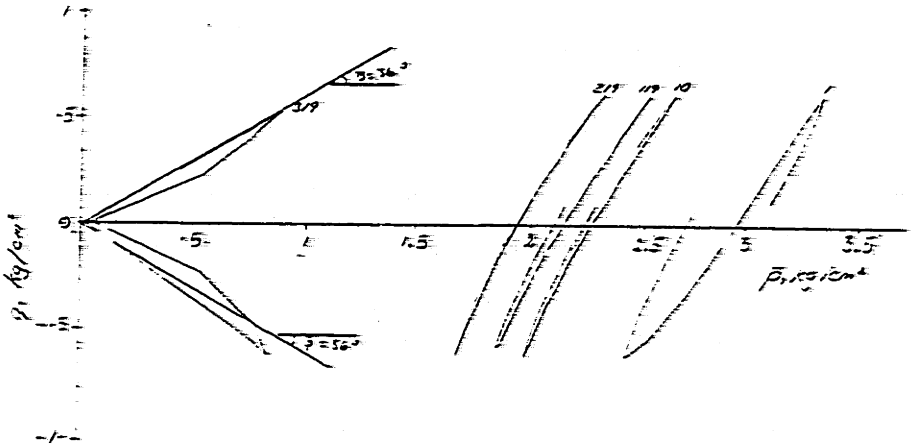

EFFECTIVE STRESS PATH

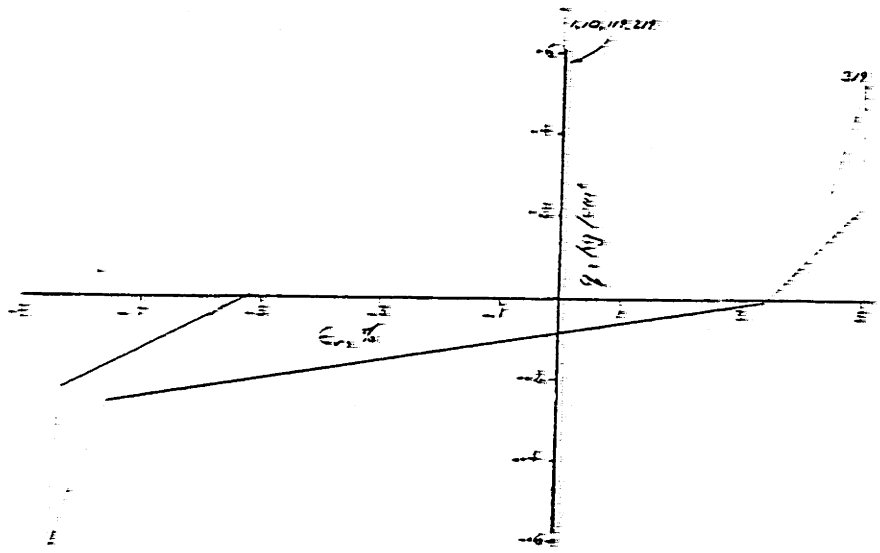

STRESS vs. STRAIN

FIGURE F-97

FIGURE F-98

OOSTERSCHELDE SAND, LC-121

$\bar{\sigma}_{ic}$ = 2.50 kg/cm², $\bar{\sigma}_{hc}$ = 1.50 kg/cm², η_c = 41.0 %, ϕ = 36.7°

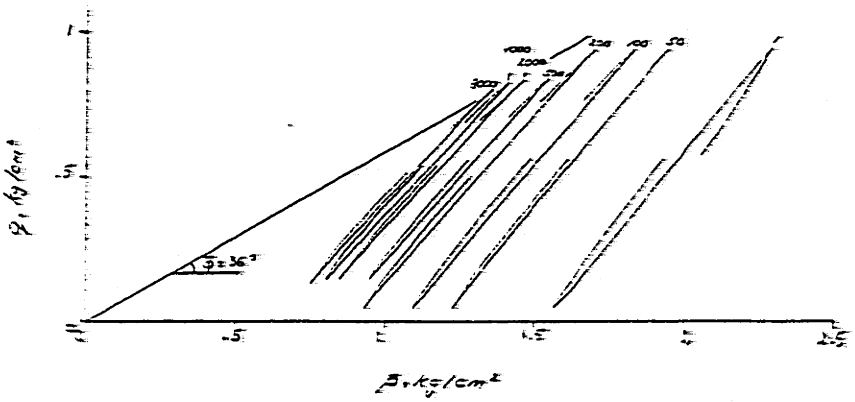

EFFECTIVE STRESS PATH

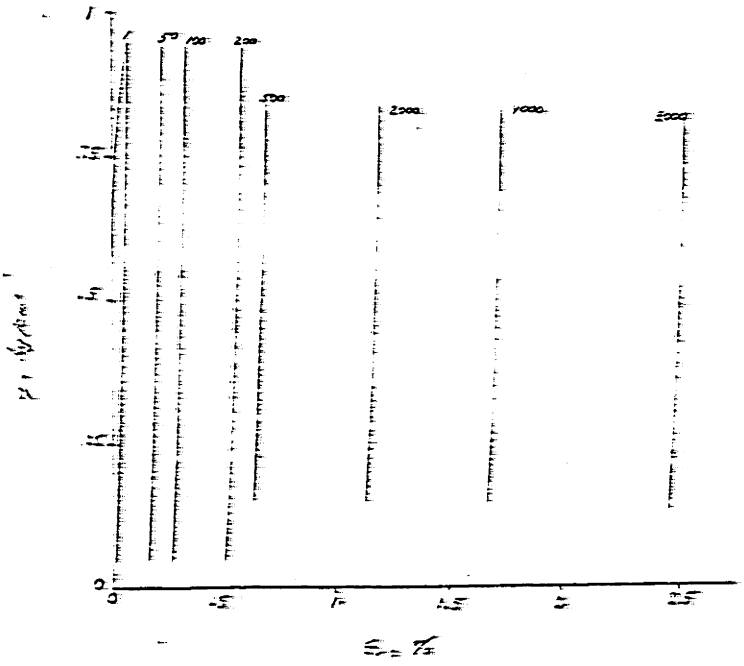

STRESS vs. STRAIN

FIGURE F-30

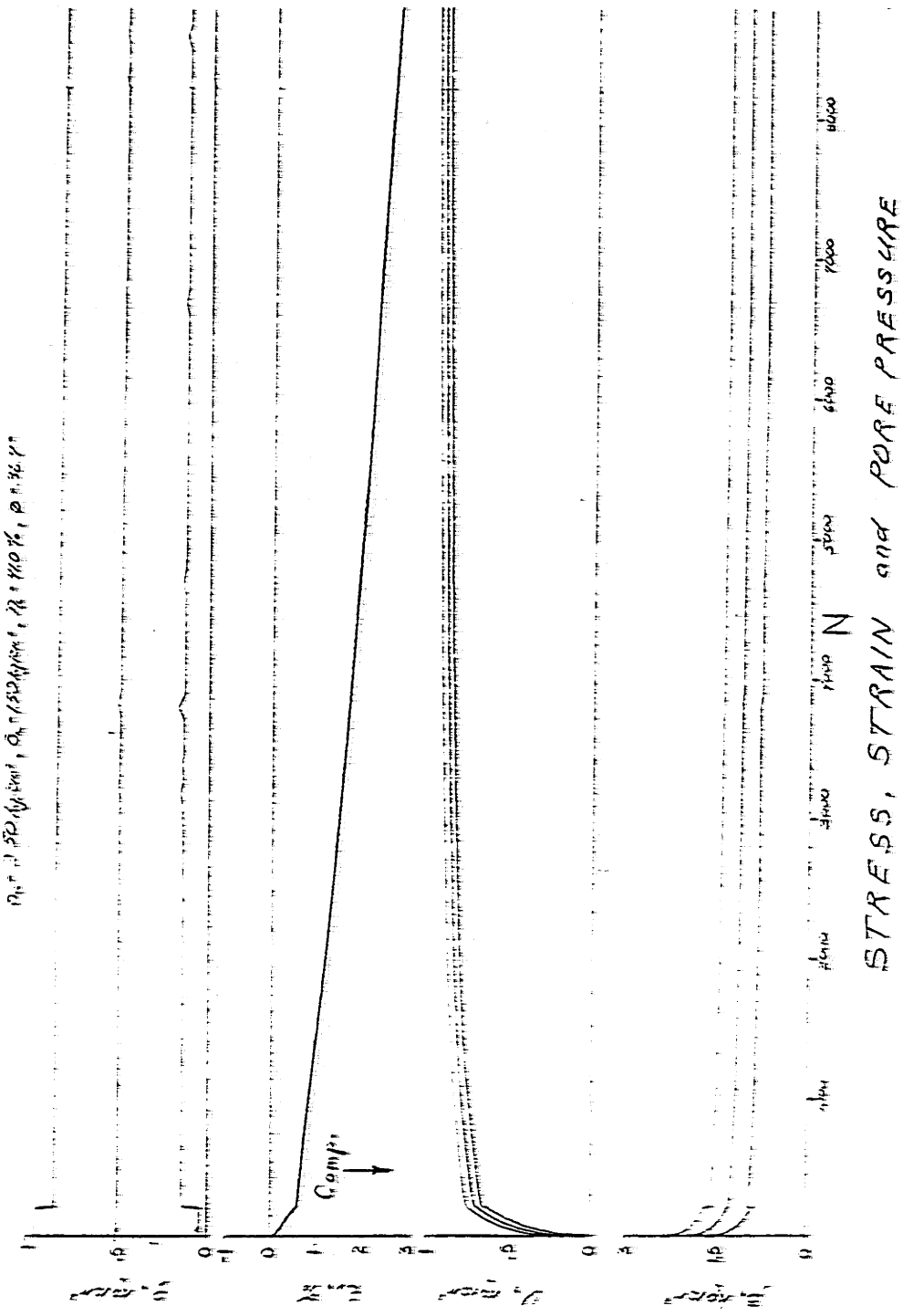
OOSTERSCHELDE SAND, LC 121
Comp.
N
STRESS, STRAIN and PORE PRESSURE

FIGURE F-100

OOSTERSCHELDE SAND, LC-122

$\bar{\sigma}_{1c} = 2.50 kg/cm^2$, $\bar{\sigma}_{3c} = 1.50 kg/cm^2$, $\eta_c = 41.1\%$, $\phi = 38.9°$

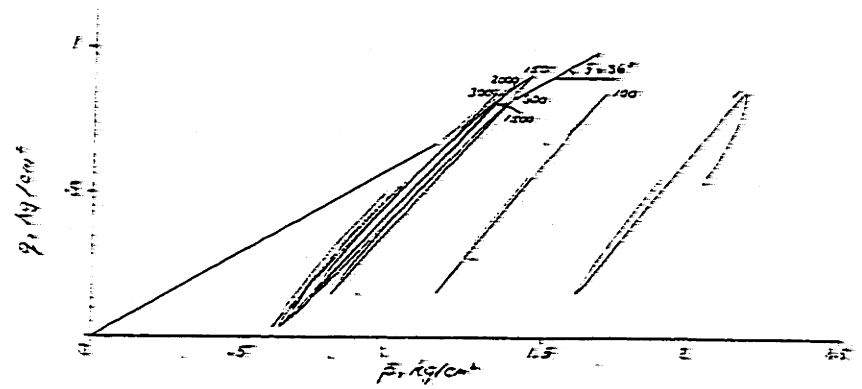

EFFECTIVE STRESS PATH

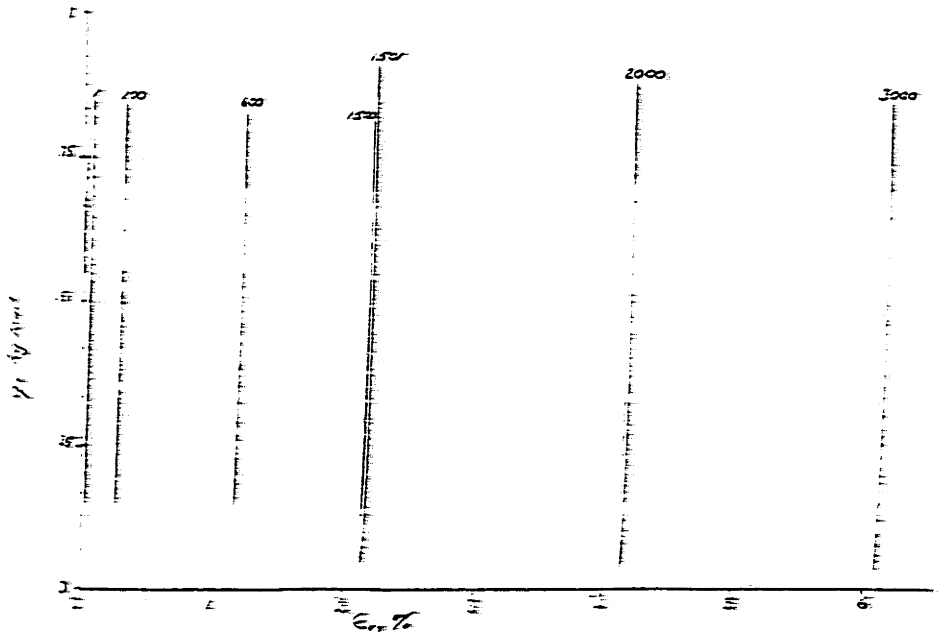

STRESS vs. STRAIN

FIGURE F-101

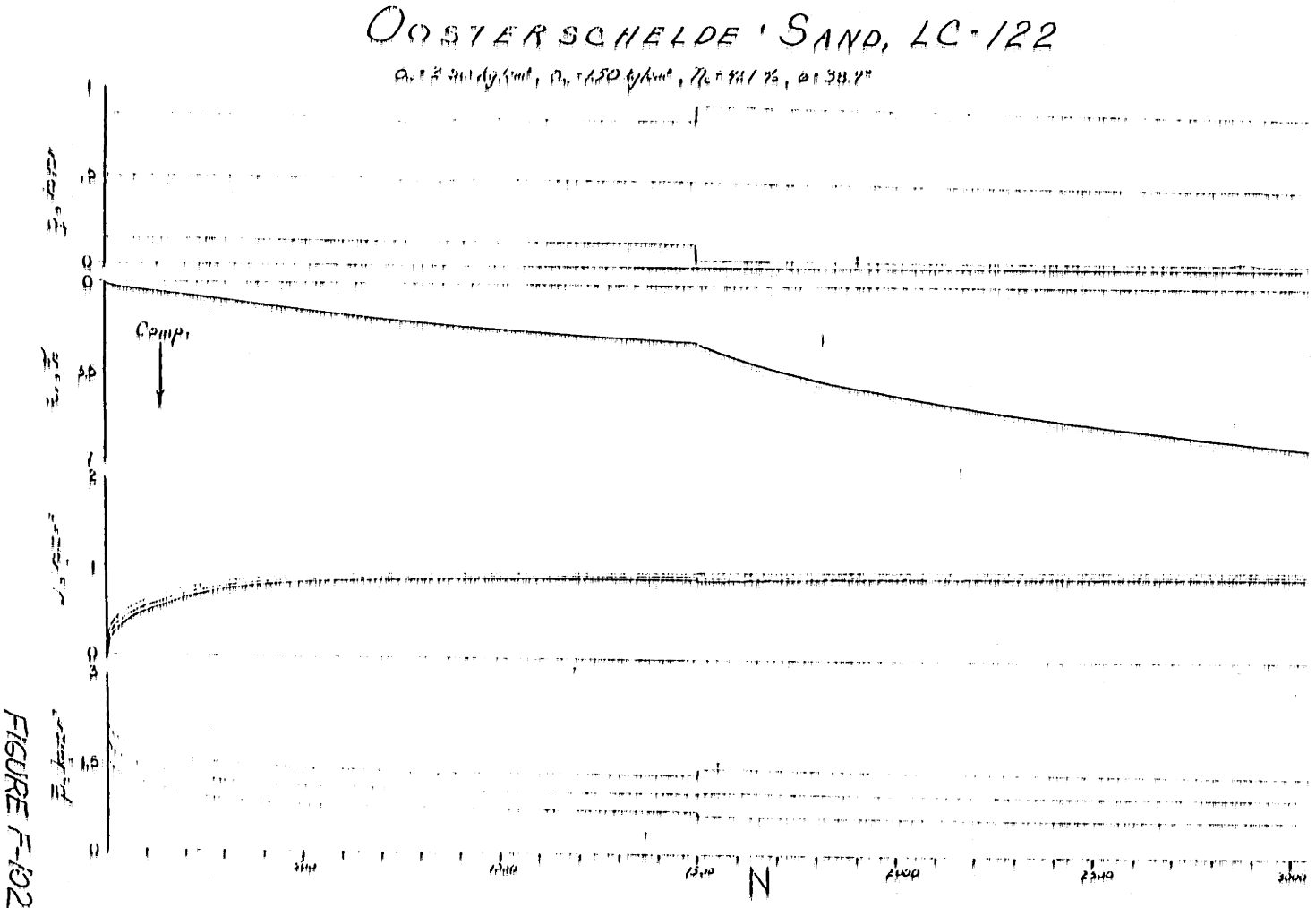

FIGURE F-102

STRESS, STRAIN and PORE PRESSURE

OOSTERSCHELDE SAND, LC-124I

$\bar{\sigma}_{3c} = 2.50$ kg/cm², $\bar{\sigma}_{1c} = 1.50$ kg/cm², $D_c = 41.3\%$

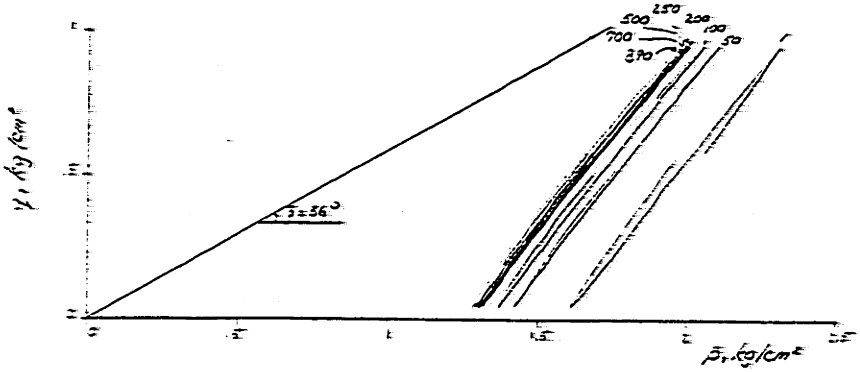

EFFECTIVE STRESS PATH

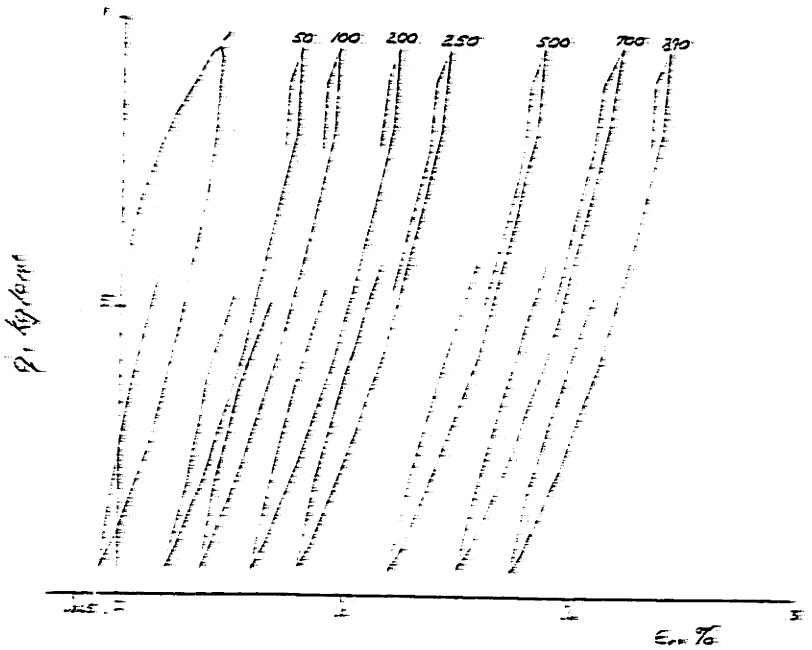

STRESS vs. STRAIN

FIGURE F-103

OOSTERSCHELDE SAND, LC-1241
STRESS, STRAIN and VOLUME CHANGE

FIGURE F-[illegible]

OOSTERSCHELDE SAND, LC-124II

$\bar{\sigma}_{vc}$ = 2.50 kg/cm², $\bar{\sigma}_{hc}$ = 1.50 kg/cm², η_c = 49.5, η_o = , $\bar{\phi}$ = 38.0°

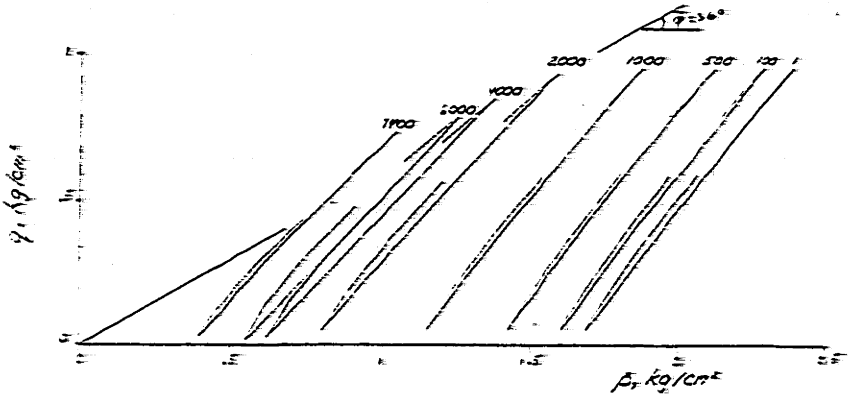

EFFECTIVE STRESS PATH

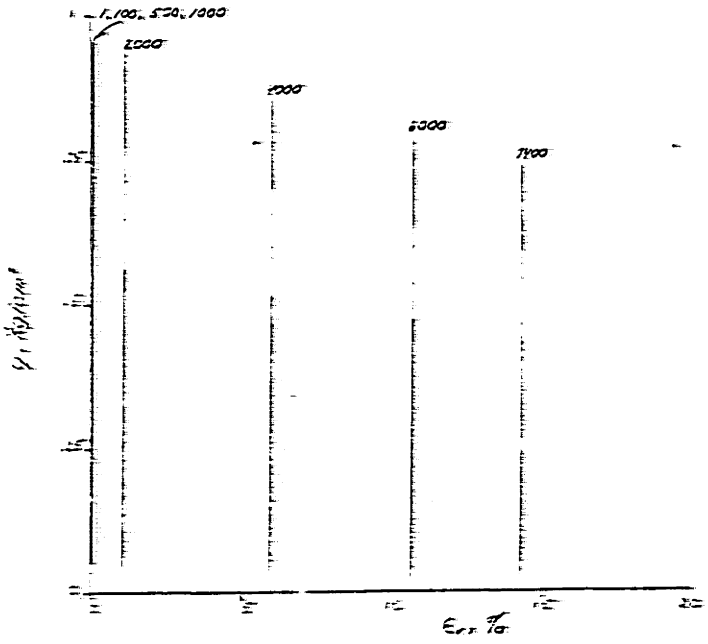

STRESS vs. STRAIN

FIGURE F-105

OOSTERSCHELDE SAND, LC-124II

$\bar{\sigma}_{ic}$ = [illegible] kg/cm², $\bar{\sigma}_{hc}$ = [illegible] kg/cm², n_c = [illegible] %, ϕ = [illegible]°

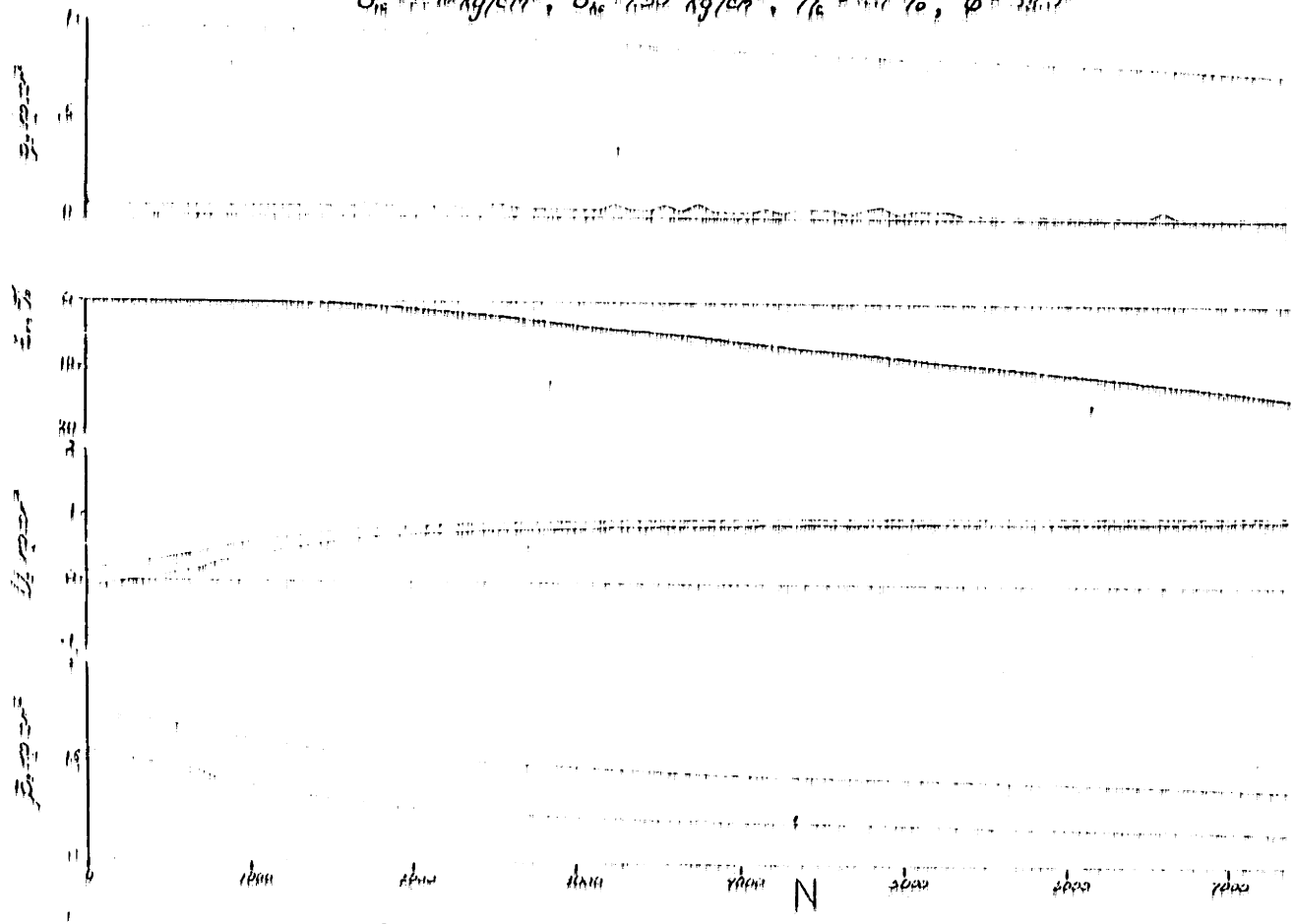

N

STRESS, STRAIN and PORE PRESSURE

FIGURE F-102

OOSTERSCHELDE SAND, LC-125

$\bar{\sigma}_{hc}$ = 2.50 kg/cm², $\bar{\sigma}_{hc}$ = 1.50 kg/cm², η_c = 41.2 %, ϕ = 33.5°

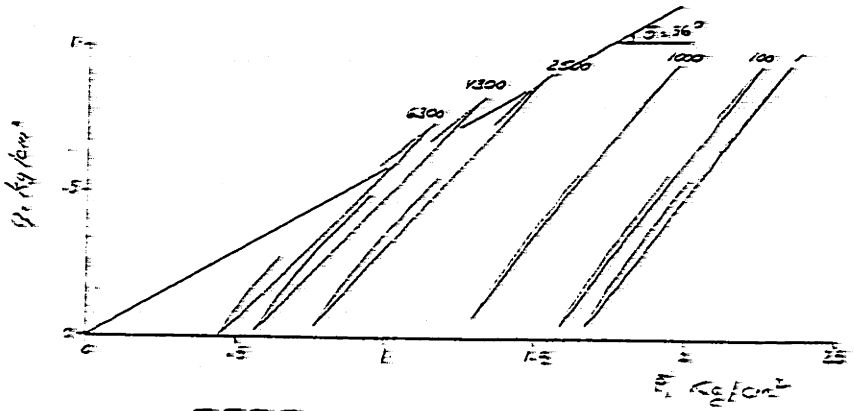

EFFECTIVE STRESS PATH

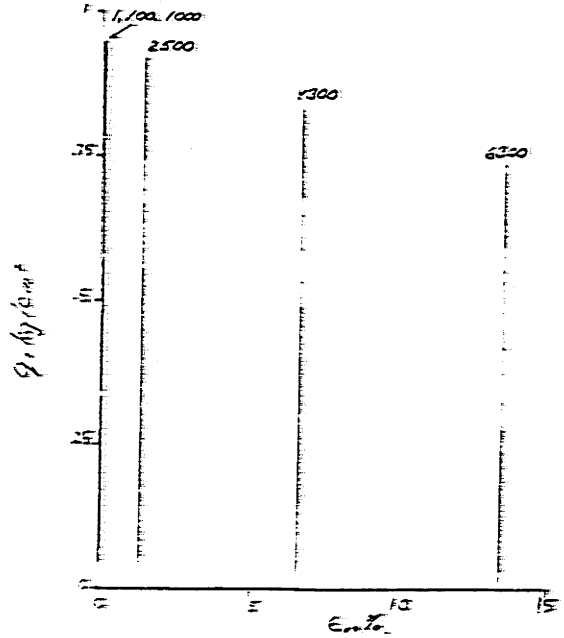

STRESS vs. STRAIN

FIGURE F-107

OOSTERSCHELDE SAND, LC-125

σ_{1c} = 2.50 kg/cm², σ_{3c} = 1.50 kg/cm², η_c = 77.2 %, ϕ = 38.4°

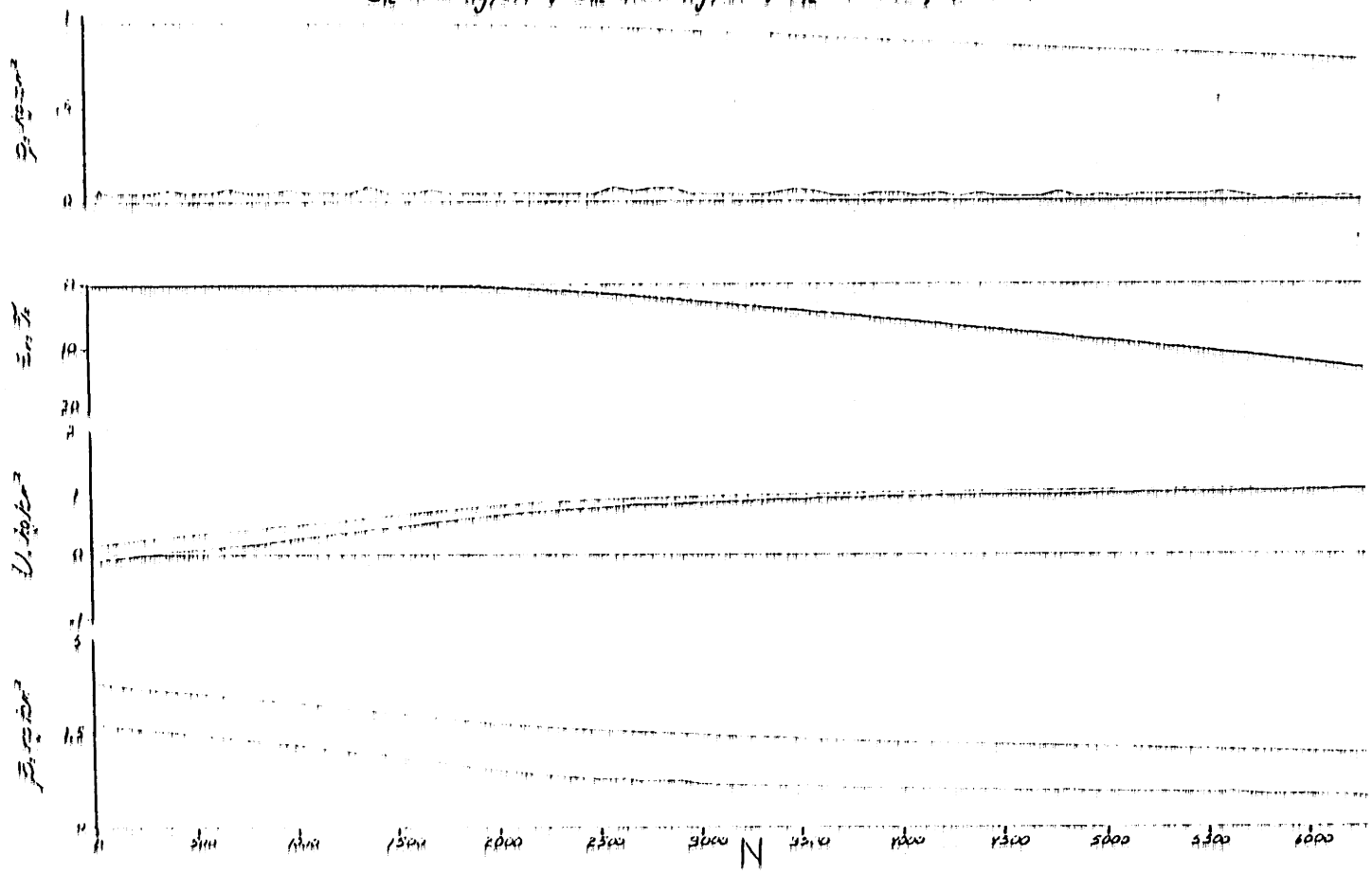

STRESS, STRAIN and PORE PRESSURE

FIGURE F-108

OOSTERSCHELDE SAND, LC-126

$\bar{\sigma}_{3c} = 2.50 kg/cm^2$, $\bar{\sigma}_{3c} = 1.50 kg/cm^2$, $\eta_c = 41.0\%$,

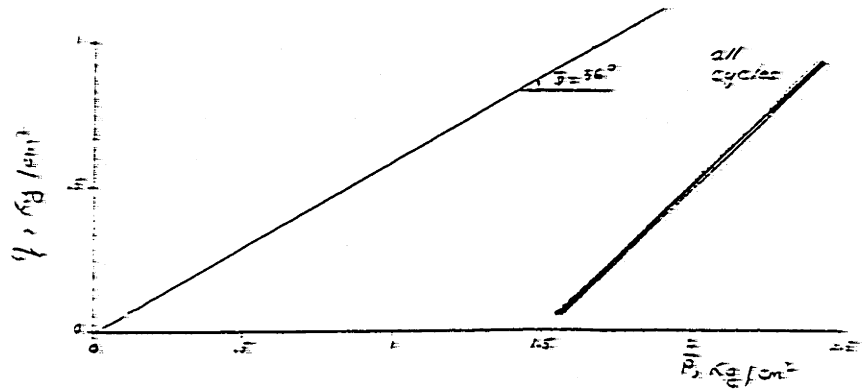

EFFECTIVE STRESS PATH

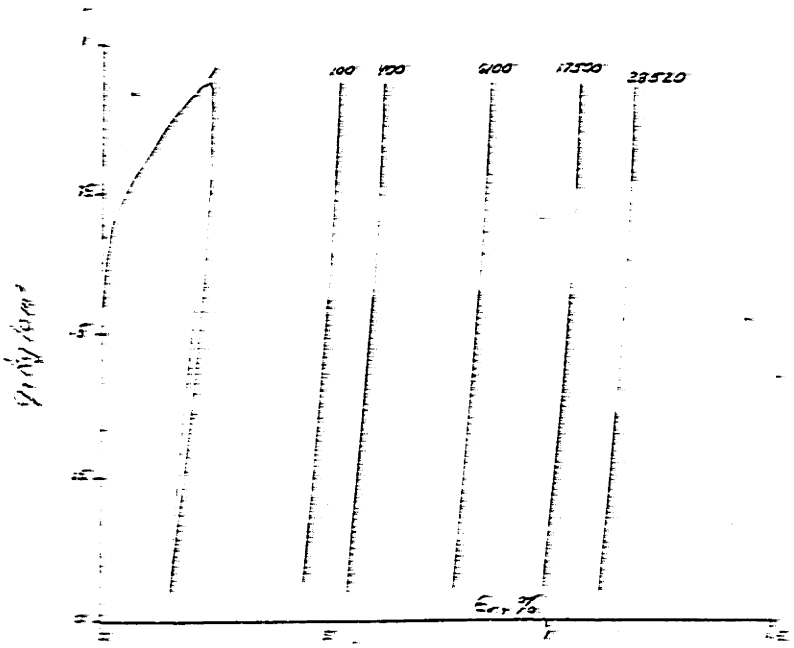

STRESS vs. STRAIN

FIGURE C-109

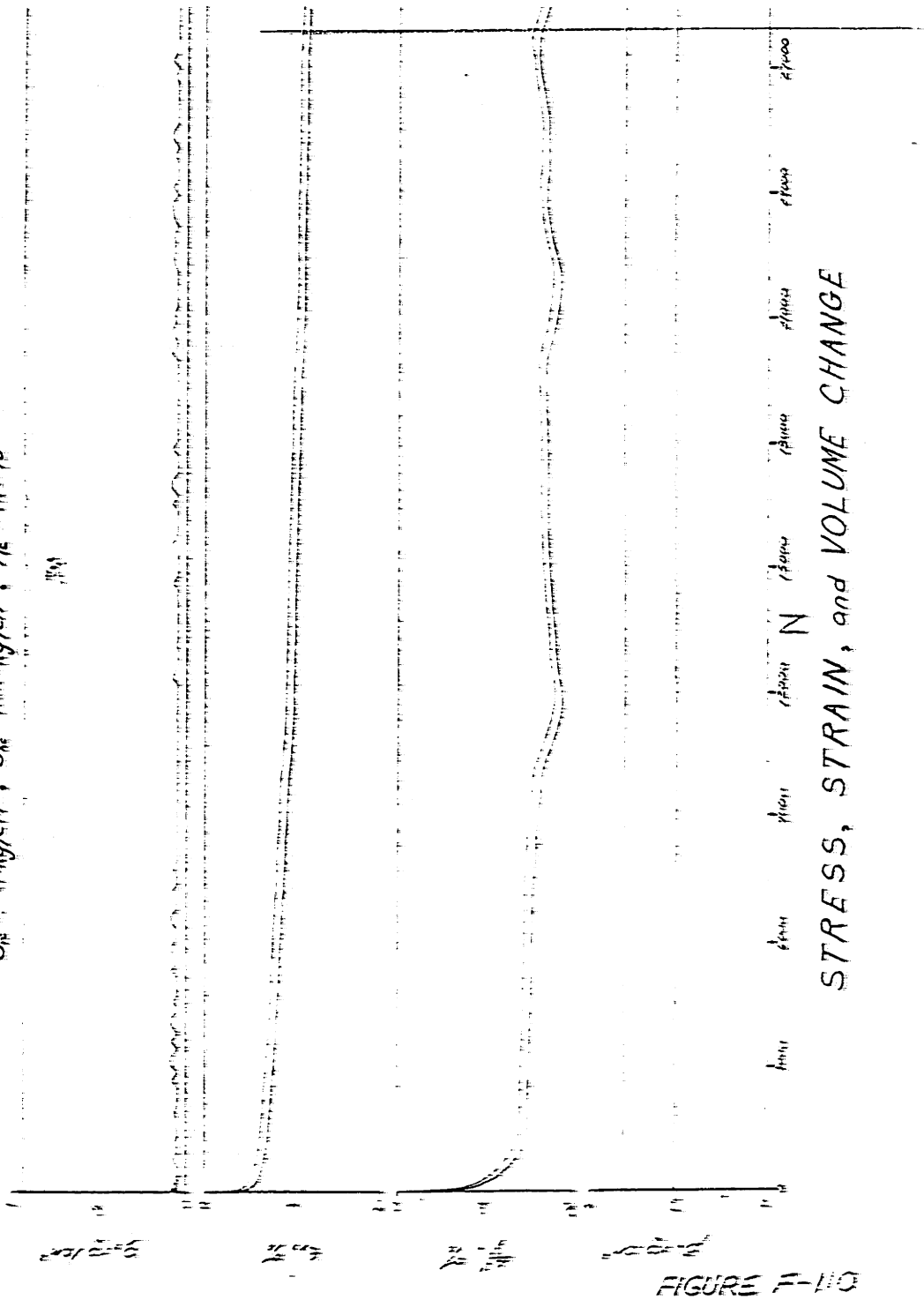
OOSTERSCHELDE SAND, LC-126
STRESS, STRAIN, and VOLUME CHANGE
N

FIGURE F-110

OOSTERSCHELDE SAND, LC-127

$\bar{\sigma}_{hc}$ = 5.33 kg/cm², $\bar{\sigma}_{hc}$ = 5.33 kg/cm², n_c = 41.2 %

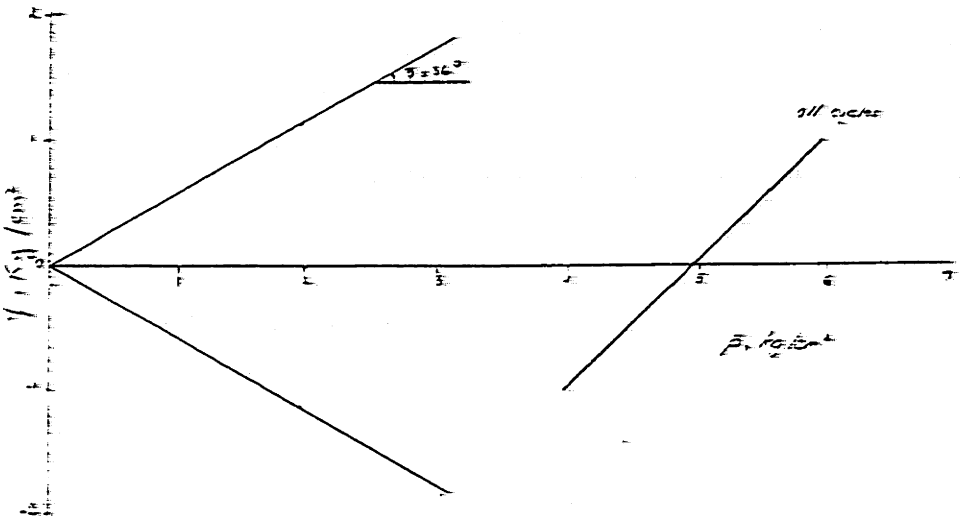

EFFECTIVE STRESS PATH

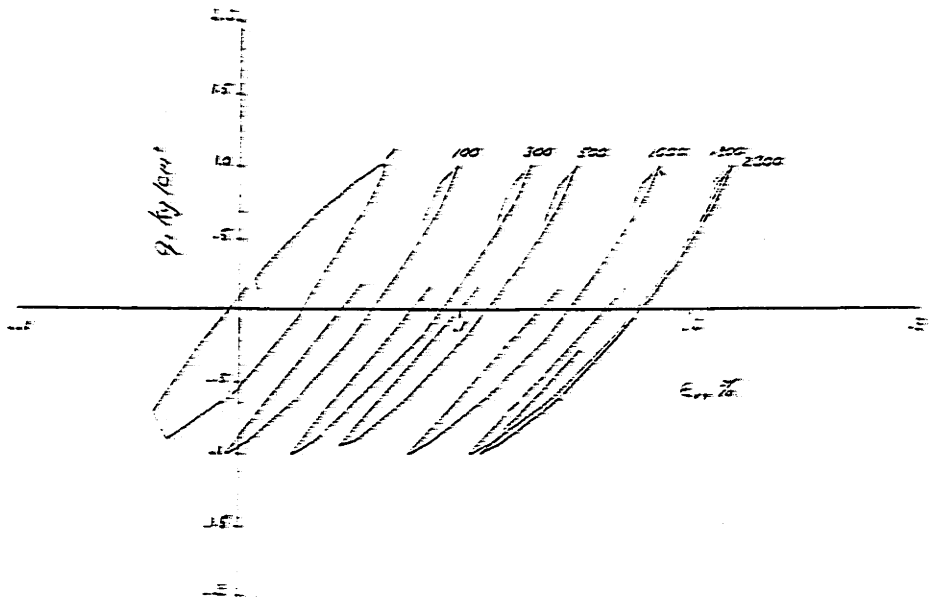

STRESS vs. STRAIN

FIGURE F-III

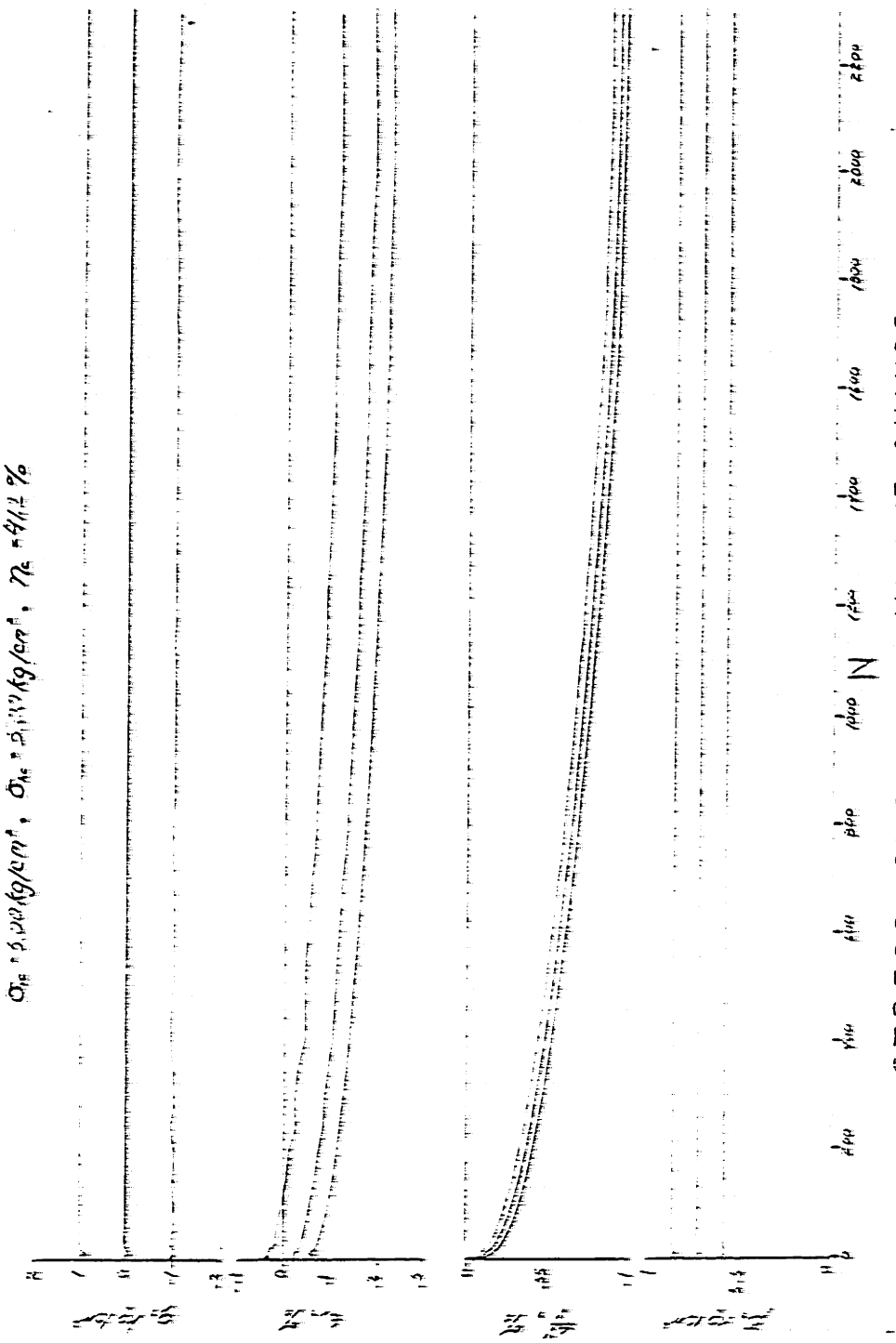
OOSTERSCHELDE SAND, LC-127
STRESS, STRAIN, and VOLUME CHANGE
N

FIGURE F-112

OOSTERSCHELDE SAND, LC-128I

$\bar{\sigma}_{1c} = 2.50$ kg/cm², $\bar{\sigma}_{3c} = 1.50$ kg/cm², $n_c = 41.7\%$

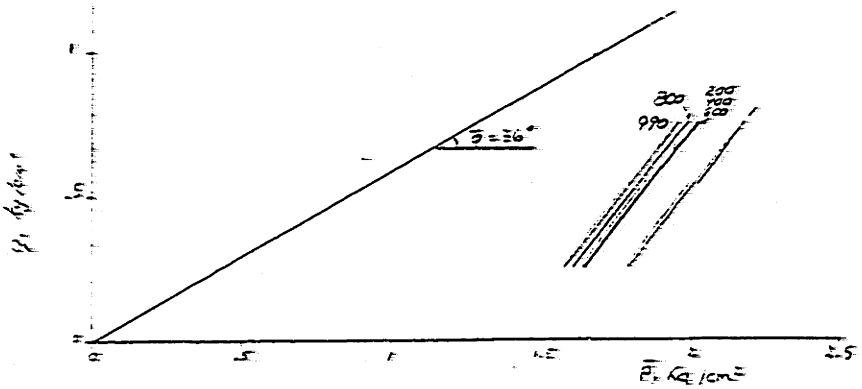

EFFECTIVE STRESS PATH

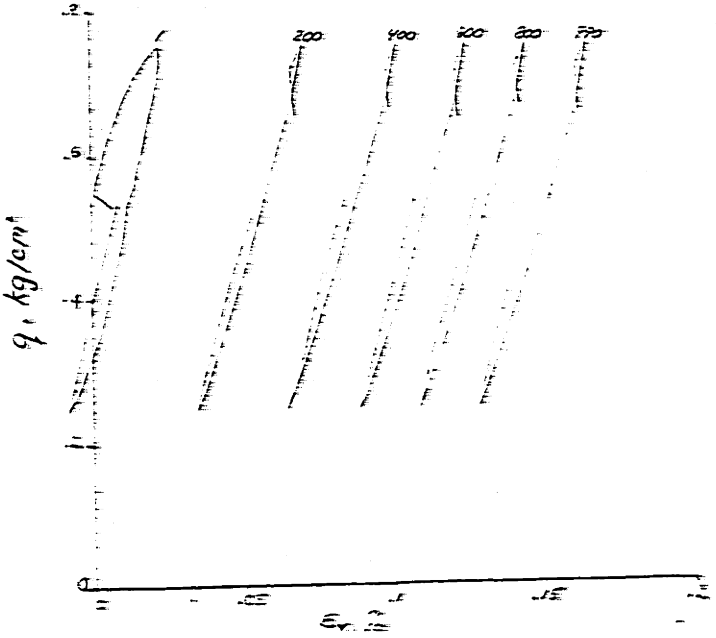

STRESS vs STRAIN

FIGURE F-113

OOSTERSCHELDE SAND, LC-128I

σ_{3c} = 2.52 kg/cm², σ_{3c} = 1.512 kg/cm², n_c = 47.30 %

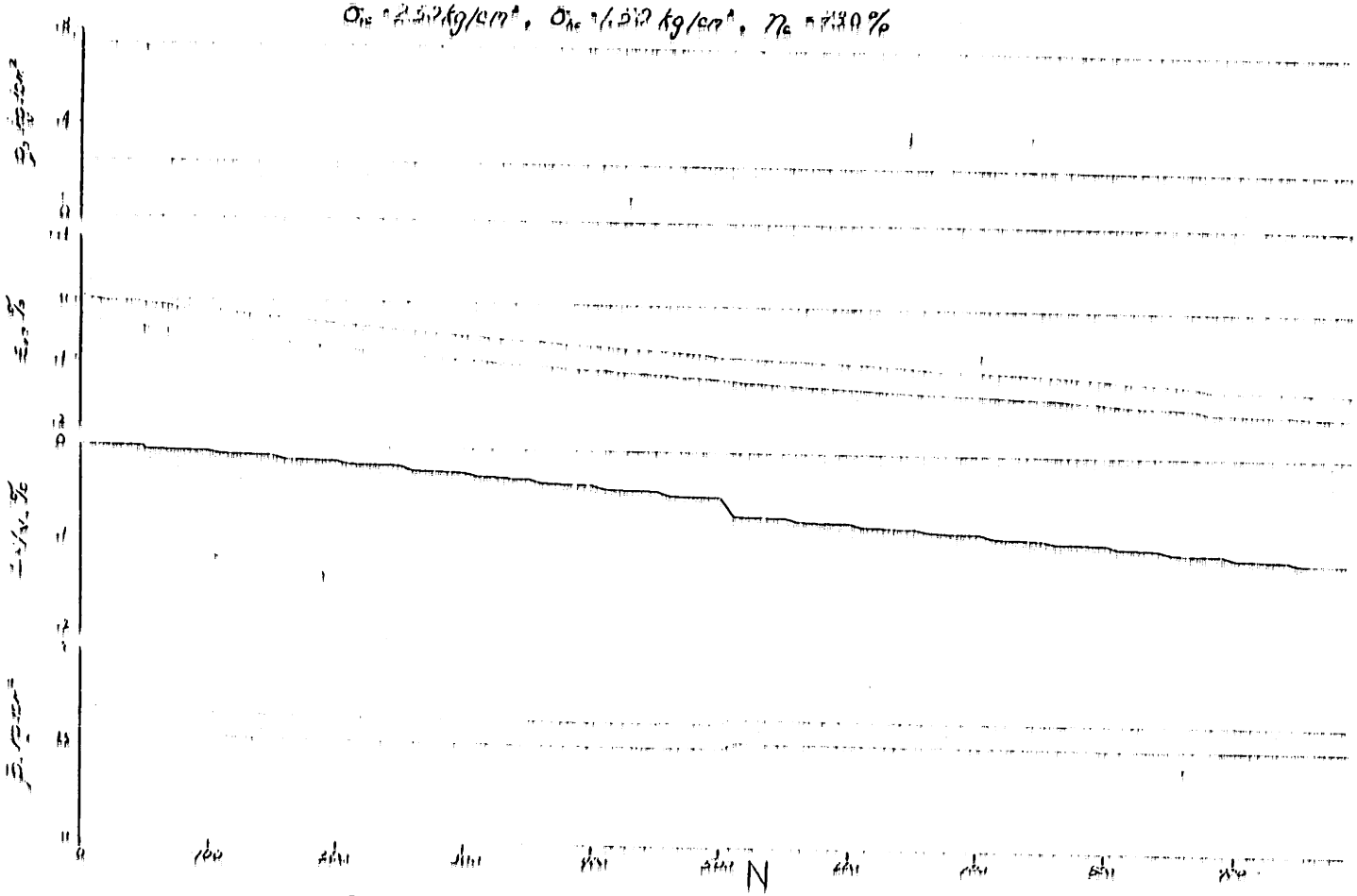

STRESS, STRAIN and VOLUME CHANGE

FIGURE F-128I

OOSTERSCHELDE SAND, LC-128II

$\bar{\sigma}_{hc} = 2.50\ kg/cm^2$, $\bar{\sigma}_{hc} = 1.50\ kg/cm^2$, $n_c = 42.5\%$, $\phi = 35.5°$

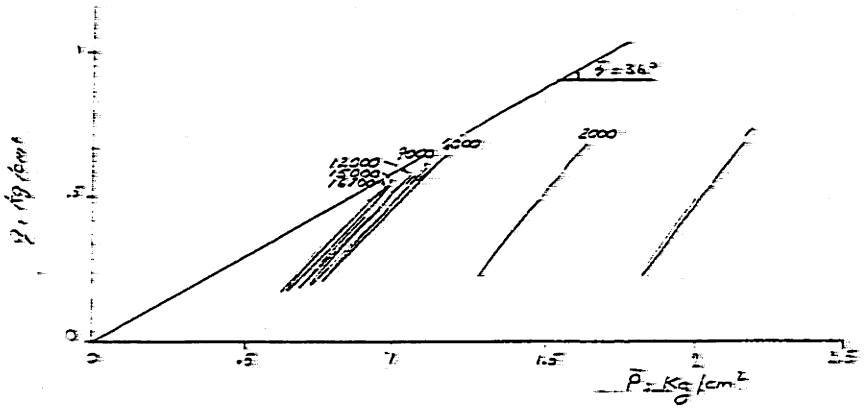

EFFECTIVE STRESS PATH

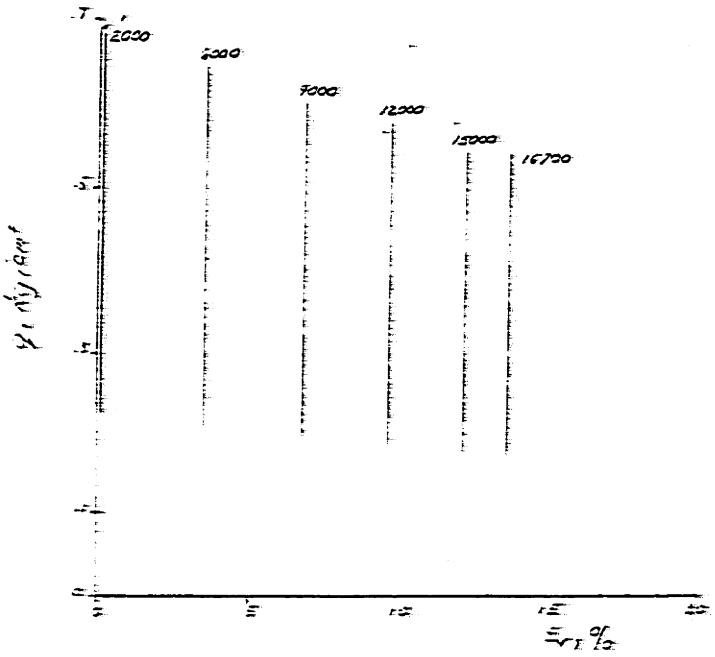

STRESS vs. STRAIN

FIGURE F-115

OOSTERSCHELDE SAND, LC-128II

$\bar{\sigma}_{1c}$ = 2.30 kg/cm², $\bar{\sigma}_{3c}$ = 1.50 kg/cm², n_c = 43.6 %, ϕ = 35.2°

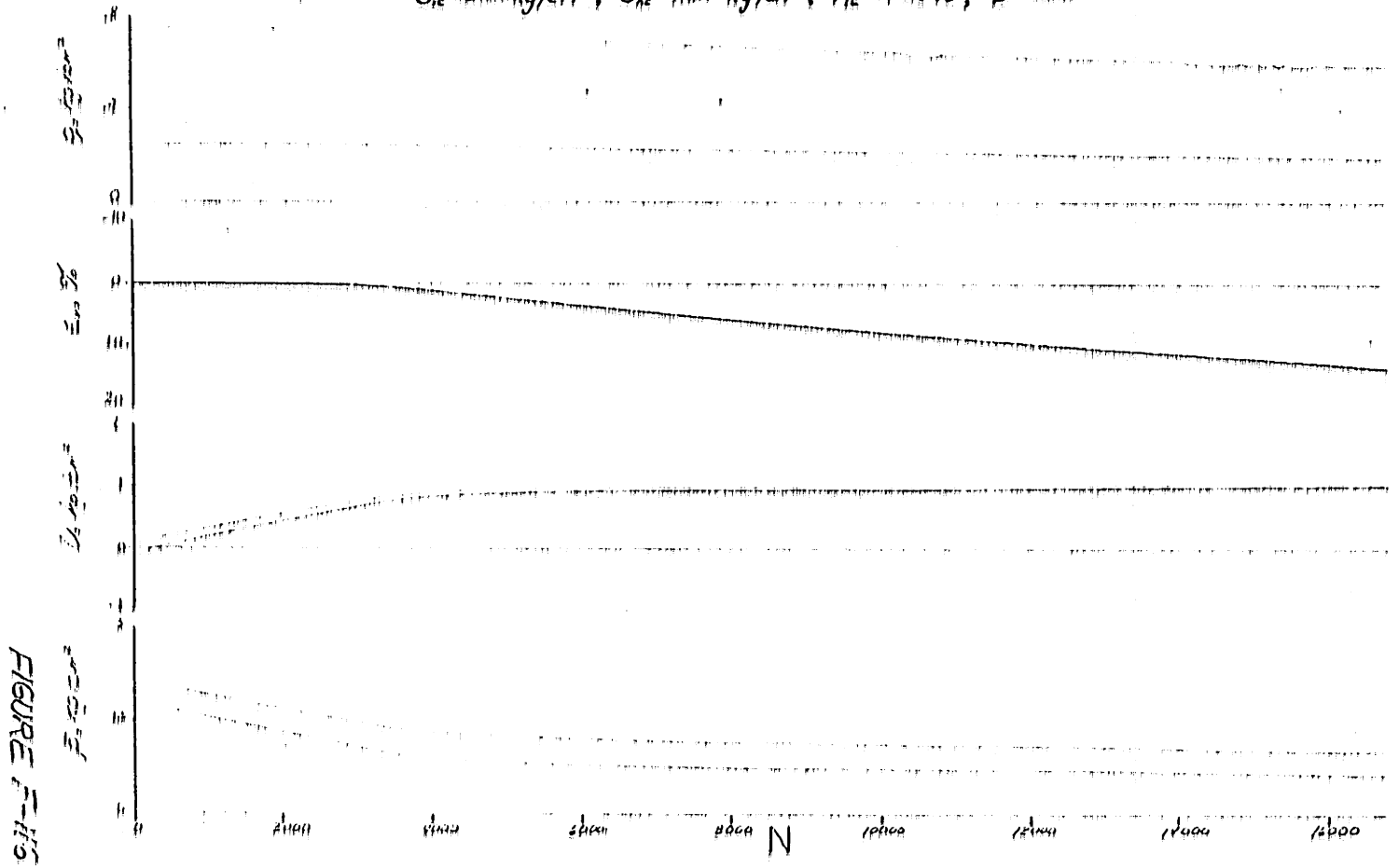

FIGURE 7-115

STRESS, STRAIN and PORE PRESSURE

OOSTERSCHELDE SAND, LC-133

$\bar{\sigma}_{3c} = 3.00 \text{ kg/cm}^2$, $\bar{\sigma}_{3c} = 1.50 \text{ kg/cm}^2$, $\eta_c = 41.3\%$

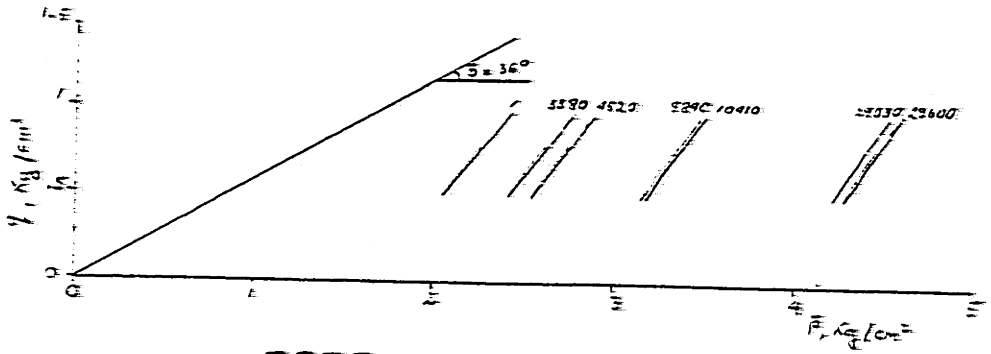

EFFECTIVE STRESS PATH

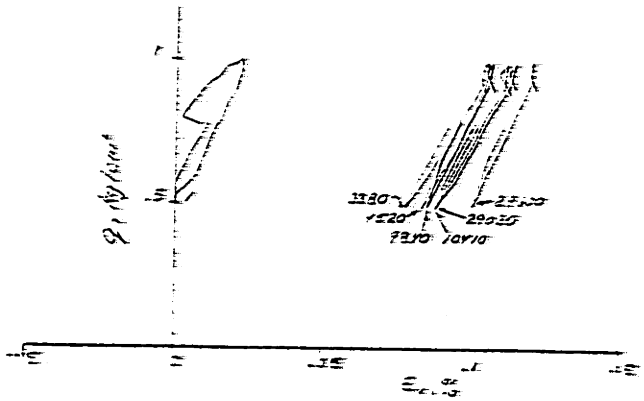

STRESS vs. STRAIN

FIGURE F-117

OOSTERSCHELDE SAND, LC-133
STRESS, STRAIN and PORE PRESSURE
N

FIGURE F-118

OOSTERSCHELDE SAND, LC-141

$\bar{\sigma}_{hc}$ = 2.50 kg/cm², $\bar{\sigma}_{hc}$ = 1.50 kg/cm², η_c = 15.1%

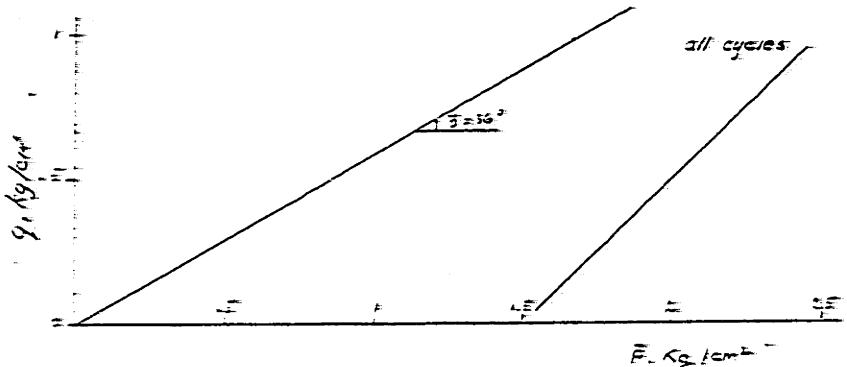

EFFECTIVE STRESS PATH

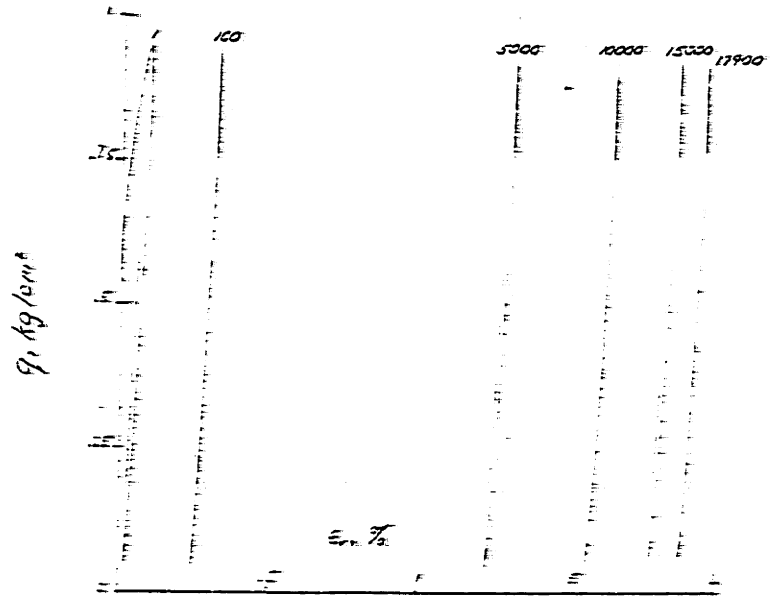

STRESS vs. STRAIN

FIGURE F-119

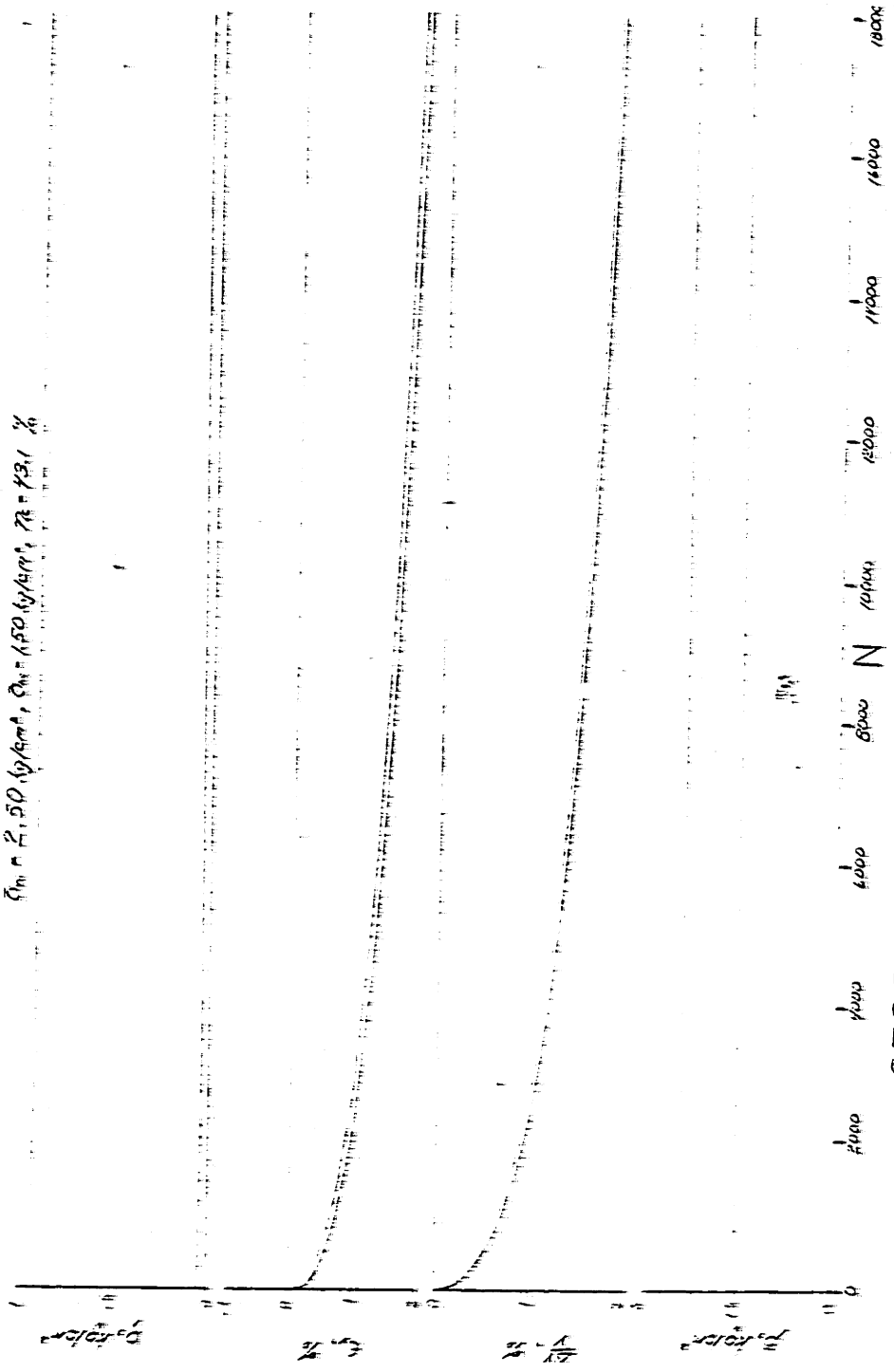
OOSTERSCHELDE SAND, LC-141
STRESS, STRAIN, and VOLUME CHANGE
N

FIGURE F-120

OOSTERSCHELDE SAND, LC-155

$\bar{\sigma}_{1c} = 3.50 kg/cm^2$; $\bar{\sigma}_{3c} = 2.50 kg/cm^2$, $n_c = 45.4\%$

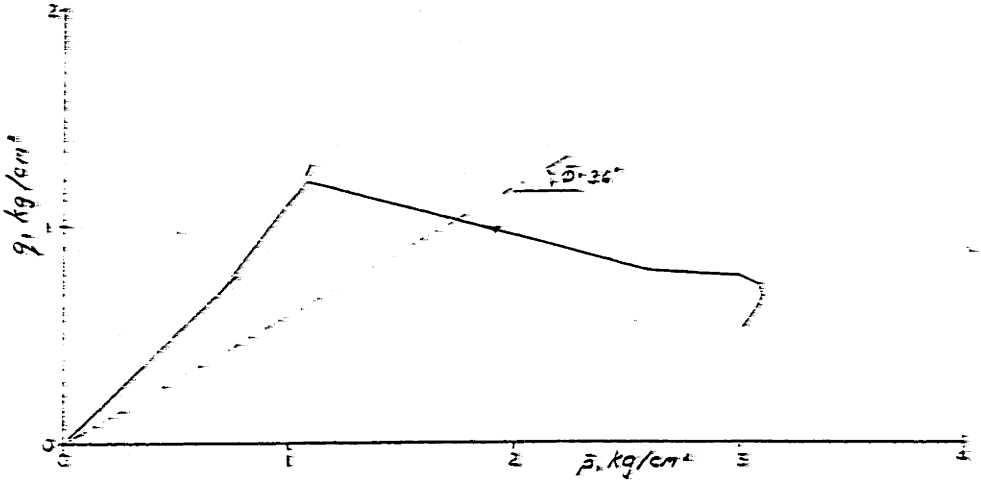

EFFECTIVE STRESS PATH

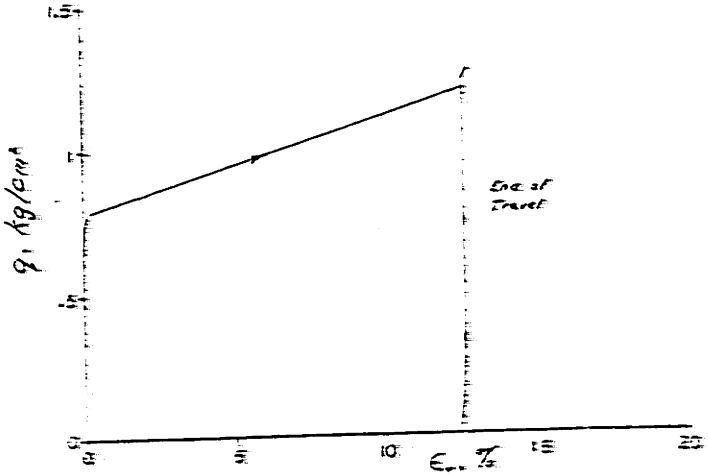

STRESS vs. STRAIN FIGURE F-121

OOSTERSCHELDE SAND, LC-156

$\sigma_{3c} = 3.50 kg/cm^2$, $\sigma_{1c} = 2.50 kg/cm^2$, $n_c = 45.0\%$, $\phi = 31.9°$

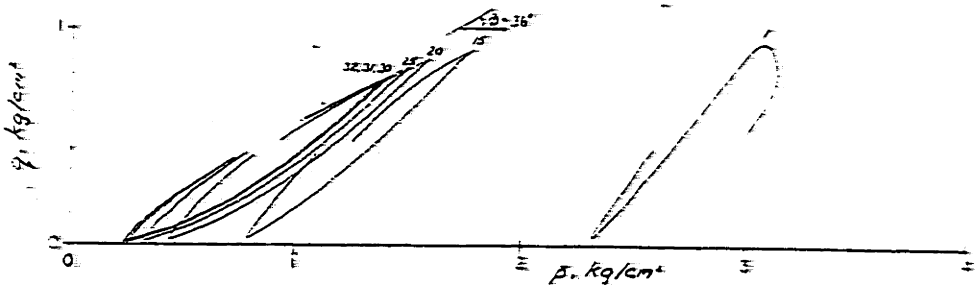

EFFECTIVE STRESS PATH

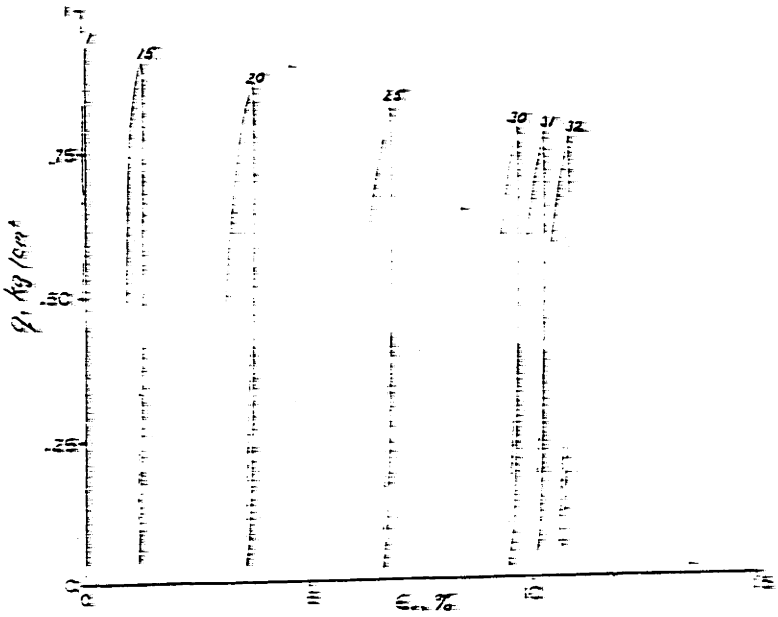

STRESS vs. STRAIN

FIGURE F-122

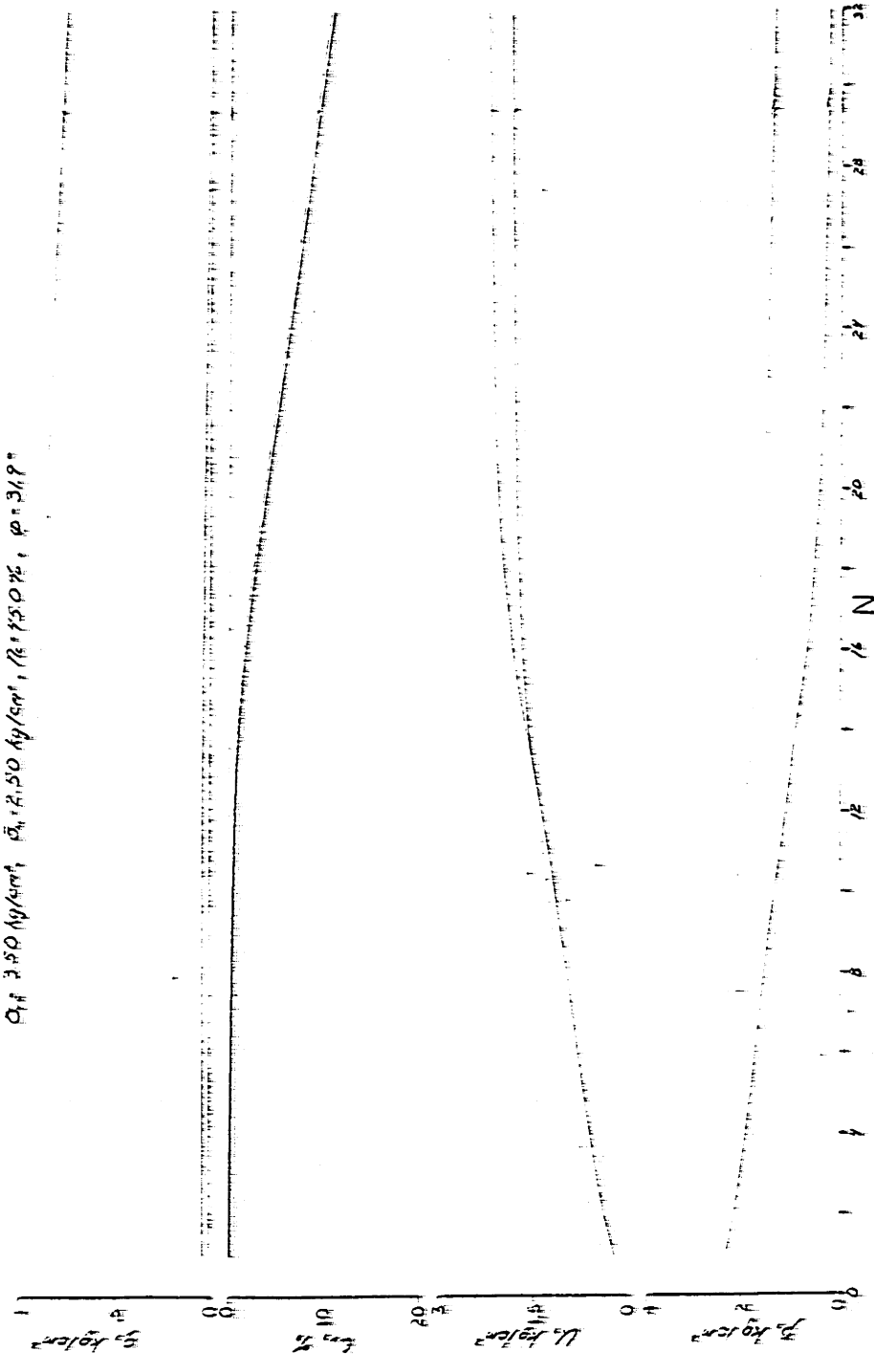
OOSTERSCHELDE SAND, LC-156
STRESS, STRAIN and PORE PRESSURE
N

FIGURE F-123

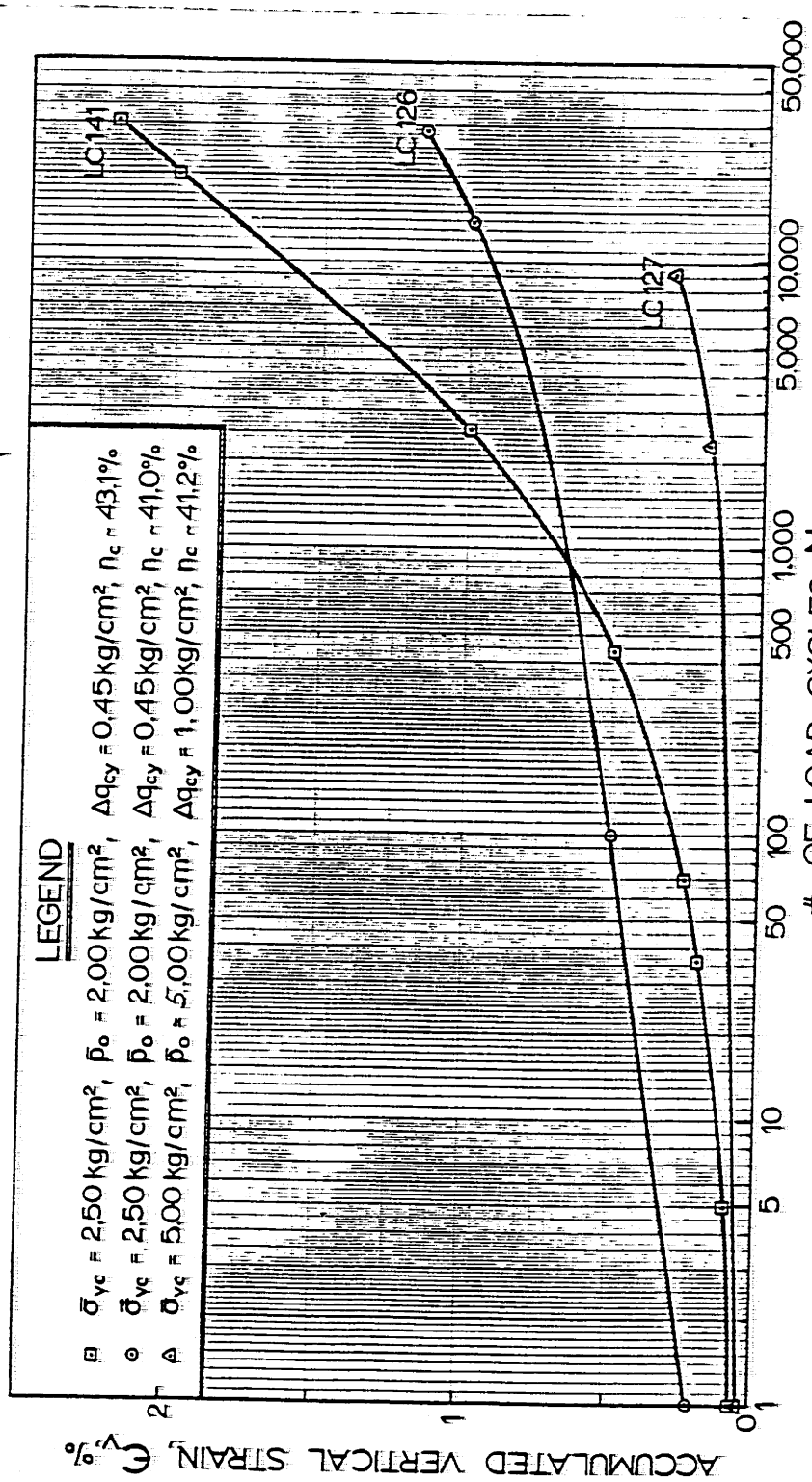

STRAIN DEVELOPMENT IN DRAINED TESTS

FIGURE F-124

APPENDIX G

Cyclic Oedometer Tests

G.1 Test Plots and Tabulations

Figures G.1 to G.7 show plots of cyclic oedometer tests (testing procedure given in Appendix B). Vertical strain is plotted versus vertical stress for selected cycles. The cycle numbers are all given at the right end of the cycle. Table G.1 gives pertinent data for the tests.

All the oedometer test samples were placed in a very loose state in the oedometer ring. The placement of the top cap on the sample therefore caused 2-3% vertical strain in the dry samples (Figures G.1 to G.5), but none in the wet compacted samples. The wet samples, however, strained about 2% by saturation (Figures G.6 and G.7), whereas the dry only strained 0.5 - 1%. At the end of the first loading, the samples had strained between 4 and 8% vertically. The tests were ended at strains beteen 11 and 16%.

CYCLIC OEDOMETER TEST TABULATION

Test # LC-		n %	$\bar{\sigma}_{vm}$ kg/cm^2	$\pm\Delta\bar{\sigma}_v$ kg/cm^2	$\Delta\bar{\sigma}_{vm}/\bar{\sigma}_v$	N, #	REMARKS
4-0		46.6	1.23	1.21	0.98	4460	Fine sand, poured dry
5-0	I	47.2	3.74	1.25	0.33	3120	Fine Sand
	II		1.23	1.21	0.98	33.830	Poured dry
6-0	I	46.5	0.65	0.63	0.97	35.660	Fine sand
	II		1.30	1.24	0.95	83.560	Poured dry.
8-0	I	47.0	7.18	1.24	0.17	20.082	Fine sand
	II		1.27	1.24	0.98	1750	Poured dry
9-0	I	46.3	1.76	1.24	0.71	23.440	Fine sand
	II		1.27	1.24	0.98	48.060	Poured dry
12-0		47.1	1.27	1.24	0.98	16.300	Medium sand, compacted moist
13-0		47.8	1.27	1.24	0.98	43.140	Fine sand, compacted moist

Table G.1

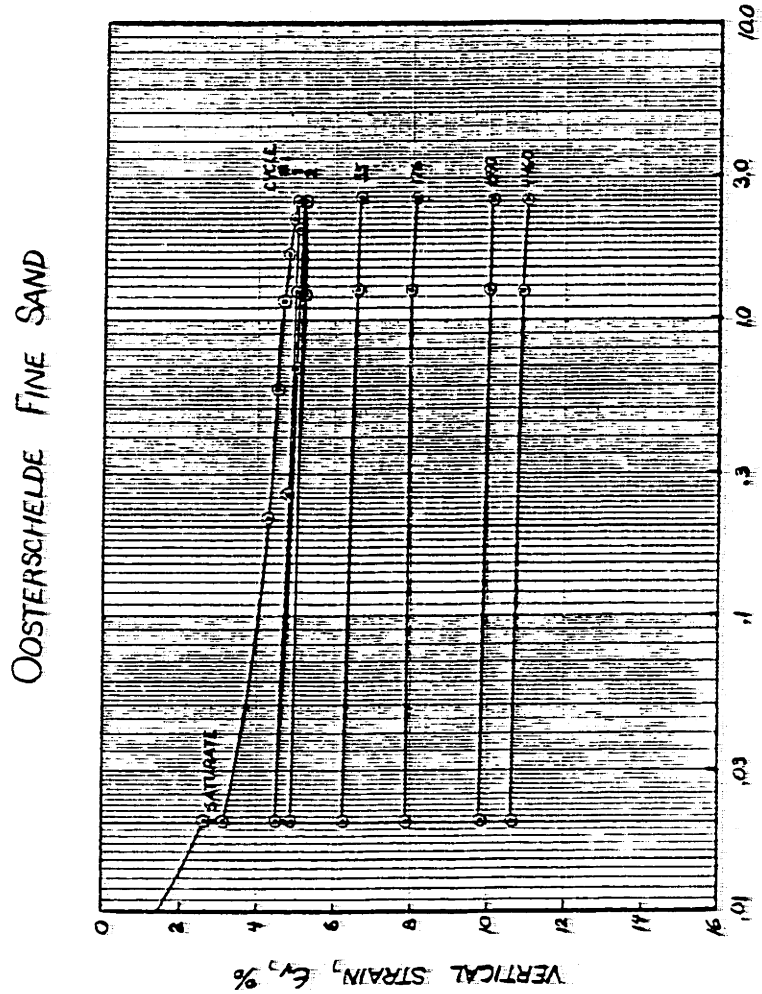
OOSTERSCHELDE FINE SAND
CYCLIC OEDOMETER TEST LC-4-O
VERTICAL STRAIN, ε_v, %
$\overline{\sigma_v}$, kg/cm²
SATURATE
CYCLE
1
3
10
100
1000
3000
0
2
4
6
8
10
12
14
16
.01
.03
.1
.3
1
3
10
100

FIGURE G-1

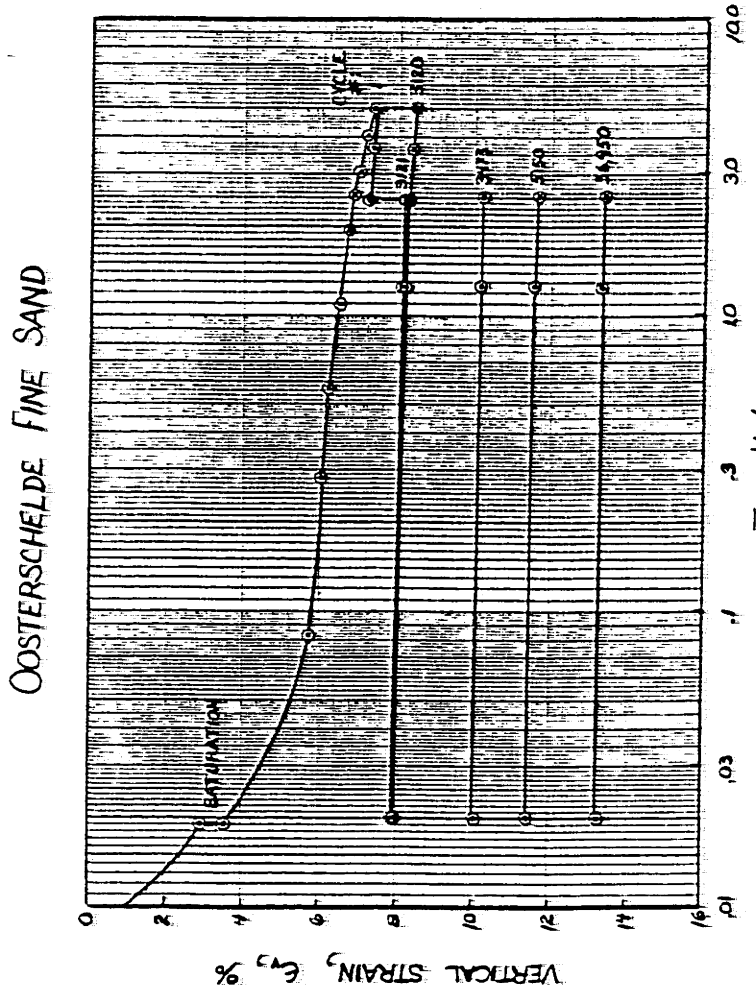
OOSTERSCHELDE FINE SAND
CYCLIC OEDOMETER TEST LC-5-0
VERTICAL STRAIN, ε_v %
$\bar{\sigma}_v$, kg/cm²
SATURATION
CYCLE #1
310
3481
3473
3760
14,950
0
2
4
6
8
10
12
14
16
.01
.03
.1
.3
1.0
3.0
10.0

FIGURE 6-2

OOSTERSCHELDE FINE SAND

CYCLIC OEDOMETER TEST LC-6-0

FIGURE 6-3

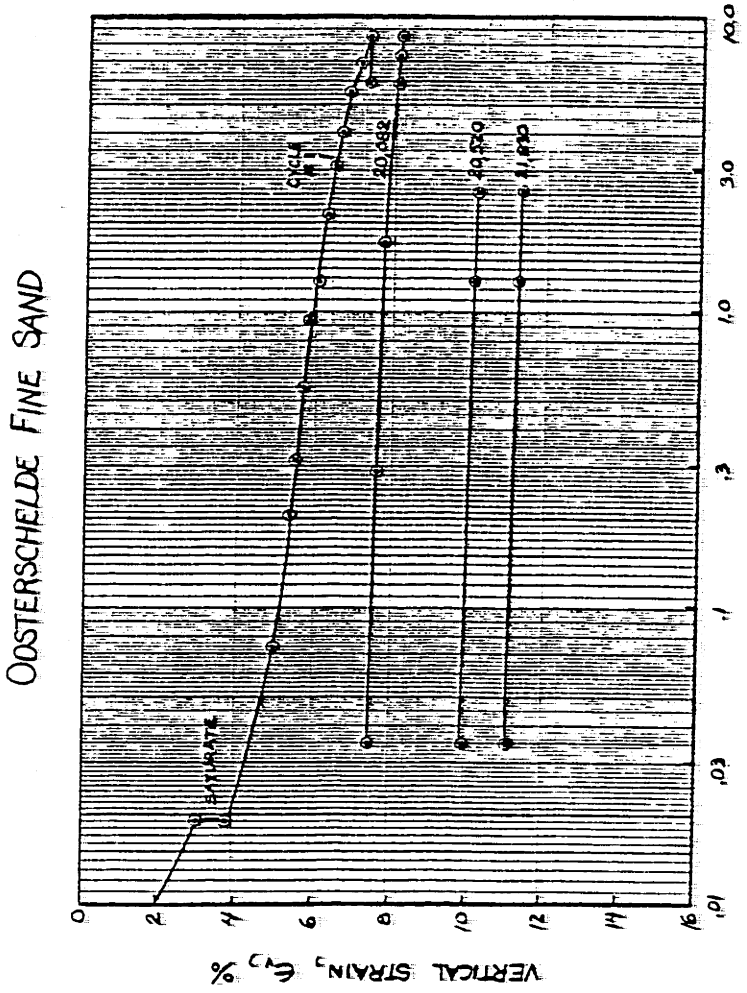
OOSTERSCHELDE FINE SAND
VERTICAL STRAIN, ϵ_v %
$\bar{\sigma}_v$, kg/cm²
CYCLIC OEDOMETER TEST LC-8-0
CYCLE #1
20,032
29,520
41,880
SATURATE

FIGURE G-4

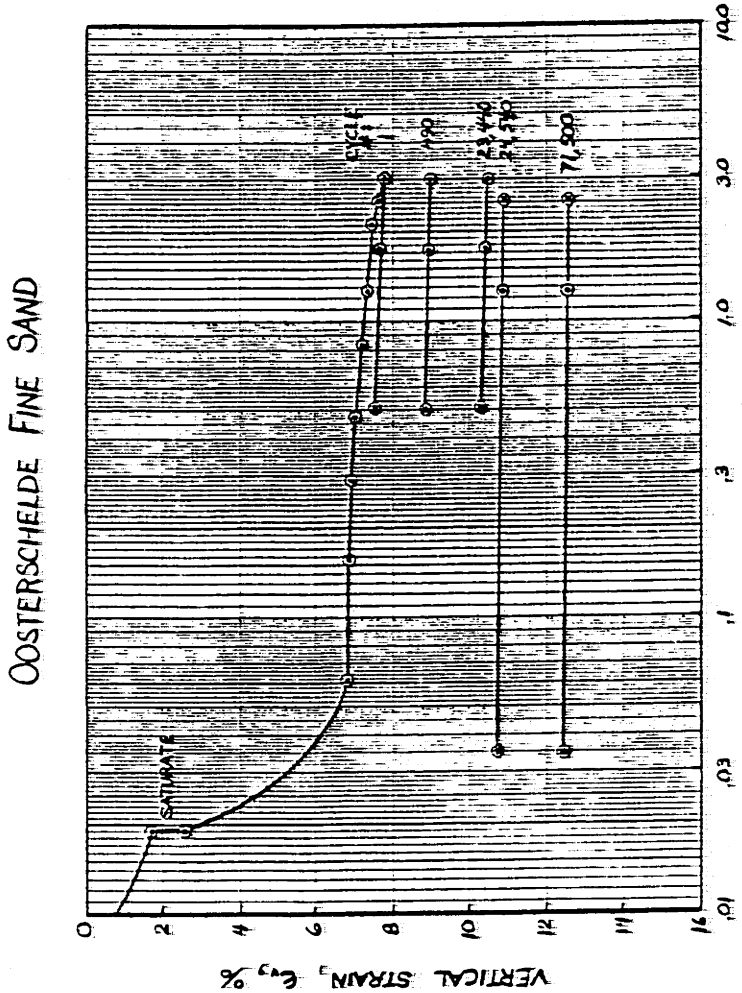
OOSTERSCHELDE FINE SAND
CYCLIC OEDOMETER TEST LC-9-O
VERTICAL STRAIN, ε_v, %
$\overline{\sigma_v}$, kg/cm²
SATURATE
EXCESS
1
180
23,440
24,540
71,500

FIGURE 4-5

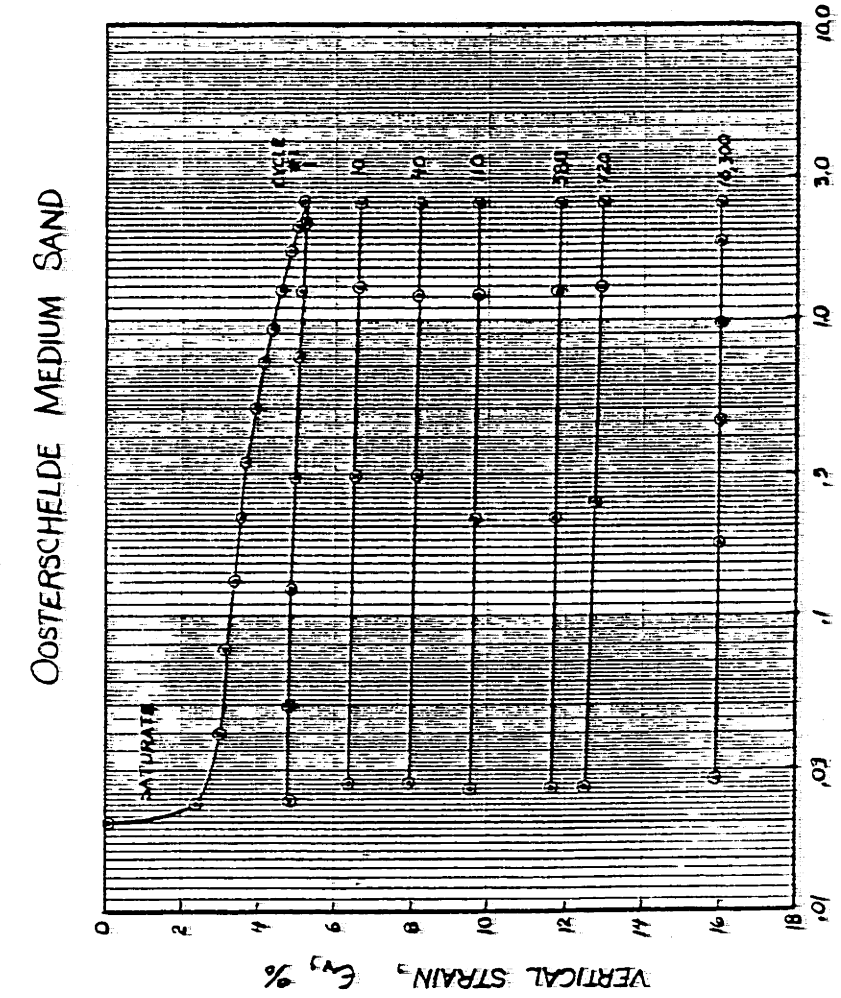
OOSTERSCHELDE MEDIUM SAND
CYCLIC OEDOMETER TEST LC-12-O
SATURATED
CYCLE
1
9
40
10
360
720
6,300
VERTICAL STRAIN, ε_v %
$\overline{\sigma_v}$, Kg/cm²
0
2
4
6
8
10
12
14
16
18
,01
,03
,1
,3
1
3,0
10,0

FIGURE 6-6

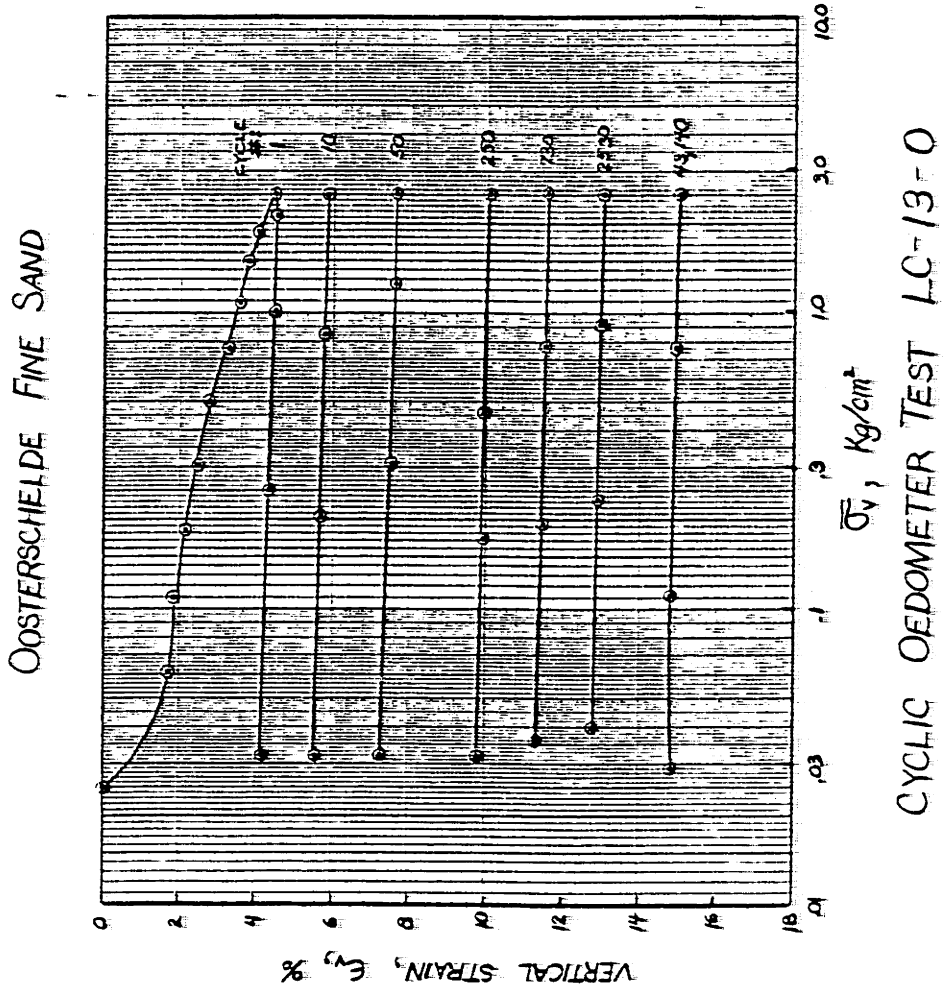
OOSTERSCHELDE FINE SAND
CYCLIC OEDOMETER TEST LC-13-O
VERTICAL STRAIN, ε_v, %
$\bar{\sigma}_v$, kg/cm²
FIELD
#1
10
20
40
80
160
320
640
0
2
4
6
8
10
12
14
16
18
.01
.03
.1
.3
1
3
10
30
100

FIGURE 6-7

Appendix H

PREDICTION EXAMPLE

Suppose there is an element in the foundation of an offshore structure with a porosity of 40.4%, a mean normal stress of 0.75 kg/cm^2 and a mean shear stress of 0.33. The design storm loading of that structure may be represented by 100 load cycles, each producing a cyclic shear stress ratio of 0.267.

The procedure to predict strain and pore pressure for a triaxial test modeling that field condition is then as follows (see Chapter V):

(1) Enter Figure H.1 with the porosity of 40.4% and cyclic shear stress ratio of 0.267. The test plots within the contractive range, so the prediction procedure is valid for this case.

(2) Enter Figure H.2 at n_c = 40.4% to find $C_{n\varepsilon}$ = 2.40 and C_{nu} = 2.70. Enter Figure H.3 at $\Delta q_{cy}/\bar{p}_o$ = 0.267 to find $C_{\Delta q\varepsilon}$ = 0.068 and $C_{\Delta qu}$ = 0.082. Enter Figure H.4 at $\bar{p}_o$ = 0.75 kg/cm^2 to find $C_{\bar{p}\varepsilon}$ = 4.5 and $C_{\bar{p}u}$ = 5.2.

(3) Calculate $N_\varepsilon = N/C_{n\varepsilon} \cdot C_{\Delta q\varepsilon} \cdot C_{\bar{p}\varepsilon}$ = 100/2.40 · 0.068 · 4.5 = 136 cycles, and $N_u = N/C_{nu} \cdot C_{\Delta qu} \cdot C_{\bar{p}u}$ = 100/2.70 · 0.082 · 5.2 = 87 cycles.

(4) Enter Figure H.5 at N_ε = 136 and $q_m/\bar{p}_o$ = 0.33 to

find an accumulated vertical strain of 0.092% and Figure H.6 at N_u = 87 cycles to find a pore pressure ratio of 0.31.

Test LC66 was performed at the same porosity and stress path as the example above. From Figure F.2c in Appendix F is found by interpolation that M = 0.41 and ε_v = 0.06% was measured in test LC66. The measured pore pressure ratio thus exceeds the predicted by a factor of 1.32, whereas the predicted strain exceeds the measured by a factor of 1.53.

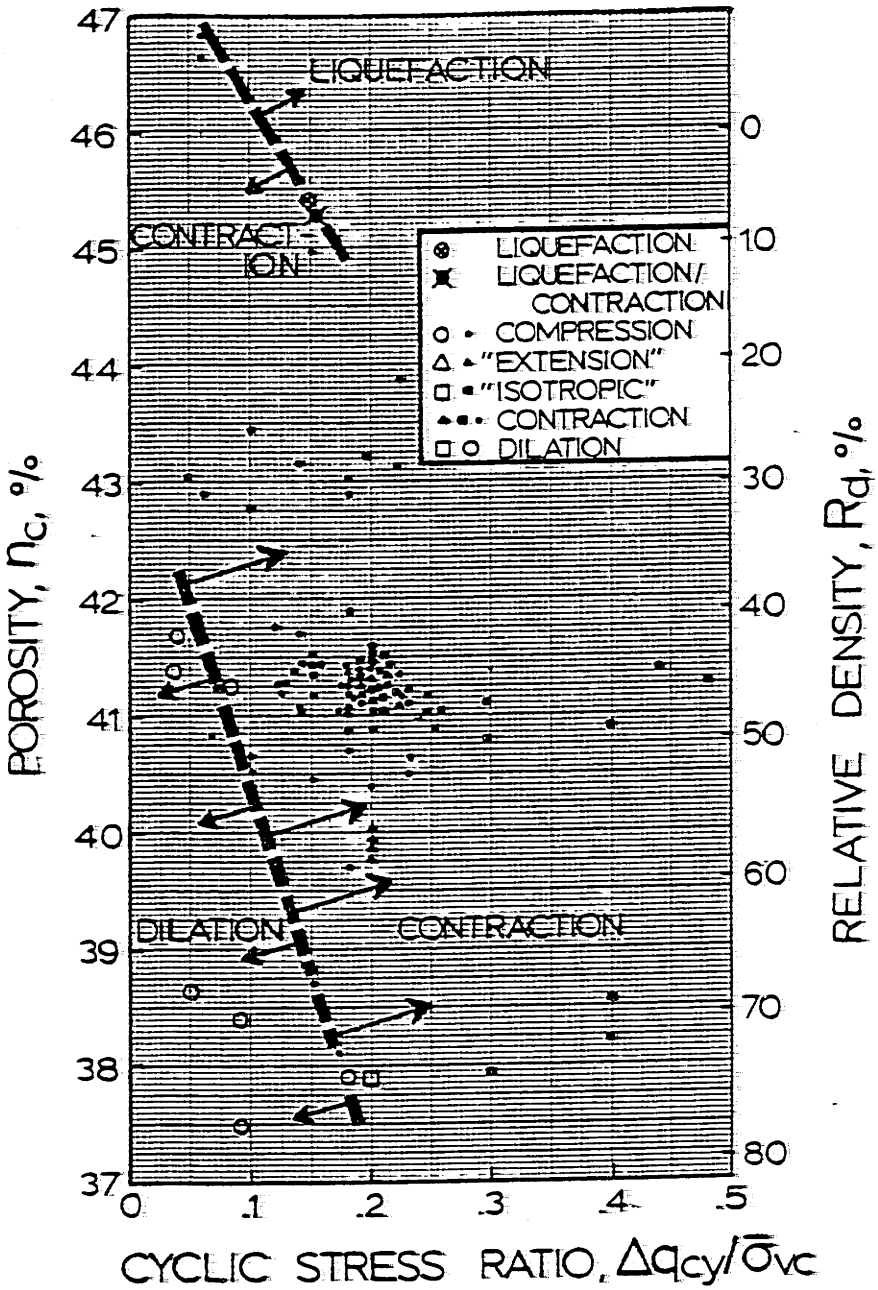

SUMMARY OF CYCLIC TRIAXIAL TESTS

FIGURE 4-1

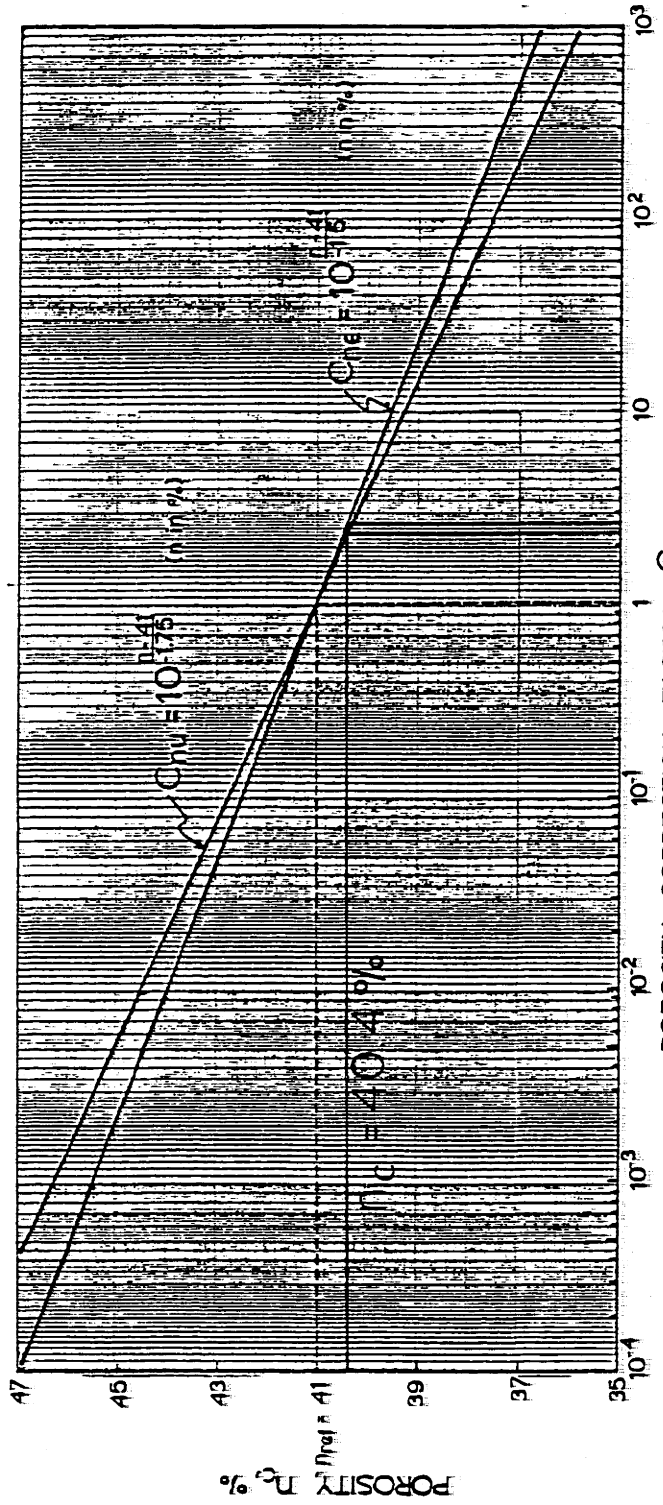

POROSITY CORRECTION FACTORS FOR CYCLIC COMPRESSION TESTS

FIGURE H-2

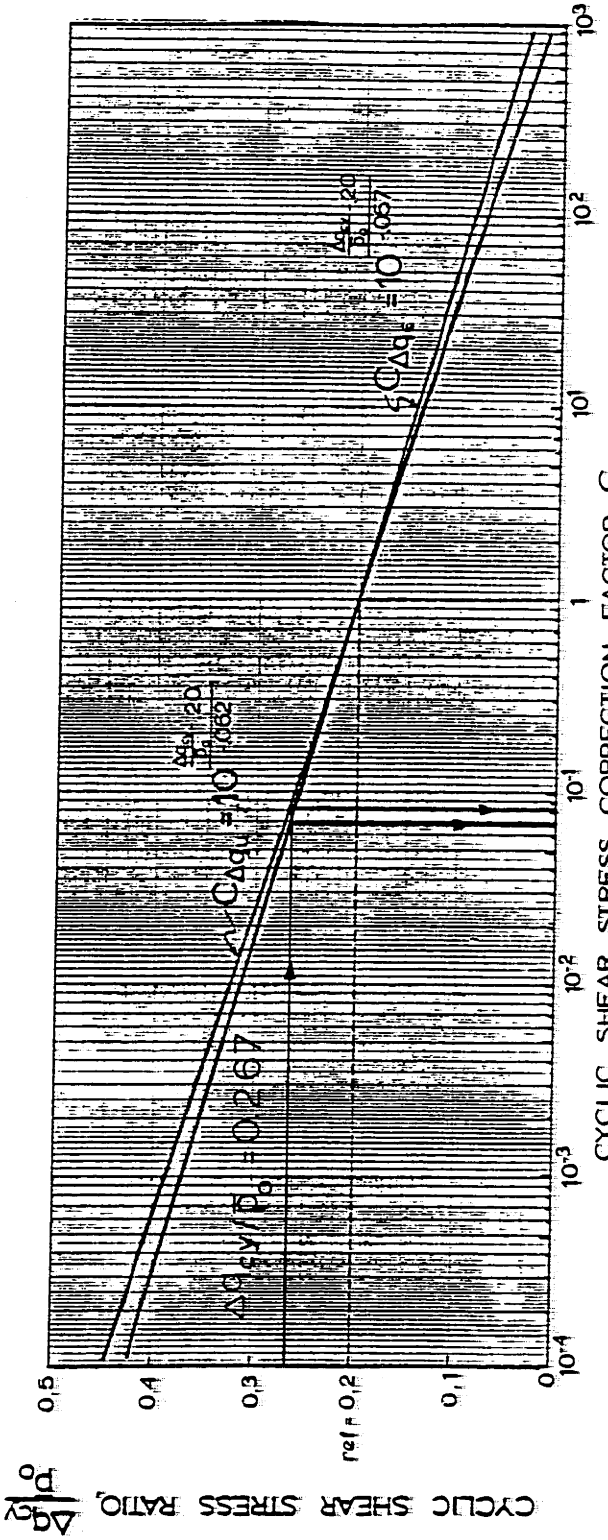

CYCLIC SHEAR STRESS RATIO CORRECTION FACTORS FOR CYCLIC COMPRESSION TESTS

FIGURE H-3

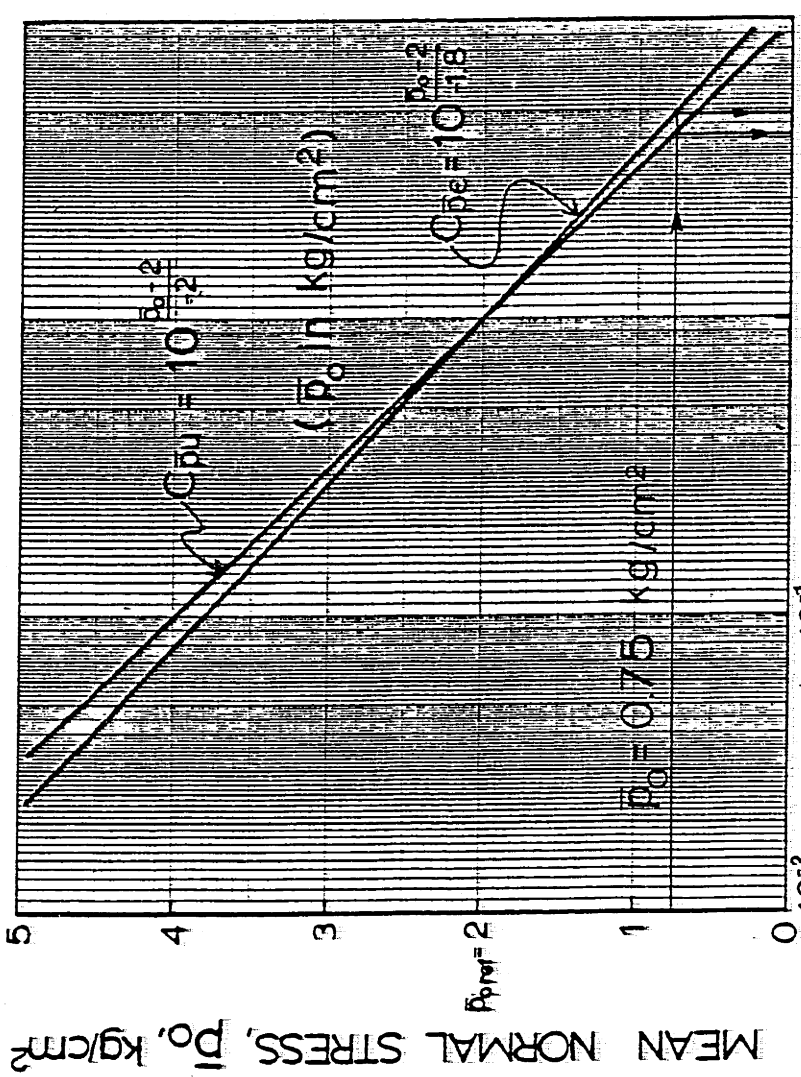

MEAN NORMAL STRESS CORRECTION FACTOR FOR CYCLIC COMPRESSION TESTS

FIGURE H-4

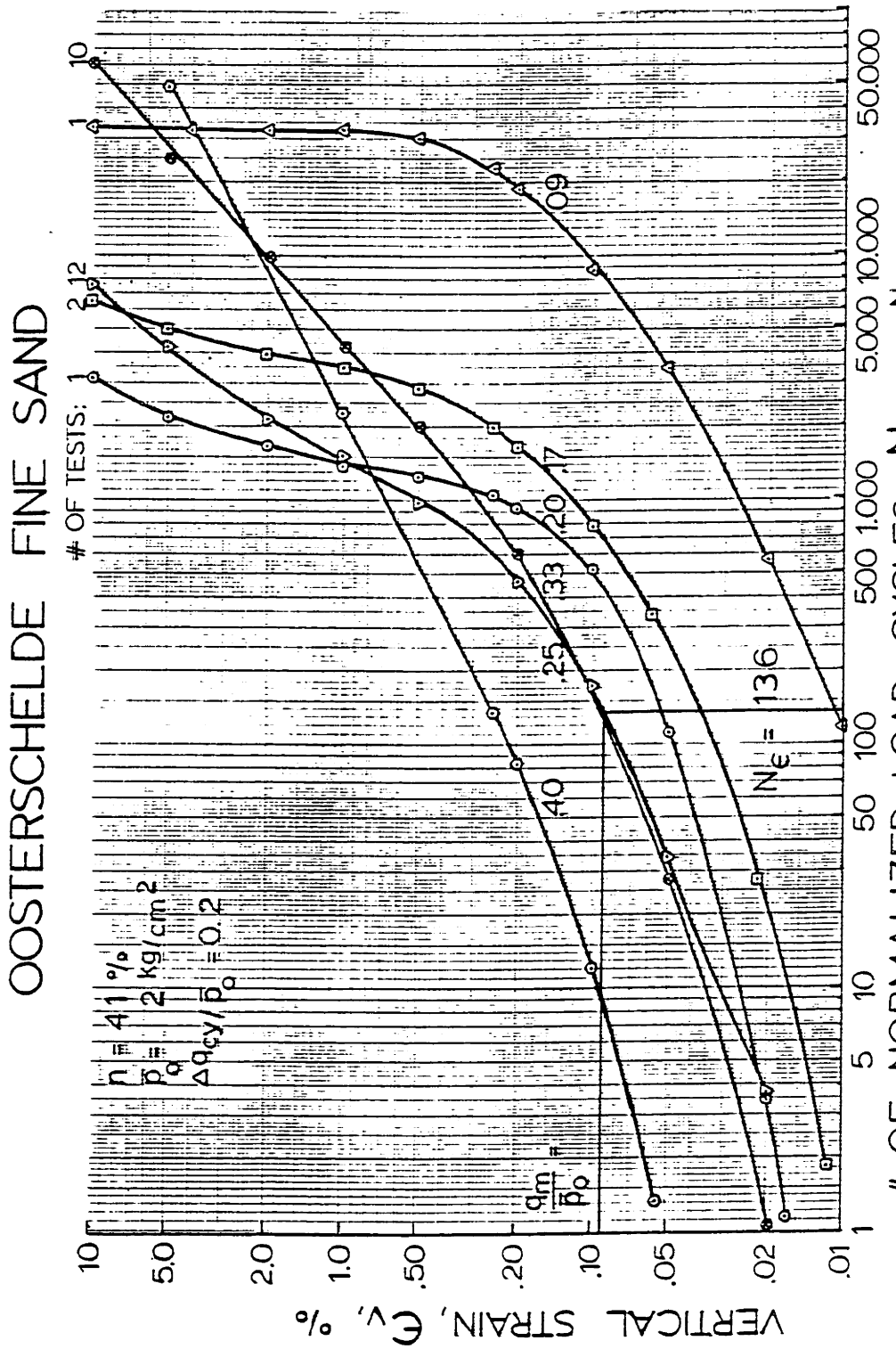

STRAIN PREDICTION PLOT FOR COMPRESSIVE STRESS STATE

FIGURE H-5

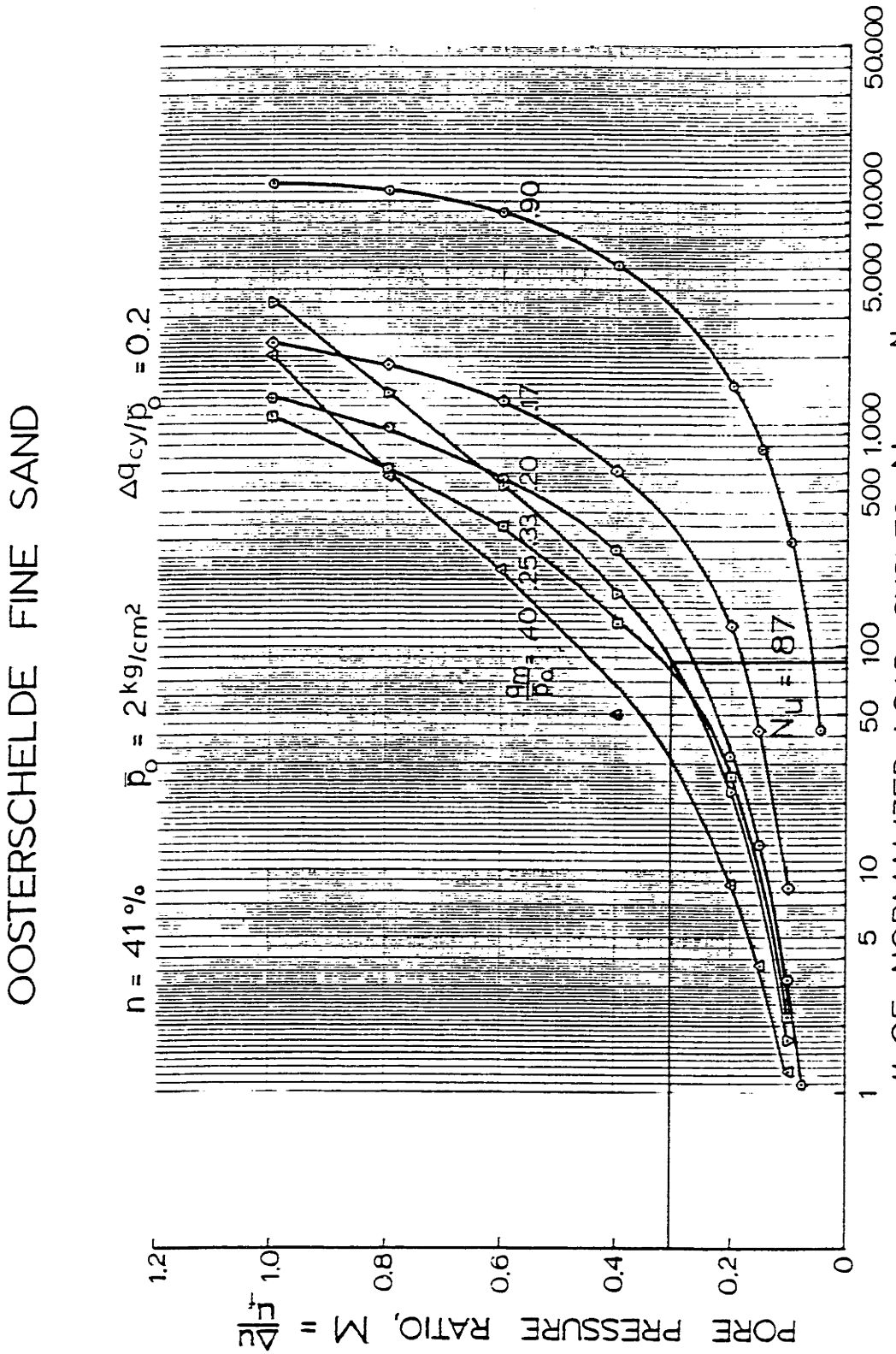

PORE PRESSURE PREDICTION PLOT FOR COMPRESSIVE STRESS STATE

FIGURE H-6

BIOGRAPHY

Jan Hedberg was born in Sarpsborg, Norway on May 21, 1947. He lived there until finishing high school in 1966; then he moved to Darmstadt, Germany to study civil engineering. In 1972 he received his diploma at the Technische Hochschule Darmstadt (Dipl.-Ing.), married and started working at the Norwegian Geotechnical Institute in the field instrumentation division. In 1973 he left N.G.I. to study at the Massachusetts Institute of Technology, where he received his Master of Science in Civil Engineering (M.Sc.) in 1975. Jan Hedberg speaks English, German and the Scandinavian languages. With his wife, Mimi, they have a daughter and a son, born in 1973 and 1975.


OF FILM
E REWIN